Annual Report 2001

Institut für Kernphysik and COSY Research

Cover Picture

An outstanding milestone has been reached at COSY when the first beam with a momentum of 1.57 GeV, which was electron cooled at injection energy, was transported to BIG KARL, an external target station. The left picture shows a tv-screen shot taken from a viewer for an uncooled beam, the right picture shows the result of the electron cooling process. The tick marks shown are 2 mm from the center. The shrinking effect visible on these pictures does not fully reflect the real reduction due to the high brightness of the cooled beam spot and the subsequent strong blooming caused by the tv-camera. More telling was the difference in countrate measured by a veto scintillator detector close to the target, having a small hole through which the beam passed. The veto counting rate at this position, which was a limiting factor in previous experiments, was reduced by nearly two orders of magnitude for the cooled beam. This breakthrough will enable the investigation of reactions in external experiments hitherto unapproachable.

Berichte des Forschungszentrums Jülich ; 3978
ISSN 0944-2952
Institut für Kernphysik Jül-3978

Zu beziehen durch: Forschungszentrum Jülich GmbH · Zentralbibliothek
52425 Jülich · Bundesrepublik Deutschland
☎ 02461/61-5220 · Telefax: 02461/61-6103 · e-mail: zb-publikation@fz-juelich.de

Preface

The current annual report summarizes the research of the Institut für Kernphysik (IKP) at the Forschungszentrum Jülich (FZJ) in the fields of nuclear and hadron physics for the year 2001. In particular, it covers the experimental activities at the major facility of the institute, the Cooler Synchrotron (COSY), and at various external German and international research facilities.

COSY has been running very reliable again during 2001, similar to the years before, delivering proton beams – unpolarized or polarized, electron or stochastically cooled, slowly or fast extracted – for internal and external experiments with a total operation time close to 7300 hours. For about 30% of that time, polarized proton beams were provided, a significant increase compared to previous years, which testifies the performance level reached with the polarized source. Other highlights of the accelerator include:

- Extraction of a cooled proton beam with significantly reduced phase space (see figure on front page).
- Different beam extraction modes: fast kicker (~300 ns), and stochastic (20 – 1000 s)
- Long stored beam lifetime (~ 100 hrs).
- Increase in maximum momentum from 3.4 to 3.65 GeV/c.
- First deuteron beam, accelerated up to 3.3 GeV/c.

In response to these new possibilities, experiments utilizing the high energy proton and the new deuteron beam are scheduled for the beginning of 2002.

The experiments at the internal and external target positions of COSY have made use of the proton beam for more than 5500 hours. You will find many interesting and exciting results from these measurements in the pages to follow, like e.g.:

- ANKE has been able to identify the production of a scalar meson (a_0 (980)) in proton-proton collisions via its decay into the two main decay channels.
- COSY-11 has performed a first measurement of η-production with a polarized proton beam.
- EDDA has finished its program of measurements of proton-proton elastic scattering with very successful double-polarisation runs.
- GEM has taken simultaneously high statistics data for pd → ^{3}He π° and ^{3}H $\pi+$ at the η-threshold, which will significantly improve the knowledge on π°–η mixing.
- JESSICA, a mock-up target station experiment for the European Spallation Neutron Source (ESS), has used a mercury target and a water moderator to obtain first spectra of moderation time as function of the neutron energy.
- MOMO has obtained high quality data for K^+K^- and ϕ-meson production in pd → ^{3}He X reactions.
- PISA, a new internal beam set-up for nuclear spallation physics, has started commissioning.
- At TOF first successful data was taken with the big new calorimeter and meson identifier in pp → pp$\pi^+\pi^-$.

Members of the institute are also participating in external collaborations: in the anti-hydrogen experiment ATRAP at the anti-proton decelerator (AD) at CERN, in nuclear spectroscopy investigations with EUROBALL, in pionic-atom measurements at PSI, in photonuclear reaction experiments with TAPS at MAMI, in experiments using hadronic interactions with WASA at CELSIUS, in high energy measurements with ZEUS at DESY and atomic physics experiments at GSI. Results of these activities are also found below.

The theory group of the institute has been active in a broad range of research fields with a focus on hadronic physics in the realm of non-perturbative Quantum Chromo-dynamics (nPQCD) and special emphasis on results from COSY. This is done in the framework of phenomenological models and effective theories. These activities are further strengthened by a strong visitors program and numerous world-wide collaborations. The diversity of the research of the theory group is demonstrated in the corresponding chapter below.

COSY has the status of a "Large Scale Facility" by the European Commission within the framework "Support for Access to Research Infrastructure". Together with its partner laboratories, KVI Groningen and TSL Uppsala, it forms the joint organization LIFE ("Light Ion Facility Europe"), which coordinates the studies with hadronic probes.

Since drastic changes are starting to evolve with respect to funding the "Helmholtz-Centers" – to which FZJ belongs – we, as part of this, are on the verge of serious new challenges, but we will take these as an opportunity to sharpen our program and strengthen our efforts even further. We are in a good shape for the immediate and intermediate future, since we have received funds for building a new linac to replace the old injector cyclotron, and we have been given green light selecting successors for two of the four directors of our institute after their retirement in 2003 and 2004.

In closing, I would like to thank all my colleagues from within the institute and FZJ as well as the many outside users – from universities and other institutions in Germany, Europe and worldwide – for their support and dedication in helping to make COSY a world class facility for hadron physics. Without the support from various partners, in particular from the user organization CANU and from many different funding agencies, the successful operation of such a research facility would not have been possible. I'm also much obliged to our advisory committees (Beirat and PAC) for their guidelines and recommendations. Finally, I thank the board of directors of the Forschungszentrum Jülich for their commitment for COSY and the research at our institute.

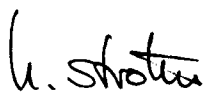

Hans Ströher

INSTITUTE FOR NUCLEAR PHYSICS

Forschungszentrum Jülich GmbH

D-52425 Jülich, Germany

Managing director:	Prof.Dr.H.Stöher
Experimental Nuclear Physics I, director:	Prof.Dr.K.Kilian
Accelerator division, head of the:	Prof.Dr.R.Maier
Experimental Nuclear Physics II, director:	Prof.Dr.H.Stöher
Theoretical Physics, director:	Prof.Dr.J.Speth

CONTENTS

I. Experimental Hadron Physics

1.2 Experiments at External Facilities

2. NUCLEAR SPECTROSCOPY

II. Theoretical Nuclear Physics

3. MEDIUM AND HIGH ENERGY PHYSICS

4. NUCLEAR PHYSICS AND OTHER TOPICS

III. Accelerator Division

5. COOLER SYNCHROTRON COSY

6. ION SOURCES, BEAM TRANSPORT, AND LINAC INJECTOR

7. SPECTROMETER BIG KARL

8. RADIATION PROTECTION

IV. EUROPEAN SPALLATION NEUTRON SOURCE (ESS)

9. TARGET PHYSICS

10. ACCELERATOR COMPONENTS

V.Technical Developments

11. ELECTRONICS,SEMICONDUCTOR DETECTORS

I. Experimental Hadron Physics

1. MEDIUM ENERGY PHYSICS

1.1 Experiments at COSY

1.2 Experiments at External Facilities

2. NUCLEAR SPECTROSCOPY

1.1 Experiments at COSY

Elastic pp Scattering: Recent Results from the EDDA Experiment

J. Bisplinghoff, F. Hinterberger, H. Rohdjeß and W. Scobel for the EDDA collaboration[1]

Proton-proton elastic scattering with projectile energies up to 800 MeV has been studied thoroughly in the past to an extent that there is now a comprehensive database [2]. In terms of meson exchange and potential models, this determines the long and medium range part of the nucleon-nucleon (NN) force. In particular recent precision measurements at IUCF of rare spin observables for projectile energies $T_p \leq 450$ MeV [3, 4, 5] added valuable information. The data are well described by the results of phase shift analyses (PSA) [2, 6] which show only little variations among each other in this energy regime [3, 5, 7]. Modern meson exchange potential models provide adequate descriptions of the data up to the pion production thresholds [8]. The extension of these models to higher energies requires the inclusion of contributions from inelastic channels. Using relativistic transition potentials the restriction to a coupling of NN, NΔ and ΔΔ channels leads to a reasonable description of the data up to 1 GeV [9]. However, meson exchange models will break down once the hadron substructure cannot be neglected any more. At higher energies larger momentum transfers contribute, thus probing smaller distances (< 0.8 fm), so that genuinely new processes involving the dynamics of the quark-gluon constituents may be important. A related problem is the nature of the strong repulsive core of the NN interaction needed to explain scattering data at low energies. Another important problem is the question of dibaryons. Accordingly, proton-proton scattering at 0.5 – 2.5 GeV is ideally suited to sample the short range part of the NN interaction with spatial resolutions of about 0.15 fm and to study the role of heavy-meson exchanges [9].

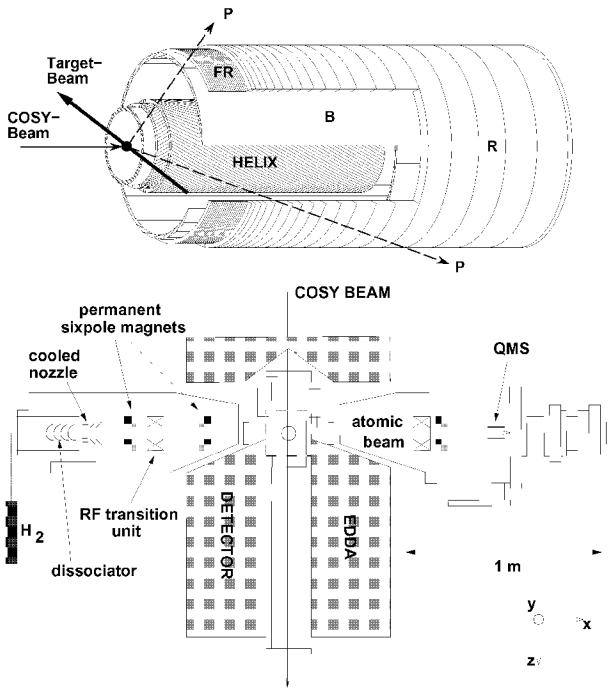

Fig. 1: Scheme of the EDDA detector (top) and its combination with the atomic beam target (bottom).

When the EDDA experiment started in 1994, the experimental data base was incomplete for energies $T_p > 1.0$ GeV, and normalization discrepancies of angular distributions obtained at discrete energies gave rise to systematic errors. Therefore, the concept of the EDDA experiment is to measure excitation functions in small energyy steps with a high relative accuracy using an *internal* target at the proton cooler synchrotron COSY (FZ Jülich) [10]. Data taking proceeds *during the synchrotron acceleration ramp*, such that a complete excitation function is measured during each acceleration cycle. Statistical accuracy is obtained by averaging over many thousand cycles (multi-pass technique).

In *phase 1* of the experiment unpolarized differential cross sections have been measured [11] using 4 μm × 5 μm CH_2 fiber targets. The number of recirculating protons was reduced to some 10^7 yielding luminosities of typically $5{\cdot}10^{29}$ $cm^{-2}s^{-1}$. In *phase 2* the analyzing power A_N was measured [12] using a polarized atomic beam target in conjunction with the unpolarized proton beam with up to $3{\cdot}10^{10}$ protons in the flattop. This method is in contrast to the conventional use of a polarized proton beam and an unpolarized hydrogen target. It has the advantage to avoid systmatic uncertainties due to depolarizing resonances crossed in the acceleration ramp. The absolute value of the target polarization is constant during the full acceleration cycle. In the final *phase 3* the spin correlation coefficients A_{NN}, A_{SS}, and A_{SL} were measured with a polarized atomic beam target of about 80 % effective polarization and a polarized proton beam of typically 55 - 80% polarization, up to $1.3{\cdot}10^{10}$ circulating protons and luminosities up to $3{\cdot}10^{27}$ $cm^{-2}s^{-1}$. The final production run was in 2001. The data analysis is in progress.

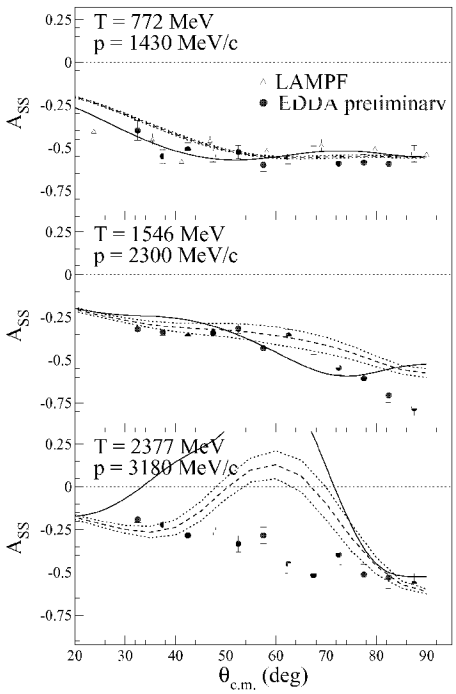

Fig. 2: Preliminary spin correlation parameter A_{SS}, from EDDA at p_p = 1430, 2300 and 3180 MeV/c. The SAID solution SM00 is given as a solid line, the Saclay-Geneva solution [20] as dashed line. The open symbols at 1430 MeV/c are data from LAMPF.

In order to access A_{SS}, A_{NN} and A_{SL} the target polarization was changed cyclewise between $\pm x$, $\pm y$, and $\pm z$, and the beam polarization from $+y$ to $-y$, resulting in 12 different relative spin orientations. These lead to different modulations of the scattering rates with the azimuthal angle Φ; the resulting asymmetries between the four quadrants $\Delta\Phi = 90°$ can be used to determine the spin correlation parameters as well as target and beam polarizations.

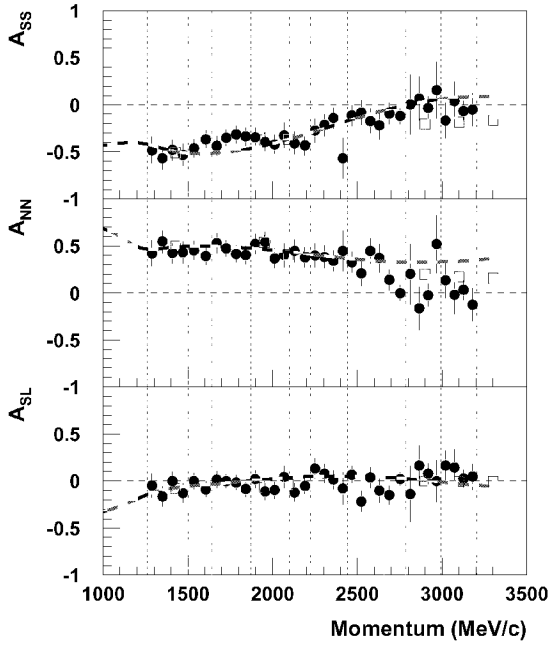

Fig. 3: Preliminary excitation functions for the spin correlation coefficients A_{SS},A_{NN}, and A_{SL} measured during beam acceleration (closed symbols) with Δp_p = 60 MeV/c and Θ_{cm} = 37.5°± 2.5°. Also shown are results from high statistics flattop measurements (open symbols) and the SAID solution FA00 (solid line). Depolarizing resonances are indicated by the dotted lines.

A first measurement was carried out at T_p = 772 MeV, the highest energy, for which some data for all three correlation coefficients exist already. Our data were found to be in good agreement with them as well as with the PSA solutions FA00. The measurements have then been extended to higher energies with data collection in the momentum ramp and the following flattop. With the completion of data taking in 2001, a total of 10 different flattop energies have been accessed. Angular distributions of A_{SS} at three energies are shown in Figure 2. Excitation functions at $\Theta_{cm} = 37.5°$ are shown in Figure 3. The predictions of phase shift analyses of the George Washington University (previous VPI) [21] and the Saclay-Geneva [20] group for the regions not yet covered with data show for A_{SS} large deviations from the data as well as from each other. Obviously the experimental data base at higher energies as of 2000 does not allow a precise and unambiguous determination of phase shifts, rendering the predictive power of PSA questionable in the energy regime. This is supported by attempts to reconstruct the scattering amplitudes directly from experimental data [20] where different sets of amplitudes were found to describe the data. We have conducted such an analysis at 2.1 GeV (2900 MeV/c) and find that primarily new data on A_{SS} will reduce the number of possible solutions for the scattering amplitudes. If this will allow for an unambiguous determination of phase shifts has yet to be seen, when these new data have been included in the PSA.

The concept of EDDA as a dedicated experiment for the measurement of elastic pp, $p\vec{p}$ and $\vec{p}\vec{p}$ scattering on an internal target during the acceleration of the recirculating COSY beam has proven feasible. It yielded precise data for c.m. scattering angles from 30° to 90° and quasicontinuous energies from 0.5 GeV to 2.5 GeV. Each set of excitation functions for (i) spin averaged cross sections, (ii) analyzing powers, and (iii) spin correlation coefficients led to distinct extensions and modifications of the then actual PSA solutions in regions with low or no data coverage. In retrospective are these deviations larger - and the predictive power of interpolated or extrapolated phase shift solutions smaller - than anticipated at the beginning of the EDDA experiment.

The EDDA collaboration gratefully acknowledges the great support received from the COSY accelerator group, and the financial support by the BMBF, Contracts 06BN664I(6) and 06HH952, and the FZ Jülich, Contracts FFE 41126803 and 41126903.

References:

[1] Spokespersons: J. Bisplinghoff, F. Hinterberger, W. Scobel. See http://www.iskp.uni-bonn.de/edda.html and http://kaa.desy.de.
[2] R.A. Arndt et al., Phys. Rev. C **56**, 3005 (1997).
[3] F. Rathmann et al., Phys. Rev. C **58**, 658 (1998).
[4] B. von Przewoski et al., Phys. Rev. C **58**, 1897 (1998).
[5] B. Lorentz et al., Phys. Rev. C **61**, 054002 (2000).
[6] V. G. J. Stoks et al., Phys. Rev. C **48**, 792 (1993).
[7] V. G. J. Stoks and J. J. de Swart, Phys. Rev. C **52**, 1698 (1995).
[8] R. Machleidt and I. Slaus, R. et al., J. Phys. G: Nucl. Part. Phys. **27**, 69 (2001) and references therein.
[9] R. Machleidt, Adv. in Nucl. Phys. **19**, 189 (1989).
[10] R. Maier, Nuclear Physics News **7/4**, 5 (1997).
[11] D. Albers et al., Phys. Rev. Lett. **78**, 1652 (1997).
[12] M. Altmeier et al., Phys. Rev. Lett. **85**, 1819 (2000).
[13] P. D. Eversheim et al., Nucl. Phys. **A626**, 117c (1997).
[14] M. Garçon et al., *Nucl. Phys.* **A445**, 669 (1985).
[15] R. A. Arndt, I. I. Strakovsky, and R. L. Workman, Phys. Rev. C **50**, 2731 (1994).
[16] G. G. Ohlsen and P. W. Keaton, Nucl. Instr. and Meth. **109**, 41 (1973).
[17] M. W. McNaughton et al., Phys. Rev. C **41**, 2809 (1990).
[18] C. E. Allgower et al., Phys. Rev. C **60**, 054001 (1999).
[19] C. E. Allgower et al., Phys. Rev. C **60**, 054002 (1999).
[20] J. Bystricky, C. Lechanoine–LeLuc and F. Lehar, Eur. Phys. J. C **4**, 607 (1998).
[21] R. A. Arndt, I. I. Strakovsky, and R. L. Workman, Phys. Rev. C **62**, 034005-1 (2000).

Study of η′-Meson Production in the Reaction pd → ^{3}He η′ at COSY-11

H.-H. Adam[1], A. Khoukaz[1], T. Lister[1], R. Santo[1] and S. Steltenkamp[1] for the COSY-11-Collaboration

At COSY-11 [1], measurements on the η- and η′-meson production in proton-proton scattering have been recently extended by production measurements in the proton-deuteron interaction, i.e. studies on the reaction channels pd → ^{3}He η, η′ [2,3].
Different to elementary nucleon-nucleon reactions the production of mesons on heavier targets provides the possibility to study reaction processes with more than only one involved target nucleon. Such data sets in the near threshold region are valuable for the understanding of the η- and η′-meson production in hadronic interactions [4,5,6] and may also be important in the context of understanding the production processes for these mesons in heavy ion collisions.

In earlier beam times the COSY-11 collaboration took data on the reaction channel pd → ^{3}He η at excess energies of Q = 5, 11, 15, 20 and 40 MeV, which are currently under final evaluation. Additionally, during one of these beam times first measurements on the η′-meson production in pd collisions have been carried out successfully at excess energies of Q = 10 MeV and Q = 40 MeV.
Here we present first preliminary results from a two days measurement on the η′-production obtained at an excess energy of Q = 10 MeV.

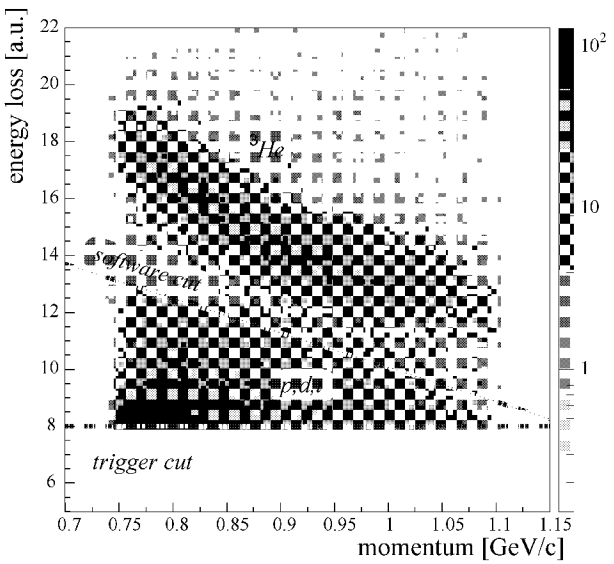

Fig. 1: Energy loss of positively charged particles as function of the reconstructed momentum, obtained at a beam momentum of p = 2.457 GeV/c (logarithmic z-axis). The cut at about 8 MeV is caused by the trigger used in the experiment. As indicated, the ^{3}He nuclei can be easily separated from other particles (software cut).

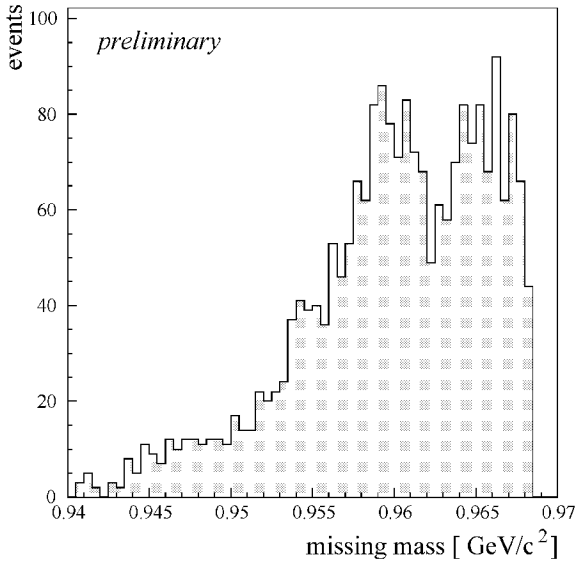

Fig. 2: Missing mass spectrum of the reaction pd → ^{3}He X, obtained at an η′ excess energy of Q = 10 MeV, integrated over a range of ^{3}He cms scattering angles of $-0.6 \leq \cos\theta^* \leq 0.6$.

The COSY-11 standard procedure for particle identification is the track reconstruction for positively charged particles through the well known magnetic dipole field by means of a set of two drift chambers, yielding a precise momentum determination, followed by a time-of-flight measurement using a set of two scintillator hodoscopes (S1, S3).
Detected ^{3}He nuclei can be separated from protons, deuterons and tritium, due to the comparatively large energy loss of the ^{3}He nuclei in the scintillation detector S1, as demonstrated in the ΔE/p plot in figure 1.
In figure 2 a preliminary missing mass distribution of accepted events with one detected particle, identified as ^{3}He nucleus, is presented. Close to the η′ literature mass a clear signal of the pd → ^{3}He η′ production is obvious, corresponding to ~ 340 detected η′ mesons.

References:

[1] S. Brauksiepe et al., Nucl. Instr. & Meth. A 376 (1996) 397.
[2] H.-H. Adam, diploma thesis, Universität Münster (2000).
[3] I. Geck, Staatsexamensarbeit, Universität Münster (2001).
[4] G. Fäldt and C. Wilkin, Nucl.Phys. A 587 (1995) 769.
[5] K. Kilian and H. Nann, AIP Conf. Proc. Vol. 221 (1990) 185.
[6] M. Betigeri et al., Phys. Lett. B 472 (2000) 267.

[1] Institut für Kernphysik, Universität Münster

Luminosity determination at COSY-11 using the proton-deuteron elastic scattering

S. Steltenkamp*, H.-H. Adam*, A. Khoukaz*, T. Lister*, R. Santo* for the COSY-11 collaboration

Measurements on the near-threshold η and η' meson production in the reaction $pd \rightarrow {}^3HeX$ have been performed at the internal beam experiment COSY-11 [1, 2]. To extract total and differential cross sections from the data, the luminosity will be determined by the simultaneously measured pd elastic scattering. For this purpose events with one proton detected in both drift chambers and the scintillation detector S1 and one deuteron hit in the monitor detector [3] have been selected.

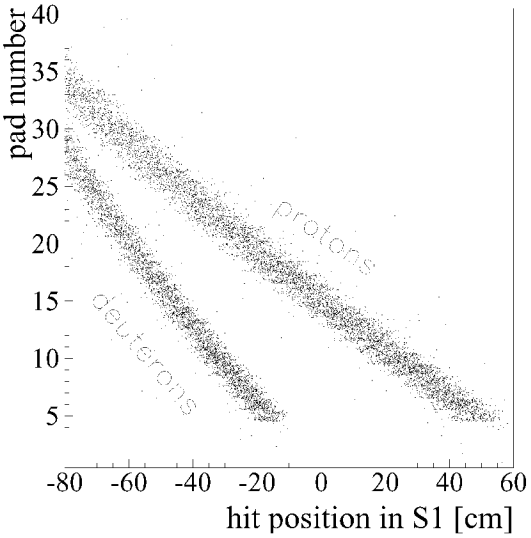

Fig. 1: Correlation between the hit position in the scintillation detector S1 and the pad number of the silicon monitor detector of the pd elastic scattering (MC simulation).

Figure 1 presents results of Monte-Carlo simulations on pd elastic scattering, performed at a beam momentum of $p_{beam} = 1.581\,\mathrm{GeV/c}$, corresponding to an excess energy of $Q \sim 11\,\mathrm{MeV}$ relative to the $pd \rightarrow {}^3He\eta$ threshold. The upper and the lower band correspond to events with a proton or a deuteron detected in the scintillation detector S1. Due to the comparatively large momentum transfer, the deuteron band is not expected to be visible in experimental data.

Data plotted in figure 2a expose two bands, the lower one is the signal of pd elastic scattering with protons detected in S1 and the upper one corresponds to events of the quasi-free proton-proton scattering. As expected the deuteron band is suppressed.

Due to two-body kinematics the S1 hit position of protons from elastic pd scattering is directly correlated with their momentum transfer t. At beam momenta close to the $pd \rightarrow {}^3He\eta$ threshold, momentum transfers of $-1.2\,(\mathrm{GeV/c})^2 < t < -0.2\,(\mathrm{GeV/c})^2$ are accessible at COSY-11.

In figure 2b the hit distribution in the monitor pad detector is presented for events with both a hit in the S1 and the monitor pad detector and a reconstructed proton momentum transfer of $-0.8\,(\mathrm{GeV/c})^2 < t < -0.7\,(\mathrm{GeV/c})^2$. On top of a smooth background arising from the quasi-free pp scattering a clear signal of scattered deuterons from pd elastic scattering is obvious.

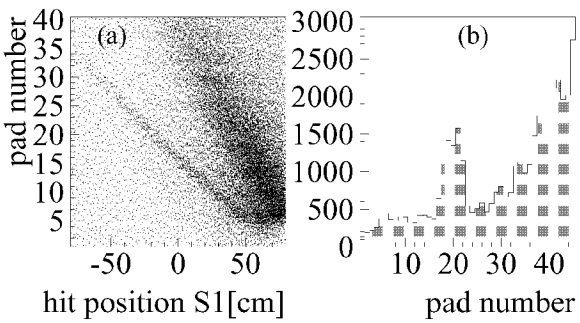

Fig. 2: a) Correlation as shown in figure 1 based on real data obtained at a beam momentum of $p_{beam} = 1.593$ GeV/c. b) Hit distribution in the monitor pad detector for protons with a momentum transfer of $-0.8\,(\mathrm{GeV/c})^2 < t < -0.7\,(\mathrm{GeV/c})^2$.

Therefore a luminosity determination for proton-deuteron scattering experiments at COSY-11 is possible using pd elastic scattering.

References:

[1] H.-H. Adam, diploma thesis, Universität Münster (2000)

[2] I. Geck, Staatsexamensarbeit, Universität Münster (2001)

[3] S.Brauksiepe et al., Nucl. Instr. & Meth. **A 376**, 397 (1996)

* Institut für Kernphysik, Universität Münster.

Dalitz-plot distribution of the $pp \to pp\eta$ reaction at excess energy Q = 15.5 MeV

P. Moskal[1] for the COSY–11 collaboration

A close to threshold measurement of the $pp \to pp\eta$ reaction allows to study the interaction of the η-meson with the proton. At small excess energies the final state particles are in the range of the strong interaction much longer than 10^{-23} s i.e. the typical life-time of N^* and Δ baryon resonances. Thus their mutual interaction may significantly influence the distributions of their relative momenta [1]. In order to study this effect the COSY–11 collaboration has carried out a measurement of the $pp \to pp\eta$ reaction at an excess energy of Q = 15.5 MeV. Figure 1 presents the missing mass spectrum, with the clear signal originating from ~24000 events of the

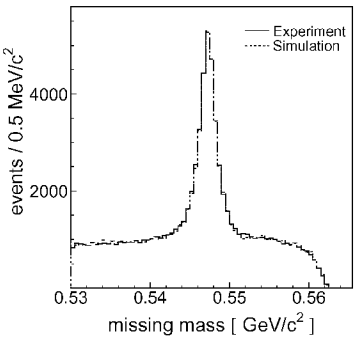

Fig. 1: Missing mass spectrum for the $pp \to ppX$ reaction determined at a beam momentum of 2.0259 GeV/c. The mass resolution amounts to 1 MeV/c^2 (σ).

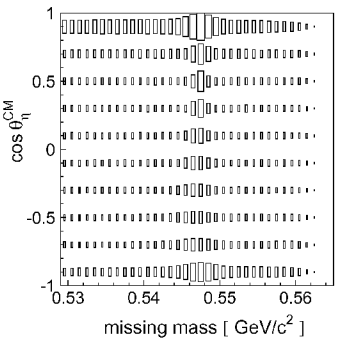

Fig. 2: Distribution of the center-of-mass polar angle of the produced system X as a function of the missing mass.

$pp \to pp\eta$ reaction seen on a flat distribution due to multipion production. By means of the simultaneous measurement of elastically scattered protons not only the luminosity but also the synchrotron beam geometrical dimensions and its position relative to the target have been monitored [2]. This, and the correction for the mean beam-momentum-changes [3] determined by means of the Schottky-spectrum and the known beam optics, allow to reproduce exactly the observed missing mass distribution as it is shown by the dashed line in Figure 1, which is hardly distinguishable from the real data. Figure 2 shows that the full range of the η meson center-of-mass polar scattering angles has been covered by the detection system acceptance. This permitted to determine the angular distribution of the created η meson which, as can be seen in Figure 3, is completely isotropic within the shown statistical errors. The observed distribution is consistent with the previous measurement performed at an excess energy of Q = 16 MeV at the CELSIUS facility [4]. However, it improves the former statistics by a factor of 80. The determination of the four-momentum vectors for both outgoing protons of each registered event gives the complete information of the ηpp-system allowing for investigations of the ηp and ηpp interactions. Figure 4 shows the Dalitz plot of the identified $pp\eta$ system corrected for the detection acceptance and the proton-proton interaction. The enhancement from the η-proton interaction at small $m^2_{p\eta}$ is evident.

The quantitative analysis aiming at the determination of the ηp and ηpp interaction parameters is in progress.

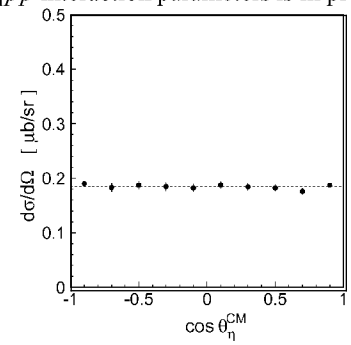

Fig. 3: Differential cross section of the $pp \to pp\eta$ reaction as a function of the η meson center-of-mass polar angle.

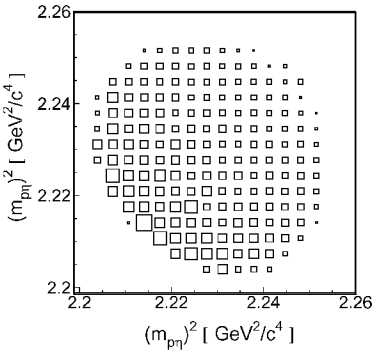

Fig. 4: Dalitz-plot distribution corrected for the detection acceptance and the proton-proton FSI. For this plot only events with a mass differing by no more than 1 MeV/c^2 from the real η meson mass were taken into account. The proton-proton FSI enhancement factor was calculated as a square of the on-shell proton-proton scattering amplitude derived according to the modified Cini-Fubini-Stanghellini formula including Wong-Noyes Coulomb corrections [5].

References:

[1] more extensive motivation of the measurement can be found in proceedings of the 9th International Symposium on Meson - Nucleon Physics and the Structure of the Nucleon (MENU 2001), Washington, District of Columbia, 26-31 Jul 2001; P. Moskal et al., e-Print Archive: nucl-ex/0110018.

[2] P. Moskal et al, Nucl. Instr. & Meth **A 466** (2001) 448.

[3] P. Moskal et al., Ann. Rep. 2000, IKP, FZ-Jülich, Jül-3852 (2001) 46.

[4] H. Calén et al, Phys. Lett. **B 458** (1999) 190.

[5] H. P. Noyes, H. M. Lipinski, Phys. Rev. **C 4** (1971) 995.

[1] Institute of Physics, Jagellonian University, 30–059 Cracow, Poland

First measurement of the analysing power A_y in the reaction $\vec{p}p \to ppη$ at COSY-11

P. Winter for the COSY-11 collaboration

Data on the η meson production with a polarised proton beam in the reaction $\vec{p}p \to pp\eta$ have been taken at the internal experiment facility COSY-11. The measurement was performed with a proton beam momentum p = 2.096 GeV/c corresponding to an excess energy of Q = 40 MeV. Due to interference effects, polarisation observables – such as the analysing power A_y – are very sensitive to the influence of higher partial waves. Especially in the threshold region, where the s-wave meson production is expected, the onset of p- and d-waves could be observed.

The event selection requires the identification of two protons in the exit channel. The four-momentum determination of positively charged ejectiles allows a full kinematical reconstruction for the $\vec{p}p \to ppX$ reaction. An identification of the meson X is done via the missing mass method.

The averaged beam polarisation was measured at the internal experiment EDDA [1] and amounted ≈50%. The analysing power was determined as a function of the polar angle θ_q of the η meson in the center of mass system [2]. The relative luminosity of both spin states was extracted based on the simultaneous measurement of the elastic proton-proton scattering. The angular dependence of A_y is shown in Figure 1. Though the data are consistent with $A_y = 0$ within the errorbars given, there seems to be a slight increase of A_y towards backward scattering angles.

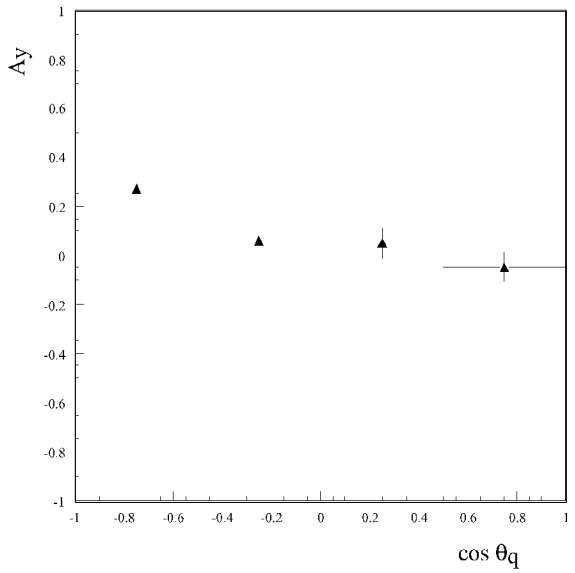

Fig. 1: Angular dependence of the analysing power A_y in the center of mass system for the reaction $\vec{p}p \to pp\eta$.

In Figure 2 a comparison of the data (solid triangles) with theoretical predictions for Q = 37 MeV from Fäldt and Wilkin [3] (dotted line) and Nakayama [4] (solid line) is shown. In addition, the theoretical calculations for Q = 10 MeV are plotted. Both models are based on the one meson exchange model. While Fäldt and Wilkin predict a dominance of ρ exchange, Nakayama concludes a dominant π and η exchange.

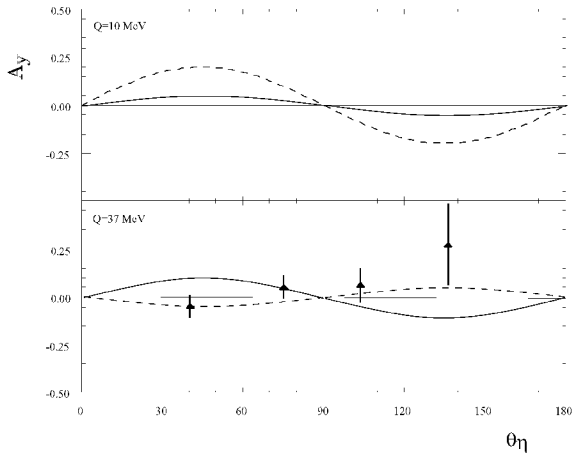

Fig. 2: Theoretical predictions for the analysing power according to [3] (dotted line) and [4] (solid line) for Q = 10 and 37 MeV. The solid triangles represent the measured values [2] at Q = 40 MeV.

The first results of the analysing power differ from both theoretical calculations although the predictions of [3] show a quite good match. For a more precise statement further measurements are needed. These measurements could benefit from higher polarisation available at COSY. Therefore, smaller errorbars with the same statistics can be achieved.

Besides a measurement at Q = 40 MeV for higher statistics, a new run at Q = 10 MeV is motivated by a theoretically expected higher value of A_y [3]. Furthermore, the sign of the analysing power should change in case of dominant ρ exchange (see Fig. 2).

References:

[1] M. Altmeier et al., Phys. Rev. Lett., 85 (2000) 1819 and F. Bauer, private communication.

[2] P. Winter, Erste Messung der Analysierstärke A_y in der Reaktion $\vec{p}p \to pp\eta$ am Experiment COSY-11, Diplomarbeit, Rheinische Friedrich-Wilhelms-Universität Bonn, 2001.

[3] G. Fäldt and C. Wilkin, Phys. Scripta 64 (2001) 427.

[4] K. Nakayama, e-Print archive: nucl-th/0108032 (2001).

Investigations on overlapping scalar resonances $f_0(980)$ and $a_0(980)$ produced at threshold in p-p collisions

P. Moskal* and W. Oelert for the COSY-11 collaboration

A study of the $1\,\mathrm{GeV/c^2}$ mass range is motivated by the continuing discussion on the nature of the scalar resonances $f_0(980)$ and $a_0(980)$, which have been interpreted as exotic four quark states [1], conventional $q\bar{q}$ [2, 3] or molecular like $K\bar{K}$ bound states [4, 5].

We briefly [6] report here the first experimental investigation, which concerns the close to threshold production of the broad resonances in the $1\,\mathrm{GeV/c^2}$ mass range. Moreover, till now we have restricted our investigations to the f_0 and a_0 mass range below the $K\bar{K}$ threshold, where they can decay into non-strange mesons only.
It is obvious that for the excitation of a broad resonance the phrase "close to threshold" is not well defined and implies here that the beam momentum is such that masses just in the range of the resonance can be excited.
In the missing mass spectra of the $pp \to ppX$ reaction a mass bin corresponding to $\mathrm{Q} = 5\,\mathrm{MeV} \pm \Delta\mathrm{Q}$ with $\Delta\mathrm{Q} = 5\,\mathrm{MeV}$ was chosen in the analysis. The number of events per mass bin has been calculated for seven measurements and after the correction for the detection efficiency has been normalized to the corresponding integrated luminosity, leading to a counting rate of $N(\sqrt{s})$.
Subsequently, the well known values of $d\sigma/dm(\eta', \sqrt{s})$ [7] were subtracted. Further, in order to account for the contribution from the multi-pion and $\pi\eta$ production we subtracted from each $N(\sqrt{s})$ the value determined for the lowest measured energy, assuming changes of the cross section for the multi-pion and $\pi\eta$ production to be negligible (which is justified, since the measurements were performed about 560 MeV and 300 MeV above the 3π and $\pi\eta$ thresholds, respectively). The values of $\Delta N(\sqrt{s})$ are shown in figure 1, which also represents calculations approximating the spectral function by the Breit-Wigner distribution and demonstrates that the data are sensitive to the average mass of the created meson or mesons but rather non-sensitive to the width of an assumed Breit-Wigner structure.
The parameters of the mesons $f_0(980)$ and $a_0(980)$ are very similar to each other [8]:

$f_0(980)$: $m = 980 \pm 10$, $\Gamma = 40$ to 100
$a_0(980)$: $m = 985.2 \pm 1.5$, $\Gamma = 50$ to 100

and therefore we can not distinguish between these two resonances in a missing mass analysis.

The fit to the resonance like structure of figure 1 results in **preliminary** values of:
$m = 970$, $\Gamma = 65$ and $\sigma_{primary} \approx 400\,\mathrm{nb}$.

It is worth to note, that the obtained structure is in line with the measurements of the $\pi^+\pi^-$ invariant mass distribution of J/Ψ decays into the $\phi\pi^+\pi^-$ system.
This result encourages us for further investigations. We plan to perform a similar analysis with the data taken during the measurements of the K^+K^- [9] and ϕ meson production. This will allow us to extend the mass range of figure 1 up to $1043\,\mathrm{MeV/c^2}$.
It should be noted that the given estimate of the cross section is certainly only an upper limit. Influences of reactions like $pp \to pp\omega\pi$ for instance will reduce this value further.

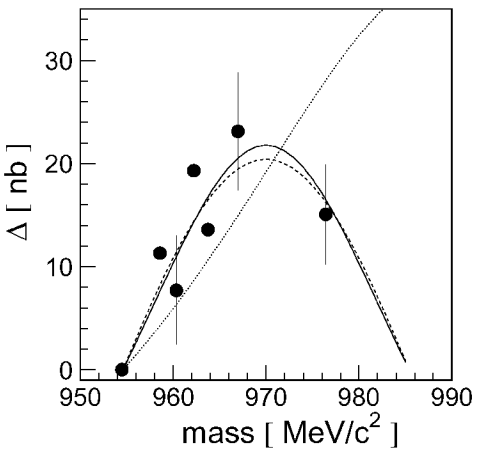

Fig. 1: Points: Number of events, measured at the 10 MeV upper bin of the missing mass spectrum for the $pp \to ppX$ reaction normalized to the integrated luminosity. The value obtained at $959.6\,\mathrm{MeV/c^2}$ was subtracted from each point. The x-axis denotes the mass corresponding to Q = 5 MeV.
Lines: Simulations of the $pp \to ppX$ reaction, with X being the Breit-Wigner type meson resonance of the following parameters:
(dotted line) M = 990 MeV/c², Γ = 65 MeV/c², and $\sigma_{primary} = 750\,\mathrm{nb}$,
(solid line) M = 970 MeV/c², Γ = 40 MeV/c², and $\sigma_{primary} = 400\,\mathrm{nb}$,
(dashed line) M = 970 MeV/c², Γ = 65 MeV/c², and $\sigma_{primary} = 1200\,\mathrm{nb}$.

References:

[1] R. Jaffe, Phys. Rev. **D 15** (1977) 267.
[2] D. Morgan, M.R. Pennington, Phys. Rev. **D 48** (1993) 1185.
[3] F. Kleefeld et al., e–Print Archive: hep–ph/0109158.
[4] J. Weinstein, N. Isgur, Phys. Rev. **D 41** (1990) 2236.
[5] Z.S. Wang, S. Krewald, J. Speth, Nucl. Phys. **A 684** (2000) 429c.
[6] for a more extensive discussion, please see: P. Moskal and W. Oelert, contribution to the COSY–11 Collaboration meeting, Kraków, 20 – 24 June 2001,to be published in: Schriften des Forschungszentrums Jülich, Eds.: P. Moskal and M. Wolke
[7] P. Moskal et al., Phys. Lett. **B 474** (2000) 416.
[8] D.E. Groom et al., Eur. Phys. J. **C 15** (2000).
[9] C. Quentmeier et al., Phys. Lett. **B 515** (2001) 276.

*on leave from Institute of Physics, Jagellonian University, Kraków, Poland

Track reconstruction in the hexagonal drift chamber at COSY-11

C. Kolf for the COSY-11 collaboration

In summer 2000, a drift chamber with hexagonal cells [1] was added to the COSY-11 detection system. Placed along the dipole magnet, it increases the momentum acceptance of COSY-11 towards lower momenta. Due to its smaller distance to the target (compared to the drift chambers D1 and D2, see figure 1), the detection efficiency for kaons also increases. This report describes the reconstruction software developed for this drift chamber [2].

To investigate the drift behaviour in hexagonal drift cells,

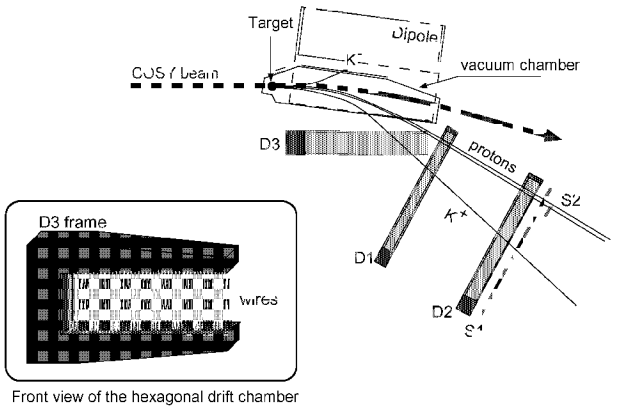

Fig. 1: The new hexagonal drift chamber (D3) in the COSY-11 setup. The tracks of a $pp \rightarrow ppK^+K^-$ event at threshold are sketched.

the simulation programme GARFIELD [3] was used. It turns out that due to the special arrangement of the drift cells in the chamber the isochrones are not completely radially symmetric and thus for high drift times (200-300 ns) the distance-to-drifttime relation depends on the track angle of the particle crossing the chamber. After digitization of the calculated isochrones, angle-dependant *lookup tables* were created as starting calibrations (see 'GARFIELD simulations' in figure 2). According to the 'uniform irradiation method' [4], which is already used for the drift chambers D1 and D2, another starting calibration was calculated ('integrated drift time spectrum' in figure 2).

The new track reconstruction software for the hexagonal

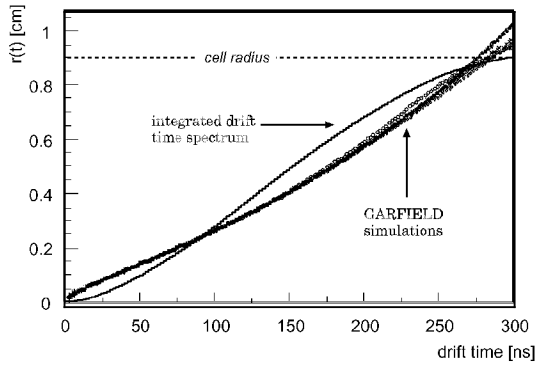

Fig. 2: Different starting calibrations for the reconstruction.

chamber provides the three-dimensional reconstruction of the particle tracks. A two-dimensional hit display is used to control the hit distribution and detection inefficencies already online during the experiment (see figure 3). In the

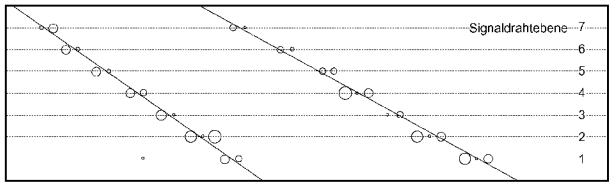

Fig. 3: 2-dimensional event display for the hexagonal chamber.

offline analysis, starting from the raw data, a track recognition routine combines every hit in the first and last detection plane to a track candidate, rejecting combinations which did not register hits in the other planes within a corridor around the connecting line. Thus, the number of track candidates (and therefore CPU time) is reduced by a factor of 2-3 without losing real physical tracks. In the next step, a fit routine minimizes the distance of the assumed track projection to the isochrones for every wire orientation. The resulting planes (spanned by the calculated track projection and the direction of the wire) are combined to a line in three-dimensional space. A matching routine separates the real result from combinatorial background.

With a data sample of the COSY-11 beam time in March 2001, the distance-to-drifttime relation was calibrated, using an iterative procedure (described in [5]). A position resolution in the order of 450 μm was achieved, determined as the standard deviation of the experimental data.

Besides the reconstruction software, a two-dimensional and a three-dimensional event display are now available for the hexagonal chamber. The substantial reconstruction and visualization routines can be used for other drift chambers, for instance for the new COSY-11 deuteron detector, which also uses a drift chamber with hexagonal cells for track reconstruction and will be added to the COSY-11 detection system in January 2002.

References:

[1] J. Smyrski, Additional drift chamber for the COSY-11 facility, Annual Report 1998, Jül-3640, p.41

[2] C. Kolf, Spurrekonstruktion in der Hexagonal-Driftkammer am Experiment COSY-11, Diplomarbeit, Rheinische Friedrich-Wilhelms-Universität Bonn, Dezember 2001

[3] R. Veenhof, GARFIELD, Simulation of gaseous detectors, Version 7.04, CERN Program Library Writeup W5050, CERN, Geneva, Switzerland

[4] A. Breskin et al., Further results on the operation of high accuracy drift chambers, Nucl. Instr. & Meth., **119**,9–28, 1974

[5] B. Gugulski et al., Construction and Test of Drift Chambers for the New Jülich Accelerator COSY, Technical Report, KFA-IKP(I), 1992.

Ratio of the Λ / Σ^0 hyperon production via the excitation of the $N^*(1650)S_{11}$ resonance

P. Kowina* and W. Oelert for the COSY–11 collaboration

In a simple constituent quark model the two hyperons Λ and Σ^0 have a rather similar structure consisting of the light up and down quarks and the heavier strange quark. Having the same total spin S = 1/2 these two hyperons differ in the spin coupling of the two light quarks and the isospin.

First order isospin arguments would suggest that the cross section ratio for the Λ/Σ^0 production is in the order of three. In fact, such values of the ratio were observed in proton–proton scattering experiments at high excess energies [1] as well as in antiproton–proton annihilations leading to $\bar{\Lambda}$–Λ, $\bar{\Sigma}^0$–$\Lambda + c.c.$ and $\bar{\Sigma}^{\pm}$–$\Sigma^{\mp}$ as performed by the experiment PS185 at LEAR [2, 3].

However, the ratio of the total cross sections for the Λ and Σ^0 production near threshold was measured at COSY–11 [4] via the reactions $pp \to pK^+\Lambda(\Sigma^0)$ and the most remarkable feature of the data is that – at the same excess energy – the total cross section for the Σ^0 production appears to be about a factor of 28^{+6}_{-9} smaller than for the Λ particle.

It was suggested [4] that strong $\Sigma^0 p$ final state interactions, and in particular a $\Sigma N \to \Lambda p$ conversion, were the likely cause of the depletion in the Σ^0 signal. This hypothesis is in line with other experimental evidence.

Still, a quantitative explanation of the relatively low Σ^0 production rate observed in pp collisions near threshold must await detailed theoretical efforts. In any case, the first COSY–11 data stimulated several theoretical investigations.

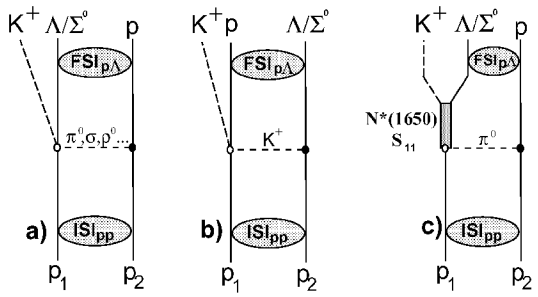

Fig. 1: Graphs for the hyperon production.

Calculations within a meson exchange model taking into account pion and kaon exchange (Fig. 1 **a)** and **b)**) reproduce the measured ratio by a destructive interference of π and K exchange amplitudes [5]. While the Λ production channel appears to be dominated by the K exchange, the interference becomes significant in the Σ^0 case. Even the absolute production cross section is described when employing a reasonable initial and final state interaction. The authors [5] claim that the data calls for a destructive interference of the π and K exchange contributions independently of the hyperon–nucleon potential used.

Within a factor of two also other models describe the data by including heavier exchange mesons and/or nucleon resonances [6, 7, 8].

Here we present an additional idea for a qualitative understanding. If the $N^*(1650)S_{11}$ is excited in the first step of the reaction it decays either into the $K^+\Sigma^0$ or the $K^+\Lambda$ channel (Fig. 1 **c)**). Other possible channels will not be considered.

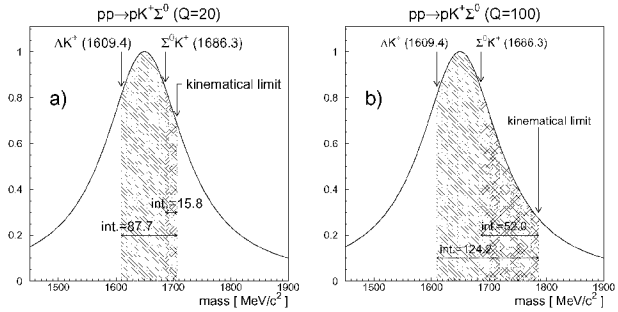

Fig. 2: The Breit–Wigner distribution of the $N^*(1650)S_{11}$ resonance. The available phase space for the decay into the K-hyperon channel at the smaller **a)** and larger **b)** excess energy is depicted by the dashed areas.

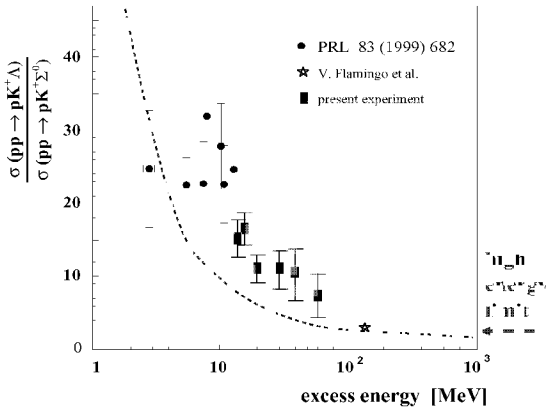

Fig. 3: Cross section ratio of the Λ/Σ^0 production as a function of the excess energy. The dashed line depicts the ratio of the integration of the phase space available for the decay into the $K-\Lambda$ and $K-\Sigma^0$ channels.

One can estimate the probability for the decay into one of the two channels with the available phace space by integrating the Breit–Wigner distribution [9] in the range of the kinematical limit and the rest mass of the $K^+\Sigma^0$ or $K^+\Lambda$ systems, respectively, see Fig. 2 **a)** and **b)**.

In Figure 3 the calculated ratio of the available phase space for the two channels considered is plotted by the dashed line together with the experimental data. Please note that no absolute normalization of the ratio has been included. Still, the shape of the excitation function for the production ratio is well described by the simple model presented.

References:

[1] V. Flaminio et al., CERN HERA **84–01** (1984).
[2] P. Barnes et al., Phys.Rev. **C 54** (1996) 2831.
[3] P. Barnes et al., Phys. Lett. **B 402** (1997) 227.
[4] S. Sewerin et al., Phys. Rev. Lett. **83** (1999) 682.
[5] A.M. Gasparian et al., Phys. Lett. **B 480** (2000) 273.
[6] R. Shyam et al., Phys. Rev. **C63** (2001) 022202.
[7] A. Sibirtsev et al., nucl-th/0004022.
[8] J.-M. Laget, hep-ph/0101047.
[9] Eur. Phys. J. **C 15** (2000), 705.

* on leave from: Institute of Physics, Silesian University, Pl-40-007 Katowice, Poland

Monitoring of the relative beam polarization at COSY–11

P. Kowina* for the COSY–11 collaboration

At COSY–11 the determination of the luminosity is based on the comparison of the differential cross section for the proton–proton elastic scattering [1] with the measured rate of events recognized as elastically scattered protons.
In the COSY–11 detector setup [2] the forward scattered proton deflected by the magnetic field of the dipole is registered in drift chambers D1 D2, scintillator arrays and S1 and S3. The second branch of this two body reaction is detected in a position sensitive silicon pad detector. The reaction plain is more or less parallel to the plain of COSY.
In measurenents with a polarized proton beam aiming for the determination of the *analysing power*, beside the luminosity the beam polarization has to be known. This can not be extracted from a measurement in the COSY plain alone. The beam polarization has to be taken from simultaneous measurement at e.g. the EDDA [3] installation.
Another solution could be the registration of elastically scattered protons perpendicular to the COSY plain. Such a luminosity measurement is independent of the orientation of the spin of the beam protons. For this purpose a **Luminosity Monitor System** has been installed at COSY–11.

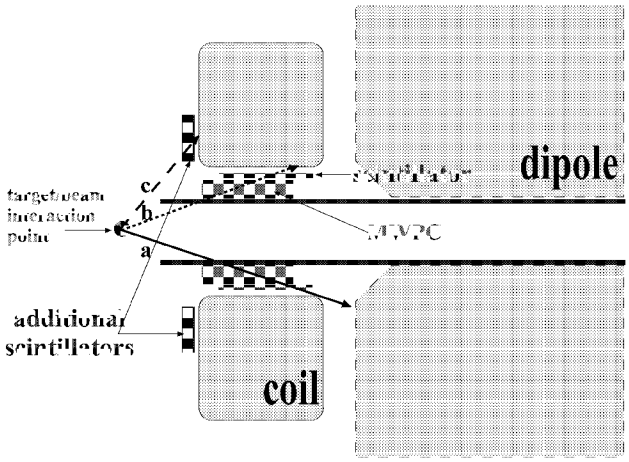

Fig. 1: Luminosity Monitor System extended by two additional scintillators. Trajectory **a** and **b** are valid for 2620 *MeV/c*. For lower beam momentum (2096 *MeV/c*) tracks **a** and **c** are suitable.

Figure 1 shows the used detection system together with an example of the trajectory for elastically scattered protons. The Luminosity System, described precisely in [4], was designed and optimized for beam momenta in the 3 *GeV/c* range. An event for such a beam momentum is presented in Fig. 1 by the vectors **a** and **b**. Both protons cross a MWPC and scintillator. The opening angle of protons in the exit channel for lower beam momentum is larger than for the higher one. At lower beam momenta only one of the protons (**a**) is registered in MWPC, the second (**c**) hits the additional scintillator installed in front of the coil.
First data with polarized beam were taken at COSY-11 in January 2001 during first measurement of the analysing power for the η production in the proton–proton scattering [5]. COSY was operated in the super cycle mode with 15 min. cycles of alternating opposite proton polarization. First results obtained from on-line monitoring are presented

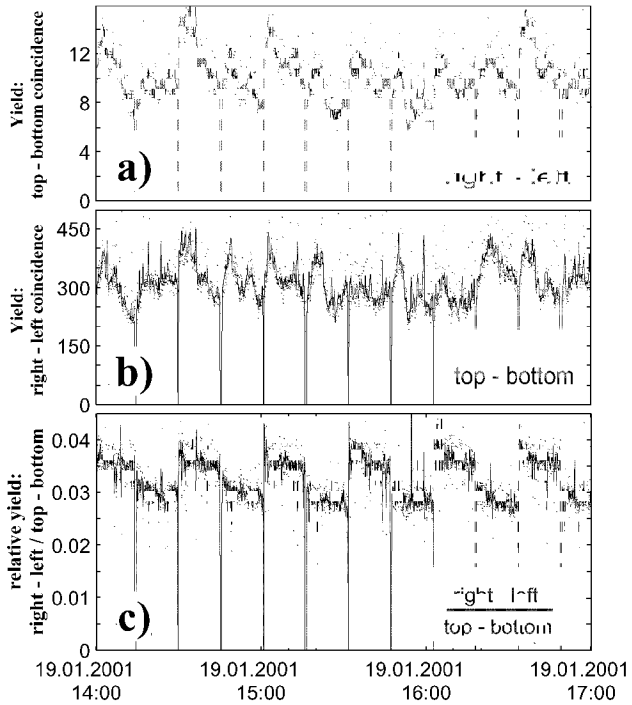

Fig. 2: On-line observation of the effect due to the polarized beam at COSY–11 in January 2001 (description see text).

in Figure 2. Figure 2**a)** shows the coincident event rate registered with the detectors in the COSY plain. It seems that the event rate differs for subsequent cycles of opposite polarization. In Figure 2**b)** the rate measured by means of the Luminosity Monitor System is presented. Changes in the number of events are rather independent on the cycles, so the event rate does not depend on the spin orientation of the beam protons.
Finally, Figure 2**c)** is a result of the normalization of the counting rate of Figure 2**b)** to the one of Figure 2**a)**. Now it is clearly seen, that the normalized number of events is changing from cycle to cycle. With more detailed analysis, the described systems can be used as a monitoring of the beam polarization.

References:

[1] D. Albers et al., Phys. Rev. Lett. **78** (1997), 1652,
[2] S. Brauksiepe et al., Nucl. Instr. & Meth. **A 376** (1996) 397.
[3] M. Altmeier et al., Annual Report 2000, IKP, Forschungszentrum Jülich, Jül-3852 (2001) 59
[4] I.-A. Pellmann, Diploma Thesis at Westfälische Wilhelms-Universität Münster (1999), Jül-3686
[5] P.Winter, contribution to this Annual Report.

* Institute of Physics, Silesian University, Pl-40-007 Katowice, Poland

Production of ω-Mesons at COSY-11

D. Grzonka, G. Schepers
for the COSY-11 collaboration

Within meson exchange models the production of ω mesons in the $pp \rightarrow pp\omega$ reaction is essentially driven by both mesonic and nucleonic exchange currents [1]. To separate the contributions from the different exchange currents total cross section data are not sufficient but differential observables like angular distributions are needed.

At the COSY-11 system the reaction $pp \rightarrow pp\omega$ has been measured at excess energies of 25, 50 and 107 MeV in order to extract angular distributions of the ω emission angle as a function of the excess energy.

The COSY-11 installation is optimized for threshold studies where a full 4 π solid angle acceptance is achieved in the cm system. With increased excess energy the detection efficiency is decreasing. But due to the large exit window at the COSY-11 dipole even for high excess energies the full azimuthal angular distribution is covered if the reaction plane is parallel to the COSY dipole plane. Therefore the full angular distribution for the ω emission is measurable. To extract the angular distribution the missing mass distribution has to be generated for separate bins in $\cos\Theta^*_\omega$, the ω emission angle in the cm system with respect to the beam direction. For each $\cos\Theta^*_\omega$ bin the number of ω events has to be determined and compared to corresponding Monte Carlo data samples. The Monte Carlo data are generated assuming a pure s-wave phase space distribution including the known pp final state interaction. Deviations from these assumed s-wave behaviour which are certainly expected at such high excess energies would modify the $\cos\Theta^*_\omega$ distribution by the efficiency variations as a function of the other relevant kinematic variables. Therefore double differential distributions have to be studied.

An instructive variable is given by the orientation of the ejectile plane relative to the beam axis. The yield of the ω production can vary with the angle of the ejectile plane which would result in a modification of the $\cos\Theta^*_\omega$ distribution extracted at COSY-11.

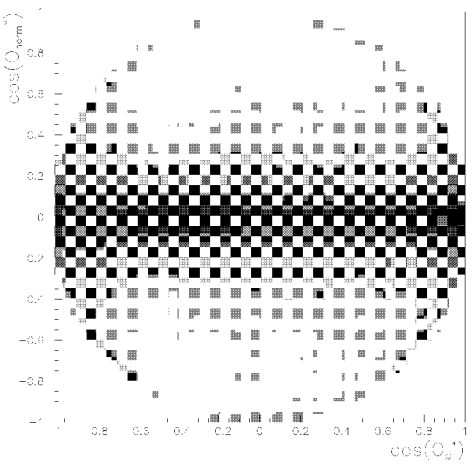

Fig. 1: Two dimensional distribution in the cm system for the ejectile plane perpendicular versus the ω emission angle for the data at ε = 107 MeV.

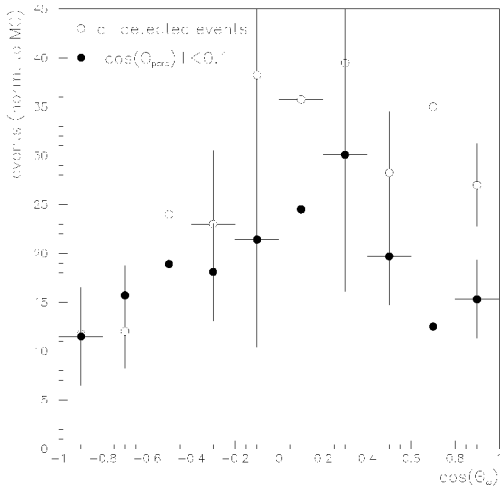

Fig. 2: Angular distribution of the produced ω mesons at ε = 107 MeV including the full data sample (open symbols) and with a cut on the ejectile plane orientation $|\cos\Theta^*_{perp}| < 0.1$ (full symbols).

In Fig. 1 the distribution of events in the field of the cosine of the ejectile plane perpendicular $\cos\Theta^*_{perp}$ versus the $\cos\Theta^*_\omega$ is shown for the data at ε = 107 MeV. Mainly the region around $\cos\Theta^*_{perp} = 0$ is populated with events, i.e. when the ejectile plane is parallel to the COSY dipole plane.

To detect possible modifications of the $\cos\Theta^*_\omega$ distribution due to a dependency of the ω production from the orientation of the ejectile plane the angular distribution is determined for different cuts on the ejectile plane perpendicular $\cos\Theta^*_\omega$. Fig. 2 shows the distributions with a cut on $|\cos\Theta^*_{perp}| < 0.1$ (filled symbols) and for the full data sample (open symbols). The distributions show differences indicating a non uniform ω production with regard to the ejectile plane orientation. Therefore double differential event selection for the extraction of angular distributions is required. Only the data points with a restriction on the ejctile plane orientation show the physically expected symmetry around 0 but the extracted angular distribution is not consistent with recent data from the TOF collaboration [2] and DISTO data [3].

To reduce the errors on the data the analysis is continued. The background substraction in the missing mass distribution will be improved by Monte Carlo data and different binnings in the double differential distributions will be studied.

References:

[1] K. Nakayama et al., Phys. Rev. C**57**, 1580 (1998).
[2] S. Abd El-Samad et al., Phys. Lett. B**522**, 16 (2001).
[3] F. Balestra et al., Phys. Rev. Lett. **81**, 4572 (1998), Phys. Rev. C **63**, 024004 (2001).

Energy Dependence of the pp → ppK$^+$K$^-$ Total Cross Section Close to Threshold

M. Wolke for the COSY–11 Collaboration

Recently, a first value of the total cross section for the reaction $pp \to ppK^+K^-$ below the Φ production threshold at an excess energy of 17 MeV has been published by the COSY–11 collaboration [1]. The obtained result shown as filled square in figure 1 encouraged us to study the energy dependence of the total cross section [2, 3]. Any deviations from the behaviour expected from four–body phase space modified by the proton–proton final state interaction might be attributed to either changes in the primary production amplitude or FSI effects in the kaon–nucleon, antikaon–nucleon or kaon–antikaon subsystems.

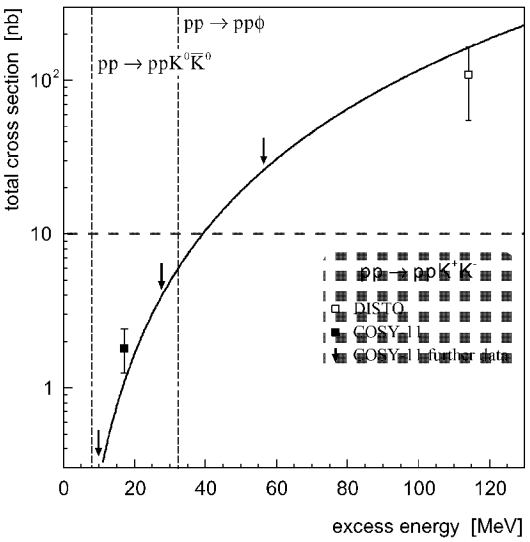

Fig. 1: Total cross section for K^+K^- production in proton–proton scattering close to threshold. Data are from [1, 4], and include both statistical and systematical errors. The solid line corresponds to an energy dependence of the total cross section based on four–body phase space modified by proton–proton FSI [5], fitted to the available data. The dashed lines indicate the $K^0\overline{K^0}$ and Φ production thresholds, respectively.

Here we report on preliminary results from a two weeks measurement at an excess energy of Q = 28 MeV with respect to the K^+K^- threshold ($p_{beam} = 3.390$ GeV/c)[1].
Positively charged particles are identified by combining the reconstructed momenta and the time–of–flight information from the COSY–11 drift chamber and scintillator arrangements [6]. Preliminary missing mass distributions with respect to the detected (ppK^+) subsystem are presented in figure 2.
A signal at the expected position of the charged kaon mass is evident and stands out of a broad background structure (fig. 2 left), which in case of the published data has been well reproduced by contributions from misidentified pions and the excitation of the hyperon resonances $\Lambda(1405)$ and $\Sigma(1385)$, with one of the identified protons originating from the weak decay of a previously produced hyperon [1].
Requiring an additional hit in the dedicated negative particle detection system mounted inside the gap of the momentum analysing dipole leads to independent proof: The background structure in the region of lower missing masses is suppressed drastically, and a clean signal at the K^- mass is obvious (fig. 2 right), the latter with a reduction quantitatively in good agreement with Monte Carlo simulations. Although measured and expected hit positions of the associated K^- in the highly granulated silicon pad detectors have not yet been compared at this stage of the analysis, the final result is expected to be as free of background as shown for the measurement at Q = 17 MeV (fig. 3 in [1]). A value of the total $pp \to ppK^+K^-$ cross section at Q = 28 MeV has to await the analysis of proton–proton elastic scattering data measured simultaneously.
To conclude studies on the energy dependence of the total cross section further data taking at an excess energy of 10 MeV is scheduled in January 2002. This measurement close to the elementary antikaon production threshold is especially motivated by recent theoretical investigations [7].

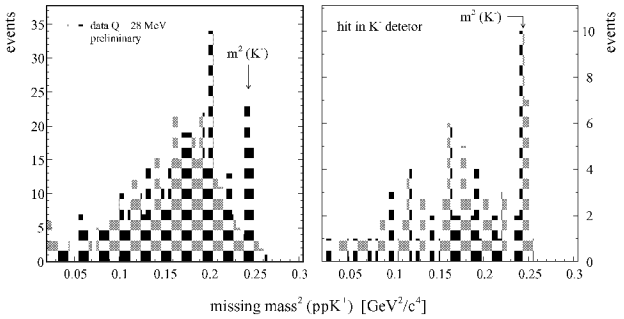

Fig. 2: Missing mass squared with respect to an identified (ppK^+) subsystem at an excess energy of 28 MeV without (left) and with (right) the additional requirement of a registered hit in the negative particle detection system.

References:

[1] C. Quentmeier et al., Phys. Lett. **B 515** (2001) 276.
[2] M. Wolke et al., COSY–Proposal No. 61, May 1998; M. Wolke, C. Quentmeier et al., COSY–Proposal No. 61.2, May 2000.
[3] P. Winter, M. Siemaszko et al., COSY–Proposal No. 61.3, Nov 2001.
[4] F. Balestra et al., Phys. Rev. **C 63** (2001) 024004.
[5] G. Fäldt, C. Wilkin, Z. Phys. **A 357** (1997) 241.
[6] S. Brauksiepe et al., Nucl. Instr. & Meth. **A 376** (1996) 397.
[7] A. Sibirtsev, M. Wolke, contribution to the proceedings of the COSY–11 Collaboration meeting, Kraków, 20 - 24 June 2001, to be published in: Schriften des Forschungszentrums Jülich, eds.: P. Moskal and M. Wolke.

[1] Preliminary results on Φ production are given in a separate report.

Close–to–threshold Φ production at COSY–11

M. Wolke for the COSY–11 collaboration

Studies of Φ meson production in nucleon–nucleon collisions are especially motivated by possible violations of the Okubo–Zweig–Iizuka rule [1]. Any significant deviation from the expected suppression of Φ compared to ω production in hadronic interactions might be interpreted as a hint for a strangeness component in the nucleon [2]. Large violations of predictions based on the OZI rule have been found in $p\overline{p}$ annihilation at LEAR (as reviewed in [2]), where it is the spin triplet fraction in the entrance channel which is strongly correlated to the Φ yield as shown in [3]. Similarly, in proton–proton collisions, for close–to–threshold Φ production, the entrance channel must be in a spin triplet $^3P_1$ state.

The exclusive production ratio has been determined in the reaction $pp \to pp\Phi/\omega$ at a beam momentum of 3.67 GeV/c corresponding to excess energies of 82 MeV and 319 MeV to the Φ and ω thresholds, respectively [4]. However, angular distributions indicate already a P–wave component in the pp–system in the final state at this energy. Thus, the influence of the spin triplet entrance channel might be diluted in the presently available data and would be expected to be more prominent in the production closer to threshold.

As a study of feasibility, the reaction $pp \to pp\Phi$ has been measured at the COSY–11 facility at a beam momentum of $p_{beam} = 3.481$ GeV/c, i.e. at an excess energy of 24 MeV with respect to the Φ production threshold [5].

The analysis of experimental data focuses on events with two protons and one K^+ meson identified in the final state. The (squared) invariant mass distribution of a third positively charged ejectile in addition to two identified protons is shown versus the missing mass (squared) of the identified (ppK^+) subsystem in figure 1.

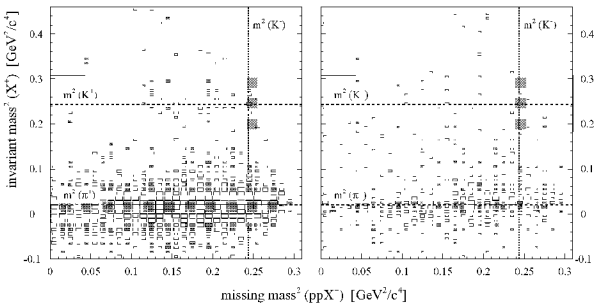

Fig. 1: Invariant mass squared of a third positively charged particle in addition to two identified protons versus missing mass squared with respect to the assumed (ppK^+) subsystem without (left, logarithmic scale) and with (right, linear scale) requiring an additional hit in the K^- scintillator. Solid lines denote the cut on the kaon mass used for the K^+ identification, and the shaded area corresponds to the mass range expected for the ppK^+K^- final state.

On the scale of the invariant mass, positively charged kaons appear rather well separated from the dominant pion signal (fig. 1 left). A group of 39 events with an identified (ppK^+) subsystem stands out close to the K^- mass as expected for a ppK^+K^- final state.

Requiring an additional hit in the dedicated K^- scintillator mounted inside the dipole gap cleans the spectrum especially in the regions of $(pp\pi^+)$ events and lower missing mass values (fig. 1 right, note the change to linear scale). Within the resolutions expected for the kaon invariant mass and for the (ppK^+) missing mass ten events in total remain consistent with a ppK^+K^- final state.

The (ppK^+) missing mass is shown in figure 2 as a function of the (K^+K^-) invariant mass. Without requiring a detected signal of the K^-, a slight enhancement close to the Φ mass is obvious (fig. 2 left). However, the signal disappears when demanding an additional K^- consistent hit (fig. 2 right), although the detection efficiencies for non–resonant K^+K^- production and the reaction $pp \to pp\Phi \to ppK^+K^-$ are comparable (54 % and 46 %, respectively).

The total number of candidates for a ppK^+K^- final state falls short of the estimations based on the available total cross section data [4] and acceptance studies by a factor of two. This, however, might be easily accounted for by the integrated luminosity, which so far has not been determined accurately.

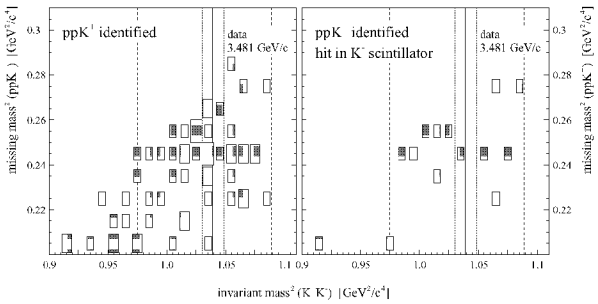

Fig. 2: Missing mass squared with respect to the identified (ppK^+) subsystem versus (K^+K^-) invariant mass squared without (left) and with (right) requiring an additional hit in the dedicated K^- scintillator. Dashed lines mark the kinematical limits of K^+K^- production. The solid line denotes the squared mass of the Φ meson, dotted lines indicate its finite width.

Despite the low statistics, the study of feasibility performed at the COSY–11 facility should allow to determine an upper limit on Φ production in proton–proton scattering at a beam momentum of $p_{beam} = 3.481$ GeV/c and thus on the Φ/ω ratio. The analysis of ω production at the same excess energy is in progress [6].

References:

[1] S. Okubo, Phys. Lett. **5**, 165 (1963); G. Zweig, Report CERN–TH–412 (1964); J. Iizuka, Prog. Theor. Phys. Suppl. **37–38**, 21 (1966).

[2] J. Ellis et al., Phys. Lett. **B 353**, 319 (1995); Nucl. Phys. **A 673**, 256 (2000).

[3] A.M. Bertin et al., Phys. Lett. **B 388**, 450 (1996).

[4] F. Balestra et al., Phys. Rev. **C 63**, 024004 (2001).

[5] G. Schepers et al., COSY Proposal No. 78, Nov 1998.

[6] D. Grzonka, P. Kowina, G. Schepers et al., Annual Report 1999, IKP, FZ Jülich, Jül–3744 (2000) 47.

Dependence of the excess energy distribution for the quasi-free $pn \to pn\eta'$ reaction on the deuteron wave function model

R. Czyżykiewicz[1], P. Moskal[1] for the COSY-11 Collaboration

The η and η' meson production in the collisions of protons with neutrons will be measured by the COSY-11 collaboration in March 2002 [1] using a COSY proton beam and a deutron cluster target. The experimental aim is to determine the total cross section for the reactions $pn \to pn\eta$ and $pn \to pn\eta'$ as a function of the excess energy Q. A simultaneous measurement of the fast neutron and proton as well as the slow backwards flying spectator proton will allow to identify the reaction and to determine the excess energy for each event. However, in order to extract the total cross section from the number of identified reactions at a given Q value, the knowledge of the geometrical acceptance and efficiency of the detection system alone will not be sufficient. It will require an assumption of the nucleon momentum distribution in the target deuteron. There exist several models that describe the distribution of the nucleon momentum inside the deuteron [2–6]. In order to estimate the systematical uncertainty of the cross section determination due to the choice of the model a Monte-Carlo simulation of the quasi-free $pn \to pn\eta'$ reaction for Paris and CD-Bonn potentials have been performed. For the calculations the S- and D-wave components of the deuteron wave function were parametrized analytically in the momentum space according to the prescription given in reference [2]:

$$\frac{\psi_0(p)}{p} = \sqrt{\frac{2}{\pi}} \sum_{j=1}^{n} \frac{C_j}{p^2 + m_j^2} \; ; \quad \frac{\psi_2(p)}{p} = \sqrt{\frac{2}{\pi}} \sum_{j=1}^{n} \frac{D_j}{p^2 + m_j^2} \qquad (1)$$

where the coefficients C_j and D_j can be found in [2] and [3] for the Paris and CD-Bonn potential, respectively. By means of the above equations the probability density of finding a nucleon with a Fermi momentum p inside a deuteron (see fig. 1) can be expressed as: $f(p) = p^2[(\psi_0)^2 + (\psi_2)^2]$, where the parameters C_j and D_j were chosen such that $\int_0^\infty f(p)dp = 1$.

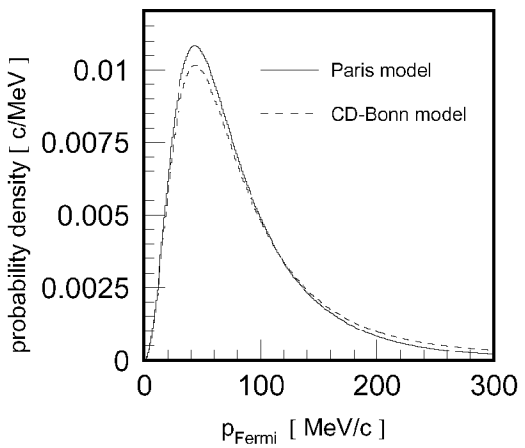

Fig. 1: Momentum distribution inside the deuteron as obtained for Paris (full line) and CD–Bonn (dotted line) potentials.

In the experiment, only spectators with total momenta up to 130 MeV/c will be registered [1]. In this momentum range the Fermi momentum distributions deduced from Paris and CD-Bonn potentials differ no more than by $\sim 6\%$. The resulting systematical error for the total cross section energy dependence originating from the choice of the deuteron potential may be estimated from the difference between solid and dashed line shown in Figure 2. In the performed simulations of the $pd \to p_{sp}pn\eta'$ reaction, it was assumed that the proton from a deuteron does not take part in the reaction and is on it mass shell at the moment of interaction. Thus in the framework of this impulse approximation the spectator proton is a physical particle and due to the energy and momentum conservation the reacting neutron is off its mass shell.

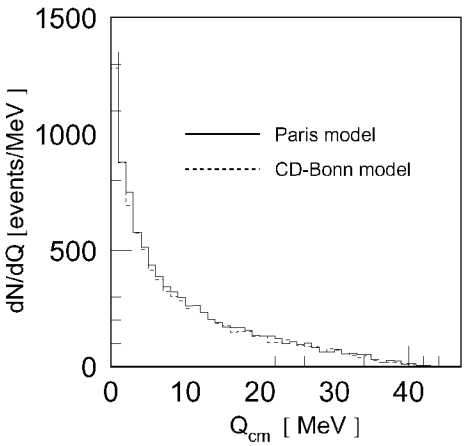

Fig. 2: Distribution of the excess energy Q_{cm} for the quasi-free $pn \to pn\eta'$ reaction as simulated with the COSY-11 detection system at a beam momentum of $p_{beam} = 3.350$ GeV/c. Calculations have been performed assuming the target diameter equal to 0.9 cm, and standart deviations of 0.2 cm and 0.4 cm for the horizontal and vertical beam spread, respectively. The distance between the centre of spectator detector's pad and the centre of target was assumed to be $\Delta Z_{SD} = -3.4$ cm [7]. The neutron detector was set at the distance of 430 cm from the target. The figure shows the number of reconstructed events per 1 MeV bin out of $5 \cdot 10^6$ generated $pd \to p_{sp}pn\eta'$ reactions.

Summarizing: The uncertainty, originating from the differences between the CD-Bonn and Paris potentials, in the correction factor ($F(Q) = dN/dQ \,/\, 5 \cdot 10^6$) necessary for the determination of the total cross section from a data, amounts to about 4 % only.

References:

[1] P. Moskal, T. Johansson et al., COSY Proposal#100, April 2001, see also e-Print Archive: nucl-ex/0110001.
[2] M. Lacombe et al., Phys. Lett. **B 101** (1981) 139.
[3] R. Machleidt, Phys. Rev. **C 63** (2001) 024001.
[4] R.B. Wiringa et al., Phys. Rev. **C 51** (1995) 38.
[5] V.G.J. Stoks et al., Phys. Rev. **C 49** (1994) 2950.
[6] F. Gross et al., Phys. Rev. **C 45** (1992) 2094.
[7] R. Czyżykiewicz et al., contribution in this report.

[1] Institute of Physics, Jagellonian University, 30–059 Cracow, Poland

Time resolution of the COSY–11 neutron detector tested via the $pp \rightarrow pn\pi^+$ reaction

P. Moskal[1] for the COSY–11 collaboration

In order to study charged hyperon production, for example Σ^+ via the reaction $pp \rightarrow nK^+\Sigma^+$ or quasi free meson production in proton-neutron interactions, the COSY–11 facility was extended by a neutron detector. At the present stage it consists of twelve modules each built out of eleven plates of plastic scintillator with dimensions of 270 x 90 x 4 mm^3 interlayed by lead plates [1]. The scintillators are read out on one side by a light guide manufactured from one solid block of plexiglass, which changes smoothly its shape from rectangular to cylindrical. This enables to collect the scintillation light on a circular (4 cm diameter) photocathode of a photomultiplier.

During the measurement of the $pp \rightarrow ppK^+K^-$ reaction [2] in April 2001, one day of beam time was devoted for the test of the performance of the neutron detector. For this purpose we measured the $pp \rightarrow pn\pi^+$ reaction registering outgoing protons and neutrons in coincidence. The neutron detector was positioned behind the COSY–11 dipole magnet downstream the beam at a distance of 4 m from the target location as shown in the accompanying report [3]. In order to identify the $pn\pi^+$ final state the momentum vectors of the registered protons and neutrons have been determined for each event. Proton momenta have been reconstructed by tracking back trajectories, registered by drift chambers, to the interaction point [4].

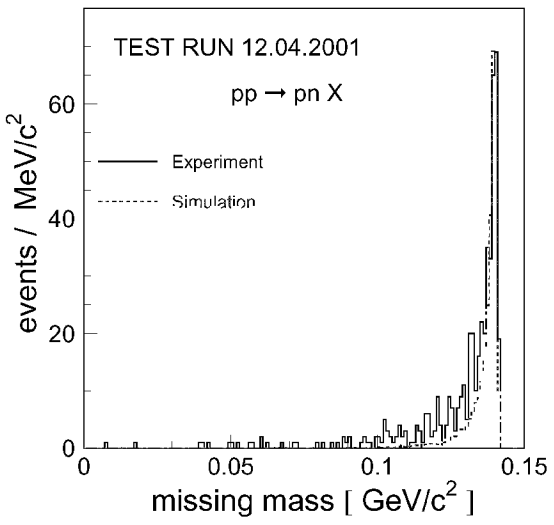

Fig. 1: Missing mass spectrum of the $pp \rightarrow pn\pi^+$ reaction. The data shown by the solid line are compared to the result of Monte-Carlo simulations indicated by the dashed line. The FWHM of the peak amounts to $\sim 4\ MeV/c^2$.

The neutron momenta have been determined from the time of flight between the target and neutron detector and the angle defined by the centre of the hit segment. The neutron detector granularity allows to determine the horizontal hit position with an accuracy of ± 4.5 cm. Figure 1 shows a missing mass spectrum with respect to the measured proton-neutron system. The obtained distribution is clearly peaked at the mass corresponding to the mass of the π^+ meson ($\sim 140\ MeV/c^4$) and because there is no physical reaction which could contribute to this spectrum one can assign the observed events to the $pp \rightarrow pn\pi^+$ reaction, especially since its shape agrees well with Monte-Carlo simulations. The simulations have been performed with the time resolution of the neutron detector as free parameter, which determines the width of the missing mass spectrum. By the fit to the data the time resolution of the detector was established to be 0.5 ns (rms).

Taking into account the number of registered events, the detection efficiency and the luminosity we determined the total cross section for the $pp \rightarrow pn\pi^+$ reaction at the kinetic beam energy of 296.7 MeV. The result – shown in Figure 2 – agrees within the error bars with the measurements performed at other laboratories [5–7].

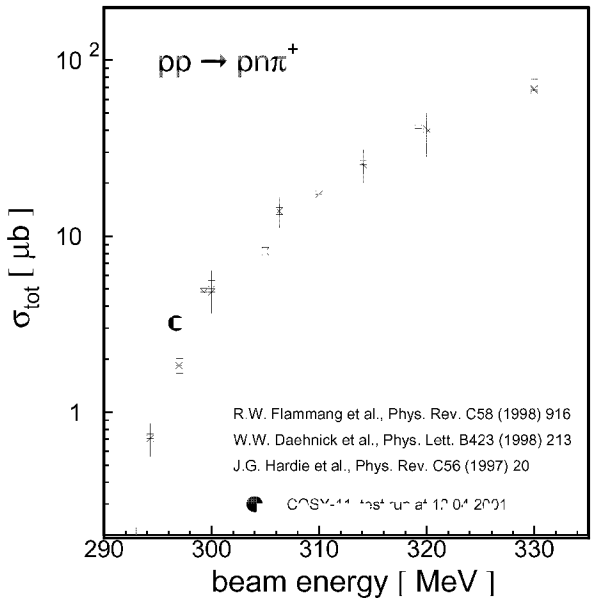

Fig. 2: Total cross section for the $pp \rightarrow pn\pi^+$ reaction. Full circle shows the result of the test run juxtaposed with the existing data.

References:

[1] P. Moskal et al., Ann. Rep. 1996, IKP, FZ-Jülich, Jül-3365, (1997) 35.
[2] M. Wolke, contribution to the COSY–11 Collaboration meeting, Kraków, 20 – 24 June 2001, to be published in: Schriften des Forschungszentrums Jülich, Eds.: P. Moskal and M. Wolke.
[3] R. Czyżykiewicz et al., contribution in this report.
[4] S. Brauksiepe et al., Nucl. Inst. & Meth. **A 376** (1996) 397.
[5] R. W. Flammang et al., Phys. Rev. **C 58** (1998) 916.
[6] W. W. Daehnick et al., Phys. Lett. **B 423** (1998) 213.
[7] J. G. Hardie et al., Phys. Rev. **C 56** (1997) 20.

[1] Institute of Physics, Jagellonian University, 30–059 Cracow, Poland

Optimization of the spectator detector arrangement for the $pn \to pn\eta'$ measurements at COSY-11

R. Czyżykiewicz[1], D. Grzonka, J. Majewski[1], P. Moskal[1] for the COSY-11 Collaboration

In order to investigate the quasi-free η' meson production the COSY-11 setup will be extended by the silicon pad counters used succesfully at the CELSIUS storage ring for tagging of the quasi-free $pn \to pn\pi^0$ and $pn \to d\pi^0$ reactions [1].

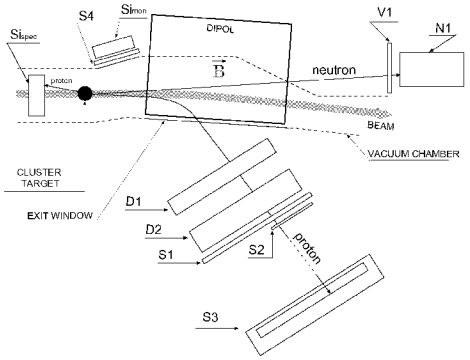

Fig. 1: Schematic view of the COSY-11 detection setup with the new spectator detector denoted as Si_{spec}.

In Figure 1 a shematic view of the COSY-11 facility together with a spectator counter is presented. The tagger shown in more details in Figure 2 consits of four modules each divided into six groups of three close laying strips. The active area of a unit strip amouts to 20 mm x 5 mm.

The study of the $pn \to pn\eta'$ reaction will be realized by means of the COSY proton beam with a fixed momentum and by utilizing a deuteron cluster target as a source of neutrons. The spectator detecor will be used for tagging the quasi-free proton-neutron interaction and for the determination of the total energy available in the center of mass of the interacting nucleons, since this will vary from event to event due to the Fermi motion of the nucleons inside a deuteron. The excess energy of the ejectiles of the quasi-free $pn \to pn\eta'$ reaction will be determined inderectly by the measurment of the emission angle and the kinetic energy of the spectator proton which will allow to deduce the four-momentum vector of the neutron at the moment of the interaction.

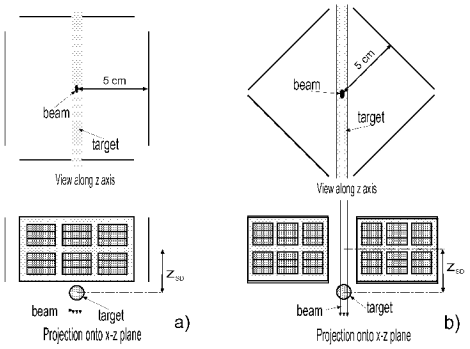

Fig. 2: Spectator detector arrangement. Z_{SD} denotes the distance (along the beam axis) between target and detector center. Simulations have been performed varying the parameter Z_{SD} but keeping the distance between the proton beam and the detector to be constant and equal to 5 cm. This is a compromise between the coverage of the solid angle, angular resolution for the measurement of the spectator proton and the technical needs for the installation.

At a given beam momentum the position of the spectator detector determines the maximum in the excess energy spectrum of the tagged $pn \to pn\eta'$ reactions. For example, installing the detector upstream the target as shown in Figure 1, the $pd \to p_{sp}pn\eta'$ event can be tagged only if the spectator proton is moving opposite to the beam proton, and hence the neutron inside the target deuteron is escaping the beam proton which results in the excess energy lower than it would be in the case with tagger being placed downstream the beam and the neutron moving against it. Due to the geometry of the standard COSY-11 setup the most appropriate excess energy range to be studied is between 0 MeV and 30 MeV. In order to find out an optimum position for the installation of the spectator detector which would give the maximum at this excess energy range a Monte-Carlo calculation have been performed varying a distance Z_{SD} along the beam axis between the target and the spectator counter.

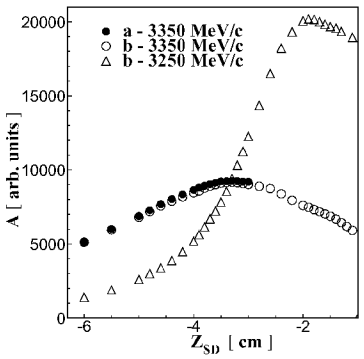

Fig. 3: Detection efficiency for the $pd \to p_{sp}pn\eta'$ reaction as a function of the Z_{SD} – distance measured along the beam axis between target and spectator detector. Circles (triangles) show calculations at P_{beam} = 3350 MeV/c (3250 MeV/c) for both configuration depicted in Figure 2 **a**(filled symbols) and **b**(open symbols). Neutron detector was placed 430 cm from the target and we assumed 0.2 cm and 0.4 cm standard deviations for the horizontal and vertical beam spread, respectively [2].

Figure 3 shows the fraction out of $5 \cdot 10^6$ generated $pd \to p_{sp}pn\eta'$ events which give signals in the detection system necessary to identify a quasi-free $pn \to pn\eta'$ reaction. The calculations have been performed for the two different detector configurations shown in Figure 2. It was found that at P_{beam} = 3350 MeV/c the maximum of the detection efficiency is obtained at Z_{SD} = -3.3 cm independently of the choice of a configuration. However, at the lower beam momentum of P_{beam} = 3250 MeV/c a maximum of the determined efficiency is about two times larger than this at P_{beam} = 3350 MeV/c. This preliminary results show that the detection efficiency for registering quasi-free $pn \to pn\eta'$ reaction depends strongly on both position of the spectator detector and momentum of the proton beam.

References:

[1] R. Bilger et al., Nucl. Instr. & Meth. **A 457** (2001) 64.
[2] P. Moskal et al., Nucl. Instr. & Meth. **A 466** (2001) 448.

[1] Institute of Physics, Jagellonian University, 30–059 Cracow, Poland

Preparation of silicon pad detectors for measurements of the $pn \to pn\eta$ and $pn \to pn\eta'$ reactions at COSY–11

J. Majewski[1], E. Białkowski[2], R. Czyżykiewicz[1], O. Felden, G. Fiori, P. Moskal[1], D. Protić for the COSY–11 collaboration

For measurements of the meson production in quasi-free proton-neutron reactions at COSY-11 a silicon detector system will be installed close to the target region. The detector setup consisting of four modules with a total active area of 72 cm^2 [1] will be positioned at a distance of 5 cm from the interaction region between beam and target [2], and hence will cover about 22 % of the full solid angle. The detectors, manufactured by ELMA [3] Research Association have been used previously in experiments at the CELSIUS storage ring of The Svedberg Laboratory by the PROMISE/WASA collaboration. Its adoption to the COSY-11 setup needs, however, few significant changes. First of all, the geometry of the COSY-11 facility requires 80 cm long cables to transfer the signals from vacuum to the outside of the scattering chamber, which is by 50 cm longer then those used at the PROMICE/WASA setup. The prolongation of the vacuum compatible printed circuit board is desinged and will be manufactured by the STRASCHU company [4]. The additional transmission circuit will increase the capacitance of the detection setup by about 40% which will increase the noise and hence reduces the capability of identification of the low energetic spectator protons. At the PROMISE/WASA experiments the minimum energy of the spectators which still could have been identified was about 0.5 MeV [1], a value at which the distribution of the nucleons' kinetic energy inside a deuteron reaches its maximum as shown in Figure 1.

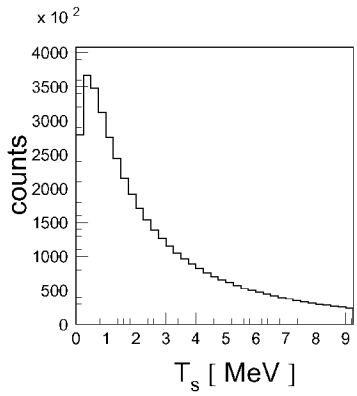

Fig. 1: Kinetic energy distribution of the nucleons in the deuteron, generated according to the analytical parametrization of the deuteron wave function [5].

The growth of that limit could diminish significantly the fraction of the spectators which can be identified. Therefore, to compensate the increase of the noise due to the inevitable extension of the signal transmitters the preamplifiers used previously have been modified and the signal to noise ratio was improved by a factor of 2. This has improved the energy resolution by about the same factor.

Tests of the energy resolution of each of the 96 silicon pad (with still short transmission cables) have been performed using Plutonium, Americium and Curium elements. The detectors and sources of alpha particles have been positioned inside the recovered scattering chamber which was used at the former experiments at the Jülich-Cyclotron [6]. Figure 2 is an example of the obtained energy distribution for one of the tested pads. It can be seen that the energy resolution (FWHM) is about 50 keV. Assuming conservatively that the extension of cables and the operation at the COSY ring will deteriorate this value to 100 KeV Monte-Carlo calculations of the $pd \to pnp_s\eta'$ reaction have been performed which resulted in a missing mass distribution of about 8 MeV for excess energies Q lower than 20 MeV, as depicted in Figure 3.

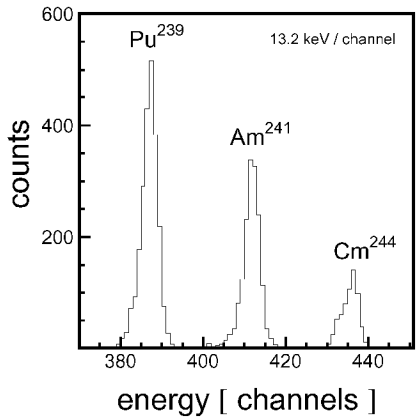

Fig. 2: Energy spectrum of alpha particles emitted from ^{239}Pu, ^{241}Am and ^{244}Cm with mean kinetic energies of 5.15 MeV, 5.48 MeV and 5.80 MeV, respectively.

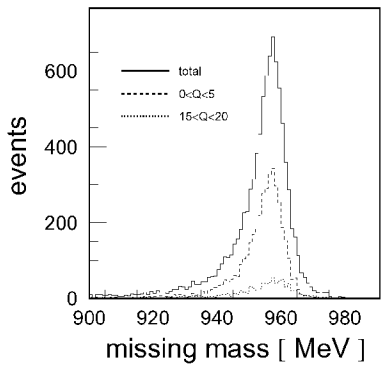

Fig. 3: Missing mass distribution with respect to the pn subsystem of the quasi-free $pn \to pn\eta'$ reaction as reconstructed from $5 \cdot 10^6$ simulated events. The neutron detector was placed at a distance of 430 cm from the target. The spectator detector was positioned at $Z_{SD} = -3.3$ cm [2]. The distance between the silicon pads and the reaction vertex was 5 cm.

References:

[1] R. Bilger et al., Nucl. Instr. and Meth. A **457** (2001) 64.
[2] R. Czyżykiewicz et al., contribution in this report.
[3] Research and Production Association ELMA, Zelonograd, Russia.
[4] Straschu Leiterplatten GmbH 26135 Oldenburg, Germany.
[5] M. Lacombe et al., Phys. Lett. **101B** (1981) 139.
[6] U. Schmidt-Rohr, Die Deutschen Teilchen Beschleuniger, p. 56 ff, Neumann Druck, Heidelberg.

[1] Institute of Physics, Jagellonian University, 30–059 Cracow, Poland
[2] Institute of Nuclear Physics, 31–342 Cracow, Poland

Estimation of the radiation damages of the Uppsala spectator detector

E. Białkowski[1], J. Majewski[2], P. Moskal[2], J. Uehlemann for the COSY–11 collaboration

The preparation of the Uppsala spectator detector [1] for use at the forthcoming COSY-11 experiments [2] was described in details in accompanying reports [3]. Here we present tests on the radiation damages due to the operation at the PROMISE/WASA facility, where the detector elements have been positioned at a distance of 11 cm from the interaction region of the circulating CELSIUS proton beam and the deuteron cluster target. At such circumstances an absorption of a high radiation dose which could cause significant structural defects in semiconductor material is expected. Therefore, it is important to identify its influence and accordingly perform a temperature annealing before the next application.

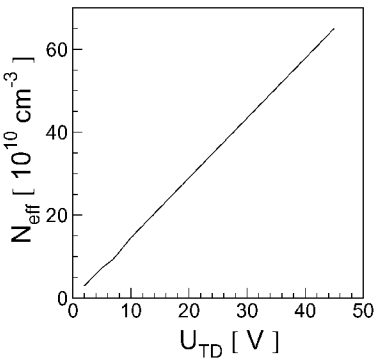

Fig. 1: Relation between total depletion bias voltage and the doping concentration for n-type silicon semiconductors [4].

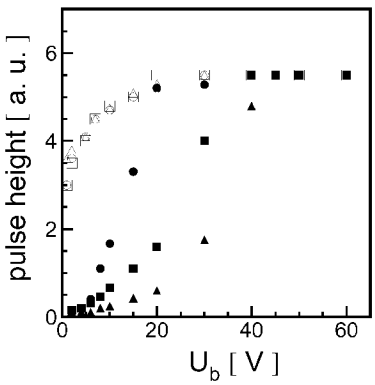

Fig. 2: Pulse height of the detector signals due to the illumination by monoenergetic alpha particles from the front (open symbols) and rear (full symbols) side, as a function of the applied bias voltage. As examples, result for three different detection pads is shown.

The appraisal of the irradiation can for example be performed by measuring the effective impurity concentration which diminishes with the growing number of defects in the active volume of the detector. One can uniquely relate the doping concentration to the thickness of the depleted region and the applied external bias voltage [4]. This dependence is shown in Figure 1 for the case of a 300 μm thick depletion for n-type material. Thus, knowing the detector thickness and the total depletion voltage one can estimate the effective impurity concentration in the detector. Since the total depletion voltage of the considered n-type 300 μm semiconductor silicon detectors, before usage in the Uppsala experiments, amounted to U_{TD} = 45 V, the impurity concentration was about 6.5 x 10^{11} cm^{-3}. For the estimation of the present value of the total depletion voltage we have irradiated the front and rear electrodes of the detector by short range monoenergetic 5.5 MeV (~ 25 μm in silicon) alpha particles emitted from a ^{241}Am isotope. Figure 2 shows that already at bias voltages U_b about 10 V a total depletion is achieved. Such a low total depletion voltage (U_{TD} = 10 V) indicates that the detectors were exposed to the radiation fluence which reduces the impurity concentration about a factor of ten. A similarly small value for U_{TD} was determined from the measured C-V characteristics. The irradiation was most probably caused by electrons since the last experiment with the detector was finished more than two years ago, and during that time the effect of self annealing at room temperature would be much stronger if the damages had been caused by protons or neutrons. Though at present, as shown in accompanying reports, the detectors still permit measurements with sufficient energy resolution, in order to ensure operability for next years a temperature enhanced annealing will be applied.

In order to optimize the bias voltage for the use in the COSY–11 experiments we checked also the changes of the signal width as a function of U_b. The ADC converters which will be used in the experiment [5] allow for the integration of signals up to 2 μs. Therefore, as can be deduced from Figure 3, bias voltages lower than 40 V should be avoided.

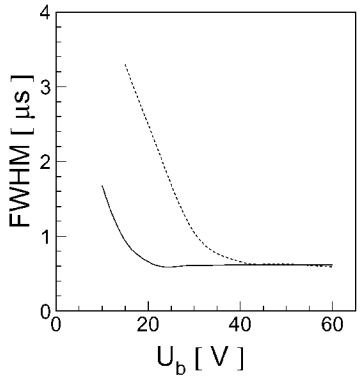

Fig. 3: Full signal width at half maximum as a function of an applied bias voltage. For pads of dimensions: 0.5 x 2.0 x 0.03 cm^3 (solid line) and 1.5 x 2.0 x 0.03 cm^3 (dashed line).

References:

[1] R. Bilger et al., Nucl. Instr. and Meth. A **457** (2001) 64.
[2] P. Moskal, T. Johansson et al., COSY Proposal#100, April 2001, see also e-Print Archive: nucl-ex/0110001.
[3] J. Majewski et al., and R. Czyżykiewicz et al., contributions in this report.
[4] D. E. Groom et al., Eur. Phys. J. **C 15** (2000) 1.
[5] ADC 1885F, LeCroy Corporation, 700 Chestnut Ridge-Road, Chestnut Ridge, New York 10977, USA.

[1] Institute of Nuclear Physics, 31–342 Cracow, Poland
[2] Institute of Physics, Jagellonian University, 30–059 Cracow, Poland

Summary of Cosy–13 results

P. Kulessa[1,2] and B. Kamys[3] for the COSY-13 collaboration

The COSY–13 experiment was devoted to the measurement of the lifetime of heavy hypernuclei. This was achived by using the recoil shadow method as described in [1], which is appropriate for fissioning hypernuclei, i.e. the hypernuclei with mass number A $\sim$ 180 - 225.

Lifetime of hypernuclei produced in proton induced reactions on three targets (Au, Bi, U) has been measured in six experimental runs performed since 1995. The obtained results are summarized in the table and presented in Fig. 1.

Target	τ_Λ / ps	Ref.
Au	130±13(stat.)±15(syst.)	[2]
Bi	161 ±7(stat.)±14(syst.)	[3]
U	138 ±6(stat.)±17(syst.)	[4]

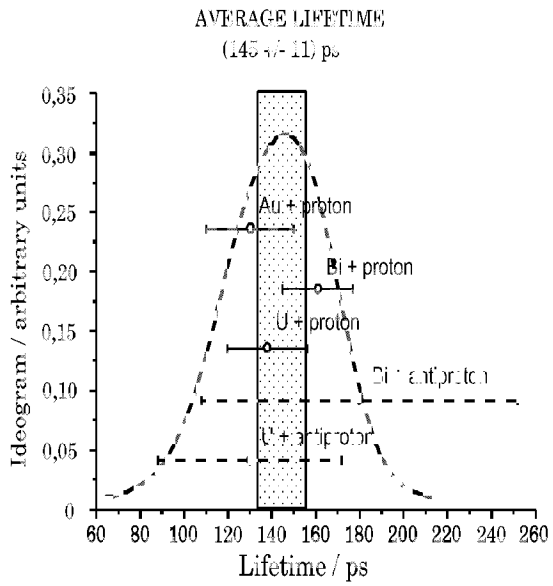

Fig. 1: The lifetimes of hypernuclei produced in proton (COSY–13) and antiproton [7] induced reactions on Au, Bi and U targets. The horizontal bars present the statistic and systematical errors added in quadrature. The position of gray vertical bar displays the overall average value for the lifetime of heavy hypernuclei and its width gives the error. The ideogram was evaluated as proposed in Ref.[8].

Investigation of the mass dependence of the hypernucleus lifetimes enabled us to test the validity of the fenomenological $\Delta I=1/2$ rule – which was found for mesonic decay of the hyperons – for the case of nonmesonic decay [5]. A ratio of the neutron to proton induced decay rate $R_n/R_p > 2$ indicates the violation of the $\Delta I=1/2$ rule. We conclude that this rule is violated at a confidence level of 0.98 for the nonmesonic decay of the Λ hyperon[6].

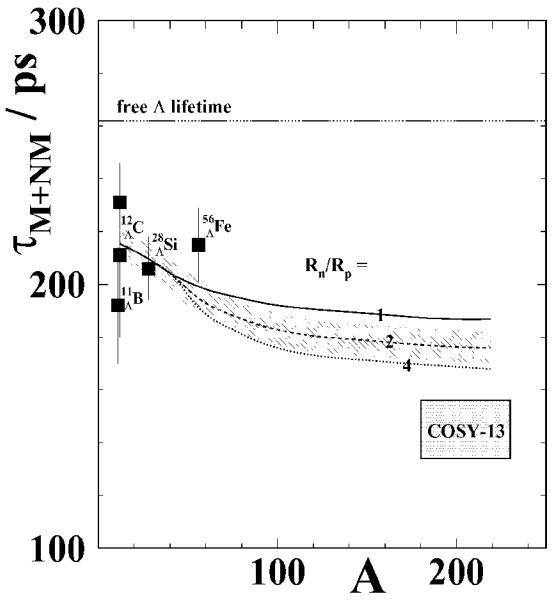

Fig. 2: Mass dependence of the lifetime of hypernuclei. Theoretical curves are plotted for R_n/R_p ratios of 1, 2 and 4 together with COSY–13 data (box) and data for light hypernuclei(full squares). The width and height of the "COSY-13" box represent the range of hypernucleus masses involved and the error of the lifetime determination, respectively. The hatched area around the dashed line shows the one standard deviation uncertainty of the normalization of theoretical values (from [6]).

References:

[1] K. Pysz, et al., NIM **A420** (1999) 356
[2] B. Kamys, et al., Eur. Phys. J. **A 11** (2001) 1
[3] P. Kulessa, et al., Phys. Lett. **B427** (1998) 856
[4] P. Kulessa, et al., nucl-ex/0108027, in press Acta Physica Polonica **B**
[5] Z. Rudy, et al., Eur. Phys. J. **A5** (1999) 127
[6] W. Cassing, et al., nucl-ex/0109012
[7] T. A. Armstrong et al., Phys. Rev.**C47** (1993) 1957
[8] Particle Data Group, Eur.Phys.J.**C15**(2001)1

[1]H. Niewodniczański Institute of Nuclear Physics, PL-31342 Cracow, Poland
[2]Institut für Kernphysik, Forschungszentrum Jülich, D-52425 Jülich, Germany
[3] M. Smoluchowski Institute of Physics, Jagellonian University, PL-30059 Cracow, Poland

Pionic Fusion on the Deuteron

The GEM Collaboration

There has been considerable effort to understand the pionic absorption in nucleus-nucleus interactions. However, even for the simple case

$$p + A \rightarrow (A + 1) + \pi^+$$

the underlying reaction mechanism is not well understood. Modelling of this reaction favors the assumption of the absorption of the proton on a quasi-deuteron as the dominant process with little dependence upon the nuclear structure. This makes the reaction

$$p + d \rightarrow {}^3H + \pi^+$$

as well as the isospin related reaction

$$p + d \rightarrow {}^3He + \pi^0$$

interesting. Because $p + d \rightarrow {}^3H + \pi^+$ is believed to be related to the $p + p \rightarrow d + \pi^+$ reaction, we have a chain of bootstrap reactions pictured in Fig. 1.

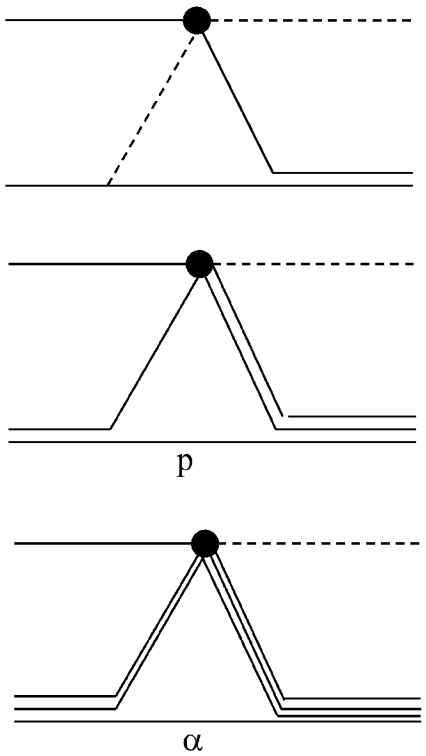

Fig. 1: Bootstrap reactions producing a two body final state with one particle being a pion. The upper graph is the $p + p \rightarrow d + \pi^+$ reaction with the underlying elementary $\pi^0 + p \rightarrow \pi^+ + n$ or $\pi^+ + p \rightarrow \pi^+ + p$ reaction. The middle graph is the $p + d \rightarrow {}^3H + \pi^+$ reaction with the underlying $p + p \rightarrow d + \pi^+$ reaction, the indicated proton is a mere spectator. The lower graph shows the reaction $p + {}^6Li \rightarrow {}^7Li + \pi^+$ with $p + d \rightarrow {}^3H + \pi^+$ as the underlying reaction and an a-particle as spectator.

Starting from single pion exchange the chain goes up to pionic fusion of the proton on ${}^6Li$. The $p + p \rightarrow d + \pi^+$ reaction was recently studied by the GEM collaboration with emphasis on differential cross sections (see Ref. [1]).

It then becomes evident that the reactions $p + d \rightarrow {}^3H + \pi^+$ and $p + d \rightarrow {}^3He + \pi^0$ are the key reactions to study models of pionic fusion. Numerous measurements of the differential cross sections have been reported, however, the agreement between results at the same energy is not always good. The same is true for the inverse reactions. The situation on the theoretical side was characterized by Fearing [2] "where by qualitative (fit to the data) one means an overall normalization correct to a factor of 5 or so and angular distributions differing at some angles by an order of magnitude", and more recently by Falk [3] "In general, theoretical descriptions of $pd \rightarrow Xp$ reactions have not been particularly successful, despite great efforts by many groups over the years".

The GEM collaboration has therefore studied the two reactions of interest by simultaneous measurement of the recoiling A=3 nuclei. This was done with the Germanium wall and for nuclei being emitted at zero degree in the laboratory (180 degree in the center of mass system) by the magnetic spectrograph BIG KARL. The set-up of the Germanium wall is described in Ref. [5]. Further details can be found in a first publication [4] dealing with a part of the data. The total yields are shown in

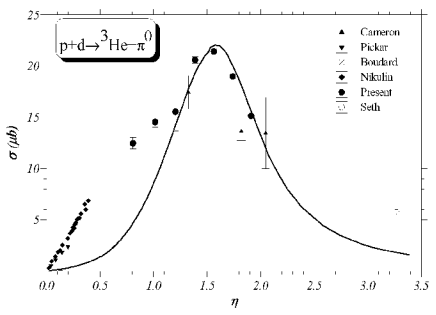

Fig. 2: Excitation function of the indicated reaction. The present data are compared with previous data, shown by different symbols. The solid curve is the excitation function for the $p + p \rightarrow d + \pi^+$ reaction, scaled down by a factor of 145.5.

Fig. 2 together with previous results as function of $\eta = p/m$ with p and m the pion center of mass momentum and its mass. The data points have significantly smaller error bars than previous measurements in this energy range, except for the point at $\eta = 1.2$ corresponding to a beam momentum of 850 MeV/c. In this experiment, we had an energy threshold due to a hardwired coincidence between quirl and pizza detector. The present data show an increase in yield up to a local maximum around $\eta \approx 1.6$ corresponding to a proton beam momentum of 950 MeV/c. In order to study whether the

bootstrap model shown in Fig. 1 may be applicable, we have also plotted in Fig. 2 the excitation function for the $p + p \rightarrow d + \pi^+$ reaction downscaled by a factor of 145.5 to match the order of magnitude of the present data. The data points for the higher momenta fall on this curve while those for the two lower momenta do not. The local maximum is in both excitation functions and hence due to the excitation of the $\Delta(1232)$ resonance. There is a clear disagreement between this curve and the data close to threshold. In order to study this effect further we compare the differential cross sections as function of the momentum transfer $q = p_p + p_\pi \cos(q)$ with the incident and final momenta in the center of mass system. Some selected data sets are shown in Fig. 3.

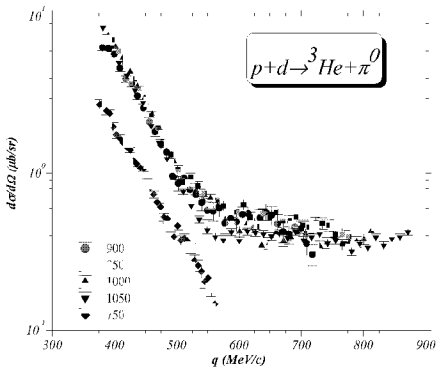

Fig. 3: Differential cross sections in the center of mass system as function of the transferred momentum for the indicated momenta.

The behavior of the distributions seems to be the same as for the dependence on $\cos(q)$: an almost exponential with an additional flat component for the higher beam momenta. However, the exponential part seems to be almost independent of the bombarding energy, where the integrated data are in agreement with the downscaled $p + p \rightarrow d + \pi^+$ curve. In order to get rid of trivial phase factors we extract the matrix element $|M(s, t(q))|$ in a relativistic formulation with s and t the Mandelstam variables. The matrix elements show the same behavior as the cross sections, as expected. In order to be quantitative we fitted the function

$$|M(s, t(q))|^2 = a \ \exp(bt) + c$$

to the extracted matrix elements. The slope parameter in the exponent was found to be independent of the bombarding energy

$$b = -(16.86 \pm 0.17) \ (GeV/c)^{-2}.$$

The momentum dependence of the parameters a and c is shown in Fig. 4.

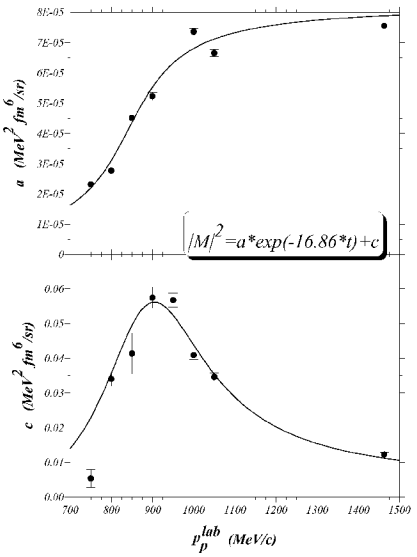

Fig. 4: Beam momentum dependence of the parameters fitted to the matrix elements as function of the four momentum transfer squared t.

Differential cross sections in the center of mass system as function of the transferred momentum for the indicated momenta. Here we have added data from K. Seth (private communication) taken at a beam momentum of 1463.3 MeV/c. The strength parameter of the exponential a tends to saturate for energies above the resonance. It is interesting that the parameter c related to the high momentum transfer again shows the dependence as one expects for an intermediate D-excitation. A possible reaction mechanism may, therefore, be a two step process: pion production in the first step is followed by scattering on the spectator nucleon in the second step. However, also scattering of the pion radiated off the projectile proton can scatter on the deuteron. Additional measurements of polarization observables - there are four independent quantities- may help to disentangle the reaction mechanisms.

References

[1] M. Drochner *et al.*, Phys. Rev. Lett. **77** (1996) 454, Nucl. Phys. **A 626** (1998) 63, Phys. Rev. **C 63** (2001) 044011.

[2] Fearing, Phys. Rev. **C 11** (1977) 1210.

[3] W. Falk, Phys. Rev. **C 61** (2000) 034005.

[4] M. Betigeri *et al.*, Nucl. Phys. **A 690** (2001) 473.

[5] M. Betigeri *et al.*, Nuclear Instr. Methods in Physics Research **A 421** (1999) 447.

A precision experiment to measure the η – meson mass

The GEM Collaboration

The goal of this investigation is a precise measurement of the ηmeson mass. Unique Big Karl properties and a kinematical coincidence with a calibration reaction makes it possible to obtain beam momentum and Big Karl central momentum with very good accuracy. Simultaneous detection of ^3He from the $pd \rightarrow {}^3He\eta$ reaction allow one to obtain very precise ηmass value. The proposed method makes it possible to reduce the ηmass error to the level of 0.03 MeV, which is four times smaller than reported by Particle Data Group. According to Particle Data Group the η-meson mass is poorly known [1]. In addition, a recent measurement of the decay $\eta \rightarrow 3\pi^0 \rightarrow 6\gamma$ by the NA48 collaboration at CERN resulted in a shift of 523 ± 59 keV compared to the PDG value. Therefore, a new measurement with a very small systematic error is required in order to obtain a precise value for the η-mass. The idea of the experiment is the simultaneous detection of three forward outgoing particles produced in two different reactions, thus permitting the measurement of beam momentum, spectrograph setting and η mass. The first of these two possibilities are the reactions

$$p + p \rightarrow d + \pi^+ \quad (1)$$

$$p + p \rightarrow \pi^+ + d \quad (2)$$

$$p + d \rightarrow {}^3He + \eta. \quad (3)$$

The second possibility will make use of

$$p + d \rightarrow {}^3H + \pi^+ \quad (4)$$

$$p + d \rightarrow \pi^+ + {}^3H \quad (5)$$

$$p + d \rightarrow {}^3He + \eta. \quad (6)$$

It is always the third particle which will be detected. While the second reaction set needs a deuterium target for the the first set a mixed hydrogen-deuterium target is required. As an example the first possibility is shown in Fig. 1.

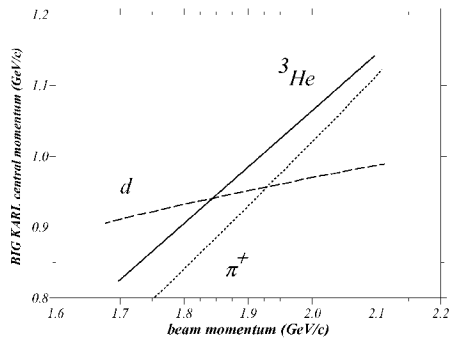

Fig. 1: Big Karl central momentum versus beam momentum: for the reactions $p + p \rightarrow d\pi^+$, $p + p \rightarrow \pi^+ + d$, and $p + d \rightarrow {}^3He + \eta$.

Both reactions were employed. A proton beam interacted with 2 mm thick target filled with liquid hydrogen, deuterium or their mixture. The magnetic spectrograph Big Karl was used to analyze the momenta of the particles obtained in the interactions. It operated in angle sensitive mode, allowing measurements of particles emerging under small angles from a target, placed in the focus of the spectrograph. Besides production runs, test runs were performed which included beam luminosity monitoring measurements and Big Karl calibration measurements. In order to control the magnetic field of Big Karl with a high precision it was measured periodically using nuclear magnetic resonance probes.

Until now the data from the deuterium target are analyzed only. In Fig. 2 the ^3He missing mass distribution is shown. It is obtained from interaction of deuterons with the proton beam. The sample shown includes only events, where the emerging ^3He particles have vertical angels less then 30 mrad only, which allows to decrease the background significantly. The peak from $pd \rightarrow {}^3He\,\eta$ reaction is seen with signal to background ratio 1:1. The background originates mainly from $pd \rightarrow {}^3He\,\pi^+\pi^-$ reaction with small admixture from $pd \rightarrow {}^3He\,\pi^+\pi^-\pi^0$. The result of its Monte Carlo simulation is shown by dashed line in the same figure. The statistical error of the η meson mass obtained from these data is about 0.02 MeV. When the data from the target with a mixture deuterium and hydrogen will be included this will decrease the error to 0.015 MeV. In order to obtain the unbiased η meson mass, analysis of all experimental data set is needed.

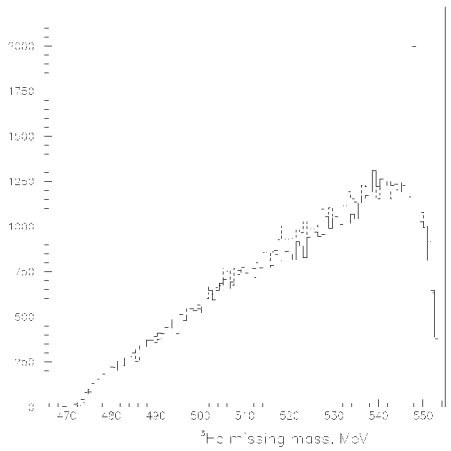

Fig. 1: ^3He missing mass distributions obtained from events where the particles have vertical angels less then 30 mrad. The simulated background is shown by dashed line.

References

[1] D. E. Groom *et al.*, Eur. Phys. Jour. **C 15** (2000) 1.

[2] NA48.

First results of $\pi^0 - \eta$ mixing angle measurement

The GEM Collaboration

A detailed motivation for $\pi^0 - \eta$ mesons mixing angle measurement via isospin symmetry breaking was given in our original proposal [1]. Various solutions of QCD give theoretical predictions for its value of about 0.015. However, the mixing angle was never measured in spite of the fact that it may play an important role in investigation of CP violation sources and in the analysis of B meson decays.

The calculations performed in the framework of a simple model [2] predict that a strong effect due to $\pi^0 - \eta$ mixing may be observed in the ratio of the cross sections for p+d$\rightarrow{}^3$H+π^+ and p+d$\rightarrow{}^3$He+π^0 reactions. As suggested in Ref. [2] such a strong effect may be due to existence of a quasi-bound ^{3}He-η state. This ratio has to be studied for the beam momenta close to the η meson production threshold, and the ^{3}H/^{3}He cross section ratio should be measured at large relative angles between the incident proton and outgoing pion. While isospin symmetry predicts the ratio of the cross sections to be equal 2, $\pi^0 - \eta$ mixing leads to deviations from this value. In order to extract the mixing angle it is necessary to measure the beam energy dependence of the cross sections ratio.

The applied method of determining the energy dependence of the ratio of cross sections is based on simultaneous detection of ^{3}H and ^{3}He nuclei. Therefore, it ensures high accuracy of the results, allowing to study even quite small effects of isospin symmetry breaking. The simultaneous detection of ^{3}He and ^{3}H is achieved by detecting helium nuclei at the focal plane and tritons at the first dipole yoke hole. The experimental set-up and the results of the test measurements were presented in Refs. [3–7].

In the run analyzed recently we have measured the ^{3}H/^{3}He cross section ratio for two beam momenta. The beam momentum of 1.57 GeV/c is close to the η production threshold, where the symmetry breaking effect should be maximal. For the second beam momentum of 1.59 GeV/c the expected symmetry breaking effect should be much smaller. The obtained ratio of the cross section is shown in Fig. 1 together with calculations using the model of Ref. [2], however, employing a mixing angle of 0.030. Further measurements were performed at beam momenta of 1.571 (exactly at η threshold), 1.56 and 1.70 GeV/c. The analysis of these new data is in progress. However, the already existing points show large isospin symmetry breaking and suggest the $\pi^0 - \eta$ mixing angle to be much larger than expected from QCD calculations.

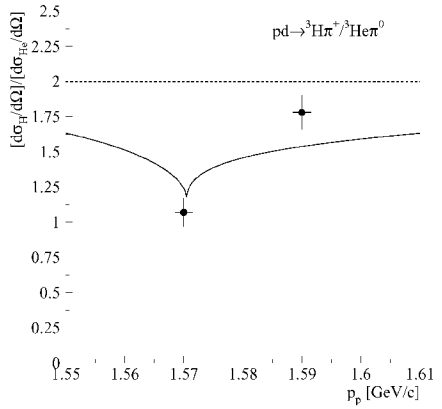

Fig. 1: Experimental ratio of the cross sections for p+d$\rightarrow{}^3$H+π^+/^{3}He+π^0 reactions. The theoretical solid curve is from the model of Ref. [2] using $\pi^0 - \eta$ mixing angle equal 0.030.

References

[1] A. Magiera, COSY - Proposal No. 59 (1997).

[2] A. Magiera and H. Machner, Nucl. Phys. A674 (2000) 515.

[3] GEM Collaboration, Annual Report 1998, KFA-IKP, 1999, p. 28.

[4] GEM Collaboration, Annual Report 1998, KFA-IKP, 1999, p. 30.

[5] GEM Collaboration, Annual Report 1999, KFA-IKP, 2000, p. 58.

[6] GEM Collaboration, Annual Report 1999, KFA-IKP, 2000, p. 60.

[7] GEM Collaboration, Annual Report 2000, KFA-IKP, 2001, p. 56.

Eta-nucleus final state interaction studies

The GEM collaboration

As a part of our experimental programmes on the understanding of eta-nucleus interaction, the reaction p+^{6}Li $\rightarrow$ ^{7}Be+η is under investigation at Big Karl. The details of the physics motivation are reported in the previous year's report [1]. The available experimental information on the eta-nucleus final state interactions for nuclei heavier that ^{4}He is scarce. The only measurement on the present reaction exists, to the best of our knowledge, at T_p= 684 MeV [2]. The measurement in this experiment was performed by detecting eta-decay products (two forward going gammas) . The efficiency of the measurement was about only 2% and the energy resolution was not sufficient to resolve various excited states of ^{7}Be. The detection of heavy recoil nucleus, for reaction

close to threshold, is somewhat more convenient as the particles are emitted in a small forward cone. A good energy resolution can also be achieved by employing the high precision magnetic spectrograph Big Karl.

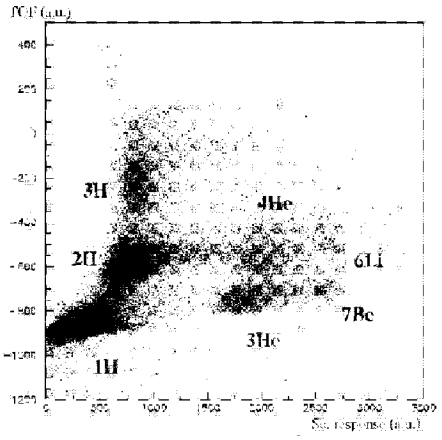

Fig. 1: Time of flight vs. scintillator light output spectrum.

The identification of p+^{6}Li $\rightarrow$ ^{7}Be+η events can then be followed by constructing invariant mass of unobserved η particles. In our test run performed at a beam momentum close to the reaction threshold (3 MeV/c above threshold), ^7Be particles were detected using Big Karl and a new set of focal plane detectors [1](plastic scintillators in the form of long bar and two such layers were placed in vacuum for time of flight measurement). A very good time of flight resolution obtained from such measurement allowed us to achieve particle separation(see Fig.1) and to estimate the upper limit of production cross section. However, the position resolution was not as good as expected and did not allow us to identify ^{7}Bη events in the missing mass spectrum. In order to enhance the position resolution, a multi-wire avalanche counter (MWAC) is under construction and will be used along with the scintillators. The advantage of MWAC, in contrast to multi-wire proportional counter (MWPC), is that the former works at very low pressure ($\approx$ few mb) making it suitable for the detection of such strongly ionizing particles. The MWAC, in its present design, consists of two layers of wire (546 wires in each layer) inclined by 45 deg, very thin Mylar windows(6 μm) and has an over all dimension of 728 x 228 x 22 mm. The expected position resolution is $\approx$ 0.5 mm which sufficient enough for the present purpose. A schematic diagram of the detector is shown in Fig.2. Two such thin stacks of MWAC will be mounted at the Big Karl exit which will be followed by ΔE-E plastic scintillator detectors for time of flight information. The detector is expected to be ready in the beginning of 2002.

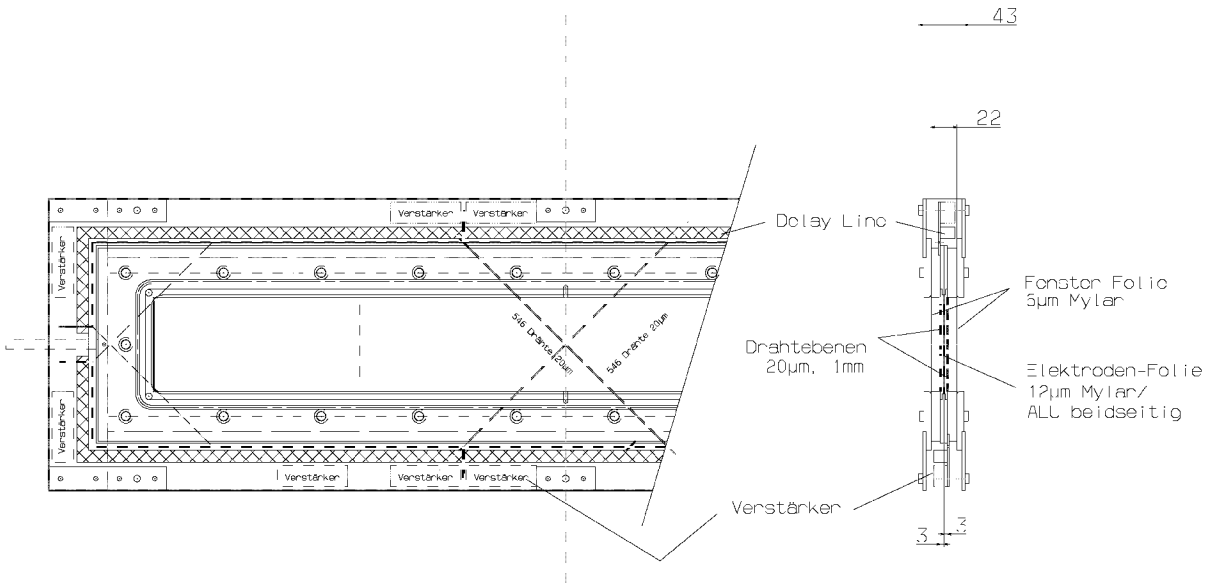

Fig. 2: Schematic diagram of multi-wire avalanche counter.

References

[1] GEM collaboration, IKP, FZ annual report (2000) 57

[2] Scomparin et al, J.Phys. G19 (1993) L51

Eta-nucleus bound state study and the detector ENSTAR

The GEM collaboration

In contrast to the π -nucleon interaction, the η-nucleon interaction is strong and attractive at low energies (S-wave). This is linked to the N*(1535) S_{11} baryon resonance, which lies just above the η +N threshold (1488 MeV), and has a large branching ratio to the η -N channel (30-55%). Due to this, the cross section for η production in nucleon-nucleon collisions at threshold is expected to be large and the η-nucleus potential would be attractive. This provides an interesting possibility of the existence of the eta-nucleus bound states, and their production in near threshold η production in proton nucleus collisions. We plan to produce these η-nuclei in p+$^{A}_{Z}$X $\rightarrow$ ^{3}He+$^{A-2}_{Z-1}Y_{\eta}$ or p+$^{A}_{Z}$X $\rightarrow$ d+$^{A-1}_{Z}X_{\eta}$ reactions by choosing the "magic momentum" of the proton-beam and the detection angle of ^{3}He such that the η is produced with very small momentum. The "magic momentum" for protons is around 1.75 GeV/c in the p+d $\rightarrow$ ^{3}He+η reaction and 3.02 GeV/c in the p+n $\rightarrow$ d+η reaction, which are well within the COSY limit. The target can be of solid target (^{12}C, ^{6}Li etc) as well as liquid (^{14}N).

The estimated cross section for η-mesic nucleus formation is only about a few nano barns [1]. On the other hand the background ^{3}He events due to other reactions can be an order of magnitude larger. In order to detect the η -mesic nucleus events in the presence of large background, it would be necessary to demand a triple coincidence of ^{3}He and the η -mesic nucleus decay particles, namely, protons and pions. The η -mesic nucleus decay is related to the N*(S_{11}) decay, resulting in one of the following branches.

$$\eta + N \rightarrow N^{*} \rightarrow \begin{matrix} \pi^{-} + \mathrm{p} \\ \pi^{o} + n \\ \pi^{o} + p \\ \pi^{+} + n. \end{matrix}$$

In order to tag the η -mesic nucleus ($\tau \sim 10^{-22}$ sec) through its decay products, a large acceptance detector "ENSTAR" [2] is being built in Mumbai, India. Phase space calculations to simulate eta-mesic nucleus decay events have been performed using a Monte Carlo event generator program GENBOD. The reaction studied was p+^{16}O $\rightarrow$ ^{3}He+$^{14}N_{\eta}$ at a momentum close to the magic momentum. The simulations were done in two steps. In the first step, Monte Carlo events were generated for p+^{16}O $\rightarrow$ ^{3}He+^{14}N*. An excitation energy of 547 MeV, equal to the mass of eta meson, was given to ^{14}N. Only those ^{14}N events for which corresponding ^{3}He is within the BIG KARL acceptance ($\theta_{lab}(^{3}\mathrm{He}) \leq$ 6 deg.) were considered. In the next step the decay of N* to pπ^{-} was simulated. A mass of N* equal to the mass of a nucleon plus the mass of a eta meson was assumed. The N*, before its decay, was moving with the same velocity as that of the recoil ^{14}N plus a modification by the Fermi momentum. The π,p opening angle distribution shows a peak at around 150 deg. with a width of 40 deg. The energy spectrum for proton peaks at T_p= 100 MeV with a width (FWHM) of 120 MeV while the π^{-} has a peak at 320 MeV with a similar width. The ENSTAR design was based on the results of the present simulation.

The detector (Figs.1 and 2) is made up of two identical cylinders, each consisting of three layers of plastic scintillator. The two cylinders are to be placed on either side of target leaving sufficient space to enable mounting of targets. Each layer is split into a number of pieces in order to obtain θ and ϕ information. Signals from the various layers will be used to generate ΔE-E spectrum for particle identification and to obtain total energy information for the stopped particles. The scintillator read out using wave length shifting optical fibres (BCF-91A, manufactured by Bicron, USA) has been planned.

The detector fabrication is at an advanced stage at BARC, Mumbai and will be shipped to Jülich immediately after the completion of the construction work.

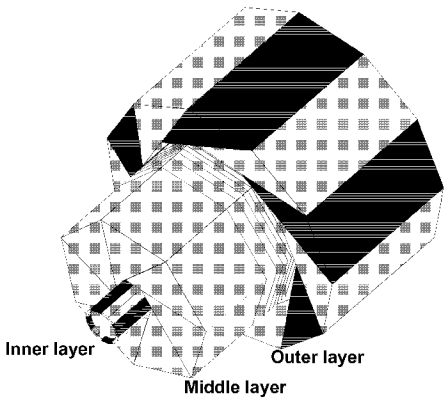

Fig. 1: An assembly drawing of ENSTAR detector.

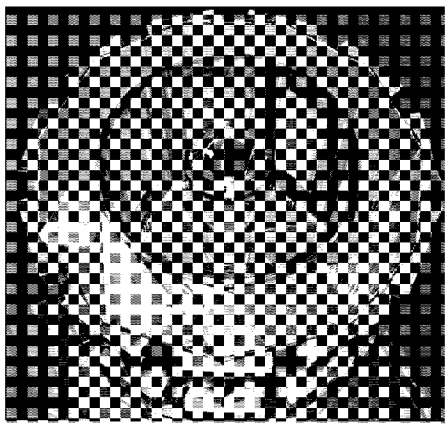

Fig. 2: ENSTAR with its support structure.

References

[1] L.C.Liu, Private communication

[2] B.J.Roy et al, BARC External Report No BARC/2000/E/004

ω meson production at the Time-Of-Flight spectrometer[&]

K.-Th. Brinkmann* for the COSY-TOF collaboration

In a first attempt to study the production of vector mesons in collisions between protons, data taken with the TOF spectrometer during an experiment in early 2000 were evaluated with respect to a signal for ω meson production [1]. The beam momenta of 2950 and 3200 MeV/c were chosen with the focus on associated hyperon production [2]. They correspond to excess energies of ε = 92 and 173 MeV, respectively, above the threshold for pp → ppω.

Events with a characteristic topology in the TOF detector were selected from the data sample for further inspection. The required pattern includes two hits at small angles, which could be associated with the protons from the pp → ppX reaction, and an additional pair of hits at angles larger than that allowed for protons. The latter were assumed to be decay pions from , e.g., $\rho^0 \to \pi^+\pi^-$ (BR 100%) or $\omega \to \pi^+\pi^-\pi^0$ (BR 89%) decay. ρ^0 production contributes appreciably to the background because of its similar central mass compared to ω. The missing mass of particle X and its momentum was calculated using the mass assignment of the two proton candidates and their measured velocity vectors. An additional cut on the coplanarity of the decay pions with respect to the resonance X was used to reject events that meet the condition that the charged pions were emitted back to back in the center-of-momentum frame defined by X (→ $\pi^+\pi^-$). The remaining spectrum of ω candidates is shown in figure 1.

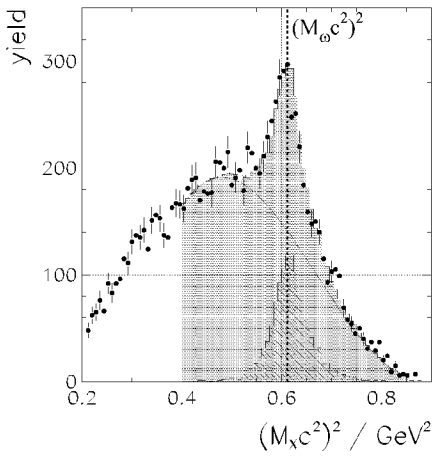

Fig. 1: Spectrum of the squared missing mass deduced from the two detected proton candidates. The ω peak at $(Mc^2)^2 \approx 0.6$ GeV^2 is clearly visible.

A clean signature of ω production is visible at $M^2 = M_\omega^2$. The hatched peak at the same position shows the simulated response function of the TOF detector. It nicely agrees in shape with the ω signal above background, as demonstrated by the shaded area that is a sum of the parametrized background as indicated and the Monte Carlo ω signal.

Using the simulated detector acceptance for events of the chosen type and a luminosity calibration extracted from elastic proton-proton scattering events, which are measured over a large angular range in the TOF setup, total cross sections for ω production were deduced. These are shown in figure 2 together with data from the literature [3, 4, 5]. Error bars shown in the figure represent statistical as well as systematic errors, which were added quadratically.

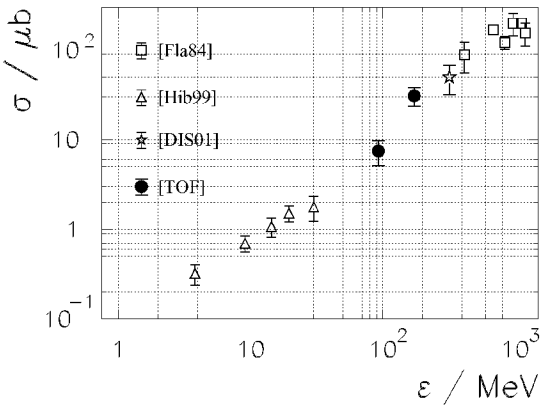

Fig. 2: Excitation function of pp → ppω. The filled circles are the present data, while the open triangles are from [3] and the star is from [4]. The open squares represent data adopted from a compilation of cross sections [5].

The present data nicely fill the gap between the SPES3 measurements [3] below ε = 30 MeV and the DISTO result [4] at ε = 320 MeV. The DISTO experiment not only measured ω production but also took data on the production of φ mesons. According to the SU(3) mixing scheme, the quark content of the φ meson is almost exclusively $s\bar{s}$, while the ω wave function contains $u\bar{u} \oplus d\bar{d}$. Hence, φ meson production should be strongly suppressed in pp collisions. According to the OZI rule [6], $\sigma_\phi/\sigma_\omega$ is given by the small deviation from perfect decoupling of s and u/d and should not exceed a value of 0.4%. The DISTO result [7] suggested a violation of this rule by one order of magnitude, but the finding relied on an extrapolation for the ω cross section to ε = 85 MeV. The present work gives a value for the cross section at an energy closeby, so that the ratio can now be determined without further assumptions. We find $\sigma_\phi/\sigma_\omega = (2.5\pm1.0)\%$, which is about a factor of 7 above the naive SU(3) expectation.

References:

[1] COSY-TOF collaboration, Phys. Lett. B **522**, 16 (2001).
[2] W. Eyrich et al., this report.
[3] F. Hibou et al., Phys. Rev. Lett. **83**, 492 (1999).
[4] DISTO collaboration, Phys. Rev. C **63**, 024004 (2001).
[5] V. Flaminio et al., Compilation of Cross-Sections, CERN-HERA 84-10 (1984).
[6] S. Okubo, Phys. Lett. **5B**, 165 (1965); G. Zweig, CERN Report No 8419/Th 412; I. Iizuka, Prog. Theor. Phys. Suppl. **37-38**, 21 (1966).
[7] DISTO collaboration, Phys. Rev. Lett. **81**, 4572 (1998).

* Institut für Kern- und Teilchenphysik, Technische Universität Dresden, D-01062 Dresden, Germany
[&] supported in part by BMBF and FZ Jülich

Λ-Hyperon Production at COSY-TOF *

W. Eyrich, M. Fritsch, W. Schroeder, F. Stinzing, M. Wagner and S. Wirth
Physikalisches Institut, Universität Erlangen-Nürnberg
for the COSY-TOF Collaboration

The exclusive measurement of associated strangeness production in elementary proton induced reactions has been being studied extensively for several years at the COSY-TOF spectrometer. The modular apparatus combines high efficiency and acceptance for charged tracks with an energy and momentum resolution of a few percent.

So far, the $pp \rightarrow K^+\Lambda p$ reaction has been investigated at seven beam momenta between 2.5 and 3.2 GeV/c covering the full phase space. The complete measurement of primary and delayed hyperon decay particles allows the extraction of differential observables including Dalitz plots and invariant mass spectra of 2-particle subsystems. As an example for the quality of the data, figure 1 shows angular distributions of the Λ-hyperon at four different beam momenta together with Legendre fits; as expected, growing p-wave contributions are observed with increasing beam momentum. Total cross section values of 7.4±0.3 μb, 8.6±0.3 μb, 12.0±0.4 μb and 18.7±0.5 μb are obtained at the four beam momenta shown in figure 1 ([1], [2]).

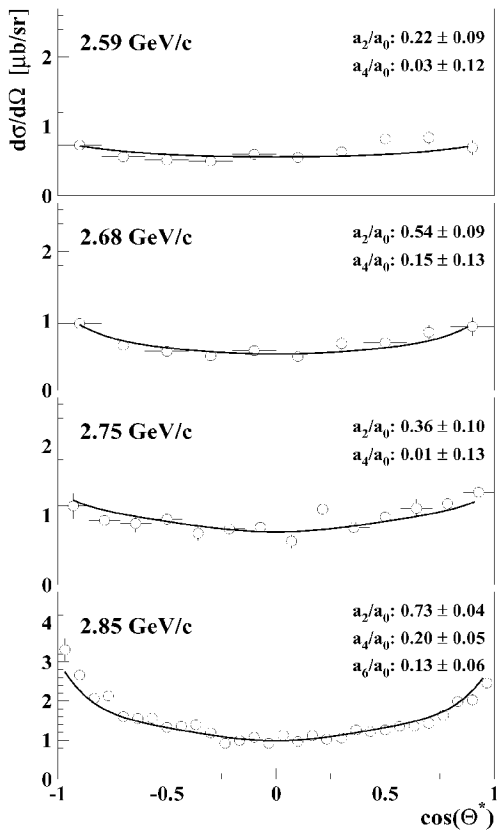

Fig. 1: angular distributions of Λ-hyperons at various beam momenta with coefficients of the Legendre fits

From the analysis of the Dalitz plots and the 2-particle invariant mass spectra at 2.75 and 2.85 GeV/c (see figure 2) there is clear evidence of the Λ final-state interaction which shows up as an enhancement on the left side of the $p\Lambda$-spectra. The shift to higher masses in the $K\Lambda$-spectrum gives some indication on the influence of N^*-resonances as proposed in resonance model calculations [3].

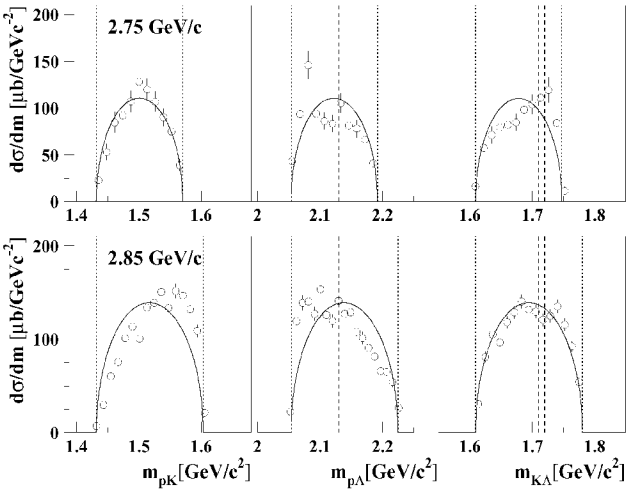

Fig. 2: invariant mass spectra for 2-particle subsystems with phase space limits (dotted), Σ^0 threshold (dashed line in $p\Lambda$), and $N^*(1710)$, $N^*(1720)$ (dashed lines in $K\Lambda$)

After the upgrade of the TOF spectrometer by ring and barrel hodoscopes, which significantly increased the detector acceptance as well as time and angular resolution, a high statistics run was performed at beam momenta of 2.95 and 3.20 GeV/c. For subsamples at both measured momenta Λ missing mass distributions are shown in figure 3. A total yield of about fifty thousand fully reconstructed Λ-events almost free from background contributions is expected.

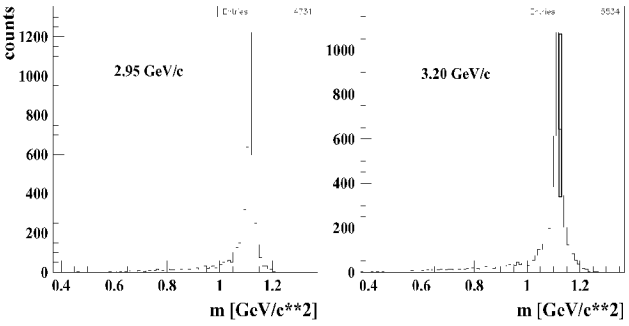

Fig. 3: missing mass spectra for reconstructed Λ-hyperons at 2.95 and 3.20 GeV/c

The next step for future hyperon measurements at COSY-TOF will be the use of a polarized beam.

References:

[1] D. Hesselbarth, PhD Thesis, Berichte des FZ Jülich; 3849 (2001)
[2] R. Bilger et al., Phys. Lett. B **420**, 217 (1998)
[3] A. Sibirtsev, K. Tsushima and A.W. Thomas, Phys. Lett. B **421**, 59 (1998)

*supported by German BMBF and FZ Jülich

Σ-Hyperon Production at COSY-TOF *

W. Eyrich, M. Fritsch, W. Schroeder, F. Stinzing, M. Wagner and S. Wirth
Physikalisches Institut, Universität Erlangen-Nürnberg
for the COSY-TOF Collaboration

Besides the measurement of Λ-hyperons the production of Σ-hyperons is investigated at the COSY-TOF spectrometer. The Σ^0 is observed in the reaction $pp \to K^+\Sigma^0 p$ via its decay into $\Lambda\gamma$. As the γ cannot be detected with the TOF detector, this reaction has to be distinguished from the Λ-production by using additional energy loss information of the various start and stop detector components. This allows a strong reduction of the Λ-background in the Σ^0 region and the extraction of total cross sections; for the measured beam momentum of 2.85 GeV/c a value of $\sigma_{tot}(K^+\Sigma^0 p) = 2.0\pm0.3\,\mu$b is derived. Σ^+-hyperons are investigated in two channels: the first is $pp \to K^+\Sigma^+ n$, where the neutron is detected in a large area neutron-wall, which is installed behind the TOF spectrometer (for details of this reaction see [1]). For the channel $K^0\Sigma^+ p$, the combination of the delayed decays $K^0 \to \pi^+\pi^-$ and $\Sigma^+ \to \pi^+ n$ or $\pi^0 p$ gives a unique signature for the event identification.

Figure 1 shows reconstructed missing mass peaks for three beam momenta. As demonstrated for the beam momentum of 2.85 GeV/c the shape of the distribution is in very good agreement with Monte-Carlo simulations. The shaded area marks the Λ-background in this channel.

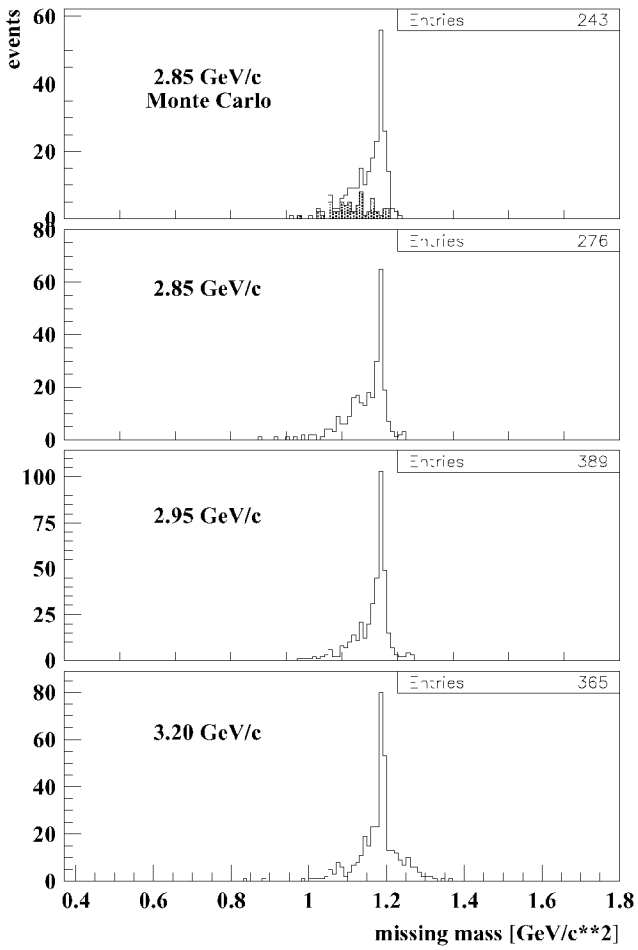

Fig. 1: missing mass distributions for reconstructed Σ^+-events at beam momenta of 2.85 GeV/c, compared to MC-events (shaded: Λ-background) and preliminary results of subsamples at 2.95 and 3.20 GeV/c

*supported by German BMBF and FZ Jülich

From the data at 2.85 GeV/c for the first time in the threshold region a value for the total cross section in the channel $K^0\Sigma^+ p$ could be extracted: $\sigma_{tot} = 5.6\pm1.0\,\mu$b. In figure 2 this result is shown together with the existing COSY data (filled symbols) and older data at higher beam momenta [2] for the Λ and Σ^0-channels.

Together with the value of $18.7\pm0.5\,\mu$b for the Λ-channel at 2.85 GeV/c (see [3]) it is now possible to compare total cross sections of the Λ, Σ^0 and Σ^+-production.

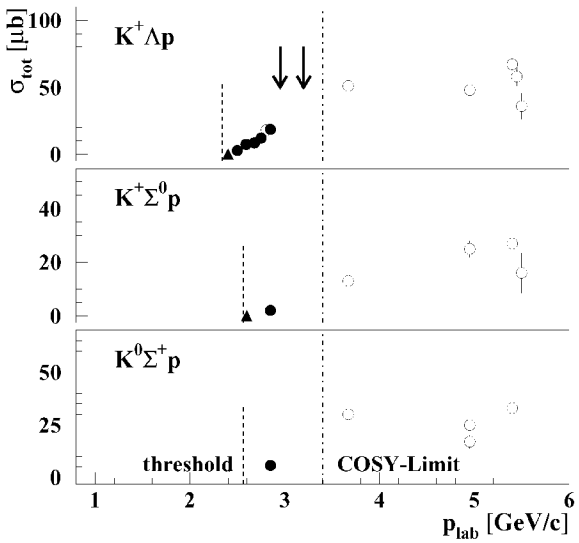

Fig. 2: total cross sections for the reactions $K^+\Lambda p$, $K^+\Sigma^0 p$ and $K^0\Sigma^+ p$; filled triangles: COSY-11 (see e.g. [4]), filled circles: COSY-TOF; the arrows mark the recent measurements at 2.95 and 3.20 GeV/c

For the newer data in the channel $K^0\Sigma^+ p$ at beam momenta of 2.95 and 3.20 GeV/c a total number of 2000 events is expected allowing the study of differential observables as well. A detailed analysis of the full sample will give information on the reaction mechanism, especially the role of final state interaction and N^*-resonances. Moreover, there is a special interest in an exotic $qqqq\bar{q}$ resonance called Z^+, which is proposed in the soliton model [5]. It should show up in the reaction $pp \to K\Sigma^+ N$ as a narrow peak in the mass spectrum of the KN subsystem and will be sought in the Dalitz plots of the different momenta.

References:

[1] P. Schönmeier et al., contr. to this report
[2] CERN-HERA Rep. 84-01, (1984)
[3] W. Eyrich et al., contr. to this report
[4] S. Sewerin et al., Phys. Rev. Lett. **83**, 682 (1999)
[5] M.V. Polyakov et al., Eur. Phys. J. A **9**, 115-118 (2000)

Investigation of the $pp \to nK^+\Sigma^+$ reaction*

Peter Schönmeier** for the COSY-TOF collaboration

Reactions of the type pp $\to$ NKY are presently studied at COSY in very detail, in particular the channels Y = (Λ,Σ^0). Data on Σ^+,Σ^- are not known close to threshold.

A measurement of the channnel $pp \to nK^+\Sigma^+$ was performed with the short version of the COSY-TOF spectrometer, which consisted of the Erlangen start and vertex detectors, the neutron detector COSYnus and the Quirl. The Erlangen start detector supplies the time-of-flight reference (two layers of 1mm thick scintillator wedges at a distance of z=23mm from the target). The vertex detector consists of a silicon-microstrip detector at z=30mm and two double-layer scintillating fiber hodoscopes at z=100mm and z=200mm downstream of the liquid hydrogen target.

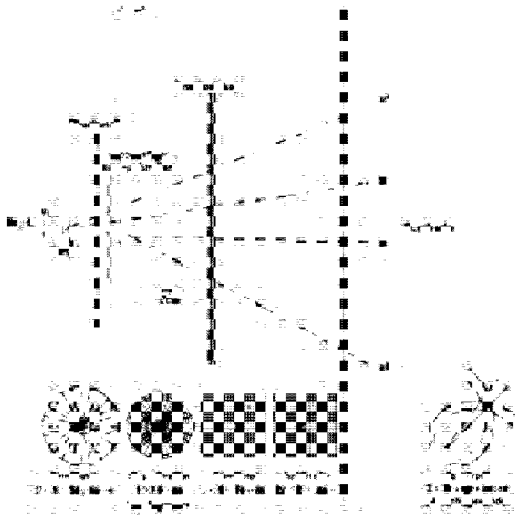

Fig. 1: Experimental setup (start and vertex detectors) used in the experiment

In contrast to more recent TOF experiments on strangeness production, the stop detector (Quirl) was mounted rather close (1m) to the target, hence the time of flight resolution limits the velocity resolution, and the selection of good events rests (besides the detection of the primary neutron) mainly on geometry. This suffices due to the good spatial resolution of the Erlangen vertex detector, the neutron detector and the grannularity of the Quirl.

For the detection of a K^+-track at least two spatial points (e.g. one hit in the Erlangen vertex detector and one in the Quirl) are required. A Σ^+ is identified by one hit in the microstrip detector without any hit in a given $\theta - \phi$ region behind it. The track of the charged decay particle of the Σ^+ (either p or π^+) is constructed from the remaining hits which were not used for the reconstruction of the K^+-track. The decay point of the Σ^+ is given by the point of closest approach between the Σ^+ track and the track of the charged decay particle. For $nK^+\Sigma^+$-events this point should be between the microstrip detector and the first fiber hodoscope.

The neutron is detected in a scintillator wall (3m downstream of the target) which measures the position of impact and time-of-flight [1]. The directions of the primary neutron and all primary charged particles in conjuction with a hypothesis on their masses are used to reconstruct the kinematics. The large background due to $pp \to np\pi^+$ is suppressed by various cuts on kinematic variables and time of flight of the primary neutron.

For the final inspection of the selected events, a 3-D display software is used. It allows to plot a 2 dimensional projection of the detector and all of its elements from any given observation point, e.g. the target position or the decay point of the Σ^+. Furthermore it is possible to plot the fitted tracks of n, K^+ and Σ^+, thus allowing to check visually the fitting algorithm to have worked properly.

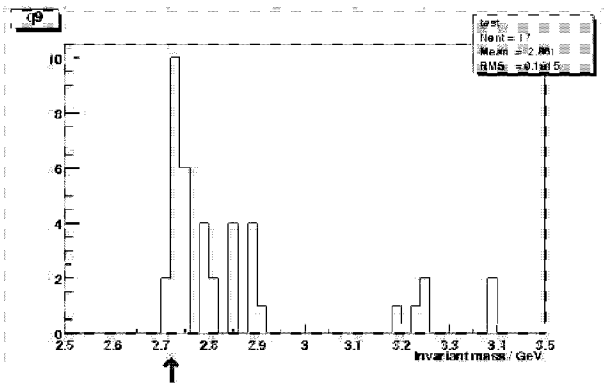

Fig. 2: Invariant mass spectrum of the $nK^+\Sigma^+$ -system

Fig. 2 shows the invariant mass plot of events which fulfill all selection criteria. A Σ^+ -signal is clearly visible at 2.718 GeV (marked with an arrow). The remaining events are due to $pp \to np\pi^+$ background which is almost completely suppressed.

References:

[1] A. Böhm, Ph.D. thesis, Dresden 1998

* supported by FZ Jülich and BMBF

** Institut für Kern- und Teilchenphysik, Technische Universität Dresden, 01062 Dresden

Status of the analysis of the $\vec{p}p \to pp\gamma$ reaction channel

A.Wilms* for the COSY-TOF Collaboration

In December 1998 COSY extracted its first polarized proton beam with a beam momentum of 798.0 MeV/c for the external TOF experiment.
The detector setup consisted of the Rossendorf start-detector MARS, the barrel, the three layer ring- and the three layer quirl-spectrometer.
The events of the three particle reactions of interest ($pp \to pp\gamma$ and $pp \to pp\pi^0$) were selected by the missing-mass method, in which the mass of the third neutral ejectile is reconstructed from the four-momenta of the charged ejectiles. Figure 1 (upper plot) shows the missing-mass distribution of the two measured three-body reactions for full-target runs (black) underlayed with the normalized background evaluated from empty-target runs (grey). The difference between full-target and empty-target events is shown in the lower plot.

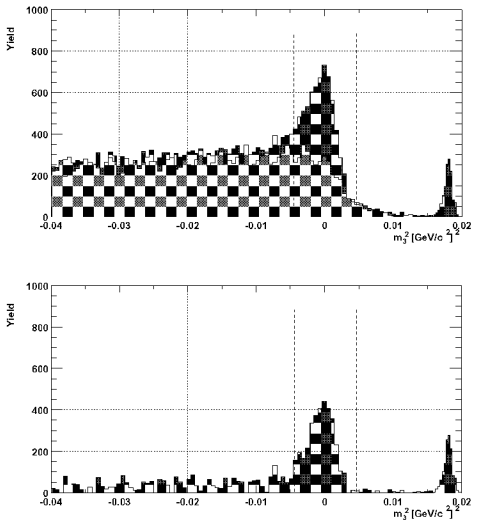

Figure 1: *Missing-mass distribution for the analyzed three particle reactions: The lower histogram shows the distribution after subtracting the normalized background shown in the picture above.*

To calculate the total cross-section of a reaction the integrated luminosity $\mathcal{L}$ has to be determined. This was done by using the counting rates N_{el} of the elastic proton scattering measured in a well-defined solid angle range $\Delta\Omega$, and the differential cross-section $\left(\frac{d\sigma}{d\Omega}\right)_{el}$ of this reaction. The value of the integrated luminosity was determined to be $\mathcal{L} = (1402 \pm 131)\,\mu b^{-1}$.
The angular distribution of the reconstructed photons and the fit using the first two even Legendrian coefficients a_0 and a_2 is shown in figure 2.
The total cross-section of the reaction $pp \to pp\gamma$ was determined to be

$$\sigma_\gamma = (4.45 \pm 0.62 \pm 0.22)\,\mu b\,. \qquad (1)$$

Taking into account the different errors this value is

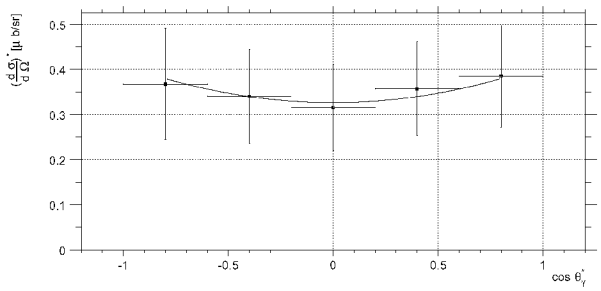

Figure 2: *Differential cross-section of the reaction $pp \to pp\gamma$ as a function of the polar angle in the CMS.*

in agreement with the total cross-section determined in [1]: $\sigma_\gamma = (3.5 \pm 0.3 \pm 0.2)\,\mu b$.
The contributions of the different partial waves found in this reaction channel can be determined by calculating the coefficients of the Legendrians. They depend on the energy of the reconstructed photons. The energy dependence of these values is shown in figure 3.

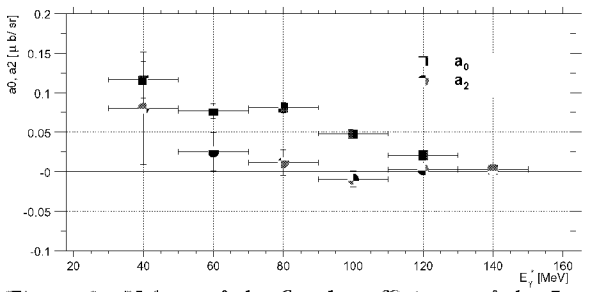

Figure 3: *Values of the fitted coefficients of the Legendrians from the analysis of the reaction $pp \to pp\gamma$ as function of the photon energy in the CMS-frame.*

The polarization of the incident proton beam was determined for every run taken during the beam time by using the "super-asymmetry" method [2] and the analyzing-power of the elastic scattering at a well-defined polar-angle of one detected proton. The analyzing-power was taken from [3]: $A_y = 0.32 \pm 0.02$.
Taking into account the varying durations of the runs the average value of the polarization was estimated to be $P_y = (36.7 \pm 0.5)$ % and will be used for the determination of the analyzing-power of the reaction $\vec{p}p \to pp\gamma$ which is still in progress.

Supported by BMBF and FZ Jülich

References

[1] Peter Herrmann Ph.D. thesis Inst. für Exp. Physik I Bochum 1997

[2] Andrea Wilms Annual Report 2000, KFA Jülich

[3] EDDA homepage: http://said-hh.desy.de

*Inst. f. Experimental Physics I, Ruhr-Universität Bochum

Studies of η Production in Proton Proton Collisions with the Time Of Flight Spectrometer

E. Roderburg for the COSY-TOF collaboration

The data of pp→ppη, which were measured in 1999 at excess energies of 15 MeV and 41 MeV, are analyzed in respect to differential observables as invariant mass and angular distributions. Both protons of the reaction are detected with the time of flight detector with nearly 100 % acceptance. The η is reconstructed with the missing mass technique. In Fig. 1 the missing mass distribution is compared with a Monte Carlo Simulation of the detector response to this reaction [1].

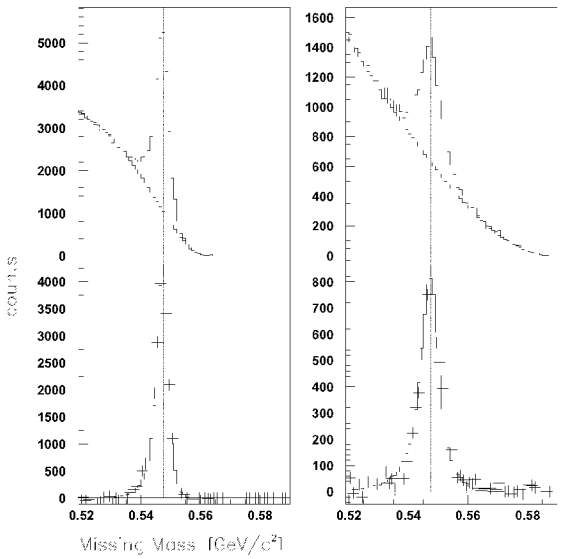

Fig. 1: The missing mass distribution at an excess energy of 15 MeV (first column) and 41 MeV (second column). Upper figure: Raw data with fitted background. Lower figure: Missing mass distribution from Monte Carlo calculations (solid line) in comparison with data after background subtraction (crosses).

The width of the η signal in the missing mass distribution, which stems from the finite detector resolution, is very well described by the monte carlo calculation. In order to enrich the η events in comparison to the background - which comes mainly from multiple pion production - a cut in the missing mass with ±0.3% of the η mass was applied.
The Dalitz plots for both excess energies of this data sample are shown in Fig. 2. Due to the proton proton final state interactions strong deviations from phase space are seen in the region of low proton - proton invariant mass. But comparing the phase space modified merely with this fsi shows that other mechanism play an important role. Under discussions are the effects of the S_{11} resonance - which pole is at the maximum of the proton-proton invariant mass of the 41 MeV excess energy - and the η-nucleon interaction.

References:

[1] E. Roderburg et al. Acta Physica Polonica **31** (2000) 2299

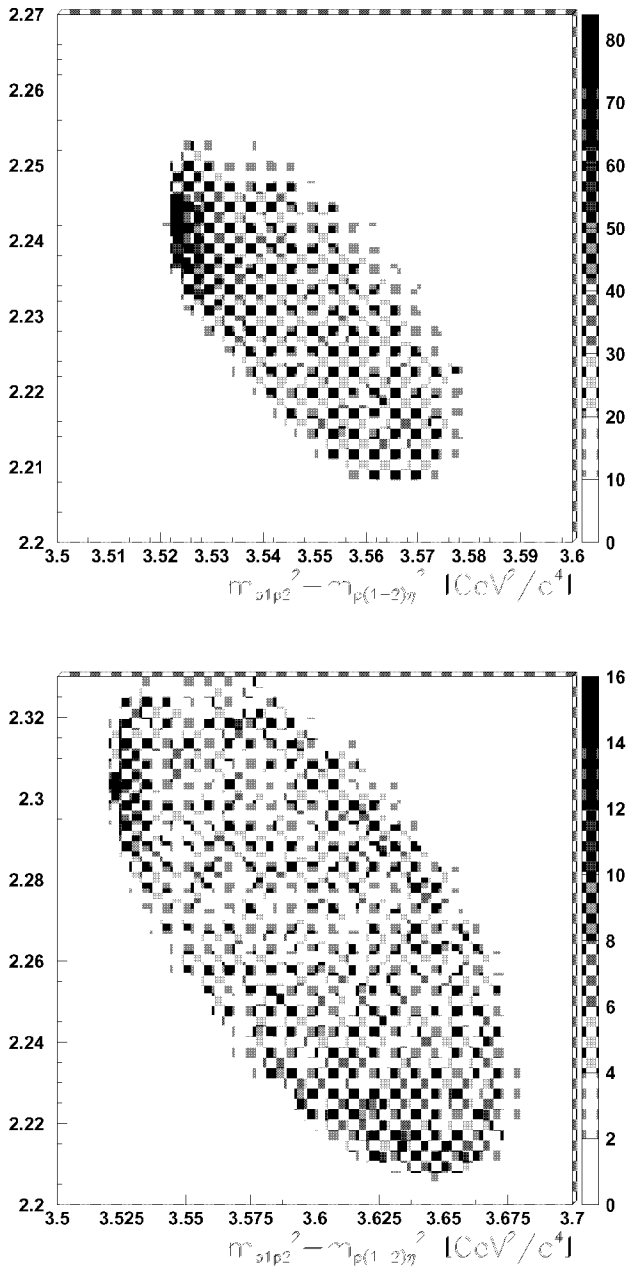

Fig. 2: The upper figure shows the dalitzplot for the excess energy of 15 MeV, the lower one the dalitzplot for the excess energy of 41 MeV. On the abscissa the squared invariant mass of the proton-proton system and on the ordinate the squared invariant mass of the proton-η system is plotted. As the protons can't be distinguished the invariant masses of proton1+η and proton2+η are filled into the histogram for each event.

Search for a quasi-bound $\eta - {}^3$He state with the COSY-TOF spectrometer

A. Gillitzer for the COSY-TOF collaboration

We plan to study the $pd \to ppp\pi^-$ reaction below the ^{3}Heη threshold with the COSY-TOF spectrometer in order to search for signatures of a quasi-bound state in the ^{3}Heη system. An experimental proposal [1] was recently presented to the COSY-PAC which granted two weeks of beamtime in 2002 (scheduled for July) for exploratory studies.

The study is motivated by the peculiar behavior of the cross section of the $pd \to {}^3$Heη reaction close to threshold. The significant enhancement of the squared amplitude $|f|^2 = \frac{p_p}{p_\eta}\left(\frac{d\sigma}{d\Omega}\right)$ towards the threshold first observed at SATURNE [2] has been interpreted as a consequence of the existence of a quasi-bound $\eta - {}^3$He state [3, 4] close to the continuum region. In order to clarify this question, experimental information complementary to studies of continuum η production, such as from a formation experiment below the ^{3}Heη threshold is required.

The in-medium decay of an η meson is distinctly different from the free η decay, and is expected to be dominated by the $\eta N \to \pi N$ channel. η absorption from the neutron results in the 4-charged particle final state $ppp\pi^-$, which has a characteristic kinematical topology: it consists of a $p\pi^-$ pair approximately back-to-back in the center of mass frame with an invariant mass close to the $N\eta$ mass, and a pp spectator pair with small relative energy nearly at rest in the *cm* frame. The TOF detector is ideally suited to study this reaction since it has both the large acceptance required for the detection of the $p\pi^-$ pair thanks to the ring and barrel detectors, and the particle identification capability for the pp spectators thanks to the new forward scintillator calorimeter. The experimental task is to measure an excitation function of the $pd \to ppp\pi^-$ reaction in an energy region from a few tens of MeV below the ^{3}Heη threshold up to a few MeV above it in sufficiently small steps. A quasi-bound state would manifest itself as a resonance-like shape of the cross section. Thus the deduced η binding energy and width is not affected by the energy resolution of the TOF spectrometer, but only by the knowledge of the absolute COSY beam energy and its energy spread at the interaction point in the target.

Binding energy B_η and width Γ_η of the quasi-bound state are closely related to the η-nucleon scattering length $a_{\eta N}$, for which theoretical literature values vary from 0.25 fm to 1.1 fm and from 0.15 fm to 0.37 fm for the real and the imaginary part, respectively. From these values a rough estimate for B_η and Γ_η is found by using the Schrödinger equation with a first-order-in-density optical potential

$$U_\eta(r) = -\frac{4\pi}{2\mu}\left(1+\frac{m_\eta}{M_N}\right) a_{\eta N}\rho(r). \qquad (1)$$

Bound states were found for $Re\, a_{\eta N}$ larger than 0.35 fm, giving confidence in their observability. The width not only depends on the imaginary part, but also strongly on the real part which determines the overlap of η and nucleon wavefunctions. For low values of $Re\, a_{\eta N}$ which are related to small binding energies and more extended η wavefunctions, the width may be only few MeV. For the larger values of $a_{\eta N}$ values of several tens of MeV for both B_η and Γ_η were obtained. The value $a_{\eta N} = 0.52 + i0.25$ fm deduced in Ref. [3] corresponds to $B_\eta \simeq 1$ MeV and $\Gamma_\eta \simeq 8$ MeV.

Detailed simulations were done for both the $pd \to {}^3\mathrm{He}_\eta \to ppp\pi^-$ reaction and for possible background reactions. The simulation includes the internal momentum distributions of nucleons in d and ^{3}He, and of the η in $^3\mathrm{He}_\eta$, where relevant, and the finite acceptance and resolution of the TOF detector. As physical background the $pd \to ppp\pi^-$ reaction was considered *(a)* according to pure phase space, *(b)* as quasi-free π^- production on the neutron with a spectator proton, and *(c)* as twostep process with rescattering of either a nucleon or the pion. As instrumental background with mis-identified or unobserved particles in the final state we simulated the reactions *(d)* $pd \to dp\pi^+\pi^-$, *(e)* $pd \to t\pi^+\pi^+\pi^-$, *(f)* quasi-free $\pi^+\pi^-$ production from the proton with an unobserved spectator neutron, and *(g)* quasi-free double pion production from the neutron with the spectator proton observed, and either the neutron or the π^0 unobserved. The results of the simulations are encouraging. The acceptance fraction for the quasi-bound $^3\mathrm{He}_\eta$ formation reaction including appropriate software cuts was obtained to be 0.35. Furtheron, the simulations demonstrate that the overlap in phase space between the $^3\mathrm{He}_\eta$ formation reaction and the considered physical background reactions is sufficiently small, and that all instrumental background reactions can be suppressed by at least four orders of magnitude.

Since so far no predictions exist for the cross section of quasi-bound $^3\mathrm{He}_\eta$ formation in $p+d$ collisions, one has to rely on simple estimates. The magnitude of the cross section for η production very close to threshold in $pd \to {}^3$He of a few hundred nb [2] suggests that the peak formation cross section should have the same order of magnitude. Independently, we can estimate the resonance cross section from the Breit-Wigner formula

$$\sigma_{BW} = \frac{(2J+1)}{(2S_1+1)(2S_2+1)}\,\frac{\pi}{k^2}\,\frac{B_{in}B_{out}\Gamma_{tot}^2}{(E-E_R)^2+\Gamma_{tot}^2/4}, \qquad (2)$$

where k is the *cm* momentum, E is the *cm* energy, and B_{in} and B_{out} are the branching ratios of the resonant state into the entrance and the exit channel, respectively. B_{out} can be easily estimated to be 2/9 from isospin coupling and n to p number ratio, whereas B_{in} can be seen as probability for the non-pionic η absorption channel $^3\mathrm{He}_\eta \to pd$. This branching ratio is not known. Assuming B_{in} to be between 10^{-3} and 10^{-2} we obtain $\sigma_{peak} = 290\,\mathrm{nb} \cdots 2.9\,\mu\mathrm{b}$. Taking into account a peak cross section $\sigma_{peak} = 500$ nb, an incident proton beam intensity $I_p = 10^7$/s, and a total detection efficiency of 0.1, we obtain a count rate of 770 events per day at the center of the resonance, which leaves room for smaller branching ratios and additional instrumental losses.

References:

[1] A. Gillitzer *et al.*, COSY proposal #102 (2001).

[2] J. Berger *et al.*, Phys. Rev. Lett. **61** (1988) 919; B. Mayer *et al.*, Phys. Rev. C **53** (1996) 2068.

[3] C. Wilkin, Phys. Rev. C **47** (1993) R938.

[4] L. Kondratyuk, A.V. Lado and Yu.N. Uzikov, Proc. Int. Conf. "Mesons and Nuclei at Intermediate Energies", Dubna, Russia, May 3-7, 1994, p. 714.

Performance of the Central Calorimeter of the COSY-TOF Detector

J. Kress, A. Erhardt, H. Clement, G. J. Wagner for the COSY-TOF collaboration
Physikalisches Institut, Universität Tübingen

The central calorimeter has been assembled and integrated into the vacuum tank of the Time-Of-Flight spectrometer directly behind the Quirl detector (Fig. 1). It consists of 84 hexagonal plastic scintillator blocks each with a width of 14 cm and a length of 45 cm. Protons are stopped therein up to kinetic energies of $T_p = 320$ MeV, the maximum energy for stopping charged pions is about $T_\pi = 160$ MeV. For first measurements with this calorimeter the short version of the TOF setup has been used as shown in Fig. 1. This way the calorimeter can cover a large solid angle with $\Delta\theta \approx 50°$.

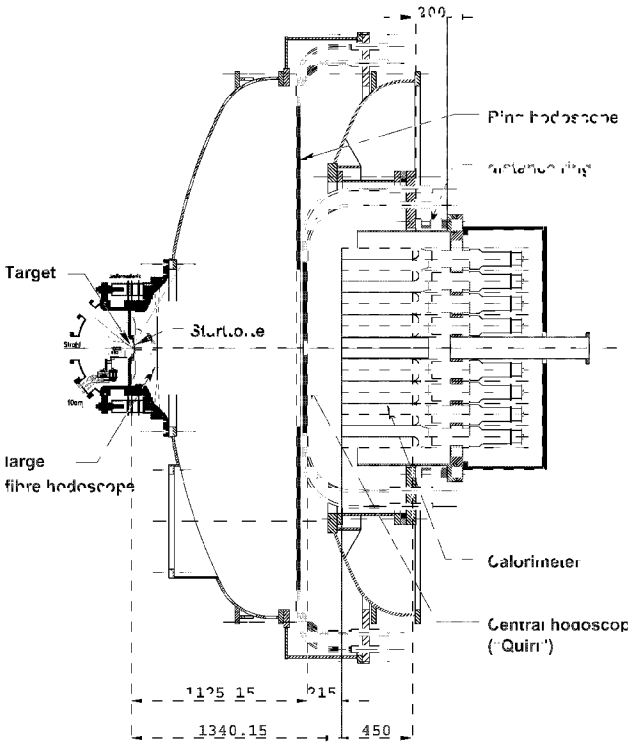

Fig. 1: Setup of the short version of the TOF spectrometer as used for the measurements in 2000 and 2001

With this setup four runs have been carried out in the years 2000 and 2001 at proton kinetic energies of $T_p = 400$ MeV, 750 MeV and 800 MeV. The first run at $T_p = 400$ MeV was for the commissiong of the calorimeter. The single pion production reactions $pp \to d\pi^+$, $pp \to pp\pi^0$ and $pp \to pn\pi^+$ are used to calibrate the calorimeter where the first order energy calibration is done with cosmics. The other runs at higher energies (two runs at 750 MeV, one at 800 MeV) have been carried out with a beam of polarized protons. They have been dedicated runs to investigate the $\pi^+\pi^-$ production in proton-proton collisions.

Fig. 2 shows a ΔE-E scatter plot for events resulting from 750 MeV protons incident on LH_2 target. Since the time-of-flight resolution is superior to the ΔE resolution of the Quirl detector, the quantity $1/\beta^2$ is plotted along the ordinate in-

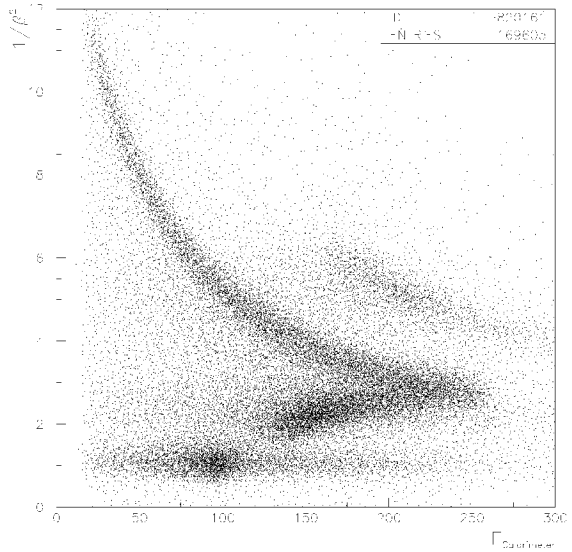

Fig. 2: ΔE-E plot for two-track events; there is also a cut for the polar angle included here with $10° < \theta < 20°$ for both tracks.

stead of ΔE. On the abscissa the energy deposited (and not yet corrected for quenching effects) in the calorimeter is plotted. Deuterons, protons and pions appear in well separated bands and can thus be easily identified. Fast protons, which are not stopped in the calorimeter lead to a back-bending of the proton band. Fast pions resulting from the $pp \to d\pi^+$ reaction have $\beta \approx 1$ and are close to minimum ionizing. They are also not stopped in the calorimeter and cause a pronounced peak at the bottom of the ΔE-E spectrum.

In the last run in September 2001 multihit-TDCs for Quirl and calorimeter could be integrated into the new Data Acquisition System. This provides the posibility to identify positive pions stopped in the calorimeter by observing the μ^+ decay following the decay of the π^+ in the calorimeter (delayed pulse technique).

Implementation of a new Data Acquisition System at COSY-TOF

Mathias Drochner[b], Arthur Erhardt[c], Thomas Sefzick[a], Peter Wuestner[b],
for the COSY-TOF collaboration

Triggered by the need to install Lecroy LRS 1877 Multihit TDCs on the TOF spectrometer's Quirl and Calorimeter subdetectors, the collaboration decided to build a new DAQ based on the EMS[1, 2] data acquisition. EMS, which has been developed at the Zentrallabor für Elektronik, is a modular, object-oriented, scalable, distributed data acquisition system. To implement EMS at the COSY TOF experiment, there were several tasks to accomplish:

- DAQ electronics had to be partially replaced and extended.
- A new central control workstation has been installed and configured accordingly.
- Several diskless single board computers running NetBSD/i386 have been installed replacing the old m68k based VME CPU's.
- New software had to be developed for beam monitoring, data conversion and analysis.

As far as VME or Fastbus controllers are concerned, the VME CPU boards have been replaced by a two-component solution: one controller board inside the VME crate or VME to Fastbus adapter, connected via glass fibre to a 32bit PCI card inside the mainboard of a diskless single board computer, thus reducing future upgrade costs from the price of a new VME CPU to the price of a new diskless single board computer (SBC). The components planned for use are VME to PCI interfaces designed by Struck Innovative Systems[3] and the Zentrallabor für Elektronik at Jülich. For the first tests and beamtimes Bit3 [4] components from COSY-11 have been used.

For CAMAC components a similar approach has been used, only that CAMAC components deliver much less data. Therefore faster controlling computers for these components are not necessary for the forseeable future.

For the central workstation replacing the old IBM RS6000/220 standard PC hardware has been selected because of price/performance ratio considerations and easy component availability. Linux as operating system has been chosen for the workstation because of source code and development tools availability.

For the SBC's controlling the crates, NetBSD/i386 has been chosen as operating system, because, for driver development the full source code availability was even more important than for the software on the control workstation, and there were already working drivers for most electronics components available that have been developed and tested at other COSY experiments.

After replacing the data-taking hard- and software, it was necessary to connect the beam monitoring software to the new DAQ. After evaluating the old beam monitoring software based on the interviews toolkit[5], the decision was taken to write new software for that task: a java applet can show the beam profile in different subdetectors in any (java-enabled) web browser, reading its scaler data from a tcp port of the control workstation. The scaler data is read from the VME controlling SBC of the scaler crate and is compiled into a simplified event format by an event deflector running on the control workstation.

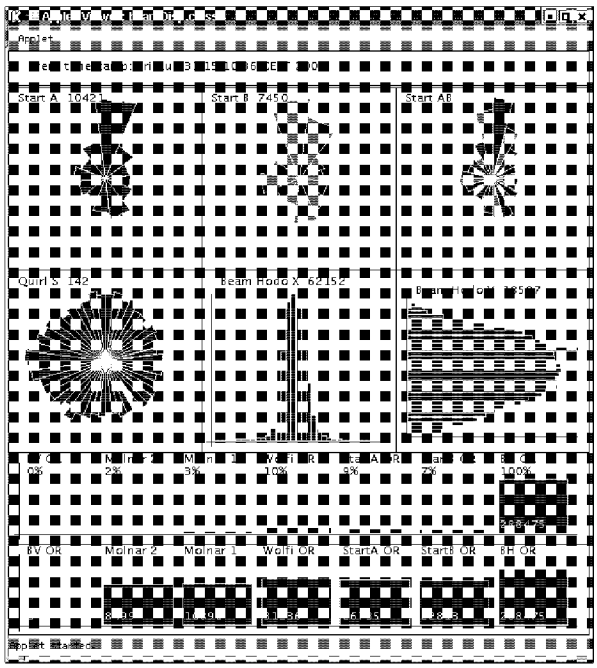

Fig. 1: Screenshot of beamDisp applet during 08/2001 beamtime.

The new DAQ has shown good performance and very high reliability in the last two COSY TOF beam times. The LRS 1877 multihit TDCs for the delayed pulse technique have been successfully included in the DAQ. Performance will further increase with the availability of the Struck VME interfaces.

References:

[1] Mathias Drochner, Aufbau eines flexiblen Datenaufnahmesystems für das GEM Experiment am Jülicher Beschleuniger COSY und Messungen der Reaktion $pp \to \pi^+ d$ nahe der Produktionsschwelle, Dissertation, TU Dresden, 1996

[2] Peter Wüstner, Die Produktion des η-Mesons am Jülicher Beschleuniger COSY und Entwicklung eines optimierten Datenaufnahmesystems, Dissertation, Universität Bochum, 1998

[3] `http://www.struck.de/`

[4] `http://www.sbs.com/computer/products/function.shtml`

[5] `http://interviews.stanford.edu/`

[a]Forschungszentrum Jülich, IKP
[b]Forschungszentrum Jülich, ZEL
[c]Physikalisches Institut, Universität Tübingen

Cryogenic Heat Pipe-Target with Aluminum condenser for the COSY - TOF Experiment

M. Abd El-Bary, S. Abd El-Samad, K. Kilian, J. Uehlemann
for the COSY – TOF collaboration

In our former cryo targets we used metal conductors (Aluminum, Copper, and Silver) between a cold head and the target region [1]. Recently, a gravity assisted 32-cm long, 1.6-cm diameter heat pipe system [2,3] has been developed, where the target liquid is used as the heat transport medium. In a first version it worked safely with a Copper condenser.

The main objects to change from metal conductor to heat pipe were to decrease the cool down time and the amount of material in the target region. The time, which is needed to liquefy a gas, depends on the mass, the heat capacity and thermal conductivity of the condenser material, the available cooling power, the thermal load and the desired final temperature. By replacing the copper condenser by aluminum we expected and achieved further improvements. Soldering the stainless steel gas tube to the aluminum condenser is difficult and was avoided by soldering the gas tube to the heat pipe tube directly.

Table (1) allows to compare the characteristics for the heat pipe with Aluminum and Copper condensers for H_2, D_2, N_2, and CH_4 as working and target medium.

Figure (1) shows in detail the time dependence of the temperatures measured at the condenser and at the evaporator (target) for LH_2 operation with Aluminum and Copper condenser.

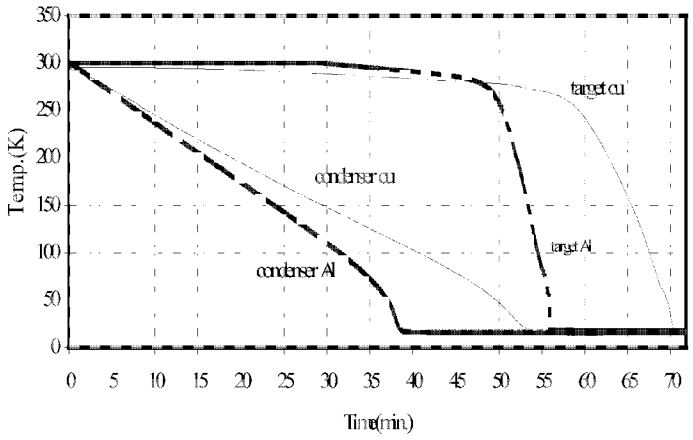

Figure 1: The time dependence of the temperatures of Cu and Al condensers and the target during cool down for LH2.

characteristics	**Aluminum condenser**	**Copper condenser**
Weight (g)	20	100
Thermal conductivity	at 15 k 35 W/cm.K	at 15 k 12 W/cm.K
Heat capacity	2.95 kJ from 295-15 K for 20 g	7.28 kJ from 295-15 K for 100 g
Condensation area	3400 mm^2	2500 mm^2
cool down to 15 k	38 min	52 min.
H_2 (15 K)	56 min.	70 min.
D_2 (18.9 K)	48 min.	62 min.
N_2 (64.5 K)	38 min.	53 min.
CH_4 (95 K)	34 min.	45 min.

Table 1: Thermal characteristics of Al and Cu condensers and times needed to get liquid in the target cell.

The conclusion is that the Al condenser has clearly better performance.

References:

[1] V. Jaeckle et al, "A liquid hydrogen / deuterium target with very thin windows", Nucl. Inst. and Methods, **A349** (1994).

[2] S. abdel-Samad et al., "New Developments in the COSY Cryogenic Target System", IKP Ann. Rep.99, FZ Juelich, 16 (1999).

[3] S. abdel-Samad et al.," Cryogenic Heat Pipe Target Cooling System for the COSY/TOF Experiment", IKP Ann. Rep.2000, FZ Juelich, 13 (2000).

Status Report of the Straw Tracking Detector for COSY–TOF

W. Erven[2], D. Filges[1], K. Kilian[1], V. Kozlov[3], I. Mohos[1], R. Nellen[1], S. Orfanitski[3], T. Sefzick[1], P. Wuestner[2], K. Zwoll[2], and P. Wintz[1] for the COSY–TOF Collaboration
[1]Institut für Kernphysik, [2]Zentralabteilung Technologie, [3]Moskow State University

A new workshop for straw tube mass production was set up and 250 straws per month were assembled including tests of gas leakage and wire tension of each single straw tube. Fig.1 shows the wire tension of 200 straws measured by the mechanical resonance frequency of the wire with alternating current inside a magnetic field. Over a pressure range from 2.3 bar (absolute) down to 1 bar (atmosphere) the wire tension showed a well–defined constant slope.

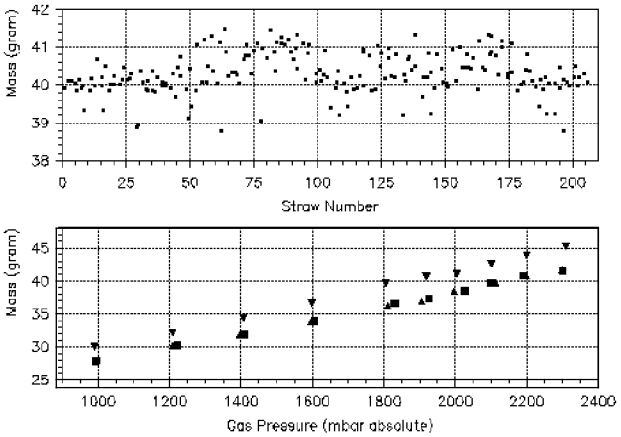

Fig. 1: Wire tension (sigma 0.5g) at 1 bar overpressure inside the tubes (top) and tension versus gas pressure (bottom) for 3 single straws.

The high–voltage operation of single straw tubes filled with an Ar/CO_2 (90/10%) gas mixture was tested. Fig.2 shows typical pre–amplified signals of an anode wire exposed to ^{55}Fe γ–radiation of 5.9keV energy.

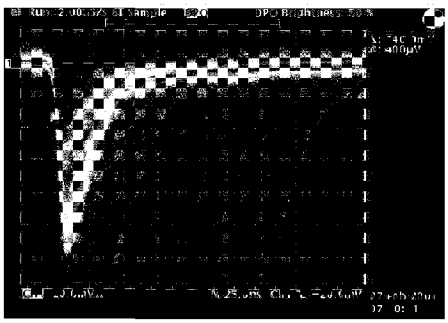

Fig. 2: Signal of a straw wire exposed to ^{55}Fe γ–radiation (oscilloscope self–triggered, infinite persistence mode, threshold at –20mV).

The 2 voltage peak heights are –120mV and –60mV corresponding to ionization energies of 5.9keV and 2.9keV the latter with roughly 10–15% probability coming from the escape of an Ar–$E_{k\alpha}$–γ. Notice the clear separation of the 2 voltage peaks indicating a nice energy resolution and excellent signal characteristics of the drift tube. The signals leading edge had a rise time below 10ns. Time spread at the threshold set was a few ns, only. A gas gain around $A=10^5$ was measured.

A first full prototype detector containing 168 straws was built (Fig.3) demonstrating the feasibility of a new ultra low–mass detector design. Although single tubes exhibit a pressure dependent twisting [1] they could be glued together in firm, self–supporting double–layer packages of 2×4 straws using a new dedicated point–gluing technique. The packages were put in a surrounding frame which only had to support the straw weight.

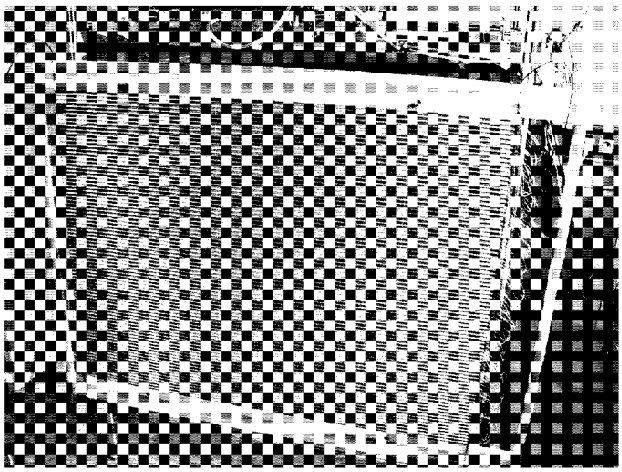

Fig. 3: First prototype detector containing a double–layer of 168 straws.

No fixing or clamping of the straw packages increasing the weight was necessary. Flexible springs were used for electric cathode contact to Cu–covered thin belts on both sides, necessary to allow a small lengthening of the straw tubes with increasing pressure inside.
New dedicated Rohacell–CF sandwich bars [2,3] for a next frame were developed with improved strength but still lower density of only 0.15 g/cm^3.
The full detector will consist of a stack of 15 frames each with a double–layer of 208 straws giving more than 3000 detector cells within an active volume of 1/3 m^3. The total weight will be less than 20kg including the front–end pre–amplifier electronic and high–voltage boards, signal and high–voltage cabling and gas distribution tubes.

References:

[1] P. Wintz et al., IKP Ann. Rep. 2000, Jül–3852, p. 12.
[2] Plexiglas Röhm GmbH&Co. KG, Germany.
[3] Sulzer–Innotec AG, Switzerland.

The TofRoot Project - Status and Perspectives

M.Schulte-Wissermann*, L.Karsch*, Ch.Plettner*, S.Dschemuchadse*, K.-Th.Brinkmann*, for the COSY-TOF-Collaboration

The COSY-TOF spectrometer is a modular detector system which, besides other merits, stands out for versatility. At present, each modification requires new calibration and the adaption of the data analysis software. This rather cumbersome and time consuming procedure will be extremely simplified by the use of the TofRoot environment [1]-[3]. When fully implemented, TofRoot will provide a professional environment for the collaboration, making available a general data format, calibration procedures, and analyzing tools. It can be easily adapted for any experimental setup and, thus, will significantly speed up data analysis.
Some properties are presented in the following.

General Routines

Using C++, the routines (algorithms) are not written 'plain text' into the code or stored in simple function collections, but are rather *incorporated into classes*. The (member) functions of the classes have defined input and output, and are easy to use by everyone without ever having to touch the code. Furthermore, these functions are checked and debugged by all users and, therefore, are much more trustworthy than code written by a single user. E.g., calibration routines were developed for almost all sub-detectors of the TOF-detector. Big effort was put into the automatic generation of control histograms to supervise the calibration process.

Track-finding algorithms

The start-detector region of COSY-TOF consists of a tracking device. Algorithms were developed to identify tracks from the hit pattern. The algorithms are based on existing functions developed within the collaboration, but they were rewritten to accommodate the needs of an object oriented approach to data analysis. A detailed documentation is provided for the users in the Internet.

Online monitoring capabilities

Recently, the Juelich EMS DAQ-system was implemented at COSY-TOF. An interface between this new system and ROOT was developed. A simple GUI was established to display control histograms. Since the speed of the online analysis is comparable with the data rate, it is planed to combine the EMS2ROOT interface and the existing TofRoot classes to allow true online control, e.g. not only monitoring of single channels (TDC, QDC), but performing online calibration and then displaying physical observables, e.g. angular distributions of pp-elastic and missing-mass-spectra. An example of what could be viewed online during future beam times is shown in Fig 1. Besides the optimization of our detector, the improved online-control will also help the COSY-team to optimize the beam for our special needs.

Team-Work capability

The TofRoot philosophy is not only to initiate team-work but to demand it. Due to the modularity of the code, tasks can simply be separated and later integrated into the whole system. Each contributor is strongly encouraged to use the existing routines and forced to obey the TofRoot rules. This

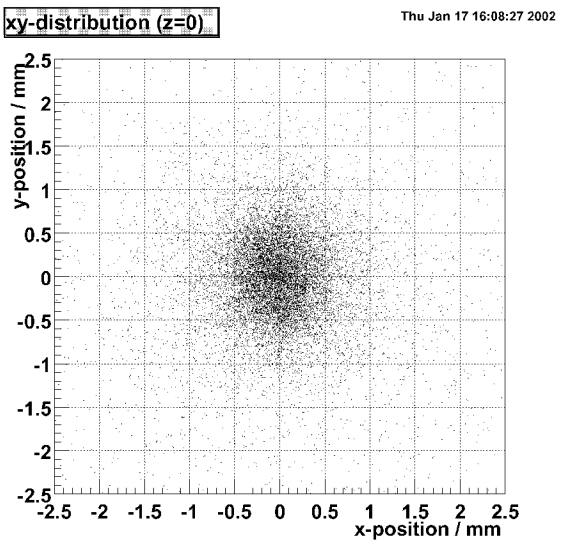

Fig. 1: *Distribution of intersection points of all reconstructed tracks with the xy-plane in the center of the target. This can be interpreted as an image of the spacial distribution of the beam. The beam spot size in this specific beam time is below* $FWHM = 1mm$.

implies intensive discussions with other users, wrapping of routines into TofRoot-Classes, and the (online) documentation. Only then it is possible to efficiently use the work of others and to integrate new members into the TofRoot team.

Online Documentation

High quality documentation is essential for effective and efficient team-work. ROOT provides the possibility to automatically create online (WWW) documentation. This holds true for classes, but also for programs and further documentation. The automatic linkage to the ROOT web site combined with the automatic linkage between the self-written classes is an extrodinary help towards efficient programming and team work.

Outlook

The TofRoot-project has successfully passed the first phase of development. In addition efforts are being made to integrate Monte Carlo simulation and online monitoring into the TofRoot framework. With this, TofRoot will be a generalized toolkit for three phases of an experiment: planing, doing and final data analysis.

References:

[1] ROOT - root.cern.ch (1995-2002)
[2] C. Plettner, annual report 2000;
[3] ROOT In Nuclear Physics - M. Schulte-Wissermann, http://www-root.fnal.gov/root2001/presentations/session2

* Institut für Kern- und Teilchenphysik, TU Dresden, 01062 Dresden, Germany
Supported by BMBF and FZ-Juelich

Simulation of neutron detector efficiencies[&]

B. Jakob[1] and B. Naumann[1] for the COSY-TOF collaboration

Different codes for the calculation of efficiency corrections for neutron detectors in the energy range up to $500\,MeV$ exist. For the neutron detector COSYnus [?] at COSY-TOF, results obtained with the three different codes Modeff [?], FLUKA [?] and LasVegas [?] were compared. All these programs have their advantages and shortcomings. Modeff is a widely used and tested code in the lower energy region ($1-20\,MeV$), but only extrapolations from the low energy regions are used to remedy the lack of experimental cross sections for neutron interactions at higher energies.

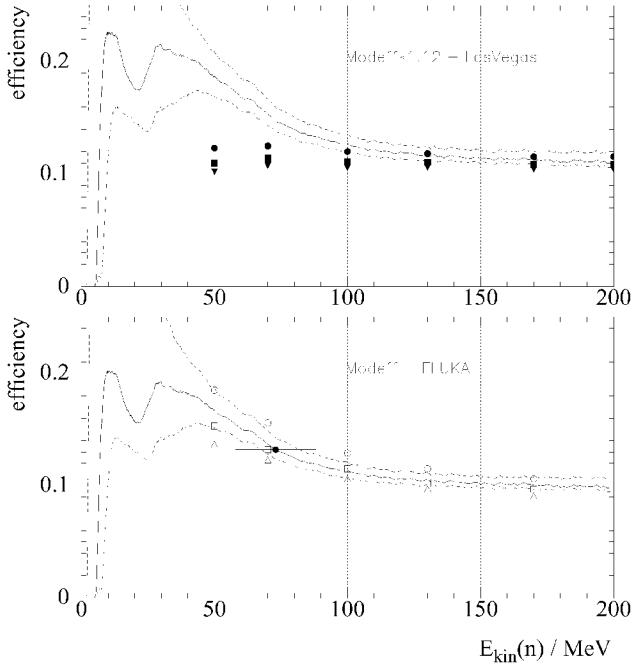

Fig. 1 *Comparison of neutron detection efficiencies obtained with Modeff (lines), LasVegas (filled symbols) and FLUKA (open symbols). The results are shown for the threshold energies $E_{th} = 2\,MeV_{pe}$ (dotted lines or circles), $E_{th} = 5\,MeV_{pe}$ (dashed or squares) and $E_{th} = 7\,MeV_{pe}$ (dash-dotted or triangles). The upper plot shows LasVegas results in comparison with Modeff simulations. The latter are scaled by a factor 1.12 [?] in this plot. In the lower frame, the good agreement between FLUKA and Modeff (not scaled in this case) is shown. The experimental value for neutrons with a kinetic energy of $(73 \pm 16)\,MeV$ was obtained by measuring all three particles of the reaction $pp \rightarrow pn\pi^+$ at a beam energy of $T = 300\,MeV$ ($E_{th} = 5\,MeV_{pe}$) [?].*

With the FLUKA code, neutron interactions in the energy range from thermal neutrons up to $E_n \approx 20\,TeV$ can be simulated, but implementing the full TOF geometry in FLUKA would be very complicated. In the LasVegas code, which is a Monte Carlo code designed for TOF, neutron interactions can only be incorporated through the use of the INC-Code of Cloth [?] which is based on the INtranuclear Cascade model of Bertini [?]. The results of the calculations are shown in Figures 1 and 2. They were obtained for three different detection thresholds requiring a light deposit of at least $E_{th} = 2,5$, and $7\,MeV_{pe}$ in the scintillator. Obviously, the LasVegas results for energies less than about $100\,MeV$ are too low, since at these energies nuclear reactions play an important role, which are not well described in cascade type models.

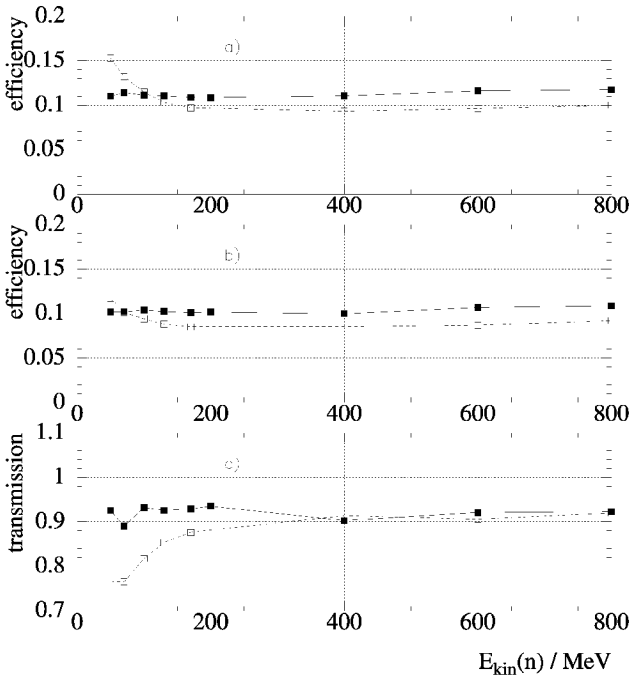

Fig. 2 *Comparison of detection efficiencies obtained with LasVegas (filled symbols) and FLUKA (open symbols) for high neutron energies using $E_{th} = 5\,MeV_{pe}$: a) without the influence of the vacuum vessel, b) with vacuum vessel (i.e. 1.5 cm Fe) and c) the transmission through the iron wall.*

Experimental data, in particular for the high energy region, are needed but are not yet available. First results obtained with COSYnus [?] show large statistical uncertainties and do not allow to distinguish between different simulations. For the time being, LasVegas can be used for simulations of the TOF detector but a systematic uncertainty of 10% for the neutron efficiency should be taken into account in absolute normalizations. For a more detailed discussion see also [?].

References:

[1] A. Böhm, Dissertation, Dresden 1998
[2] R. A. Cecil et al., Nucl. Instr. and Methods, 161:439-447, 1979
[3] A. Fasso et al., Proc. of the III Spec. Meeting on Shielding Aspects, Sendai (1997)61-74.
[4] U. Zielinski, Dissertation, Bochum 1998
[5] P. Cloth, Programm INC77, Version 1.0, FZ Jülich 1992
[6] H. W. Bertini, Phys. Rev., 131:1801-1821, 1963 and Phys. Rev., 188:1711-1730, 1969
[7] L. Karsch et al., Nucl. Instr. and Methods, A460:362-367, 2001
[8] B. Jakob, Dissertation, Dresden 2001
[9] K. Knoche, Dissertation, Hamburg 1994

[1]Institut für Kern- und Teilchenphysik, TU Dresden
[&]supported by FZ Jülich and BMBF

Search for a quasi-bound $\eta-{}^3$He state with the COSY-TOF spectrometer

A. Gillitzer for the COSY-TOF collaboration

We plan to study the $pd \to ppp\pi^-$ reaction below the ^{3}Heη threshold with the COSY-TOF spectrometer in order to search for signatures of a quasi-bound state in the ^{3}Heη system. An experimental proposal [1] was recently presented to the COSY-PAC which granted two weeks of beamtime in 2002 (scheduled for July) for exploratory studies.

The study is motivated by the peculiar behavior of the cross section of the $pd \to {}^3$Heη reaction close to threshold. The significant enhancement of the squared amplitude $|f|^2 = \frac{p_p}{p_\eta}\left(\frac{d\sigma}{d\Omega}\right)$ towards the threshold first observed at SATURNE [2] has been interpreted as a consequence of the existence of a quasi-bound $\eta-{}^3$He state [3, 4] close to the continuum region. In order to clarify this question, experimental information complementary to studies of continuum η production, such as from a formation experiment below the ^{3}Heη threshold is required.

The in-medium decay of an η meson is distinctly different from the free η decay, and is expected to be dominated by the $\eta N \to \pi N$ channel. η absorption from the neutron results in the 4-charged particle final state $ppp\pi^-$, which has a characteristic kinematical topology: it consists of a $p\pi^-$ pair approximately back-to-back in the center of mass frame with an invariant mass close to the $N\eta$ mass, and a pp spectator pair with small relative energy nearly at rest in the *cm* frame. The TOF detector is ideally suited to study this reaction since it has both the large acceptance required for the detection of the $p\pi^-$ pair thanks to the ring and barrel detectors, and the particle identification capability for the pp spectators thanks to the new forward scintillator calorimeter. The experimental task is to measure an excitation function of the $pd \to ppp\pi^-$ reaction in an energy region from a few tens of MeV below the ^{3}Heη threshold up to a few MeV above it in sufficiently small steps. A quasi-bound state would manifest itself as a resonance-like shape of the cross section. Thus the deduced η binding energy and width is not affected by the energy resolution of the TOF spectrometer, but only by the knowledge of the absolute COSY beam energy and its energy spread at the interaction point in the target.

Binding energy B_η and width Γ_η of the quasi-bound state are closely related to the η-nucleon scattering length $a_{\eta N}$, for which theoretical literature values vary from 0.25 fm to 1.1 fm and from 0.15 fm to 0.37 fm for the real and the imaginary part, respectively. ¿From these values a rough estimate for B_η and Γ_η is found by using the Schrödinger equation with a first-order-in-density optical potential

$$U_\eta(r) = -\frac{4\pi}{2\mu}\left(1+\frac{m_\eta}{M_N}\right) a_{\eta N}\rho(r). \qquad (1)$$

Bound states were found for $Re\ a_{\eta N}$ larger than 0.35 fm, giving confidence in their observability. The width not only depends on the imaginary part, but also strongly on the real part which determines the overlap of η and nucleon wavefunctions. For low values of $Re\ a_{\eta N}$ which are related to small binding energies and more extended η wavefunctions, the width may be only few MeV. For the larger values of $a_{\eta N}$ values of several tens of MeV for both B_η and Γ_η were obtained. The value $a_{\eta N} = 0.52 + i0.25$ fm deduced in Ref. [3] corresponds to $B_\eta \simeq 1$ MeV and $\Gamma_\eta \simeq 8$ MeV.

Detailed simulations were done for both the $pd \to {}^3\mathrm{He}_\eta \to ppp\pi^-$ reaction and for possible background reactions. The simulation includes the internal momentum distributions of nucleons in d and ^{3}He, and of the η in ${}^3\mathrm{He}_\eta$, where relevant, and the finite acceptance and resolution of the TOF detector. As physical background the $pd \to ppp\pi^-$ reaction was considered *(a)* according to pure phase space, *(b)* as quasi-free π^- production on the neutron with a spectator proton, and *(c)* as twostep process with rescattering of either a nucleon or the pion. As instrumental background with mis-identified or unobserved particles in the final state we simulated the reactions *(d)* $pd \to dp\pi^+\pi^-$, *(e)* $pd \to t\pi^+\pi^+\pi^-$, *(f)* quasi-free $\pi^+\pi^-$ production from the proton with an unobserved spectator neutron, and *(g)* quasi-free double pion production from the neutron with the spectator proton observed, and either the neutron or the π^0 unobserved. The results of the simulations are encouraging. The acceptance fraction for the quasi-bound ${}^3\mathrm{He}_\eta$ formation reaction including appropriate software cuts was obtained to be 0.35. Furtheron, the simulations demonstrate that the overlap in phase space between the ${}^3\mathrm{He}_\eta$ formation reaction and the considered physical background reactions is sufficiently small, and that all instrumental background reactions can be suppressed by at least four orders of magnitude.

Since so far no predictions exist for the cross section of quasi-bound ${}^3\mathrm{He}_\eta$ formation in $p+d$ collisions, one has to rely on simple estimates. The magnitude of the cross section for η production very close to threshold in $pd \to {}^3$He of a few hundred nb [2] suggests that the peak formation cross section should have the same order of magnitude. Independently, we can estimate the resonance cross section from the Breit-Wigner formula

$$\sigma_{BW} = \frac{(2J+1)}{(2S_1+1)(2S_2+1)}\,\frac{\pi}{k^2}\,\frac{B_{in}B_{out}\Gamma_{tot}^2}{(E-E_R)^2+\Gamma_{tot}^2/4}, \qquad (2)$$

where k is the *cm* momentum, E is the *cm* energy, and B_{in} and B_{out} are the branching ratios of the resonant state into the entrance and the exit channel, respectively. B_{out} can be easily estimated to be 2/9 from isospin coupling and n to p number ratio, whereas B_{in} can be seen as probability for the non-pionic η absorption channel ${}^3\mathrm{He}_\eta \to pd$. This branching ratio is not known. Assuming B_{in} to be between 10^{-3} and 10^{-2} we obtain $\sigma_{peak} = 290\,\mathrm{nb} \cdots 2.9\,\mu\mathrm{b}$. Taking into account a peak cross section $\sigma_{peak} = 500\,\mathrm{nb}$, an incident proton beam intensity $I_p = 10^7$ /s, and a total detection efficiency of 0.1, we obtain a count rate of 770 events per day at the center of the resonance, which leaves room for smaller branching ratios and additional instrumental losses.

References:

[1] A. Gillitzer *et al.*, COSY proposal #102 (2001).

[2] J. Berger *et al.*, Phys. Rev. Lett. **61** (1988) 919; B. Mayer *et al.*, Phys. Rev. C **53** (1996) 2068.

[3] C. Wilkin, Phys. Rev. C **47** (1993) R938.

[4] L. Kondratyuk, A.V. Lado and Yu.N. Uzikov, Proc. Int. Conf. "Mesons and Nuclei at Intermediate Energies", Dubna, Russia, May 3-7, 1994, p. 714.

Two - Kaon Production at the ϕ – Threshold with MOMO

F. Bellemann[1], J. Bisplinghoff[1], G .Bohlscheid[1], J. Ernst[1], F. Hinterberger[1], R. Ibald[1], R. Jahn[1], L. Jarczyk[2], R. Joosten[1], A. Kozela[3], H. Machner, A. Magiera[2], R. Maschuw[1], T. Mayer-Kuckuk[1], G. Mertler[1], J.Munkel[1], D. Rosendaal[1], P. v. Rossen, H. Schnitker[1], J. Smyrski[2], A. Strzalkowski[2], R. Tölle, and C. Wilkin[4]

The MOMO experiment focuses on near threshold meson production via the reactions pd $\rightarrow$ ^{3}He $\pi^+\pi^-$ and pd $\rightarrow$ ^{3}He K^+ K. The setup consists of a high granularity scintillating fibers meson detector near the target with a ± 45 deg. opening angle, and the spectrometer Big Karl, which is used for ^{3}He-identification. The large solid angle and high resolution of this detection method will yield precision data on the low energy (T<80 MeV) meson-meson interaction and probe into questions like meson-nucleon resonances and KK-molecule.

After completion of the two pion program, the MOMO - collaboration measured two kaon production at beam momenta of 2.620 GeV/c, 2585 GeV/c and 2574 GeV/c (corresponding to c.m. energies above production threshold of Q = 56 MeV, 40 MeV and 35 MeV, respectively). The beam intensity was about 5 x 10^8/s and the beam halo was negligible (< 10^{-4}). At all energies the reaction pd $\rightarrow$ ^{3}He K^+ K^- was measured at four largely overlapping Big Karl momentum settings, so that the full phase space of the reaction was obtained. The ^{3}He - particles could be unambiguously identified by time of flight and energy loss measurements. The two - kaon hits on the vertex wall were uniquely identified by their hit patterns and energy loss. Good events must be coplanar in respect to the total meson momentum axis, which is defined by the beam and the ^{3}He momenta. The newly implemented 16 – fold circular scintillator hodoscope behind the vertex detector enables good kaon identification and pion separation. In total, some 6000 two kaon events were observed.

Fig.1 shows the obtained two kaon invariant mass spectra. The clear signal of the ϕ – meson is evident. In all figures, the dashed lines correspond to phase space. In contrast to our two pion data, no significant deviation from phase space (plus ϕ – production) can be observed. The obtained total cross sections are:

Q_{KK} = 56 MeV : 17.5 ± 1.8 nb
Q_{KK} = 40 MeV : 9.6 ± 1.0 nb
Q_{KK} = 35 MeV : 7.5 ± 1.0 nb

Q_ϕ = 24 MeV : 1.4 ± 0.6 nb
Q_ϕ = 8 MeV : 0.9 ± 0.2 nb
Q_ϕ = 2.8 MeV : 0.7 ± 0.2 nb

The Q – dependence of these cross sections scales well with the assumption of s – wave two kaon ($\sigma \sim Q^2$) and ϕ ($\sigma \sim \Theta^{1/2}$) production. It is interesting to note, that no indication of p – waves is present in the mass spectra and angular distributions, in contrast to our two pion data, where a p – wave dominance was observed

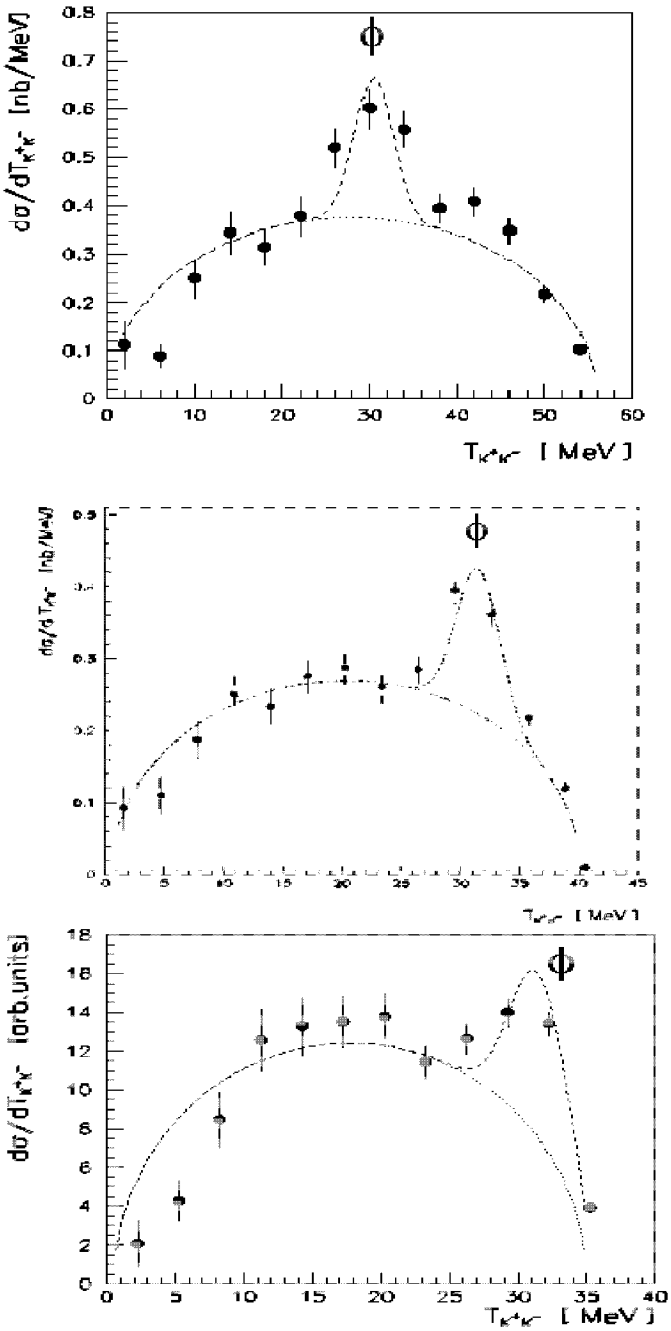

Fig. 1: K^+ K^- invariant mass spectra from the reaction pd $\rightarrow$ ^{3}He K^+ K^- at 56 MeV,40 MeV and 35 MeV above threshold plotted in units of K^+ K^- relative energy.

[1] Institut für Strahlen- und Kernphysik, Universität Bonn
[2] Institute of Physics, Jagellonian University, Cracow, Poland
[3] Institute of Nuclear Physics, Cracow, Poland
[4] Physics & Astronomy Department, University College London

Status Report ANKE*

M. Büscher for the ANKE collaboration

The measurements of inclusive K^+ production in pA collisions under forward angles were completed during beam times in Oct. and Dec. '01. Data for beam energies $T = 1.0, 1.2, 1.5, 1.75, 2.0, 2.3$ GeV and C, Cu, Ag and Au targets are now available [1, 2]. Even at the lowest beam energy, far below the free nucleon-nucleon threshold at T_{NN}=1.58 GeV where the signal-to-background ratio is $\sim 10^{-6}$, double-differential cross sections $\mathrm{d}^2\sigma/\mathrm{d}\Omega\mathrm{d}p$ covering the full momentum range of the produced kaons could be extracted from the data, see Fig. 1. The spectra reveal a high degree of collectivity

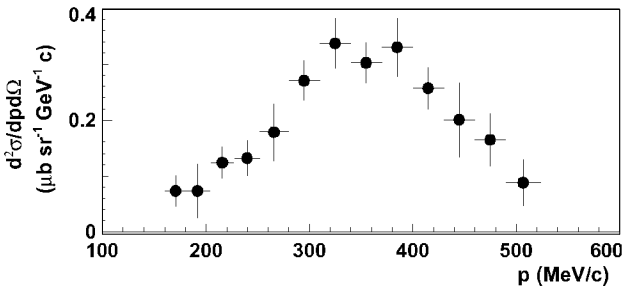

Fig. 1: Double differential cross section for the production of K^+ mesons in $p^{12}C$ reactions under forward angles $\vartheta \leq 12^\circ$ at $T = 1.0$ GeV [3].

in the target nucleus, e.g., a simple kinematical analysis shows that 6 target nucleons (at rest) are needed to produce kaons with the highest observed momenta [3]. The low-momentum parts of the spectra at high energies are strongly sensitive to Coulomb effects and the repulsive nuclear K^+-potential. As a next step the measurement of correlated K^+p and K^+d events is foreseen. The feasibility of such studies has already been shown during the beam time in Oct. '01.

Scalar-meson studies have begun in a two-weeks beam time (Jan./Feb.) during which $p(2.65\ \mathrm{GeV})p \rightarrow dK^+\overline{K}^0$ and $\rightarrow d\pi^+\eta$ reactions where measured [4]. The data allow to determine the production cross section for the $a_0^+(980)$-resonance for the two main a_0^+ decay channels ($K\bar{K}$ and $\pi\eta$) and, thus, will supply novel information about the structure of light scalar resonances [5]. During this beam time the Münster cluster-jet target was used and high luminosities of $\sim 3 \cdot 10^{31}\ \mathrm{cm}^{-2}\mathrm{s}^{-1}$ could be achieved. The experiments will be continued in spring 2002 with measurements at energies up to 2.8 GeV.

The investigation of the deuteron-breakup process $pd \rightarrow (pp)_S\, n$ with emission of a fast forward S-wave proton pair has begun [6]. The first measurements in Feb. '01 showed that such processes can be investigated at ANKE and that novel information about short-range effects in the deuteron breakup can be expected. In Sept. '01 the first ANKE beam time with polarized beam took place, aiming at the measurements of the vector analyzing power of the deuteron-breakup process.

Data on the production of ω mesons in pn collisions were taken in Aug. '01. The measurement was performed with a deuterium cluster-jet target and target-near semiconductor counters [7] for spectator-proton detection. The data are currently being analyzed [8].

Data from previous beam times on the reactions $p(492\ \mathrm{MeV})p \rightarrow d\pi^+/pn\pi^+$ show that for small relative energies of the pn pair the spin-singlet contribution to the cross section is at most a few percent [9].

Two new targets are currently in preparation for ANKE: The *polarized target (ABS)* [10], to be operated with a storage-cell which will allow to use polarized hydrogen and deuterium as target material and, thus, make possible double polarization measurements. The *pellet target* for high luminosity studies which, during test runs in 2001, produced droplets of liquid hydrogen [11].

The experimental program with ANKE in 2002 will focus on the following measurements: • ϕ-meson production in pp collisions [12]. For these measurements a new detection system for K^- mesons will be installed at ANKE. • $\pi^0\eta$-production in pn interactions [13]. Further measurements under preparation are: • Investigation of neutral scalar mesons a_0/f_0 [14]; • Measurement of η-meson production in $dd \rightarrow \alpha\eta$ reactions close to threshold [15]; • Investigation of spin effects in the charge-exchange deuteron-breakup reaction $dp \rightarrow (pp)n$ [16].

During the year 2002 a new scattering chamber, developed at the ZAT of the FZJ, will be installed in the target area of ANKE. This large chamber will, e.g., be used for storage-cell tests. Further technical developments comprise: • New target-near position sensitive Si(Li) counters [7]. First test with such counters have already been performed in 2001. • The ANKE photon detector [17] made of $PbWO_4$ crystals. First tests of prototype arrays will be performed at MAMI and ANKE. • New readout electronics for the ANKE MWPCs (ZEL, FZJ).

References:

[1] M. Nekipelov et al., contr. to this report
[2] Proc. Workshop on Strangeness Production in pp and pA Interactions at ANKE, Berichte des FZ-Jülich Jül-3922, ISSN 0944-2952, Editors M.Büscher, V.Kleber, P.Kulessa and M.Nekipelov
[3] V. Koptev et al., Phys. Rev. Lett. **87**, 022301 (2001)
[4] V. Kleber et al., contr. to this report
[5] V. Bratkovskaya et al., contr. to this report
[6] S. Dymov et al., contr. to this report
[7] A. Mussgiller et al., contr. to this report
[8] S. Barsov et al., contr. to this report
[9] V.Abaev et al., Phys. Lett. B **521**, 158 (2001); V. Abaev et al., contr. to this report
[10] M. Mikirtychiants et al., contr. to this report
[11] M. Büscher et al., contr. to this report
[12] M. Hartmann et al., contr. to this report
[13] A. Khoukaz et al., COSY proposal #94 (2000)
[14] M. Büscher et al., COSY proposal #97 (2001)
[15] A. Wrońzka et al., contr. to this report
[16] V. Glagolev et al., contr. to this report
[17] V. Hejny et al., contr. to this report

*Work partially supported by BMBF, DFG, INTAS, ISTC and RFFI

Effects of Coulomb and kaon nuclear potentials on soft K^+ production from nuclei.

M.Nekipelov, V.Koptev, M.Büscher, W.Cassing, Z.Rudy, K.Sistemich, H.Ströher, C.Wilkin

K^+-meson production in pA collisions is of utmost importance to learn about either cooperative nuclear phenomena or high momentum components of the nuclear many-body wave function. If the incident beam energies are far below the free nucleon-nucleon threshold, kaons are produced with rather low momentum ($< 600\,\mathrm{MeV/c}$). Therefore, for a large part of the kaon momentum spectra consideration of the in-medium Coulomb and kaon potentials becomes essential. The importance of taking into account these potentials for pion and kaon production in pA interactions has been discussed by several groups [1, 2, 3]. Since most of the measurements resulted in high pion and kaon momenta, the experimental data are not very informative from the point of view of both Coulomb and kaon potentials. This has changed with ANKE, which is currently the only spectrometer which is able to measure kaons with momenta down to $150\,\mathrm{MeV/c}$. Classically, if a particle with mass m is produced at the edge of a nucleus of radius R, then as it escapes to infinity it must aquire the energy $T = V$ due to the repulsive potential V, so that it must have a minimum momentum of $p_{min} = \sqrt{2mV}$. In the absence of any nuclear kaon potentials, this momentum is fixed by the Coulomb energy and yields $p_{min} \approx 130\,\mathrm{MeV/c}$ for a gold target. The momentum shift for a carbon target is ≈ 3 times smaller. This effect should be observed in the heavy-to-light cross-section ratios as a steep rise starting at the p_{min} of the heavy target.

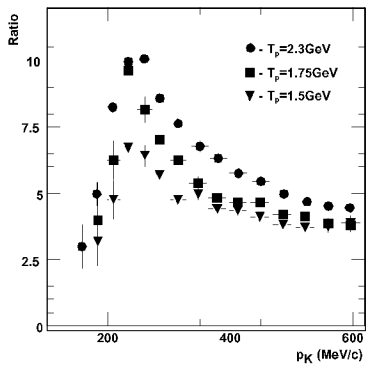

Fig. 1: Ratios of K^+ production cross sections for Au and C measured at different energies as a function of kaon momentum.

Ratios of kaon-production cross sections measured at different energies and with several target nuclei are presented in Fig. 1,2,3. All ratios exhibit similar shapes, rising with decreasing kaon momenta, passing a maximum and falling down at low momenta. The position of the maximum is practically independent of the incident proton beam energy (Fig. 1), but varies with the mass of the target nucleus, giving 245, 230, 205 MeV/c for Au/C, Ag/C and Cu/C, respectively (see Fig. 2).

The ratios for Au/C are compared to calculations made within the framework of the CBUU transport model, taking into account different mechanisms of the kaon production, rescattering effects and realistic density distributions (Fig. 3). Without including the Coulomb and kaon potentials (shaded area in Fig. 3) the ratio should exhibit a smooth momentum

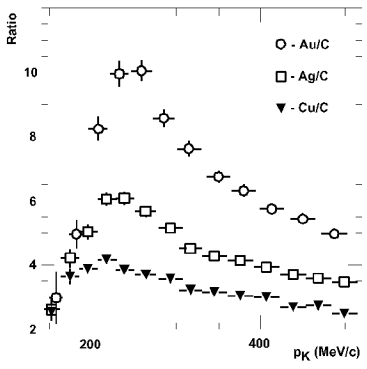

Fig. 2: Ratios of the K^+ production cross sections for the different targets (measured at $T_p = 2.3\,\mathrm{GeV}$) as a function of kaon momentum.

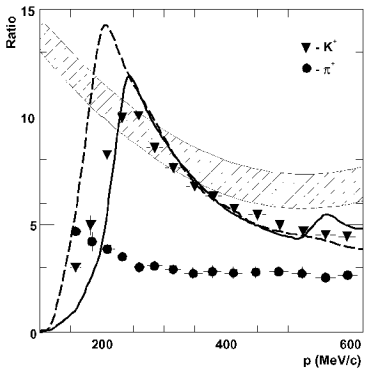

Fig. 3: Ratios of π^+ and K^+ production cross sections for Au/C at $T_p = 2.3\,\mathrm{GeV}$ as a function of meson momentum. The dashed line is obtained from CBUU calculations with Coulomb and baryon potentials included, the solid line shows the result with the kaon potential included in addition, while the shaded area corresponds to calculations without Coulomb and kaon potentials (width shows statistical theoretical uncertainty).

dependence with a steady increase towards low momenta, resulting from the stronger rescattering processes for heavy nuclei. This phenomenon is observed in pion production, where the influence of the Coulomb potential is expected to show up below $p_\pi \approx 80\,\mathrm{MeV/c}$. For kaons the Coulomb interaction leads to a distortion of the momentum spectrum and provides a maximum at $p \approx 200\,\mathrm{MeV/c}$ for Au/C, which is still lower than the experimental data. Finally, when the repulsive kaon potential of 20 MeV is also considered in the calculations, a reasonable agreement with the experiment is achieved (solid curve in Fig. 3). We expect that further analysis of the experimental data and more detailed comparison with CBUU calculations will permit us to measure the strength of the kaon potential more accurately.

References:

[1] J.F.Crawford et al., Phys.Rev.C 22, 1184(1980).
[2] A.Sibirtsev, W.Cassing, Nucl.Phys.A 641, 476(1998).
[3] S.Teis et al., Z.Phys.A 359, 297(1997).

Phenomenological Analysis of K^+-Meson Production in Proton-Nucleus Collisions*

M. Büscher, B.L. Ioffe[a], L. Kondratyuk[a], V. Koptev[b], M. Nekipelov, A. Sibirtsev, J. Speth, H. Ströher

In a recent publication [1] we analyzed whether the differential cross sections of K^+-meson production in pA collisions, see Table 1, can be described as a function of (few) simple kinematical variables. It was shown

Table 1: Data on K^+-production in pA collisions at various beam energies T_p, kaon momenta p_K and emission angles θ_K obtained by several groups.

T_p (GeV)	p_K (GeV/c)	θ_K (°)	Meas. at
0.842–0.99	*total cross sections*		PNPI [2]
2.1	0.35–0.75	15–80	LBL [3]
1.2, 1.5, 2.5	0.5–0.7	40	SATURNE [4]
1.2	0.165–0.255	90	CELSIUS [5]
1.7–2.91	1.28	10.5	ITEP [6]
2.9	0.545	17	ITEP [7]
1.0	0.171–0.507	≤ 12	ANKE [8]
2.5, 3.5	0.3–1.05	40	KAOS, [9]
1.2, 2.0, 2.3	0.171–0.507	≤ 12	ANKE, *prelim.*

that the spectra follow an exponential scaling behaviour when plotted as a function of the four-momentum transfer t, which is illustrated in Fig.1. Apart from the data

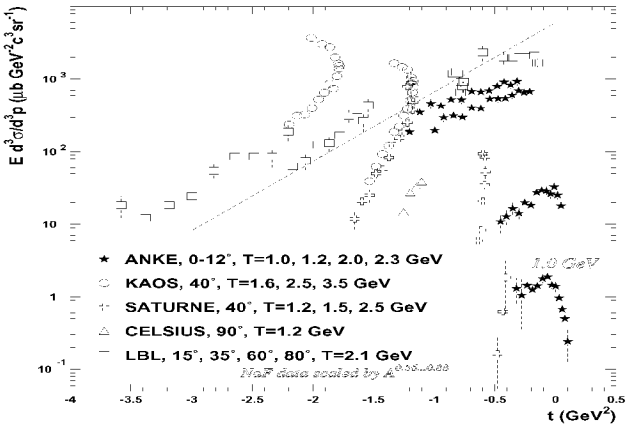

Fig. 1: Invariant $p^{12}C \to K^+X$ cross sections for as a function of the four-momentum transfer t between the beam proton and the outgoing kaon. The data from LBL [3], measured with a NaF target, were scaled according to Ref.[1].

taken with ANKE at T=1.0 GeV all spectra cover the range of negative t. The sharp fall-off of the cross sections from ANKE towards positive values of t was explained [1] by the fact that the data were taken very close to the kinematical limit for hyper-nucleus formation at t=0.145 GeV^2 which is usually accompanied by very small cross sections. For t<0 the different data sets show exponential dependences like

$$E\frac{d^3\sigma}{d^3p} = c_0 \exp\left[b_0 t\right], \qquad (1)$$

with parameters c_0 and b_0 given in Ref.[1]. It has been speculated [1] that deviations from the exponential behaviour (see, e.g., the data from KAOS and SATURNE [4] in Fig.1) reflect a dependence on the kaon-emission angles or, equivalently, the excitation energy of the target nucleus, Δm=$m_X - m_A$ (m_X (m_A) being the mass of the target nucleus before (after) the reaction process) and the available c.m. energy s. Based on Regge phenomenology the following formula has been suggested:

$$E\frac{d^3\sigma}{d^3p} \propto f(t, m_X^2) \exp\left[b_0 t \cdot \ln\left(s/s_0\right)\right] . \qquad (2)$$

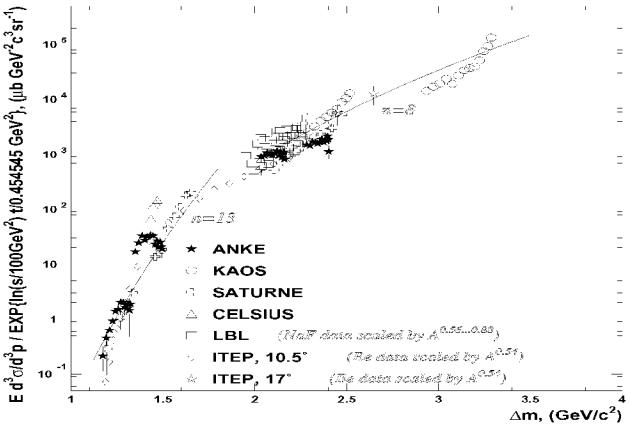

Fig. 2: Invariant $p^{12}C \to K^+X$ cross sections as a function of the excitation energy Δm of the target nucleus. The data from LBL [3] (ITEP [6, 7]) were measured with NaF (Be) targets and were scaled according to Ref.[1].

Figure 2 shows the invariant cross sections devided by an average t dependence using b_0 = 2.2 GeV^{-2} (indicated by the dashed line in Fig.1) and s_0 = 100 GeV^2. It can be seen that all data follow the same dependence on the excitation energy m_X as indicated by the lines in Fig.2 corresponding to phase space behaviour $\sigma \propto (m_X)^{(3n/2-5/2)}$ with n particles in the exit channel. Thus we suggest the following parametrization of the K^+-production cross sections in $p^{12}C$ interactions:

$$E\frac{d^3\sigma}{d^3p} = \sigma_0 \cdot m_X^{N_0} \cdot \exp\left[b_0 t \cdot \ln\left(s/s_0\right)\right] , \qquad (3)$$

with N_0=17, σ_0=25 nb GeV^{-3}c^{3}sr^{-1} below the free nucleon-nucleon threshold (T_{NN}=1.58 GeV) and N_0=9.5, σ_0=1 μb GeV^{-3}c^{3}sr^{-1} above threshold.

References:

[1] M.Büscher et al., Phys. Rev. C **65**, 014603 (2002)
[2] N.K. Abrosimov et al., JETP **67**, 2177 (1988)
[3] S.Schnetzer et al., Phys. Rev. C **40**, 640 (1989)
[4] M.Debowski et al., Z. Phys. A **356**, 313 (1996)
[5] A.Badalà et al., Phys. Rev. Lett. **80**, 4863 (1998)
[6] A.V.Akindinov et al., JETP Lett. **72**, 100 (2000)
[7] M.Büscher et al., Z. Phys. A **335**, 93 (1996)
[8] V.Koptev et al., Phys. Rev. Lett. **87**, 022301 (2001)
[9] W.Scheinast et al., Ann. Rep. 2000 FZR-319, 47 (2001)

[a] ITEP, Moscow, Russia
[b] PNPI, Gatchina, Russia

*Supported by: A.v.Humboldt foundation, BMBF, DFG, RFFI and RMS

Investigation of the $a_0^+(980)$ Resonance at ANKE

V. Kleber, M. Büscher, P. Fedorets, V. Koptev, M. Nekipelov

In a recent ANKE beam time (Jan./Febr. 2001) a first experiment on the production of scalar mesons in pp collisions was performed. The goal of this experiment is to investigate the charged $a_0(980)$ resonance, a candidate for the scalar meson nonet, in the reaction $pp \to da_0^+$.

The $a_0(980)$ is known to decay in $K\overline{K}$, $\pi\eta$ and 2γ [1]. At ANKE the deuteron in coincidence with the decay K^+ or π^+ can be detected. Kaons and pions are identified by the side detection system (SD) [2] via their TOF and energy loss. The TOF between the start and stop counters is shown in Fig. 1, left side. The fast pions cause the left peak, protons the right. To select pions it is sufficient to cut on their TOF. Cutting on energy loss in the ΔE counter reveals a kaon peak on a background distribution between the pion and proton peaks (small inset). This background is almost completely suppressed by requiring a coincident deuteron in the forward detection system (FD). Deuterons are distinguished from other fast particles by their TOF relative to a pion or kaon in the SD. The TOF of forward particles relative to pions detected in the sidewall counters is shown in figure 1, right side. Two bands from protons and deuterons are seen. Cutting along the deuteron band allows to investigate the a_0^+ with a missing mass analysis.

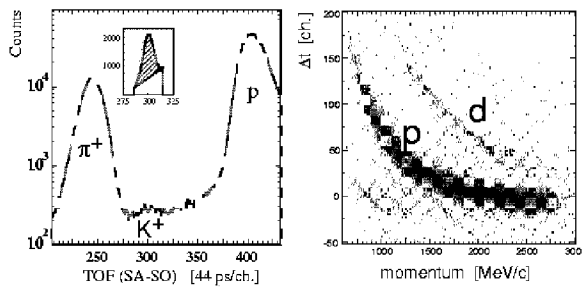

Fig. 1: Identification of particles in the SD and FD of ANKE.

If a deuteron and a K^+ are detected from pp collisions at T=2.65 GeV the missing particle must be a $\overline{K}^0$ due to energy and strangeness conservation. In fact the missing mass distribution $m(pp,dK^+)$ of the coincident dK^+ events (see Fig. 2, left side) shows a clear peak around the $\overline{K}$ mass containing about 600 events. There is only very little background from misidentified particles (<3%).

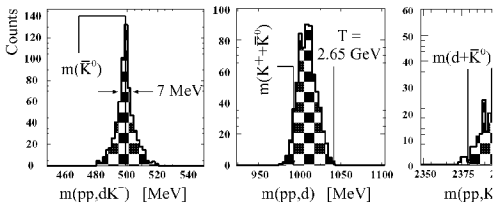

Fig. 2: Missing mass distributions of $pp \to dK^+\overline{K}^0$ events.

In the missing mass distribution $m(pp,d)$ the a_0^+ should be seen (see Fig.2, middle). However, the available phase space is limited by the $K^+\overline{K}^0$ threshold ($m_{\min}$=991 MeV) and the COSY beam energy T=2.65 GeV ($m_{\max}$=1038 MeV). Therefore one can hardly distinguish whether the $K^+\overline{K}^0$ events originate from an a_0^+ decay or from non resonant production. In any case the missing mass distribution would look similar. The $dK^+\overline{K}^0$ events offer the possibility to investigate the $d\overline{K}$ FSI which is supposed to be strong [3]. The corresponding missing mass distribution $m(pp,K^+)$ is shown in figure 2 (right side). All mass distributions are not yet corrected for detection efficiencies and acceptances. It is assumed that both corrections do not have a strong influence on the distributions except for $m(pp,K^+)$.

The observed 600 $dK^+\overline{K}^0$ events correspond to a total cross section of ~40 nb. This value is still preliminary due to the ongoing analysis.

For events with a coincident deuteron-pion pair the missing mass distribution $m(pp,d\pi^+)$ shows a huge background distribution increasing with the mass (Fig.3, left side). At 550 MeV a peak is visible due to $d\pi^+\eta$ events. The peak contains about 2300 η mesons and has a width of ~16 MeV.

In the missing mass distribution $m(pp,d)$ a shoulder at the mass of the a_0^+ a background distribution is seen (Fig.3, right side). Assuming that background events left and right to the η peak have the same behavior as the background below the peak this background can be subtracted. In the missing mass histogram $m(pp,d)$ only the shaded events survive with a peak at the a_0^+ mass and a width of about 40 MeV.

The result of this experiment will be determination of the total cross sections of the reactions $pp \to dK^+\overline{K}^0$ and $pp \to da_0^+ \to d\pi^+\eta$ at T=2.65 GeV. In February 2002 a second beam time on a_0^+ production will be performed at higher beam energies [4] corresponding to wider missing mass intervals which seem to be essential to determine the ratio of resonant and non resonant $K^+\overline{K}^0$ pair production. Moreover we hope to be able to determine the a_0^+ width, the ratio of $a_0^+ \to K^+\overline{K}^0$ and $a_0^+ \to \pi^-\eta$ decays and to draw conclusions on the $d\overline{K}$ FSI.

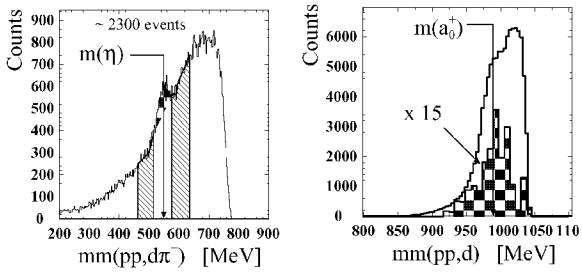

Fig. 3: Missing mass distributions of $pp \to d\pi^+X$ events.

References:

[1] C. Caso et al. (Particle Data Group), Eur. Phys. J. **C 15** (2000) 1.

[2] M.Büscher et al., NIM A in print

[3] E. Oset et al., nucl-th/0109050.

[4] M. Büscher et al., Beam time request for COSY proposal #55, 2001; available via http://ikpd15.ikp.kfa-juelich.de:8085/doc/Proposals.html.

Near threshold production of a_0-mesons in the reactions $pp \to ppK^+K^-$ and $pp \to pnK^+\bar{K}^0$: Is the $a_0(980)$ a $q\bar{q}$ state or a threshold cusp?*

E.L. Bratkovskaya[a], V. Yu. Grishina[b,c], L.A. Kondratyuk[c], M. Büscher, and W. Cassing[a]

In our recent paper [1] we have considered a_0 production in the reaction $\pi N \to a_0 N$ near threshold and at GeV energies. An effective Lagrangian approach as well as the Regge-pole model were applied to investigate different contributions to the cross section of the reaction $\pi N \to a_0 N$. The results have been used in Ref. [2] for an analysis of a_0 production in NN collisions. Within the framework of the one-pion exchange approximation the cross sections of the reactions $pp \to ppa_0^0$, $pp \to pna_0^+$, $pn \to pna_0^0$ and $pn \to ppa_0^-$ were expressed through two independent amplitudes of the reaction $\pi N \to a_0 N$ describing the channels with isospin I =1/2 and 3/2. It was found that near threshold the u-channel exchange mechanism with intermediate nucleon exchange gives the dominant contribution. This leads to the specific prediction that due to the favorable isospin Clebsh-Gordan coefficients the cross section of the reaction $pp \to pna_0^+$ is expected to be much larger than the one of the reaction $pp \to ppa_0^0$.

The production cross section in each channel depends on the cut-off parameter Λ_N for the virtual nucleon. In Refs. [1, 2] we used for the nucleon propagator (i.e. for the combined vertices a_0NN and πNN) the form factor $F_N(s) = \Lambda_N^4/[\Lambda_N^4 + (s - m_N^2)^2]$, which at large s behaves as $\simeq s^{-2} \simeq q_N^{-4}$. For brevity let's denote it by monopole form factor. In Ref. [1] we fixed Λ_N in the interval 1.2–1.3 GeV for the monopole form using experimental data on the forward differential cross section of the reaction $pp \to da_0^+$ at $3.8 \div 6.3$ GeV/c from Ref.[3] (see Fig.1).

Since there is no strict rule for the power of the nucleon form factor some authors (studying meson production in πN reactions) used a dipole form factor $[F_N(s)]^2$. Here we note that using a dipole form factor and readjusting the cut-off to the data of Ref. [3] only slightly modifies the results presented in Ref. [2]. In Fig. 1 we show the sensitivity of the forward differential cross section for the reaction $pp \to da_0^+$ to the choice of the nucleon and pion form factors. First of all, we see that an increase of $\Lambda_{\pi NN}$ from 1.05 to 1.3 GeV changes the cross section by about 30 % or less (compare the corresponding thin and bold curves). For the monopole nucleon form factor the Berkeley data from Ref. [3] can be reasonably fitted using $\Lambda_N = 1.2 - 1.24$ GeV (solid curves in Fig. 1). However, when employing a dipole FF with the same cut-off Λ_N, the predicted cross section will be lower than the data by a factor ~ 5 or more (lower long dashed curves in Fig. 1), which proves the cut-off to be inadequate in this case. The description of the data is regained (for the dipole FF) if we use $\Lambda_N = 1.55 - 1.6$ GeV (short dashed curves in Fig. 1). Therefore, using the Berkley data on the reaction $pp \to da_0^+$ we can fix the cut-off Λ_N for both cases: i.e. the monopole FF as well as the dipole FF.

The relevant question now is, if the resulting cross sections for the ppa_0^0 and pna_0^+ final states differ significantly. In Ref. [2] we calculated the total cross sections for four different channels of the reaction $NN \to NNa_0$

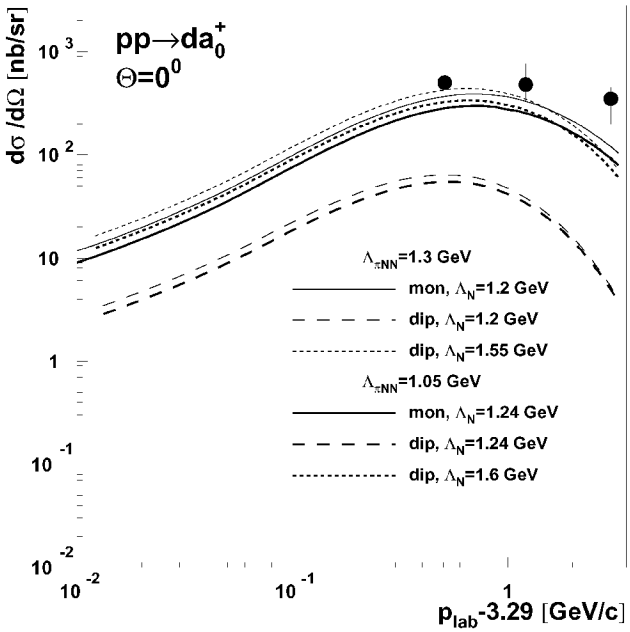

Fig. 1: Forward differential cross section of the reaction $pp \to da_0^+$ as a function of $(p_{lab} - 3.29)$ GeV/c. The bold and thin solid curves are calculated at $\Lambda_{\pi NN}$=1.05 and 1.3 GeV respectively. The solid curves correspond to a monopole nucleon form factor with Λ_N= 1.2 (thin) and 1.24 GeV (bold). The long-dashed and short-dashed curves are calculated using the dipole nucleon form factor for different values of Λ_N as shown in figure. The experimental data are taken from Ref. [3].

using a monopole nucleon FF with Λ_N = 1.24 GeV. If we take the dipole FF with the same Λ_N we again find the cross section to be 6–10 times smaller for the channels $pp \to pna_0^+$, $pn \to pna_0^0$, $pn \to ppa_0^-$, where the u-channel exchange mechanism is dominant and u-s interference is not very important. If we increase Λ_N to 1.55–1.6 GeV (as dictated by the Berkeley data) the cross sections are roughly the same as in the case of the monopole FF with Λ_N = 1.24 GeV (compare the solid and dotted curves). This behaviour of the cross section (with Λ_N) is very similar to the case of the reaction $pp \to da_0^+$. Only for the channel $pp \to ppa_0^0$ we find a slightly different cross section. For the dipole FF the cross section becomes somewhat larger than for the monopole FF, which is related to a strong destructive interference of the s- and u- exchange mechanisms. Due to this large cancellation of amplitudes by interference our predictions for the $pp \to ppa_0^0$ channel have a larger (systematic) uncertainty than for the other channels. Nevertheless, our basic result, that the a_0 production in the reaction $pp \to pnK^+\bar{K}^0$ will be much more abundant (by a factor of 10) than in the reaction $pp \to ppK^+K^-$ holds also in case of the dipole FF. This is demonstrated

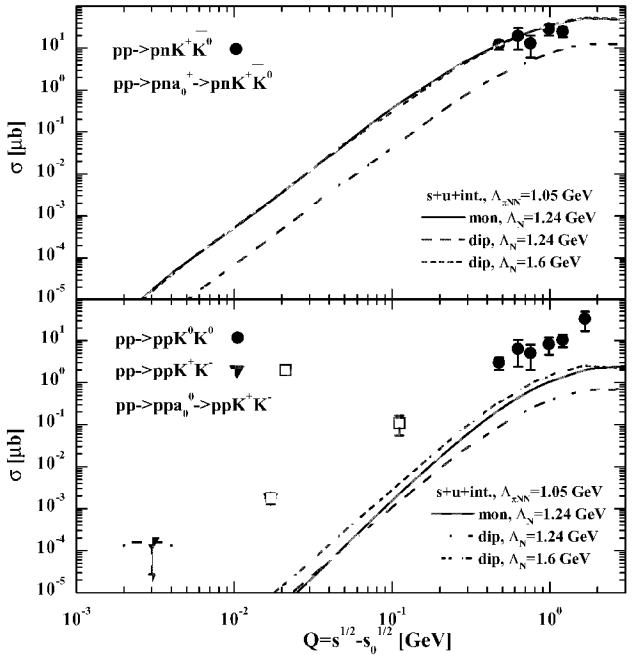

Fig. 2: Upper part: calculated total cross section for the reaction $pp \to pna_0^+ \to pnK^+\bar{K}_0$ in comparison to the experimental data for $pp \to pnK^+\bar{K}_0$ (solid dots) from Ref. [4] as a function of $Q = \sqrt{s} - \sqrt{s_0}$. The solid and long-dashed lines correspond to the coherent sum of the contributions from $s(N)$ and $u(N)$ channels with $\Lambda = 1.24$ GeV and are calculated using monopole (solid) and dipole (long-dashed) nucleon form factors; the short-dashed line is calculated using the dipole form factor with $\Lambda = 1.6$ GeV. Lower part: calculated total cross section for the reaction $pp \to ppa_0^0 \to ppK^+K^-$ as a function of $Q = \sqrt{s} - \sqrt{s_0}$ in comparison to the experimental data. The solid dots indicate the data for $pp \to ppK_0\bar{K}_0$ from Ref. [4], the open square for $pp \to ppK^+K^-$ from Ref. [5]; the full down triangels show the data from Ref. [6]. The legends of the lines are the same as in the upper part.

in Fig.2 where we display the calculated total cross sections for the reactions $pp \to pna_0^+ \to pnK^+\bar{K}^0$ and $pp \to ppa_0^0 \to ppK^+K^-$ as a function of $Q = \sqrt{s} - \sqrt{s_0}$ in comparison to the experimental data. For the a_0 mass distribution we used a Flatté formula with $\Gamma_{a_0\pi\eta}$=70 MeV and $BR(K\bar{K})$=0.187. We note also that our predictions for the cross sections $pp \to ppa_0 \to ppK^+K^-$ (using the dipole FF) do not exceed the upper limits on this cross section imposed by the DISTO data at $Q \simeq 100$ MeV and COSY-11 at $Q = 17$ MeV as well as by data at $Q \leq 2$ GeV. There is also no contradiction with the available data in other channels.

The structure of the lightest scalar mesons $a_0(980)$ and $f_0(980)$ is still under discussion. Different authors interpreted them as unitarized $q\bar{q}$ states or as four-quark cryptoexotic states or as $K\bar{K}$ molecules or even as threshold cusps. Experimental data on the a_0 production in NN collisions might give new information on the a_0 structure. According to Atkinson et al. [7] a relatively strong production of the a_0 (the same as for the $b_1(1235)$) in non-diffractive reactions can be considered as evidence for a $q\bar{q}$ state rather than a $qq\bar{q}\bar{q}$ state. For example the cross section of a_0 production in γp reactions at 25–50 GeV is about 1/6 of the cross sections for ρ and ω production. Similar ratios are found in the two-body reaction $pp \to dX$ at 3.8–6.3 GeV/c where $\sigma(pp \to da_0^+) = (1/4 \div 1/6)\sigma(pp \to d\rho^+)$ [3].

In our case we can compare a_0 and ω production. Our model predicts $\sigma(pp \to pna_0^+) = 30 \div 70$ μb at $Q \simeq 1$ GeV (see Fig. 7 in Ref.[2]) which can be compared with $\sigma(pp \to pp\omega) \simeq 100 - 200$ μb at the same Q. If such a large cross section could be detected this would be a serious argument in favour of the $q\bar{q}$ model for the a_0 meson.

To distinguish between the threshold-cusp scenario and a resonance model one can exploit different analytical properties of the a_0 production amplitudes. In case of a genuine resonance the amplitude of $\eta\pi$ and $K\bar{K}$ production through the a_0 has a pole and satisfies the factorization property. This implies that the shapes of the invariant mass distributions in the $\eta\pi$ and $K\bar{K}$ channels should not depend on the specific reaction in which the a_0 is produced (for $Q \geq \Gamma_{\rm tot}$). On the other hand, for the threshold cusp scenario the a_0 bump is produced through the $\pi\eta$ final state interaction. The corresponding amplitude has a square-root singularity and in general cannot be factorized (see e.g. Ref. [8] where the factorization property was disproved for pp FSI in the reaction $pp \to ppM$). This means that for a threshold bump the invariant mass distributions in the $\eta\pi$ and $K\bar{K}$ channels are expected to be different and will even depend on kinematical conditions (i.e. initial energy and momentum transfer) at the same excess energy, e.g. $Q \geq \Gamma$.

References:

[1] V.Yu. Grishina et al. Eur. Phys. J. A **9**, 277 (2000)
[2] E.L. Bratkovskaya et al., nucl-th/0107071
[3] M.A. Abolins et al., Phys. Rev. Lett. **25**, 469 (1970) S. Flatté, Phys. Lett. **B 63**, 224 (1976)
[4] Landolt-Börnstein, *New Series*, ed. H. Schopper, I/12 (1988)
[5] F. Balestra et al., Phys. Rev. C **63**, 024004 (2001)
[6] C. Quentmeier et al., Phys. Lett. **B 515**, 276 (2001)
[7] M. Atkinson et al., Phys. Lett. **B 138**, 459 (1984)
[8] V. Baru et al., Phys. Atom. Nucl. **64**, 579 (2001)

[a] Institut für Theoretische Physik, Universität Giessen, D-35392 Giessen, Germany
[b] Institute for Nuclear Research, 60th October Anniversary Prospect 7A, 117312 Moscow, Russia
[c] Institute of Theoretical and Experimental Physics, B.Cheremushkinskaya 25, 117259 Moscow, Russia

*Supported by DFG and RFFI

Measuring the life-time of a_0-mesons by their excitation function in pN reactions

E.L. Bratkovskaya[a], V.Yu. Grishina[b,c], L.A. Kondratyuk[c], M. Büscher, and W. Cassing[a]

The structure of the lightest scalar mesons $a_0(980)$ and $f_0(980)$, which carry the quantum numbers of the QCD vacuum, is still under discussion. They have been interpreted as unitarized $q\bar{q}$ states, as four-quark cryptoexotic states, as $K\bar{K}$ molecules or even as vacuum scalars (Gribov's minions). Although it is possible to describe them as ordinary $q\bar{q}$-states, other options cannot be ruled out up to now. There is no doubt that new data on a_0^0 and a_0^+/a_0^- production in πN and NN reactions will help to shed light on the a_0 structure and the dynamics of its production.

The a_0 production in $NN \to NNa_0$ reactions has been studied recently in Ref. [1] (cf. Ref. [2] for $\pi N \to a_0 N$ reactions). Using an effective Lagrangian approach with one-pion exchange we have analyzed different contributions to the cross section corresponding to t-channel diagrams with $\eta(547)$- and $f_1(1285)$-meson exchanges as well as s and u-channel graphs with an intermediate nucleon. In Ref. [1] we additionally have considered the t-channel Reggeon exchange mechanism. These results have been used to calculate the contribution of a_0 mesons to the cross sections of $pp \to pnK^+\bar{K}^0$ and $pp \to ppK^+K^-$ reactions. Due to the isospin Clebsh-Gordan coefficients as well as rather strong destructive interference of the s- and u-channel contributions our model gives quite small cross sections for a_0^0 production in the $pp \to ppK^+K^-$ reaction. The a_0^+ production cross section in the $pp \to pna_0^+ \to pnK^+\bar{K}^0$ reaction should be larger by about an order of magnitude. Therefore the experimental observation of a_0^+ in the reaction $pp \to pnK^+\bar{K}^0$ is much more promising than that of the a_0^0 in the reaction $pp \to ppK^+K^-$.

We have also analyzed invariant mass distributions of the $K\bar{K}$ system in the reaction $pp \to pNa_0 \to pNK\bar{K}$ at different excess energies Q not far from threshold. Our analysis of the DISTO data on the reaction $pp \to ppK^+K^-$ at 3.67 GeV/c has shown that the a_0^0-meson is practically not seen in $d\sigma/dM$ at low invariant masses, however, the f_0-meson gives some contribution. In this respect the possibility to measure the a_0^+ meson in $d\sigma/dM$ for the reaction $pp \to pnK^+\bar{K}^0$ (or $\to dK^+\bar{K}^0$) looks much more promising not only due to a much larger contribution for the a_0^+, but also due to the absence of the f_0 meson in this channel.

As shown in Ref. [1] the mass distribution of the final $K\bar{K}$ system can be written as a product of the total cross section for a_0 production (with 'running' mass M) in the $NN \to NNa_0$ reaction ($\sigma_{a_0}(s,M)$) and the Flatté mass distribution function

$$\frac{d\sigma_{K\bar{K}}}{dM^2}(s,M) = \sigma_{a_0}(s,M) \times C_F \frac{M_R \Gamma_{a_0 KK}(M)}{(M^2 - M_R^2)^2 + M_R^2 \Gamma_{tot}^2(M)} , \quad (1)$$

with $\Gamma_{tot}(M) = \Gamma_{a_0 K\bar{K}}(M) + \Gamma_{a_0 \pi\eta}(M)$. The partial widths $\Gamma_{a_0 K\bar{K}}(M) = g^2_{a_0 K\bar{K}} q_{K\bar{K}}/(8\pi M^2)$, $\Gamma_{a_0\pi\eta}(M) = g^2_{a_0\pi\eta} q_{\pi\eta}/(8\pi M^2)$ are proportional to the center-of-mass decay momenta $q_{K\bar{K}}$, $q_{\pi\eta}$. The coupling constant $g_{a_0\pi\eta}$ is defined by $\Gamma_{a_0\pi\eta}(M_R)$, whereas the parameters C_F and $g_{a_0 K\bar{K}}$ are fixed by the unitarity condition and the branching ratio $Br(a_0 \to K\bar{K}) = 0.187$ is in line with Ref. [3].

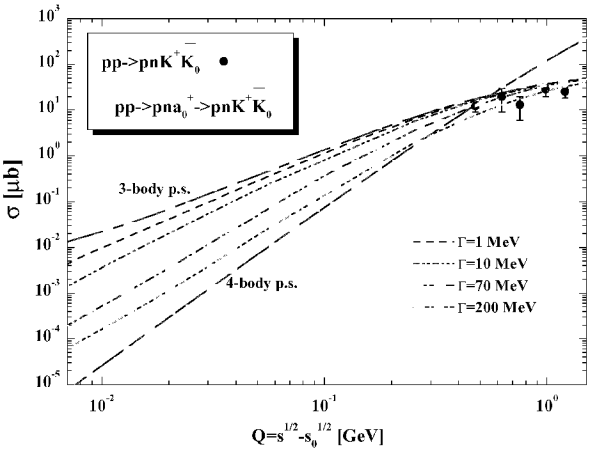

Fig. 1: The total cross section for the reaction $pp \to pna_0^+ \to pnK^+\bar{K}_0$ calculated for different a_0 widths in comparison to 3- and 4-body phase space.

In Fig. 1 we show the total cross section as a function of the excess energy $Q = \sqrt{s} - \sqrt{s_0}$ for the reaction $pp \to pna_0^+ \to pnK^+\bar{K}^0$ calculated for different a_0 widths ($\Gamma = 1, 10, 70, 200$ MeV) in comparison to 3- and 4-body phase space (normalized to the first two experimental data points). According to the quantum mechanical uncertainty relation this cross section approaches the limit of 3-body phase for a long life time of the a_0 (i.e. $\Gamma = 1$ MeV). On the contrary, for very short lived a_0 mesons or large off-shell contributions from the a_0 propagator the excitation function follows approximately 4-body phase space as shown in Fig. 1. Thus, apart from a direct measurement of the a_0 width via invariant $K\bar{K}$ mass spectra the excitation function of the resonant (via a_0) $K\bar{K}$ cross section provides valuable information on the a_0 life time.

References:

[1] E.L. Bratkovskaya et al., nucl-th/0107071.
[2] V.Yu. Grishina et al., Eur. Phys. J. A 9 (2000) 277.
[3] J. Adomeit et al., Phys. Rev. D 57 (1998) 3860.

[a]Institute for Theoretical Physics, University of Giessen, D-35392 Giessen, Germany
[b]Institute for Nuclear Research, 60th October Anniversary Prospect 7A, 117312 Moscow, Russia
[c]Institute of Theoretical and Experimental Physics, B. Cheremushkinskaya 25, 117259 Moscow, Russia

Efficiency of the second scintillator plane of the ANKE forward detector*.

P. Fedorets[a], M. Büscher, V. Chernyshev[a], S. Dymov[b], V. Komarov[b]

The aim of this work is to determine the efficiency of the second scintillator plane of the ANKE forward detector(FD) for the a_0^+ beam time (Jan./Feb. 2001). We used data from 4 runs 3347, 3348, 3350, 3352 obtained with on-line "trigger 2", i.e. a signal from the first scintillator layer of the FD. For track reconstruction the information of the FD MWPCs 1 and 2 was used and only events with a single reconstructed track were accepted for the analysis.
For the suppression of scattered background (i.e. from the vacuum pipe between D2 and D3) geometrical criteria were applied [1]:

- Horizontal and vertical limitation of the track coordinate on the D2 exit window.
- Vertical cut on the target ($Y'Y$ distribution).
- Horizontal and vertical limitation for the track coordinate on the scintillator surface.

Furthermore, events with only one cluster per each wire plane in FD-MWPCs 1 and 2 were selected. This allows to reject multiparticle events with only a single reconstracted track.
The surface of the second scintillator plane was divided into cells of 5x5 mm^2. The coordinate of the crossing point was calculated from the MWPC information. The criteria of the hit was the presence of time signals from both photomultiplier tubes. If the crossing point is closer than 6 mm to the edge, the possibility of a hit in the neighbouring counter was allowed (the accuracy of the crossing point coordinate is about 5 mm and 1 mm is the mean gap value).
Figure 1 shows the efficiency of the second hodoscope plane. Over the whole surface it is close to 100%. The spatial distribution of the events which are not detected in the second scintillator plane is shown in Fig.2. There are the very few events on the counter surfaces, the four distinct counter boundaries and the areas in the upper and lower parts of the plot. The latter areas are mostly connected with the difference in the vertical acceptance between the first and the second hodoscope planes. The coordinates of these areas are close or beyond the counter edges.
In order to test the criteria near the counter boundaries, it was demanded that no hit was present in all second plane counters, which excludes all coordinate uncertainties. The same areas as in Fig.2 are seen.
From the runs 3347, 3348, 3350, 3352 a total of 390870 events were selected for the efficiency study. 384552 events have hits in the second plane. Thus the average efficiency of the second hodoscope plane is 98.4%. 6318 events have no hits. 3004 (47.5%) of them belong to the boundaries between the scintillators. 1478(23.4%) events belong to the upper and lower areas of a certain counter without a hit.
The determination of the first hodoscope plane efficiency is not possible, because this plane was used to generate

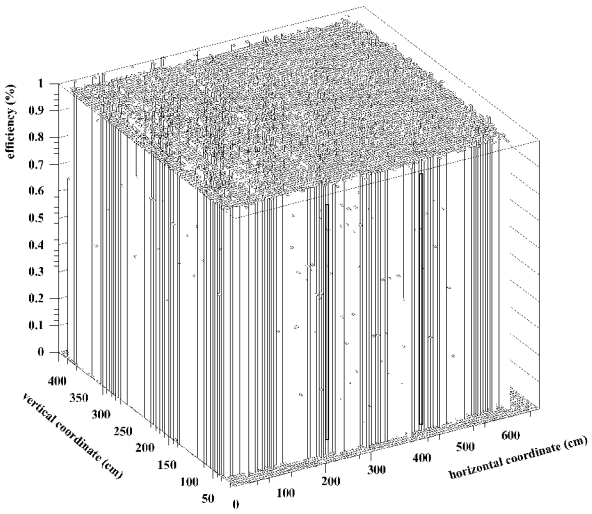

Fig. 1: Efficiency of the second plane in the hodoscope.

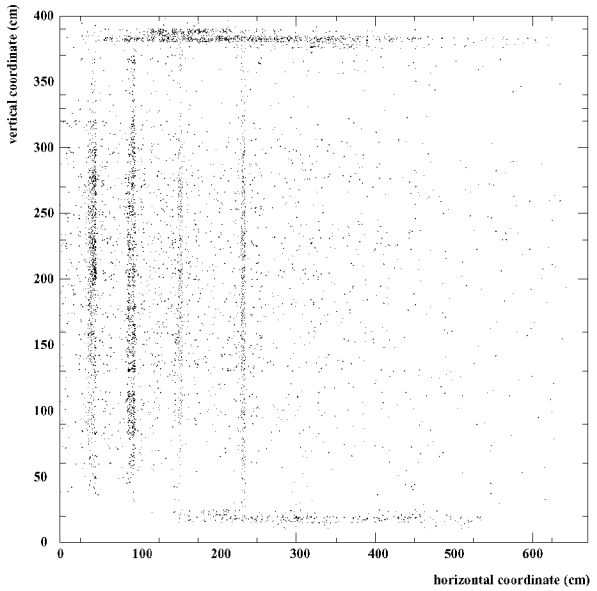

Fig. 2: Spatial distribution of the events which are not detected in the second scintillator plane

the trigger signal. However, the same high efficiency can be expected.

References:

[1] S. Dymov et al.,"Luminosity estimation in a_0 January 2001 beam time."(internal report)

[a]ITEP, Moscow, Russia
[b]JINR, Dubna, Russia
Supported by grants RFFI99-02-18179a, DFG-443RUS-113, WTZ-RUS-684-99, RFFI99-0204034, INTAS-98-500, ISTC-1966

Observation of the deuteron break-up pd $\rightarrow (pp)_S + n_{backward}$ with forward emitted S-wave proton pair

S. Dymov[a], A. Kacharava[b,c], V. Komarov[d], A. Kulikov[d], V. Kurbatov[d], G. Macharashvili[c,d], A. Petrus[d,†], F. Rathmann, H. Seyfarth, Yu. Uzikov[d,e,††], S. Yaschenko[b,d] for the ANKE collaboration

The ANKE Experiment No. 20 [1] aims at a study of the proton-induced deuteron break-up at high momentum transfer to deduce information on the short-range nucleon-nucleon interaction. Whereas later measurements will use polarized protons stored in COSY to bombard a polarized deuterium gas target, first experiments [2] have been performed with unpolarized and polarized beams incident on the deuterium-cluster jet target [3]. The process pd $\rightarrow (pp)_s+n$ with forward emission of a fast S-wave proton pair and backward neutron emission is a novel approach to study short-range effects in deuteron break-up [4]. Its kinematics is similar to pd backward elastic scattering, whereby the interpretation is simplified, because the one-nucleon exchange mechanism is expected to dominate the process. First results from measurements with polarized beam are given elsewhere [5]. Here results of the analysis of data are presented, which were obtained in the first one-week beam time with unpolarized proton beam in February 2001.

The experiment was carried out (i) to investigate the two-proton momentum resolution, achievable with the three multi-wire proportional chambers (MWPC's in Fig. 1) of the ANKE forward detector system (FD), and (ii) to measure the energy dependence of the differential cross section. A pronounced minimum is predicted [6] around an incident beam energy of $T = 0.8$ GeV, and a broad plateau for $T > 1.2$ GeV. In order to study the energy dependence, measurements were carried out at beam energies of 0.5, 0.6, 0.7, 0.8, 0.95, 1.35, and 1.9 GeV.

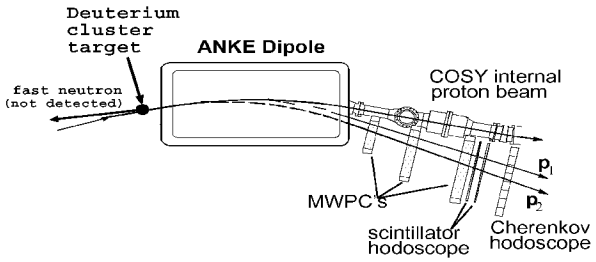

Fig. 1: Scheme of the ANKE FD system used in $pd \rightarrow (pp)_S + n$ experiment.

The experimental setup at ANKE, used in the experiment, is shown in Fig. 1. Further details, e.g. about the FD wire chambers, can be found in Ref. [7]. Track reconstruction provides a complete determination of the kinematics for each event. The obtained missing-mass spectra for the process pd $\rightarrow$ ppX reveal a clear peak at the neutron mass at all beam energies. Figure 2 shows an example. Events inside the missing-mass peak exhibit a distribution of relative forward proton-pair energies predominatly below 3 MeV, as shown in Fig. 3 for a beam energy of $T_p = 500$ MeV. The shape of the spectrum in this region is well reproduced by the Migdal-Watson approach for the S-wave FSI in the proton pair.

The obtained results confirm that the deuteron break-up reaction, accompanied by high momentum transfer, is well identified by the ANKE FD system. The data are currently processed in order to determine the cross sections based on a procedure of luminosity determination described in Ref. [8].

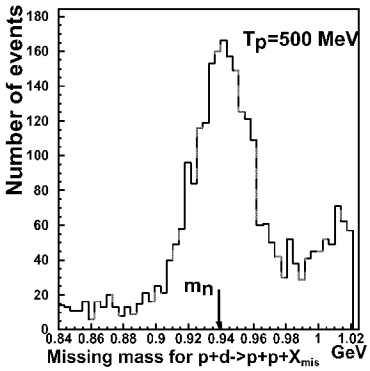

Fig. 2: Example of the missing mass distributions for pd $\rightarrow$ ppX.

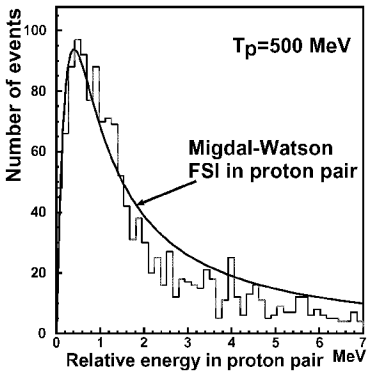

Fig. 3: Distribution of relative energies in proton pairs for events inside the missing-mass peak of Fig. 2.

References:

[1] S.V. Dshemuchadze *et al.*, COSY Experiment Proposal 20.2 (1991), spokesperson V. Komarov.

[2] V. Abazov *et al.*, COSY Experiment Proposal 20.3 (1999), spokespersons V. Komarov, F. Rathmann (local contact).

[3] A. Khoukaz *et al.*, Eur. Phys. J. **D5**, 275 (1999).

[4] A.V. Smirnov and Yu.N. Uzikov, Phys. At. Nuclei **61**, 361 (1998).

[5] F. Rathmann *et al.*, contribution to the present report.

[6] Yu.N. Uzikov *et al.*, Annual Report IKP and COSY 2000, report Jül-3852 (Berichte des FZ Jülich, 2001), p.36.

[7] S.Barsov *et al.*, Nucl.Inst. and Meth.A462 364(2001).

[8] S.Yaschenko *et al.*, contribution to the present report.

[a]PhD student from JINR, Dubna, Russia.
[b]Friedrich-Alexander-Universität Erlangen, Germany.
[c]High Energy Physics Inst., Tbilisi State Univ., Georgia.
[d]JINR, Dubna, Russia.
[e]Kazakh State University, Almaty, Kazakhstan.
†supported by FZJ (FFE, contract 41419786).
††supported by BMBF, Germany (WTZ grant KAZ 99/001) and Heisenberg-Landau program.

Momentum correlation of particles recorded in the ANKE forward detector

S. Dymov[a,b], A. Kacharava[c,d], V. Komarov[b], S. Yaschenko[b,c]

The absolute momentum values (p_1 and p_2) of two particles in any three-particle final-state process are strictly correlated if they are emitted into fixed directions (θ_1,ϕ_1 and θ_2,ϕ_2). The correlations are to some extent conserved if the precise directions are changed by some restricted solid angles. The ANKE forward detector (FD) accepts the secondaries with a polar emission angle from zero up to about 16°. However, the angular range is substantially reduced for particles of definite momentum (see Fig.1, which presents the ejectile momentum p versus the projection of the polar angle θ_{xz} on the median plane), and, moreover, it is limited to 5° for particles with full 2π azimuthal angle acceptance. Therefore, one may expect the existence of a significant kinematical correlation for particles recorded in this detector even without any additional kinematical cuts. Fig.2 shows the correlated momentum distributions for particle pairs produced in a hydrogen cluster target and both particles recorded in the FD. The momenta of the two ejectiles were calculated from the information on hit wires in the forward MWPCs. The correlations well correspond to the one expected from simulation (Fig.3) and are caused by the dominant processes with two positively charged particles: $pp \to pp\pi^0, pp \to pn\pi^+, pp \to d\pi^+$. The distributions are very useful for calibration purposes. They give a good overview of the experimental conditions like intensity of the main recorded processes, their momentum ranges and possible overlaps, background, etc. The distributions with the deuterium target (Fig.4 and Fig.5) show that the same processes as obtained with the hydrogen target are clearly observable with the deuterium target in a quasifree mode. As expected, some additional processes show up with deuterium.

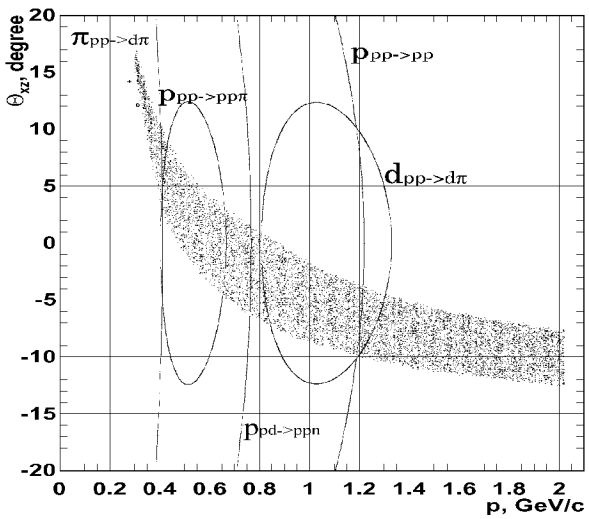

Fig. 1: FD angular-momentum acceptance

[a] IKP FZ-Jülich, Germany
[b] JINR, Dubna, Russia
[c] Universität Erlangen, Germany
[d] HEPI TSU, Tbilisi, Georgia

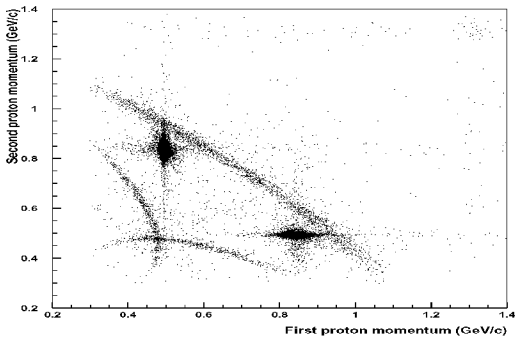

Fig. 2: Momentum of the two particles detected in the FD (experimental data, H_2 target, T_p=0.7 GeV).

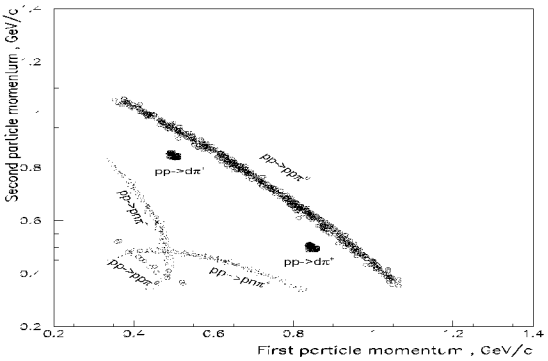

Fig. 3: Simulation for experimental conditions of Fig.2

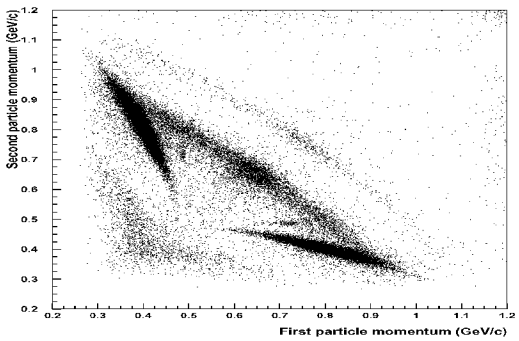

Fig. 4: Same as Fig.2 for D_2 target and T_p=0.6 GeV.

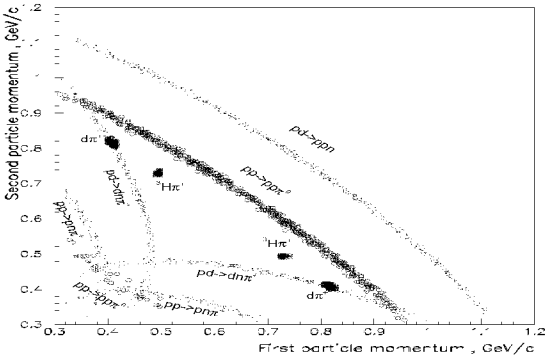

Fig. 5: Simulation for experimental conditions of Fig.4

Determination of the ANKE forward detector MWPC efficiency

S.Dymov, V.Komarov[a], A.Petrus[a], S.Yaschenko

The three MWPCs of the ANKE forward detector (FD) provide the reconstruction of track and momentum of positively charged forward-emitted ejectiles in several experiments. The layout of the FD is shown in Fig. 1(a). Each of the chambers is made of two wire (X and Y) and two strip planes, the latter being inclined under $\pm 18^\circ$ to the vertical axis, and separated by a thin supporting film from the corresponding wire planes (see Fig. 1(b)). The wire planes have 1 mm step (wire distance), and the strip planes ≈ 3 mm.

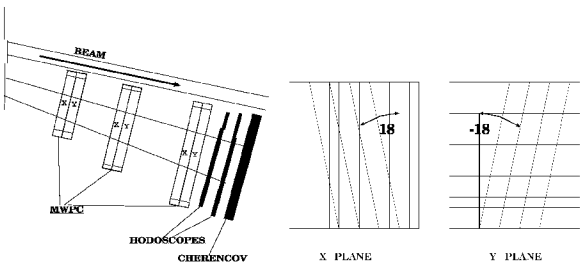

(a) (b)

Fig. 1: Sketch of the ANKE forward detector and structure of the MWPC.

For processing experimental data with the aim to determine differential cross-sections and various polarization observables, it is necessary to know the efficiency of particle registration. The efficiency of proportional chambers demands a special investigation, in contrast to scintillation counters which usually have efficiency close to 100%. Furthermore, the efficiency could be inhomogeneous over the sensitive plane due to the non-standard construction, e.g. a weakly conducting supporting film, positioned between the wires and strips.

In this connection, a procedure to determinate the chamber efficiency is developed. A particle track is reconstructed using the information from the other wire/strip planes, and only events with one cluster per each plane are considered. The reconstructed tracks are checked for coincidence with the fired hodoscopes and must pass all background cuts. This allows one to uniquely reconstruct particle tracks as well as to circumvent complications caused by multi-track events and electronic noise. Then the crossing point of the track with the sensitive plane under study is determined and the presence of a hit wire (strip) is checked in the area around the crossing point. In order to determine the dependence of the chamber efficiency over area of the sensitive plane, the plane is divided into cells. If the crossing point of the track occurs inside a cell, the event is regarded as belonging to the cell. A typical efficiency distribution obtained by this method is shown in Fig. 2. Since the number of MWPC's used in data taking was different during different beam times, various combinations of wire and strip planes were used for building tracks. In one case all three MWPC's operated, and the wire planes of two of them could be used to estimate the efficiency of the third one. In the second case only two chambers operated, and one had to use also a strip plane for reconstruction. A similar situation occured when only the first MWPC and the Y plane of the second MWPC operated.

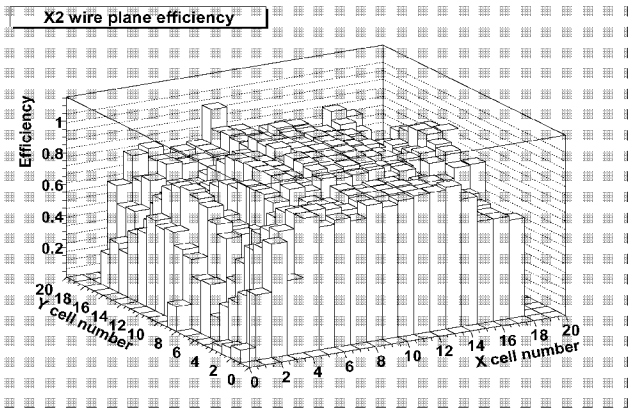

Fig. 2: Typical efficiency distribution over a wire plane.

These three situations lead to a significantly different spacial resolution of the reconstructed tracks and effectiveness of the track selection criteria. A comparison of the three methods on the same data has shown a rather good coincidence of the results for the efficiencies.

In order to check how well one can correct data for the MWPC inefficiency we compared model and experimental $pp \to pp$ angular distributions at $T_{beam} = 2.65$ GeV and a H_2 target, with one ejectile proton detected in FD. To obtain the model distribution we used the differential cross-section, calculated by SAID, and traced the particles through the setup with a GEANT-based program. The experimental events were selected from the momentum reconstructed distribution, in which this reaction yields a prominent peak at the proper position. The efficiency correction was done by assigning a weight for each event according to the coordinates of the track crossings with the MWPC's. In Fig. 3 distributions over the azimuthal angle are shown. The uncorrected experimental histogram is scaled by a factor 2.5 for better visual comparability.

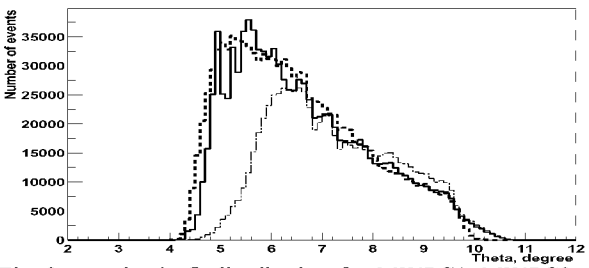

Fig. 3: pp-elastic Θ distribution for MWPC1–MWPC3: uncorrected (thin, dash-dotted), corrected (thick solid) experimental and model (thick dashed).

One can see that even in the chamber region with a strong efficiency drop (small Θ) the correction allows one to reproduce the expected shape. We also used the data with all three chambers in operation and found that the corrected results are in a good agreement for the cases when the tracks were reconstructed by MWPC1–MPWC2 and MWPC1–MWPC3 pairs.

This shows that the developed method can be used for effective reconstruction of experimental spectra.

[a] JINR, Dubna, Russia

Beam Polarization Measurement for the ANKE deuteron break-up experiment

F. Rathmann, S. Dymov†, A. Kacharava[a,c], V. Komarov[b], A. Kulikov[b], V. Kurbatov[b], B. Lorentz, G. Macharashvili[b,c], A. Petrus[b], H. Rohdjess[d], H. Seyfarth, D. Prasuhn, Yu.Uzikov[b,e], S.Yaschenko[a,b]

The first polarization study at ANKE has been carried out in Sept 2001 to measure the proton vector analyzing power A_y^p of the deuteron break-up process $p + d \to (pp)_S + n_{\text{backward}}$ [1] at a beam energy of 0.5 GeV. To that aim, the Münster deuterium cluster target [2] was bombarded with polarized protons. The beam polarization was measured with the EDDA detector [3]. A calibrated measurement of the beam polarization at EDDA is possible only at energies above $\approx$ 0.7 GeV (1343 MeV/c). In addition, the employed polyethylene targets do not tolerate beam intensities exceeding about $5 \cdot 10^8$ stored protons. Since initially, we wanted to perform a measurement of A_y^p at 0.5 *and* at 1.0 GeV, a macro cycle was realized, which consisted of two flattops at 0.5 and 1.0 GeV (Fig. 1). The beam polarization was

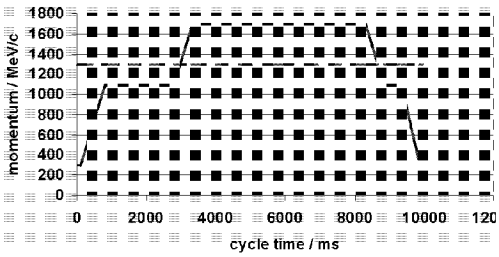

Fig. 1: Schematic picture of the cycle with two flattops, at $T = 0.5/1.0$ GeV (1.090/1.696 GeV/c).

measured in separate cycles with appropriately reduced intensity (micro-pulsing), but otherwise identical to the data-taking cycles. At 0.5 GeV for instance data were taken for 10 min, subsequently the beam was ramped to a very short 1 GeV flattop. The beam polarization was alternated from cycle to cycle. Polarization data with EDDA were recorded once or twice per day, *a)* during flattop at 1 GeV to monitor the polarization and *b)* during the ramp, with modified flattop durations. Since between 0.5 and 0.7 GeV the depolarizing resonances in COSY are understood and compensated, this procedure provides the beam polarization at 0.5 and at 1.0 GeV.
Since the polarization data recorded with EDDA did not provide a continuous monitoring of beam polarization, the beam spin up/down ($\uparrow$, $\downarrow$) asymmetry of protons scattered off the deuterium target was measured with ANKE. Elastically and quasi-elastically scattered protons between $\theta_{\text{lab}} = 5^\circ \ldots 11^\circ$ were registered in the Forward Detector (FD). At the same time proton pairs from the break-up process under study were recorded. The relative luminosity $\mathcal{L}_\uparrow/\mathcal{L}_\downarrow$ was determined from inelastically scattered protons near zero degree, simultaneously detected in the FD. Online track reconstruction provided information (angle and momentum) to select the scattered protons. Both proton count rates and observed asymmetry were sufficiently large to monitor the beam polarization during the run. The resulting polarizations (EDDA) and asymmetries (ANKE)

$$\varepsilon(\uparrow,\downarrow) = \frac{N_\uparrow/\mathcal{L}_\uparrow - N_\downarrow/\mathcal{L}_\downarrow}{N_\uparrow/\mathcal{L}_\uparrow + N_\downarrow/\mathcal{L}_\downarrow}$$

are shown in fig. 2. The asymmetries from ANKE were obtained for 2 h runs carried out right after the EDDA polarization measurements. The data are quite stable in time, thus averaging is justified and yields:

T [GeV]	P_{beam}^{EDDA}
0.7	0.645 ± 0.009
1.0	0.577 ± 0.001

The measured asymmetries at ANKE are given below:

T [GeV]	$\varepsilon(\uparrow,\downarrow)$	$[\varepsilon(\uparrow,\uparrow) + \varepsilon(\downarrow,\downarrow)]/2$
0.5	0.294 ± 0.006	-0.002 ± 0.009

Here $\varepsilon(\uparrow,\uparrow)$ and $\varepsilon(\downarrow,\downarrow)$ denote false asymmetries by analyzing cycles with the same polarization direction. The effective analyzing power of ANKE, given by the ratio $\varepsilon(\uparrow,\downarrow)/P_{beam}^{\text{EDDA}}$, is thus $A_y^{\text{eff}} = 0.456 \pm 0.011$. The data at 0.5 GeV are currently processed to arrive at a first measurement of the vector analyzing power in the break-up process. Unfortunately, the low beam intensity during the run did not permit to record deuteron break-up data at 1.0 GeV.

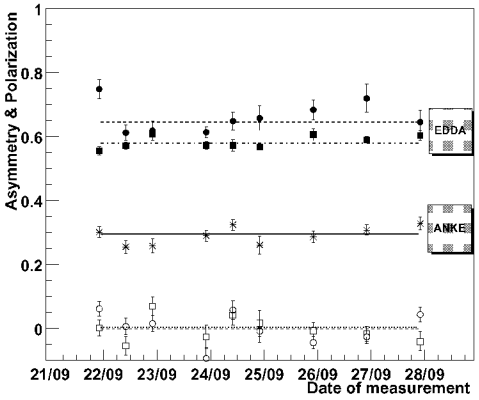

Fig. 2: EDDA beam polarization and asymmetry measured at ANKE. Filled circles denote the measured beam polarization at 0.7 GeV at EDDA, filled squares the 1 GeV flattop polarization. Stars indicate the asymmetry of small-angle scattered protons off the deuteron target, and the open symbols correspond to the measured false asymmetries $[\varepsilon(\uparrow,\uparrow)$ and $\varepsilon(\downarrow,\downarrow)]$.

The first measurement with polarized beam at ANKE, described here, became possible only through help from the EDDA collaboration, which we hereby gratefully acknowledge.

References:

[1] S. Dymov *et al.*, contribution to this report.
[2] R. Santo *et al.*, NIM **A386**, 228 (1997).
[3] H. Rohdjess, AIP Conf. Proc. **421**, 99 (1998).

[a]Physikalisches Institut II, Universität Erlangen; [b]JINR, Dubna, Russia; [c]HEPI TSU, Tiflis, Georgia; [d]Inst. Strahlen u. Kernphysik, Universität Bonn; [e]Kazakh State University, Almaty, Kazakhstan; †PhD student from[b].

Singlet-to-triplet ratio in the deuteron breakup reaction pd → pnp at 585 MeV *

Yu. Uzikov[a,b], V. Komarov[a], F. Rathmann, H. Seyfarth

Recent analyses of experimental data on $\pi-$meson production, employing the largely model-independent approach of Ref. [1], show that the formation of the final spin-singlet np-pair is strongly suppressed in the $pp \to pn\pi^+$ reaction at proton kinetic energies between 300 and 800 MeV (see [2, 3] and reference therein).

The measured pion-production cross section in pp collisions allows one to estimate the singlet-to-triplet (s/t) ratio in the deuteron breakup reaction $pd \to \{pn\}p$, when the quasi-bound $\{pn\}$ pair is observed in the final-state interaction (fsi) region at high momentum transfer. If one assumes that the triangle diagram of one-pion exchange with the subprocess $pp \to d\pi^+$ [5] dominates in the $pd \to \{pn\}p$ reaction at large scattering angles, one would expect in this reaction a similar s/t ratio of a few percent. For the Δ mechanism in the $pd \to pnp$ reaction, which dominates the one-pion exchange triangle diagram, the product of spin and isospin factors yields a s/t ratio of $\frac{1}{27}$ [6]. In contrast, one should expect the s/t ratio of about $\frac{1}{3}$ for the one-nucleon exchange mechanism of the deuteron breakup.

Available data on the formation of a singlet $(np)_s$ pair were obtained in a few semi-inclusive measurements of the reaction $dp \to pnp$. The only exclusive $pd \to pnp$ experiment has been performed in Virginia [7] at a proton beam energy of $T_p = 585$ MeV and with a low relative energy of the final neutron-proton pair ($E_{np} = 0 - 5$ MeV) and a large scattering angle of the second proton ($\theta_{cm} \sim 90°$). The data from Ref. [7] are shown in Fig. 1 as a function of the momentum of the detected proton. At energies E_{np} of about 1 MeV the cross section is strongly influenced by the np fsi. The shape of this peak is well described by the Migdal-Watson formulae [4], which take into account the nearby poles in the fsi triplet (t) and singlet (s) $pn-$scattering amplitudes

$$d\sigma_{s(t)} = FSI_{s(t)}(k) \cdot K \cdot |A_{s(t)}|^2. \quad (1)$$

Here $A_{s(t)}$ is the production matrix element for the singlet (triplet) state, K is the kinematical factor, and $FSI_{s(t)}$ is the well known Goldberger-Watson factor. Important new information on the mechanism of $pd \to pnp$ and off-shell properties of the NN system is hidden in the matrix elements $A_{s(t)}$, in particular in the ratio $\zeta = |A_s|^2/|A_t|^2$. One can find the following parametrization for the full singlet plus triplet cross section

$$d\sigma_{s+t} = \left(1 + \zeta \frac{FSI_s}{FSI_t}\right) d\sigma_t, \quad (2)$$

where $d\sigma_t$ is the triplet cross section. The second term in the brackets of Eq. (2) corresponds to the singlet contribution.

Using the Fäldt-Wilkin extrapolation [1], which relates bound and scattering S-wave functions in the triplet state at short pn distances $r < 1$ fm, and by taking into account the short-range character of the interaction mechanism, one can find a definite relation between the matrix elements of the $pd \to \{pn\}_t p$ and $pd \to dp$ reactions [1]. Thus, the triplet cross section can be calculated in a largely model-independent way in terms of the large angle proton-deuteron elastic scattering. This approach was employed in Ref. [8] to reanalyze the data of Ref. [7]. The result is shown in Fig. 1. After smearing over the experimental resolution we obtain good agreement both in the shape and in the absolute value between the data and a pure triplet contribution of the final pn pair with $\chi^2 = 0.7$. A small singlet contribution, corresponding to $\zeta = 0.02$, does not contradict the data ($\chi^2 = 0.9$), whereas the assumption of Ref. [7] about the statistical weight of the singlet $\zeta = \frac{1}{3}$ results in a too large cross section in the vicinity of $E_{np} = 0$.

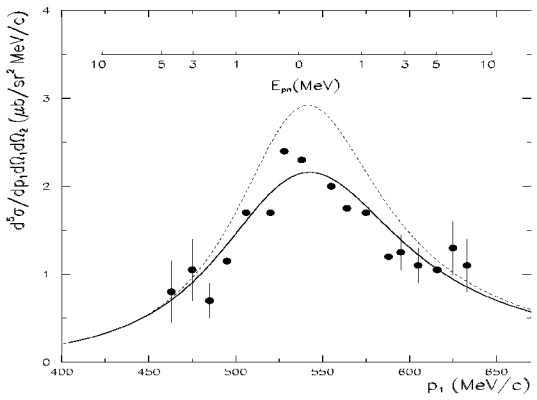

Fig. 1: Experimental cross section (points) of the $pd \to pnp$ reaction from Ref.[7] at a beam energy 585 MeV and proton laboratory scattering angles $\theta_1 = 41°$, $\theta_2 = 61°$ as function of the momentum of proton 1 measured at θ_1 in comparison with our calculations. The pure triplet contribution is calculated with corrections taking into account the experimental resolution (full line) and without (dashed). The upper scale shows the relative energy of the pn pair for $\theta_1 = 41°$.

The direct measurement of the singlet channel in the reaction $\vec{pd} \to (pp)n$ is in progress at ANKE, COSY (Exp. No. 20).

References:

[1] G.Fäldt and C.Wilkin, Physica Scripta **56**, 566 (1997).
[2] Yu.Uzikov and C.Wilkin, Phys. Lett. **B511**, 191 (2001).
[3] V.Abaev *et al.*, Phys. Lett **B 521**, 158 (2001).
[4] K.M.Watson, Phys. Rev. **88**, 1163 (1952); A.B.Migdal, Sov. Phys. JETP **28**, 3 (1955).
[5] N.S.Craigie, C.Wilkin, Nucl. Phys. B **14**, 477 (1969).
[6] Yu.N.Uzikov, nucl-theor/0006067.
[7] T.Witten *et al.*, Nucl. Phys. **A254**, 269 (1975).
[8] Yu.N.Uzikov, V.I. Komarov, F. Rathmann, H. Seyfarth, Phys. Lett. **B524**, 303 (2002).

[a] Joint Institut for Nuclear Researches, Dubna, Moscow reg. 141980 Russia
[b] Kazakh State University, Almaty, Kazakhstan

*Supported by BMBF, Germany (WTZ grant KAZ 99/001 and Heisenberg-Landau program)

Identification of Deuterons with High Momenta at ANKE

S. Barsov[a], S. Dymov[b], V.Komarov[b], I. Lehmann, G.Macharashvili[b,c] and R. Schleichert

Apart from the full three momentum determination of fast ejectiles, the forward detection system[1] [1] provides direct particle identification at ANKE. Protons, deuterons and even pions with momenta around 1 GeV/c can be well separated using their energy losses, due to a good resolution in the forward scintillation hodoscope [1]. However, there is a strong need to distinguish particles at higher momenta. E.g. in the reaction: pd $\rightarrow$ $p_{sp}d\omega$ at threshold [2] one has to distinguish deuterons with $\approx$ 2 GeV/c momentum from a 100 times larger proton background.

To allow deuteron and proton separation under such conditions, inclined Čerenkov counters have been installed [3]. As the response of these detectors is strongly momentum dependent, a dedicated procedure has been developed, to calibrate the proton suppression and deuteron efficiency within the momentum range of interest in order to equalise their proton suppression factors [4]. The scatter plot in Fig. 1 was produced from data obtained during the above mentioned experiment at 2.77 GeV/c beam momentum after the suppression of protons by Čerenkov detectors to less than 5% of their initial amount. Despite of the clear indication on the deuteron band the contribution of protons is still significantly stronger.

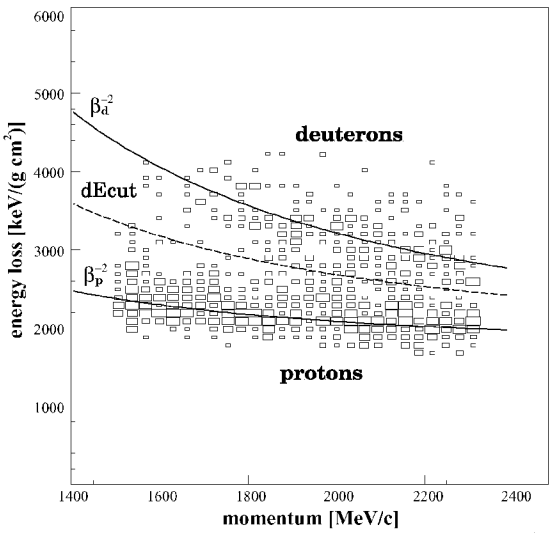

Fig. 1: Momentum dependent cut on the energy loss in the 1st layer of the forward hodoscope after 97% proton suppression; the bands from protons and deuterons can be approximated well by functions of β^{-2}.

It is necessary to take into account, that at high proton-suppression efficiencies by the Čerenkov counters also some part of the deuterons are rejected. An optimal combination of the ΔE-cut and the proton-suppression factor providing a negligible loss of deuterons was found by simultaneous varying the ΔE-cut level and the Čerenkov-efficiency level. Using the chosen suppression factor, Fig. 2 shows projections along the β_d^{-2}-line of a plot as in Fig. 1 but for the 2nd hodoscope layer (dotted line). If one applies the energy-loss cut in the 1st layer (marked "dEcut" in Fig. 1), the contribution of protons under the deuteron peak decreases already below 20%(solid line). Moreover, the remaining proton background can be easily determined using the energy loss distribution of suppressed particles (scaled)(dashed line). To more than 95% those events are protons.

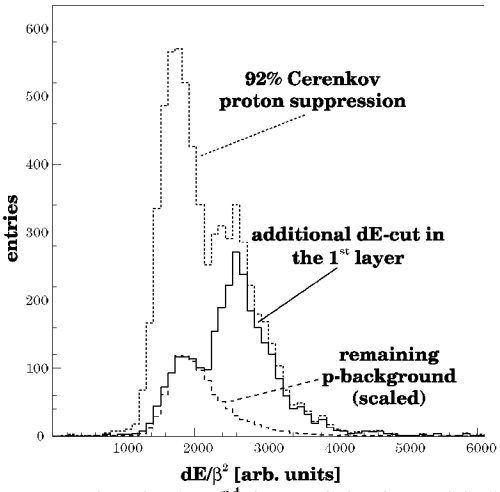

Fig. 2: Energy loss in the 2nd layer of the forward hodoscope (scaled with β_d^{-2}) using only Č-suppression (dotted), dE-cut in the first layer (solid), proton contribution extrapolated by an active selection of these particles and scaled (dashed)

To apply this subtraction for other physical observables, one has to prove that the corresponding distributions for the background protons (to be subtracted) are not affected by the cuts applied to select deuterons. As an example Fig. 3 shows the momentum and polar angle distribution with 60 and 90% efficiency for the proton identification in the Čerenkov counters. As the vast majority of particles selected by this method are protons, one can treat them as background. The curves in Fig. 3 scale with the efficiencies, but their ratios are constant within the statistical errors.

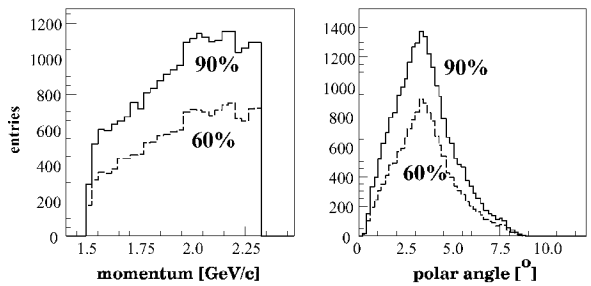

Fig. 3: Momentum and angular distributions of the background (mostly protons) for 60% (dashed) and 90% (solid) proton-identification efficiency in the Čerenkov counters; the shape does not change with the applied cut level.

Thus, deuteron identification at momenta around 2 GeV/c proves to be feasible with the ANKE forward-detection system alone. Also the remaining background of less than 20% can be subtracted on a statistical basis.

References:

[1] V.Komarov et al. *Binary process ... forward scintillation hodoscope ...*, IKP Ann. Rep. 2000, page 21.

[2] Cosy-Proposal #75

[3] A.Kachavara et al. *Beam Test of Cerenkov...*, NIM A376, 356 (1996)

[4] M.Büscher et al. *Momentum dependent efficiency of ... Čerenkov counters ...*, IKP Ann. Rep. 2000, page 22.

[a]PNPI, Gatchina, Russia; [b]JINR, Dubna, Russia; [c]HEPI TSU, Tiblisi, Georgia.

[1] consisting of three multi-wire proportional chambers (MWPC), two layers of scintillators and 16 Čerenkov counters

Model-independent analysis of the neutron-proton final-state interaction region in the pp → pn π^+ reaction*

Yuri N. Uzikov[a] and C. Wilkin[b]

Inclusive $pp \to \pi^+ X$ data in the 400 MeV to 1 GeV range generally show two structures. There is a broad peak due to quasi-free production of the Δ-isobar. There is also an enhancement near the edge of phase space arising from the strong neutron-proton final-state interaction (fsi) in either the spin-triplet or singlet S-wave which comes when the np excitation energy, $E_{np} = k^2/m_N$, is only a few MeV. The details of the fsi region are hard to investigate in a single-arm experiment, where only the π^+ is measured, because of contamination from the much larger two-body $pp \to d\pi^+$ reaction. This difficulty can be overcome by measuring the exclusive $pp \to pn\pi^+$ reaction. This has been studied at ANKE where, at a beam energy of 492 MeV, both the proton and π^+ were detected close to the forward direction [1]. Due to the good resolution of a fraction of an MeV in the proton-neutron excitation energy E_{np}, a clear fsi enhancement could then be identified.

One way to extract the spin-singlet fraction in the final state of the ANKE data involves comparing the cross section with that for $pp \to d\pi^+$. We have developed a formalism to accomplish this [2] and tested it on exclusive differential cross sections measured with poorer resolution at LAMPF [3].

Starting from the Fäldt-Wilkin extrapolation theorem [4], we predict that the triplet contribution to the laboratory five-fold differential cross section for the detection of a pion at an angle θ_π and a proton at an angle θ_p should be

$$\frac{\mathrm{d}^5\sigma_t(pp \to pn\pi^+)}{\mathrm{d}p_p\,\mathrm{d}\Omega_p\,\mathrm{d}\Omega_\pi} = \frac{1}{16\pi^3}\, s_{pp}\frac{q_p^*}{q_{\pi d}^*}\,\Phi \times$$

$$\frac{2\pi\, m_N}{\alpha_t(k^2+\alpha_t^2)}\,\frac{\mathrm{d}\sigma}{\mathrm{d}\Omega_\pi^*}(pp \to d\pi^+)\,,$$

where $\alpha_t = 0.232$ fm^{-1} is determined by the deuteron binding energy. The phase-space factor is

$$\Phi = \frac{p_p^2 p_\pi^3}{p_0\, m_p\, E_p\, |p_\pi^2\, E_n - \mathbf{p}_\pi \cdot \mathbf{p}_n E_\pi|}\,.$$

p_0 is the beam momentum and the E_i and p_i are final state laboratory energies and momenta.

The pion production angles in the laboratory (θ_π) and cm (θ_π^*) systems are related by

$$E_0\, E_\pi - p_0\, p_\pi \cos\theta_\pi = \varepsilon_0\, \varepsilon_\pi - q_p^*\, q_\pi^* \cos\theta_\pi^*\,,$$

where $\varepsilon_\pi(\varepsilon_0)$ and q_π^* are the energy of the pion (incident proton) and 3-momentum of the pion in the overall cm system and E_0 is the total laboratory energy of the incident proton.

The formula, which should be valid at low relative energies E_{np}, does not depend upon the details of the pion production dynamics and automatically includes the fsi in the triplet pn system.

Since our predictions reproduce most of the magnitude of the fsi peak at this and other angles, this is strong evidence that the vast bulk of the LAMPF data corresponds to np triplet final states. The superior ANKE data [1] confirm this at 492 MeV, where our approach shows that the singlet contribution must be below about 10%. This agrees with an analysis in terms of the shape of the fsi peak [1].

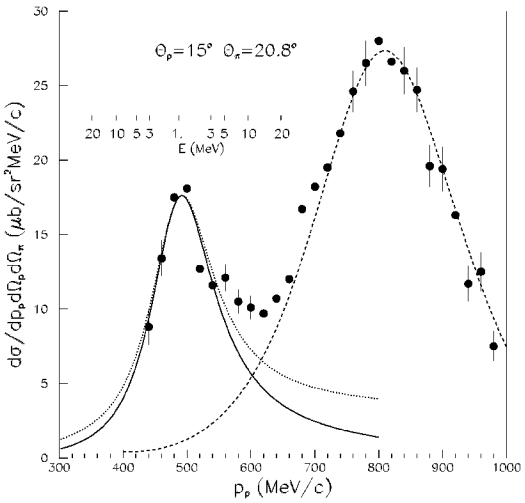

Fig. 1: Differential cross section for the $pp \to pn\pi^+$ reaction at 800 MeV at fixed proton and pion laboratory angles of $(\theta_p, \theta_\pi) = (15°, 20.8°)$ as a function of the measured proton momentum [3]. The peak on the right is due to quasi-free Δ production; that on the left is a reflection of the strong np fsi, which can be calculated (solid curve) from the $pp \to d\pi^+$ cross section. A scale is given showing the np excitation energy at the geometry corresponding to the centres of the counters.

References:

[1] V. Abaev et al., Phys. Lett. **B521**, 158 (2001).
[2] Yu.N. Uzikov and C. Wilkin, Phys. Lett. **B511** (2001) 191.
[3] J. Hudomalj-Gabitzch *et al.*, Phys. Rev. C **18** (1978) 2666.
[4] G. Fäldt and C. Wilkin, Physica Scripta **56** (1997) 566.

[a]JINR, LNP, Dubna, 141980 Russia and Kazakh State University, Almaty, 480121 Kazakhstan
[b]UCL, London, WC1E 6BT, UK
*Work partially supported by Forschungszentrum Jülich and BMBF (WTZ grant KAZ 99/001).

Spin-triplet final-state dominance in the pp → pn π^+ reaction at 492 MeV

V. Abaev[a], M. Büscher[b], S. Dymov[b,c], M. Hartmann[b], A. Kacharava[c,d], V.I. Komarov[c], V. Koptev[a], V. Kurbatov[c],
S. Mikirtychiants[a], M. Nekipelov[a,b], A. Petrus[b,c], H. Ströher[b], Yu N. Uzikov[c,*], C. Wilkin[e], and S. Yaschenko[c]

Pion production in the $pp \to pn\pi^+$ reaction has been studied at ANKE by measuring the proton in the side wall and the pion in telescope #14 of the side detection system. By comparing results obtained with C and CH_2 targets, a clear neutron peak was seen with very little background.

The published results [1] shown in Fig. 1 were obtained using different angular cuts around the forward direction. The intrinsic resolution of our system for small np excitation energies E_{np} is about 160 keV but, because of limited statistics, this is worsened by summing over angular ranges.

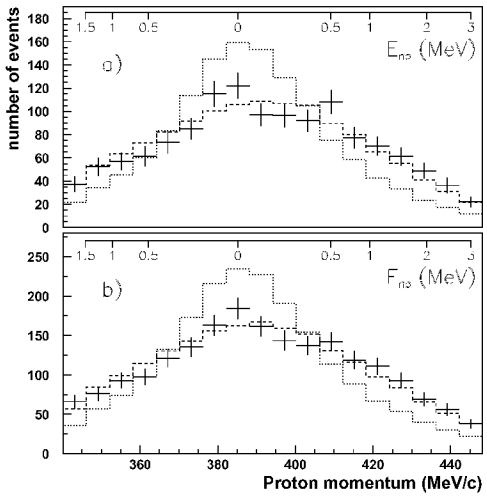

Fig. 1: Raw proton-momentum spectra of $pp \to pn\pi^+$ events (points with statistical errors), for events with $\theta_\pi \leq 2°$. The relative np energy is indicated for protons and pions emitted at 0°. Figure a) is for $\theta_p \leq 2°$ and b) for $\theta_p \leq 2.5°$. The dashed histogram is a Monte Carlo simulation assuming pure spin-triplet final state. A statistical mixture of spin states, leads to the dotted histograms with χ^2/ndf =151.2/17 for a and χ^2/ndf =178.2/17 for b.

Data were obtained for $E_{np} \leq 3$ MeV, which is the region where the spin-singlet and -triplet final-state-interactions give rise to strong peaking. Since the spin-singlet peak is much narrower ($\approx$ 0.5 MeV) than the triplet ($\approx$ 2 MeV), the *shape* of the spectrum is sensitive to the fraction of spin-singlet in the final state. After taking the angular averaging into account, the data in Fig. 1 are consistent with complete dominance by spin-triplet np final states with the singlet contributing at most 10%.

The same conclusion can be drawn from the *magnitude* of the cross sections shown in Fig. 2. The overall normalisations of these were obtained by measuring the $pp \to d\pi^+$ cross section in parallel. Here the deuteron was not detected but events were selected where there was no proton in the side detector. Using the Fäldt-Wilkin extrapolation theorem [2] it was possible to estimate the spin-triplet contribution to the $pp \to pn\pi^+$ cross section in terms of that for $pp \to d\pi^+$ in a largely model-independent way [3].

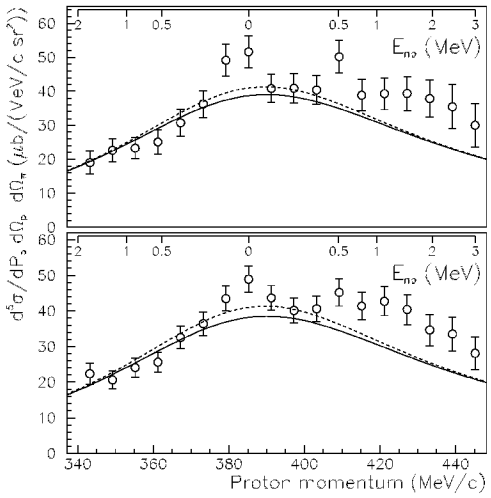

Fig. 2: Five-fold differential cross section for the $pp \to pn\pi^+$ reaction as a function of the measured proton momentum for events with $\theta_\pi \leq 2°$. The np excitation energy is indicated for protons and pions emitted at 0°. Figure a) is for $\theta_p \leq 2°$ and b) for $\theta_p \leq 2.5°$. The solid (dashed) curves correspond to predictions for the spin-triplet contribution to the fsi peak after (before) averaging over the resolution. The estimates are expected to be only weakly model-dependent [3]

The good agreement to the data of Fig. 2 given by this approach is consistent with our claim that any singlet contribution to the cross section is at most 10% and probably much smaller.

The ANKE spectrometer is capable of simultaneously measuring fsi effects in $pp \to pn\pi^+$ and $pp \to pp\pi^0$ at different beam energies which would give even a more direct measure of the small spin-singlet contribution to the final state.

References:

[1] V. Abaev et al., Phys. Lett. **B521** (2001) 158.
[2] G. Fäldt and C. Wilkin, Physica Scripta **56** (1997) 566.
[3] Yu.N. Uzikov and C. Wilkin, Phys. Lett. **B511** (2001) 191.

[a] PNPI, Gatchina; [b] IKP, FZJ; [c] JINR, Dubna;
[d] HEPI TSU, Tbilisi; [e] UCL, London.
* Work supported by WTZ grant KAZ 99/001.

Luminosities in ANKE experiments with heavy nuclear targets

H.R.Koch

The A-dependence of proton induced subthreshold K^+-production was studied at ANKE in experiments with strip targets of C, Cu, Ag and Au [1]. It is expected that for targets of nuclear charge $Z \geq 6$ the lifetime of the circulating beam is limited by Coulomb-scattering. Scattering angles scale roughly with Z^2. Thus the luminostiy integrated over the beam life time should decrease with Z as $LT \equiv \int Ldt \sim 1/Z^2$. However in the ANKE experiments a weaker dependence was observed: $LT \sim 1/Z^{1.2}$ [2], suggesting that other particle-loss mechanisms contribute. In order to accomplish optimal accelerator conditions in future K^+, K^-experiments a better understanding of energy loss in the target is needed.

A rough estimation of LT can be obtained from integral formulae, which yield a Gaussian distribution of multiple scattering through small angles and the mean energy loss (Bethe-Bloch). The calculation shows that for the relevant COSY ring parameters and for a particle momentum acceptance of $\Delta p/p<0.3\%$ particle loss through energy degradation may occur for targets of $Z \leq 6$. Recently the energy loss induced by the ANKE H_2 clustertarget could be measured directly [3]. Beam life times deduced fom the integral formulae alone may differ significantly from reality as the tails of the probability distributions ($1/\theta^3$ for the scattering angle θ, $1/\Delta E^2$ for the energy losses ΔE) are not reproduced. In particular the coupling of transversal and longitudinal phase space is missing. Dispersion somewhere in the ring reduces the accepted transversal phase space. E.g. for a beam momentum shift dp/p=0.2%, a dispersion D=20m, and a free beam tube diameter of 120 mm the beam axis is shifted by 40 mm, which reduces for the x-acceptance to 1/9 of the value relevant for dp/p=0 particles.

More precise luminosities are obtained through MC simulations, in which the full probability distributions for energy loss and angular scattering for thin targets are reproduced. Starting from routines which were used in the design phase of ANKE for the study of the beam target interaction [4] a C program has been developed in which particle deflection by the target follows from the sum of elementary scattering processes. The Coulomb cross section is given by

$$\sigma_{Cb} = 4\pi \, (Z_1 \cdot Z_2 \cdot e^2 / p \cdot c \cdot \beta \cdot \alpha)^2$$

with Z_1, Z_2: nuclear charge numbers, p: particle momentum, β: particle velocity, α: atomic screening angle. Single scattering angles Θ are deduced from a random numbers RN (0<RN<1) through $\Theta = \alpha\sqrt{1/RN - 1}$ [5]. Energy loss is chosen according to the Landau distribution [6].

The calculations show, that for typical thin solid state targets (10 to 1000 $\mu g/cm^2$) LT is independent of target thickness and geometry. Therefore -for certain target and ring parameters- LT can be determined through MC calculations assuming a thin target of any geometry.

The following parameters were used for the heavy target luminosity calculations:

- beam energy: T=1 GeV
- beta functions at target: βx=4m, βy=5m
- transv. accept. of COSY: Ax=50, Ay=16π·mm·mrad
- figure of merit [4]: FM=1/(βx/Ax+βy/Ay)=2.5
- target thickness: 1mg/cm²
- injection: ring filled to transversal ring acceptance
- acceleration: beam emittance shrinks with 1/p
- momentum acceptance: $\Delta p/p$ = 0.1% or = 0.3%
- compens. of mean energy loss in target: ON or OFF

The ANKE experiments were made with a coasting beam. Thus energy loss was not compensated. Results of the calculations are given in table 1.

Target	Z	LT $cm^2/10^{20}$ dp/p=0.3% with dE compens.	LT · Z^2 $cm^2/10^{24}$ dp/p=0.3% with dE compens.	LT $cm^2/10^{20}$ dp/p=0.1% without dE compens.	LT · $Z^{1.2}$ $cm^2/10^{20}$ dp/p=0.1% without dE compens.
C	6	1130	4.1	270	2320
Cu	29	56	4.7	39	2220
Ag	47	25	5.5	19	1970
Au	79	9.8	6.1	8.4	1590

Tab. 1: Calculated integrated luminosities LT per circulating particle for the ring momentum acceptance dp/p=0.3% with compensation of the mean energy loss for each target crossing and for dp/p=0.1% without compensation of the mean energy loss.

LT changes roughly as expected for $Z \geq 6$, if the mean energy loss in the target is compensated (column 4). If energy loss is not compensated (coasting beam) and if the momentum acceptance of the storage ring is low (0.1%) luminosities are strongly reduced for Z=6 targets (factor of 4) and slightly reduced for Z=29 targets (factor of 1.4, column 5). The luminosity obtained with an Au-target is only reduced by a factor of 1.16. The observed Z-dependence of LT is roughly given by $Z^{-1.2}$ (column 6). The precise value of the exponent was not determined, because it has no physics relevance. It depends on COSY beam optics which probably will change in different beam experiments.

The conclusion of the present study is, that for experiments with coasting beam energy loss in the target must be taken into account for targets of $Z \leq 29$. In future experiments energy loss compensation should be applied, if maximum luminosity is desired.

References:

[1] M.Nekipelov et al., contribution to this Annual Report
[2] V. Koptev, preliminary analysis of ANKE data
[3] H.J.Stein, D.Prasuhn, Determination of Effective Target Thickness and Luminosity from Energy Loss at the ANKE Cluster Target, contribution to this Annual report
[4] H.R.Koch, Reaction Rates in Internal Solid State Targets, Proc. 105th International WE-Heraeus-Seminar on Hadronic Processes at Small Angles in Storage Rings (1993) 67
[5] H.O.Meyer, NIM B10/11 (1985) 342
[6] L.Landau, Journal of Physics 8 (1944) 201

Luminosity determination via pp elastic scattering for the ANKE beam time on a_0^+ production*

P. Fedorets[a], M. Büscher, V. Chernyshev[a], S. Dymov[b], V. Komarov[b], Yu. Uzikov[b]

Proton-proton elastic scattering was used for the determination of the luminosity, of the ANKE experiment on a_0^+ production at a beam energy of T=2.65 GeV with a H_2 cluster-jet target. Only those events were used for our analysis which were obtained on-line with a single forward-detector (FD) trigger. The corresponding efficiency (dead time) of the DAQ was taken into account. The events belonging to pp elastic scattering reaction were selected from momentum spectra obtained from the MWPC information in the region of $\theta = (5.5 - 9°)$ [1]. The background in pp peak was fitted and subtracted (see fig. 1). The background level in the pp peak was estimated as ≈10%. The acceptance from the azimuthal angle distribution is in a good agreement with the GEANT simulations [1](see Fig 2). The tracks were reconstructed with forward MWPCs (FD-MWPC 1 and 2).

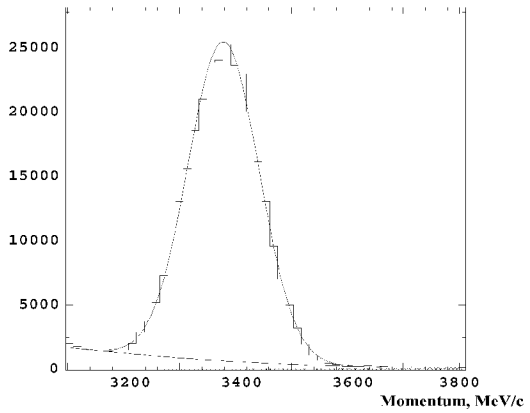

Fig. 1: pp-elastic momentum distribution after taking into accout the FD-MWPC efficiency.

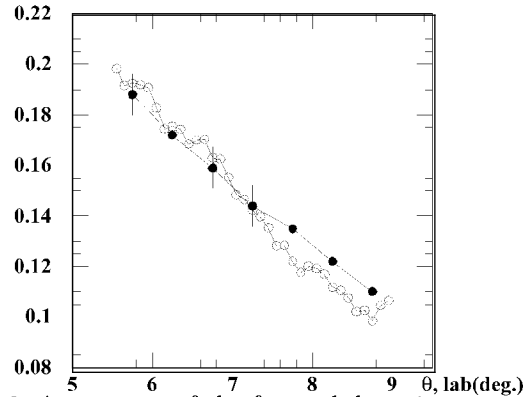

Fig. 2: Acceptance of the forward detection system for the pp elastic events. The solid circles are the acceptances from the azimuthal angle distribution, the empty circles are the acceptances from GEANT simulations.

The data were divided into three groups according to the monitor ratio criteria:

Run	monitor2/monitor3	Npp/trigger2 in
3276-3310	not stable	not stable
3311-3324	stable	not stable
3326-3369	stable	stable

The efficiency maps for these chambers were calculated [2] for each run. Figure 3 shows the average efficiency of the chambers 1 and 2 for the pp elastic events during the January 2001 beam time.

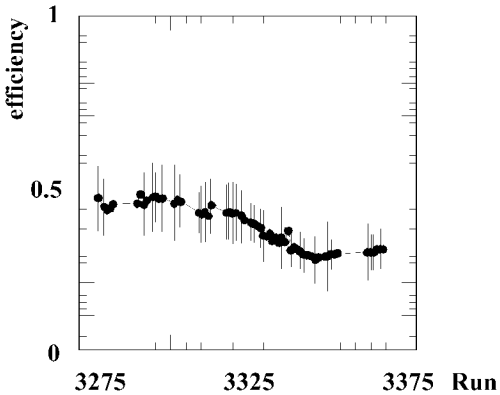

Fig. 3: FD-MWPC efficiency for the pp elastic events in the a_0^+ beam time

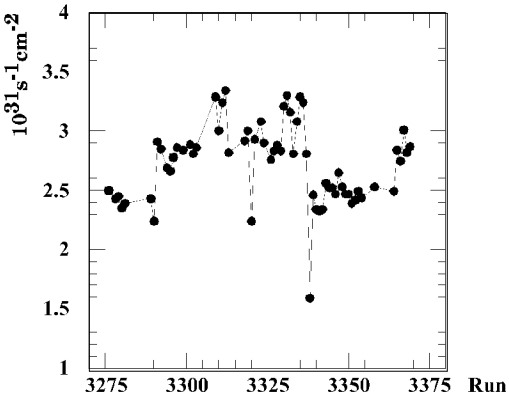

Fig. 4: Luminosity in the a_0^+ beam time

The luminosity was calculated for each run (see Fig. 4) and for all groups.

Run	luminosity ($10^{31}s^{-1}cm^{-2}$).
3276-3310	$2.73 \pm 0.55 \pm 0.55$
3311-3324	$2.95 \pm 0.6 \pm 0.55$
3326-3369	$2.69 \pm 0.55 \pm 0.55$

The first error contains all statistical uncertainties, while the second includes the systematical errors. The average luminosity for the a_0^+ beam time is $L = (2.70 \pm 0.55 \pm 0.55) \times 10^{31}$ $s^{-1}cm^{-2}$. A check of the luminosity determination procedure (including aceptance calculation and the chambers efficiency determination) can be done at lower beam energies where the $pp \to d\pi^+$ reaction is be compared with the pp elastic results [3].

References:

[1] S. Dymov et al.,"Luminosity estimation in a_0 January 2001 beam time."(internal report)

[2] S. Dymov,"Determination of the FD MWPC efficiency."(internal report)

[3] P. Fedorets et al.,"Test of the luminosity determination procedure for the ANKE beam time on a_0^+ production."contribution to this Annual Report,p

[a]ITEP, Moscow, Russia

[b]JINR, Dubna, Russia

Supported by grants RFFI99-02-18179a, DFG-443RUS-113, WTZ-RUS-684-99, RFFI99-0204034, INTAS-98-500, ISTC-1966

Test of the luminosity determination procedure for the ANKE beam time on a_0^+ production*.

P. Fedorets[a], M. Büscher, V. Chernyshev[a], S. Dymov[b], V. Komarov[b], Yu.Uzikov[b]

The average luminosity during the last a_0^+ beam time has been estimated using the pp elastic scattering reaction at T=2.65 GeV with one proton detected in the ANKE forward detector (FD). The value found is $L = (2.70 \pm 0.55 \pm 0.55) \times 10^{31}$ s^{-1}cm^{-2} [1]. It was proposed to test this method by comparing with the luminosity deduced from the reaction $pp \to d\pi^+$ at the same beam energy. However, this is not possible yet, because the two-track algorithm for the forward detection system is under development (both particles, d and π^+, must be detected in the ANKE forward detector at this beam energy). Therefore, the check of the pp elastic method was done at T=500 MeV (run 2864, September 2000 beam time), where for the reaction $pp \to d\pi^+$ only one particle (deuteron) is going into the forward detector.

At this energy all three reactions (pp elastic scattering, $pp \to$ d(forward)π^+, $pp \to$ d(backward)π^+) can be clearly separated using the energy-loss distributions in the forward hodoscope as a function of the particle momenta (Fig. 1).

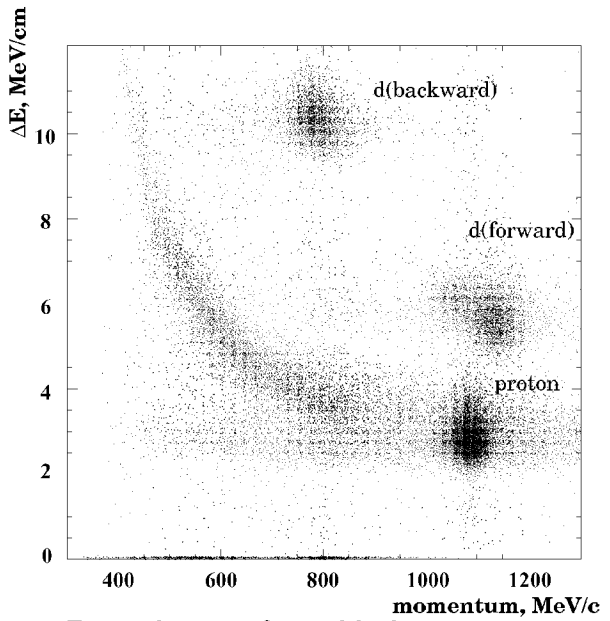

Fig. 1: Energy losses in forward hodoscope versus particle momentum at T=500 MeV

The background was subtracted using a fit of the momentum spectrum [1]. While the background level for the pp elastic events was ≈19%, this correction was less than 5% for the two branches of the $pp \to d\pi^+$ process. The acceptance for each process was calculated from the azimuthal angle distribution as function of the scattering angle θ. For the luminosity calculation we selected the region of θ where the acceptance changes smoothly. The accepted region of θ at 500 MeV for the pp elastic events was $\theta = (4.0{-}10.0°)$, for d(forward) $\theta = (4.5 - 10.0°)$, for d(back) $\theta = (1.0 - 7.5°)$. The kinematical limit for deuterons is $\theta_{max} = 10.7°$.

In the September 2000 beam time FD-MWPCs 1 and 2 were used for the track reconstruction. The FD-MWPCs efficiencies for each process were deduced for events with the corresponding energy losses in the forward hodoscope. It should be noted that the MWPC efficiency maps for the three different process are almost identical. The inefficiency of the forward hodoscope counters was neglected [2]. The cross sections at this beam energy were calculated with the SAID program. The DAQ inefficiency was taken into account.

The luminosity results for 500 MeV beam energy are:
$L = (0.49 \pm 0.08 \pm 0.08) \times 10^{30}$s^{-1}cm^{-2} for pp elastic;
$L = (0.45 \pm 0.08 \pm 0.08) \times 10^{30}$s^{-1}cm^{-2} for d(forward);
$L = (0.41 \pm 0.08 \pm 0.08) \times 10^{30}$s^{-1}cm^{-2} for d(backward).
Thus within errors the different reactions yield the same results for the luminosity, even if for a certain reaction (e.q. pp) a efficiency map of a different one (e.q. d(backward)) is used.

References:

[1] P.Fedorets et al.,"Luminosity determination via pp elastic scattering for the ANKE beam time on a_0^+ production."contribution to this Annual Report,p

[2] P.Fedorets et al.,"Efficiency of the second scintillator plane of the ANKE forward detector." contribution to this Annual Report,p

[a]ITEP, Moscow, Russia
[b]JINR, Dubna, Russia

Supported by grants RFFI99-02-18179a, DFG-443RUS-113, WTZ-RUS-684-99, RFFI99-0204034, INTAS-98-500, ISTC-1966

Determination of Effective Target Thickness and Luminosity from Beam Energy Losses at the ANKE Cluster Target

H.J. Stein, D. Prasuhn

The cluster target is one of the four targets in use or to be used at the ANKE spectrometer facility. It provides a 12 mm long and 5 mm wide beam of hydrogen or deuterium vertically crossing the p beam 300 mm in front of the D2 spectrometer magnet [1] The cluster target was first used in Sept. 1999. During the a_0 beamtime in Jan./Febr. 2001, the hydrogen cluster target operated with a very high particle density so that the energy loss of the p beam due to the beam-target interaction was measurable with good accuracy via the shift of the revolution frequency of the p beam.

This was possible because - at least up to now - ANKE experiments are using a coasting beam without stochastic cooling. Since the dispersion at the ANKE position can be minimized due to a special lattice setting, the p beam does not shift away from the target when the beam energy decreases. The beam intensity, however, may fall off after some time when emittance growth and dispersion in the arcs cause particle losses due to the acceptance limits. In the Sept. 2000 run the 1.97 GeV COSY beam could be used in one-hour cycles with only 5% beam losses. In the a_0 run in Febr. 2001 with 2.65 GeV beam energy the intensity started to decrease rapidly already after 5 to 6 min, an indication of very high target density [2]. The cycle time was therefore reduced to 5 min. Due to the sufficiently low vacuum pressure in the ring, mean value ~ 5 x 10^{-9} mbar, the beam losses with cluster beam off were not detectable. The operational status of the cluster target showed up in the vacuum pressure in the ANKE region, increasing from about 10^{-8} up to almost 10^{-6} mbar. The pressure rise is caused by hydrogen gas not completely trapped in the gas catcher. Since the pressure rise in the beam tube is extended over a distance of 10 to 20 m, its contribution to the energy loss has to be examined.

The shift Δf of the revolution frequency f_0 in the time interval Δt, detected by a Schottky pick-up and analyzed by a high-performance fast-Fourier transformer [3], is related to the momentum shift Δp and the energy loss ΔT by the two Eqs. (1). The energy loss dT per a single target traversal, divided by the stopping power and the mass of the proton, Eqs. (2), yield the number n of hydrogen atoms interacting with the proton beam.

$$\frac{\Delta p}{p_0} = \frac{1}{\eta}\frac{\Delta f}{f_0} \qquad \frac{\Delta T}{T_0} = \frac{1+\gamma}{\gamma}\frac{\Delta p}{p_0} \tag{1}$$

$$dT = \frac{\Delta T}{f_0 \Delta t} \qquad n = \frac{dT}{(dE/dx)m_P} \tag{2}$$

For the case considered here the following numbers apply:

T_0	= 2.650 GeV	the beam energy,
p_0	= 3.463 GeV/c	the beam momentum,
f_0	= 1.577 MHz	the revolution frequency,
η	= − 0.13	the measured slip factor
γ	= 3.82	the Lorentz factor,
dE/dx	= 4.1 MeV·cm^2·g^{-1}	the stopping power [5],
m_P	= 1.67 x 10^{-24} g	the proton mass.

It should be noted that due to the D = 0 setting in the straight sections COSY is operating above transition energy, T_{trans}= 1.3 GeV. Therefore, the slip factor η is negative and the frequency shift positive.

Figure 1 shows the frequency shift measured at different times during a 5 min cycle. The relation is linear yielding Δf = 198 Hz per 300 s and consequently n = 9.97 x 10^{14} atoms/cm^2.

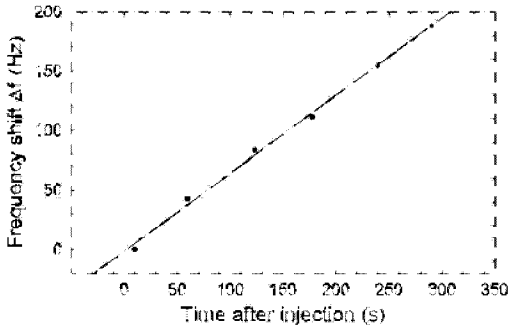

Fig. 1: Revolution frequency shift Δf due to energy loss of the p beam in the hydrogen cluster target at ANKE.

As a systematic correction one has to subtract the fraction of straying hydrogen atoms in the beam tube around ANKE. The estimate based on the measured pressure rise yields at most 10%. The 1σ statistical errors of the slope of the $\Delta f(t)$ relation and of η are 5%. dE/dx may also have 5% error. All other error contributions are negligible. The "effective " areal target density n_T is then given as:

$$n_T = (9 \pm 1) \text{ x } 10^{14} \text{ atoms/cm}^2$$

This value, also considering an incomplete beam-target overlap, is more than a factor of 10 higher then expected from earlier runs [1]. If the p beam current is known during the time period of the frequency shift measurement, one may obtain a rather reliable value for the luminosity because n_T contains only those target particles which do interact with the p beam, no matter whether there is a complete beam target overlap.

$$L = i_p \, n_T \tag{3}$$

In the 5 min period of the reported Δf measurement 3.1 x 10^{10} protons (i_p = 4.9 x 10^{16} p/s) where circulating in the COSY ring (ANKE Run No. 3217), resulting in a luminosity

$$L = (4.4 \pm 0.8) \text{ x } 10^{31} \text{ s}^{-1} \cdot \text{cm}^{-2}.$$

The practical application of this procedure in a long running experiment needs a continous recording and the evaluation of the p beam current and a typical target monitor rate in order to take into account p beam or target beam intensity variations.

References:

[1] H.-H. Adam et al., IKP Annual Report 1999, Jül-3744, p.20.
[2] H.J. Stein, ANKE Collaboration Meeting 2001.
[3] A. Schnase et al., IKP Annual Report 1997, Jül-3505, p. 188.
[4] Physical Reference Data, see http://physics.nist.gov.

Luminosity determination for the deuteron breakup experiment

S. Yaschenko[a,b], S. Dymov[†], A. Kacharava[a,c], V. Komarov[b], G. Macharashvili[b,c], A. Petrus[b], F. Rathmann, Yu. Uzikov[b,d]

During the *pd* breakup beam time (February 2001) experimental data were obtained with deuteron cluster target at incident proton beam energies of 600, 700, 800, 950, 1350, and 1900 MeV. The luminosity was calculated using *pd* forward scattering at low transferred momenta with one proton registered in the ANKE Forward Detector (FD).

The *pd* scattering cross section is composed of elastic and inelastic contributions. It is not possible to separate them experimentally in ANKE FD, due to the very similar kinematical parameters of forward scattered protons and the limited FD momentum and angular resolution. Therefore, theoretical calculations of differential cross sections were carried out [1] in Glauber-Sitenko diffraction theory approximation. The calculations are within 10% with existing experimental data.

The event selection of *pd* forward scattering was done among single track events in the data taken with FD trigger. (Multiple track events are rare.) For track reconstruction the first and third FD MWPC were used. The horizontal and vertical limitations of the track coordinate on the exit window of the D2 magnet and the FD scintillation counter were applied together with a vertical cut on the target position [2].

The particle type selection was done by particle mass calculated using energy losses in two planes of FD scintillation counters and the particle momentum. In Fig. 1a the particle mass in the first plane of the scintillation hodoscope is plotted vs the mass in the second plane.

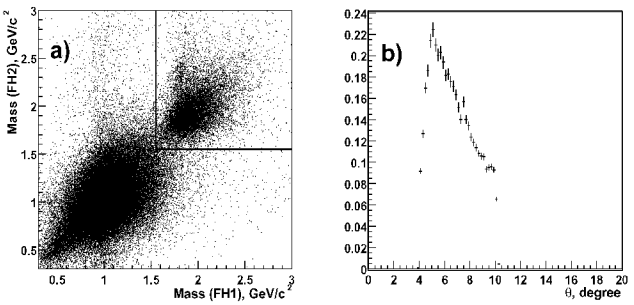

Fig. 1: Particle mass calculated from energy loss in the first layer of FD hodoscope vs mass calculated from energy loss in the second layer (a), FD angular acceptance (b).

After selection of protons from energy loss vs momentum for different polar angle intervals (1 degree bins) for $\theta_{lab} = 5 \ldots 10°$, the data were fitted by the sum of a gaussianand an inclinded line. Events were selected within 2σ from the fitted average momentum value. In Fig. 2a an example of such a fit is shown.

The determination of the efficiency of the FD MWPCs is described in [3]. For each event the track efficiency was calculated and a correction to the analyzed momentum was applied.

The FD acceptance was calculated using a GEANT-based simulation program. The events with *pd* elastic kinematics were generated within the polar angle range of $0 - 20$ degree of the forward emitted proton, with ϕ randomly distributed over 2π. The probability to hit the FD was obtained as a function of polar angle (Fig. 1b). The limiting values of θ coincide well with the experimental data.

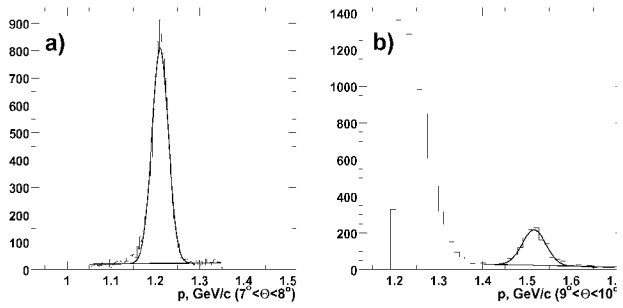

Fig. 2: Momentum distributions of protons from *pd* forward scattering (a) and deuterons from *pd* backward scattering (b).

The luminosity was calculated for individual polar angles. In Table 1 the mean values of the luminosity averaged over all angles is listed. The errors correspond to rms value. Errors of this type are one source of systematics. A second source is the accuracy of the theoretical calculation of the cross section, estimated to be $\approx 10\%$. The statistical errors are negligible in comparison with the systematic ones.

Table 1. The luminosity determined using *pd* forward and backward scattering.

T_p [MeV]	L_{forw} [cm^{-2}s^{-1}]	L_{back} [cm^{-2}s^{-1}]
600	$(0.540 \pm 0.030)\cdot 10^{30}$	$(0.45 \pm 0.09)\cdot 10^{30}$
700	$(0.298 \pm 0.017)\cdot 10^{30}$	$(0.30 \pm 0.06)\cdot 10^{30}$
800	$(0.350 \pm 0.015)\cdot 10^{30}$	$(0.34 \pm 0.07)\cdot 10^{30}$
950	$(0.305 \pm 0.010)\cdot 10^{30}$	
1350	$(0.399 \pm 0.010)\cdot 10^{30}$	
1900	$(0.516 \pm 0.019)\cdot 10^{30}$	

The method was tested by comparing the results with the luminosity determined from the $pd \to dp$ process with the deuteron registered in the ANKE FD. After track and energy loss selection, clear peaks in the momentum spectra are seen for beam energies of 600, 700, and 800 MeV (Fig. 2b). Using existing experimental data [4] and calculations similar to those described in [5]. The luminosity was determined for these energies (third column of table 1). The results are in good agreement with results obtained from the *pd* forward scattering process.

References:

[1] Yu. Uzikov, ANKE Internal report, 2001.
[2] S. Dymov *et al.*, ANKE Internal report, 03.2001.
[3] S. Dymov, ANKE Internal report, 10.05.2001.
[4] E.T. Boschitz *et al.*, Phys. Rev. C**6**, 547 (1972); E. Winkelmann *et al.*, Phys. Rev. C**21**, 2535 (1980).
[5] Yu. Uzikov, Elem. Particl. and Nuclei, 29, 1405 (1998).

[a]Universität Erlangen.
[b]JINR, Dubna, Russia.
[c]HEPI TSU, Tbilisi, Georgia.
[e]Kazakh State University, Almaty, Kazakhstan.
[†]PhD student from[b].

Diffraction *pd*-scattering at COSY energies

Yu. Uzikov[a,b,*]

Diffraction theory of hadron-nucleus scattering at high energies (see [?] and references therein) is used here to calculate the cross section of *pd*-scattering in forward direction at energies 0.6–2.5 GeV. This cross section can be used to determine the luminosity in experiments with a deuteron target at ANKE, where for beam energies T_p =0.6–2.5 GeV the forward detector system registers protons with scattering angles of $\theta_{\rm cm} = 10^\circ - 20^\circ$.
The *pd*-scattering cross section $\mathrm{d}\sigma^{sc}/\mathrm{d}\Omega$ consists of elastic ($\mathrm{d}\sigma^{el}/\mathrm{d}\Omega$) and inelastic ($\mathrm{d}\sigma^{inel}/\mathrm{d}\Omega$) terms. The general expression for $\mathrm{d}\sigma^{sc}/\mathrm{d}\Omega$ was obtained in Ref. [?] in closure approximation, which includes the sum over the complete set of final *pn* states. Final-state pn-interaction (fsi) is properly taken into account in this approach. The cross sections $\mathrm{d}\sigma^{sc}/\mathrm{d}\Omega$ and $\mathrm{d}\sigma^{el}/\mathrm{d}\Omega$ are written in [?] in terms of the deuteron elastic form factor $S(q)$, the deuteron wave function $\phi(\mathbf{r})$ and the pN-scattering amplitudes $f_{pN}(\mathbf{q})$,

$$f_{pN}(\mathbf{q}) = \frac{k}{4\pi}\sigma_N(i+\alpha_N)\exp\left[-\frac{1}{2}\beta_N\, q^2\right], \qquad (1)$$

where σ_N, α_N and β_N are the parameters of the pN amplitude determined from the experimental data. The inelastic cross section can be calculated as

$$\frac{d\sigma^{inel}}{d\Omega} = \frac{d\sigma^{sc}}{d\Omega} - \frac{d\sigma^{el}}{d\Omega}\ . \qquad (2)$$

In the numerical calculations presented here we use for the deuteron nuclear density, (*i*) the one-gaussian approximation, (*ii*) the renormalized S-component of the Reid soft-core (RSC) wave function, and (*iii*) the three gaussian (ABB) form factor from Ref. [?]. The parameters of the pN-scattering amplitudes are taken from Ref. [?].

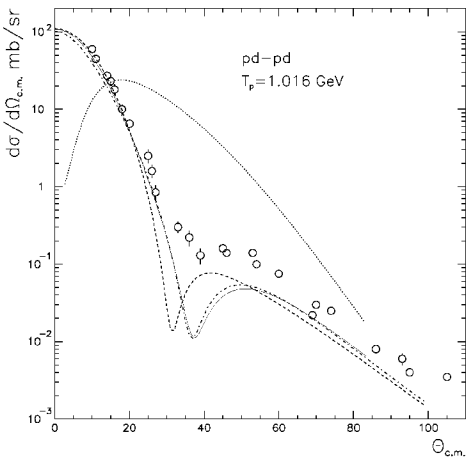

Fig. 1: Experimental data [?] on the elastic $pd \to pd$ cross section vs scattering angles $\theta_{\rm cm}$ at T_p = 1.016 GeV in comparison with those obtained from Glauber theory with (*i*) the one gaussian w.f. (dashed line), (*ii*) the renormalized S-wave RSC w.f. (dashed-dotted), and (*iii*) the ABB-formfactor from [?] (solid). The inelastic cross section calculated with the ABB form factor is shown by the dotted line.

Examples of the numerical results are shown in Figs. ?? and ??. The full set of calculated cross sections, covering the COSY beam energies, can be found elsewhere [?]. The calculated elastic cross section at c.m. scattering angles $\theta_{\rm cm}$<30° is in a good agreement with the data at energies available at COSY (Fig. ??). The experimental data on the inelastic cross section of *pd* scattering ($pd \to pnp$) at 0.95 GeV [?] are also in a reasonable agreement with the present calculation (Fig. ??). As shown in Fig. ??, the elastic and inelastic cross sections are comparable at scattering angles $\theta_{\rm cm} \sim 10^\circ - 20^\circ$. We found that the inelastic cross section from Eq. (2) coincides with that obtained on the basis of the approximation from Ref. [?]. According to an explicite formula

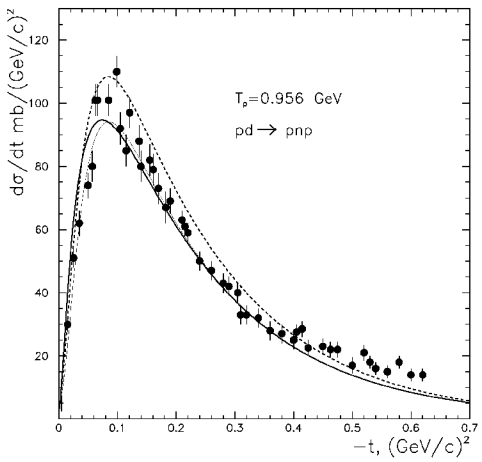

Fig. 2: Experimental data [?] on the inelastic $pd \to pnp$ cross section at T_p = 0.956 GeV in comparison with the Glauber calculations using (*i*) the RSC form factor (full thick), (*ii*) the ABB form factor (full thin), and (*iii*) according to approximation from [?] with the ABB formfactor [?] (dashed).

for $\mathrm{d}\sigma^{inel}/\mathrm{d}\Omega$ from Ref. [?], the inelastic cross section vanishes at zero transferred momentum due to orthogonality of the deuteron bound state and the *pn*-scattering wave function in the spin-triplet state. This feature is not taken into account in the Born approximation (or spectator model), which leads to a wrong result in the fsi region.

References:

[1] V. Franco, R.J. Glauber, Phys. Rev. **142**, 1195 (1966).
[2] B.S. Aladashvili et al., J. Phys. G **3**, 1 (1977).
[3] Particle Data Group Report, UCRL 20000 NN, (1979).
[4] G.W. Bennet et al., Phys. Rev. Lett. **19** , 387 (1967).
[5] Yu. Uzikov *et al.*, FZJ report, in preparation.

[a]JINR, Dubna, Russia.
[b]Kazakh State University, Almaty, Kazakhstan.
*Supported by BMBF (WTZ grant KAZ 99/001).

Beam Properties of the ANKE Atomic Beam Source

M. Mikirtytchiants[1], R. Emmerich[2], R. Engels[2], H. Kleines[3], V. Koptev[4], P. Kravtsov[4], J. Ley[2], B. Lorentz, S. Lorenz[5], M. Nekipelov[1], V. Nelyubin[4], H. Paetz gen. Schieck[2], F. Rathmann, J. Sarkadi[3], H. Seyfarth, E. Steffens[5], H. Ströher, A. Vassiliev[4], K. Zwoll[3]

The polarized atomic beam source (ABS) [1] will be utilized in future experiments at the magnetic spectrometer ANKE to feed a storage cell gas target.

Investigations of the polarized atomic beam intensity have been carried out under various conditions using a compression tube located such as to match the position of the storage cell feeding tube (10 mm diameter, 100 mm length) in future experiments. The obtained absolute beam intensity as a function of the nozzle temperature is shown in Fig. 1. The maximum of $(6.9 \pm 0.3) \cdot 10^{16}$ H atoms per second is achieved around 72 K at primary H_2 flow of 1 mbar·l/s, O_2 admixture of 0.1% and 300 W dissociator power. The measured slope is reproduced well by the result of a trajectory calculations [5], which assumed a constant degree of dissociation, verified through earlier measurements. The discrepancy at lower temperatures may be explained by increasing intra-beam and rest-gas scattering, which is not taken into account in the simulations. The present results are compared with the maximum intensities given for the sources operated at HERMES (DESY) [2], PINTEX (IUCF) [3], and the polarized ion source at tandem accelerator in Munich, Germany [4]. In addition to the absolute beam intensity the atomic

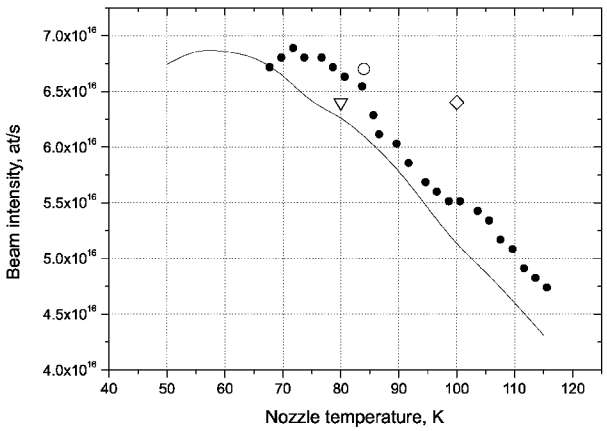

Fig. 1: Absolute beam intensity as a function of the nozzle temperature. For comparison, data from the HERMES ABS (◇) and PINTEX (○) ABS and Munich ion source (▽) are shown on the figure. The solid line represents results of simulations (scaled).

beam profile has been measured. These studies were carried out with a compression tube of 5 mm diameter and 50 mm length at two positions: 300 mm (1) and 337 mm (2) behind the last magnet. Figure 2 shows the *xy*-distribution of the pressure in the compression volume measured 300 mm behind the last magnet. Both measured distributions (1) and (2) can be reproduced by assuming gaussian beam profiles with $\sigma_1 = 2.85 \pm 0.42$ mm and $\sigma_2 = 2.95 \pm 0.43$ mm, respectively.

A medium and a weak field rf-transition unit (MFT, WFT) have been designed and built at the University of Erlangen [6]. The MFT is currently being tested and an efficiency of 0.90 ± 0.05 has been measured for the 2-3 transition with the compression tube.

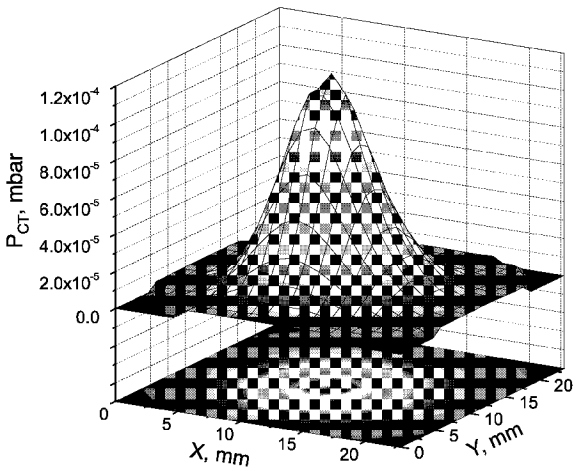

Fig. 2: *xy*-distribution of the pressure in the compression volume measured with a narrow (5 mm diameter) compression tube 300 mm behind the last magnet.

For future experiments at COSY with polarized internal targets a Lamb-shift polarimeter has been designed, built and tested at the University of Cologne [7]. In order to complete the commissioning of the polarimeter with a polarized beam, it has been installed at the ABS. Measurements of the nuclear polarization of the atomic hydrogen beam, produced by the MFT unit, yield a value of $P_z = 0.889 \pm 0.009$. A first measurement of the vector and tensor polarization of the deuterium beam has been performed.

The work was supported by BMBF (contracts RUS 99/686 and 06 ER 831), by DFG (contract 436 RUS 113/430), by FZ Jülich (FFE, contract 41149451), and by the Russian Ministry of Sciences.

References:

[1] R. Emmerich *et al*, Annual Report IKP and COSY 2000, report Jül-3852, p.32
[2] J. Stewart *et al*, AIP Conf. Proc. **421**, 69 (1998).
[3] F. Rathmann *et al*, AIP Conf. Proc. **421**, 89 (1998).
[4] R. Hertenberger *et al*, Proc. 8th Int. Workshop on Polarized Sources and Targets (PST99), Erlangen, 1999. Edt. A. Gute, S. Lorenz, E. Steffens (Universität Erlangen-Nürnberg, 1999) , p. 52.
[5] Based on a code obtained from D. Toporkov, BINP Novosibirsk.
[6] S. Lorenz, Diploma thesis, Universität Erlangen-Nürnberg (1999).
[7] R. Engels, PhD thesis, Universität zu Köln, (2002); contribution to the present report.

[1] PhD student from Petersburg Nuclear Physics Institute, 188300 Gatchina, Russia
[2] Universität zu Köln, 50937 Köln, Germany
[3] Zentrallabor für Elektronik, FZ Jülich
[4] Petersburg Nuclear Physics Institute, 188300 Gatchina, Russia
[5] Friedrich-Alexander-Universität, 91058 Erlangen, Germany

The Lamb-shift Polarimeter for the Polarized Gas Target at ANKE

R. Engels[a], R. Emmerich[a], P. Kravtsov[b], J. Ley[a], M. Mikirtytchiants, H. Paetz gen. Schieck[a], F. Rathmann, H. Seyfarth, A. Vassiliev[b]

The Lamb-shift polarimeter [1] was tested with an unpolarized beam of protons and deuterons at the University of Cologne and, since the beginning of 2001, at the Forschungszentrum Jülich with the polarized atomic hydrogen and deuterium beams from the atomic beam source of the polarized gas target for ANKE [2].

The polarimeter is based on measuring the ratios of Lyman-α transition intensities after Stark quenching of spinfilter selected Zeeman hyperfine states (HFS). The nuclear polarization of the atomic beam is deduced by applying a series of correction factors. For the polarized beam these values could be determined by varying the operating conditions:

1. Unpolarized protons from the residual gas in the ionizer reduce the measured peak ratios. The correspondig correction factor k_1 is ~ 1.005.

2. The same effect by unpolarized protons, produced from recombined H_2 molecules in the ionizer results in a correction factor $k_2 \sim 1.095$.

3. The magnetic flux density in the ionizer is $B = 133\,\mathrm{mT} = 2.6 \cdot B_{\mathrm{crit.}}$. Thus the conservation of the polarization is only 93.5% for the Zeeman states 2 and 4 ($k_3 = 1.07$).

4. The magnetic field in the Wienfilter is not perfectly homogeneous. Therefore the spin rotation is not the same for different trajectories of the protons ($k_4 = 1.008$).

5. The magnetic flux density in the Cs cell is B= 55 mT=9 $\cdot$ $B_{crit.}$ resulting in $k_5 = 1.005$ for all metastable Zeeman states.

6. The transmission of the metastable atoms through the spinfilter is not the same for the different Zeeman states ($k_6 = 1.002$ for HFS 2/3 and $k_5 = 0.998$ for HFS 1/4)

The total correction factor amounts to between 1.1 and 1.2 depending on the occupation numbers of the hyperfine states.

The nuclear polarization of atomic beams of hydrogen (Fig. 1) and deuterium (Fig. 2) is determined with an accuracy of $\leq 1\%$ within a few seconds for beams of $\sim 3 \cdot 10^{16}$ atoms/s in one hyperfine state. Its error is dominated by the systematic errors of the various correction factors and will be lowered to $\approx 0.5\%$ using a recently developed new ionizer.

The sensitivity of the polarimeter is such that even for a beam intensity reduced to 10%, the polarization could be determined reliably. The new ionizer will lower this sensitivity limit to $\leq 3\% \doteq 10^{15}$ atoms/s. With this sensitivity it appears feasible to measure the polarization in the planned storage cell of ANKE by extracting a small fraction of the atoms.

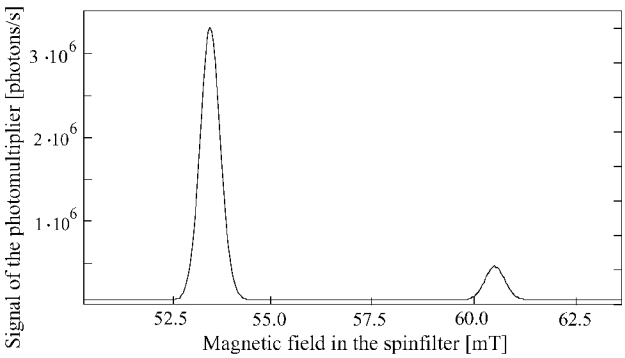

Fig. 1: Lyman-α spectrum of a polarized hydrogen beam. The polarization of the atomic beam was $p_z = 0.889 \pm 0.009$.

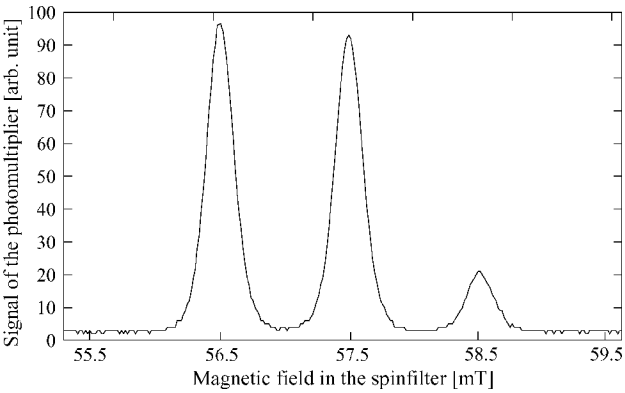

Fig. 2: First Lyman-α spectrum of a polarized deuteron beam measured with a preliminary setup.

In an ISTC-project the Lamb-shift polarimeter will be used to measure the polarization of H_2 and D_2 molecules after the recombination of polarized atoms in a storage cell [3].

References:

[1] R. Engels, *Entwicklung eines universellen Lamb-shift-Polarimeters für polarisierte Atomstrahl-Targets wie an ANKE/COSY*, PhD thesis, Universität zu Köln (2002).
[2] R. Emmerich et al., contribution to this report.
[3] H. Seyfarth et al., contribution to this report.

[a] Institut für Kernphysik, Universität zu Köln, Zülpicher Str. 77, D-50937 Köln
[b] High Energy Physics Dept., St. Petersburg Nucl. Physics Inst., 188350 Gatchina, Russia

Nuclear Polarization of Hydrogen Molecules from Recombination of Polarized Atoms

T. Wise[a], J. T. Balewski[b], J. Doskow[b], W. Haeberli[a], B. Lorentz, H. O. Meyer[b], P. V. Pancella[c], R. E. Pollock[b], B. v. Przewoski[b], P.A. Quin[a], F. Rathmann, T. Rinckel[b], Swapan K. Saha[d], B. Schwartz[a], T. G. Walker[a], A. Wellinghausen[b]

The question to what extent the nuclear polarization of atoms is preserved after recombination is interesting. A recent measurement with deuterium [1] reported that molecules partially retain the tensor polarization of the atoms (fraction polarization retained = 0.81 ±0.31). The present report is about a first measurement with H atoms, carried out by PINTEX at IUCF [2]. The idea of the experiment is to compare the nuclear polarization P_{at} of atoms from an atomic beam source to the nuclear polarization P_{mol} of molecules when the atoms are allowed to recombine on a copper surface. The nuclear polarization is measured by passing a 203 MeV polarized proton beam through a target cell (Fig. 1) containing the gas to be analyzed. The beam of polarized H atoms (state 1, m_J = 1/2, m_J= 1/2) enters a recombination cell through a tapered entrance tube. In the recombiner, which is made of copper, atoms encounter enough wall collisions to lead to almost complete recombination. The H_2 molecules diffuse out of the recombiner into a thin-walled Al target cell through which the proton beam passes. The recombination cell is separated from the target cell by a remotely operated valve. To measure P_{at} the valve is closed, in which case the atoms from the polarized beam source diffuse into the target cell with negligible loss in polarization, because they encounter only the Teflon-coated surfaces of the recombiner valve and the target and entrance tubes, which are known to strongly inhibit depolarization and recombination. The present measurements determine the polarization P_{mol} of the H_2 molecules, relative to the polarization of the atoms before recombination, $R = P_{mol}/P_{at}$. The magnetic field is provided by a superconducting coil (Fig. 1) which produces fields up to 0.66 T at the recombiner. Thus the available field is large compared to the critical field of the hyperfine interaction in H of 50.7 mT. To avoid the large distortion of the proton closed orbit that a transverse B-field would have entailed, B was chosen longitudinal (z-direction). Forward wire chambers and scintillators detected protons from pp elastic scattering at lab angles in the range 30° - 60°. Event identification depended on detection of two protons in coincidence, with the requirement that they be coplanar. Parity conservation requires the longitudinal analyzing power to be zero. Consequently, to measure the longitudinal target polarization, one needs to resort to a spin correlation measurement (polarized beam *and* polarized target) . The number of observed pp coincidences for longitudinal beam polarization p and target polarization P can be written as $Y = kt(\alpha)[1 + pPA_{zz}(\theta)]$ where the dependence of Y on proton beam current was removed by dividing the observed number of counts by the integrated beam current obtained from a current transformer. In the above equation, target polarization P stands for either P_{open} or P_{closed}, depending on whether the recombiner valve is open or closed, and the constant k contains factors like the pp cross section and detector efficiencies. The spin correlation coefficient A_{zz} [3] is near 1 in the vicinity of θ_{lab} =45°. Exact values of p and A_{zz} are unimportant here because they cancel in the ratio P_{open} / P_{closed}. The target thickness $t(\alpha)$ is a function of the degree of dissociation of the target gas because the conductance depends on the mass of the target particles.

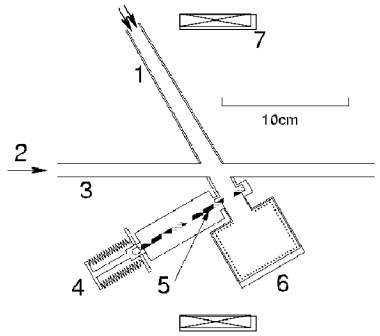

Fig. 1: Schematic scale drawing of recombiner volume and target cell. (1) tapered Teflon-coated entrance tube for polarized H atoms; (2) 203 MeV proton beam; (3) Teflon-coated Al target cell; (4) pneumatic valve actuator; (5) Teflon valve; (6) copper recombiner; (7) superconducting current loop. Figure from ref. [2].

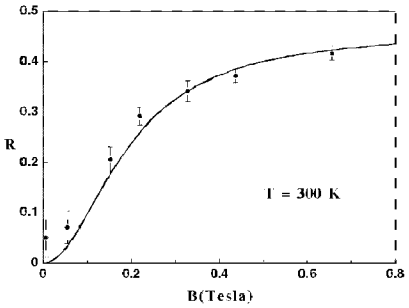

Fig. 2: Fraction R of proton polarization of the H atoms that is retained in the H_2 molecules after recombination on a room temperature copper surface in a magnetic field B. The error bars are probable errors that include the uncertainty from statistics as well as the systematic uncertainty from the incomplete knowledge of α_{open} and α_{closed} (see text).

The fraction R of polarization retained in the molecules shows a strong dependence on magnetic field B applied to the recombiner and target cell (Fig. 2). As the magnetic field is varied from 5 mT to 0.66 T, the nuclear polarization retained by the molecules rises from near zero to R = 0.42 ±0.02.

References:

[1] J. F. J. van den Brand *et al.*, Phys. Rev. Lett. **78**, 1235(1996).
[2] T. Wise *et al.*, Phys. Rev. Lett. **87**, 042701 (2001).
[3] B. Lorentz *et al.*, Phys. Rev. C **61**, 54002(2000).

[a]University of Wisconsin–Madison, WI 53706; [b]Indiana University Cyclotron Facility, Bloomington, IN 47405; [c]Department of Physics, Western Michigan University, Kalamazoo, MI 49008; [d]Department of Physics and Astronomy, University of Pittsburgh, Pittsburgh, PA 15260.

The Nuclear Polarization of Molecules from Recombined Polarized Hydrogen and Deuterium Gas Atoms – New Measurements in the Framework of an International Science and Technology Center Project

H. Seyfarth, R. Engels[a], P. Kravtsov[b], B. Lorentz, M. Mikirtytchiants[c], H. Paetz gen. Schieck[a], F. Rathmann, H. Ströher, N. Tchernov[b,†,*], A. Vassiliev[b,††,*]

During the past decade, polarized atomic H and D gas targets have been successfully applied at storage rings. In order to increase the target thickness over that obtained with an atomic jet, the beam from a polarized atomic beam source is directed into an open storage-cell tube in which the atoms make several hundred collisions before they escape from the target tube [1]. However, a fraction of the polarized atoms recombines in the wall collisions. The nuclear polarization, of the molecules is not directly accessible with a Breit-Rabi polarimeter (as used at HERMES), only the polarization of the atoms extracted from the cell can be measured. In order to overcome the resulting systematic uncertainty in the total overall nuclear polarization of the target gas, in an earlier measurement [2] the nuclear tensor polarization in recombined D_2 molecules in spite of the high statistical uncertainty was found to be retained partially (fraction 0.81 ± 0.31). The nuclear polarization of recombined H_2 molecules was recently studied in a separate experiment [3, 4]. A high value has been found for a strong external magnetic holding field.

In the framework of an ISTC project [5, 6], additional investigations of polarized hydrogen and new studies of polarized deuterium molecules are being prepared. The scheme of the set-up, which is developed, built, and tested in Gatchina and then will be transferred to Jülich, is shown in

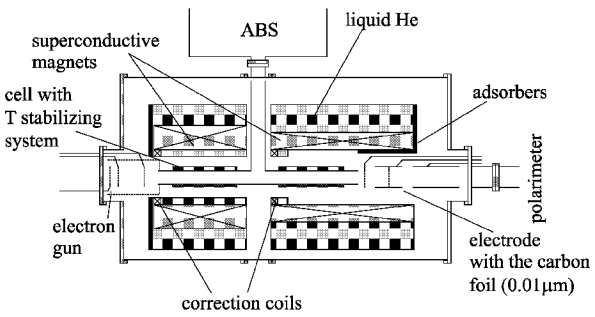

Fig. 1: Schematic drawing of the set-up, being developed in Gatchina in the framework of the ISTC project, in its position between the polarized atomic beam source and the Lamb-shift polarimeter after the transfer to Jülich.

Fig. 1. The storage cell will be fed by the H or D beam from the polarized atomic beam source (ABS, [7]), built for the polarized gas target of the ANKE/COSY spectrometer and to be used for the present studies between the beam times. Following a suggestion by W. Haeberli [8], $H(D)^+$ and $H(D)_2^-$ ions are produced from atoms and molecules in the storage-cell by electron bombardment, which are then accelerated to 50 keV a the strong longitudinal magnetic holding field (up to 5 T) onto a thin carbon foil. There, still in the strong field, the $H(D)_2^+$ ions are stripped, leaving two protons of 25 keV each, contrary to the protons from atomic hydrogen whose energy is 50 keV. Appropriate choice of the electric potentials of the electron gun, the cell, and the electrode supporting the carbon foil yields either protons from gas atoms or protons from gas molecules of 500 eV required for the analysis by the Lamb-shift polarimeter. In the first mode the protons from molecular dissociation cannot reach the polarimeter, in the second case the protons from atomic hydrogen of about 25 keV cross the polarimeter essentially without interaction in the Cs charge-exchange region of the Lamb-shift polarimeter. The polarimeter has been developed, built, and tested at the Universität zu Köln [9, 10]. For the final commissioning it has been installed at the polarized atomic beam source for ANKE.

The studies will focus the dependence of the nuclear polarization, maintained in the recombined molecules, on the cell-wall material and temperature and on the strength of the magnetic field on the cell. Effects from variation of the average number of wall collisions can be studied by changing of the cell dimensions. Most important will be to investigate the difference in the recombination process for $\vec{H}$ and $\vec{D}$. For hydrogen the lowest ortho-molecular state is the J=1 rotational state, whereas for deuterium it is the J=0 rotational ground state. The present status of the project is described in ref. [11].

The authors and all the members of the project group acknowledge the valuable help by G. Lincks and R. Wagner (FZ Jülich), by D. Gambier and H. Ihssen (European Commission, Brussels), by G. Kulikov and U. Meyer (ISTC Moscow) in establishing and starting the project).

References:

[1] W. Haeberli, in: Free and Stored Beams as Internal Targets, AIP Conf. Proc. **128** (AIP, New York, 1984), p. 251.
[2] J.F.J. van den Brand et al., Phys. Rev. Lett. **78**, 1235 (1997).
[3] T. Wise et al., Phys. Rev. Lett. **87**, 042701 (2001).
[4] T. Wise et al., contribution to the present report.
[5] International Science and Technology Center, project no. 1861.
[6] Information to the ISTC initiative is found under www.istc.ru.
[7] M. Mikirtytchiants et al., contr. to the present report.
[8] Private communication.
[9] R. Engels, PhD thesis, Universität zu Köln (2002).
[10] R. Engels et al., contribution to the present report.
[11] Internal report on the 3rd project meeting December 19 and 20, 2001. Available from the ANKE ABS group.

[a] Institut für Kernphysik, Universität zu Köln, 50937 Köln, Germany
[b] High Energy Physics Department, St. Petersburg Nuclear Physics Institute (PNPI), 188300 Gatchina, Russia
[c] PhD student from PNPI
[†] Leading Manager of the ISTC project
[††] Scientific Leader of the ISTC project
[*] The names (N.T., A.V.) stand for a group of about 25 scientists and technicians working for the project in Gatchina

Hydrogen droplet production with the ANKE pellet target*

V. Balanutsa[1], W. Borgs, M. Büscher, A. Bukharov[2], V. Chernetsky[1], V. Chernyshev[1], M. Chumakov[1], P. Fedorets[1],A. Gerasimov[1], V. Goryachev[1], L. Gusev[1], Z. Khorguashvili[3] and S. Podchasky[1]

The main goal of the pellet-target activities during the year 2001 was to achieve stable production of liquid hydrogen jets and to break up these jets into micro-droplets of about 50 μm diameter by acoustical excitation. First attempts into this direction were made already in the beginning of 2000 at ITEP, and short-term injection of hydrogen jets into the target cryostat [1] was achieved [2]. These results could be reproduced in Nov. 2000 and in the beginning of 2001, during test runs with the target cryostat at the test setup in the COSY hall. During the first tests short pulses of hydrogen jets and, consequently, only the production of single droplets was observed. It was concluded that adequate temperature and pressure conditions inside the triple-point chamber (TPC), needed for the production of hydrogen droplets, were reached, but that the stability of those parameters was insufficient. These problems could be solved in May and Dec. 2001, and stable production of hydrogen jets was achieved. Simultaneously, a sonic generator for the breakup of the jets into droplets was tested.
Both, the cryogenic nozzle for jet production as well as the sonic generator were developed and tested at MPEI. These tests were performed with water instead of hydrogen: it is expected that hydrogen jets can be broken into droplets at the same generator power since the surface tension of hydrogen is lower than that of water. Our test confirmed this expectation and it could be shown that droplet formation from water and hydrogen takes place under similar conditions. The operation frequency during all tests was around 3 kHz.
For the test runs with hydrogen a nozzle having an injection hole of 60 μm diameter was used. Fig. 1 shows the break-up of the hydrogen jet into droplets of $\sim$ 70 μm diameter. Stable droplet production, as shown in the figure, was achieved over long time periods of several hours. From the picture the jet and droplet velocities can be estimated. The former depends on the pressure in the supply channel for the liquid hydrogen. In order to decrease the distance between individual droplets, the generator frequency must be increased (and, simultaneously, to guarantee stable droplet produciton the jet velocity). Systematical investigations of frequency and velocity boundary conditions for stable droplet production are foreseen for future tests. During the test runs in Dec. 2001 it could also be verified that with the existing target cryostat it will be possible to produce droplets of liquid nitrogen.
In order to achieve stable hydrogen-jet production the temperatures and pressures inside the cryostat must be stabilized on a level of not worse than 5%. New temperature and pressure control systems have been developed for this purpose. Currently, the temperatures are measured at 8 points with silicon diode sensors DT-470 and DT-471 (Cryophysics). They provide an average accuracy for the temperature measurements of about 10 mK. The pressures are measured at 12 points with APR260, TPR260 and PKR250 sensors and MaxiGauge controllers (PFEIFFER). The data from all sensors can

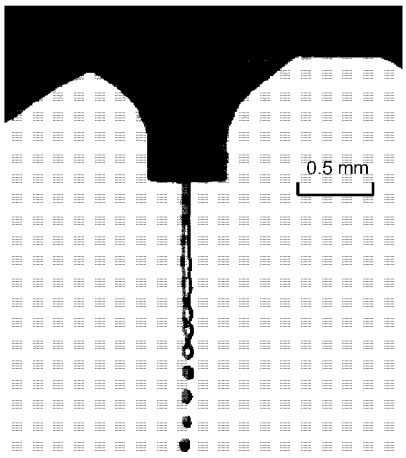

Fig. 1: Stroboscopic picture of liquid hydrogen-droplet production in the triple-point chamber (TPC) of the ANKE pellet target. The temperature (pressure) in the TPC were $T = 14$ K ($p = 100$ mbar).

be transfered to a PC-based visualizing system using LabView for further analyses.
During the year 2001 the target cryostat has been substantially modified. In order to decrease the temperature gradient along the gas condensation system a new, more effective, heat eschange head was installed. To allow for more precise measurements of the temperare and pressures, sensors were installed inside the heat exchange lines of the hydrogen and helium flows. This required to design and build special housings for the temperature sensors and of capillars for the pressure sensors. For a better control of the gas flows, low power heaters were installed in the hydrogen and helium supply lines.
The main tasks for the target development during the year 2002 will be:

- A fast, high-resolution diagnostic system will be installed allowing to measure the size and velocity of the produced droplets and/or pellets.
- Production of frozen pellets from the droplets.

References:

[1] A.Boukharov et al., Annual Report 1998 of the IKP, Berichte des Forschungszentrums Jülich, Jül-3505, p.63 (1998).
[2] V.Balanutsa et al., Annual Report 2000 of the IKP, Berichte des Forschungszentrums Jülich Jül-3852, p.34 (2001).

[1]ITEP, Moscow
[2]MPEI, Moscow
[3]IPH GAS, Tbilisi
*Supported by grants: RFFI99-02-18179a, RFFI99-0204034, DFG-443RUS-113, WTZ-RUS-684-99, INTAS-98-500, ISTC#1966

Study of liquid hydrogen jet properties close to triple-point conditions*

V. Balanutsa[1], W. Borgs, M. Büscher, A. Bukharov[2], V. Chernetsky[1], V. Chernyshev[1], M. Chumakov[1], P. Fedorets[1], A. Gerasimov[1], V. Goryachev[1], L. Gusev[1], Z. Khorguashvili[3] and S. Podchasky[1]

The goal of our measurements was a study of boundary conditions for stable hydrogen-jet production in the ANKE pellet target. The experiments were performed at the test set-up of the pellet target in May 2001. Jet modifications in dependence of pressure deviations from the triple-point value ($\sim$ 100 mb) were studied.

A photo camera and a strobe light source were used to observe the jet inside the triple-point chamber (TPC), with equal frequencies of the light source and the droplet generator. The liquid hydrogen jet was produced with a nozzle of 60 μm diameter[1]. During our measurements the jet velocity was stabilized at a level of about 1 m/s. To fix the gas temperature inside the TPC, the temperature of the nozzle and the liquid hydrogen channel were measured and stabilized with an accuracy of about 10 mK. The temperatures were measured with silicon diode sensors DT-470 (Cryophysics). One sensor was mounted at the nozzle, a second one was placed on the generator flange. The gas pressures were measured at 12 points of the target system with APR260, TPR260, PKR250 sensors and MaxiGage controllers (PFEIFFER). To stabilize the gas pressure, MKS pressure and flow control systems 640A, 641A, 1359C, 647 were used. The stabilization of the hydrogen flow and pressure during our tests was not worse than 5%.

A stable hydrogen jet is generated in the target chamber only close to triple point conditions, $T = 14$ K and $p =$ 100 mbar [1]. The jet is broken into droplets with the help of a sonic generator.

A pressure decrease to 85 mbar leads to unstable jet movements. The gas evaporation from the liquid surface increases and the skin of jet and droplets is cooled intensively. Thus, the jet position in the TPC is no longer stable and a part of the droplets freezes at the bottom of the TPC. If the pressure in the TPC is decreased further to 75 mbar, the surface of the jet is completely frozen, but a liquid jet is still moving inside the solid hydrogen. This process is shown in the upper photo of Fig. 1. Intuitively, this operation of the target has been called "macaroni mode".

The hydrogen jet freezes completely at a pressure of about 50 mbar and spontaneous growing of hydrogen icicles is observed. The onset of this process is shown in the lower photo.

The performed measurements and observations are very important for understanding of solid hydrogen pellet production processes from liquid droplets. These studies are progress at the ANKE pellet-target test setup.

References:

[1] V.Balanutsa et al., Contr. to this Ann.Rep., p.

[1]ITEP, Moscow
[2]MPEI, Moscow
[3]IPH GAS, Tbilisi

*Supported by grants: RFFI99-02-18179a, RFFI99-0204034, DFG-443RUS-113, WTZ-RUS-684-99, INTAS-98-500, ISTC#1966

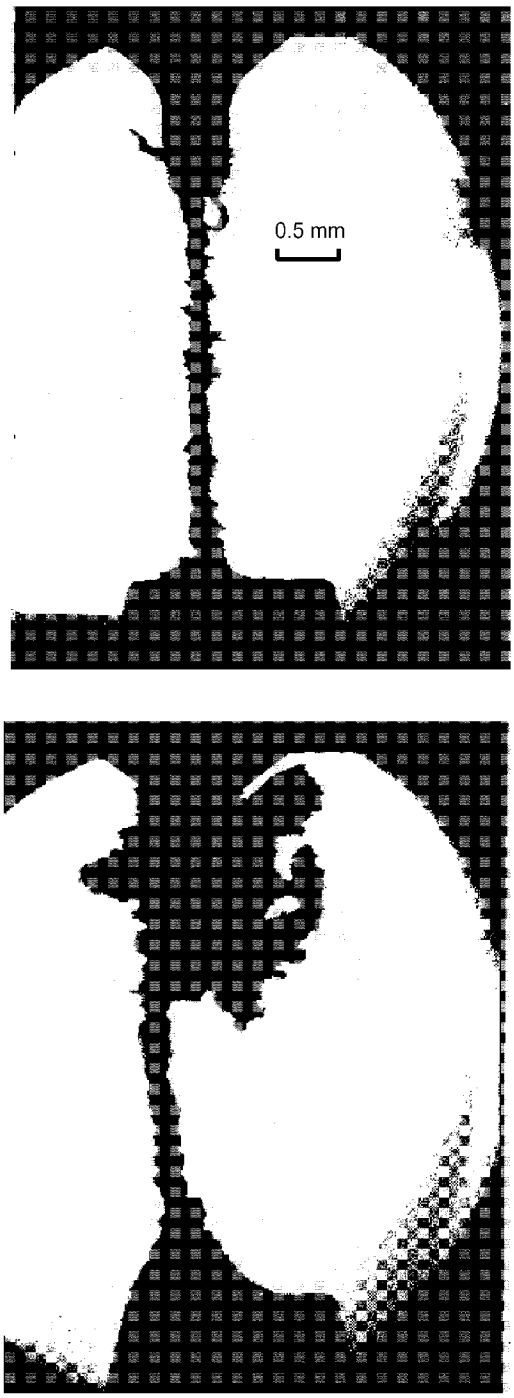

Fig. 1: Hydrogen-jet production in the TPC of the ANKE pellet target under different conditions. The surface of the hydrogen jet freezes at $T =$ 14 K and $p = 75$ mbar (upper photo). At $T =$ 14 K and $p = 50$ mbar spontaneous growing of hydrogen icicles is observed (lower).

The ANKE Silicon Spectator Tracker ASiST

S. Barsov[1], G. Fiori, T. Krings, I. Lehmann, S. Merzliakov[2], H. Metz, A. Mussgiller, D. Protic, R. Schleichert

The identification and tracking of low energy protons allows to use deuterium as an effective neutron target. Once the polarized **A**tomic **B**eam **S**ource ABS [1] will be installed at the ANKE spectrometer, also polarized proton-proton and proton-deuteron collisions can be studied. Especially the polarized deuteron gas of the ABS allows to study reactions of the type $\vec{p}\vec{n} \to pnX$ or $\vec{p}\vec{n} \to dX$.

For this purpose a vertex detector based on double-sided silicon strip detectors inside the vacuum of the COSY ring is under development [2]. Its barrel region will be based on modular silicon tracking telescopes that provide

- ΔE/E proton identification from 2.5 up to 40MeV. The telescope structure of 65/300/300/5500μm thick double-sided Si-strip detectors, read out by high dynamic range electronics [3], allows ΔE/E particle identification over a wide dynamic range.
- self-triggering capabilities. The telescopes identify a particle passage within ≤100ns and provide in combination with the self-triggering chips a fast hit pattern recognition [3].
- particle tracking over a wide range of energies, either 2.5MeV spectator protons or minimum ionizing particles.
- high rate capability with a read-out pitch of ~200μm.

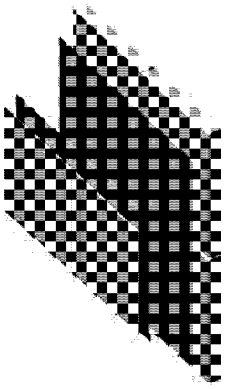

Fig. 1: The ASiST telescope arrangement of the double-sided silicon-strip detectors: Two 65μm thick detectors as inner layer, two and four 300μm thick detectors as middle layers[1] and four 5500μm thick Si(Li) detectors as outer layer. Protons will be tracked and identified from 2.5MeV up to 40MeV.

The basic detection concept of a telescope is to combine proton identification and particle tracking over a wide energy range. The tracking of particles is accomplished by the use of double-sided silicon strip detectors. Measuring the energy loss in the individual layers of the telescope allows to identify stopped particles by the ΔE/E method. The minimum energy of a proton to be tracked is given by the thickness of the most inner layer. It will be detected as soon as it punches through the inner layer with a minimum energy loss in the second layer. The maximum energy of protons to be identified is given by the range within the telescope and therefore by the total thickness of all detection layers. Especially the recent development of very thick (≥5mm) double-sided micro structured Si(Li) [4] and very thin (≤65μm) double-sided Si-detectors provides the use of the telescopes over a wide range of particle energies. The self-triggering capability of all detectors introduces the options to start a read-out on a particle passage and to set fast timing coincidences with other detector components of the ANKE spectrometer. Figure 1 shows the principle arrangement of the detectors within a single telescope.

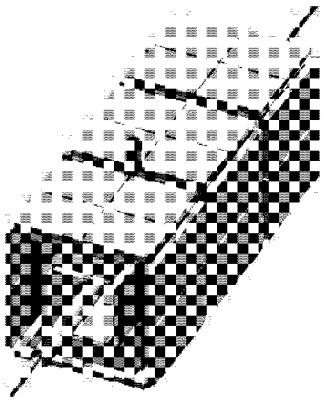

Fig. 2: 12 telescopes are arranged around the 40cm long storage cell of the polarized atomic beam source.

12 of these telescopes are foreseen to cover the barrel region of the ANKE vertex detector. Figure 2 shows a possible arrangement of these telescopes around a 40cm long ABS storage cell.

The assembly of the UHV compatible read-out boards for the ASiST telescopes is described in [5], first measurements are reported in [6]

References:

[1] M. Mikirtytchiants et al., *Beam Properties of the ANKE Atomic Beam Source*, contribution to this report.

[2] R. Schleichert et al., *Combined Spectator and Vertex Detection at ANKE*, Annual Report 2000 of the IKP, FZ-Juelich (2000), p.26.

[3] A. Mussgiller et al., *Evaluation of front-end Chips for Silicon Strip Detectors*, Annual Report 1999 of the IKP, FZ-Juelich (1999), p.31.

[4] D. Protic et al., *Development of Double-sided Microstructured Si(Li)-Detectors*, contribution to this report.

[5] L. Conin et al., *A Flexible Printed Board for the ASiST Chip Readout*, contribution to this report.

[6] A. Mussgiller et al., *Experimental Results from an ASiST Prototype*, contribution to this report.

[1] PNPI Gatchina, Russia

[2] JINR Dubna. Russia

[1] The 3rd layer is optional to guaranty redundancy in the case of multiple track events.

Current status of the photon-detector project for ANKE/COSY

V.Hejny, J.Bacelar[1], M.Büscher, V.Chernyshev[2], M.Hoek[3], H.R.Koch,
H.Löhner[1], H.Machner, A.Magiera[4], R.Novotny[3], H.Ströher, A.Wrońska[4]

In November 2000 the proposal for building a dedicated photon detector for COSY [1] has been accepted by PAC. Since the requirements on the setup are very stringent, various activities are currently going on in order to find the best suited components for this device.

Scintillator material

Although it became clear quite early that $PbWO_4$ is the only material, which meets our requirements in density and radiation length, it was questionable for some time whether crystals of the appropriate sizes could be manufactured in one piece. While the crystals for CMS at CERN are produced with cross sections of about 2x2cm^2, the very compact design for ANKE requires a pronounced trapezoidal cross section with an inner radius of - at least - 3.2x3.2cm^2 at the outer end surface of the detector ball (see below). This has been settled recently, when crystals with an even larger diameter have been grown at the Bogoroditsk Technical Chemical Plant (Russia) [2]. For further tests we already have received 18 crystals of size 12x3.2x3.2cm^2.

Photon sensors

The strength of the stray magnetic field of the ANKE dipole magnets in the target region has triggered the discussion whether Avalanche Photo Diodes can be used as it is done for CMS. This has been ruled out due to the available sizes and the problems concerning stability and high noise level. Therefore, the final solution will be based on fine-mesh photo tubes, most probably Hamamatsu R5505. However, there are also investigations on an equivalent type of multiplier produced in Russia.

The necessity of shielding the transverse component of the magnetic field (with respect to the photomultiplier axis) requires the use of shielding tubes (see fig. 1). While initial tests at ANKE have already shown that soft-iron tubes with a wall thickness of 3mm are sufficient, more detailed studies and optimisation have started recently at ITEP, Moscow. The size of the shielding tubes will finally determine the geometry of the crystals.

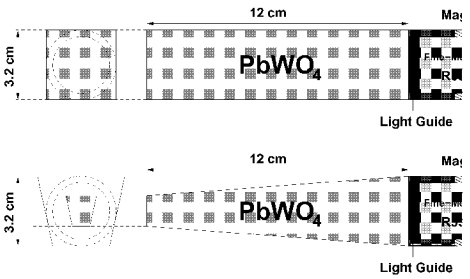

Fig. 1: Tentative geometry of one test module including crystal, photo tube and high-voltage base (upper part). As discussed in the text a light guide might be added between photo tube and crystal. Rather than quadratic, the final setup will have a trapezoidal cross section and, in addition, the crystals will be tilted (lower part).

In the final layout the tubes have to extend the photo cathode by at least a few millimeters to provide a proper shielding of the magnetic field. This problem has been solved, for example, in the TAPS spectrometer by using BaF_2 crystals with a cylindrical endcap. Unfortunately, the mechanical properties of $PbWO_4$ do not allow processing to have a cylindrical extension on the backward end of each crystal. Therefore a thin light guide between multiplier and crystal is forseen as shown in Fig. 1.

Concerning high-voltage dividers for photomultipliers, systems from two different companies are under investigation: *iseg Spezialelektronik GmbH, Rossendorf*, and *HVSys, Dubna, Russia*. Those made by HVSys are in use at the WASA detector at CELSIUS/Uppsala. Both systems provide active high-voltage generation in the base by means of Cockroft-Walton devices and remote control over serial lines. Currently, conditions for the production of prototypes are discussed.

Further activities

In summer 2001 the particle response of $PbWO_4$ has been tested at COSY using a secondary target behind the TOF setup. Results are presented in [3].

One reaction, which was proposed to be measured with the photon detector at ANKE, is charge symmetry breaking in $dd \rightarrow {}^4He\pi^0$ [1]. A proposal to measure $dd \rightarrow {}^4He\eta$ at ANKE will be prepared for the PAC in April 2002 [4]. Besides the physics output this experiment will give us the opportunity to study the background conditions for the π^0 measurement.

Currently, the 18 crystals are assembled in the University of Gießen in 2 separate arrays (3x3 modules each) using Hamamatsu R5505 photo tubes and magnetic shieldings. One of the test arrays will include light guides to test the feasibility of such a design. The arrays will be tested first at the tagged photon facility of the electron accelerator MAMI (University of Mainz) to check the response function and energy resolution of the complete setup (January 2002). The next step will be a parasitic test in the experimental environment of ANKE during one of the beam times in 2002.

References:

[1] M. Büscher et al., COSY Proposal #83: A photon detector for COSY, November 2000.
[2] M. Korzhik, Institute for Nuclear Problems, Minsk, private communication.
[3] M. Hoek et al., "Detection of charged particles with $PbWO_4$", contribution to this Annual Report.
[4] A. Wrońska et al., "Simulation of the $dd \rightarrow \alpha\eta$ reaction at ANKE", contribution to this Annual Report.

[1]Kernfysisch Versneller Instituut, Groningen, The Netherlands
[2]Institute of Theoretical and Experimental Physics, Moscow, Russia
[3]II. Physikalisches Institut, Universität Gießen, Germany
[4]Institute of Physics, Jagellonian University, Cracow, Poland

Detection of charged particles with $PbWO_4$

M.Hoek[1], V.Hejny, R.Novotny[1], K.Römer[1]

As part of the development for the Photon Ball at ANKE the response of $PbWO_4$ (PWO) to charged particles has been investigated. In a parasitic experiment behind the TOF experiment at COSY an external proton beam of 1.2 GeV kinetic energy was hitting an aluminum target. Elastically and inelastically scattered protons as well as charged secondary reaction products were detected with a PWO-matrix comprising 25 individual crystals, which was set up in a distance of 2.9 m behind a start-detector for particle identification via time-of-flight measurement. The detector system was positioned at a scattering angle of $\approx 8°$ with respect to the beam axis (see Fig. 1). For each module, which is individually read-out with a photomultiplier tube, time and energy information were recorded. In addition, cosmic rays were detected to provide a relative energy calibration. The required trigger of the start counter, a fast plastic scintillator, excluded automatically neutral particle events.

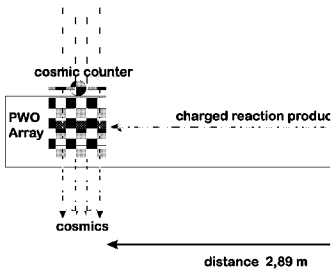

Fig. 1: The experimental set-up.

The absolute energy calibration relies on the position of the minimum ionizing peak caused by fast protons. The absolute value of 160 MeV was taken from GEANT3 simulations. The time-of flight was calibrated via the known geometry and particle kinematics. The charged particle identification was based on the correlation between time-of-flight and kinetic energy, which holds true for all particles being completely stopped in the crystal (length 15 cm).
As shown in Fig. 2, protons, deuterons, pions and kaons are distinctly separated. For protons with kinetic energies up to 365 MeV, which deposit their energy completely within the PWO-matrix, an energy resolution of

$$\left(\frac{\sigma}{E}\right)_{proton} = \left(\frac{(0.9 \pm 0.2)}{\sqrt{E\,/\,GeV}} + (3.7 \pm 0.6)\right)\%$$

was extracted.
The results between 50 MeV and 250 MeV are comparable to previous measurements carried out with the same PWO-matrix at MAMI (Mainz) detecting electromagnetic showers due to photons up to 850 MeV [1] as illustrated in Fig. 3.
These results, obtained for the first time, establish the applicability of PWO even as charged particle detector in the medium-energy regime. However, fig. 2 indicates a strong discrepancy of the energy calibration

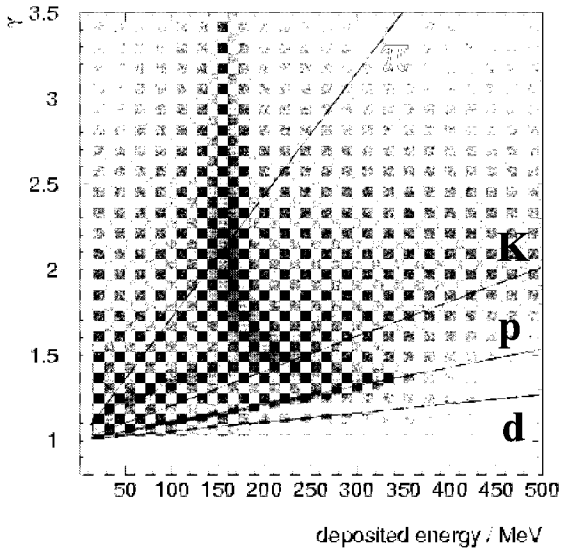

Fig. 2: Measured kinematical correlation between time-of-flight and deposited energy. The lines show the calculated correlations for different particles based on the applied energy calibration (see text).

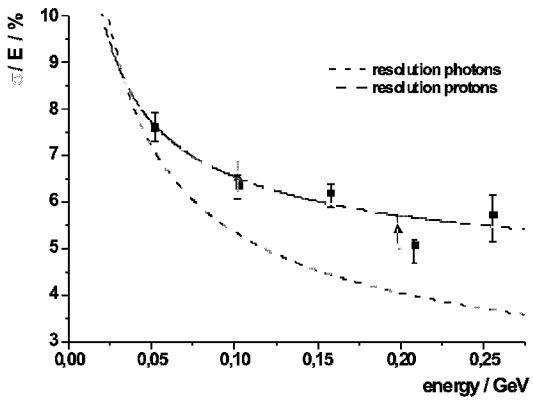

Fig. 3: Energy resolution for protons in comparison to the results for electromagnetic probes.

when applied to charged pions. The detailed analysis leads to a strong quenching of the scintillation light for hydrogen isotopes compared to pions, which requires further investigations.

References:

[1] K. Römer, diploma thesis: Vergleich verschiedener Szintillationsmaterialien zum optimierten Nachweis hochenergetischer Photonen, Giessen, 2001.
[2] M. Hoek, diploma thesis: Nachweis geladener Teilchen mit $PbWO_4$, Giessen, 2001

[1] II. Physikalisches Institut, Universität Gießen

An Improved Gas Mixture for the Side-Detector Wire Chambers at ANKE

H. Ohm, Chr. Schneider [a]

In an attempt to make the operation of wire chambers of the ANKE side detector more stable we have made investigations which aim at the improvement of the gas mixture. Multiwire proportional chambers have to be filled with a proper gas mixture which guarantees sufficient gas amplification, fast response of the chamber and stability against high-voltage break downs. Furthermore, possible ageing effect define additional boundary conditions for chambers operated in an high-rate environment.

For the ANKE side detector large multi-wire proportional chambers have been built at Forschungszentrum Rossendorf. Usually they are continously flushed with the standard gas mixture of 70% Ar and 30% CO_2 at a total flow rate of 200 ml/minute. The advantage of this gas is that there are no ageing effects. However, in particular at instantaneous high counting rates under beam conditions there is a strong tendency for high-voltage break downs during which sometimes wires break resulting in a short curcuit and failure of the chamber.

We have added to the standard gas mixture in various quantities isobutane or let a fraction of the gas flow through liquid pentane or hexane in order to investigate their quenching properties. When the chamber is irradiated with Sr-90 β-particles the total current increases to a good approximation exponentially due the increase of the gas multiplication. In Fig. 1. the current is normalized to the current measured with the standard gas mixture and it is presented as a function of the operating voltage. When allowing part of the gas to flow through liquid hexane then the current increases already at low concentrations. This increase in the gas amplification is probably due to the Penning effect in which excited Ar atoms deexcite in collisions with Hexane molecules thereby releasing electrons. Hexane in larger concentrations absorbs photons more efficiently thus reducing the current which is due to photoelectrons.

Similar but less pronounced effects are observed with pentane and i-butane admixtures to the gas. The backbending effect towards the highest voltage and the increase of the gas amplification at intermediate voltage is strongest for hexane. Both effects are desirable since they allow operation of the chamber at reduced voltage and limit the current at high ionization density. Therefore hexane is considered to be the best admixture to our standard gas. A gas mixture with 70 ml/min. out of the total gas flow of 200 ml/min. passing through liquid hexane is chosen as the optimum. This corresponds to a flow of gaseous hexane of 11 ml/min.

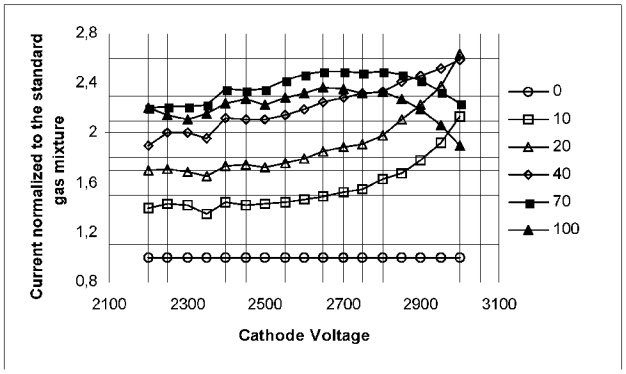

Fig. 1 : The current flowing through the wire chamber under irradiation with a Sr-90 source. The base gas mixture is 140 ml/min. Argon and 60 ml/min. CO_2. The gas flow which passes through liquid hexane is given in the legend. The current is given in units of the current which is measured with the standard gas mixture.

The effect of the gas composition on the detection efficiency is examined for a similar chamber, see Fig. 2. This chamber is smaller and it is equipped with 20 μm anode wires instead of 25 μm like the chamber mentioned before. Already small admixtures of hexane shift the characteristics to lower voltages. For the standard gas the efficiency decreases seemingly near the end of the plateau. This effect is due to events with several clusters of wires firing upon the passage of a single particle. The corresponding events are rejected during the data analysis since no unambigous assignment of the hit position is possible. The reason for the phenomenon are afterpulses due to electrons released by photons. Hexane reduces this

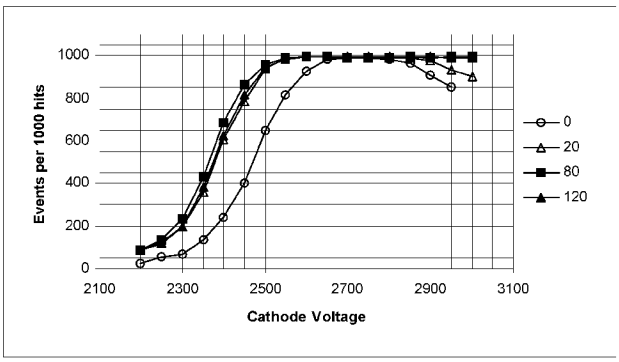

effect by absorbing photons in the ultraviolet region.

Fig. 2 : The detection efficiency of the small ANKE side-detector wire chambers. The standard gas mixture with a total flow of 200 ml/min. is used while the flow given in the legend is bypassed through liquid hexane.

[a] Forschungszentrum Rossendorf

Measurement of the Wire Tension in MWPCs

A. Volkov[a], H. Ohm, Chr. Schneider[b]

The wires in multiwire proportional chambers have to be held under proper mechanical tension which is in large chambers usually close to the limit defined by the tensile strength of the wire. Too a low tension leads to deviation of the wires from the ideal position which results in changes of the gas amplification of the chamber thereby affecting the detection efficiency and it reduces the high-voltage stability of the chamber. On the other hand, too a strong tension can pull the wires out of the joints which hold them in place or break the wires

Usually the wire tension T is derived from the resonance frequency f of the wire via the relationship:

$$T = 4\, f^2 L^2 \cdot \rho_L$$

with L being the length of the wire and ρ_L the wire mass per length unit. The oscillations are usually excited with a low-frequency AC current which is driven through the wire in the presence of a magnetic field. This requires access to both ends of each wire which is in most cases only possible when the chamber is disassembled.

In order to make routine checks of the wire tension while the chamber is in operating condition we applied a technique which is schematically described in Fig.1.

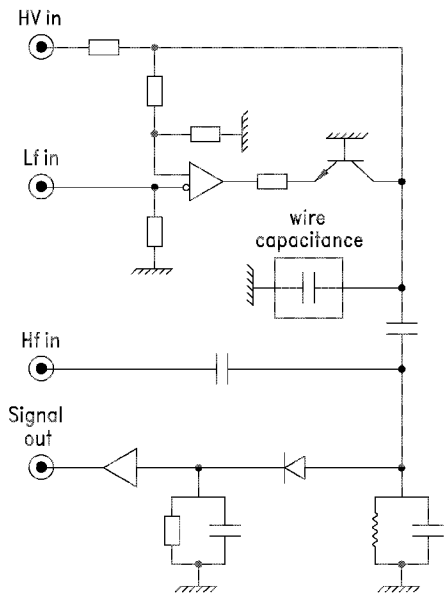

Fig. 1: Circuit for the measurement of the wire resonance frequency. In the upper part of the scheme DC high voltage is modulated with a low frequency signal which is fed into the chamber. The wires under measurement are coupled with a high-frequency resonance circuit in the lower part of the scheme.

Access is needed only to single wire ends. Mechanical oscillations of the wires are excited with a low frequency (typicaly 200 - 300 Hz) high-voltage signal which is applied to a pair of neighbouring wires one of them being grounded. This signal with amplitudes up to 1500 Volt is generated with a HV transistor in the upper part of the scheme. The resonance of the wire is identified via changes of the capacitance between the wires which is modulated with the frequency of the oscillating wire. This capacitance is made part of a high-frequency resonance circuit which is shown in the lower part of Fig. 1. It is excited with a low-voltage signal the frequency of which is close to the Hf resonance of the circuit of about few MHz. Mechanical oscillations of the wire result in a spread of the hf amplitude which is largest at the wire resonance. The resonance condition is made visible on an oscilloscope. The setup is schematically shown in Fig. 1.

We have systematically investigated the side detector chambers of the ANKE spectrometer which have been build at Forschungszentrum Rossendorf. For these the precise information about the wire tension is particularly important since the chambers are large and had to be built with fairly narrow frames due to space limitations at the experiment. As a consequence the frames are deformed under the force of the wires and have to be pre-bent before the wires are mounted. Fig. 2 shows as an example the results for one of the large chambers at ANKE. The actual values of the wire tension are rather close to the design value of 0.8 Newton which indicates that high precision has been achieved in the winding and production process of the chamber.

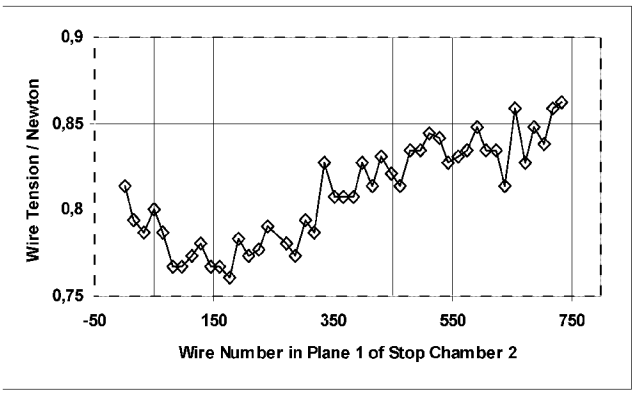

Fig. 2: Wire tension in a plane with vertical wires. Only every 16th wire is shown

[a] JINR Dubna, Russia
[b] Forschungszentrum Rossendorf

Investigation of the φ-meson production in *pp* and *pn* collisions at ANKE

M. Hartmann, R. Koch, Y. Maeda, J. Haidenbauer, A.A. Sibirtsev

The Okubo-Zweig-Iizuka (OZI) rule states that processes with disconnected quark lines in the initial or final state are suppressed. Accordingly, the production of φ-mesons from initial non-strange states is expected to be substantially suppressed relative to the ω-meson production. The cross-section ratio for φ- and ω-meson production under similar kinematical conditions should then be in the order of $\sigma_\phi/\sigma_\omega \cong R = \tan^2\alpha_V = 4.2 \times 10^{-3}$ [1, 2], where $\alpha_V = 3.7^\circ$ is the deviation from the ideal φ−ω mixing angle [3]. However, existing experimental data show an apparent excess of the cross-section ratio over the OZI estimation R and thus indicate a possible violation of the OZI rule. This could be due to an intrinsic $s\bar{s}$ component in the nucleon, which would manifest itself in a φ production cross section significantly exceeding the limits given by the OZI rule.

Data on the reaction $\bar{p}p \to \phi\pi^0$ from the LEAR facility show a strong dependence on the initial spin state of the proton-antiproton system. Specifically the production rate from the spin-triplet state is 15 times larger than the one from the spin-singlet state [4]. It has been argued that the larger production rate of the spin-triplet state can be explained by a negatively polarized intrinsic $s\bar{s}$ component in the nucleons through a *rearrangement* process [5]. Such a situation could also occur in the φ-meson production in nucleon-nucleon collisions in the threshold region. In case of the reaction $pp \to pp\phi$ the entrance channel becomes a pure spin-triplet state close to threshold. Thus if the negatively polarized strangeness hypothesis is correct, the φ/ω ratio in *pp* collision should be increased.

There is only one experiment for $pp \to pp\phi$ at low excess energy (ε=83 MeV) and the reported φ/ω ratio is enhanced by about a factor 5 over the estimation from the OZI rule [6]. Furthermore, the fraction of initial spin-triplet states is only around 70∼80% due to contributions from higher partial waves. Therefore, a measurement of the total cross section at excess energies much closer to threshold would be very useful to map out the energy dependence of the φ/ω ratio and, in particular, could provide important information about the origin of the strange sea quarks as well as the OZI violation.

In addition, the φ-meson production in *pn* collision, i.e. the reactions $pn \to pn\phi$ and $pn \to d\phi$, could also be sensitive to the intrinsic strangeness. Close to threshold the proton-neutron entrance channel contains both spin-triplet and spin-singlet channel whereas in $pn \to d\phi$ case only a spin-singlet state is present. Therefore, following the arguments of Ref. [5], a cross section ratio $\sigma_{pn\to pn\phi}/\sigma_{pp\to pp\phi} \approx 0.5$ is expected and in addition $\sigma_{pn\to d\phi}/\sigma_{pp\to pp\phi}$ should be strongly suppressed according to the negatively polarized strangeness hypothesis. In contrast, meson exchange models predict $\sigma_{pn\to pn\phi}/\sigma_{pp\to pp\phi} \sim 5$ [7] and also the ratio $\sigma_{pn\to d\phi}/\sigma_{pp\to pp\phi}$ was found to be sizable [8]. Experimental data on these ratios close to threshold would allow to discriminate between those theoretical models.

At the ANKE facility the measurement of the total cross section for $pp \to pp\phi$ will be carried out at the proton beam energies of 2.65 GeV(ε=18.5 MeV) and 2.70 GeV(ε=34.6 MeV). The energy dependence of the φ/ω ratio can then be obtained by utilizing available SPES-III results [9] of ω-meson production at comparable excess energies. The K^+K^- pair from the φ-meson decay is detected. Simulated invariant mass spectra of the K^+K^- system are shown in Fig.1. For details, see our proposal [10].

For φ-meson production in *pn* collision, the $pn \to d\phi$ reaction can be identified by detecting the fast deuteron in coincidence with the K^+K^- pairs from the φ decay using the deuterium target [11, 12, 13]. First measurements are foreseen at the end of 2002.

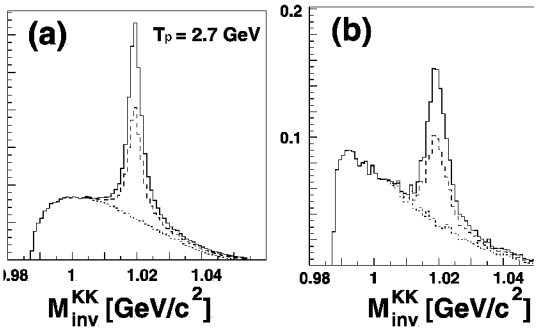

Fig. 1: Expected invariant spectra of the K^+K^- system at the beam energy of 2.70 GeV. The dotted lines show the contribution of the nonresonant process ($pp \to ppK^+K^-$). The solid and dashed lines show the total spectra with and without final-state interaction of protons, respectively. Figures (a) and (b) show the simulated result without and with the ANKE acceptance, respectively.

References:

[1] H.J. Lipkin, Phys. Lett. B**60**, 371 (1976).
[2] J. Ellis et al., Phys. Lett. B**353**, 319 (1995).
[3] Particle Data Group, Eur. Phys. J. C**3**, 1 (1998).
[4] A.Alberico et al., Phys. Lett. B**438**, 430 (1998).
[5] J. Ellis et al., Phys. Lett. B**673**, 256 (2000).
[6] F.Balestra et al., Phys. Rev. C**63**, 024004 (2001).
[7] A.I. Titov et al., Eur. Phys. J. A**7**, 543 (2000).
[8] K.Nakayama et al., Phys.Rev.C**60**, 055209 (1999); Phys. Rev. C**63**, 015201 (2000).
[9] F. Hibou et al., Phys. Rev. Lett. **83**, 492 (1999).
[10] M. Hartmann et al., COSY Proposal No.104.*
[11] M. Büscher et al., Ann. Rep. 2000 of IKP, 37 (2001).
[12] V. Yu. Grishina, et al., Phys. Atom. Nuclei, **63**, 1824 (2000).
[13] M. Büscher et al., COSY Proposal No.92. *

* available via http://www.fz-juelich.de/ikp/anke

The cross-section estimate for non-resonant K^+K^- production in pn collisions

Y.Maeda, M.Hartmann, A.A.Sibirtsev

At ANKE the total cross-section for the $pn \to d\phi$ reaction will be measured using deuterium target [1]. Nonresonant K^+K^- production, i.e. the $pn \to dK^+K^-$ reaction, will be the main background. Therefore, the magnitude of this cross section determines whether the resonant peak can be identified. The total cross-section for the $pp \to ppK^+K^-$ reaction was measured at low excess energies of ε=17 MeV [2] and 114 MeV [3], respectively. In the following, the total cross-section for the $pn \to dK^+K^-$ reaction is deduced from the experimental data for $pp \to ppK^+K^-$ taking into account the S-wave final-state interaction of the spin-singlet pp state and -triplet $d(pn)$ state (pn denotes the scattering state). According to Ref.[4], if the reaction process is dominated by short-range effects (r<1fm), the scattering wave function of the final nucleons at short distance can be factorized from the total amplitude. Thus the ratio of the scattering amplitudes for the spin-singlet and -triplet state is proportional to the ratio of the final-state wave functions (ϕ) with relative momentum (k), i.e.:

$$\frac{|\phi_s|}{|\phi_t|} \propto g(k) = \frac{|\sin\delta_s(1-r_b/a_s)/C|}{|\sin\delta_t(1-r_b/a_t)|}, \qquad (1)$$

where a_s and a_t shows the scattering length of the spin-singlet and -triplet state, respectively and δ_i is the phase shift as a function of k. C is the Coulomb penetration factor [4]. We set $r_b \simeq 1$ fm. Following the arguments of Ref.[5], the spin-triplet scattering wave function at short distances is approximated by the bound state wave function. Thus by using eq.(1) the total cross-section for the final pp-, pn- and d-states are determined by the d-state amplitude (M_d) :

$$\sigma_{pn} = |M_d|^2 \int h(k)(1+Ag^2(k))d\rho_n/f, \qquad (2)$$

$$\sigma_{pp} = A|M_d|^2 \int h(k)g^2(k)d\rho_n/f, \qquad (3)$$

$$\sigma_d = |M_d|^2 \int d\rho_{n-1}/f, \qquad (4)$$

where ρ_n and f are n-body phase-space and flux factor, respectively [6]. $h(k) = 2\pi m_N/[\alpha_t(k^2+\alpha_t^2)]$, α_t=0.232 fm^{-1} and m_N is twice the np reduced mass [5]. A is a parameter, which gives the relative magnitude of the spin-singlet and -triplet state amplitude. Our model is applied to single meson production (n=3), i.e. $NN \to NN(d)\pi$, η and ω, at lower excess energies ε<100 MeV. The results are shown in Fig.1. In the case of π and η production, data for the final pn- and pp-state are fitted by using eqs.(2) and (3), while the total cross-section for the final deuteron state is evaluated using eq.(4). In case of ω production, there are no data available for the final pn-state as well as d-state. Therefore the amplitude $|M_d|^2$ is obtained by fitting eq.(3) to the pp data with fixed $A=\frac{2}{9}$ assuming that the production mechanism is dominated by isovector interaction. The result for the d-state is compared with theoretical calculations [7, 8]. Our model is in qualitative agreement with measured and predicted cross-section for the final d-state.

The kaon and pion exchange mechanisms give a satisfactory description of $pp \to ppK^+K^-$ data [9]. We assume that these mechanisms also dominate for $pn \to dK^+K^-$. In a model independent way we deduce the total cross-section for $pn \to dK^+K^-$ from each $pp \to ppK^+K^-$ data point independently. The expected upper limit of the total cross-section at the beam energy of 2.69 GeV (ε=66.4 MeV) is $\sigma \simeq 0.04\mu$b. On the other hand, the predicted total cross-section for $pn \to d\phi$ at this beam energy (ε=34.6 MeV, where the $pp \to pp\phi$ reaction will be measured at the same excess energy [1]) is 0.3−0.6μb [7, 8]. Therefore we conclude that the resonance peak can be identified on top of a low background of non-resonant K^+K^- production (Fig.2(b)).

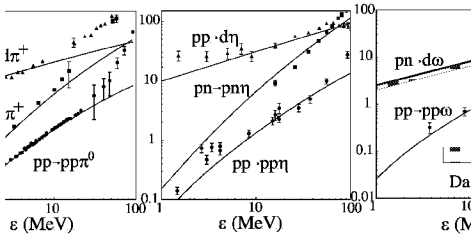

Fig. 1: Total cross-section for the $NN \to NN(d)\pi,\eta$ and ω reactions. Data for π, η and ω production are taken from Refs.[10], [11] and [12], respectively.

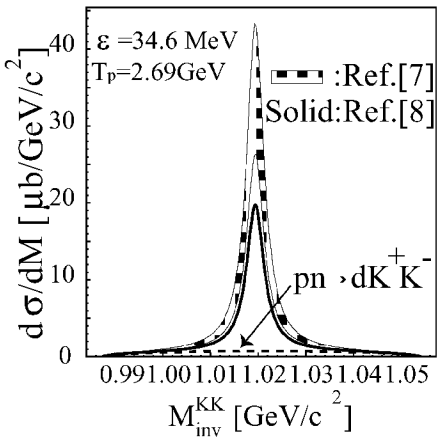

Fig. 2: Expected invariant mass spectra of the K^+K^- system.

References:

[1] M.Hartmann *et al.*, Ann. Rep. 2001 of IKP, (2002).
[2] C.Quentmeier *et al.*, Phys. Lett. **B515**, 276(2001).
[3] F.Balestra *et al.*, Phys. Rev. **C63**, 024004(2001).
[4] R.J.N. Philips *et al.*, Nucl. Phys. **53**, 650(1964).
[5] G. Fäldt *et al.*, Physica. Scripta **56**, 566(1997).
[6] Particle Data Group, Eur. Phys. J. C**3**, 186(1998).
[7] V.Yu.Grishina *et al.*, Phys. Atomic. Nucl **63**, 1824(2000).
[8] K.Nakayama *et al.*, Phys. Rev. **C63**,015201(2000).
[9] A. Sibirtsev *et al.*, Z. Phys. **A358**, 101(1997).
[10] H. Machner *et al.*, J. Phys. G: Nucl. Part. Phys. **25**, R231(1999) and references therein.
[11] H.Calen *et al.*, Phys. Rev. **C58**, 2667(1998) and references therein.
[12] F. Hibou *et al.*, Phys. Rev. Lett. **83**, 492(1999).

Simulations of the dd → αη reaction at ANKE

A. Wrońska[a], V. Hejny, A. Magiera[a], H. Ströher, C. Wilkin[b]

Deuteron acceleration in COSY has been achieved successfully during the year 2000. The tests showed that both quality and intensity of the deuteron beam were similar to the proton case [1]. This opens new fields for research at COSY, among others investigation of η-meson production in the dd → αη reaction. So far only near-threshold data for the total cross section of this reaction are available [2, 3], information on angular distributions and data for higher Q values are missing (see Fig. 1). Currently used values for the α-η scattering length - crucial e.g. in the discussion about η-nucleus bound states - were extracted under the assumption of pure S-wave production. The goal of the proposed investigation is to study the contribution of higher partial waves in the near threshold region and, in particular, to determine the energy, at which the P-wave channel opens (c.m. angular distribution becomes anisotropic). Thus, this measurement will test the validity of the S-wave approximation.

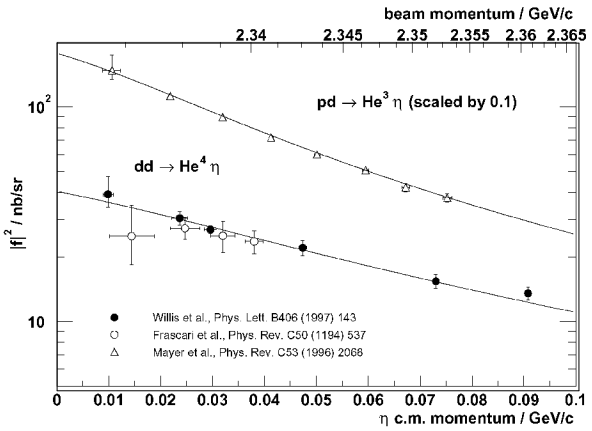

Fig. 1: Extracted reaction amplitudes for pd → ^{3}Heη and dd → ^{4}Heη. The curves taken from [3] follow from a combined S wave optical model fit. In case of pd → ^{3}Heη, new data show a deviation from this fit starting at $p_{\eta,\mathrm{c.m.}} \approx 0.15$GeV/c [4]

To check the feasibility of such a measurement using the ANKE detection system, Monte Carlo simulations have been carried out. For a beam momentum of 2.35 GeV/c ($p_{\mathrm{d,thr.}} = 2.335$GeV/c) a total cross section of 13.5 nb and a luminosity of $5 \cdot 10^{30}$ cm^{-2}s^{-1} (deuterium-cluster-jet target) were assumed. The background, which is considered to be mainly 2-pion production ($\sigma_{tot} \approx 2\mu$b), was generated on the basis of parameterised data from [5]. Only the α particle will be detected in ANKE, the η will be reconstructed by a missing-mass analysis.

Figure 2 presents the results containing statistics for 2 days of beam time expected under the conditions listed above. In the left picture the η peak in the missing-mass spectrum is clearly visible on top of the background. Thus, the resolution of the forward multiwire chambers is sufficient to identify the η meson in the proposed measurement. The right picture, showing the transverse momentum distribution of the produced α-particles with a cut on the η missing mass, will serve for the η c.m.-momentum determination independent from the beam momentum information provided by COSY. Using ANKE a resolution of $\Delta p_{\eta,\mathrm{c.m.}} \approx \pm 5$ MeV/c can be

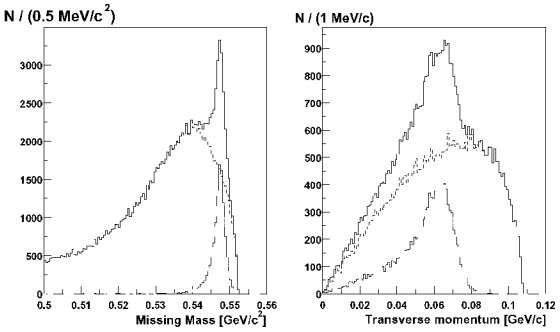

Fig. 2: Results of the simulations for dd → αη at a beam momentum of 2.35 GeV/c. Left:missing mass spectrum; right: transverse momentum distribution with a cut on missing mass ($m > 0.54$ GeV/c). The dotted histogram indicates the signal, the dashed one shows the background from 2-pion production.

achieved. This corresponds to an uncertainty of the beam momentum of $\Delta p_{\mathrm{d}}/p_{\mathrm{d}} \approx \pm 1 \cdot 10^{-3}$.

At the investigated beam momentum all α-particles from the reaction dd → αη can be detected in the forward detector of ANKE. The hardware trigger will be based on the forward hodoscope response. Since the mean energy losses of α's in the hodoscope are 8 times larger than those of protons and 4 times larger than those of deuterons of the same rigidity, high threshold settings will reduce the trigger rate to a level, which can be handled by the ANKE DAQ. In off-line analysis events with an α-particle in the exit channel will be selected by a combined energy loss - momentum cut. The reaction dd → αη will be identified - as shown above - by the missing-mass method.

The discussed method of the dd → αη measurement at ANKE does not require the installation of any additional detectors. However, such a possibility has been taken into consideration as well. Namely, it is possible to take advantage of the near-target vertex detector which is going to be constructed. As the final setup of this detector has not been fixed yet, several different, preliminary layouts were checked, that could be built and installed on a short time scale. In the optimal setup (4 silicon detectors, 5cm×6cm each), demanding an α in the forward detectors together with no other charged particle in ANKE or the vertex detector, this would lead to a further background supression: the signal-to-background ratio would improve by a factor of 1.5.

In view of the presented results we decided to apply for a beam time in the second half of 2002. The proposal will be submitted for the PAC meeting April 2002.

References:

[1] *Operating Report of COSY in 2000*, IKP/COSY Annual Report 2000, FZ-Juelich (Jül-3852), p.143
[2] R.Frascaria *et al.*, Phys. Rev. C 50 (1994) R537
[3] N.Willis *et al.*, Phys. Lett. B 406 (1997) 14
[4] Bilger *et al.*, submitted to Phys. Rev. C
[5] J.Banaigs *et al.*, Nucl. Phys. B 105 (1976) 52

[a]Insitute of Physics, Jagiellonian University, Cracow, Poland
[b]Physics & Astronomy Department, University College London, UK

Spin Effects in the Deuteron Charge-Exchange Break-up reaction

V. Glagolev[a], A. Kacharava[b,c], V. Komarov[a], G. Macharashvili[a,c], M. Nioradze[c], F. Rathmann, H. Seyfarth

We consider the possibility of using the ANKE spectrometer to investigate the spin structure of the elementary $np \to pn$ charge-exchange (CE) process by measuring the deuteron CE break-up reaction: $dp \to (pp)n$. Following the mathematical formalism developed in [1], the relation between the effective cross sections of this reaction and the elementary $np \to pn$ charge-exchange process in the framework of the impulse approximation can be written as a sum of spin-independent (index 1) and spin-dependent (index 2) parts of the elementary $np \to pn$ process: $(d\sigma/dt)_{dp\to(pp)n} = [1 - S(t)](d\sigma/dt)_1 + [1 - 1/3S(t)](d\sigma/dt)_2$, where t is the momentum transferred to the neutron and $S(t)$ is the deuteron form-factor. At zero momentum transfer from the target proton to the neutron $(d\sigma/dt)_{dp\to(pp)n} = 2/3(d\sigma/dt)_2$. Thus, this reaction in forward direction is completely determined by the spin-dependent part of the elementary $np \to pn$ process. A first attempt to measure the spin-dependent part for the amplitude of the $np \to pn$ reaction was made in a Hydrogen Bubble Chamber experiment [2] at a deuteron beam momentum of 3.34 GeV/c. The results showed an important role of spin effects in the $np \to pn$ process at small scattering angles. At present an experiment, STRELA [3], is in progress at the Nuclotron deuteron beam in Dubna. The STRELA set-up can detect a proton pair with small relative momentum close to 0°. However, this is not sufficient to observe the dynamics of the differential cross section change near 0°. To clarify the different behaviour of the deuteron CE and direct break-up (DIR) reactions at low momentum transfer, the result from ref.[2] is presented in Fig. 1. The differential cross section is shown for events, when both protons are emitted in a narrow 3° forward cone (shaded histogram). Here t is the momentum transfer from the target-proton to the recoil nucleon. A clear peak can be seen around $t \approx 0$, whereas the differential cross section for the direct break-up, when a proton-neutron pair is emitted in the same forward cone, vanishes at low t. As a first step we intend to use the unpolarized deuteron beam. Both fast protons, emitted into a narrow forward cone with typical momenta around half of the deuteron beam momentum, will be detected by means of the forward detector (FD) of the ANKE spectrometer. For estimation of the FD efficiency in registration and for studying the background, a simulation based on data from [2] as GEANT event generator was carried out. The angular-momentum acceptance of the FD is shown in Fig. 2. It presents the ejectile momentum p versus the projection of the polar angle on the median plane θ_{xz} of ANKE. The curves show the kinematical locus for protons and deuterons from several processes. The label $dp \to ppn$ denotes the deuteron CE break-up with emission of a forward proton pair with zero relative momentum. The acceptance region is centered at $\theta_{xz} = 0°$ in a polar angle range of -4° to +4°. Simulation results show that the main count rate in the FD is expected from one-proton events. However, even if all inclusive protons are registered, the count rate is not larger than 220 per two-proton event, when the selection aperture is 3°. Background of two proton events is left only from the channel $dp \to ppn\pi^0$, but an unambigous identification of the reaction is possible using a missing-mass criterion. One can conclude that the ANKE spectrometer is well suited to study the deuteron CE break-up reaction at small momentum transfer and allows one to measure the spin-dependent part of the amplitude of the $np \to pn$ process. Further development of this investigation is connected with polarization experiments, which allows one to estimate the two spin-dependent terms in the amplitude of the $np \to pn$ process under 0° and their relative phase.

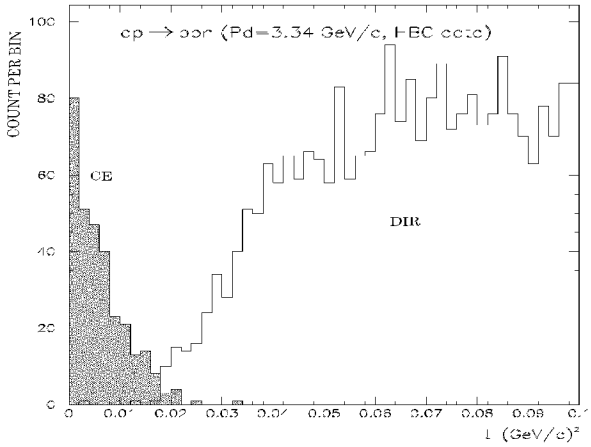

Fig. 1: Events from the bubble chamber experiment [2], interpreted as due to charge exchange (CE) and direct (DIR) deuteron break-up.

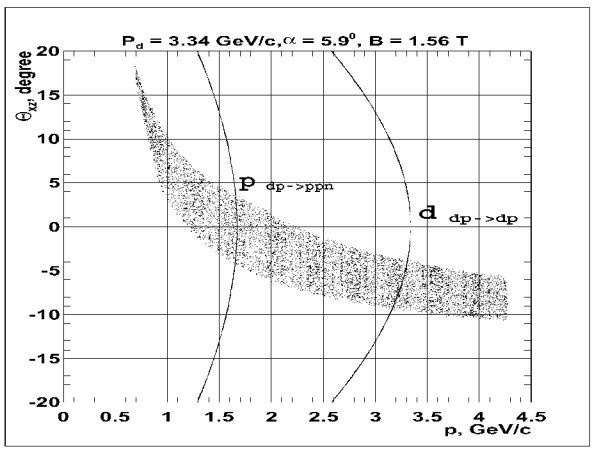

Fig. 2: FD angular-momentum acceptance for a 3.34 GeV/c deuteron beam as used in ref.[2] (α and B denote ANKE-operation parameters).

References:

1. N.W. Dean Phys. Rev. D5 (1972) 1661; D5 (1972) 2832.
2. B. Aladashvili et al. Nucl. Phys. B86 (1975) 707.
3. V. Glagolev et al., Research Program JINR-LHE-0941-1 (1999) 29.

[a] JINR, Dubna, Russia
[b] Universität Erlangen, Germany
[c] HEPI TSU, Tbilisi, Georgia

1.2 Experiments at External Facilities

ATRAP on the way to cold Antihydrogen

T. Götz, D. Grzonka, W. Oelert, G. Schepers, T. Sefzick
for the ATRAP-collaboration

The aim of the ATRAP experiment [ATR97] at the Antiproton Decelerator AD at CERN is a high precision test of the CPT theorem when comparing observables from hydrogen and antihydrogen. If the frequency of the meta stable 1S-2S two photon transition could be measured on the antihydrogen with a similar precision as on a beam of cold hydrogen atoms, i.e. $1.8 \cdot 10^{14}$ [MPQ00], this would be by far the most accurate test of the CPT invariance using a combined baryon/lepton system.

In the first phase of the experiment – being in operation – the formation of antihydrogen in a Penning ion trap situated in the bore of a 6 Tesla superconducting magnet is aimed for. Two most promising schemes for producing antihydrogen atoms, the Pulsed Field Recombination [AMS00] and Three Body Recombination, were studied [ATR01a]. In the next year the Laser Induced Recombination method will be a further part of the investigations.

Successful trials of the recombination as well as losses of particles during the recombination procedure are observed by a set of Jülich scintillation detectors consisting of a fiberdetector [ATR99] and large area scintillation paddles. As sketched in figure 1 the recombination trap is surrounded by three layers of scintillating fibers which indicate in coincidence with the scintillator paddles around the magnet (not shown) the charged pions from an antiproton annihilation with a proton of the atoms of the trap material supressing most effectively the physical background coming from cosmics, background radiation in the experimental area, and single noise signals.

In the second phase [ATR00a] which is presently under construction a magnet with a bore diameter as large as 0.5 m will be used so that a gradient field Ioffe trap can be added for holding the once formed neutral antiatoms.

After a successful start of first measurements in fall 2000 [ATR00c] that resulted in the first ATRAP publication about positron cooling [PLB01] the ATRAP-Experiment used the beam period during 2001 for refining and optimizing the trapping of antiprotons and positrons and systematical studies of their interaction [ATR01a].

Accompanied by simultaneous improvements of the antiproton beam of the AD, i.e. a higher intensity and smaller emittance of the extracted beam, the trapping rates could be increased to values of regularly 15000 antiprotons every 110 sec. Another important step towards an efficiency increase of the experiment was the new procedure allowing to fill antiprotons from the AD and positrons from the Na^{22} source simultaneously what was before only possible in sequent delaying steps. For this purpose a ball-valve [PLB01] between the positron– and the antiproton trap (figure 1) was employed which was closed during the loading of both antiprotons and positrons and which was opened when bringing the positrons and antiprotons together.

Once trapped a lot of effort was put into the understanding of the manipulation and shifting of both small numbers of particles as well as of big particle clouds between the electrodes of the trap, shown together with the inner detectors in figure 1. Using the fiber charged particle detector a map of particle velocities transition times and rates of launching and recatching of the particles between the different (in location and type) electrodes was achieved. Furthermore, with help of the special ball-valve that has a small opening diameter of 0.5 cm compared to the ring electrodes with 1.2 cm inner diameter the properties of the particle clouds could well be examined. Driving the antiprotons through this valve and back cleaned the cloud considerably so that thereafter no losses were observed. Free of background conditions without antiproton losses during the trapping periode are crucial for any recombination experiments.

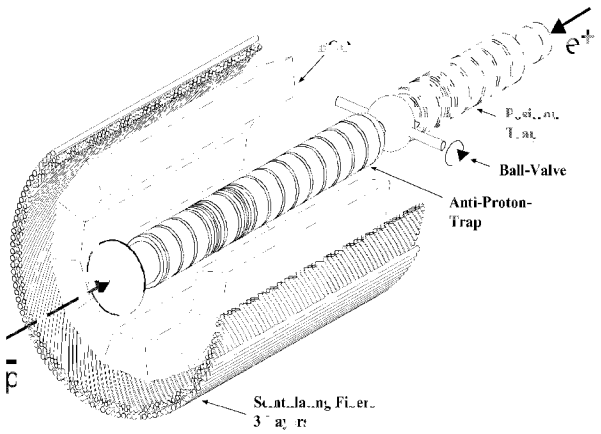

Fig. 1: Sketch of the inner setup of the ATRAP-Experiment (Phase I)

As described in the last years progress report [ATR00c] the light guides of the BGO detector for the measurement of the 2×511 keV gammas from the positron annihilation showed a low light output and had to be improved. New light guides were constructed and built in the mechanical workshop of the IKP-Jülich. Tests of the new BGO detector (see [ATR01b]) performed in Jülich and in place at the experiment showed the strong improvement of the light output.

References:

[ATR97] Proposal of the ATRAP collaboration, CERN-SPSC 97-8/P306.
[ATR00c] ATRAP, after half a year of operation, Annual Report 00
[ATR01a] ATRAP Studies of interactions between $\bar{p}$ and e^+, this Annual Report
[ATR01b] Studies on the Bismuth-Germanate-detector of the ATRAP-experiment, this Annual Report
[ATR99] Jülich fibre detector, Annual Report 99
[ATR00a] ATRAP II, Annual Report 00
[MPQ00] M.Niering et al., Phys. Rev. Lett. 84, 5496 (2000).
[AMS00] C.Wesdorp et al., Phys. Rev. Lett. 84, 3799 (2000).
[PLB01] G.Gabrielse et al., Phys. Lett. B 507, 1 (2001)

Studies on the Bismuth-Germanate-detector of the ATRAP-experiment

T. Götz, D. Grzonka, H. Hadamek, W. Oelert, G. Schepers, T. Sefzick
for the ATRAP collaboration

The ATRAP [1] collaboration focuses its attention to the great challenge of comparing hydrogen and antihydrogen to high accuracy. The current assumption, that reality is invariant under CPT transformations, is based in large part upon the success of quantum field theories, which themselves rely on reasonable presumptions as causalilty, locality and Lorentz invariance. Theoretical investigations of possible CPT violations are discussed in the context of string theory [2].

The studies at the ATRAP-experiment require the simultaneous identification of antiprotons and positrons. The antiproton annihilates with a proton to multi pion events, whereas the signature of a positron is given by the two 511 keV gammas when annihilating with an electron. Since in practice the antiproton annihilation on a copper nucleus of the trap material produces numerous secondary particles, including the generation of positrons in the interaction cascade, a unique identification of the primary positron through the detection of the 511 keV photons is not possible. Thus the identification of an antihydrogen event on the base of a single event is not feasible. The antihydrogen detection is only possible on a statistical basis with an event sample.

Various studies have been done in order to optimize the performance of the BGO-detector of ATRAP-I, consisting of 12 BGO crystals readout with light guides on PM's.

Basic measurements regarding the light coupling have been performed, in which parameters like surface structure, light guiding and temperature dependence of the light emission were studied. Concerning the surface of the BGO crystals, polishing and painting with white reflective colour improves the light output by a factor of 3.2.

The optimized BGO-detection system allows a clear separation of the 511 keV photon line from noise. An energy resolution of $\sigma = 17.3\%$ was obtained, which is certainly not outstanding but could not be improve due to the limitation given for the light guides.

The studies of the temperature dependence show, that the

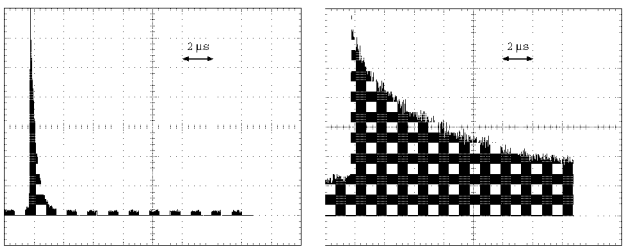

Fig. 1: Time distribution of the recorded BGO signals, each with a time axis of 20 μs. In the left part the histogram at room temperature (T = 298.9 K) is shown, the right part presents the distribution at 91.3 K. The y-axes are scaled in arbitrary units.

decay time of the scintillating components in the BGO increases drastically (see Fig. 1) with decreasing temperature. As an example the ADC gate width has to be set to 3 μs, in order to achieve at temperatures of 100 K a light intensity, which is comparable to the one at a temperature of 300 K (see Fig. 2).

The photon detection system of ATRAP-II was studied

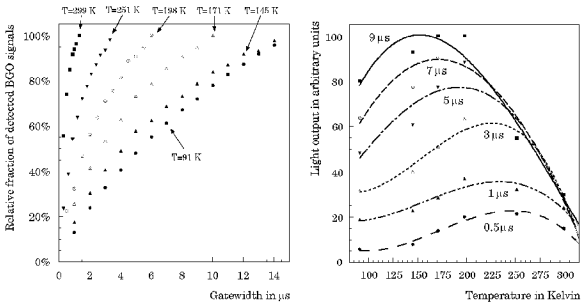

Fig. 2: Left: Fraction of the detected light versus ADC gate width for different temperatures. Right: Light output depending on temperature for different ADC gate widths using the data of [3] for the temperature dependent light output.

with the help of Monte Carlo simulations. Based on the experience of ATRAP-I a new detector configuration with BGO-bars as used but with a ϕ-segmentation of 32 is sufficient. Thereby the height determines via the coverage of the solid angle the detection efficiency.

Both, the amount of the registered single photons in the 511 keV peak as well as the amount of coincidently detected photons of the positron decay can be used for the detection of antihydrogen. Regarding the photon detection system independently of the system for the charged particles single photon and coincident photon identification are comparable. Ideally 45 antihydrogen events are sufficient for the case of single photon detection of the production of antihydrogen with a probability of 99.73% (3-σ-effect), whereas detecting the photons coincidently requires 75 antihydrogen annihilations.

Considering additionally the information of the position of the annihilation resulting from the tracks of the charged particles, the situation gets drastically improved. Via an event selection through the distance between the position of the antiproton annihilation and the connection line of two photon events the amount of the necessary produced antihydrogen atoms is reduced to 8 for a comparable probability.

Acknowledgements:

We would like to thank D. Protic and his laboratory team for the extensive help and lots of support during the experiments.

References:

[1] ATRAP Proposal, CERN-SPSC 97-8 / P 306

[2] J. Ellis, N.E. Mavaromatos and D.V. Nanopoulos, Phys. Lett. **B 293** (1992), 142
V. Kostelecky and R. Potting, Phys. Rev. **D 51** (1995), 3923

[3] M.J. Weber and R.R. Monchamp. Luminescence of $Bi_4Ge_3O_{12}$. Journal of Applied Physics, 44:5496,1973.

ATRAP Studies of interactions between $\bar{p}$ and e^+

D. Grzonka, W. Oelert, G. Schepers, T. Sefzick
for the ATRAP-collaboration

The ATRAP collaboration at the new antiproton decelerator (AD) at CERN aims for comparing observables of hydrogen to those of antihydrogen. The first observation of positron cooling of antiprotons, the closest approach yet to the production of cold antihydrogen, has been published by the collaboration [1]. During the year 2001 considerable progress has been achieved with respect to the manipulation of the antiproton – and positron clouds and the studies to their interaction. Here we present a systematic investigation of the cooling of antiprotons with positrons which in principle is similar to electron cooling of hadrons in general. By Coulomb collisions the motional energy of the trapped antiprotons is transferred to the lighter trapped positrons which cool rapidly via synchrotron radiation.

A schematic potential well containing electron–cooled antiprotons and positrons in a nested well structure is shown in Fig. 1. These overlaying clouds of the two species of antihydrogen were allowed to interact for different time intervalls before opening the potential well. The energy distribution of the trapped antiprotons was registered by a scintillation detector arrangement when slowly lowering the potential barrier as indicated by the arrow in the figure. When no positrons

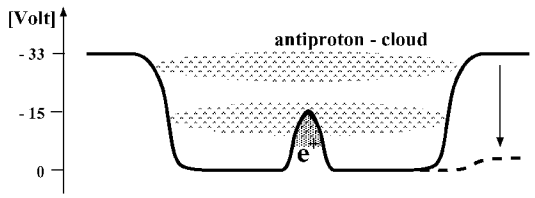

Fig. 1: Schematical view of the potential distribution for antiprotons in a trap together with positrons.

are present in the nested trap, as shown by the top spectrum of the 14 spectra presented in Fig. 2, the antiprotons had kinetic energies distributed around 33 eV. With increasing interaction time the antiprotons cool further and seem to group during the time intervall from 535 ms to 910 ms at around 21 eV whereas after 910 ms suddenly a strong yield for antiprotons with kinetic energies around 17 eV is observed. This is the lowes kinetic energy expected due to the potential hight for the positrons – as shown in Fig. 1 – which might be slightly diminished by the space charge of the positively charged positrons.

Surprisingly enough a further cooling was observed down to kinetic energies of about 10 eV of the antiprotons after an interaction time of more than 2000 ms. This observation might be explained by evaporation cooling where two antiprotons with similar kinetic enegy scatter and distribute the kinetic energy unequally.

In further experiments the collaboration investigated both the field–induced – [2] and the three body recombination. Still, some substantial simulations of the experiments are going on and no final conclusion can be given here.

However, it might be possible that cold Rydberg antihydrogen has been produced but the collaboration is not yet ready to claim that such states have been observed and have been

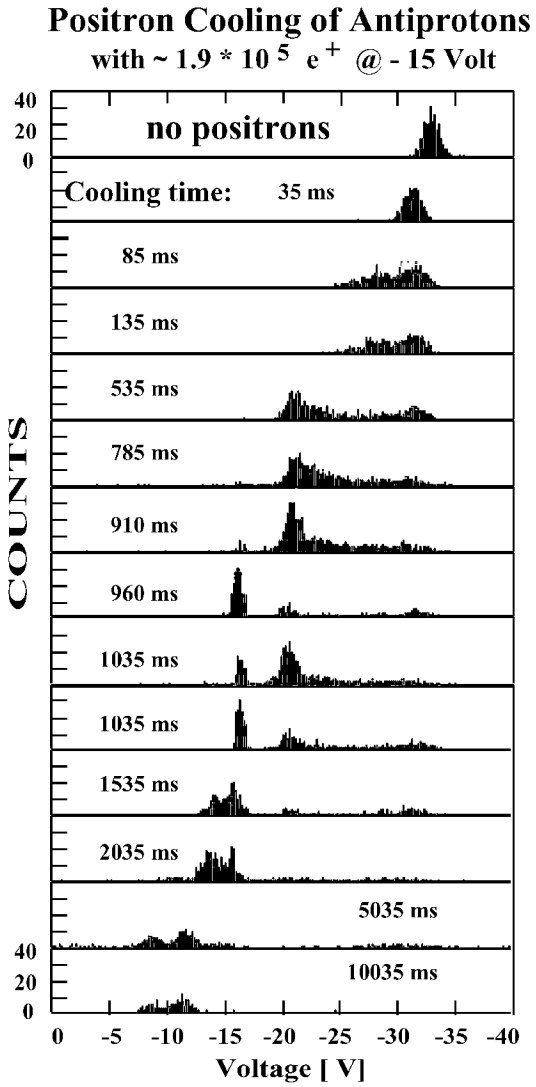

Fig. 2: Variation of the cooling time for antiprotons in a trap together with $\approx 1.9 \times 10^5$ positrons in a nested trap of - 15 Volt depth.

distinguished from a cold neutral plasma of antiprotons and positrons.

In any case, the ATRAP collaboration achieved at least to produce and observe a kind of cold neutral plasma of antiprotons and positrons which is a very promissing base for forming cold antihydrogen. Furthermore, it is difficult to see how to prevent the formation of cold antihydrogen in such a neutral plasma and certainly the environment is ready for investigations with laser induced recombination and cooling of antihydrogen. This is the aim for the research of the next year.

References:

[1] G. Gabrielse et al., Phys. Lett. **B 507**, 1 (2001)
[2] C. Wesdorp et al., Phys. Rev. Lett. **84**, 3799 (2000)

Pressure Dependence of Ground-state shift and Width in Pionic hydrogen

D. F. Anagnostopoulos[a], W. Breunlich[b], H. Fuhrmann[b], D. Gotta, A. Gruber[b], M. Hennebach,
P. Indelicato[c], Y.-W. Liu[d], B. Manil[c],V. Markushin[d], N. Nelms[e], A. J. Rusi El Hassani[f],L. M. Simons[d], H. Zmeskal[b]

The new pionic hydrogen experiment [1,2] at PSI has started with a detailed study of the pressure dependence of the ground-state shift in the pionic hydrogen atom. The aim of these measurements is to identify or exclude molecular effects which falsify the shift value attributed to the strong interaction.

Molecular effects on level energies may come from excited πp systems bound into complex structures forming $[(\pi pp)p]_{ee}$ molecules [3]. Radiative decay from such states – with binding energies decreased by up to 4.5 eV – leads to reduced X-ray energies. Only rough estimates for the formation rates exist at present and though deexcitation is expected to occur dominantly by Auger emission, even low-intensity satellites can cause a center-of-gravity shift of the line that is noticable at the envisaged accuracy of the experiment. Finally, the new experiment aims for an improvement by a factor of about 5 compared to the previous one [4].

The πH(3p-1s) transition (Fig. 1) was measured in the pressure range equivalent to 4 bar up to liquid by using a cryogenic target. This experiment was the first observation of X-ray emission from liquid hydrogen.

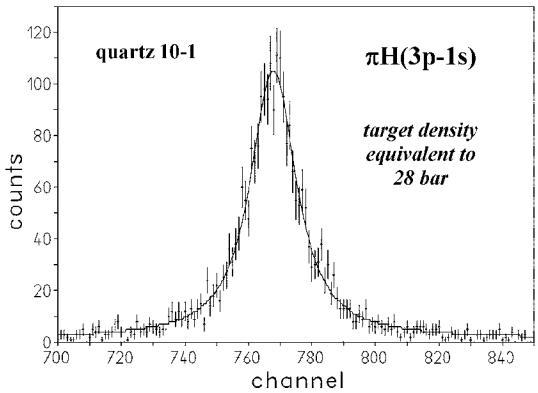

Figure 1. πH(3p-1s) transition with a peak-to-background ratio of 40 to 1 at a count rate of 15 per hour for the hydrogen line. One channel correponds to 60 meV.

At low density the energy calibration line $\pi^{16}O$ (6h-5g), which is not affected by the strong interaction, was measured simultaneously with the πH line as described in [1]. At higher hydrogen densities the measurement was performed alternately with pure hydrogen gas and a mixture of helium and oxygen (80%/20%) at higher temperature. Helium is needed to reduce self absorption of the X-rays in oxygen. The oxygen fraction itself was a mixture of ^{16}O and ^{18}O, which allowed to check the angular dispersion of the crystal spectrometer (Fig.2).

The spectrometer response was determined from πC (Fig. 3), because πO transitions are Doppler broadened by Coulomb explosion [5]. Coulomb explosion is negligibly small for molecules like CH_4 because the hydrogen atoms are weakly bound and the mass ratio C/H is large. The measurements were performed with a spherically bent quartz crystal cut along the 10-1 plane.

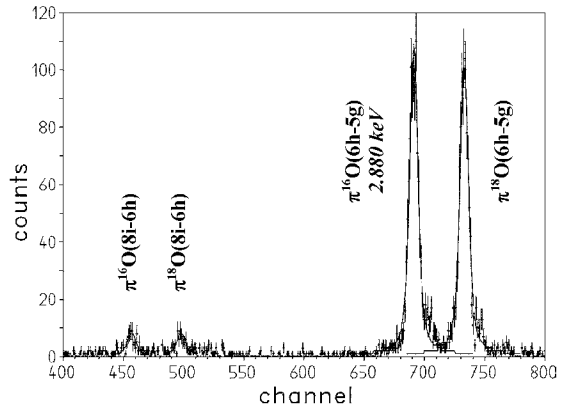

Figure 2. The πO reflections from the ^{16}O and ^{18}O mixture are used for energy calibration.

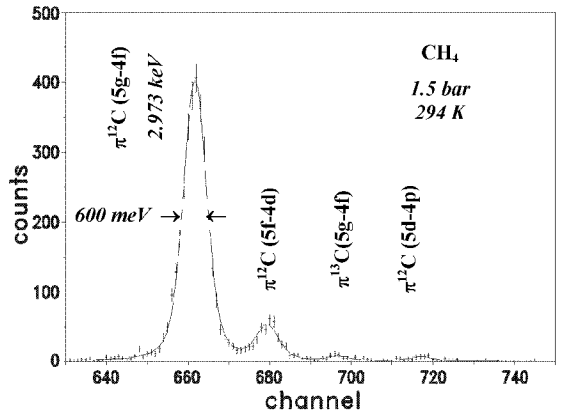

Figure 3. Crystal spectrometer response function.

No pressure dependence was found for the energy of the πH(3p-1s) transitions. The preliminary result for the hadronic shift is also in agreement with the value of the previous experiment performed at 15 bar equivalent density [4]. Evidence for an increased line width, however, was observed for liquid hydrogen which points to a strength for Coulomb deexcitation even beyond the predictions from cascade calculations [6]. The forthcoming high-statistics measurement in summer 2002 will yield an improved value for the hadronic shift. Liquid hydrogen will be remeasured to confirm the increased line width.

[1] IKP annual report 2000, p. 71
[2] PSI exp. R-98.01; http://pihydrogen.web.psi.ch
[3] S. Jonsell et al. Phys. Rev. A 59 (1999) 3440
[4] H.-Ch. Schröder et al., Phys. Lett. B 469 (1999) 25
[5] T. Siems et al., Phys. Rev. Lett.84 (2000) 4573
[6] T. Jensen and V. Markushin, priv. comm.

[a] Dept. of Material Science, Univ. of Ioannina, Greece
[b] IMEP, Österr. Akademie der Wiss., Vienna
[c] Lab. Kastler-Brossel, Univ. P. et M.Curie, Paris
[d] Paul-Scherrer-Institut (PSI),Villigen, Switzerland
[e] Dept. of Physics and Astronomy, Univ.of Leicester
[f] Dept. De Physique, Tanger, Morocco

Precision Determination of the Charged Pion Mass

D. F. Anagnostopoulos[a], G. Borchert, J.-P. Egger[b], D. Gotta, M. Hennebach,
P. Indelicato[c], Y.-W. Liu[d], B. Manil[c], N. Nelms[e], L. M. Simons[d]

The mass of the negatively charged pion has been measured with pionic atom X-ray transitions by using a new calibration method. The experiment uses the fact that the muon mass is known to an accuracy of 0.05ppm [1]. Energies of the (5-4) transitions in pionic nitrogen and muonic oxygen are 4.055 and 4.023 keV and, hence, differ by only 32 eV. This allows the simultaneous measurement of both lines with a reflection-type crystal spectrometer. Such a set-up reduces substantially the sources for systematic errors arising from instabilities during long measuring periods.

Nitrogen and oxygen targets are used in gaseous form, which leads to a well pronounced X-ray cascade. The line yield of the (5-4) transitions is about 40% and most of the intensity is collected in the circular transitions (5g-4f) (Fig. 1). In gases, screening effects from remaining electrons are negligibly small, thus avoiding systematic uncertanties caused by the use of solid targets [2].

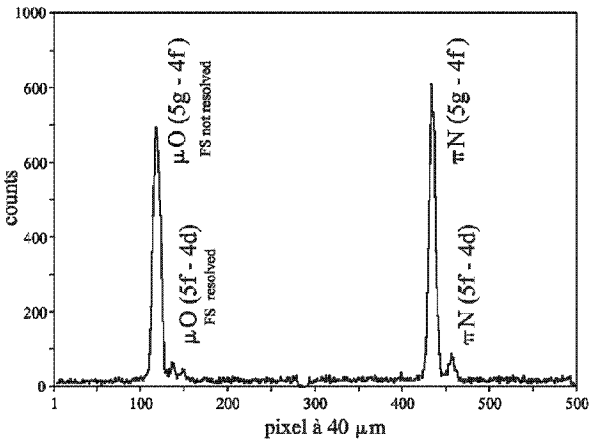

Figure 1. Simultaneously recorded reflections of the pionic oxygen and nitrogen (5-4) transitions measured with an O_2/N_2 gas mixture. The Bragg angles are 52.8 and 53.4 degrees, respectively. One channel corresponds to 2 CCD pixels of 40 μm or 102 meV.

The pion beam of the πE5 area at PSI was injected into the new cyclotron trap. The gap between the magnet coils of the new trap is almost a factor of 2 wider than the one of the previously used device. This allows to stop about one order of magnitude more muons which stem from the decay of slow pions inside the trap. However, the low count rate for muons is one of the limiting factors of the experiment. In the set-up optimized for pions up to 250 X-rays per hour were achieved for the π(5-4) transition.

The second limitation originates from a large Doppler broadening of the πN and μO transitions due to Coulomb explosion. The acceleration of the charged ions during the separation of the molecules – for the first time directly observed by this experiment [3] – doubles the line widths as expected from the spectrometer resolution of 500 meV. Consequently, a factor of 4 higher statistics is required to achieve the same accuracy for the line positions.

X-rays emitted from the target were reflected in second order by a spherically bent silicon crystal cut along the 110 plane. For a bending radius of 3 m, the μO and πN reflections are separated by 25 mm. They were measured in a large area X-ray detector built up of six 25 mm × 25 mm CCD chips set up for this experiment [4]. The gaps between the chips were determined from a mask with high precision slits and irradiated with 2.3 keV sulphur X-rays excited in a target at about 4 m distance by means of an X-ray tube [5].

For the simultaneous measurement an oxygen/nitrogen gas mixture of 90%/10% at 1.4 bar was used yielding a count rate of 15 per hour both for the μO and the πN (5g-4f) transition. More than 8000 events were recorded in each of the circular transitions. The error for the value of the pion mass is dominated by statistics for the measurement with the O_2/N_2 gas mixture. It amounts to 1.7ppm for 75% of the total statistics analyzed up to now. The systematic contributions to the error are small. From the curvature of the reflections an uncertainty of ± 0.1ppm arises. Temperature and bending corrections are both of the order of 0.1ppm only because of the small difference of the Bragg angles. The uncertainty stemming from the determination of the gaps between the CCDs with the slit mask is at present 0.5ppm, but will be negligible after a remeasurement with improved statistics.

A second energy calibration has been performed for consistency reasons by using the copper fluorescence radiation. The method follows the line as described in our preliminary experiment of the pion mass [6]. An accuracy of about 2ppm is expected here.

To summarize, the pion mass has been remeasured by comparing the wavelengths of pionic and muonic X-ray transitions. Finally we expect an accuracy of about 1.5ppm for the new determination of the pion mass. The final value will be available after a precise calibration of the spectrometer dispersion early in 2002.

[1] D.E.Groom et al. (PDG), Eur. Phys. J. C 15 (2000) 1
[2] B. Jeckelmann, P. F. A. Goudsmit, H. J. Leisi, Phys. Lett. B 335 (1994) 326
[3] T. Siems et al., Phys. Rev. Lett. 84 (2000) 4573
[4] N. Nelms et al., to be published in Nucl.Instr.Meth.
[5] D. Gotta et al., this report
[6] S. Lenz et al., Phys. Lett. B 416 (1998) 50

[a] Dept. of Material Science, Univ. of Ioannina, Greece
[b] Inst. de Physique, Univ. de Neuchâtel, Switzerland
[c] Lab. Kastler-Brossel, Univ. P. et M.Curie, Paris
[d] Paul-Scherrer-Institut (PSI),Villigen, Switzerland
[e] Dept. of Physics and Astronomy, Univ.of Leicester

Alignment measurement of the CCD array installed at the PSI crystal spectrometer

D. Gotta, M. Hennebach, P. Jones[a], B. Leoni[b], L. Simons[b]

In the recent precision measurement of the mass of the charged pion (m_π) at PSI [1], a 2 x 3 array of CCD detectors [2] was used. The crucial measured value is the position difference between the lines of the 5g→4f transitions in pionic nitrogen (πN) and in muonic oxygen (μO). Since these lines are positioned on different columns of the CCD array, the gaps between individual CCDs must be considered when calculating the position difference. These gaps are mainly caused by a 5–pixel–wide "dead zone" at the CCD edges. Furthermore, the CCDs are not perfectly aligned mechanically, which means there are slight rotations in addition to the gaps. To reach the envisaged accuracy of ~1 ppm for m_π, the relative CCD positions must be known better than 4 μm or 1/10th of a pixel.

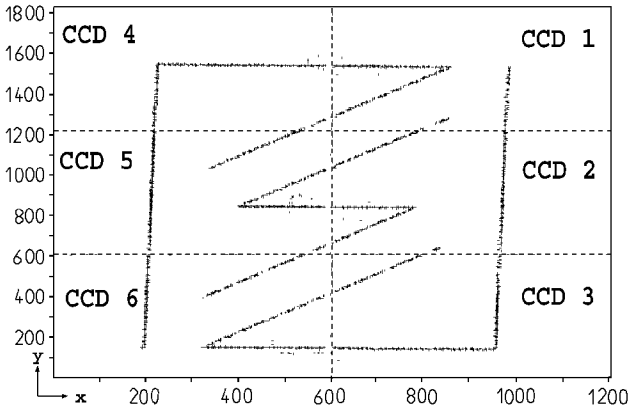

Fig. 1: The 3 x 2 CCD array with mask data (not in scale). Rotation and translation corrections are already applied.

The experimental approach for this alignment measurement is to place a mask with several horizontal, vertical and diagonal slits over the detector array. The mask has a thickness of 1 mm, the slits are wire eroded with a width of 0.1 mm. The detector array, shielded by the mask, is irradiated with X–rays from a sulphur fluorescence target, which produces mainly 2.3 keV X–rays; an energy low enough to keep charge splitting effects small. The target (activated with an X–ray tube) was placed as far away as possible (3.3 m) to reduce distortion of the mask image by parallax effects. A collimator with a diameter of 5 mm was put in front of it to provide a point–like source. After optimizing the X–ray tube for rate and a good peak/background ratio, about 30 hours of data taking followed. In total, about 600 000 events were collected, the final data is displayed in Fig. 1.

Changes to the software for processing and displaying the detector data had to be made to represent the rotation and translation of individual CCDs. Basically, the position of each event within a pixel is determined randomly before it is rotated and translated. The process for extracting the CCD positions from the mask data is as follows:

1. Get the individual rotations of the CCDs from linear fits to the mask slits by comparing the inclinations for the same slit on different CCDs. The fit is done by calculating the center of gravity (COG) for each CCD row (or column for fitting a horizontal line) and then making a linear regression through them. The error of the COGs is based upon a rectangular distribution with a width equal to the width of the slits of the mask. With N as the number of events and w as the slit width, $\Delta x = \frac{w}{\sqrt{12 \cdot N}}$.

2. After correcting the differences in the relative rotations, make new linear fits to find the crossing points of each mask slit with the CCD edges. The horizontal and vertical offsets of the CCDs follow from the condition that each slit has to continue without a jump from one CCD to an adjacent one (see Fig. 2).

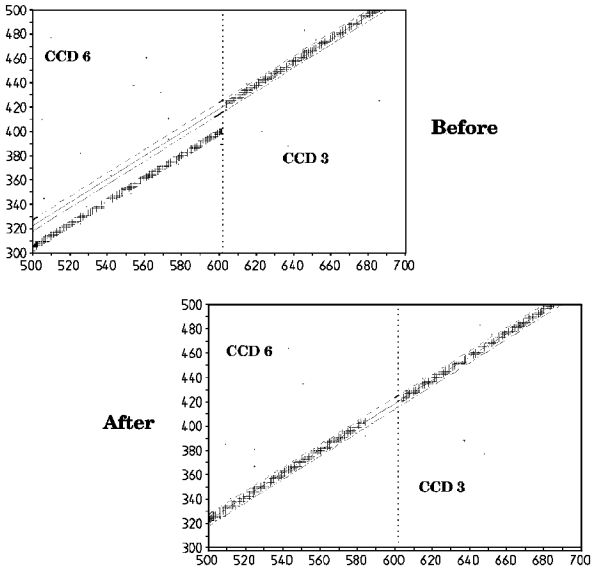

Fig. 2: Mask detail before and after position corrections

The final results for the individual CCD positions are given in Table 1. Note that the crucial values, the x–offsets for CCDs 4-6, all have an accuracy of roughly 4/100th of a pixel or ~1.6 μm. This level of precision is already near to what is achievable with optical methods, which would have required dismantling and transporting the detector. The result presented here is, in principle, accurate enough not to contribute noticably to the systematic error in the measured pion mass, but another mask measurement will take place in early 2002 to confirm these values.

CCD	x/y-Offset [pixel]	Rotation [mrad]
1	-2.585(26) / 22.535(92)	0.094(110)
2	-0.990(17) / 10.904(64)	0.343(56)
3	0 / 0	0
4	-14.545(46) / 21.108(95)	1.861(109)
5	-14.637(42) / 12.225(70)	2.984(91)
6	-16.410(39) / 1.270(22)	6.660(93)

Table 1: CCD position corrections (relative to CCD 3)

[a] Dept. of Phys. and Astr., Univ. of Leicester, England
[b] Paul–Scherrer–Institut (PSI), Villigen, Switzerland

[1] Annual report, IKP 2000, p. 72
[2] N. Nelms et al., to be published in Nucl. Instr. Meth.

Observation of deeply bound pionic states in Sn isotopes

A. Gillitzer, M. Fujita[a], H. Geissel[b], H. Gilg[c], R.S. Hayano[d], S. Hirenzaki[a], K. Itahashi[e], M. Iwasaki[e], P. Kienle[c], L. Maier[c], M. Matos[b], G. Münzenberg[b], T. Ohtsubo[f], M. Sato[e], M. Shindo[d], K. Suzuki[d], T. Suzuki[d], H. Weick[b], M. Winkler[b], T. Yamazaki[g], T. Yoneyama[e]

An experimental study of the ^{208}Pb(d,^{3}He) reaction at the GSI Fragment Separator (FRS) had led to the discovery of the deeply bound pionic states $2p$ and $1s$ in ^{207}Pb [1]. These states are inaccessible in electromagnetic cascades subsequent to the capture of stopped negative pions. In this first experiment the $2p$ state was observed as a distinct peak whereas the $1s$ state, populated with smaller strength, was only visible as a bump at the shoulder of the $2p$ state in the excitation energy spectrum. The poor separation of the two pionic states was partially due to the $3p_{1/2} - 3p_{3/2}$ doublet structure in the neutron hole spectrum in ^{207}Pb.

In a following experiment pionic states in ^{205}Pb were populated in the ^{206}Pb(d,^{3}He) reaction. ^{206}Pb was purposely chosen as a target because in this case a much smaller $3p_{1/2}$ contribution was expected from shell model systematics. Together with an improved energy resolution of $\sim$ 300keV, this allowed a clear separation of the pionic $1s$ state from the $2p$ state in the excitation energy spectrum. The data analysis of this experiment was completed and pionic binding energies and widths $B_{1s} = 6.768 \pm 0.061$MeV, $\Gamma_{1s} = 0.778^{+0.160}_{-0.141}$MeV, $B_{2p} = 5.110 \pm 0.045$MeV, and $\Gamma_{2p} = 0.371 \pm 0.060$MeV were deduced for the $1s$ and the $2p$ state, respectively [2].

Since the pionic $1s$ binding energy and width is almost exclusively determined by the s-wave pion-nucleus potential, the central potential V_0 can be deduced to be $\sim$ 27MeV (repulsive) [2], which indicates a significant additional repulsion as compared to the value deduced from the free πN scattering lengths. The experiment does however not allow to decide whether this additional repulsion is due to the isoscalar or the isovector part of the interaction. In order to experimentally separate both parts, one has to compare deeply bound pionic states in nuclei with different neutron to proton number ratio. In this respect the study of pionic states in Sn isotopes was considered particularly promising, an expectation which was supported by theoretical studies [3]. Sn has the advantage of having both a long chain of stable isotopes ranging from $A = 112$ to $A = 124$ and a well-suited neutron level scheme with low-lying $3s_{1/2}$ neutrons. This opens the possibility of populating quasi-substitutional configurations where the $s_{1/2}$ neutron is replaced by a negative pion in the $1s$ state. These configurations are preferentially formed at vanishing momentum transfer, a condition which is achieved in (d,^{3}He) transfer reactions at a deuteron incident kinetic energy close to 500 MeV.

In a beam time in May 2001 the population of deeply bound pionic states in Sn isotopes was studied at the FRS at GSI in the (d,^{3}He) reaction. The Sn isotopes $A = 112, 116, 120, 124$ were irradiated with a d beam at $T_d = 503.388$MeV. One of the prerequisites for the experiment was a high quality of the d beam, which was delivered from SIS with an intensity of $1.5 \cdot 10^{11}$ per spill (average intensity $\sim 0.5 \cdot 10^{11}$/s), a momentum spread $\delta p/p = 3 \cdot 10^{-4}$, and a horizontal beam spot $\delta x \simeq$ 1mm. In order to achieve the aspired energy resolution of 300 keV, thin strip targets of 1.3 mm width and 20 mg/cm^2 were used. The ^{3}He energy at the FRS focal plane was calibrated by using the non-pionic ^{112,116,120,124}Sn(d,^{3}He)^{111,115,119,123}In$_{(g.s.)}$ reactions, and independently by using the $p(d,^3\mathrm{He})\pi^0$ reaction from a thin mylar layer attached to the down-stream surfaces of the Sn targets. Fig. 1 shows the observed energy spectra (acceptance corrected) of ^{3}He in the ^{116,120,124}Sn(d,^{3}He) reactions. The three distinct peaks in the middle part correspond to the $1s$ states in ^{115,119,123}Sn, respectively. The large skewed peaks close to 371 MeV arise from the $p(d,^3\mathrm{He})\pi^0$ reaction, and are subject to a large kinematical shift and broadening. They not only assured that there was no long term drift in the experiment but also provided an independent energy calibration which turned out to be consistent with the calibration with the Sn(d,^{3}He)In reactions. Further analyses to deduce the binding energies, widths, isotope shifts and cross sections are in progress.

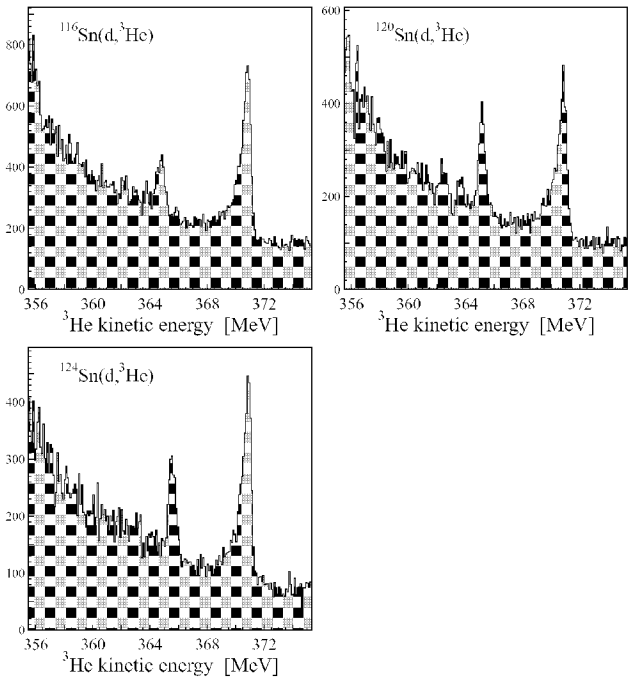

Fig. 1: Acceptance corrected ^{3}He kinetic energy spectra measured in ^{116,120,124}Sn(d,^{3}He) reactions at $T_d = 503.388$MeV. See text for further explanation.

References:

[1] T. Yamazaki *et al.*, Z. Phys. **A355** (1996) 219; H. Gilg *et al.*, Phys. Rev. C **62** (2000) 025201; K. Itahashi *et al.*, Phys. Rev. C **62** (2000) 025202.

[2] H. Geissel *et al.*, accepted by Phys. Rev. Lett.

[3] Y. Umemoto, S. Hirenzaki, K. Kume and H. Toki, Phys. Rev. C **62** (2000) 024606.

[a]Nara Women's University, [b]GSI Darmstadt, [c]Technische Universität München, [d]University of Tokyo, [e]Tokyo Institute of Technology, [f]Niigata University, [g]RI Beam Science Lab., RIKEN

Simulations on a general purpose detector to be used at the High Energy Storage Ring at GSI

V.Hejny, S.Ganzhur[1], O.Hartmann[2], U. Lynen[2], J.Ritman[3], C.Schwarz[2]

During the last year a Conceptual Design Report has been worked out presenting the plans for a major new international research facility at GSI Darmstadt, Germany [1]. The proposed facility consists of a 100/200 Tm double-ring synchrotron and a system of associated storage rings for beam collection, cooling, phase space optimization and experimentation. One major topic is the study of hadronic matter at the sub-nuclear level with beams of antiprotons in the energy range of 1 GeV to 15 GeV. They will be stored in the High-Energy Storage Ring (HESR) for in-ring experiments, which will be used for charmonium spectroscopy, for the search of hybrids and glueballs, the interaction of hidden and open charm particles with nucleons and nuclei, experiments with strange hypernuclei and CP violation studies.

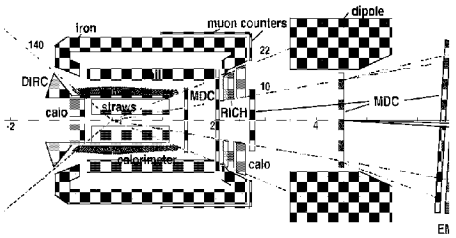

Fig. 1: Top view of the general purpose spectrometer. The detector is divided in a target spectrometer (solenoid section) and a forward spectrometer (dipole section).

Simulation techniques

For the main part of the programm a general purpose detector will be provided (Fig. 1). The detector design has to incorporate most recent technologies to reach the required performance criteria with regard to mass, momentum, and energy resolution, hit resolution, particle identification and solid-angle coverage. Therefore, it is a basic requirement to investigate the detector properties using a full simulation already at the planning stage. For the simulations the OO-based package Geant4 [2] has been chosen, together with PLUTO++ [3] for primary event generation and ROOT [4] for further data analysis. Geant4 and ROOT libraries have been combined successfully in order to transfer the output into ROOT data structures directly from the simulation. The output files are processed in separate ROOT sessions performing track and shower reconstruction and particle identification.

Currently, the components of the target spectrometer are fully implemented in the simulation. The target is surrounded by 4 diamond or silicon start detectors (each 20x30 mm^2) followed by 5 layers of a silicon micro-vertex detectors. Starting from a radial distance of 12 cm from the beam line, up to 42 cm, 15 double-layers of crossed straw tubes are arranged as a barrel, that extends from 40 cm upstream to 110 cm downstream of the target. At a radial distance of 45 cm a layer of DIRC Cherenkov detectors is placed surrounded by an electromagnetic calorimeter. This calorimeter consists of $PbWO_4$ crystals which are read out with avalanche photodiodes (APD). In the region between the calorimeter and the end cap there are 2 sets of mini drift chambers (MDC) with 6 active planes each. The TS is contained in a 2.5 m long and 80 cm radius solenoid. Behind the return yoke scintillating strips for muon identification are used. Code development for the forward spectrometer has not yet been started.

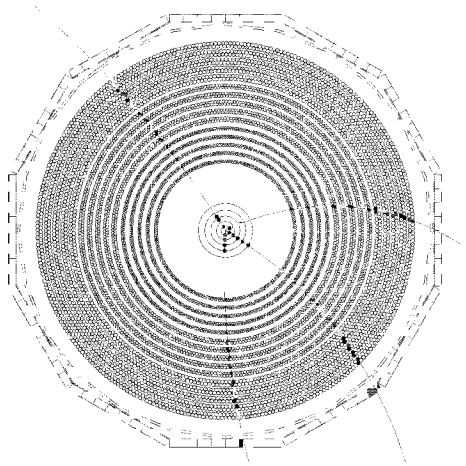

Fig. 2: View of the inner detectors. The tracks show an event of type $\bar{p}p \rightarrow \Phi\Phi$.

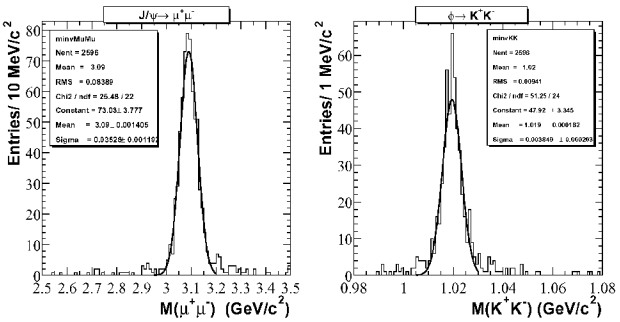

Fig. 3: Invariant mass distribution of $\mu^+\mu^-$ pairs and K^+K^- pairs from the reaction $\bar{p}p \rightarrow J/\psi + \Phi$.

Results

Only a few results obtained from the simulation can be shown here for illustration. The tracking of particles in the inner detectors of the target spectrometer is depicted in Fig. 2. The four tracks - bent in the field of the solenoid magnet of 2T - represent the final state of the reaction $\bar{p}p \rightarrow \Phi\Phi \rightarrow K^+K^-K^+K^-$. This momentum information in combination with particle identification in, for example, DIRC or RICH can be used to reconstruct the invariant mass. The resolution for a $\Phi \rightarrow K^+K^-$ invariant-mass spectrum is shown in Fig. 3 together with one for the decay $J/\psi \rightarrow \mu^+\mu^-$. A more detailed discussion of simulation results and the general detector properties can be found in [1].

References:

[1] "An International Accelerator Facility for Beams of Ions and Antiprotons", Conceptual Design Report, GSI, 2001, (http://www.gsi.de/GSI-Future).
[2] see http://wwwinfo.cern.ch/asd/geant4, CERN.
[3] see http://www-hades.gsi.de, GSI.
[4] see http://root.cern.ch, CERN.

[1]Inst. f. Experimentalphysik,Universität Bochum, Germany
[2]GSI Darmstadt, Germany
[3]II. Physikalisches Institut, Universität Gießen, Germany

2. Nuclear Spectroscopy

Gamma-ray Imaging with Segmented Tracking Detectors

W. Gast, L. Mihailescu, R.M. Lieder

Introduction

Gamma-ray imaging devices based on the Compton-camera principle theoretically could provide the highest detection efficiency, since they do not require any kind of collimation or masking. However, until now the large volume detectors needed for good efficiency, the high granularity needed for precise localization of the Compton interactions, and the high energy resolution needed for the reconstruction of the scattering angles made them incompetitive for practical implementation with respect to other approaches. With the advent of a new technical concept, the gamma-ray tracking detector, this situation changes. The tracking detector is a large volume high resolution semiconductor detector with relatively low granularity, but combined with advanced digital signal processing methods it is able to provide an effective position sensitivity being two orders of magnitude higher than that given by the physical granularity. The signal processing employs the WPC (Wavelet transform - Pattern recognition - Correlation analysis) method which decomposes and extracts multiple interactions occuring in the detector by analyzing the features of the digitized detector segment signals. Applying Based on the knowledge which we collected during the development of a coaxial, segmented tracking detector we studied the relevant criteria for a Compton- camera design based on tracking detector principles with planar Ge diodes.

Compton Camera Design

The basic concept of a Compton camera comprises a detector system made of two parts, a scatterer and an absorber. The direction of incident γ-rays, Compton-scattering from the scatterer to the absorber, is reconstructed by analysing the interaction positions and deposited energies in both detectors, i.e. by extracting the scattering angle, and applying the Compton formula. Hence the most relevant design criteria are:

* Maximize the probability that the incident γ-rays scatter by just a single scattering interaction from the scatterer to the absorber and that they are absorpt in the latter. This determines the total detection efficiency and hence the sensitivity of the Compton camera.

* Minimize the uncertainty with which the positions and energies of the γ-ray interactions are determined and maximize the distance between scatterer and absorber. This maximizes the accuracy of determining the scattering angle and hence optimizes the resolution of the Compton camera.

It is obvious, that these are partly conflicting requirements, and careful optimizations on the basis of Monte-Carlo simulations had to be made.

The best choice for the scatterer appears to be a planar detector, since its thickness can be easily varied. The thickness and the material of the scatterer detector, as well as the energy of the incident γ-ray determine its probability of undergoing a single forward scattering. Figure 1 shows the absolute number out of 100 000 Monte Carlo simulated events, which scatter frontward only once whithin a planar detector volume, as function of detector thickness for three different γ-ray energies (180, 511, and 1000 keV) and detector materials (CdZnTe, Ge, and Si), respectively. According to this, a Ge detector of 2.0 cm thickness appears to be a good choice

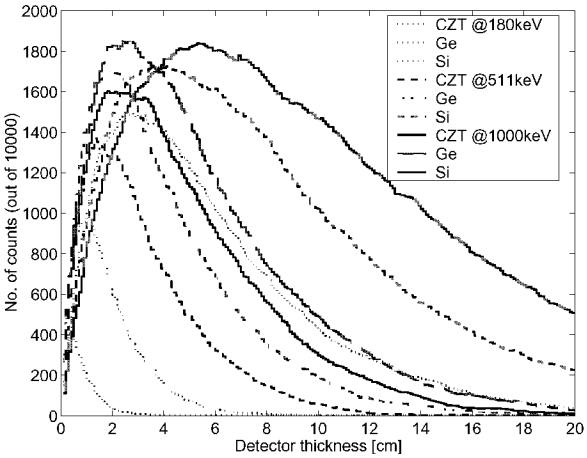

Fig. 1: Efficiency of a scatterer detector (see text)

for a broad range of energies. In addition Ge provides an adequate energy resolution, and the technical possibility to build planar detectors as thick as 2.5 cm with full depletion at a reasonable bias potential (approx. 2000V).

Ideally the absorber should be as big and efficient as possible. Since Ge offers the best price per volume and efficiency and a planar geometry the most favourable sensitive area-to-thickness ratio, and because of design simplicity and other reasons, which become clear later, we chose a stack of two 2.0 - 2.5 cm thick planar Ge detectors as absorber.

The ultimate resolution achievable for such a Compton camera is limited by the Compton profile, which reflects the fact that the γ-rays are scattered by electrons, which are not at rest, but moving in an unknown direction, and by the finite spatial distribution of the charge carriers, which are created during the ionization process by the recoiling electron. Both put natural limits on the energy and position resolution requirements being meaningful for our technical realization of the camera, i.e. energy resolutions better than 3 keV and 3D position resolutions better than 1 mm^3 is overkill. However, an optimal design should approach these limits.

Concerning the energy resolution our choice of a planar Ge-diode just provides the right order of magnitude. Concerning the 3D position resolution and taking a rectangular planar detector of 80x80x20 mm as an example, it means, that we have to provide an effective granularity of 128000 voxels per detector!

For a planar detector, we can consider the x,y coordinates (surface) and the z coordinate (depth) separately, when we discuss, how to achieve this granularity. The x,y granularity usually is obtained by segmenting either one or both electrodes into either pixels or orthogonal stripes, respectively. For a 1 mm raster this would mean 80x80 segments in case of a pixel detector and 80+80 segments in case of a strip detector. But even choosing the more economic strip detector as basis for our design, both solutions are unrealistic, considering, that each segment has to be equipped with a high resolution signal processing and data acquisition channel.

The advanced digital pulse shape analysis developed in the framework of the TMR project "Development of Gamma-Ray Tracking Detectors for 4*pi* Gamma-Ray Arrays" offers a solution to that problem. It allows to provide an effective position sensitivity being two orders of magnitude higher than that given by the physical granularity of the detecor by analyzing the features of the digitized "real charge" and "mirror charge" signals of the irradiated detector segments, and their neighbours with only influenced charges, respectively.
In this approach the signal-to-noise (S/N) ratio of the low amplitude induced current "mirror charge" signals, which are crucial for the x,y position identification, represents an important limiting factor, especially if a position resolution of the order of 1 mm for energies of $\leq$100 keV should be guarantied. Assuming a given noise the S/N ratio improves with increasing signal power. Amplitudes and shapes of the induced current signals depend on the profile of the weighting field along which the charge carriers drift, which field in turn depends mainly on the segment size, i.e. strip width. Figure 2 represents the profiles of the weighting fields along

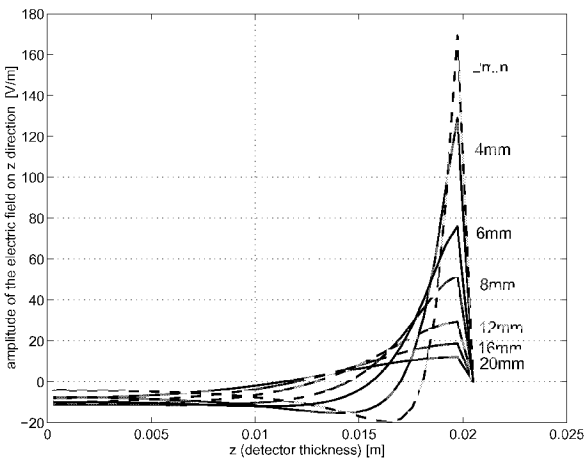

Fig. 2: Profile of the weighting fields at different strip widths for a planar Ge strip-detector of 20 mm thickness.

the virtual charge carrier drift path placed in the middle of the first neighbouring segment with respect to the one whose weighting field is considered. Smaller segments create better featured induced signals, but would also give rise to an increased number of segments. However, for segments smaller than $\approx$5mm, the steep variations might not be evident experimentally due to the limited bandwidth of the preamplifier and detector capacitance. A further reduction of the segment size would therefore bring no advantage in terms of a better profile of the induced signal anymore. With our γ-ray energy range of interest in mind we deduced a strip width of 8 mm as reasonable compromise between performance and price.
The depth of interaction, i.e. the z-coordinate of the 3D position identification, can only be obtained by pulse shape analysis, preferably by analysis of the real charge signals of the irradiated segments. If the above discussed limiting criteria for the mirror charge signals are fulfilled, the real charge signals have enough power to allow easily an extraction of the z-coordinate with at least 1 mm precision.

Pulse Shape Analysis
As in the case of the coaxial tracking detector the use of advanced digital signal processing and pulse shape analysis methods is the key to obtain high position sensitivity for large volume, planar semiconductor detectors. Taking the output of the preamplifier as signal source the signal processing starts by conditioning this non-ideal output signal for the analog-to-digital converter (ADC) via an anti-aliasing filter to fulfil the Nyquist theorem, and a differentiator to maintain the dynamic range at high rate. The resolution and sampling speed of the ADC itself has to be carefully selected to convert all the information contained in the analog signal into its digital representation without losses.
The pulse shape analysis system consists of three main processing steps: *Wavelet transform* + *Pattern recognition* + *Correlation analysis* (WPC). First the sampled signals are preprocessed using a specially designed wavelet transform. This processing has the important property of isolating and emphasizing the signal features, making their recognition less dependent on the noise level, and in the same time making a decomposition of multiple interactions possible.
The output of this transform, the wavelet coefficients, represent the data which are used in a pattern recognition system which determines the positions of interaction. This means that a data base has to be constructed which has to cover the various expected classes, i.e. signal types corresponding to a particular interaction position, and the recognition system has to identify to which class the experimental data pertain. Due to the not negligible probability of observing multiple interactions the problem is even more demanding, since then not only a single class within the experimental data, but a superposition of different classes with different weights has to be identified.
Therefore, and since an interaction in one segment will actually induce transient signals in all neighbouring segments, another important ingredient for a correct positioning is a correlation analysis, which correlates the pattern identification results of an irradiated segment with its neighbouring segments. In particular the x,y coordinates of an interaction are obtained from this analysis.
The WPC pulse shape analysis system is described in detail in ref. [1]. The average 1mm position resolution obtained using the WPC method fulfills the requirements for efficient γ-ray imaging. This position resolution corresponds to the targeted effective granularity of 128000 voxels for a planar detector with the dimensions $20\times80\times80$ mm^3, while in fact a physical segmentation into only $10+10=20$ segments is needed.

This work is partly supported by the EU in the framework of the TMR program under the contract ERB FMR XCT 970123.

References:

[1] L. Mihailescu, PhD Thesis, FZ-Jülich, (2001);

Design of the Advanced Gamma Tracking Array AGATA

R.M. Lieder and the TMR Gamma-Tracking Detector Collaboration

In order to carry out high-precision γ-ray spectroscopy using radioactive ion beams (RIB) or high-spin spectroscopy with stable beams with a sensitivity which is ≈ 100 larger than that of EUROBALL a new γ-ray detection system utilizing the concept of γ-ray tracking is required. For RIB applications stringent design criteria for a new γ-detector array are imposed. They result from limited beam intensities, a wide range of recoil velocities (up to $v/c = 50\%$), high γ-ray and particle backgrounds and γ-ray multiplicities up to $M_\gamma = 30$. A 4π γ-ray array with highest efficiency, selectivity and energy resolution is required which is capable of high event rates. The main properties for $E_\gamma = 1$ MeV and $v/c \leq 50\%$ can be summarized as follows:

Photo-peak efficiency $P_{ph}(M_\gamma = 1) = 40\%$
Photo-peak efficiency $P_{ph}(M_\gamma = 30) = 25\%$
Peak-to-total ratio $P/T(M_\gamma = 1) = 65\%$
Peak-to-total ratio $P/T(M_\gamma = 30) = 50\%$
Angular resolution $\Delta\Theta_\gamma(\Delta E/E \leq 1\%) \leq 1^\circ$

These features can only be achieved with a close-packed arrangement of Ge detectors, i.e., a 4π shell consisting of γ-ray tracking detectors. This new generation of Ge detectors has been developed in the framework of the TMR Network Project "Development of Gamma-Ray Tracking Detectors for 4π Gamma-Ray Arrays" (contract nr. ERBFMRXCT970123). They consist of high-fold segmented Ge detectors and a front-end electronics, based on digital signal processing techniques, which allows to extract energy, timing and spatial information on the interactions of a γ ray in the Ge detector by pulse shape analysis of its signals. Utilizing the information on the positions of the interaction points and the energies released at each point the tracks of the γ rays in a Ge shell can be reconstructed in three dimensions on the basis of the Compton scattering formula.

In order to achieve a large tracking efficiency the positions at which the γ rays interact inside the detector volume, should be determined with an accuracy of 1-2 mm. This corresponds to an effective granularity of approximately 30000 voxels per Ge detector. It is impossible to achieve such a granularity by a physical segmentation of the detector. However, pulse shape analysis methods have been developed, which can provide this position accuracy together with high resolution energy and time information. These methods require a medium level segmentation of the outer detector contact. The segments are read out via individual preamplifiers and can be considered as separate detectors.

The design of the Advanced Gamma Tracking Array AGATA with the properties defined above has been carried out [1]. The geometry of AGATA is based on the geodesic tiling of a sphere with twelve regular pentagons and 180 hexagons. For this design three slightly different irregular hexagons are needed. Owing to the geometry these three hexagonal detectors can be mounted in a common cryostat and the 180 hexagonal detectors can be arranged in 60 equal cryostats. Each Ge detector is encapsulated and has 36 segments. The total solid angle covered by Ge material is close to 80%.

The total number of segments in the array is 6780. Together with pulse shape analysis, this provides unprecedented position sensitivity. A key feature of AGATA is the high precision for determining the emission direction of the detected γ quanta of $\leq 1^\circ$ corresponding to an effective granularity of $\geq 5 \cdot 10^4$. This ensures an energy resolution better than 0.5% for transitions emitted by nuclei recoiling at velocities as high as 50% of the speed of light. This value is only a factor of two bigger than the intrinsic resolution of Ge detectors. With respect to EUROBALL the improvement under these conditions is a factor of 10.

The 36-fold segmented Ge detector of AGATA with six azimuthal and six longitudinal segmentations has a cirular shape at the rear side with a diameter of 8 cm and a hexagonal shape at the front face. The length of the detector is 10 cm. An AGATA module is a cryostat containing three segmented Ge detectors.

The preamplified detector signal has to be digitized with at least 12 bit resolution and at a speed of at least 40 MSPS (million samples per second) in order to preserve all relevant features of the signal in its digital representation. It is the task of the digital processing electronics to digitize the preamplifier signal using a sampling ADC and to provide digital signal processing hardware powerful enough for on-line processing of the signals. Under optimum conditions the whole information should be reduced to only five values per interaction: E_γ, t_γ and the three coordinates of the interaction point. Methods for a determination of the interaction positions of γ-rays in segmented Ge detectors have been developed. They take into account the shapes of the induced "real" and "mirror" signals. Real signals are measured at the electrodes of the segment, in which an interaction takes place. Mirror signals are measured on the electrodes of the neighbouring segments, where no interaction takes place and are due to a capacitative coupling between these segments and the moving charges. With a pattern recognition system based on the wavelet transform of the preamplifier signals a position resolution of the order of 1 mm^3 for single events was obtained. Multiple hits may be resolved if they lie more than 2 - 3 mm apart. The position resolution depends on the noise. The limit of the position resolution is the dimension of the charge carrier cloud produced in an interaction, being ≈ 1 mm.

Tracking requires powerful computer algorithms that takes into account the physical characteristics of the γ-ray interactions in the detector. The development of such algorithms follows two successful lines. In the so-called "clusterization" mthod a preliminary identification of interaction-point clusters is followed by a comparison of all possible scattering angles within a cluster against the Compton-scattering formula. The second approach starts from those points likely representing the last interactions and goes back, step by step, to the origin of the incident γ rays. This "backtracking" method allows, in principle, to disentangle the interaction points of two γ rays which enter the detector very close to one another. Furthermore, long-range scattering such as backscattering across the target region may also be recovered. The optimal tracking algorithm may be a combination of both methods including features such as pair production and neutron rejection. These tracking algorithms achieve a reconstruction efficieny of up to 60%, depending on the assumed accuray for the determination of the interaction positions.

References:

[1] AGATA Proposal, GSI Darmstadt (2001)

Evaluation of critical input angular momenta in the ^{114}Cd+^{36}S and ^{100}Mo+^{48}Ti reactions from fold spectra

A.A. Pasternak[1], R.M. Lieder, W. Gast, E.O. Podsvirova[1], D. Bazzacco[2], S. Lunardi[2], R. Menegazzo[2], C. Rossi Alvarez[2], G. de Angelis[3], D. Napoli[3] and T. Rzaca-Urban[4]

To deduce the critical input angular momenta Lcr for the ^{114}Cd(^{36}S,xn)^{144,145,146}Gd (E=182MeV) and ^{100}Mo(^{48}Ti,xn)^{143,144,145}Gd (E=215 MeV) reactions a global fit of experimental fold spectra [1] has been carried out. The calculation procedure is briefly described in [1-3]. Three values of Lcr for each reaction, viz. 48, 53, 58 $\hbar$ for the ^{100}Mo + ^{48}Ti reaction and 53, 61, 69 $\hbar$ for the ^{114}Cd + ^{36}S reaction have been chosen. For each residual nucleus experimental fold spectra have been fitted and the optimum value of the parameter Smr, defined in [1], has been deduced. After a subtraction of the unstretched transitions of statistical and mixed interband nature for each case the value %M1 = stretched M1/stretched M1+E2 contributions has been found. Since the location of the entry state population distributions are close for ^{144}Gd and ^{145}Gd, respectively, in the ^{114}Cd+^{36}S and ^{100}Mo+^{48}Ti reactions the parameters, representing the relative population probability for magnetic rotational bands, should also be close. Based on this hypothesis the parameters %M1 have been evaluated for ^{144}Gd and ^{145}Gd (Fig 1. Top). Subsequently it was possible to evaluate Lcr independently for each nucleus and both reactions. For each reaction the Lcr values obtained in the analysis of the fold distributions for ^{144}Gd and ^{145}Gd agree with each other, but the sensitivity for the case of ^{145}Gd is higher due to the larger angular momenta of the entry states as compared to the ^{144}Gd case. The results are presented in Tabl. 1. An indirect evidence for the validity of the deduced parameters Lcr and %M1, responsible for the population and deexcitation of the entry states in case of the ^{114}Cd(^{36}S,5n)^{145}Gd reaction, is the agreement of the calculated time distribution for the population of the yrast superdeformed band at high spins with the experimental value for the effective side feeding time [3]. In case of the ^{48}Ti+^{100}Mo reaction the value obtained for Lcr seems to be close to the data obtained for the ^{50}Ti + ^{118}Sn and ^{94}Zr + ^{74}Ge reactions leading to the ^{168}Hf compound nucleus [4, 5]. In spite of indirect arguments for the validity of our analysis the difference in Lcr obtained for our reactions (61 $\hbar$ and 53$\hbar$, for ^{114}Cd+^{36}S and ^{100}Mo+^{48}Ti respectively) seems to be unexpectedly large.

The work was partly funded by the Russian-German Cooperation in Science and Technology project RUS-99/191.

[1] A.F. Ioffe PTI, RU-194021, St.-Petersburg, Russia
[2] INFN, Sezione di Padova, I-35131 Padova, Italy
[3] INFN, Lab. Naz. di Legnaro, I-35020 Legnaro, Italy
[4] Warsaw University, PL-00-681, Warsaw, Poland

References:

[1] R.Lieder et al., IKP Ann. Rep. 2001
[2] A.A. Pasternak et al., IKP Ann. Rep. 2001
[3] A.A. Pasternak et al., IKP Ann. Rep. 2001
[4] J. Domscheit et al., Nucl. Phys. A 689 (2001) 655
[5] J.N. Wilson et al., submitted to EPJA (2001)

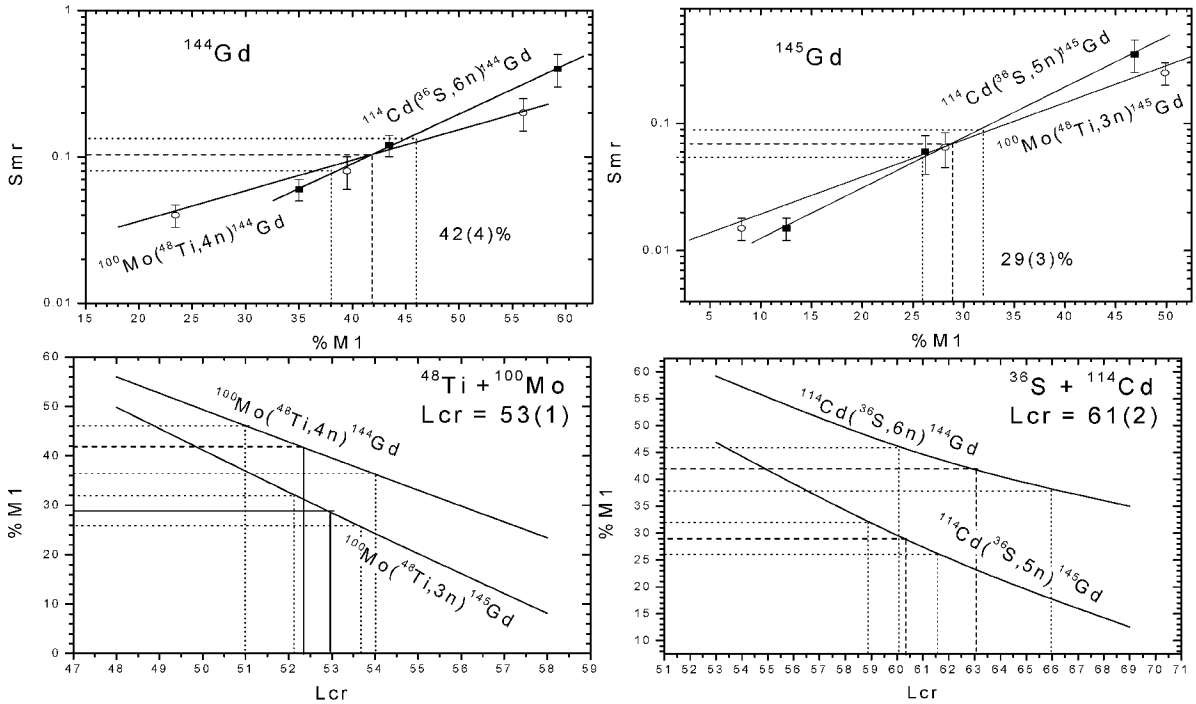

Figure 1. Top – Smr vs. %M1 dependences for ^{144}Gd and ^{145}Gd as measured in the ^{114}Cd+^{36}S and ^{100}Mo+^{48}Ti reactions and evaluation of %M1 for the ^{144,145}Gd nuclei. Bottom – Evaluation of Lcr for both reactions from the %M1 results.

Reaction	Gate, keV	L_{cr}	$I_{1/2m}$	S_{mr}	M_{sum}	M_{E2}	M_{E1}	M_{M1sm}	M_{M1str}	$\%M1_{str}$
^{100}Mo(^{48}Ti,5n)^{143}Gd	1023 (19/2$^-$)	53	46	0.04	18.6	9.6	3.0	1.4	4.6	32
^{114}Cd(^{36}S,6n)^{144}Gd	715 (11$^+$)	61	50	0.10	20.7	9.3	3.3	1.4	6.7	42
^{100}Mo(^{48}Ti,4n)^{144}Gd	+1017 (12$^+$)	53	50	0.10	24.2	11.0	3.8	1.4	8.0	42
^{114}Cd(^{36}S,5n)^{145}Gd	1553	61	55	0.07	27.1	15.7	3.4	1.6	6.4	29
^{100}Mo(^{48}Ti,3n)^{145}Gd	(13/2$^+$)	53	54	0.07	29.4	17.1	3.7	1.6	7.0	29
^{114}Cd(^{36}S,4n)^{146}Gd	1579 (3$^+$)	61	60	0.09	32.7	19.7	3.7	1.7	7.6	28

Tabl. 1. Results of fold spectra analysis. L_{cr} and $I_{1/2max}$ — positions at half maxima of the input and entry state spin distributions , M_{**} — multiplicity data with respective indices, M1sm – unstretched M1 transitions (statistical and mixed).

Side feeding pattern calculations including stretched M1 cascades and superdeformed bands in the continuum

A.A. Pasternak[1], R.M. Lieder, W. Gast, E.O. Podsvirova[1] and D. Bazzacco[2]

Our previous work [1] on side feeding pattern calculations has been extended. In the calculations using Monte-Carlo methods all possible side feeding cascades starting from the entry states region are taken into account assuming that side feeding is not only defined by the competition between stretched E2 bands (including the rotational damping effect) and statistical E1 transitions but that additional mechanisms can play important roles. Now the side feeding pattern calculations have been considerably improved both for DSAM applications (time dependence of the side feeding population probability) and for calculations of other measurable quantities like sum energy spectra and multiplicity distributions.

The improved Monte-Carlo code takes typically 10^6 entry state events, simulated by the code COMPA [2] taking into account the formation and decay of compound nuclei, and simulates the side feeding cascades between the entry states and the considered levels. The standard level density parameterization has been used [3]. Additionally to the stretched E2 bands and statistical E1 transitions statistical M1and E2 transitions as well as M1and E2 transitions between mixed bands have been included in the calculations. For the case of the near-magic nuclei $^{142\text{-}146}$Gd several special hypotheses have been made which allow to consider the influence of superdeformed bands (SDB) and the existence of a large amount of particle-hole excitations in the entry state region which generate magnetic rotational bands with shears effects [4]. The mechanism to form shears bands in the continuum region as well as results of the calculations of effective side feeding times in case of the investigated ^{114}Cd(^{36}S,5n)^{145}Gd reaction [5] are presented in Figs. 1, 2. Parameters for the calculations have been taken from the analysis of multiplicity distributions [6].

The work was partly funded by the Russian-German Cooperation in Science and Technology project RUS-99/191.

[1] A.F. Ioffe PTI, RU-194021, St.-Petersburg, Russia
[2] INFN, Sezione di Padova, I-35131 Padova, Italy

References:

[1] A.A. Pasternak et al., IKP Ann. Rep 2000, Jül-3852 (2001) 79
[2] A.A. Pasternak et al., IKP Ann. Rep. 2001
[3] T. Døssing and E. Vigezzi, Nucl. Phys. A587 (1995) [4]
[4] R.M. Clark and A.O. Macchiavelli, Ann. Rev. Nucl. Part. Sci. 50 (2000) 36
[5] T. Rzaca-Urban et al., Nucl. Phys. A677 (2000) 25
[6] R.Lieder et al., IKP Ann. Rep.2001

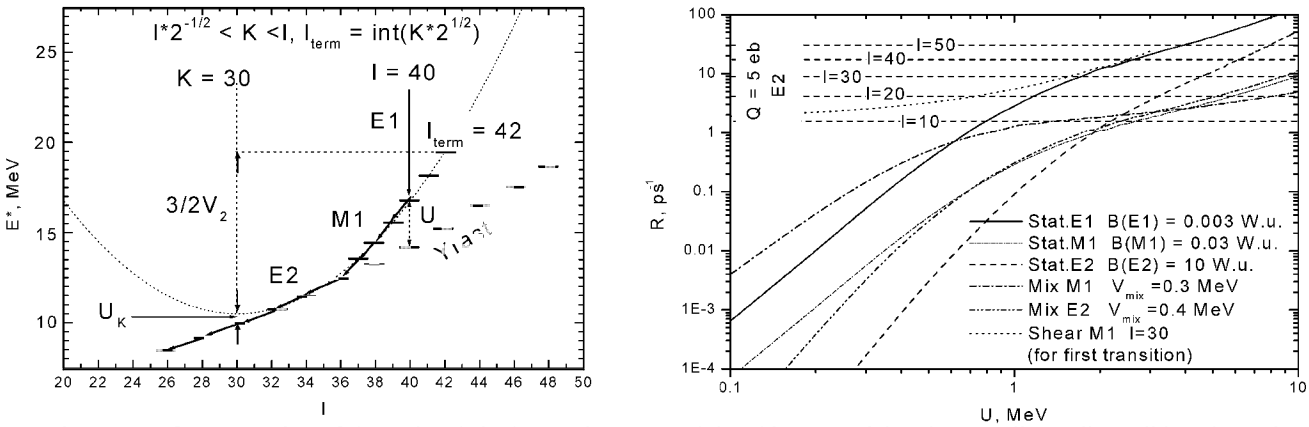

Figure 1. Left – Formation of shears bands in the continuum. Each band is tangential to the yrast line. All possible values of K are taken into account. Right – γ-transition probabilities for different types of γ-radiation versus excitation energy U above the yrast line.

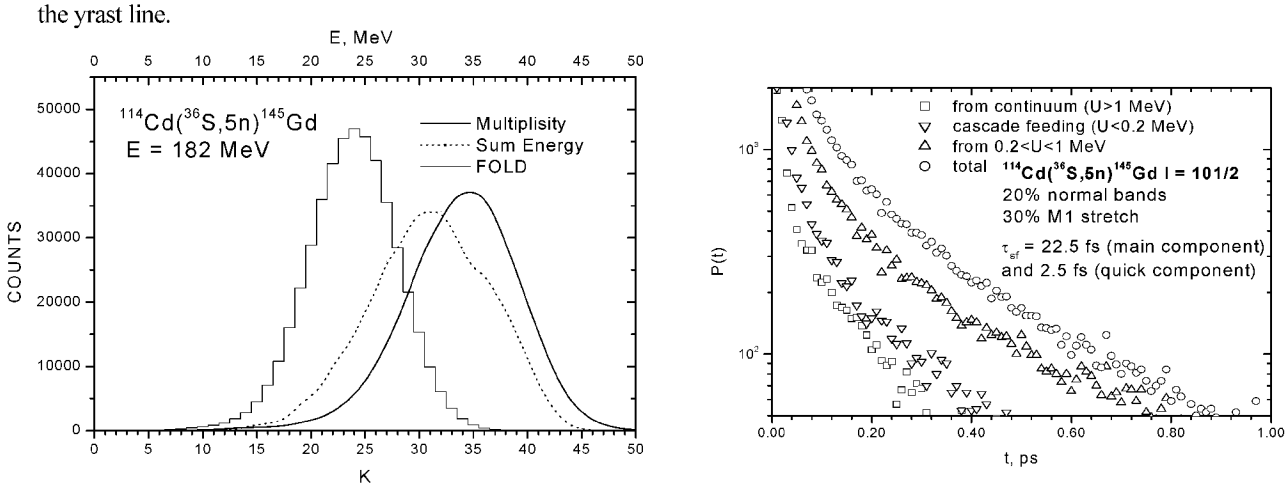

Figure 2. Left - Calculated multiplicity, sum energy and fold distributions for the ^{114}Cd(^{36}S,5n)^{145}Gd reaction studied with GASP. Right – Time population curves, calculated for the yrast SDB of ^{145}Gd. The experimental value [5] is $23\ ^{+12}_{-7}$ fs.

Side-feeding time-distributions for the 26^+ level of ^{144}Gd populated in the ^{114}Cd(^{36}S,6n) reaction at E = 182 MeV

R.M. Lieder, A.A. Pasternak[1], W. Gast, E.O. Podsvirova[1], D. Bazzacco[2], S. Lunardi[2], R. Menegazzo[2], C. Rossi Alvarez[2], G. de Angelis[3], D. Napoli[3], T. Rzaca-Urban[4] and W. Urban[4]

A new approach for the investigation of continuum γ-ray cascades has been developed. It is based on Monte-Carlo simulations of entry-state population distributions and the deexcitation of the entry states using a few parameters for the simultaneous fitting of different types of experimental data, e.g., statistical distributions of γ-ray cascades like γ-multiplicity, distributions and DSA γ-lineshapes, being sensitive to the time-distribution of side-feeding cascades. For the case of the ^{114}Cd(^{36}S,6n)^{144}Gd reaction at E = 182 MeV, studied with the γ-spectrometer GASP at the LNL, Italy, the parameter, responsible for the relative density of stretched magnetic bands as compared to that of the E2 bands (Smr = 0.08±0.02) and a critical input angular moment (Lcr = 61±2) have been found from a fit of experimental fold distributions [1-4]. Side-feeding time distributions have been calculated for different values of a third parameter, viz. Sb being the relative density of stretched E2 bands for a normal deformation (Qo = 4 eb) as compared to the full density including SD bands (Qo = 14 eb) in the high spin region (I > 26 ħ) where the yrast SD band crosses the normal deformed yrast states (Fig.1a.). The experimental value of the parameter Sb has been evaluated by the DSA lineshape analysis of the 837 keV γ-line, corresponding to the E2 transition from the 26^+ state in ^{144}Gd which is to 70% populated by side feeding. Unfortunately it is in this case impossible to evaluate the lifetime (τ) of the 26^+ state independently since the population of the band at high spins is too weak for a lineshape analysis using the "gating above" technique [5] or the "narrow gate on transitions below" procedure [6], which allows to bypass the side-feeding problem. Besides, at least three background lines contaminate the Doppler-broadened γ-line of interest (Fig 1b).

Therefore, the parameter Sb and the lifetime τ were evaluated by the analysis the difference spectra obtained by subtracting the spectra measured with backward ring detectors from those of the corresponding forward ring detectors. In this case the unshifted components of the lines of interest as well as all unshifted background lines are removed and the lineshape becomes anti-symmetric around a zero mean value (Fig.1c). The final lineshape, suitable for fitting has been constructed by summing the negative left and positive right components of this line after two subsequent reflection operations (Fig.1d).
The preliminary result is that up to an excitation energy of U ~1 MeV above the SD yrast line a large number of (about 80%) SD continuum bands contribute. A lifetime of τ = 0.38 ± 0.09 ps has been obtained for the 26^+ state in ^{144}Gd .

The work was partly funded by the Russian-German Cooperation in Science and Technology project RUS-99/191.

[1] A.F. Ioffe PTI, RU-194021, St.-Petersburg, Russia
[2] INFN, Sezione di Padova, I-35131 Padova, Italy
[3] INFN, Lab. Naz. di Legnaro, I-35020 Legnaro, Italy
[4] Warsaw University, PL-00-681, Warsaw, Poland

References:

[1] R.Lieder et al., IKP Ann. Rep. 2001
[2] A.A. Pasternak et al., IKP Ann. Rep. 2001
[3] A.A. Pasternak et al., IKP Ann. Rep. 2001
[4] A.A. Pasternak et al., IKP Ann. Rep. 2001
[5] A. Pasternak et al., EPJ A09 (2000) 293
[6] F. Brandolini, R.V. Ribas, Nucl. Instr. & Meth. A 417 (1998) 150

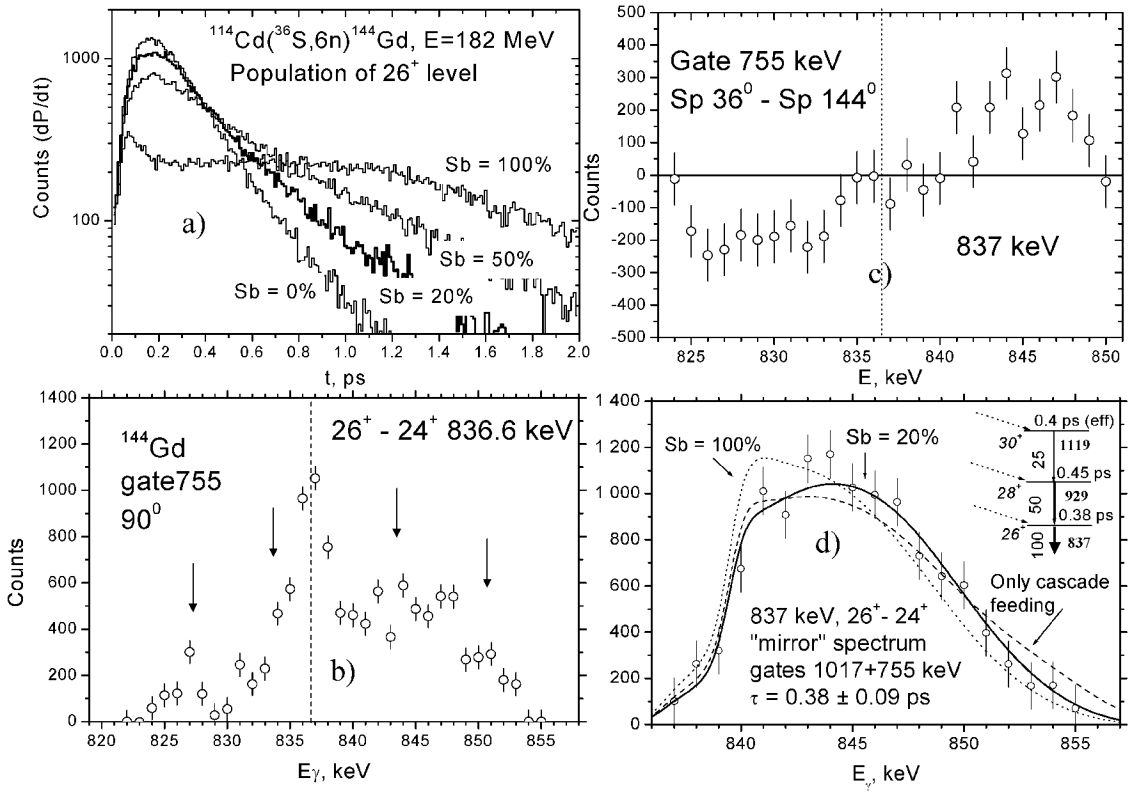

Fig. 1. a) Side-feeding time distributions for the population of the 26^+ state in ^{144}Gd for four values of Sb. b) Partial spectrum containing the 837 keV line measured at 90°; arrows mark contamination lines. c) Spectrum obtained by subtracting the spectrum for the 144° ring from that of the corresponding 36° ring. d) Fit of the lineshape to a spectrum obtained by two subsequent reflections.

Analysis of fold distributions in the $^{114}Cd(^{36}S,xn)^{144-146}Gd$ and $^{100}Mo(^{48}Ti,xn)^{143-145}Gd$ reactions

R.M. Lieder, A.A. Pasternak[1], W. Gast, E.O. Podsvirova[1], D. Bazzacco[2], S. Lunardi[2], R. Menegazzo[2], C. Rossi Alvarez[2], G. de Angelis[3] and D. Napoli[3]

On the basis of high statistics Monte-Carlo simulation calculations of the formation of entry state distributions [1] and their γ-ray de-excitation taking into account shears bands [2], multiplicity distributions have been calculated for the $^{114}Cd(^{36}S,xn)^{144-146}Gd$ (E=182 MeV) and $^{100}Mo(^{48}Ti,xn)^{143-145}Gd$ (E=215 MeV) reactions. Experimental fold distributions for the 3n – 6n reaction channels have been obtained from data measured with the spectrometer GASP by gating on transitions characteristic for the respective final nuclei. For the comparison of calculated multiplicity and experimental fold distributions a deconvolution of the measured fold distributions using the response function of the BGO ball of GASP for high-multiplicity events is required. But since the parameters of this transformation depend on the γ-ray energy this procedure is not accurate enough as the cascades contain E2 (≈1 MeV), E1 (≈2-3 MeV) and M1 (≈0.5 MeV) transitions. Therefore, the multiplicity distributions have been folded with the calibration response function to obtain fold distributions, which can be compared with the experimental results.

The main factors, important for the reproduction of the experimental fold distributions, are the critical input angular momentum Lcr [1] defining the position of the entry state population distribution in the E vs. I plane and the multiplicities of the stretched M1 cascades. The evaluation of Lcr is described in [3]. The multiplicities of the M1 cascades depend on the relative density of stretched magnetic bands as compared to that of the E2 bands. As an input parameter to define this multiplicity, the suppression factor Smr = R(M1rot)/R(M1rot$_{max}$) was used — being the relative probability for the first γ-transition to populate a M1 cascade as compared to the maximal possible value, calculated under the assumption that for each point of the entry state population distribution all possible values of K can be realized.

As an example in the left portion of Fig. 1 experimental and calculated fold distributions for the $^{100}Mo(^{48}Ti,4n)^{144}Gd$ reaction are shown. The experimental fold distributions were obtained by gating on the 1017 and 715 keV transitions feeding the 10^+ isomer, the 395 keV 18^+ - 17^+ transition in the strongest dipole band and the 755 keV 20^+ - 18^+ transition member of the strongest quadrupole band. With one parameter set it is possible to reproduce rather well all experimental fold distributions. In the right portion of Fig. 1 the corresponding multiplicity distributions are shown.

The work was partly funded by the Russian-German Cooperation in Science and Technology project RUS-99/191.

[1] A.F. Ioffe PTI, RU-194021, St.-Petersburg, Russia
[2] INFN, Sezione di Padova, I-35131 Padova, Italy
[3] INFN, Lab. Naz. di Legnaro, I-35020 Legnaro, Italy

References:

[1] A.A. Pasternak et al., IKP Ann. Rep. 2001
[2] A.A. Pasternak et al., IKP Ann. Rep. 2001
[3] A.A. Pasternak et al., IKP Ann. Rep. 2001

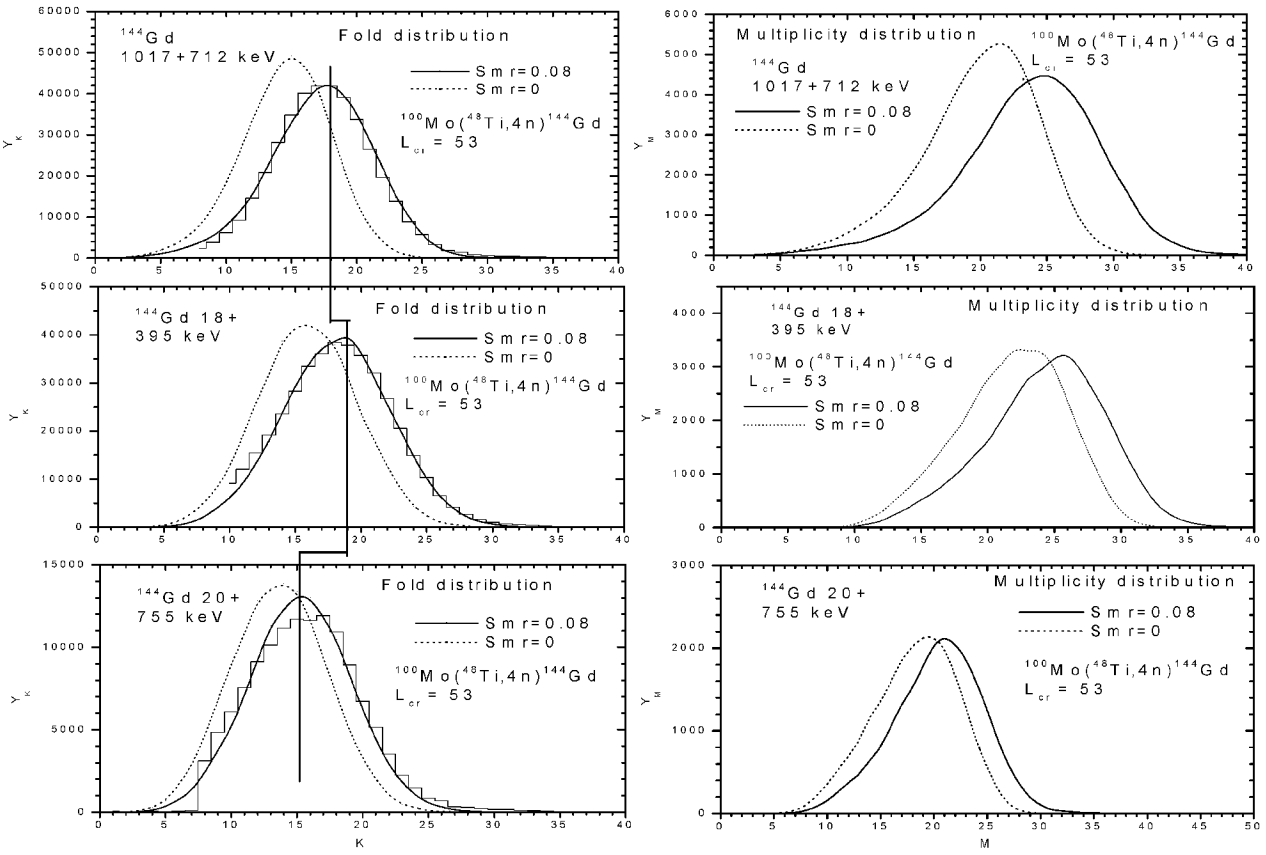

Figure 1. Left – Experimental (histograms) and calculated fold distributions for gates on different transitions in ^{144}Gd. Full and dotted lines are calculated with and without taking into account stretched M1 cascades. Right – Corresponding multiplicity distributions.

II. Theoretical Nuclear Physics

3. MEDIUM AND HIGH ENERGY PHYSICS

4. NUCLEAR PHYSICS AND OTHER TOPICS

3. MEDIUM AND HIGH ENGERGY PHYSICS

A study of η meson production in NN collisions

K. Nakayama[a)], J. Speth, and T.-S. H. Lee[b)]

The production of η mesons in NN collisions is thought to occur predominantly through the excitation (and de-excitation) of the $S_{11}(1535)$ resonance, to which the η meson couples strongly. However, the excitation mechanism of this resonance is currently an open issue. Some authors [1, 2] find the ρ exchange to be the dominant excitation mechanism of the $S_{11}(1535)$ resonance. In particular, it has been claimed [1] that ρ meson exchange is important for explaining the observed shape of the angular distribution of the $pp \to pp\eta$ reaction. Other authors [3] have found that both the π and η exchanges are the dominant excitation mechanisms. They have, however, considered only the $pp \to pp\eta$ reaction. In contrast to these findings, in Ref.[4] it is found that the dominant contribution arises not from the $S_{11}(1535)$ resonance current, but from the shorter range part of the nucleonic currents. Here, we report on another possible scenario for exciting the $S_{11}(1535)$ resonance that reproduces both the $pp \to pp\eta$ and $pn \to pn\eta$ reactions and discuss a possibility to disentangle these reaction mechanisms.

Our investigation of $NN \to NN\eta$ reaction is based on a relativistic meson exchange model of hadronic interactions. The reaction amplitude is calculated in the Distorted Wave Born Approximation. Details of our model may be found in Ref.[5]. In order to examine the differences between our model and previous works, we show in Fig. 1 the results from the calculations keeping only the $S_{11}(1535)$ resonance(solid curves) contribution. Within our model, this resonance excitation is due to the exchange of π, η, ρ, and ω. To see the relative importance between these different meson exchange mechanisms, we also show in Fig 1 the results from π exchange(dashed curves), η exchange(dash-dotted curves), and ρ exchange(dotted curves). The ω meson contribution is negligible. As can be seen, the dominant contribution is due to the π exchange followed by η exchange. The ρ exchange is very small in contrast to Refs.[1, 2] because we use a gauge invariant ρNN^* vertex rather than a gauge violating $\gamma_\mu\gamma_5$ vertex. In Fig 1 the nucleonic and mesonic currents are not included; their contribution to the total cross section is very small compared to that due to the $S_{11}(1535)$ resonance. However, their interference with the resonance current result in an angular distribution similar (although less pronounced) to that given by the ρ exchange dominance mechanism for exciting the $S_{11}(1535)$ resonance.

From the above considerations, we conclude that, at present, the excitation mechanism of the $S_{11}(1535)$ resonance in NN collisions is still an open question. It is therefore of special interest to seek a way to disentangle these possible scenarios. In this connection, spin observables may potentially help resolve this issue. As an example, we present in Fig. 2 the analyzing power at $Q = 10\ MeV$ (upper panel) and $Q = 37\ MeV$ (lower panel). The predictions of the present model are shown as the solid curves, whereas the predictions assuming the vector meson exchange dominance for exciting the $S_{11}(1535)$ resonance as the dashed curves. The different

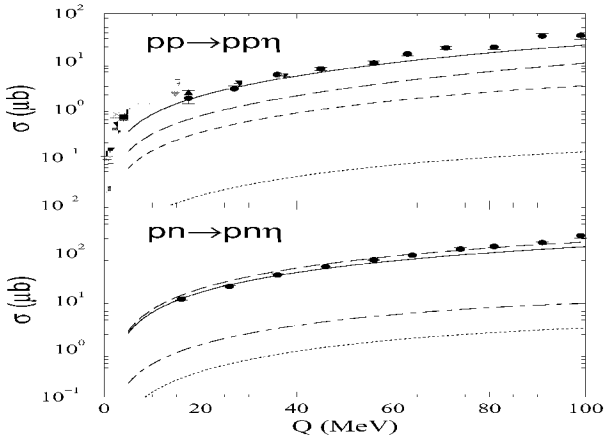

Fig. 1: $S_{11}(1535)$ resonance contribution to the total cross sections for the $pp \to pp\eta$ (upper panel) and $pn \to pn\eta$ (lower panel) reactions as a function of excess energy within our model.

features exhibited by the two scenarios for the excitation mechanism of the $S_{11}(1535)$ is evident. The dotted curve in Fig. 2 corresponds to the case of ρ exchange dominance according to Ref.[1].

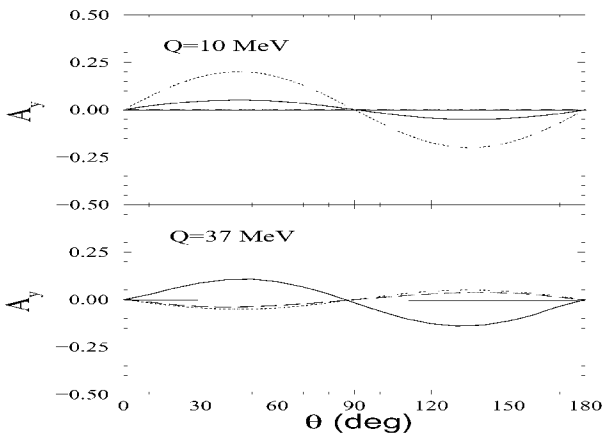

Fig. 2: Analyzing power for the reaction $pp \to pp\eta$ as a function of emission-angle of η in the c.m. frame of the total system.

References:

[1] G. Fäldt and C. Wilkin, nucl-th/0104081 and references therein.
[2] E. Gedalin, A. Moalem and L. Razdolskaja, Nucl. Phys. **A634**, 368 (1998).
[3] M. Batinić, A. Svarc and T.–S. H. Lee, *Phys.Scripta* **56**, 321 (1997).
[4] M. T. Peña, H. Garcilazo and D. O. Riska, Nucl. Phys. **A683**, 322 (2001).
[5] K. Nakayama, J. Speth, and T.-S. H. Lee, in preparation.

a) Department of Physics and Astronomy, University of Georgia, Athens, GA 30602, USA

b) Physics Division, Argonne National Laboratory, Argonne, IL 60439, USA

Neutron-Proton Final State Interaction in Incoherent Photoproduction of η mesons from Deuterium near Threshold

A. Sibirtsev, Ch. Elster, J. Haidenbauer, J. Speth

The incoherent η photoproduction on the deuteron close to threshold provides a very good scenario to investigate the final state interactions between the outgoing neutron-proton-η system. In Ref. [1] we calculated the reaction $\gamma d \to np\eta$ and included the dominant $S_{11}(1535)$ resonance and the neutron-proton (np) final state interaction. For photon energies around 680 MeV and higher the impulse approximation (IA) reproduces the η photoproduction cross section and the angular distribution of η-mesons in the photon-deuteron c.m. system quite well.

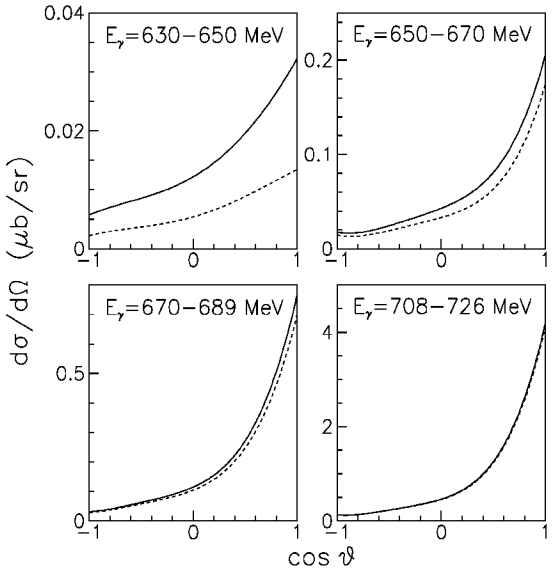

Figure 1: Angular distributions of the η mesons in the photon-deuteron c.m. system for different photon energies E_γ. The dashed line gives the IA calculation, while the solid line represents the result with the np FSI from calculated from the CD-Bonn potential [2].

At lower energies the consideration of the np FSI between the outgoing nucleons is essential to describe the relative enhancement of the cross section data with respect to the impulse approximation. It turns out that the magnitude of these np final state interactions is practically the same for different nucleon-nucleon force models considered.

Though the np FSI accounts for a large part of the observed enhancement, our analysis [1] suggests that there still remains a small discrepancy with respect to the data for very small excess energies. This discrepancy is of a similar size as found in the η production in nucleon-nucleon collisions and may be taken as signature of the ηN final state interaction close to threshold.

The angular distributions of the η mesons in the photon-deuteron center-of-mass (c.m.) system are

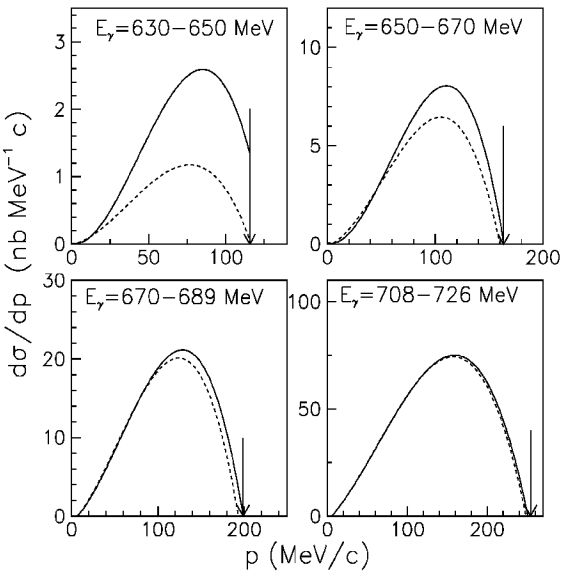

Figure 2: Momentum distributions of the η-meson in the photon-deuteron c.m. frame for different photon energies E_γ. The dashed lines shows the IA calculation, while the solid line represents the result with the np FSI from calculated from the CD-Bonn potential [2]. The arrow indicates the largest kinematically allowed momenta of the η-meson.

shown in Fig. 1. The momentum distributions of the η mesons in the photon-deuteron c.m. system are shown in Fig. 2. Both figures clearly indicate the enhancement through the np FSI with respect to the impulse approximation for photon energies close to the reaction threshold. We would like to emphasize that the theoretical results in Figs. 1 and 2 represent an average over the finite energy interval indicated in the figure. This is done in order to make the predictions comparable to experiments [3, 4], where likewise an averaging over energy bins is made.

References:

[1] A. Sibirtsev, Ch. Elster, J. Haidenbauer, J. Speth, Phys. Rev. **C64**, 024006 (2001).

[2] R. Machleidt, Phys. Rev. **C63**, 024001 (2001).

[3] V. Metag, Proceedings of the 8-th Int. Conf. on the Structure of Baryons, Bonn (1998), H. Ströher, V. Metag and J. Weiss, private communication.

[4] V. Hejny et *al.*, submitted to EPJ.

Effects of contact terms in OBE NN potentials

G. Caia, J.W. Durso, Ch. Elster, J. Haidenbauer, A. Sibirtsev, J. Speth

We examine the effects of inclusion of the contact terms that arise in one-boson exchange models based on time-ordered perturbation theory. In covariant perturbation theory one starts with a Lorentz-invariant Lagrangian density, from which one derives the Hamiltonian density and, from that, the Hamiltonian. For Lagrangians with scalar or pseudoscalar mesons without derivative coupling, the interaction part of the Hamiltonian density is just the negative of the interaction part of the Lagrangian density. For Lagrangians with derivative coupling or with vector mesons, however, non-covariant "contact" terms arise in the Hamiltonian density. These terms are necessary to cancel the non-covariant terms in the meson propagators so that, in any order of perturbation theory, the resulting amplitude is covariant [1]. From a procedural point of view, this means that in the Feynman rules one simply drops the contact terms and the non-covariant parts of the propagators.

In TOPT, however, one does not use particle propagators. They are effectively supplied by the vertex functions and energy denominators in the time-ordered diagrams. In order to obtain covariant results in TOPT starting from a Lagrangian density with derivative coupling, or with vector mesons, one must include the contributions of the contact interactions in the Hamiltonian in the appropriate order of the perturbation expansion. Therefore, for single pion exchange with pseudovector coupling in NN scattering, i.e., in second order in the coupling constant, one must include not just the meson exchange diagrams, but also the four-point nucleon-nucleon contact interaction (similarly for vector meson exchange). Only then will the result agree with covariant perturbation theory when all external particles are on their mass shells.

In order to make the comparison of different treatments of pseudoscalar meson exchange explicit, we will focus on two one-boson exchange (OBE) models of the NN interaction. One model will consider a pseudovector coupling of the pseudoscalars π and η, the other will use pseudoscalar coupling for them. All other mesons will be identical in both models, namely vector mesons ρ and ω, and scalar mesons σ and δ. Gauge terms arising in the polarization sum in vector meson exchange in TOPT will be retained. Results for some selected NN partial waves are shown in Fig. 1. The solid line corresponds to the model with pseudovector coupling and involving the contact terms (PV) and the dashed line are the phase shifts for the model with pseudoscalar coupling (PS). Evidently, both prescriptions yield a comparable and overall satisfactory description of the NN phase shifts. We should mention, however, that in both case the usual parameters of one-boson-exchange models (coupling constants of the heavier mesons, cutoff masses at the vertex form factors [2]) have been properly adjusted. In order to demonstrate the effect of the different coupling schemes we also present results were the pseudovector coupling (for the π and η-meson exchange) is replaced by pseudoscalar coupling, but without re-tuning the parameters. The corresponding phase shifts are given by the dotted line. Obviously, the coupling has basically no influence on P waves, neither on other higher partial waves [3]. This is simply a consequence of the short-ranged nature of those additional contact terms arising in the pseudovector coupling scheme. Not unexpected the strongest effects are seen in the mixing parameter ε_1. This quantity is primarily determined by the tensor force generated by the π exchange and here the two coupling scheme lead indeed to significant differences. At the same time the $^1S_0$, where this tensor force does not contribute remains essentially unchanged.

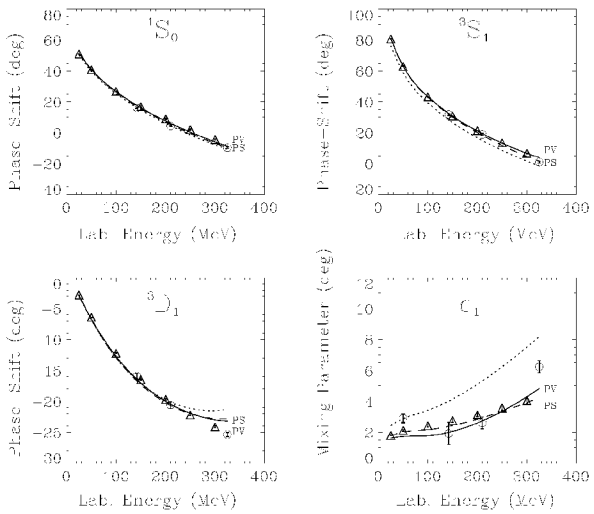

Figure 1: Phase shifts for some selected NN partial waves. The solid line represents the calculation with pseudovector coupling. The dotted line shows the results if pseudoscalar coupling is used. The dashed line are results for pseudoscalar coupling after refitting some of the model parameters.

References:

[1] S. Weinberg, *The Quantum Theory of Fields, Vol. I*, Cambridge Univ. Press, 1995, pp. 318.

[2] R. Machleidt, K. Holinde, and Ch. Elster, Phys. Rep. **149**, 1 (1987).

[3] G. Caia et al., in preparation.

Further development of the Jülich πN model

A.M. Gasparyan[1], J. Haidenbauer, C. Hanhart, and J. Speth

The existing Jülich πN model [1, 2] is based on the meson-exchange picture and contains five coupled channels, namely πN, ηN, and three effective $\pi\pi N$ channels (σN, ρN, and $\pi\Delta$). The potential consists of a set of t-channel diagrams (e.g. π, ρ, σ exchanges), u-channel pole graphs (nucleon and Δ exchanges), and also s-channel pole diagrams corresponding to the resonance contributions from the $\Delta(1232)$ and of the N^* resonances $S11(1535)$, $S11(1650)$, $D13(1520)$. This model yields a quite satisfactory description of the πN phase shifts and inelasticities as well as of the ηN differential and total cross sections in the energy range from the πN threshold up to about 1600 MeV.

The natural way to extend this model to higher energies is to include also other channels like $K\Lambda$, $K\Sigma$, and ωN which open at center of mass energies within the region 1600-1700 MeV. However, to do so one first has to apply some modifications in the πN sector of the model, because a direct extrapolation of the present scheme to higher energies produces results incompatible with the πN data (see [2]) – independently of whether additional channels are included or not.

In this work we report on the improvements of the model of Ref. [2]. First of all we added several pole contributions which are needed to describe the resonance structures in various partial waves, in particular we added the $S31(1620)$, $P13(1720)$ and $D33(1700)$ resonances, that are also known to play an important role in the pion induced strangeness production (c.f. [3, 4]). The nonresonant part of the potential or the background had to be suitably changed to describe the data far away from the position of the resonances. Our new results for the phase shifts are displayed in fig.1. Shown are the $S31$, $P13$, and $D33$ partial waves. The contributions from the background are given separately (dashed line). The results of the original Jülich πN model are shown by the dotted lines.

We also adopted a different treatment of the $S11$ resonances. The main problem which occurred in the original model was a dominant influence of the $N^*(1650)$ resonance on the near threshold region. To eliminate this we changed the πNN^* vertex structure from the scalar one used before to gradient coupling. It corresponds to the effective Lagrangian of the form

$$\mathcal{L}_{N^*N\pi} = \frac{f_{N^*N\pi}}{m_\pi}\bar{\psi}_{N^*}\gamma_\mu\vec{\tau}\psi_N\partial^\mu\vec{\Phi}_\pi + h.c.$$

This structure leads to a stronger suppression of the corresponding resonance graph at small momenta. However the main S-wave low energy contributions (ρ, σ exchanges) are fixed in our model by the dispersion relation technic. Therefore one has to introduce an additional S-wave piece to compensate for the absence of the resonance term at low energies. We solved this problem introducing a nonzero subtraction term in the dispersion relation in the σ channel.

The presented results are preliminary. Some work has yet to be done to incorporate strangeness channels as well as ωN channel.

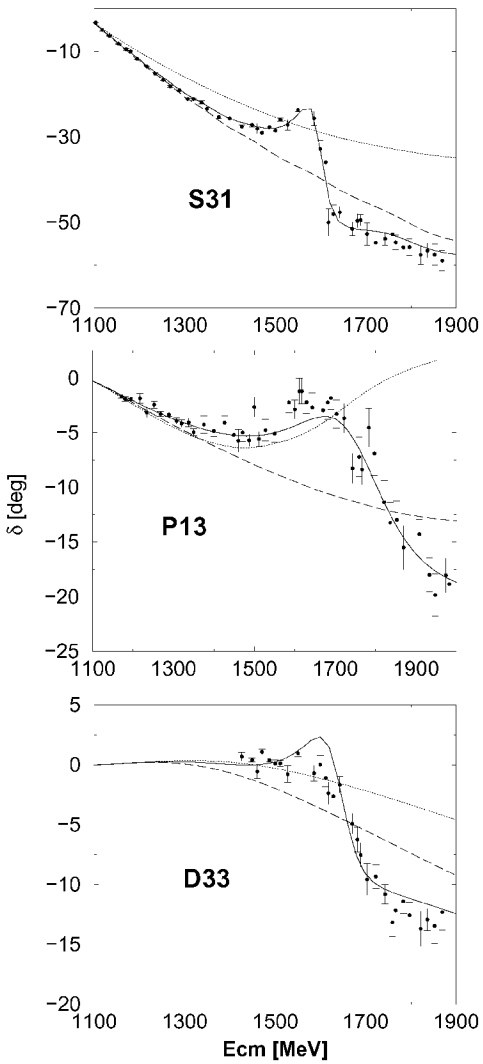

Fig. 1: πN phase shifts for S31, P13, and D33 partial waves. The dashed lines show the background contribution. Solid lines represent the total results. The dotted lines are the results of the original Jülich model [2]. The data are from [5].

References:

[1] C. Schütz et al., Phys. Rev. C **57**, 1464 (1998).
[2] O. Krehl et al., Phys. Rev. C **62**, 025207 (2000); O. Krehl, Jülich report, No. 3692 (1999).
[3] R.D. Baker et al., Nucl.Phys. B **126**, 365 (1977).
[4] D.J. Candlin et al., Nucl.Phys. B **238**, 477 (1984).
[5] SAID, current solution, Nov. 2001.

[1]also at: Inst. of Theoretical and Experimental Physics, 117258, B.Cheremushkinskaya 25, Moscow, Russia

Hard component to pion-pion scattering

A. Szczurek[1], N.N. Nikolaev and J.Speth

We evaluate the pQCD two-gluon (2G) contribution to the elastic pion-pion scattering. We treat the pion as the quark-antiquark state. A calculation of Born amplitudes in the non-relativistic approximation for the target and beam pions can be found elsewhere [1]. In the present communication we report results for elastic pion-pion scattering based on a relativistic light-cone description of the pion [2].

Making use of the Sudakov technique [3], one readily obtains the impact factor representation of the pion-pion scattering amplitude

$$A(\vec{q}) = is \cdot \frac{2}{9} \cdot \frac{1}{(2\pi)^2} \cdot \int d^2\kappa \; g_s^2(\kappa_1^2) g_s^2(\kappa_2^2) \; \Phi^{2g}_{\pi\to\pi}(\vec{q},\vec{\kappa}) \Phi^{2g}_{\pi\to\pi}(\vec{q},\vec{\kappa}) \; \frac{1}{(\vec{q}/2+\vec{\kappa})^2} \frac{1}{(\vec{q}/2-\vec{\kappa})^2} \; , \qquad (1)$$

where Φ is the two-gluon pionic impact factor, $\vec{\kappa}_{1/2} = \frac{\vec{q}}{2} \pm \vec{\kappa}$ are the exchanged-gluon momenta, which are purely transverse, 2/9 is the QCD color factor and g_s is the QCD strong charge[1].

There are four different diagrams how 2 gluons may couple to the pion. In general, both gluons may couple to the same quark/antiquark or to quark and antiquark. This leads to 16 2G exchange amplitudes for pion-pion scattering.

The anatomy of the 2G exchange amplitude is shown in more detail in Fig.1 where we present the cross section calculated in the case when gluons couple only to the same quark/antiquark (impulse approximation) and in the case when gluons couple only to different constituents of both pions. We shall call the later components Glauber-Gribov-Landshoff (GGL) terms. The IA components dominate at small to moderate values of $|t| \leq 0.5$ GeV^2, where the nonrelativistic and light-cone amplitudes are nearly identical. A comparison of the NR and LC cases shows clearly a substantial suppression of the GGL contribution by the $q-z$ correlations inherent to the LC case. The GGL mechanism dominates at $|t| \geq 1.0$ GeV where the light-cone amplitude decreases faster than the nonrelativistic one. One should note, however, that even at large $|t| \sim 4$ GeV^2 due to interference effects all contributions must be included.

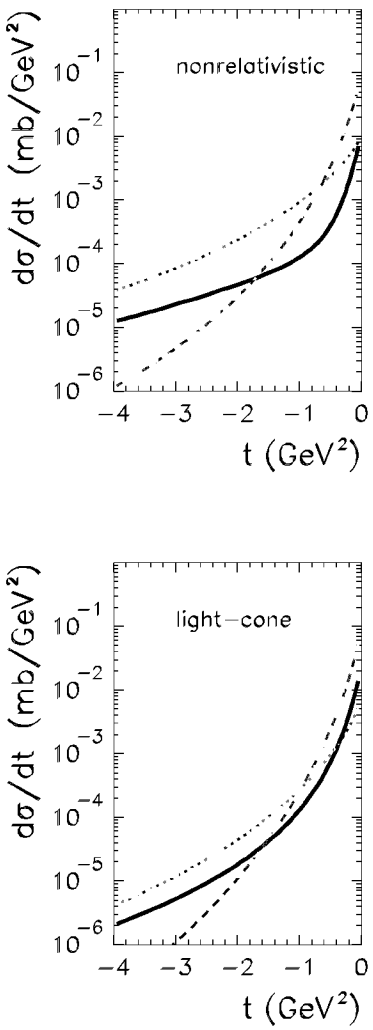

Fig. 1: The emergence of GGL dominance in elastic pion-pion scattering for the two-gluon exchange model. The dashed line is for pure IA contributions, whereas the dotted line corresponds to the pure GGL terms. The thick solid line corresponds to the full result with all terms for the impact factor.

References:

[1] J.F. Gunion and D.E. Soper, Phys. Rev. **D15**, 2617 (1977).

[2] A. Szczurek, N.N. Nikolaev and J. Speth, hep-ph/0112331.

[3] V.N. Gribov, L.N. Lipatov and G.V. Frolov, Sov. J. Nucl. Phys. **12** 543(1971).

[1]also at: Inst. of Nuclear Physics, PL-31-342 Cracow, Poland

[1]In our practical calculations the QCD coupling constant is frozen in the infra-red region.

Soft components to pion-pion scattering

A. Szczurek[1], N.N. Nikolaev and J.Speth

The understanding of the onset of hard pQCD regime requires evaluation of the large-$|t|$ tail from soft non-perturbative interactions. In the nonperturbative region of small transferred momenta in baryon-baryon and meson-baryon elastic scattering one is bound to the Regge phenomenology [1, 2].

In the case of pion-pion scattering the soft pomeron exchange must be supplemented by the subleading isoscalar (f) and isovector (ρ) reggeon exchanges. Here we resort to the simplest Regge-inspired phenomenological form:

$$\begin{aligned} A_{IP}(t) &= i\, C_{IP} \cdot (s/s_0)^{\alpha_{IP}(t)} \cdot F_{IP}^2(t)\ , \\ A_f(t) &= -\eta_f(t)\, C_f \cdot (s/s_0)^{\alpha_f(t)} \cdot F_f^2(t)\ , \\ A_\rho(t) &= -\eta_\rho(t)\, C_\rho \cdot (s/s_0)^{\alpha_\rho(t)} \cdot F_\rho^2(t)\ , \end{aligned} \quad (1)$$

where η_f and η_ρ are somewhat simplified signature factors:

$$\eta_R = \exp(i\phi_R(t))\ , \quad (2)$$

with the phase depending on the reggeon signature.

In the imupulse approximation, the Regge pole contributions to different scattering processes are related by the Regge factorization. In our case of $\pi\pi$ scattering residues at $t = 0$ can be evaluated from those for πN and NN scattering as:

$$C_i^{\pi\pi} = \frac{(C_i^{\pi N})^2}{C_i^{NN}} \quad (3)$$

for each reggeon $i = IP, f, \rho$. Then the corresponding Regge phenomenology of πN and NN scattering [3] gives $C_{IP} = 8.56$ mb, $C_f = 13.39$ mb and $C_\rho = 16.38$ mb.

Here for example we shall discuss the total cross section for both opposite-sign and the same-sign pion-pion scattering. In Fig.1 we compare our predictions with the quasi-data from [4]. While the opposite-sign pion-pion total cross section depends strongly on energy, the same-sign pion-pion total cross section is almost independent of energy. In the spirit of duality, the near cancellation of contributions from crossing-even and crossing-odd Regge exchanges in the $\pi^+\pi^+, \pi^-\pi^-$ channels is not accidental and is consistent with the absence of isotensor s-channel resonances, in close analogy to the flatness of the pp total cross section.

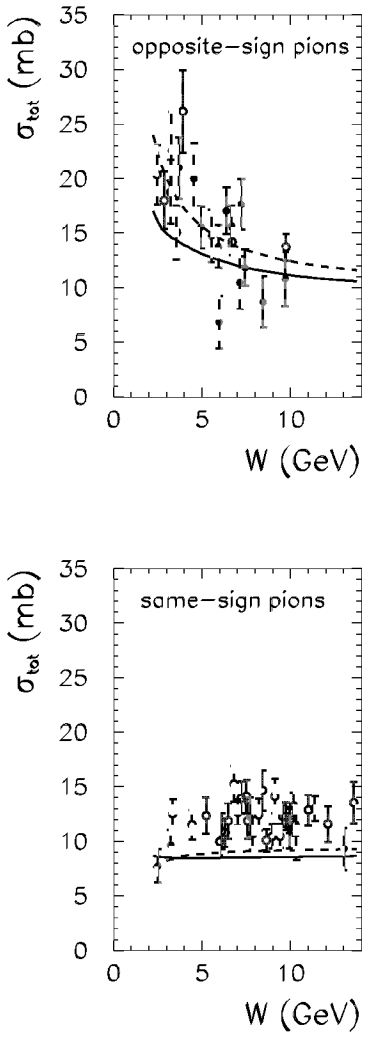

Fig. 1: Total cross section for $\pi^+\pi^-$ and $\pi^+\pi^+$ or $\pi^-\pi^-$ scattering as a function of center-of-mass energy W. The experimental data for $\pi^+\pi^-$ scattering (left panel) were extracted from $\pi^+p \to X\Delta^{++}$ (open circles) and from $\pi^+n \to Xp$ (full circles). The experimental data for $\pi^-\pi^-$ scattering (right panel) were extracted from $\pi^-p \to X\Delta^{++}$ (open circles) and from $\pi^-n \to Xp$ (full circles). The single IP and subleading reggeon exchanges are given by the dashed lines. The solid line includes absorption corrections to be discussed in the next contribution.

References:

[1] A.C. Irving and R.P. Worden, Phys. Rep. **34** 117 (1977);
A.B. Kaidalov, Phys. Rep. **50** 157 (1979).

[2] P.D.B. Collins, An Introduction to Regge Theory and High Energy Physics, Cambridge University Press, Cambridge 1977.

[3] A. Donnachie and P.V. Landshoff, Phys. Lett. **B296** 227 (1992).

[4] B.G. Zakharov and V.N. Sergeev, Sov. J. Nucl. Phys. **39** 448 (1984).

[1]also at: Inst. of Nuclear Physics, PL-31-342 Cracow, Poland

Multiple scattering effects in pion-pion scattering

A. Szczurek[1], N.N. Nikolaev and J.Speth

Absorption corrections to single reggeon+pomeron exchange have been studied actively in the past (see for instance [1] and references therein; a more recent dicussion can be found e.g. in [2]). One usually resorts to the so-called eikonal approximation. Here we restrict ourselves to the dominant double-scattering corrections which read

$$A_{ij}^{(2)}(s,\vec{k}) = \frac{i}{32\pi^2 s}\int d^2\vec{k}_1 d^2\vec{k}_2\,\delta^2(\vec{k}-\vec{k}_1-\vec{k}_2) \\ A_i^{(1)}(s,\vec{k}_1)\,A_j^{(1)}(s,\vec{k}_2)\,. \qquad (1)$$

In general, the single scattering amplitudes $A_k^{(1)}$ in (1) are not restricted to soft reggeon exchanges and hard two-gluon exchanges should be included too. Consequently in the following we shall include the (soft $\otimes$ soft), (soft $\otimes$ hard)+(hard $\otimes$ soft) and (hard $\otimes$ hard) double-scattering amplitudes. The last three double-scattering contributions are expected to be small, at least at forward angles, compared to the leading (soft $\otimes$ soft) absorption correction. In the (hard $\otimes$ hard) case the eikonal amplitude sums only a certain subset of possible four-gluon exchange amplitudes, but this contribution is entirely negligible.

For example, in Fig.1 we compare differential cross sections for single-exchanges and those including the double-scattering terms. Again one can observe rather different pattern for the opposite-sign (left panel) and the same-sign (right panel) pion-pion scattering. The dip minima for opposite-sign pion-pion scattering is due to strong destructive interference of the single- and double-scattering terms. To illustrate this better, by the dotted line we show seperately the cross section corresponding to the double-scattering amplitude alone. As can be seen from the figure the minima in the total cross section (solid) occur in the position where the cross sections corresponding to single-scattering (dashed) and double-scattering (dotted) are identical.

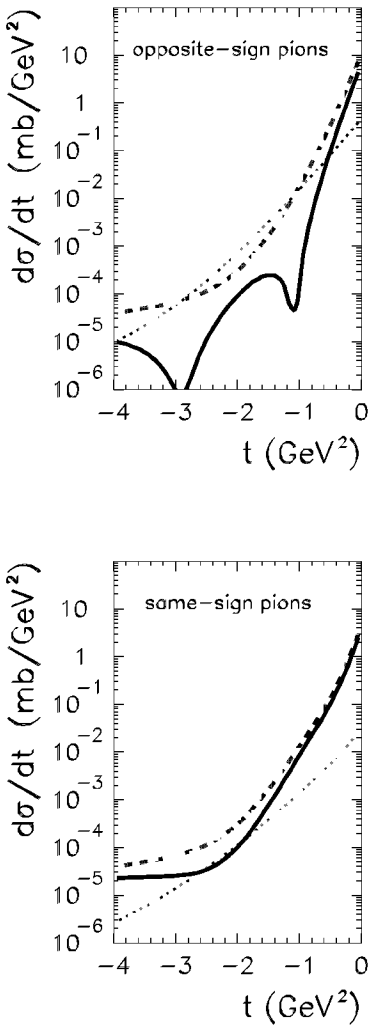

Fig. 1: The effect of the absorption corrections on the t-dependence of the elastic $\pi\pi$ cross sections for opossite-sign pions and same-sign pions for W = 4 GeV. In this calculation the slope parameter B = 4 GeV^{-2}. The cross section for single-exchange is shown by the dashed line, while the cross section which includes double-scattering effect by the solid line. By the dotted line we show the cross section calculated from the double-scattering amplitude alone.

References:

[1] K.A. Ter-Martirosyan, Sov. J. Nucl. Phys. **10** 600 (1970).

[2] E. Gotsman, E. Levin and U. Maor, Phys. Lett. **B452** 387 (1999).

[1]also at: Inst. of Nuclear Physics, PL-31-342 Cracow, Poland

a_0-f_0 mixing in the reaction $\vec{p}n \to da_0$ with polarized proton beam

A. Kudryavtsev*, V. Tarasov*, J. Haidenbauer, C. Hanhart, J. Speth

The nature of the lightest, virtually mass-degenerate, scalar mesons a_0 (980) ($I^G J^{PC} = 1^- 0^{++}$) and f_0 (980) ($0^+ 0^{++}$) is an important problem of hadron physics. The quark structure of these mesons is not well established at present time. This question is also closely related to a very interesting problem of a_0-f_0 mixing. The dynamical mechanism of this mixing close to $K\bar{K}$ threshold was suggested around 20 years ago in Ref. [1].

In a previous paper [2] we pointed out that the study of the reaction

$$p\,n \to d\,a_0^0\,. \tag{1}$$

near the threshold provides a promising opportunity to observe the a_0-f_0 mixing effect, which should manifest itself in a forward-backward asymmetry of the outgoing a_0^0 mesons in the CM system of the reaction. According to Ref. [2] the asymmetry A, defined as

$$A = \frac{\sigma_+ - \sigma_-}{\sigma_+ + \sigma_-}\,, \quad \sigma_\pm = \frac{d\sigma}{d\Omega}(z = \pm 1)\,, \quad z = \cos\theta\,, \tag{2}$$

should be of the order of 10%.

Let us discuss now what kind of effects induced by $a_0^0 - f_0$ mixing one may observe in the reaction (1) with polarized initial protons. As it will be shown below, the generalized asymmetry $A(\theta,\varphi)$ defined as

$$A(\theta,\varphi) = \frac{\sigma(\theta,\varphi) - \sigma(\pi-\theta,\varphi+\pi)}{\sigma(\theta,\varphi) + \sigma(\pi-\theta,\varphi+\pi)}\,,$$
$$\sigma(\theta,\varphi) \equiv \frac{d\sigma}{d\Omega}(\theta,\varphi)\,, \quad z = \cos\theta\,, \tag{3}$$

where θ and φ are the polar and azimutal CM angles of a_0^0-meson escape with the polar z-axis coinciding with the initial beam, gives additional information on isospin-breaking (ISB) effect in the reaction (1). This information is complementary to what could be obtained from the asymmetry A (2). The transformations $\theta \to \pi - \theta$ and $\varphi \to \varphi + \pi$ correspond to the inversion for the direction of CM momenta of the outgoing a_0 meson and the deuteron.

To obtain the expression for $A(\theta,\varphi)$ let us start from the general form of the a_0^0- and f_0-production amplitudes M_a and M_f. Here M_a corresponds to the reaction (1) and M_f to the reaction

$$p\,n \to d\,f_0\,, \tag{4}$$

respectively. In the near-threshold region of these reactions we may write M_a and M_f as

$$\begin{aligned} M_a &= a\,(\boldsymbol{p}\cdot\boldsymbol{S})\,(\boldsymbol{k}\cdot\boldsymbol{\epsilon}^*) + b\,(\boldsymbol{p}\cdot\boldsymbol{k})\,(\boldsymbol{S}\cdot\boldsymbol{\epsilon}^*) \\ &+ c\,(\boldsymbol{k}\cdot\boldsymbol{S})\,(\boldsymbol{p}\cdot\boldsymbol{\epsilon}^*) + d\,(\boldsymbol{p}\cdot\boldsymbol{S})\,(\boldsymbol{p}\cdot\boldsymbol{\epsilon}^*)\,(\boldsymbol{k}\cdot\boldsymbol{p}) \end{aligned} \tag{5}$$

$$M_f = f\,(\boldsymbol{S}\cdot\boldsymbol{\epsilon}^*) + g\,(\boldsymbol{p}\cdot\boldsymbol{S})\,(\boldsymbol{p}\cdot\boldsymbol{\epsilon}^*)\,, \tag{6}$$

where a, b, c, d, f and g are independent scalar amplitudes which can be taken to be constant near threshold; $\boldsymbol{p}$ and $\boldsymbol{k}$ are the initial and final CM momenta; $\boldsymbol{S} = \phi_1^T \sigma_2 \boldsymbol{\sigma} \phi_2$ is the spin operator of the initial NN system, where $\phi_{1,2}$ are the spinors of the nucleons; $\boldsymbol{\epsilon}$ is the deuteron polarization vector. The amplitudes (5) and (6) are obtained under the following assumption: The a_0 and f_0 mesons are produced in p and s waves, correspondingly, with respect to the deuteron, as required by selection rules [2].

The differential cross section of the reaction (1) when the $a_0^0 - f_0$ mixing process (4) is also taken into account can be presented in the form

$$\sigma(\theta,\varphi) = \frac{d\sigma}{d\Omega}(\theta,\varphi) = \frac{k}{p}\,\frac{|M|^2}{64\pi s}\,, M = M_a + \xi M_f\,, \tag{7}$$

where M is the total amplitude and ξ is the $a_0^0 - f_0$ mixing parameter [2].

The general features of $A(\theta,\phi)$ as a function of the polarization ζ of the initial proton ($0 \le \zeta \le 1$) are discussed in Ref. [3]. Here we only want to show some specific cases. For example, in forward direction ($\theta = 0^0$) and for unpolarized beam ($\zeta = 0$) we get

$$A(\theta = 0^0)_{\zeta=0} = \frac{C_1}{C_0 + C_2}\,, \tag{8}$$

where

$$C_0 = \frac{1}{2}\left(|a|^2 + |c|^2\right) p^2 k^2 + \left(|f|^2 + \frac{1}{2}|f + p^2 g|^2\right)\,|\xi|^2\,,$$

$$C_1 = pk\,\mathrm{Re}\left(\left[(a + b + c + p^2 d)^*(f + p^2 g) + 2b^* f\right]\,\xi\right)\,,$$

$$\begin{aligned} C_2 &= p^2 k^2\,[|b|^2 + \frac{1}{2}|b + p^2 d|^2 + \mathrm{Re}(a^* c \\ &+ (a + c)^*(b + p^2 d))]\,, \end{aligned} \tag{9}$$

On the other hand, at $\theta = 90^0$ and $\zeta \neq 0$ we get

$$A(\theta = 90^0,\varphi) = \frac{2\zeta\,pk\,\mathrm{Im}\left(\left[a^* f - c^*(f + p^2 g)\right]\,\xi\right)\sin\varphi}{\left(|a|^2 + |c|^2\right) p^2 k^2 + \left(2|f|^2 + |f + p^2 g|^2\right)\,|\xi|^2} \tag{10}$$

Comparison of the expressions (8) and (10) shows that the ISB effect for different angles θ and φ is expressed in terms of different invariant amplitudes. Note that in the model of a_0-meson production discussed in Ref. [2], which was based on the impulse approximation, it should be $A(90^0,\varphi) \equiv 0$, because $a = c \equiv 0$ in that model. Thus, the study of the asymmetry (3) with polarized beam provides independent information about the invariant amplitudes a, b, c, d, f and g of the a_0- and f_0-production reactions. Furthermore, it might allow to get additional information about the $a_0^0 - f_0$ mixing amplitude [3].

References

[1] N.N. Achasov, S.A. Devyanin and G.N. Shestakov, Phys.Lett. **B88**, 367 (1979).

[2] A.E. Kudryavtsev and V.E. Tarasov, JETP Lett. **72**, 401 (2000).

[3] A.E. Kudryavtsev et al., in preparation.

*Institute of Theoretical and Experimental Physics, 117258, B.Cheremushkinskaya 25, Moscow, Russia

η-meson production in nucleon-nucleon collisions

V. Baru*, A.M. Gasparian, J. Haidenbauer, C. Hanhart, A. Kudryavtsev*, and J. Speth

We have performed a microscopic calculation of the reactions $pp \to pp\eta$, $pn \to pn\eta$, and $pn \to d\eta$ in the near-threshold region [1]. The production mechanisms which have been included consist of rescattering terms with $M = \rho, \pi, \eta, \sigma$ meson exchanges and the direct η production. Effects of the final (FSI) and initial state interaction (ISI) between the nucleons are fully taken into account. For the NN interaction we utilize a version of the Bonn NN model (CCF of Ref. [2]). The main novelty of our calculation lies in the employment of a realistic model for the $MN \to \eta N$ transition amplitudes. They are taken from a coupled-channel model of the πN system developed in Jülich [3].

The results for the reactions $pp \to pp\eta$, $pn \to pn\eta$ and $pn \to d\eta$ are represented in Fig. 1 by the dashed curves. As one can observe from this figure, for the $pp\eta$ case we get an overestimation by approximately 30% whereas for $pn \to pn\eta$ the calculation underestimates the experimental data by about 40-50%. As a consequence, the experimentally observed ratio of the cross sections [4, 5] is underestimated by a factor of about 2.

It is interesting to see whether our results can be improved if we slightly extend the MN model by introducing some additional graphs. E.g., the original MN model does not contain any tree-level contributions to the $\rho N \to \eta N$ transition. Certainly, the $\rho N \to \eta N$ transition T-matrix is not equal to zero due to coupled channel effects but, in principle, tree level Born diagrams should be included as well. Since we are interested in the η-production in NN collisions near threshold, which is characterized by a strong influence of the $N^*(1535)$ S_{11} resonance, it is a natural choice to add the $\rho N \to N^*(1535) \to \eta N, \rho N, \pi N$ potentials to the model. In fact, since the $\pi N \to N^*(1535) \to \eta N$ transition potential is included in the original MN model, the coupling of the $N^*(1535)$ to the other MN channels should be taken into account anyway, for consistency reasons.

Indeed, extending the model of Ref. [3] by including these diagrams with a negative $g_{\rho NN^*}$ coupling constant allows us to achieve a better agreement for the πN inelasticity η in the S_{11} partial wave while staying as close as possible to the results for the S_{11} phase shift and the $\pi N \to \eta N$ transition cross section as predicted by the original model [1].

Interestingly, the $\rho N \to \eta N$ and $\pi N \to \eta N$ transition T-matrices, and, in particular, their relative phase changed somewhat as well. In case of the original MN model the amplitudes of the π- and ρ-exchange contributions are almost orthogonal to each other. Thus, there is practically no interference between these contributions. The additional diagrams which we introduced into the MN model yield a slight modification of the orientation of these amplitudes in the complex plane and, as a consequence, now interference effects do occur. Specifically, we observe a destructive interference for the isotriplet channel ($I = 1$) and a constructive interference for the $I = 0$ case leading to a very good agreement with the experimental data for all reaction channels, cf. the solid curves in Fig. 1.

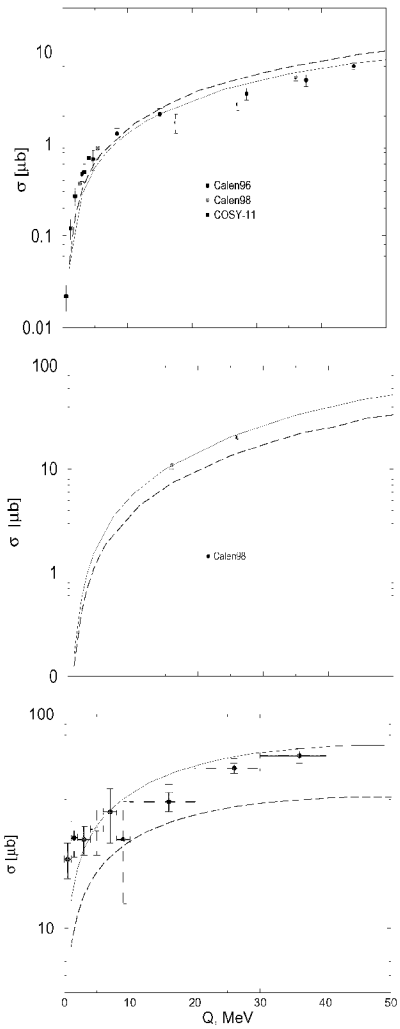

Fig. 1: Total cross section for the reaction $pp \to pp\eta$, $pn \to np\eta$ and $pn \to d\eta$. The dashed curve is the result using the original MN model [3] whereas the solid line is based on a modified MN model, cf. text. The data points are taken from Refs. [4] and [5].

References:

[1] V. Baru, Ph.D. thesis, in preparation.
[2] J. Haidenbauer, K. Holinde, and M.B. Johnson, Phys. Rev. C **48**, 2190 (1993).
[3] O. Krehl, Jülich-Report Jül-3692 (1999); O. Krehl et al., Phys. Rev. C **62**, 025207 (2000).
[4] H. Calén et al., Phys. Lett. **B366**, 39 (1996); Phys. Rev. C **58**, 2667 (1998); Phys. Rev. Lett. **80**, 2069 (1998)
[5] J. Smyrski et al., Phys. Lett. **B474**, 182 (2000).

*also at: Institute of Theoretical and Experimental Physics, 117258, B.Cheremushkinskaya 25, Moscow, Russia

Quark model study of the triton bound state

B. Juliá-Díaz*, F. Fernández*, A. Valcarce*, and J. Haidenbauer

During the last decade the development of quark-model based interactions for the hadronic force has led to nucleon-nucleon (NN) potentials that provide a fairly reliable description of the on-shell data. As a consequence of the internal structure of the nucleon, such interaction models are characterized by the presence of nonlocalities. These nonlocalities are reflected in the off-shell properties and emerge from the underlying dynamics in a natural way.

The relevance and/or necessity of considering the nonlocal parts of nucleon-nucleon potentials in realistic interactions is still under debate. Indeed, over the past few years several studies have appeared in the literature which stress the potential importance of nonlocal effects for the quantitative understanding of few-body observables and, specifically, for the triton binding energy [1, 2, 3, 4, 5]. However, the majority of these investigations [1, 2, 3, 4] explore only nonlocalities arising from the meson-exchange picture of the NN interaction. The effects of nonlocalities resulting from the quark substructure of the nucleon have only been addressed once so far [5] and more systematic studies are lacking altogether.

In this work we study the triton binding energy for a nonlocal quark-model potential, derived by means of the resonating group method [6]. The specific chiral quark cluster model for the NN interaction that is utilized in the present investigation has been widely described in the literature [7, 8, 9, 10]. Therefore we refrain from repeating this here but refer the reader to the pertinent references.

The triton binding energy is obtained by performing a five channel Fadeev calculation including the ${}^1S_0$ and ${}^3S_1 - {}^3D_1$ NN partial waves as input. Note that since in our model there is a coupling to the $N\Delta$ system, a fully consistent calculation would require the inclusion of two more three-body channels. However, their contribution to the $3N$ binding energy is known to be rather small [11] and therefore we neglect them for simplicity reasons.

To solve the three-body Faddeev equations in momentum space we first perform a separable finite-rank expansion of the $NN(-N\Delta)$ sector utilizing the EST method [12]. Such a technique has been extensively studied by one of the authors (J.H.) for various realistic NN potentials [13] and specifically for a model that also includes a coupling to the $N\Delta$ system [14]. In those works it was shown that, with a separable expansion of sufficiently high rank, reliable and accurate results on the three-body level can be achieved. In the present case it turned out that separable representations of rank 6 – for ${}^1S_0 - ({}^5D_0)$ and for ${}^3S_1 - {}^3D_1$ – are sufficient to get converged results.

Results for the triton are summarized in Table I. It is reassuring to see that the predicted triton binding energy is comparable to those obtained from conventional NN potentials, such as the Bonn or Nijmegen models. Thus, our calculations show that quark model based NN interactions are definitely able to provide a realistic description of the triton. The results also give support to the use of such interaction model for further few-body calculations. One should not forget at this point that the number of free parameters is greatly reduced in quark-model based NN interactions like the present one. In addition, the parameters are strongly correlated by the requirement to obtain a reasonable description of the baryon spectrum.

Table 1: Properties of the three-nucleon bound state.

	Quark model	Nijm II	Bonn B [13]
E_B (MeV)	−7.72	-7.65	-8.17
P_S (%)	91.49	90.33	91.35
$P_{S'}$ (%)	1.430	1.339	1.368
P_P (%)	0.044	0.064	0.049
P_D (%)	7.033	8.267	7.235

References:

[1] B.F. Gibson, H. Kohlhoff, H.V. von Geramb, Phys. Rev. C **51**, R465 (1995).

[2] J. Haidenbauer, K. Holinde, Phys. Rev. C **53**, R25 (1996).

[3] R. Machleidt, F. Sammarruca, Y. Song, Phys. Rev. C **53**, R1483 (1996).

[4] Ch. Elster, E.E. Evans, H. Kamada, W. Glöckle, Few-Body Syst. **21**, 25 (1996).

[5] S. Takeuchi, T. Cheon, E.F. Redish, Phys. Lett. **B 280**, 175 (1992).

[6] B. Juliá-Díaz, F. Fernández, A. Valcarce, J. Haidenbauer, `nucl-th/0107060` (2001).

[7] F. Fernández, A. Valcarce, U. Straub, A. Faessler, J. Phys. G **19**, 2013 (1993).

[8] A. Valcarce, A. Buchmann, F. Fernández, A. Faessler, Phys. Rev. C **50**, 2246 (1995).

[9] A. Valcarce, A. Faessler, F. Fernández Phys. Lett. **B 345**, 367 (1995).

[10] D.R. Entem, F. Fernández, A. Valcarce, Phys. Rev. C **62**, 034002 (2000).

[11] Ch. Hajduk, P.U. Sauer, Nucl. Phys. **A322**, 329 (1979).

[12] D.J. Ernst, C.M. Shakin, R.M. Thaler, Phys. Rev. C **8**, 507 (1973).

[13] W. Schadow, W. Sandhas, J. Haidenbauer, A. Nogga, Few-Body Syst. **28**, 241 (2000).

[14] S. Nemoto, K. Chmielewski, N.W. Schellingerhout, J. Haidenbauer, S. Oryu, P.U. Sauer, Few-Body Syst. **24**, 213 (1998).

*Grupo de Física Nuclear, Universidad de Salamanca, E-37008 Salamanca, Spain

A meson exchange model for the YN interaction

J. Haidenbauer, W. Melnitchouk*, and J. Speth

We have developed a new model for the hyperon-nucleon (ΛN, ΣN) interaction, derived within the meson-exchange framework. The model incorporates the standard one-boson exchange contributions of the lowest pseudoscalar and vector meson multiplets with coupling constants fixed by SU(6) symmetry relations [1]. In addition - as the main new feature of the model - the exchange of two correlated pions or kaons [2], both in the scalar-isoscalar and the vector-isovector channels, are included. In the scalar channel those contributions provide the main part of the intermediate-range interaction between two baryons, thereby eliminating the need for the fictitious sigma meson, which has been an unavoidable element of effective one-boson-exchange descriptions.

Besides replacing the conventional σ and ρ exchanges by correlated $\pi\pi$ and $K\bar{K}$ exchange, there are in addition several new ingredients in the present YN model. First of all, we now take into account contributions from $a_0(980)$ exchange. The a_0 meson is present in the original Bonn NN potential [3] and for consistency should also be included in the YN model. Secondly, we consider the exchange of a strange scalar meson, the κ, with mass ~ 1000 MeV. Let us emphasize, however, that these particles are not viewed as being members of a scalar meson SU(3) multiplet, but rather as representations of strong meson-meson correlations in the scalar–isovector ($\pi\eta$–$K\bar{K}$) [4] and scalar–isospin-1/2 (πK) channels, respectively. In principle, their contributions can also be evaluated along the lines of Ref. [2], however, for simplicity in the present model they are effectively parameterized by one boson exchange diagrams with the appropriate quantum numbers. In any case, these phenomenological pieces are of rather short range, and do not modify the long range part of the YN interaction, which is determined solely by SU(6) constraints (for the pseudoscalar and vector mesons) and by correlated $\pi\pi$ and $K\bar{K}$ exchange.

In Fig. 1 we compare the integrated cross sections for the new YN potential (solid curves) with the $YN \to Y'N$ scattering data for the channels Λp and $\Sigma^- p$. The agreement between the predictions and the data is clearly excellent. Also shown are the predictions from the original Jülich YN model A [1] (dashed curves). The main qualitative differences between the two models appear in the $\Lambda p \to \Lambda p$ channel, for which the Jülich model [1] (with standard σ and ρ exchange) predicts a broad shoulder at $p_{lab} \approx 350$ MeV/c. This structure, which is not supported by the available experimental evidence, is due to a bound state in the $^1S_0$ partial wave of the ΣN channel. It is not present in the new model.

The description of the other channels of the YN interaction is equally good, if not better, for the new model [5]. Further results and more details about the model can be found in Ref. [6].

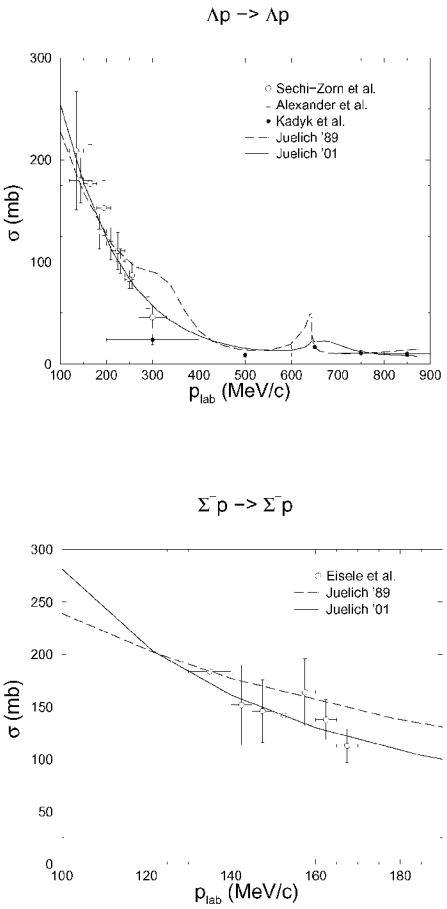

Fig. 1: Integrated cross sections for the reactions Λp and $\Sigma^- p$. The solid lines are the result of our new YN interaction. The dashed curves show the predictions of the model A of Ref. [1].

References:

[1] B. Holzenkamp, K. Holinde and J. Speth, Nucl. Phys. A500 (1989) 485.

[2] A. Reuber, K. Holinde, H.-C. Kim and J. Speth, Nucl. Phys. A608 (1996) 243.

[3] R. Machleidt, K. Holinde and Ch. Elster, Phys. Rep. 149 (1987) 1.

[4] G. Janssen, B.C. Pearce, K. Holinde, and J. Speth, Phys. Rev. D52 (1995) 2690.

[5] J. Haidenbauer, W. Melnitchouk and J. Speth, `nucl-th/0108062` (2001).

[6] J. Haidenbauer, W. Melnitchouk and J. Speth, in preparation.

* Jefferson Lab, 12000 Jefferson Avenue, Newport News, VA 23606, USA

Complete next–to–leading order calculation for pion production in nucleon–nucleon collisions at threshold

C. Hanhart and N. Kaiser †

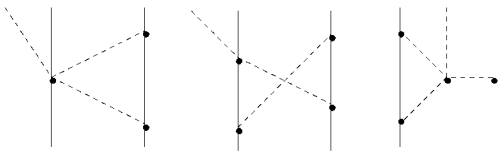

Fig. 1: Next–to–leading order contributions to s-wave production. A solid (dashed) line denotes a nucleon (pion).

Due to their nature as pseudo–Goldstone bosons the dynamics of pions is largely constrained by chiral symmetry. In the literature there are now several publications carried out within the framework of tree–level chiral perturbation theory (CHPT) including dimension two operators for neutral pion production as well as for charged pion production [1]. In addition, one loop calculations where performed for the production of neutral pions [4]. These turned out to be larger by at least a factor of two compared to the tree level diagrams. Consequently, several authors questioned the convergence of the chiral expansion for the meson production reactions in nucleon–nucleon collisions [2]. On the other hand, the chiral expansion seems to show convergence in case of the production of p–wave pions [3].

However, contrary to the kinematics of traditional chiral perturbation theory, in the meson production in nucleon–nucleon collisions an additional large scale enters, namely the initial nucleon momentum $p_i \simeq \sqrt{M_N m_\pi}$, where $m_\pi(M_N)$ denote the pion (nucleon) mass. It was argued in Ref. [3] the the counting rules have to be adopted to the appearance of the large scale. In doing so it becomes clear that some loops get pulled down in their order. In the modified counting the loops shown in Figure (1) even appear an order below the tree level rescattering diagrams. In this work for the first time we perform a complete loop calculation for the s–wave pion production using this new counting. In addition, for the first time the loops relevant for the charged pion production where calculated as well.

We find for the amplitude

$$A_n = \frac{i}{F_\pi^3}\kappa\left(\vec{\sigma}_1\cdot\frac{\vec{p}}{|\vec{p}|}\right)\left(\frac{M_N m_\pi}{128F_\pi^2}\right)(\vec{\iota}_n\cdot\vec{\phi}) \qquad (1)$$

where $\kappa = g_A^3$ and ι_n contains the isospin structure for the particular channel n.

The first observation is that the *NLO* contributions are of the order of magnitude expected by power counting, since

$$\left(\frac{M_N m_\pi}{128F_\pi^2}\right) = 0.8\chi^2\,, \qquad (2)$$

where we used $F_\pi = 92.4$ MeV and

$$\chi = \sqrt{\frac{m_\pi}{M_N}}\,. \qquad (3)$$

The power counting proposed in Refs. [3] is thus indeed capable of treating the large scale inherent to the the $NN \to NN\pi$ reaction properly. However, the loop contributions are subject to large cancellations. Explicitly, as shown in table 1, the loop contributions for the neutral pion production cancel exactly at leading order.

n	$pp \to pp\pi^0$	$pp \to (pn)^{(T=0)}\pi^+$
$a(N)$	-1	-1
$b(N)$	$+\frac{3}{2}$	$+\frac{3}{2}$
$c(N)$	$-\frac{1}{2}$	0
Σ_N	0	$+\frac{1}{2}$

Table 1: Results for the different amplitudes shown in Fig. 1. The results are given in units of $g_A^3/F_\pi^3\langle\sigma_1^z\rangle(M_N m_\pi/128F_\pi^2)$, where $\langle\sigma_1^z\rangle$ is a short hand notation for the spin matrix elements.

In Ref. [2] some pion loops were calculated fully relativistically. This calculation included diagrams 1a and b and one diagram of higher order. It is a straightforward task to expand this result, which is given analytically in eq.(16) of Ref. [2] in powers of χ, defined in eq. (3). This exercise was already carried out in the cited reference. The leading term is a constant that does not vanish in the chiral limit. We find that the next term exactly agrees with our result for the corresponding diagrams, which is an important cross check of our calculation. Also, if we neglect the constant term, the fully relativistic loop calculation, that in addition to including the nucleon kinetic energy exactly contains higher order diagrams, turns out to be nearly saturated by the leading order result. This is a clear indication that a fully relativistic calculation is unnecessary here.

Another successful check of our results was done via extracting the leading nonvanishing pieces from the calculations given in Ref. [4].

In summary, we have demonstrated that the chiral expansion, when adopted to the appearance of the large scale induced by the large inital momentum, converges for pion production in nucleon nucleon collision.

References:

[1] C. Hanhart, Acta Phys. Polon. B **31** (2000) 2213 and references therein.

[2] V. Bernard, N. Kaiser and U. Meissner, Eur. Phys. J. A **4** (1999) 259.

[3] C. Hanhart, U. van Kolck and G. A. Miller, Phys. Rev. Lett. **85** (2000) 2905.

[4] E. Gedalin, A. Moalem, L. Razdolskaya, Phys. Rev. C **60**, 31 (1999), V. Dmitrasinovic, K. Kubodera, F. Myhrer and T. Sato, Phys. Lett. **B 465**, 43 (1999), T.-S. Park, S. Ando and D.-P. Min, `nucl-th/0003004`.

† Institut für Theoretische Physik (T39), Physik–Department, Technische Universität München, D–85747 Garching, Germany

Constraints on high energy phenomena from low energy nuclear physics

U. Langenfeld*, H. Dreiner*, C. Hanhart, D. Phillips†, and S. Reddy+

The "standard model" of supernovae does an exceptionally good job of predicting the duration and shape of the neutrino pulse from SN1987a. Any mechanism which leads to significant energy-loss from the core of the supernova immediately after bounce will produce a very different neutrino-pulse shape, and so will destroy this agreement—as demonstrated explicitly in the axion case by Burrows, Brinkmann, and Turner [1]. Studies of this type showed that supernovae are extremely powerfull laboratories to deduce constraints on the coupling strength of exotic particles [2].

In any analysis of this type the first step is the calculation of the emissivity of the exotic. In our work we follow the method developed in ref. [3]. It is based on the observation that, if the radiation is soft, the production rate can be expressed in terms of the on–shell nucleon nucleon scattering data directly—the process is dominated by radiation off external legs. The leading term in such an expansion in terms of the radiation energy can be calculated for any kind of radiation model. If the radiation couples to a conserved current, however, even the next order in the expansion is fixed. This is well known for the vector current and was applied to the radiation of gravitions in ref. [4]. Obviously the kinematic requirement is best fulfilled in degenerate nuclear matter as it occurs in the late cooling phase of a PNS. It was shown in ref. [3] that our model independent approach leads to rates for neutrino–anti-neutrino bremsstrahlung that are significantly smaller than those used so far. The separation of scales is not that clear when we move to the physical conditions present in the first 20 s after the collapse. With temperatures of some tens of MeV and densities of several times nuclear matter density, matter should be expected to be neither degenerate nor non–degenerate. However, the investigations of ref. [4] suggest, that the relevant expansion parameter, namely the radiation energy in units of the average nucleon–nucleon energy, still is smaller than one even here. Using this approach emissivities where already calculated for axions [3] as well as gravition only extra dimensions (GODs) [4]. In addition the latter results where used as a basis for bounds derived on the ground of cosmological arguments [5, 6].

The methods descibed above are currently applied to derive a bound for the masses of the lightes neutralinos [7]. Supersymmetry does not prohibit a situation where they appear as pure binos and thus do not couple to the Z_0. For those kinds of supersymmetric particles no bound can be derived from current experimental data [8].

References:

[1] A. Burrows, R. P. Brinkmann, and M. S. Turner, Phys. Rev. D **39**, 1020 (1989).

[2] G.G. Raffelt, in *Stars as Laboratories for Fundamental Physics*, University of Chicago Press, Chicago (1996).

[3] C. Hanhart, D.R. Phillips, and S. Reddy, Phys. Lett. B **499** (2001) 9.

[4] C. Hanhart, D. R. Phillips, S. Reddy and M. J. Savage, Nucl. Phys. B **595** (2001) 335.

[5] M. Fairbairn, Phys.Lett. B508 (2001) 335.

[6] S. Hannestad and G. Raffelt, Phys.Rev.Lett. 87 (2001) 051301.

[7] U. Langenfeld, in preparation.

[8] D. Choudhury, H. Dreiner, P. Richardson and S. Sarkar, Phys. Rev. D **61** (2000) 095009

* Physikalisches Institut, Universität Bonn, Nußallee 12, 53113 Bonn.

† Department of Physics and Astronomy, Ohio University, Athens, OH 45701, USA.

+ Center for Theoretical Physics, Massachusetts Institute of Technology, Cambridge, MA 02139, USA.

The influence of three body cuts on the reaction $NN \to NNx$

A. Motzke, C. Elster†, C. Hanhart and J. Speth

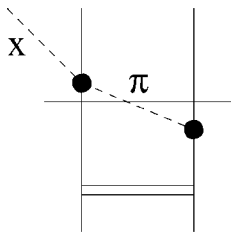

Fig. 1: *Diagram considered in the present investigation. The dashed line denotes the mesons, the single solid line the nucleon whereas the double line denotes the exchange of a heavy sigma meson. The three body cut is indicated by the dashed–dotted line.*

In recent years high quality data became available for the reaction $NN \to NNx$ close to the production threshold, where x spans the range from the lightest meson π up to mesons as heavy as the η'. Most of the theoretical work so far concentrated on pion production and, although there are still open questions, at least the production of charged pions is understood. Unfortunately, this can not be said for the production of heavier mesons where the theory is still in its infancy. Most of the studies so far did neither consider the initial state interaction between the incoming two nucleons, nor the influence of the necessarily occurring three particle cuts in the transition operators. The latter occur whenever an intermediate 3–particle state can go on–shell. The purpose of this work is to study the effect of these cuts. In this first investigation we minimize the numerical complications by working within a toy model. Note, that the gross features of the impact of the cut should not depend on the details of the interaction.

Recently a toy model suited for the present study was formulated in Ref. [1]. It is based on two distinguishable nucleons that can interact either through exchange of a scalar "pion" field or through exchange of a scalar "sigma" particle. The coupling of the latter is assumed to be weak that it only needs to be included in leading order perturbation theory. The meson–nucleon couplings are given by Yukawa couplings. In addition, the pion can interact with one of the nucleons through a seagull interaction. The diagram included is shown in Fig. (1) where the three body cut is indicated by the dashed–dotted line.

For the numerical evaluation we use a pion mass of 139 MeV and a sigma mass of 600 MeV. In order to prevent the sigma propagator to introduce an additional singularity we use a static propagator for the sigma exchange.

To demonstrate that the three body cut induced by the pion exchange indeed has a potentially large impact on the total cross section even close to the production threshold of heavier mesons, in Fig. (2) we show a comparison of the full calculation with one where the pion exchange is treated in a static approximation as well. The figure shows the total cross section in arbitrary units for a fixed excess energy $Q = \sqrt{s} - \sqrt{s_{thr}}$ as a function of m_x, the mass of the meson produced. Naturally, if we employ a static propagator the m_x dependence enters mainly through the energy dependence of the two nucleon cut. Consequently we find a weak m_x dependence. In case of the full calculation, however, the three particle cut—omitted by hand in the calculation with the static propagator—leads to a contribution that scales with the three body phase space that is available for the πNN state. Thus,

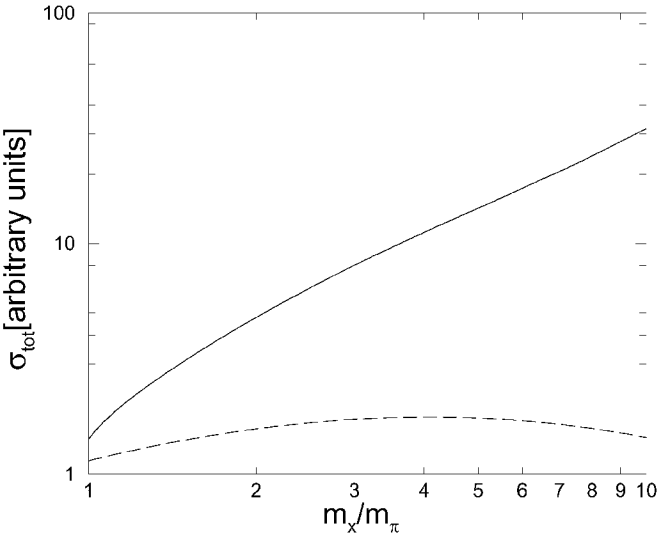

Fig. 2: *Comparison of the result of the full calculation (solid line) to the widely used static approximation (dashed line) for the pion propagator. The calculation is carried out for a fixed excess energy Q=5 MeV.*

the influence of the three body cut is getting larger and larger as the mass of the produced meson is increased: was the static propagator for the pion a good approximation for $m_x = m_\pi$ (20 % accuracy), at $m_x = 10 m_\pi$ the approximation is off by a factor of more than 20.

It should be clear that the effect of the cut is maximized by considering the diagram of Fig. (1) only, since no cut occurs in the diagram where the sigma exchange occurs in the final state instead of the initial one. In addition: in reality chiral symmetry suppresses the impact of the cut at least close to the pion production threshold, as was already pointed out in Ref. [1]. Further study in this direction is certainly necessary. For the production of heavy mesons near their thresholds one expects meson exchange currents to be important [2]. Thus, we expect the results of the present study to be relevant for those reactions. It should be stressed that simultaneously to improving the treatment of the three particle cuts in the production operator a microscopic nucleon–nucleon interaction that is capable of describing the elastic scattering data up to center of mass energies of several GeV should be developed, for a reliable initial state interaction is essential to get quantitative predictions.

References:

[1] C. Hanhart, G. A. Miller, F. Myhrer, T. Sato and U. van Kolck, Phys. Rev. C **63** (2001) 044002.

[2] K. Nakayama, "Pseudoscalar and vector meson production in N N collisions," `nucl-th/0108032`.

† also Department of Physics and Astronomy, Ohio University, Athens, OH 45701.

The reaction $\pi N \to \omega N$ revisited: the $\omega - N$ scattering length

C. Hanhart, A. Sibirtsev, and J. Speth

In Refs. [1, 2] the reaction $\pi^- p \to \omega n$ was measured at energies close to the nominal ω production threshold. In Ref. [3] it was claimed that these experiments were interpreted incorrectly. In this work we reinvestigate the experiments using an event–by–event simulation as well as an analytical calculation. The purpose of this manuscript is two fold: Besides studying, if the reaction kinematics was treated properly in Refs. [1, 2], we also take the oportunity to discuss in detail the method proposed in Ref. [1, 2] for the near threshold production of narrow resonances, for it might prove usefull for upcoming experiments at COSY and GSI.

Cross sections close to threshold depend strongly on the total energy of the reaction due to the quickly growing phase space. On the other hand secondary beams, like a π^-–beam needed for the $\pi^- p \to \omega n$ reaction, always have a sizable energy spread. To solve this discrepancy the authors of Ref. [1] suggested to run the experiment with a variable initial energy, however, keeping the final state momentum fixed in an interval of size ΔP around a central momentum P^*. This procedure removes the dependence on the ω spectral function from the equations. Therefore, the $\pi^- p \to \omega n$ cross section is given as (for details cf. Ref. [4])

$$\tilde{\sigma}(P^*, \Delta P) = \kappa \left[P^{*2} + \frac{1}{12} (\Delta P)^2 \right] |\mathcal{M}|^2 , \qquad (1)$$

with

$$\kappa = \frac{1}{2\pi E_n q_\pi \sqrt{s}} \left(\frac{\partial p_\pi}{\partial m^2} \right) , \qquad (2)$$

where $E_n = \sqrt{P^{*2} + m_n^2}$ and s denotes the invariant collision energy evaluated for the production of a stable ω–meson with center of mass momentum P^*.

The expression given in formula (1) agrees to eq. (10) of ref. [1] for an ideal detector and beam. Thus, at this stage it seems as if the experiments of refs. [1, 2, 5] where analysed properly. However, from what is written in Refs. [2] one can get the impression, that it is σ_{exp}, defined through

$$\tilde{\sigma}(P^*, \Delta P) = 2 M_\omega \left(\frac{\partial p_\pi}{\partial m^2} \right) \sigma_{exp}(P^*) . \qquad (3)$$

that is given in the data tables and not a proper cross section to be defined below.

Thus one may consider two options. *Either* the kinematics was treated properly in the experimental analysis of Refs. [1, 2, 5]. Then the strong energy dependence as shown by the solid dots in Fig. 1 is physical.

Or the experimental data were analysed improperly, namely only the Jacobian that connects the Lab–frame was included and not the terms that take care of the final resolution of the detector.

In what follows we investigate the consequences of the second option. In other words, we study the implications of the *assumption* that it was σ_{exp} defined in eq. (3) that was given in the experimental papers [2].

We can now define an effective two–body cross section σ^{eff} in terms of the cross section σ_{exp} measured in Ref. [2]:

$$\sigma^{eff} = \frac{\tilde{\mu} P^*}{P^{*2} + (\Delta P)^2/12} \, \sigma_{exp} , \qquad (4)$$

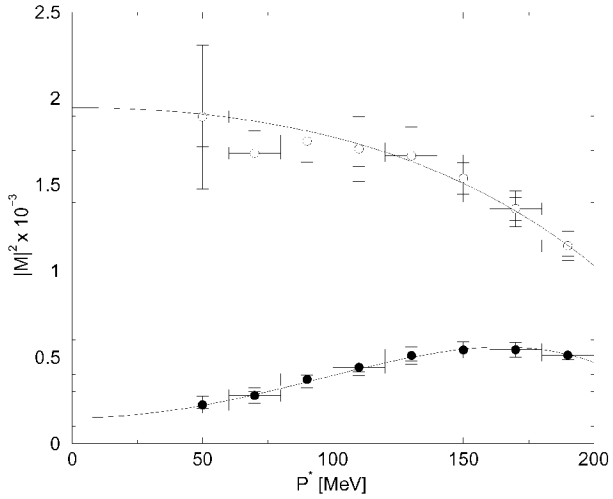

Fig. 1: The matrix element extracted from the data of Ref. [2]. The opaque circles denote the corrected matrix element using Eq. (4) whereas the filled circles show the uncorrected result. The small error bars are those from the data only, whereas the large error bars include the uncertainty in P^*, given by ΔP=20 MeV. The solid lines are polynomial fits to the data.

Therefore, the effective cross section σ^{eff} is the $\pi^- p \to \omega n$ total reaction cross section taken under the assumption that the produced ω–meson is stable with the fixed mass M_ω=781.94 MeV.

Finally we deduce for the imaginary part of the spin averanged scattering length

$$\Im a_{\omega N} \geq (0.24 \pm 0.05) \text{ fm} . \qquad (5)$$

As can be seen from Fig. 1, the value for the corrected squared matrix element at threshold changed by more than an order of magnitude. Since the lower limit for $\Im a_{\omega N}$ scales linearly with the squared matrix element, our bound naturally is significantly stronger than those present in the current literature. For instance, in Ref. [6] a value $\Im a_{\omega N} \geq 0.02$ fm is given (Note: in Ref. [6] the scattering length was deduced including the $\pi^- p$ channel only. To include the $\pi^0 n$ isotopic channel the result of Ref. [6] was multiplied with the isospin factor 3/2 to allow comparsion to our value). This change, if correct, will have a huge impact on models relevant to study the omega meson in the medium as well as omega nucelus bound states.

To resolve the problem we propose to study the reaction $\pi^- p \to \omega n$ with the HADES experiment at GSI.

References:

[1] D.M. Binnie et al. Phys. Rev. D **8**, 2789 (1973).
[2] J. Keyne et al., Phys. Rev. D **14**, 28 (1976), H. Karami et al., Nucl. Phys. B **154**, 503 (1979).
[3] C. Hanhart and A. Kudryavtsev, Eur. Phys. J. A **6**, 325 (1999).
[4] C. Hanhart, A. Sibirtsev and J. Speth, `hep-ph/0107245`.
[5] R. Wurzinger et al., Phys. Rev. C **51**, R443 (1995).
[6] B. Friman, Acta Phys. Polon. B **29**, 3195 (1998).

Supernovae as particle laboratories—a probability study

C. Hanhart, J. A. Pons*, D. Phillips†, and S. Reddy+

In the aftermath of a core collapse supernova we find a system described by extreme parameters: densities of several times nuclear matter density with simultaneous appearance of temperatures of several tens of MeV. Indeed, the matter is that dense and hot that even particles interacting as weakly as neutrinos—the by far most efficient conventional cooling mechanism—get trapped. Therefore, the cooling of the nascent proto–neutron star (PNS) has to happen on diffusion times scales of tens of seconds. It is this delayed cooling in the standard scenario that makes core collapse supernovae one of the most efficient elementary particle physics labs possible: any additional cooling mechanism will influence the time structure of the neutrino signal as long as its interaction with the medium is not too strong that it gets trapped as well [1].

To make this kind of an argument more quantitative several ingredients are in principle necessary: first one needs a reliable method to calculate the primary emission rates of the exotic under discussion in the inner core. The calculated emissivities are then to be fed into a simulation capable of describing the first several tens of seconds of a nascent PNS. The results of these simulations carried out for different coupling strengths of the additional cooling mechanism are the to be compared with the data and analyzed with the appropriate statistical method. This leads then to bounds on the coupling strength of the exotic studied. The chain of arguments is illustrated in figure (1). Also indicated in the diagram there is a possible short–cut, here labeled as Raffelt criterium. This particular criterium [1] is one of a group of criteria meant to allow to read a constraint off the emissivities directly. Although useful to get a very rough estimate of the allowed strength of an exotic one should keep in mind that the emission rates of particles in the nuclear medium are strongly temperature and energy dependent. The core temperature in the supernova, however, depends on whether or not there is an additional cooling mechanism present. Thus it is difficult if not impossible to fix a fudicial temperature and density to be used in the criteria that is valid for all kinds of particles (note that the temperature dependence of a particular production process depends on the energy/momentum dependence of the fundamental coupling vertex of the exotic to the medium and thus depends of the properties of the particle studied). Thus, to get a reliable bound, a detailed simulation is required after all. The method to calculate the emission rates of the exotic in a model independent way is described in Ref. [2]. Here we focus on the likelihood analysis. Once the emissivities are derived we have to quantify their influence on the neutrino signal of SN1987A. To do so the new energy source is implemented into a simulation of the early PNS that takes care of the neutrino diffusion [4]. Having neutrino emission rates at hand we now have to compare to the data and develop a tool that quantifies the agreement. Thus we need to define a Likelihood function. Following ref. [5] we use

$$\mathcal{L}(\{data\}|a,\kappa,I) = \prod_D \left[\prod_{i=1}^{N_D^{\rm tot}} \frac{dN_D(t_i^D)}{dt} \Delta t \right] e^{-N_D} \,, \qquad (1)$$

where N_D is the total number of observed neutrino arrivals,

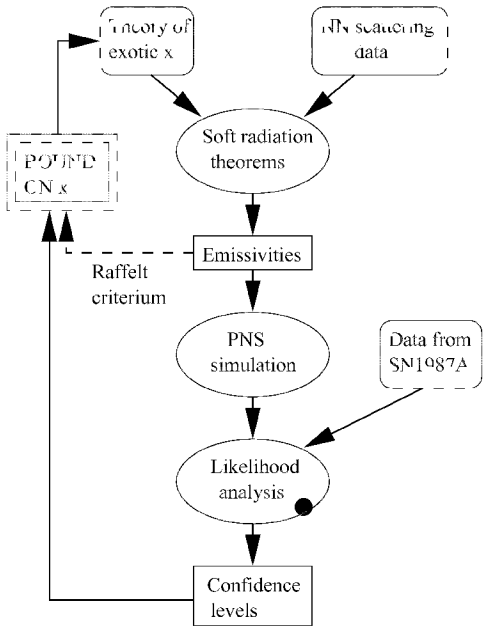

Fig. 1: *The structure of the analysis. Between input (framed in rounded boxes), calculated quantities (boxes) and analysis tools (ellipses) is explicitly distinguished.*

and $t_1^D, t_2^D, \ldots$ are the times at which neutrinos actually arrived in the detector D. $N_D(t)$ is the total number of neutrinos that the model with assumptions I, parameters κ, and exotic-coupling a predicts will have arrived in the detector D up until the time t. Δt can be any interval small enough that the probability of detecting more than one count in any one bin can be taken to be negligible. Ultimately it will be absorbed into an overall normalization constant. To actually derive a bound we now integrate (or "marginalize") over all possible values of M and $T_{\bar{\nu}_e}$, using appropriate weight functions (for details c.f. ref. [3]).

References:

[1] G.G. Raffelt, in *Stars as Laboratories for Fundamental Physics*, University of Chicago Press, Chicago (1996).

[2] C. Hanhart, D.R. Phillips, and S. Reddy, Phys. Lett. B **499** (2001) 9.

[3] C. Hanhart, J. A. Pons, D. R. Phillips and S. Reddy, Phys. Lett. B 509(2001)1.

[4] J. A. Pons, J. A. Miralles, M. Prakash and J. M. Lattimer, Astrophys. J., Astrophys. J. **553** (2001) 382.

[5] T.J. Loredo, D.Q. Lamb, in *Proceedings of the* 14^{th} *Texas Symposium on Relativistic Astrophysics*, Ann. N.Y Acad. Sci. 571 (1989) 601

* Dipartimento di Fisica "G. Marconi", Universita di Roma " La Sapienza" and Sezione INFN ROMA1, piazzale Aldo Moro 2, I–00185 Roma, Italy.

† Department of Physics and Astronomy, Ohio University, Athens, OH 45701.

+ Center for Theoretical Physics, Massachusetts Institute of Technology, Cambridge, MA 02139, USA.

Possible odderon discovery at HERA via observation of charge asymmetry in the diffractive $\pi^+\pi^-$ production

I.Ivanov[a,b], N.Nikolaev[a,c], I.F. Ginzburg[b]

The odderon, $\mathcal{O}$ (the object corresponding to the conjectured j-plain singularity with $C = -1$ and the intercept $\alpha_{\mathcal{O}} \approx 1$), has been the goal of a large number of dedicated searches, but despite all attempts it still remains elusive. On the other hand, the odderon is an integral feature of the QCD motivated picture of high energy scattering. Therefore, the experimental discovery of the odderon is crucial for the QCD theory of strong interactions.

Given the experimental fact that the odderon couples to hadrons rather weakly and, therefore, the cross sections of odderon-induced reactions are small, we propose to shift attention to high-energy processes that can proceed *both* via Pomeron and odderon exchange, and extract the Pomeron-odderon interference terms in the differential cross section. This signal of the presence of the odderon should be stronger — and therefore easier to see — than in the purely odderon-exchange processes.

To be specific, we propose [1] to investigate the high-energy diffractive photoproduction of $\pi^+\pi^-$ pairs $\gamma p \to \pi^+\pi^- X$ in the resonance region (i.e. with dipion invariant mass $M_{\pi^+\pi^-} \sim 1$ GeV). This reaction can occur via Pomeron or odderon exchange. Due to the definite C-parity of the initial photon, the Pomeron produces $\pi^+\pi^-$ pair in C-odd state, while the odderon creates the C-even dipion. Obviously, these two mechanisms do not interfere in the total cross sections, but the interference is present in the differential ones. So, our aim will be to present a method to extract this interference and to establish whether the signal obtained in this way can be statistically significant at HERA.

Since the Pomeron-odderon interference term is intrinsically C-odd, the effect, which we are looking for and which will be the definitive signal of the odderon, is the presence of *charge asymmetry* in the differential cross section. This readily suggests a method how to detect the interference: find the charge asymmetric quantities and calculate the asymmetries (cross sections integrated with a certain charge asymmetric weight). We identify two asymmetric variables, ξ and v, which are related to the longitudinal or transverse internal motion in the $\pi^+\pi^-$ system.

The C-odd $\pi^+\pi^-$ spectrum in the invariant mass region around 1 GeV is saturated by resonance, the ρ-meson being the most prominent of them. In the C-odd $\pi^+\pi^-$ spectrum a similar picture takes place, the prominent resonances being scalar f_0 and tensor f_2 mesons. Therefore, it is sufficient for us to treat the dipion production in a factorized Regge-vector-dominance manner: that is, the Pomeron or odderon exchange produces a corresponding meson, which subsequently decays into $\pi^+\pi^-$ pair. If we focus on the region around 1200 MeV, only ρ and $f_2(1270)$ meson can be taken into account. In this approach the amplitudes have form

$$\mathcal{A}^{\mathbb{P}} = \mathcal{A}^{\lambda_\gamma}_{\lambda_R} D_R(M^2) \mathcal{E}^{J,\lambda_R}_{\lambda_\gamma}\,, \quad \mathcal{A}^{\mathcal{O}} = i\mathcal{A}^{\lambda_\gamma}_{\lambda_R} D_R(M^2) \mathcal{E}^{J,\lambda_R}_{\lambda_\gamma}\,.$$

Here $\mathcal{A}^{\lambda_\gamma}_{\lambda_R}$ denote the production amplitudes of the corresponding resonances R. Their form could be written immediately, if the helicity properties of $\gamma \to R$ were known. The factors $D_R(M^2)$ describe the propagation of the resonance formed, for which we took the simple constant-width Breit-Wigner form. Finally, angular factors $\mathcal{E}^{J,\lambda_R}_{\lambda_\gamma}$ correspond to $R^{J,\lambda_R} \to \pi^+\pi^-$ decay and can be written in terms of spherical harmonics.

The presence of extra Breit-Wigner phases is a crucial point here. Without them, the Pomeron and odderon amplitudes would be almost orthogonal due to extra i, stemming from the signature of the odderon. As a result, our interference effect would occur only if the Pomeron and odderon intercepts were distinct, possessing thus small factor $\sin(\pi(\alpha_P - \alpha_O)/2)$ (see [2]). However, the final state interaction lifts this orthogonality and significantly enhances the signal. Such an effect can be viewed as an example of *severe breaking of parton-hadron duality.*

In the subsequent calculations we verified that the Pomeron-odderon interference indeed possesses longitudinal or transverse asymmetry. The asymmetries in cross section, defined as

$$\begin{aligned} \Delta\sigma^{long} &= \sigma(\xi > 0) - \sigma(\xi < 0)\,, \\ \Delta\sigma^{\perp} &= \sigma(v > 0) - \sigma(v < 0)\,, \end{aligned} \qquad (1)$$

were found to be quite significant. Within the invariant mass region $1.1 < M < 1.4$ GeV the charge symmetric background cross section is $\sigma_{bkgd} = 670$ nb, while the longitudinal asymmetry is $\Delta\sigma^{\perp} = 64$ nb. With and additional momentum transfer squared cut $\Delta^2 \geq 0.1$ GeV^2 imposed, the background cross section reduces to $\sigma^{cut}_{bkgd} = 250$ nb, while the transverse asymmetry equals to $\Delta\sigma^{\perp} = 24$ nb.

Both effects should be within the reach of HERA. We proved that no other mechanism can mimic the odderon signal at high energies, so the observation of the any type of charge asymmetry in this process would be a strong evidence for the presence of Odderon.

[a]Institut für Kernphysik, KFA-Jülich
[b]Institute of Mathematics, Novosibirsk, Russia
[c]Landau Institute for Theor. Physics, Moscow, Russia

References:

[1] I..F. Ginzburg, I.P. Ivanov, and N.N. Nikolaev, *'Possible odderon discovery at HERA via observation of charge asymmetry in the diffractive $\pi^+\pi^-$ production'*, in preparation; Workshop DIS-2001, 27 April – 1 May, 2001, Bologna, Italy.

[2] S.J.Brodsky, J.Rathsman, and C. Merino, Phys.Lett.**B461** (1999) 114-122.

Two-pion production on the nucleon

S. Schneider, S.Krewald, and J. Speth

A meson-theoretical model for two-pion production in the pion-nucleon reaction has been developped and applied in the vicinity of the reaction threshold. Both baryonic and mesonic intermediate resonances have been considered explicitly. In a first step, the model has been formulated strictly at the tree level. This version of the model could reproduce the total cross sections in the immediate vicinity of the threshold, but for kinetic energies of the incident pion above 250 MeV, the cross sections were overestimated, in particular for the reaction $\pi^+ p \to \pi^+\pi^+ n$ which is dominated by the Δ_{33}-resonance. Therefore, a proper two-body unitarization had to be implemented. In a second step, we have extended our model by replacing the sigma- and the rho-meson by correlated two-pion states which reproduce the two-pion phase shifts in the required partial waves. For the Δ_{33}-resonance we kept the non-relativistic spin-3/2 projector only. In this second version of the model, we are able to describe four of the five $\pi N \to \pi\pi N$ reaction channels up to $T_\pi = 400 MeV$.

The decomposition of the total cross sections into contributions from specific classes of intermediate states is shown in Fig.1. As expected, the $\pi^+ p \to \pi^+\pi^+ n$ reaction is entirely dominated by processes involving an intermediate Δ_{33}-resonance. The $\pi^- p \to \pi^0\pi^0 n$ rection is dominated by the decay of the intermediate correlated two-pion exchange in the scalar-isoscalar channel. In the vicinity of $T_\pi = 350 MeV$, both the intermediate Δ_{33}- and the Roper-resonance begin to make non-negligible contributions.

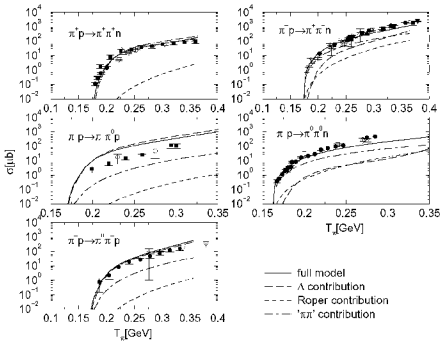

Fig. 1: Total cross sections for the reaction $\pi N \to \pi\pi N$ as a function of the Lab-energy of the incoming pion. full line: full model; long-dashed line: only intermediate Δ_{33} diagrams; short-dashed line: only intermediate Roper diagrams; dashed-dotted line: only intermediate correlated two-pion states.

The angular correlation function W is defined as the following ratio between triple and double differential cross sections:

$$W(\Theta_1, \Phi_1) = 4\pi \frac{\frac{d^3\sigma}{d\Omega_1 d\Omega_2 dT_2}}{\frac{d^2\sigma}{d\Omega_2 dT_2}}. \qquad (1)$$

In ref. [1], experimental angular correlation functions are shown for the reaction $\pi^- p \to \pi^+\pi^- n$ at a center-of-mass energy $\sqrt{s} = 1.301 GeV$. These data are compared with our model in Fig. 2.

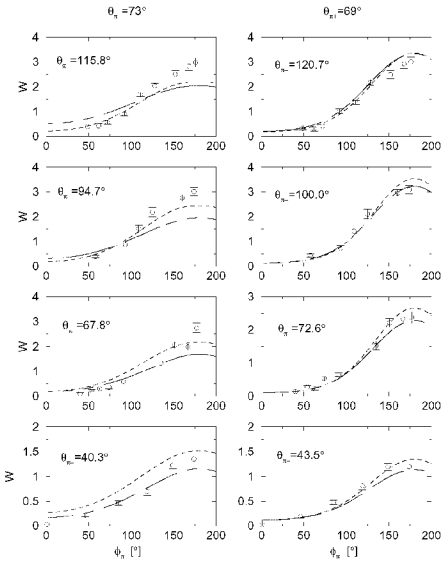

Fig. 2: Angular correlation functions for the reaction $\pi^- p \to \pi^+\pi^- n$ as a function of the angle Φ_{π^-}. full line: full model; dashed line: only intermediate correlated two-pion states.

The explicit inclusion of meson resonances in our model allows to understand the shape of the distributions qualitatively: for a fixed angle Θ_{π^-}, the angular correlation is maximal for the angle $\Phi_{\pi^-} = 180°$. The coordinate system is chosen such that $\Phi_{\pi^+} = 0°$. This means that the two produced pions tend to separate predominantly back-to-back in the $xy-$plane. We can interprete this finding as follows. Close to threshold, the intermediate meson-resonances ρ and σ are almost at rest in the center-of-mass frame. Therefore the produced pions are indeed expected to be emitted back-to-back. We can test this interpretation by simply including only those diagrams with intermediate meson resonances. The contribution of only these diagrams indeed reproduces most of the experimental cross section. There is some deviation between the dashed line and the full model because the data of ref. [1] were taken for a kinetic energy of the incident pion of $T_{\pi^-} = 0.284 GeV$ which is large enough to excite the Δ noticeably.

The model presented here is the second step in the development of a microscopic model for the one- and two-pion decay of the resonances of the nucleon. We feel encouraged to implement a simple treatment of three-body unitarity as a next step to be able to investigate the actual resonance region.

References:

[1] R. Mueller et al., Phys. Rev. C **48**, 981 (1993).

Chiral dynamics and the reactions $pp \to dK^+\bar{K}^0$ and $pp \to d\pi^+\eta$

Ulf-G. Meißner, J.A. Oller, E. Oset (Valencia)

The reaction $pp \to dK^+\bar{K}^0$ is presently the subject of experimental study by the ANKE collaboration at the Cooler Synchrotron COSY at Jülich with the aim (among others) of learning about the nature and properties of the $a_0(980)$ resonance [1]. Triggered by this, we have performed a study of the reactions $pp \to dK^+\bar{K}^0$ and $pp \to d\pi^+\eta$ [2]. We have emphasized the relevance of the final state interactions which is quite important in the present case due to the proximity of the $K^+\bar{K}^0$ system to the $a_0(980)$ resonance and the $\bar{K}^0 n$ system to the $\Lambda(1405)$ resonance. We found that the consideration of these interactions has important consequences both in the shape and strength of the invariant mass distributions. We also studied the interaction of the two final states $K^+\bar{K}^0$ and $\pi^+\eta$ by means of a coupled channel chiral unitary approach which generates both the $a_0(980)$ and $\Lambda(1405)$ resonances. Given the freedom in the primary production amplitudes we parameterize them in terms of three types of structures involving $\ell = 1$, $L = 0$ and $\ell = 0$, $L = 1$ for the $K^+\bar{K}^0$ channel and the only allowed $\ell = 1$, $L = 1$ for $\pi^+\eta$ production. This left us with two independent parameters (up to a global normalization of one total cross section) together with a subtraction constant with an expected uncertainty of about 25%.

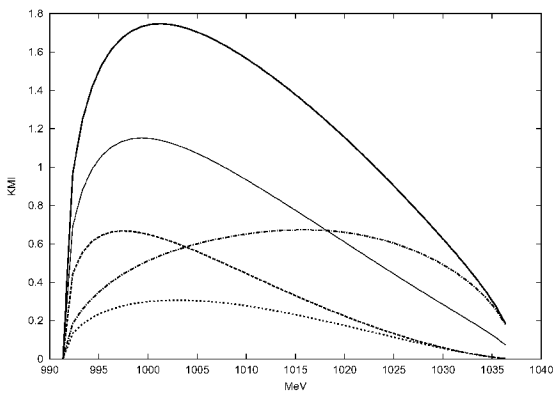

Figure 1: $d\sigma(K^+\bar{K}^0)/M_I$ for the whole range of available M_I in the reaction $pp \to dK^+\bar{K}^0$ with $\sqrt{s} = 2912.88$ MeV. The thick (thin) solid line is the full result with $a_{\bar{K}N} = -1.84\,(-1.34)$. The dashed line corresponds to including only meson-meson FSI, the dashed-dotted one includes only $\bar{K}^0 d$ FSI and the dotted line includes no FSI with a $\vec{p}_d^{\,2}$ factor for the modulus squared of the amplitude.

The sensitivity of the shapes of the $K^+\bar{K}^0$ and $\bar{K}^0 d$ distributions to those parameters was investigated anticipating that the measurements of these quantities could serve to fix them. This would allow us to make absolute predictions for $\pi^+\eta$ production due to the dynamics of coupled channels generated in the chiral unitary scheme followed here. Other quantities which might be measured could also be predicted in that case. Furthermore, we observed that the $\pi^+\eta$ production was dominated by the $a_0(980)$ resonance and that a clear signal for the relevance of the $\bar{K}^0 d$ FSI would be the observation of a peak towards low $\bar{K}^0 d$ invariant masses in the $K^+\bar{K}^0$ invariant mass distribution, see fig.1. On other hand, we have also pointed out that the $a_0(980)$ would not be clearly visible in the data for $d\sigma_{\pi+\eta}/dM_I$ because of the $|\vec{p}_d|^2$ factor due to the P-wave character of the reaction which distorts the shape of the resonance. Yet we found that the shape of the resonance was regained by dividing $d\sigma_{\pi+\eta}/dM_I$ by $|\vec{p}_d|^2$, see fig.2.

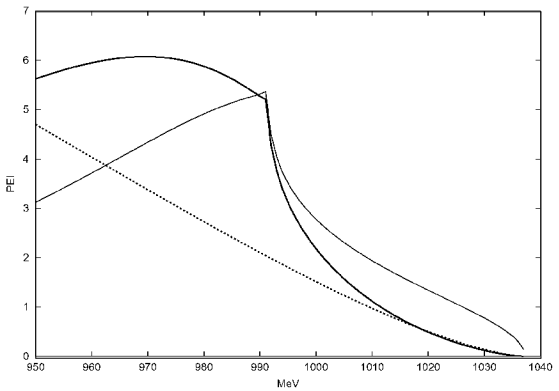

Figure 2: $d\sigma(\pi^+\eta)/dM_I$. Solid line, full result, dotted line does not include FSI, with a factor $\vec{p}_d^{\,2}$ from the modulus squared of the amplitude. The thin solid line corresponds to the full result but divided by $\vec{p}_d^{\,2}$ times 250^2 MeV^2 (to normalize the curve to the full result at the $\bar{K}K$ threshold).

Finally, we have also provided general expressions to take into account the FSI derived in this paper for any other more specific model of the primary production mechanism.

The study done here clearly shows how the measurements performed or planned with those reactions provide basic information on the strong interaction underlying the meson-meson and meson-baryon dynamics and should produce complementary and valuable information to the one obtained from other processes.

References:

[1] S. Barsov et al., Nucl. Instrum. Meth. A462 (2001) 364.

[2] E. Oset, J.A. Oller and Ulf-G. Meißner, Eur. Phys. J. A, in print, `nucl-th/0109050`.

In-medium chiral perturbation theory beyond the mean-field approximation

Ulf-G. Meißner, J.A. Oller and A. Wirzba

In [1] we have tackled the problem of establishing a chiral effective field theory in nuclear matter with explicit pions fields. We have made use of the results of ref. [2] where the generating functional for the in-medium chiral SU(2)×SU(2) Lagrangian has been derived. We have systematically studied several low–energy QCD Green functions up to next-to-leading order. The novel results obtained here can be summarized as follows:

(1) In contrast to most previous works we have established a systematic in-medium chiral counting. The counting scheme is depending on the energy flowing into the nucleon lines. This leads one to consider the standard and the non–standard case (i.e. vanishing energy flow). The chiral expansion of pion properties in the medium starts with terms at $\mathcal{O}(p^4)$ and next–to–leading order corrections appear at $\mathcal{O}(p^5)$, quite different to the in–vacuum power counting.

(2) We have also established the relevant scales of the problem when restricting ourselves to the $\mathcal{L}_{\pi\pi}$ and $\mathcal{L}_{\pi N}$ Lagrangians. In the vacuum, the pertinent scale is $\Lambda_\chi \simeq 1$ GeV$\sim 4\pi f_\pi$. In the medium, one has two new scales. These are: $\sqrt{6}\pi f_\pi \simeq 0.7$ GeV and $6\pi^2 f_\pi^2/2m_N \simeq 0.27$ GeV, in case that the standard or the non-standard counting rules apply. We point out that in case of P-wave interactions, these scales are reduced by factors $1/g_A$ and $1/g_A^2$, respectively.

(3) We have studied the quark condensates and rederived from the effective field theory point of view known results in symmetric nuclear matter, and have further extended them to the non-symmetric case.

(4) We have considered the propagation of pions in the medium obtaining the pion propagator up to $\mathcal{O}(p^5)$. In this way we have established that chiral symmetry can account for the observed shift of the mass of the negative pion in deeply bound pionic states in ^{207}Pb, our numerical result $\Delta M_{\pi^-} = 18 \pm 5$ MeV is compatible with the experimental number (from GSI), $\Delta M_{\pi^-} = 23 - 27$ MeV within errors.

(5) The wave function renormalization of the pion fields corresponding to the calculated in-medium action $\int dx \widetilde{\mathcal{L}}$ has been established making use of first principles.

(6) We have also studied the coupling of pions with axial-vector and pseudoscalar sources. In particular, it is shown that in-medium corrections up to $\mathcal{O}(p^5)$ do not spoil the validity of the Gell-Mann-Oakes-Renner relation. We have also found a decrease with increasing density for both the quark condensates and the temporal component of the pion decay constant f_t. Both effects seem indicate a partial chiral symmetry restoration with increasing density. We remark again that a systematic study of the in-medium order parameters still has to be performed. A drastic quenching with density has been also obtained for the spatial component of the pion decay constant f_s. To $\mathcal{O}(p^5)$ we have checked the QCD Ward identity relating both the temporal and spatial components of the axial-vector currents with the pseudoscalar ones and quark masses.

(7) A rapid decrease with density of the coupling of a photon to two pions, particularly in the threshold region, has been found. The derived vector current amplitudes coupled to two pions fulfill the requirement of current conservation. Furthermore, we have established the absence of in-medium renormalization up to $\mathcal{O}(p^5)$ of the anomalous $\pi^0 \to \gamma\gamma$ decay amplitude.

(8) On the other hand, $\pi\pi$ scattering has been studied as well up to $\mathcal{O}(p^3)$ since in this case the non-standard counting occurs. This implies that the in-medium corrections start at lower orders than in the standard case, here already at $\mathcal{O}(p^3)$. In addition the scale, below which the perturbative expansion is applicable, decreases. As a result the in-medium corrections increase very rapidly with density and already at $k_F \simeq 200$ MeV, or at a density of just $\sim 0.4\rho_0$, they are 100% with respect to the lowest order CHPT results.

As future challenges one should include multi-nucleon contact interactions which are enhanced because of the largeness of the S-wave scattering lengths related to the presence of shallow NN bound states as well as to calculate simultaneously pion loops necessary to determine the full $\mathcal{O}(p^6)$ contributions. On the other hand, some non-perturbative scheme that allows one to recover the scale $\sqrt{6}\pi f_\pi$ even in the case of the non-standard counting or when the multi-nucleon local interactions are included, should be pursued.

References:

[1] Ulf-G. Meißner, J.A. Oller and A. Wirzba, `nucl-th/0109026`.

[2] J.A. Oller, `hep-ph/0101204`, to appear in Phys.Rev.C.

Watson's theorem and electromagnetism in $K \to \pi\pi$ decay

Susan Gardner (Kentucky), Ulf-G. Meißner, German Valencia (Iowa)

A detailed understanding of the rich phenomenology of $K \to \pi\pi$ decays has remained elusive despite decades of effort. Although progress has been made, the dynamical origin of the $\Delta I = 1/2$ rule, as well as the strength of CP-violating parameter Re (ϵ'/ϵ), is not yet clear. Another, presumably related, puzzle stems from the apparent violation of Watson's final-state theorem. Watson's theorem emerges from unitarity and CPT-invariance, in concert with isospin symmetry, and implies that the strong phase in $K \to \pi\pi$ decay ought be given by that of $\pi\pi$ scattering. However, the S–wave $\pi\pi$ phase shift difference $\delta_0 - \delta_2$ extracted from the $K \to \pi\pi$ decay modes, using physical masses in the phase-space integrals, is about 57°, whereas its value from $\pi\pi$ scattering data, with the help of chiral perturbation theory and dispersion relations, is about 45° with an uncertainty of roughly 10%. The assumed equality of these quantities is a consequence of isospin symmetry, so that the resolution of the discrepancy has been sought in the computation of isospin-violating effects. Isospin violation can be generated by both strong (up-down quark mass difference) and electromagnetic (virtual photon) interactions, and its effects have been recently studied in great detail by various groups. While many interesting results have been obtained and many others are forthcoming, the gap between the phase-shift difference obtained from $K \to \pi\pi$ decay and $\pi\pi$ scattering has thus far eluded a detailed explanation. In the framework of chiral perturbation theory, which is the appropriate theoretical tool in this context, many new low–energy constants appear in the most general Lagrangian of Goldstone bosons coupled to virtual photons and external sources, making certain numerical predictions difficult. It is thus important to explore whether Watson's theorem can be extended in the presence of isospin violation. In Ref. [1] Watson's theorem was shown to persist through leading order in the up-down quark mass difference, so that the phase shifts from $K \to \pi\pi$ decay and $\pi\pi$ scattering ought be equal to $\mathcal{O}((m_d - m_u)^2)$. Were the phase shifts from $K \to \pi\pi$ decay and $\pi\pi$ scattering equal, the empirical phase-shift discrepancy could nevertheless be resolved, for it could be interpreted in terms of an additional amplitude in $K \to \pi\pi$ decay, of $|\Delta I| = 5/2$ in character [1]. In the isospin-perfect limit, the $K \to \pi\pi$ transition in $\mathcal{O}(G_F)$ can be of $|\Delta I| = 1/2$ or $|\Delta I| = 3/2$. In the presence of isospin violation, a $|\Delta I| = 5/2$ transition can be realized from $m_d \neq m_u$ effects in concert with a $|\Delta I| = 3/2$ weak transition or from electromagnetic effects in concert with a $|\Delta I| = 1/2$ weak transition. The empirical enhancement of the $|\Delta I| = 1/2$ weak transition suggests that the latter mechanism is of greater importance. The empirical $|\Delta I| = 5/2$ amplitude required to resolve the phase-shift discrepancy is compatible with that expected from electromagnetic effects [1], yet it is significantly larger in magnitude than and of opposite sign to that indicated by explicit estimates [2]. Moreover, including the estimated phase-shift difference from electromagnetism [2] exacerbates this discrepancy. These difficulties prompt the consideration of Watson's theorem in the presence of electromagnetism, in order to realize what constraints may exist on the strong and electromagnetically induced phase shifts in $K \to \pi\pi$ decay. This was the aim of investigation presented in [3]. We have considered the unitarity constraints on the strong and electromagnetically induced phases in $K \to \pi\pi$ decays. Assuming that the $(\pi^+\pi^-\gamma)$ final state is the only inelastic channel, and working in $\mathcal{O}(G_F)$, we have derived the constraints between the decay amplitudes A_I for $K \to (\pi\pi)_I$ decay (for isospin $I = 0, 2$) and A_γ for $K \to \pi^+\pi^-\gamma$. The corresponding S–matrix is characterized by three mixing parameters; we choose two angles $\Theta_{1,2}$ and one phase δ. The angle Θ_1 is chiefly responsible for the channel couplings $(\pi^+\pi^-\gamma) \leftrightarrow (\pi\pi)_I$, whereas δ describes the strong isospin violation effects due to the light quark mass difference, as well as any "direct" electromagnetic coupling between the $(\pi\pi)_0 \leftrightarrow (\pi\pi)_2$ states. From the general 4×4 S-matrix for K^0 decays into these three final states, one can derive a set of unitarity constraints. Most remarkably, it can be shown that the explicit coupling of the $(\pi^+\pi^-\gamma)$–channel is irrelevant to the difference between the T-conserving $\pi\pi$ phases measured in $\pi\pi$ scattering and extracted from $K \to \pi\pi$ (and $K \to \pi^+\pi^-\gamma$) decays. We have also argued that in the presence of isospin violation, the parametrization for the complex-valued decay amplitudes A_I ought be modified; we illuminate the sources of isospin breaking which give rise to the general parametrization of Ref. [1]. As a next step, it will be interesting to work out the numerical consequences of these constraints on the determination of the $|\Delta I| = 5/2$ amplitude in $K \to \pi\pi$ decay, as well as the impact on the Standard Model prediction for the CP-violating parameter Re (ϵ'/ϵ).

References:

[1] S. Gardner and G. Valencia, Phys. Rev. D 62 (2000) 094024.

[2] V. Cirigliano, J.F. Donoghue, and E. Golowich, Phys. Rev. D 61 (2000) 093001, 093002.

[3] S. Gardner, Ulf-G. Meißner and G. Valencia, Phys. Lett. B508 (2001) 44.

Near threshold neutral pion photoproduction off protons

V. Bernard (Strasbourg), N. Kaiser (München), Ulf-G. Meißner

Neutral pion photoproduction off protons and deuterons (which gives access to the elementary neutron amplitudes) belong to the premier processes to test our understanding of the chiral pion-nucleon dynamics for essentially two reasons. First, over the last decade fairly precise differential and total cross section data have been obtained at MAMI and SAL. A further experiment involving linearly polarized photons was performed at MAMI, which not only improved the differential cross sections but also gave the first determination of the photon asymmetry [1]. Second, the S-wave amplitude E_{0+} is sensitive to a particular pion loop effect. In the threshold region, the fourth order heavy baryon chiral perturbation theory calculation (HBCHPT) (which involves the sum a_1+a_2 of two low–energy constants) agrees with what is found in the multipole analysis of the data. In addition, the rather counterintuitive prediction for the electric dipole amplitude for π^0 photoproduction off the neutron, $|E_{0+}^{\pi^0 n}| > |E_{0+}^{\pi^0 p}|$ translates into a threshold deuteron amplitude E_d that was verified by a SAL experiment within 20%. Moreover, in [2] it was also shown that there are two *P-wave low energy theorems (LETs)* for the $P_{1,2}$ multipoles which show a rapid convergence based on the third order calculation. While the LET for P_1 could be tested and verified from the unpolarized data, only the recent MAMI measurement of $\vec{\gamma} p \to \pi^0 p$ allows to disentangle the contribution from the P_2 and the P_3 multipoles (the latter being largely determined by the LEC b_P at third order). It has been frequently argued that contributions from the delta isobar, that only appear at fourth order in the chiral expansion for P_1 and P_2, will not only spoil the rapid convergence of the P–wave LETs but also lead to numerically different values. This is witnessed e.g. in an effective field theory approach including the delta as an active degree of freedom in which one counts the nucleon–delta mass splitting as another small parameter. A third order analysis in that framework seems to indicate indeed large corrections rendering the agreement of the prediction for P_1 at threshold with the value deduced from the differential cross sections as accidental.

In this the work [3], we have completed the fourth order (complete one loop) analysis based on HBCHPT by evaluating the corresponding corrections for the three P-wave multipoles. We have used this framework to analyze the new data from MAMI, which confirms and sharpens previous findings concerning the electric dipole amplitude E_{0+} and sheds new light on the convergence issue of the P–wave LETs. The pertinent results of this investigation can be summarized as follows:

(i) We have given the fourth order corrections (loops and counterterms) to the three P-wave multipoles $P_{1,2,3}$. Two new low–energy constants appear, one for P_1 and the other for P_2. We have also given analytic expressions for the corrections to the low–energy theorems for the P–wave slopes $\overline{P}_{1,2} = P/|\vec{q}_\pi|$.

(ii) We have analyzed the new MAMI data [1] first in the same approximation as it was done in previous works (i.e. the P–waves to third order only). Using a realistic two parameter model for the energy dependence of the electric dipole amplitude E_{0+}, we have extracted the strength of the unitary cusp which agrees with the prediction based on the final state theorem.

(iii) Using the full one loop amplitude, one can fit the cross section data and the photon asymmetry. The combination of S–wave LECs is stable and agrees with previous determinations, leading to $E_{0+}(\omega_{\rm thr}) = -1.1 \cdot 10^{-3}/M_{\pi+}$. Two of the three P–wave LECs are not well determined because of strong correlations. More photon asymmetry data are needed to cure this situation.

(iv) We have analyzed the new LECs in the framework of resonance saturation in terms of (dominant) Δ–isobar and (small) vector meson excitations. The isobar contributions depend only on the strength of the $N\Delta$ transition magnetic moment. We have shown that for reasonable values of this constant, the 25% fourth order loop corrections to the P–wave LETs are almost completely cancelled by the isobar terms. This solidifies the third order LET predictions, which are in excellent agreement with the data.

References:

[1] A. Schmidt et al., `nucl-th/0105010`, to appear in Phys. Rev. Lett.

[2] V. Bernard, N. Kaiser and Ulf-G. Meißner, Z. Phys. C70 (1996) 483.

[3] V. Bernard, N. Kaiser and Ulf-G. Meißner, Eur. Phys. J. A 11 (2001) 209.

The generalized GDH sum rule at low photon virtualities

V. Bernard (Strasbourg), T.R. Hemmert (München), Ulf-G. Meißner

The spin structure of the nucleon has received lots of attention from the experimental as well as the theoretical side during the last few years. Measurements over a large range of photon virtualities of polarized electron-proton (neutron) scattering have been performed and are underway, e.g. at Jefferson Lab. The starting point for the theoretical investiagtions of these processes is the spin-dependent forward Compton amplitude,

$$T^{\mu\nu} = i \int d^4\xi e^{iq\cdot\xi} \langle N(p,s)|T(J^\mu(\xi)J^\nu(0)|N(p,s)\rangle \ ,$$

which can be parameterized by two functions, the forward spin-amplitudes $S_1(\nu, Q^2)$ and $S_2(\nu, Q^2)$ of $\gamma^* N \to \gamma^{*'} N$, with $\nu = p\cdot q/m_N$. In the deep Euclidean region, these are related to the spin structure functions $g_{1,2}$. At low virtualities, they can be calculated in baryon chiral perturbation theory. The pioneering third order calculation of [1] in the relativistic (using dimensional regularization) and the heavy baryon formalism led to a prediction for the slope of the generalized GDH sum rule at the photon point,

$$I_{\rm GDH} \propto \int_{\rm thr}^{\infty} \frac{\sigma_{1/2} - \sigma_{3/2}}{\nu} d\nu \ ,$$

in terms of the helicity 1/2 and 3/2 photon-proton cross section. This integral can be expressed in terms of the Born term subtracted amplitudes $\bar{S}_i$ as $\bar{S}_1 - Q^2\bar{S}_2$. Note, however, that to third order only $\bar{S}_2$ is non-vanishing. The chiral corrections to these amplitudes at fourth order were calculated in [2] employing the heavy baryon formalism. This led to sizeable corrections and a much more rapid Q^2 variation of the generalized GDH integral as expected from naive dimensional analysis, casting doubts on the convergence of the chiral expansion. Of course, it is well-known that the integrals $I_{\rm GDH}$ for the proton and the neutron are build up not only from the pion cloud but also from resonance contributions. In the difference, however, these resonance contributions should cancel to a large extent. Triggered by the results of ref.[2], we have started a systematic reevaluation of the forward spin-amplitudes in a manifestly Lorentz inavriant formulation of baryon CHPT, also called IR regularization. In this formalism, all recoil corrections are summed due to the use of the relativistic Dirac propagator, eliminating one possible source of the slow convergence of the heavy baryon formalism (as it is known already for the case of the electric form factor of the neutron). We have performed the calculation to complete one-loop accuracy, i.e. to fourth order, in the IR regularized approach [3]. The preliminary results of this study can be summarized as follows:

(1) To third order in the chiral expansion, we have completed the calculation of $\bar{S}_1 - Q^2\bar{S}_2$ and $\bar{S}_2$ for the proton and the neutron. We find sizeable differences to the third order results of heavy baryon CHPT or even to dimensionally regularized relativistic baryon CHPT, as shown e.g. for the proton GDH integral $I_p(Q^2)$ shown in the figure.

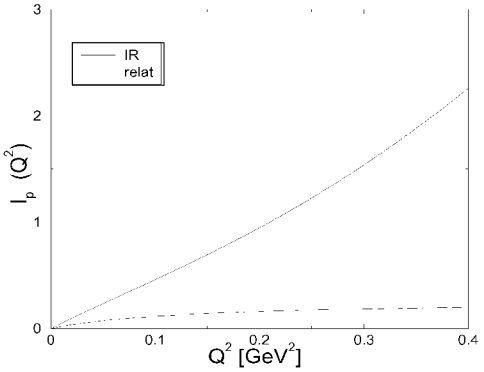

Figure 1: GDH integral for the proton. The dashed and the solid lines refer to the dimensionally and IR regularized relativistic calculation, respectively.

(2) For the neutron, we have completed the fourth order calculation of the spin-dependent amplitudes. Within the IR scheme, the fourth order corrections to $\bar{S}_2$ are well behaved for virtualities $Q^2 \leq 0.5\,{\rm GeV}^2$. Both for $\bar{S}_1$ and $\bar{S}_2$ the IR result differs markedly from the corresponding heavy baryon prediction, which can be obtained by letting the nucleon mass become very large in the IR formulation. The somewhat more elaborate calculation for the proton is close to being finsihed.

(3) We have also calculated the polarizabilities α and β and the forward spin-polarizability γ_0 in this framework. For a precise prediction of γ_0 we show that it is mandatory to retain the terms of order M_π^2 and $M_\pi^2 \ln M_\pi^2$.

(4) We are also working on the calculation of the delta contribution to the various observables based on a systematic effective field theory approach of the coupled $N\Delta\gamma$ system.

References:

[1] V. Bernard, N. Kaiser and Ulf-G. Meißner, Phys. Rev. D48 (1993) 3062.

[2] X.-D. Ji, C.-W. Kao and J. Osborne, Phys. Lett. B472 (2000) 1.

[3] V. Bernard, T.R. Hemmert and Ulf-G. Meißner, *in preparation.*

Rescattering and chiral dynamics in $B \to \rho\pi$ decay

Susan Gardner (Kentucky) and Ulf-G. Meißner

Measurements at SLAC and KEK of the time-dependent CP-violating asymmetry in $B(\bar{B}) \to \psi K_s$, yielding $\sin(2\beta)$, have conclusively established the existence of CP violation in the B meson system. The results found are consistent with Standard Model expectations, so that establishing whether the CKM matrix is the only source of CP violation in nature, as in the standard model, or not requires the empirical measurement of all the angles of the unitarity triangle.

In the work [1] we consider the determination of α through a Dalitz plot analysis of the decays $B^0(\bar{B}^0) \to \rho\pi \to \pi^+\pi^-\pi^0$ under the assumption of isospin symmetry. Ten parameters appear in the analysis, and they can be determined in a fit to the data. Nevertheless, the assumption of ρ dominance in $B \to 3\pi$ decays has no strong theoretical basis so that the contributions from other resonances in the $\rho\pi$ phase space may be important. We discuss how the isospin analysis can be enlarged to include the $\sigma\pi$ channel as well. The σ or $f_0(400-1200)$ "meson" is a broad $J = I = 0$ enhancement, close to the ρ meson in mass, so that the $\sigma\pi$ channel can potentially populate the 3π phase space associated with the $\rho\pi$ channels. The $\sigma\pi$ final state contributes preferentially to the $\rho^0\pi^0$ final state. In the context of the isospin analysis, such contributions are of consequence as they invalidate the underlying assumptions of the isospin analysis and thus mimic the effect of isospin violation. Our considerations are inspired in part by recent studies of $D^- \to 2\pi^-\pi^+$ decay: the E791 collaboration find that the pathway $D^- \to \pi^-\sigma \to 2\pi^-\pi^+$ accounts for approximately half of all $D^- \to 2\pi^-\pi^+$ decays. In [2] is was argued as a consequence that the $B \to \sigma\pi$ channel contributes significantly to the $\rho\pi$ phase space in $B \to \pi^0\pi^+\pi^-$ and modifies the ratio $\mathcal{B}(\bar{B}^0 \to \rho^\mp\pi^\pm)/\mathcal{B}(B^- \to \rho^0\pi^-)$ to yield better agreement with experiment [2]. The scalar form factor, which describes the appearance of the σ in the $\pi^+\pi^-$ final state, enters as a crucial ingredient in the assessment of the size of these effects. The scalar form factor cannot be determined directly from experiment; nevertheless, ample indirect constraints exist, permitting us to describe its features with confidence [3]. We follow Ref. [3] and adopt an unitarized, coupled-channel approach to final-state interactions in the $\pi\pi$-$K\bar{K}$ system, and match the resulting scalar form factor to chiral perturbation theory (CHPT) in the regime where the latter is applicable. The resulting form factor, in the $\pi\pi$ channel, is strikingly different from the relativistic Breit-Wigner form adopted by the E791 collaboration in their analysis of the σ in $D^+ \to \pi^+\pi^+\pi^-$ decay — the latter form factor is also used in Ref. [2]. The differences are particularly large as $\sqrt{s} \to 2M_\pi$, so that the relativistic Breit-Wigner form is at odds with CHPT in the precise region where it is working. This casts doubt on the recent conclusions, prompting new analyses incorporating a suitable scalar form factor. The generation of the σ resonance via strong rescattering effects, as in the approach we adopt, indicates that OZI effects in the scalar sector are significant. Moreover, the "doubly" OZI-violating form factor $\langle 0|\bar{s}s|\pi\pi\rangle$ is non-trivial as well; such a contribution is needed to fit the $\pi\pi$ and $K\bar{K}$ invariant mass distributions in $\psi \to \phi\pi\pi(K\bar{K})$ decay [3]. These observations give new insight on rescattering effects in hadronic B decays, generating a new mechanism of factorization breaking in $n \geq 3$ particle final states. Such effects are important for studies of CP violation because rescattering effects can potentially yield large strong phases.

The contribution of the $B \to \sigma\pi$ channel to the $B \to \rho^0\pi$ phase space can also modify the inferred empirical branching ratios in these channels. Combining the CLEO results $\mathrm{Br}(B^- \to \rho^0\pi^-) = (10.4\,^{+3.3}_{-3.4} \pm 2.1) \cdot 10^{-6}$ and $\mathrm{Br}(\bar{B}^0 \to \rho^\pm\pi^\mp) = (27.6\,^{+8.4}_{-7.4} \pm 4.2) \cdot 10^{-6}$ with the BaBar result $\mathrm{Br}(\bar{B}^0 \to \rho^\pm\pi^\mp) = 28.9 \pm 5.4 \pm 4.3$ yields, adding the errors in quadrature and ignoring correlations,

$$\mathcal{R} = \frac{\mathrm{Br}(\overline{B^0} \to \rho^\mp\pi^\pm)}{\mathrm{Br}(B^- \to \rho^0\pi^-)} = 2.7 \pm 1.2\,. \qquad (1)$$

This ratio of ratios is roughly 6 if one works at tree level and uses the naive factorization approximation for the hadronic matrix elements. The inclusion of penguin contributions can alter this result, and potentially yield better accord with theory and experiment. However, our focus will parallel that of Ref. [2]: we wish to examine how $B \to \sigma\pi \to 3\pi$ decay, given a particular scalar form factor, can effectively modify the theoretical prediction of the ratio $\mathcal{R}$. It is apparent that $B \to \sigma\pi$ is of greater impact in $B \to \pi^0\pi$ decay, so that the inclusion of such contributions ought alter the ratio of ratios. In fact, treating the various decays as two-body ones, we find $\mathcal{R} = 5.8\,(5.5)$ for the case of no (with) penguin diagrams. Proper inclusion of the final-state interaction (3-body decays) and adding the ρ and the σ contribution, which are based on the use of the consistent scalar and vector form factors, leads to

$$\mathcal{R} = 2.5\,, \qquad (2)$$

much improved compared to the number given in [2] and consistent with the data. The theoretical uncertainty is about 20%, but this needs to be sharpened.

References:

[1] S. Gardner and Ulf-G. Meißner, [hep-ph/0112281].

[2] A. Deandrea and A. D. Polosa, Phys. Rev. Lett. 86 (2001) 216.

[3] Ulf-G. Meißner and J. A. Oller, Nucl. Phys. A679 (2001) 671.

Three nucleon systems with consistent three-nucleon forces from chiral effective field theory

E. Epelbaum, H. Kamada, A. Nogga (Tucson), H. Witala (Krakau), W. Glöckle (Bochum), Ulf-G. Meißner

Chiral effective field theory can be applied successfully to the pion and the pion–nucleon systems. For processes involving more than one nucleon, the appearance of shallow nuclear bound states requires an additional non–perturbative resummation. Weinberg suggested to apply power counting to the two–nucleon (NN) potential, generating bound and scattering states from the Schrödinger or Lippmann-Schwinger (LS) equation. In [1] it was shown how to modify this power counting to generate an energy–independent hermitean potential by means of the FST-Okubo projection formalism. In addition, the so constructed wave functions are fully orthonormal. The NNLO *np* potential was constructed in [2] and shown to reproduce most *np* phase shifts to good precision up to pion production threshold. For that, the LS equation was solved using a momentum–space regulator in harmony with the underlying symmetries. Typical cut-off values range from 500 MeV to 1 GeV. In particular, the two S–waves are cut-off independent and as precisely given as in the so–called realistic potentials. With no parameter tuning, the deuteron properties can be described fairly accurately. A complication arises due to the appearance of deeply bound virtual states, which can be traced back to the very strong and singular TPEP. Therefore, in [3], we constructed the NNLO* potential which also describes the phase shifts very well but is free of these bound states. These states are of no consequence to the NN, but to the 3N and 4N systems. In a series of works [4], we have considered 3N (and 4N) systems and a **systematic** calculation of the NNLO three–nucleon forces. Our findings are:

(i) The NLO *np* potential was applied to to systems of three and four nucleons [5]. At this order, one has no three–nucleon forces (3NF) and thus obtains parameter–free predictions. For changing the cut–off between 540 and 600 MeV, the ^{3}H and ^{3}He binding energies vary between $-7.55\ldots-8.28$ and $-24.0\ldots-28.0$ MeV, respectively. 3N scattering can be solved exactly. We have considered elastic *nd* scattering at 3 and 10 MeV. While for the cross section (and also the tensor analyzing powers T_{2k}) the results using the chiral force are in agreement with what is found for high precision potentials like CD-Bonn, we find a clear improvement in the analyzing power A_y.

(ii) We have then applied the NNLO and NNLO* potentials to the same processes without including the 3NF. We find that the theoretical uncertainty decreases and is not larger than the band for the various realistic potentials. For NNL0*, the triton binding energies variees between $-8.18\ldots-8.38$ MeV. We have also shown that the NNLO* potential can even describe data at 65 MeV with good accuracy. However, the description of A_y worsens, leading to the conclusion that 3NF's are needed. For the NNLO scenario, the 3NF forces must be much stronger since the 2N contribution to the binding energy is sizeably reduced.

(iii) We have shown, contrary to what was believed before, that the leading 3NF is given in terms of *two parameters* only, one related to the exchange of a pion between a 4N vertex and a single nucleon ($\sim d_1$) and the other to a genuine 6N interaction ($\sim e_1$). With a combination of these parameters, we fit exactly the triton binding energy. Varying the other within bounds derived from naturalness, we find an improved description of A_y, but there is still some strength missing, see the figure. At N^{3}LO, the 3NF is described by new terms with however fixed parameters. We are working on the inclusion of these operators.

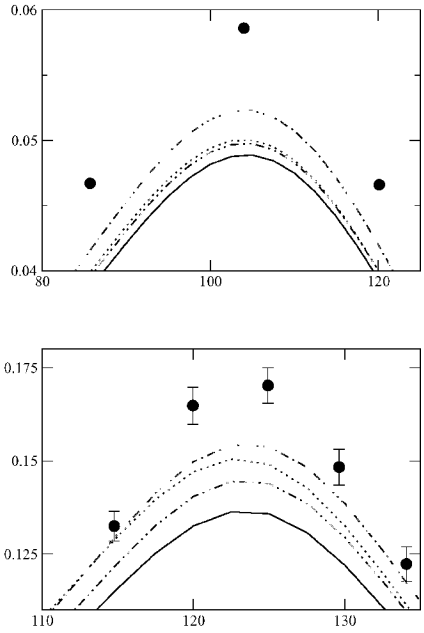

Figure 1: Maximum of A_y at $E_n = 3$ MeV (upper panel) and $E_n = 10$ MeV (lower panel). Chiral force at NNLO*: no 3NF (double-dot-dashed), $d_1 = 2$ (dotted), $d_1 = -1$ (dot-dashed) and CD–Bonn (solid curve).

References:

[1] E. Epelbaoum, W. Glöckle and Ulf-G. Meißner, Nucl. Phys. A637 (1998) 107.

[2] E. Epelbaum, W. Glöckle and Ulf-G. Meißner, Nucl. Phys. A671 (2000) 295.

[3] E. Epelbaum et al., `nucl-th/0106007`.

[4] E. Epelbaum et al., *in preparation.*

[5] E. Epelbaum et al., Phys. Rev. Lett. 86 (2001) 4787.

Limit cycle behaviour from the nucleon-nucleon interaction

E. Epelbaum and Ulf-G. Meißner

The NN potential constructed in effective field theory (EFT) based on Weinberg power counting becomes increasingly singular in coordinate space with increasing number of pion exchanges. In the attractive channels, this leads to the appearance of deeply bound virtual states. These states are well outside the limits of applicability of the effective field theory and are expected to appear on general grounds. In a simple quantum mechanical system, the behaviour of such singular potentials has recently been studied by Beane et al. [1]. It was also shown in [2] that in the pionless EFT the renormalized three-nucleon force $H(\Lambda)$ (with Λ the cut-off) shows an interesting periodic behaviour in $\ln \Lambda$, which is known as a limit cycle. In the work [3] we have studied such phenomena for the NN interaction in the pionfull theory. Starting point are the D-waves, which show a strong cut-off dependence at NNLO, but can be made cut-off independent by N^{3}LO counterterms of the form

$$C_\alpha \, p^2 p'^2 \sim \cos^2 \theta \quad (\alpha = {}^1D_2, {}^3D_1, \ldots) \; ,$$

with $p(p')$ the nucleon cms momenta and θ the scattering angle. One can now ask the question what happens if one lets the cut-off run and, in particular, what happens as $\Lambda \to \infty$? The running of the ${}^3D_2$ counterterm calculated at NNLO with Λ is shown in fig.1, at each point where the curve approaches $+\infty$ and reappears from $-\infty$, the number of bound states in this partial wave increases by one, i.e. in the limit of an infinite cut-off one has an accumulation of an infinite number of virtual bound states at very large energies. This is exactly a limit cycle behaviour. This

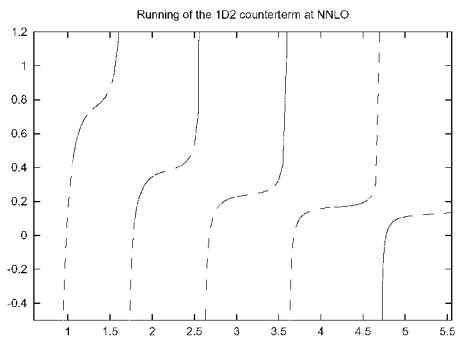

Figure 1: Running of the ${}^3D_2$ counterterm with Λ.

can also be seen in corresponding phase shift. If we fit ot the data for $E_{\rm lab} < 100\,$MeV, the phase shift at higher energies can be predicted. This is shown in fig.2 for the phase ${}^3D_2$ for $\Lambda = 0.6, 1., 2., 3.$ and 5.GeV (from bottom to top) . It clearly shows that the phase shift converges to a limiting value, interestingly, this limiting value is very close to the data

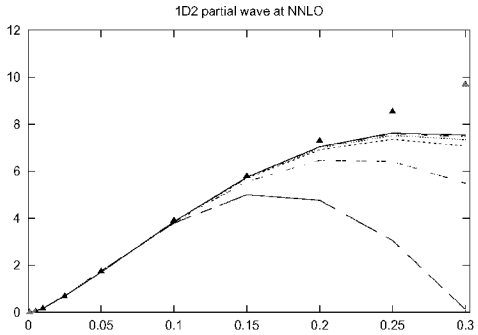

Figure 2: Prediction of the ${}^3D_2$ phase at NNLO for various valus of the cut-off as described in the text.

(or the phase shift analysis). This behaviour is also observed at NLO, but the running of the counterterms is much weaker. This can be understood from the fact that the two-pion exchange potential at NLO does not involve the large dimension two low-energy constants c_i and is thus weaker (but still singular). In fact, we have shown that this phenomenom happens in *all* partial waves, including the coupled channels. To our knowledge, that is the first time that this intriguing phenomenon has been studied for such cases. Of course, these are only the first steps for an exact renormalization scheme based on Weinberg power counting, in fact, it is not yet clear how this limiting procedure of an infinite cut-off should be understood in such a framework. A related question stems from the observation that one needs (at least) one counterterm in each partial wave, which seems to strongly limit the predictive power of such an approach. More work, also in relation to conventional renormalization group treatments, is clearly called for.

References:

[1] S.R. Beane et al., Phys. Rev. A64 (2001) 042103.

[2] P. Bedaque, H.W. Hammer and U. van Kolck, Phys. Rev. Lett. 82 (1999) 463

[3] E. Epelbaum and Ulf-G. Meißner, *in preparation.*

Effective field theory for dilute Fermi systems

L. Platter, H.-W. Hammer (Ohio) and Ulf-G. Meißner

The creation and detailed study of Bose-Einstein condensates has created novel interest in precise and systematic many-body calculations. Recently, there has also been experimental progress in creating and measuring dilute low-temperature Fermi systems, although these experiments are not yet sensitive to interactions. Besides that, the dilute Fermi gas has often served as a benchmark many-body problem. Using effective field theory (EFT), one can rederive, extend and put on firmer theoretical grounds many of the successful many-body techniques developed in the past. The prototype for such a system consists of non-relativistic fermions with a purely repulsive, spin-independent interaction of characteristic range $R = 1/\Lambda$. If these interactions are of natural size, the corresponding expansion parameter is $k_F\, R$, with k_F the Fermi-momentum. The density is related to k_F via $\rho = g k_F^3/(6\pi^2)$, with g the spin-degeneracy factor. EFT provides a model-independent description of finite density observables in terms of parameters that can be fixed from scattering in the vacuum, with no off-shell ambiguities (as they appear in many-body calculations based on potentials or pseudo-potentials). Since the system is probed with low resolution, all vertices are contact interactions, thus exchange contributions vanish.

Such a system at zero temperature has been systematically investigated by Hammer and Furnstahl [1]. They have set up a transparent power counting scheme based on a renormalization procedure employing dimensional regularization and minimal subtraction. Consequently, any Hugenholtz diagram contributes to a single, well-defined order in the low-density expansion. In particular, the ground-state energy per particle was rederived up to terms of order $(k_F a_s)^4 \ln(k_F a_s)$, with a_s the S-wave scattering length. This last terms is due to logarithmic divergences in three-to-three scattering, which can most easily be obtained using renormaliztion group methods [2]. Such methods can also be applied to obtain further $(\ln k_F)^n$ terms with $n \geq 2$. It is important to stress that such three-body contributions (and higher ones) are inevitable. Neglecting such terms leads to the unphysical off-shell dependence when employing pseudo-potentials. The power counting underlying the EFT analysis further reveals that the often used hole-line expansion for the low-density natural Fermi gas is only an artefact of a subtraction scheme that does not remove power divergences. In the EFT approach using minimal subtraction, particle-particle and particle-hole graphs contribute at the same order in k_F and are numerically comparable.

Since much more can be learned about the analytical structure of such many-body systems, we calculated [3] the complete order $(k_F a_s)^4$ contribution to the ground-state energy, which is much more complicated than the calculations in [1] due to the angular dependence appearing in the numerators. This result is new in that it was not calculated previously. We have also obtained the corresponding occupation number densities, which can simply be obtained from the Hugenholtz diagrams underlying the ground-state energy. Furthermore, based on the imaginary part of the particle self-energy, we have studied the systematic expansion of the single particle lifetime, recovering and extending results obtained from conventional many-body techniques.

References:

[1] H.-W. Hammer and R.J. Furnstahl , Nucl. Phys. A678 (2000) 277

[2] E. Braaten and A. Nieto, Phys. Rev. B55 (1997) 8090.

[3] L. Platter, H.-W. Hammer and Ulf-G. Meißner, *in preparation.*

The pion-deuteron scattering length in baryon chiral perturbation theory

S.R. Beane (Seattle),V. Bernard (Strasbourg), E.Epelbaum, Ulf-G. Meißner, D.R. Phillips (Ohio)

There has been remarkable recent progress in developing the effective field theory (EFT) relevant to multi-nucleon systems. Among the advantages of this formalism is a quantitative method for estimating theoretical errors, and the use of field theory technology, which allows one to treat scattering processes involving different numbers of nucleons in a rigorous and unified manner. The non-perturbative effects responsible for deuteron binding are accounted for in the EFT power counting, with a meaningful quantification of the theoretical error. The multi-nucleon EFT relevant to momentum transfers of order the pion mass is a straightforward generalization of single-nucleon baryon chiral perturbation theory. Nucleon-nucleon phase shifts and deuteron properties have now been computed to next-to-next-to-leading order in this expansion.

The π-deuteron (π-d) scattering length is a gold-plated observable in nuclear physics. Recent experiments with pionic deuterium allow an extraction of the π-d scattering length with an accuracy which is remarkable at the level of strong interaction physics. The Neuchatel-PSI-ETHZ (NPE) pionic deuterium measurement gives [1] $a_{\pi d} = [-0.0261(\pm 0.0005) + i\ 0.0063(\pm 0.0007)\ ]M_\pi^{-1}$. On the theoretical front, local operators which contribute to π-d scattering enter at high orders in the EFT expansion and are therefore highly suppressed. That these contributions are very small is crucial to the predictive power of the EFT, as the coefficients which determine the strength of these operators are unknown, and need therefore be determined from a seperate nuclear observable, or, at some time in the distant futurity, from lattice QCD. This suppression of local operators has an additional benefit: the π-d scattering length is sensitive to low-energy constants which contribute to the π-nucleon scattering amplitude. These parameters are fit from various partial wave analyses of π-nucleon scattering and give a rather large spread of values, π-d scattering provides an additional constraint on these parameters [2].

In baryon chiral perturbation theory the π-d scattering length can be written

$$\begin{aligned} a_{\pi d} &= \frac{(1+\mu)}{(1+\mu/2)}(a_{\pi n} + a_{\pi p}) + a_{(boost)} \\ &+ a_{(3-body)} + i\,\mathrm{Im}\, a_{\pi d}\,, \end{aligned} \qquad (1)$$

where $\mu \equiv M_\pi/m$. This was evaluated in [3] to fourth order in the chiral power counting. The first two terms refer to the scattering off a single nucleon, with the boost correction appearing first at fourth order. It depends on the low-energy constant c_2 that can be determined from π-N scattering. We leave the isoscalar π-N scattering length $a_{\pi n} + a_{\pi p} = 2a^+$ as a free parameter. The three-body contributions have a third order piece first calculated in [4], as shown in the fig. 1. To fourth order, there are 15 topologically different diagrams which, however, completely cancel. At this order, there are no local four-nucleon-two-pion operators with unknown coefficients. Eq.(1) thus allows to get an improved bound on a^+ by using the experimental number for Re $a_{\pi d}$ as input. Using the NLO and NNLO* wavefunctions from chiral effective field theory and varying the cut-off appearing in the regularized Lippmann-Schwinger eqaution within reasonable bounds and also varying the low-energy constant c_2 as determined from various fits to π-N scattering, we obtain very stable results for a^+

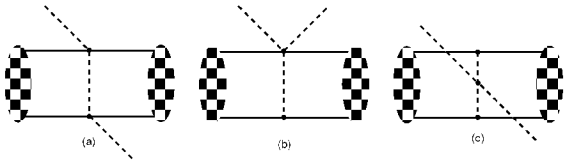

Figure 1: Leading 3-body corrections to π-d scattering.

$$\begin{aligned} \text{NLO} &: a^+ = -0.0060\ldots - 0.0049\ M_\pi^{-1}\,, \\ \text{NNLO*} &: a^+ = -0.0046\ldots - 0.0044\ M_\pi^{-1}\,, \end{aligned}$$

not including the experimental uncertainty on Re $a_{\pi d}$. These values are slightly larger in magnitude than the ones found in [2]. The smaller range at the higher order reflects the convergence of this particular calculation.

We have also calculated some fifth order corrections in [3]. It was shown that the multiple rescattering corrections appearing at that order contribute insignificantly to Re $a_{\pi d}$ and that the imaginary part of the scattering length, which is first appearing at this order, is in rough agreement with the empirical number. This reflects the usual problem of chiral perturbation theory related to the perturbative treatment of unitarity. Finally, we have also discussed the subtleties arising in the presence of deeply bound virtual states that can appear in EFT treatments (using simple regulators).

References:

[1] P. Hauser et al., Phys. Rev. C58 (1998) 1869.

[2] S.R. Beane, V. Bernard, T.S.-H. Lee and Ulf-G. Meißner, Phys. Rev. C57 (1998) 424.

[3] S.R. Beane, V. Bernard, E. Epelbaum, Ulf-G. Meißner, D.R. Philipps, *in preparation.*

[4] S. Weinberg, Phys. Lett. B295, 114 (1992).

Isospin violation in pion-kaon scattering

Bastian Kubis and Ulf-G. Meißner

One of the cleanest processes to test our understanding of the symmetry breaking pattern in the presence of strange quarks is elastic pion–kaon (πK) scattering near threshold. This reaction is interesting for a variety of reasons. First, it is very similar to $\pi\pi$ scattering in the two–flavor sector but also different in that the quark mass difference m_u–m_d can appear at leading order in the πK scattering amplitude. Second, there exist abundant data from inelastic processes which allow one to extract low–energy characteristics of the πK scattering amplitude by means of dispersion theory. The existing determinations of the S–wave scattering lengths are, however, plagued by large uncertainties, Third, the DIRAC collaboration intends to measure the lifetime of πK atoms at CERN which gives direct access to the isovector S–wave scattering length. To also pin down the isoscalar S–wave scattering length, one would have to measure the $2P-2S$ level shift, similar to what has been done for the pion–nucleon system at PSI. The precise relation between the πK atom lifetime and the scattering length (the so–called modified Deser formula) can be worked out by means of an effective field theory for hadronic bound states.

In this work [1, 2], we have considered isospin violation in pion–kaon scattering near threshold. To systematically account for such effects due to the light quark mass difference as well as electromagnetic interactions, we have made use of SU(3) chiral perturbation theory in the presence of virtual photons. The pertinent results of this investigation can be summarized as follows:

(1) Already at tree level, one has strong as well as electromagnetic isospin violation. We have considered all physical channels and found that these effects are in general small (at most two percent). In particular, the relative corrections are smaller than in the comparable case of $\pi\pi$ scattering where isospin violation at tree level is a purely electromagnetic effect. We have also stressed that considering one particular source of isospin violation only can ensue very misleading results.

(2) Because of its relevance to the lifetime of πK atoms, we have considered the one–loop corrections to the S–wave scattering length for the process $\pi^- K^+ \to \pi^0 K^0$. The fourth–order isospin symmetric corrections are moderate and the isospin violation effects at this order cancel to a large extent (for the central values of the low–energy constants used here). The uncertainty in these isospin violating contributions is mainly due to the poor knowledge of the electromagnetic LECs K_i. This uncertainty is comparable to the one in the isospin symmetric amplitude induced by the variations in the strong LECs L_i.

(3) We have also considered the radiative process $\pi^- K^+ \to \pi^0 K^0 \gamma$. We have explicitly demonstrated the cancellation of the infrared divergences. The remaining radiative cross section is strongly suppressed at threshold so that the properly redefined (finite) scattering length acquires no significant correction.

(4) We have also given the one–loop corrections for the effective range b_0 and the P–wave scattering length a_1 for this channel. The isospin violating corrections are somewhat more pronounced than for the S–wave scattering length.

(5) We have analyzed the charged channel $\pi^- K^+ \to \pi^- K^+$ by subtracting the direct photon-exchange diagrams from the full amplitude, $T = T_\mathrm{s} + T_\mathrm{ex}$. The strong amplitude T_s still contains the Coulomb pole. We therefore define the scattering length a_0 as the regular part of the amplitue T_s at threshold. The so extracted S-wave scattering length $a_0(\pi^- K^+ \to \pi^- K^+) = a_0^+ + a_0^-$ is afflicted by a sizeable uncertainty (16%) due to the appearance of the isoscalar contribution. Even when isospin violation is included, this uncertainty dominates the error for the prediction of this quantity. If, however, the aim is to extract the sum of isovector and isoscalar scattering lengths from the measurement of the strong level shift, the corresponding uncertainty in the electromagentic corrections amounts to only 3%, which is reasonable in comparison to the expected experimental accuracy.

References:

[1] B. Kubis and Ulf-G. Meißner, `hep-ph/0107199`, Nucl. Phys. A, in print.

[2] B. Kubis and Ulf-G. Meißner, `hep-ph/0112154`.

Resonance saturation for four–nucleon operators

E. Epelbaum, W. Glöckle (Bochum), Ulf-G. Meißner, Ch. Elster

Effective chiral Lagrangians can be used to investigate the dynamics of pion, pion–nucleon as well as nucleon–nucleon interactions. In all cases, one has to consider two distinct contributions, namely tree and loop diagrams, which are organized according to the underlying power counting. To a given order, one has to consider all local operators constructed from pions, nucleon fields and external sources in harmony with chiral symmetry, Lorentz invariance and the pertinent discrete symmetries. Beyond (or even at) leading order in the chiral expansion, these operators are accompanied by unknown coupling constants, also called low–energy constants (LECs). In principle, these LECs are calculable from QCD but in practice need to be fixed by a fit to some data or using some model. While in certain cases sufficient data exist allowing one to pin down the LECs, often some reliable estimate for these constants beyond naive dimensional analysis is needed. In the meson sector, the ten LECs of the chiral Lagrangian at next–to–leading order (NLO) have been determined and their values can be understood in terms of masses and coupling constants of the lowest meson resonances of vector, axial–vector, scalar and pseudoscalar character, may be with the exception of the scalar sector with vacuum quantum numbers. This is called resonance saturation, it has been used e.g. to estimate LECs at next–to–next–to–leading order (NNLO) or for the extended chiral Lagrangian including virtual photons as dynamical degrees of freedom. A similar systematic analysis exists for the finite dimension two couplings of the pion–nucleon effective Lagrangian, where it was demonstrated the LECs are saturated in terms of baryon resonance excitation in the s– and u–channel and t–channel meson resonances. Much less is known about dimension three and four couplings, but for certain processes resonance saturation has been shown to work quite well, e.g. in neutral pion photoproduction off protons.
The situation is very different concerning few–nucleon systems, where a new type of operators with $2A$ nucleon fields appears (for reactions involving $A \geq 2$ nucleons). Only recently, a complete and precise determination of the four S–wave and five P–wave (LO and NLO) LECs in neutron–proton scattering has become available [1], thus it was mandatory to ask the question whether the numerical values of these four–nucleon coupling constants can be understood from some kind of resonance saturation. This was the topic of the paper [2]. Our main findings can be summarized as follows:

(1) We have determined the LECs for the NLO and NNLO potentials, including the dominant charge–dependence effect from the pion mass difference in the one–pion exchange. To avoid the unphysical bound states at NNLO, we have argued that one has to subtract the Δ resonance contribution from the dimension two pion–nucleon LECs. This is in agreement with two–boson–exchange models, where the two–pion–exchange contribution is cancelled largely by $\pi\rho$ graphs.

(2) We have shown how to deduce similar type of contact operators from boson–exchange models in the limit of large meson masses. This allows to calculate the LECs in terms of meson–nucleon coupling constants, meson masses and (unobservable) cut–off masses. In a similar manner, one can examine the so–called high–precision potential models. We have found that in all cases, the LECs determined from these models are close to the values found in EFT, which can be considered as a new form of resonance saturation.

(3) We have shown that with the exception of one dimension zero coupling (the LEC C_T), all LECs are of natural size. The smallness of C_T is due to Wigner's spin–isospin symmetry, as was already pointed out for the case of a theory with pions integrated out or treated perturbatively.

Clearly, these findings have further–reaching consequences. On one side, they might allow to further constrain models of the nucleon–nucleon interaction applicable at energies where the EFT description can not be used. On the other hand, in case of external sources (like e.g. photons) or multi–nucleon operators (as they appear e.g. in the description of the three–body forces), these considerations will allow to at least estimate novel LECs that will appear.

References:

[1] E. Epelbaum, W. Glöckle and Ulf-G. Meißner, Nucl. Phys. A671 (2000) 295.

[2] E. Epelbaum, W. Glöckle, Ulf-G. Meißner and Ch. Elster, `nucl-th/0106007`.

Elastic electron–deuteron scattering in chiral effective field theory

Ulf-G. Meißner, M. Walzl

A new era of nuclear physics calculations was started by Weinberg in 1990 applying effective field theory (EFT) methods and chiral Lagrangians to systems of two and more nucleons. It is by now established that at very low energies, one can perform very accurate calculations using a theory of non–relativistic nucleons, whose interactions are given in terms of A-nucleon terms (A= $4, 6, \ldots$) with the pions integrated out, the so–called pionless theory. Going to higher energies, the inclusion of pions becomes of prime importance and it has been shown that Weinberg's original proposal of constructing an irreducible N–nucleon (N= $2, 3, \ldots$) potential and iterating it in a Schrödinger (Lippmann-Schwinger) equation can give a precise description of nucleon–nucleon (NN) scattering as well as static and dynamic properties of three- and four-nucleon systems. Of course, many results found in nuclear effective field theory have previously been obtained in more conventional meson-exchange approaches. These, however, cannot be formulated in a truly systematic fashion and cannot be linked simply to the symmetries of QCD, as it is the case of the chiral effective field theory employed here. In [1], we have considered elastic electron–deuteron scattering based on a Hamiltonian approach to Weinberg's formulation. The central object is the (unpolarized) scattering cross section, which in case of the deuteron is given in terms of two structure functions,

$$\frac{d\sigma}{d\Omega} = \left(\frac{d\sigma}{d\Omega}\right)_{\rm Mott} \left[A(q^2) + B(q^2) \tan\frac{\theta}{2}\right] \ , \quad (1)$$

with $q^2 = -Q^2 < 0$ the invariant momentum transfer squared, θ is the scattering angle in the centre-of-mass frame, and the QED (Mott) cross section has been separated. Alternatively, one can parameterize the response of the deuteron to an external vector current in terms of three form factors, F_C (charge), F_M (magnetic) and F_Q (quadrupole). In our approach we construct the current operators and the wave functions *simultaneously* from the same Hamiltonian. Furthermore, we study the interplay of nuclear and nucleon dynamics. Finally, this study is to be understood as the first step in a systematic investigation of the electromagnetic properties of light nuclei as on EFT methods with non-perturbative pions.

We have performed our claculations at next–to–leading and next–to–next–to–leading order. At NLO, no meson–exchange currents or four–nucleon–photon operators contribute. At NNLO, only one magnetic photon–four–nucleon operator appears, the corresponding coupling constant can be determined from a fit to the deuteron magnetic moment. The predicted static deuteron properties are collected in the table.

	LO	NLO	Exp.
$\lvert E_d\rvert$ [MeV]	2.224	2.224	2.22456612(12)
μ_d [μ_N]	0.828	0.852	0.8574382284(94)
Q_d [fm^2]	0.265	0.276	0.2859(3)

Table 1: Static properties at LO and NLO. Here, E_d, μ_d and Q_d denote the deuteron binding energy, its magnetic and its quadrupole moment.

The NLO and NNLO predictions for the electric and the quadrupole form factors coincide at NLO and NNLO because one is not yet sensitive to the NNLO wave function corrections. The EFT predictions at LO, NLO and NNLO for the structure function $B(Q^2)$ are shown in the figure. One clearly observes convergence, not only does the description improve at higher orders but also the relative corrections become smaller.

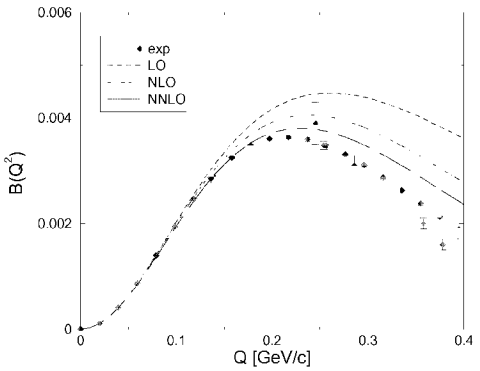

Figure 1: $B(Q^2)$ from nuclear EFT compared to the data. The dashed, dot-dashed and solid lines refer to LO, NLO and NNLO.

The accuracy of the description of the nucleon form factors limits the applicability of the effective field theory approach to the deuteron structure to momentum transfer of about $Q \simeq 0.4$ GeV. Thus an improved description of these single nucleon observables has to be obtained to extend these considerations consistently to higher photon virtualities. Obviously, as next steps one has to consider N^{3}LO corrections to the process discussed here (since only at that order sufficiently many additional contributions appear, like e.g. meson–exchange currents) as well as electron scattering of three- and four–body systems.

References:

[1] M. Walzl and Ulf-G. Meißner, Phys. Lett. B513 (2001) 37.

Nucleon properties in finite nuclei

Ulf-G. Meißner, M.Musakhanov (Tashkent), A. Rakhimov (Tashkent), U. Yakhsiev (Tashkent), A. Wirzba

The possible modification of nucleon properties in the nuclear medium is currently a much discussed topic in low energy hadron physics. One way to consider such problems is to describe the nucleon as a topological soliton and then study the influence of baryonic matter on the properties of such solitons, making use of the independent particle picture which has been so successful in describing many properties of nuclei. There exist already some works where nucleons described as Skyrme–type solitons embedded in infinite nuclear matter have been considered. The results of these studies were in qualitative agreement with experimental indications and with results of other authors using different approaches. On the quantitative level, however, there is a too large renormalization of the nucleons' effective mass in nuclear matter. The quantitative value of this renormalization is about $\sim 40\%$ for the normal nuclear matter density. It is therefore difficult to relate this modification of the nucleon self–energy in the medium to the nucleon mass in free space because such calculations consider only the special case when a nucleon is placed in the center of the heavy nucleus. The infinite nuclear matter approach allows one only to consider properties of nucleons placed near the center of heavy nuclei where the density is constant. One can expect that taking into account non-spherical effects, i.e. deformation of the skyrmion in the finite nucleus, would improve the results also on the quantitative level. Density changes play an important role when the nucleon is placed at sufficiently large distances from the center of nucleus. In [1] we consider properties of the deformed nucleon embedded in light, medium–heavy and heavy nuclei. Deformation effects are introduced by the distortion of the profile function of the chiral field under the action of the external field (which parameterizes the baryonic density within a given nucleus). Nucleons and deltas emerge as quantized solitons after performing an adiabatic rotation in coordinate and isospace which takes into account the axial symmetry of the system (leading to two different moments of inertia, $I_z \neq I_x = I_y$). In contrast to most previous investigations, we do not consider a constant nuclear density as appropriate for nuclear matter but rather the distance-dependent density as given for finite nuclei. We calculate the modifications of the nucleon properties in finite nuclei, and their dependence on the distance between the topological center of the skyrmion inside the nucleus and the geometrical center of the nucleus under consideration will be considered. The main results of this study can be summarized as follows:

(i) The density dependence of the nucleon mass shows a more realistic behavior than in the case of a uniform density as e.g. for homogeneous nuclear matter. The effective nucleon mass has its minimum at the center of the nucleus and approaches its free space value at the surface of the nucleus.

(ii) The nucleons in finite nuclei are weakly deformed. They acquire a small intrinsic quadrupole moment which, however, is strongly dependent on the distance from the center of the nucleus, e.g. the proton (neutron) deformation changes from a oblate (prolate) to a prolate (oblate) form as it is moved toward the surface of the nucleus.

(iii) Similarly, there is a direction-dependent swelling of the isoscalar and isovector root-mean-square radii. We have stressed that the concept of a uniform swelling factor is too simple a concept to apply to real nuclei.

(iv) As consequence of the axial symmetry of the system, the $|J_3| = 1/2$ Δ states ($\Delta^{0,+}$) and the $|J_3| = 3/2$ ones ($\Delta^{-,++}$) have slightly different masses in finite nuclei.

A typical result for the mass, radius and deformation parameter dependence of a nucleon embedded in two particular heavy nuclei is shown in the figure.

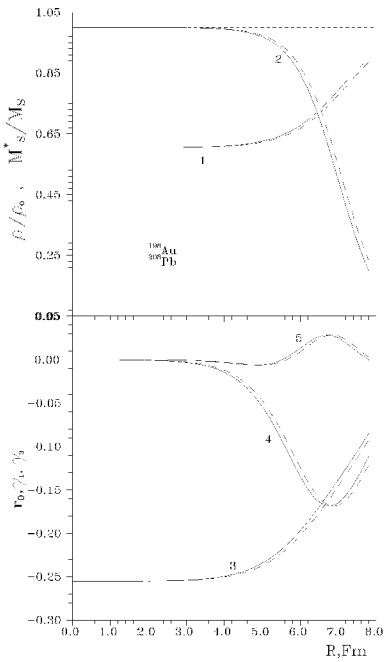

Figure 1: Effective mass (1), nuclear density (2), isoscalar radius change (in %) (3) and deformation parameters (4,5) for ^{198}Au (solid) and ^{208}Pb (dashed lines).

References:

[1] U.T. Yakhshiev et al., `nucl-th/0109008`, Nucl. Phys. A, in print.

Analysis of the pion-kaon sigma term

Matthias Frink, Bastian Kubis, Ulf-G. Meißner

In QCD, the mass terms for the three light quarks u,d, and s can be measured in the so–called sigma–terms. These are matrix elements of the scalar quark currents $m_q\bar{q}q$ in a given hadron H, $\langle H|m_q\bar{q}q|H\rangle$, with H e.g. pions, kaons or nucleons. Since no external scalar probes are available, the determination of these matrix elements proceeds by analyzing four–point functions, more precisely Goldstone boson–hadron scattering amplitudes in the unphysical region, $\phi(q)+H(p) \to \phi(q')+H(p')$ (note that the hadron can also be a Goldstone boson). The determination of the sigma–terms starts from the generic low-energy theorem for the isoscalar scattering amplitude $A(\nu,t)$ [1],

$$F^2 A(t,\nu) = \Gamma(t) + q'^{\mu} q^{\nu}\, r_{\mu\nu} \ , \qquad (1)$$

where $\Gamma(t)$ is the pertinent scalar form factor, $\Gamma(t) = \langle H(p') \,|\, m_q\bar{q}q \,|\, H(p)\rangle$, $(t = (p'-p)^2)$, which at zero momentum transfer gives the desired sigma term, $\Gamma(0) = 2M_H\,\sigma_{\phi H}$, for appropriately normalized hadron states. Furthermore, $r_{\mu\nu}$ is the so–called remainder, which is not determined by chiral symmetry. However, it has the same analytical structure as the scattering amplitude. To determine the sigma–term, one has to work in a kinematic region where this remainder is small, otherwise a precise determination is not possible. By definition, the point where the remainder takes its smallest value is the so–called Cheng-Dashen (CD) point, which e.g. for pion scattering off other hadrons is given by $t = 2M_\pi^2$, $\nu = 0$, which clearly lies outside the physical region for elastic scattering but well inside the Lehmann ellipse. The most studied reaction to determine a sigma–term is certainly elastic pion–nucleon scattering $\pi N \to \pi N$, but the best understood process is low energy pion-pion scattering $\pi\pi \to \pi\pi$ (for a beautiful sigma-term analysis for that case, see [2]). Much less is known for processes involving kaons. It is mandatory to understand the simplest process involving strange quarks, i.e elastic pion–kaon scattering. This reaction has been attracted much recent interest, mostly triggered by the intended lifetime measurement of πK atoms at CERN, but also as a theoretical laboratory to study the question whether the kaon can be considered as a heavy particle, see e.g. [3]. Therefore, we have analysed the sigma term in pion–kaon scattering. This is done in [4] in two ways. First, we use standard three flavor chiral perturbation theory, treating the pions and the kaons as (pseudo) Goldstone bosons of the spontaneously broken chiral symmetry of QCD. Then, we analyze the sigma in the heavy–kaon framework, which helps to understand the results obtained in SU(3) CHPT. In SU(3), there is an ambiguity in the choice of the decay constant F^2 appearing in the LET, i.e. one can set $F^2 = F_\pi^2$, $F^2 = F_\pi F_K$ or $F^2 = F_K^2$, with $F_K/F_\pi \simeq 1.2$. We have shown that for the first choice, the remainder at the CD-point is remarkably small (about 2%). This can be considered a true SU(2) theorem within SU(3). It can be understood in the heavy kaon framework, in which the kaon is essentially frozen and the light pion scatters off this heavy source. Even though these one-loop corrections are small, it is known that higher order corrections in the scalar channels can be substantial. We have employed the dispersive machinery set up in [5] to calculate the two-loop corrections to the real and imaginary part of the πK scalar form factor. The appearing subtraction constants were fixed from the one-loop scalar πK radius and the fact that the form factor has to be well defined in the chiral limit, i.e. by applying RGE methods. For the central values of these parameters, the tree, one-loop and two-loop results for the normalized form factor $\Gamma_K(s)/\Gamma_K(0)$ are shown in the figure. At the two-pion threshold, the two-loop corrections are fairly small, they only become important at higher energies.

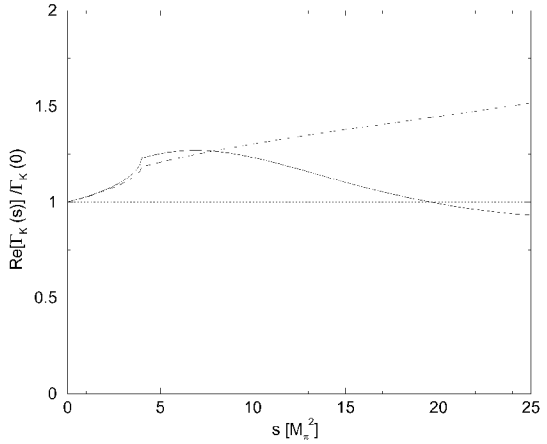

Figure 1: Real part of the normalized scalar pion-kaon form factor. The dotted, dashed and solid lines refer to the tree, one- and two-loop result, in order.

References:

[1] L.S. Brown, W.J. Pardee and R.D. Peccei, Phys. Rev. D4 (1971) 2801.

[2] J. Gasser and M.E. Sainio, in *Physcis and Detectors for DAΦNE*, Frascati Physics Series Vol. 16, S. Bianco et al. (eds) (Frascati, 1999) [hep-ph/0002283].

[3] A. Roessl, Nucl. Phys. B555 (1999) 507.

[4] M. Frink, B. Kubis and Ulf-G. Meißner, *in preparation.*

[5] J. Gasser and Ulf-G. Meißner, Nucl. Phys. B357 (1991) 90.

Complete and consistent analysis of isospin violation in pion–nucleon scattering

Nadia Fettes, Ulf-G. Meißner

Pion–nucleon scattering (πN) is one of the prime reactions to test our understanding not only of the spontaneous and explicit chiral symmetry breaking QCD is supposed to undergo, but also of isospin symmetry violation. The pion–nucleon system is particularly well suited for such an analysis, since chiral symmetry breaking and isospin breaking appear at the same chiral order. The analysis of isospin violation in πN scattering proceeds essentially in three steps. First, one ignores all isospin breaking effects, i.e. one sets $e = 0$ and $m_u = m_d$. This is the approximation on which the analysis in refs. [1, 2] was based. It is obvious that one needs a precise description of the large isospin symmetric "background" of the scattering amplitude in order to be able to pin down the small isospin violating effects. The quality of the results obtained in refs. [1, 2] makes us feel confident that we have a sufficiently accurate starting point. In the second step, one should include the leading isospin breaking terms encoded in the pion and nucleon mass differences. The mass splitting for the nucleons amounts to about 1 MeV, whereas the charged– to neutral–pion mass difference is of the order of 5 MeV. To the accuracy we are working (the third order in small momenta and charges) one has to consider such effects. The strength of chiral perturbation theory now lies in the fact that one can consistently take into account only the effect from those isospin violating low–energy constants which enter the particles' masses. This is the approximation which was considered in [3, 4]. In a third step, one has to include all virtual photon effects and directly fit to cross section data to pin down the novel electromagnetic low-energy constants. In the work [5] such a complete analysis was achieved. CHPT does not leave any doubt about the correct definition of the hadronic masses of pions and nucleons, and allows to extract the strong part of the scattering amplitude in a unique way. After determining the unknown low–energy constants by a fit to experimental data, (for pion lab momenta below 100 MeV), we switch off all electromagnetic interactions and describe QCD with unequal up– and down–quark masses and $e^2 = 0$. The so–determined strong phase shifts agree with those of Matsinos et al. [6, 7] in the P–waves, but we find a sizeably different behavior in the S–waves. We trace this difference back to the inclusion or omission of non–linear photon–pion–nucleon couplings (a typical diagramm of this type is d) in the figure). We address the question of isospin violation by studying the usual triangle relation involving elastic $\pi^{\pm}p$ scattering and the charge exchange reaction. An important advantage of the CHPT calculation lies in the fact that we can easily separate dynamical from static isospin breaking. Dynamical isospin breaking only occurs in the S–wave and is very small, $\sim 0.75\%$. Static effects do not increase the size of isospin violation in the S–wave significantly; by no means can we account for the reported 6 – 7 % isospin breaking [8, 9]. We have found large error bars on our parameter values. In order to improve this situation, we would like to fit to more experimental data. However, a third order CHPT calculation allows to describe scattering data for pion laboratory momenta not much higher than 100 MeV, a region where the data situation is not yet as good as one would hope. A fourth order calculation would certainly allow to fit to data higher in energy, but, on the other hand, would also introduce many more unknown coupling constants. Since isospin breaking effects are expected to be most prominent in the energy region we consider in this work, we do not judge it very promising to extend the analysis to full one–loop (fourth) order. Additional data for pion–nucleon scattering at very low energies would be very helpful in this respect. Also a combined fit to several reactions involving nucleons, pions, and photons, e.g. pion electro– and photoproduction, as well as $\pi N \to \pi\pi N$, would help in pinning down the fundamental low–energy constants more precisely.

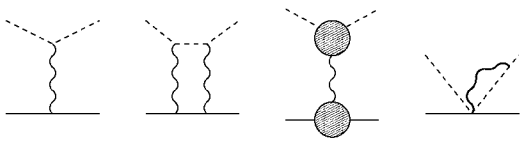

Figure 1: Electromagnetic corrections to πN scattering. See text.

References:

[1] N. Fettes, Ulf-G. Meißner and S. Steininger, Nucl. Phys. A640 (1998) 199.

[2] N. Fettes and Ulf-G. Meißner, Nucl. Phys. A676 (2000) 311.

[3] N. Fettes, Ulf-G. Meißner and S. Steininger, Phys. Lett. B451 (1999) 233.

[4] N. Fettes and Ulf-G. Meißner, Phys. Rev. C63 (2001) 045201.

[5] N. Fettes and Ulf-G. Meißner, Nucl. Phys. A693 (2001) 693.

[6] E. Matsinos, `hep-ph/9807395`; E. Matsinos, private communication.

[7] A. Gashi et al., `hep-ph/0009081`.

[8] W.R. Gibbs, Li Ai, and W.B. Kaufmann, Phys. Rev. Lett. 74 (1995) 3740.

[9] E. Matsinos, Phys. Rev. C56 (1997) 3014.

Axial structure of the nucleon

V. Bernard (Strasbourg), L. Elouadrhiri (Jefferson Lab), Ulf-G. Meißner

The nucleon as probed with the weak axial current can be parameterized in terms of two form factors, the axial, $G_A(t)$, and the induced pseudoscalar, $G_P(t)$, one:

$$\langle N(p') \, | A_\mu^a \, | N(p) \rangle =$$

$$\bar{u}(p') \left[\gamma_\mu \, G_A(t) + \frac{(p'-p)_\mu}{2m} \, G_P(t) \right] \gamma_5 \frac{\tau^a}{2} \, u(p) \; ,$$

with $t = (p'-p)^2$ the invariant momentum transfer squared and $m = (m_p + m_n)/2$ the nucleon mass. In the review [1], we have shown that precise theoretical methods based on the symmetries of QCD exist for extracting these fundamental observables from experiment. The axial form factor can be well described by a dipole, $G_A(t) = (1 - t/M_A^2)^{-2}$. The dipole mass M_A can be translated into an axial root–mean–square radius of

$$\langle r_A^2 \rangle^{1/2} = 0.67 \pm 0.01 \, \text{fm}. \qquad (1)$$

This value is consistently obtained from (anti) neutrino scattering off protons (or light nuclei), compare fig. 1, and charged pion electroproduction off protons, compare fig. 2. Clearly, more precise electroproduction data in the threshold region would be welcome to further pin down this quantity.

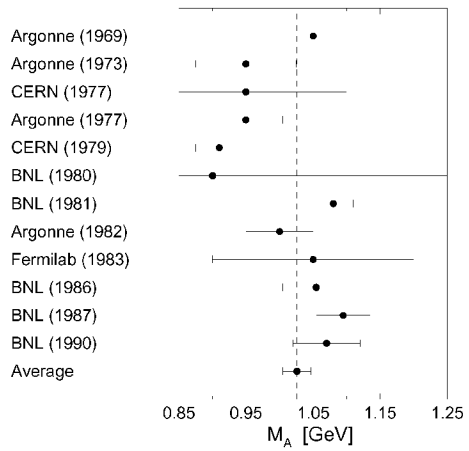

Figure 1: Axial mass M_A extractions from (quasi) elastic neutrino and antineutrino experiments. The weighted average is $M_A = (1.026 \pm 0.021)$ GeV.

The induced pseudoscalar form factor is dominated by the pion pole, but the small corrections to this leading order result have been calculated. Existing data from ordinary muon capture are consistent with these theoretical expectations but have too large error bars to cleanly test the chiral dynamics of QCD. We have argued that the result of the pioneering TRIUMF radiative muon capture experiment should be taken *cum grano salis* due to some assumptions in the analysis that are inconsistent with

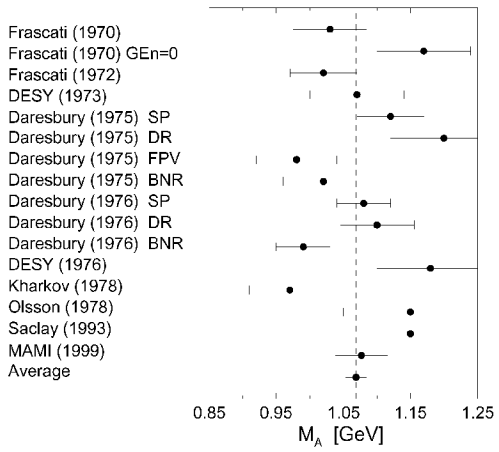

Figure 2: Axial mass M_A extractions from charged pion electroproduction experiments. The weighted average is $M_A = (1.069 \pm 0.016)$ GeV.

the power counting underlying the effective field theory of the Standard Model. However, it is fair to say that more theoretical as well as experimental effort is needed for drawing a final conclusion. The momentum–dependence of the induced pseudoscalar form factor is dominated by the pion pole which has only been tested in one electroproduction experiment so far.

Also, a better determination of strong kaon-hyperon-nucleon coupling constants $g_{K\Lambda N}$ and $g_{K\Sigma N}$ would allow for an additional stringent bound on the light to strange quark mass ratio, based on the derivations from the octet Goldberger–Treiman relations.

All this shows that precision experiments in hadron and nuclear physics indeed help to unravel the mysteries of QCD at energies where one really has to deal with *strong* interactions. Therefore, more pion and kaon electroproduction as well as muon capture experiments are called for.

References:

[1] V. Bernard, L. Elouadrihri and Ulf-G. Meißner, `hep-ph/0107088`, J. Phys. G 28 (2002) R1.

Rescattering and chiral dynamics in $B \to \rho\pi$ decay

Susan Gardner (Kentucky) and Ulf-G. Meißner

Measurements at SLAC and KEK of the time-dependent CP-violating asymmetry in $B(\bar{B}) \to \psi K_s$, yielding $\sin(2\beta)$, have conclusively established the existence of CP violation in the B meson system. The results found are consistent with Standard Model expectations, so that establishing whether the CKM matrix is the only source of CP violation in nature, as in the standard model, or not requires the empirical measurement of all the angles of the unitarity triangle.

In the work [1] we consider the determination of α through a Dalitz plot analysis of the decays $B^0(\bar{B}^0) \to \rho\pi \to \pi^+\pi^-\pi^0$ under the assumption of isospin symmetry. Ten parameters appear in the analysis, and they can be determined in a fit to the data. Nevertheless, the assumption of ρ dominance in $B \to 3\pi$ decays has no strong theoretical basis so that the contributions from other resonances in the $\rho\pi$ phase space may be important. We discuss how the isospin analysis can be enlarged to include the $\sigma\pi$ channel as well. The σ or $f_0(400-1200)$ "meson" is a broad $J = I = 0$ enhancement, close to the ρ meson in mass, so that the $\sigma\pi$ channel can potentially populate the 3π phase space associated with the $\rho\pi$ channels. The $\sigma\pi$ final state contributes preferentially to the $\rho^0\pi^0$ final state. In the context of the isospin analysis, such contributions are of consequence as they invalidate the underlying assumptions of the isospin analysis and thus mimic the effect of isospin violation. Our considerations are inspired in part by recent studies of $D^- \to 2\pi^-\pi^+$ decay: the E791 collaboration find that the pathway $D^- \to \pi^-\sigma \to 2\pi^-\pi^+$ accounts for approximately half of all $D^- \to 2\pi^-\pi^+$ decays. In [2] is was argued as a consequence that the $B \to \sigma\pi$ channel contributes significantly to the $\rho\pi$ phase space in $B \to \pi^0\pi^+\pi^-$ and modifies the ratio $\mathcal{B}(\bar{B}^0 \to \rho^\mp\pi^\pm)/\mathcal{B}(B^- \to \rho^0\pi^-)$ to yield better agreement with experiment [2]. The scalar form factor, which describes the appearance of the σ in the $\pi^+\pi^-$ final state, enters as a crucial ingredient in the assessment of the size of these effects. The scalar form factor cannot be determined directly from experiment; nevertheless, ample indirect constraints exist, permitting us to describe its features with confidence [3]. We follow Ref. [3] and adopt an unitarized, coupled-channel approach to final-state interactions in the $\pi\pi$-$K\bar{K}$ system, and match the resulting scalar form factor to chiral perturbation theory (CHPT) in the regime where the latter is applicable. The resulting form factor, in the $\pi\pi$ channel, is strikingly different from the relativistic Breit-Wigner form adopted by the E791 collaboration in their analysis of the σ in $D^+ \to \pi^+\pi^+\pi^-$ decay — the latter form factor is also used in Ref. [2]. The differences are particularly large as $\sqrt{s} \to 2M_\pi$, so that the relativistic Breit-Wigner form is at odds with CHPT in the precise region where it is working. This casts doubt on the recent conclusions, prompting new analyses incorporating a suitable scalar form factor. The generation of the σ resonance via strong rescattering effects, as in the approach we adopt, indicates that OZI effects in the scalar sector are significant. Moreover, the "doubly" OZI-violating form factor $\langle 0|\bar{s}s|\pi\pi\rangle$ is non-trivial as well; such a contribution is needed to fit the $\pi\pi$ and $K\bar{K}$ invariant mass distributions in $\psi \to \phi\pi\pi(K\bar{K})$ decay [3]. These observations give new insight on rescattering effects in hadronic B decays, generating a new mechanism of factorization breaking in $n \geq 3$ particle final states. Such effects are important for studies of CP violation because rescattering effects can potentially yield large strong phases.

The contribution of the $B \to \sigma\pi$ channel to the $B \to \rho^0\pi$ phase space can also modify the inferred empirical branching ratios in these channels. Combining the CLEO results $\mathrm{Br}(B^- \to \rho^0\pi^-) = (10.4\,^{+3.3}_{-3.4} \pm 2.1) \cdot 10^{-6}$ and $\mathrm{Br}(\bar{B}^0 \to \rho^\pm\pi^\mp) = (27.6\,^{+8.4}_{-7.4} \pm 4.2) \cdot 10^{-6}$ with the BaBar result $\mathrm{Br}(\bar{B}^0 \to \rho^\pm\pi^\mp) = 28.9 \pm 5.4 \pm 4.3$ yields, adding the errors in quadrature and ignoring correlations,

$$\mathcal{R} = \frac{\mathrm{Br}(\overline{B^0} \to \rho^\mp\pi^\pm)}{\mathrm{Br}(B^- \to \rho^0\pi^-)} = 2.7 \pm 1.2\,. \qquad (1)$$

This ratio of ratios is roughly 6 if one works at tree level and uses the naive factorization approximation for the hadronic matrix elements. The inclusion of penguin contributions can alter this result, and potentially yield better accord with theory and experiment. However, our focus will parallel that of Ref. [2]: we wish to examine how $B \to \sigma\pi \to 3\pi$ decay, given a particular scalar form factor, can effectively modify the theoretical prediction of the ratio $\mathcal{R}$. It is apparent that $B \to \sigma\pi$ is of greater impact in $B \to \pi^0\pi$ decay, so that the inclusion of such contributions ought alter the ratio of ratios. In fact, treating the various decays as two-body ones, we find $\mathcal{R} = 5.8\,(5.5)$ for the case of no (with) penguin diagrams. Proper inclusion of the final-state interaction (3-body decays) and adding the ρ and the σ contribution, which are based on the use of the consistent scalar and vector form factors, leads to

$$\mathcal{R} = 2.5\,, \qquad (2)$$

much improved compared to the number given in [2] and consistent with the data. The theoretical uncertainty is about 20%, but this needs to be sharpened.

References:

[1] S. Gardner and Ulf-G. Meißner, [hep-ph/0112281].

[2] A. Deandrea and A. D. Polosa, Phys. Rev. Lett. 86 (2001) 216.

[3] Ulf-G. Meißner and J. A. Oller, Nucl. Phys. A679 (2001) 671.

$t-$ dependence of Pionproduction in $\pi^- p \to \pi^0\pi^0 n$

F. Sassen,S. Krewald and J. Speth

Based on measurements of the S-wave intensity for the charge exchange reaction $\pi^- p \to \pi^0\pi^0 n$ by [1, 2] Anisovich et al. argued against the interpretation of the $f_0(980)$ as a $K\bar{K}$-molecule.[4] In their paper the t-dependence of the intensity distribution was modelled using only one production mechanism (π-exchange) and two interfering resonances, one broad and soft and the other hard and narrow. As Achasov et al. already mentioned, this interpretation will lead to a rather peculiar t-dependence of

$$\frac{d\sigma}{dt} = \int_{m_l}^{m_h} dm_{\pi\pi} \frac{d\sigma}{dt\, dm_{\pi\pi}} \qquad (1)$$

which then should show a dip in the region of momentum-transfers t around -0.15 GeV^2.[5] In equation (1) $m_{\pi\pi}$ denotes the invariant mass of the two exiting pions, t the square of the momentum transfer onto the nucleon and the integration limits could be chosen as $m_l = 0.8$GeV, $m_h = 0.9$GeV.

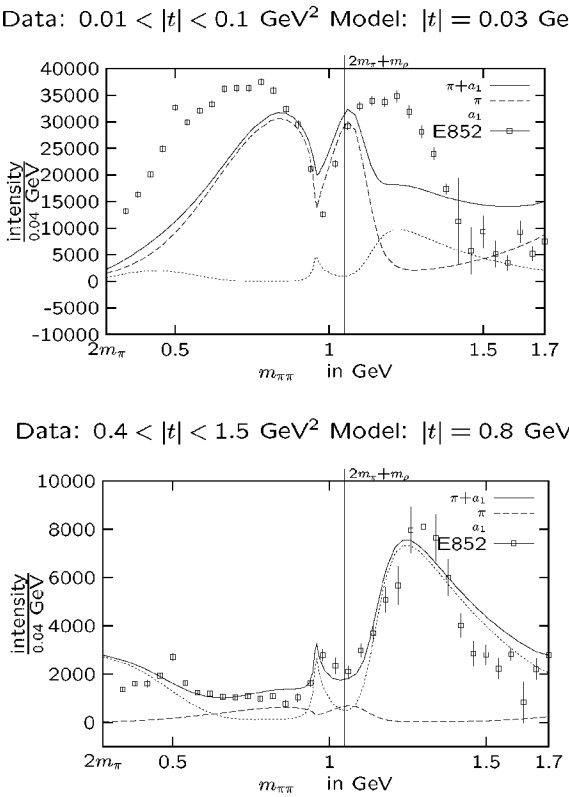

Fig. 1: Comparison of the S-wave intensity distribution in $m_{\pi\pi}$ for different momentum transfers t to the nucleon. The squares show the experimental results of [1] and the lines show the results of our calculation: The full line includes both the a_1- and the π-exchange as means of production. The dotted line shows the production via a_1 and the dashed line the production via π.

In our approach to the reaction $\pi^- p \to \pi^0\pi^0 n$ we used the a_1-exchange as well as the π-exchange as a production mechanism, which are close to non interfering since they have different spin structures. Therefore the peculiar behaviour described above is avoided. Furthermore we used the on-shell T-matrix of the extended Jülich meson-exchange-model to generate the final state interaction of the two outgoing pions. In this model we used dispersion relations for the form factor in the t-channel to remove the freedom introduced to the old model which used independent form factors for both s- and t-channel.[6] As already described in [3] this model still generates the $f_0(980)$ as a $K\bar{K}$-molecule.

Using exponential form factors at the nucleon vertices we were able to reproduce the t-dependence of the integrated intensity in figure 2. This half logarithmic plot with its two asymptotic slopes itself was already very suggestive in the direction of two competing production mechanisms. Also the t-dependence of the s-wave intensities (Figure 1) is reproduced. The intensity lacking in the low t plot (Figure 1a) is due to the 4π-vertex and the $f_0(1370)$-resonance which so far have not been included in our model. Comparing the two plots in this figure one sees nicely how the dip becomes a peak when the production via pions decreases and the production via a_1 takes over.

We conclude that there is no need for a genuine $f_0(980)$ resonance or "hard component" to account for the results of the GAMS and BNL E852 experiments, but a dynamically generated $f_0(980)$ together with π- and a_1-exchange as means of production can reproduce the data.

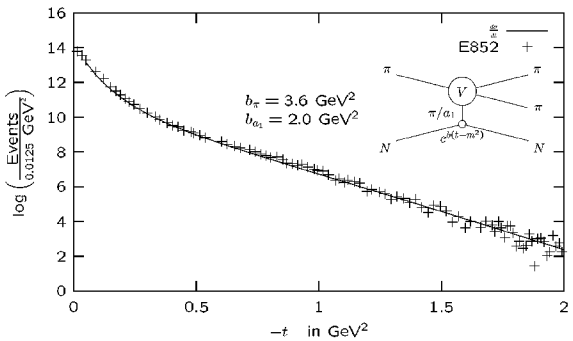

Fig. 2: Intensity distribution integrated over the full range of $m_{\pi\pi}$ (Equation 1). The + indicate the experimental results of [1] and the line shows our result. The parameters for the exponential form factors at the $pn\pi$- and pna_1-vertex are indicated.

References:

[1] J.Gunter et al., Phys.Rev.D **64**, 072003 (2001)
[2] D.Alde et al., Z.Phys.C **66**, 375 (1995)
[3] F.Sassen, S.Krewald and J.Speth, Annual Report 2000 FZ-Jülich
[4] V.V.Anisovich et al., Phys.Lett.B **355**, 363 (1995)
[5] N.N.Achasov et al., Phys.Rev.D **58**, 054011-1 (1998)
[6] D.Lohse et al., Nucl.Phys.A **516**, 513 (1990)

Invariant Mass Spectrum of the npη Final State extracted from incoherent η-Photoproduction from the Deuteron near Threshold

A. Sibirtsev, S. Schneider, Ch. Elster, J. Haidenbauer, S. Krewald, J. Speth

Incoherent photoproduction of η mesons close to the reaction threshold can provide a good scenario to investigate the final state interaction in the outgoing neutron-proton-η system. In Ref. [1] we presented a model for the reaction $\gamma d \to np\eta$, where the dominant η-production mechanism is provided through the S_{11} resonance. If one only considers the tree level contribution (i.e. the impulse approximation (IA)) then the production cross sections are well described for excess energies larger than 40 MeV above the production threshold, corresponding to photon energies around 680 MeV [2].

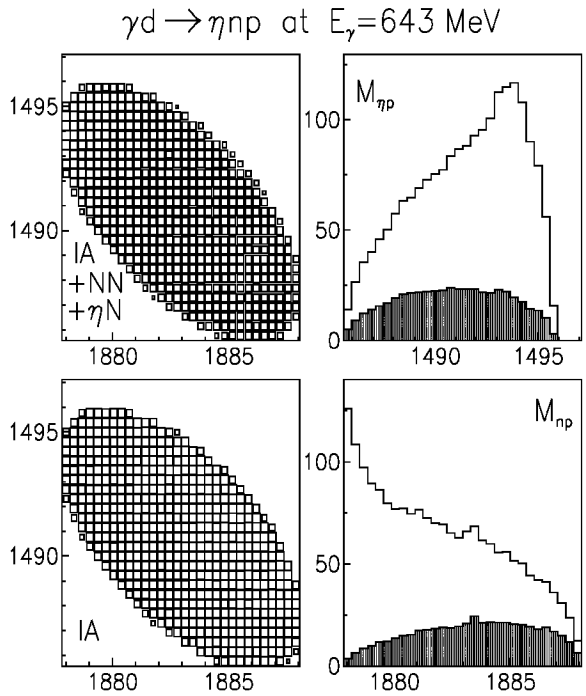

Fig. 1: Dalitz plots and invariant mass spectra for the reaction $\gamma d \to np\eta$, with an incident photon energy of 643 MeV. The upper left panel shows the Dalitz plot for the calculation where the NN and ηN final state interactions are taken into account, the lower left panel shows the Dalitz plot calculated only from the contribution of the S_{11} resonance. The upper right panel give the invariant η-p mass spectrum, the lower right panel the invariant np mass spectrum. The lower line in the two left figures represents the calculation with the S_{11} contribution alone. All units are MeV.

However, for smaller excess energies, the consideration of the final state interaction (FSI) between the outgoing particles is necessary to describe the experimental production cross section. In Ref. [1] we found that although the FSI in the np system provides the dominant contribution to the enhancement to the cross section close to threshold, the FSI in the ηN system is also important to describe the data very close to threshold. In our calculation of the np FSI effects we employ the CD-Bonn NN potential [3]. The ηN FSI is given by the Jülich meson-baryon model, whose parameter are fixed by πN data [4].

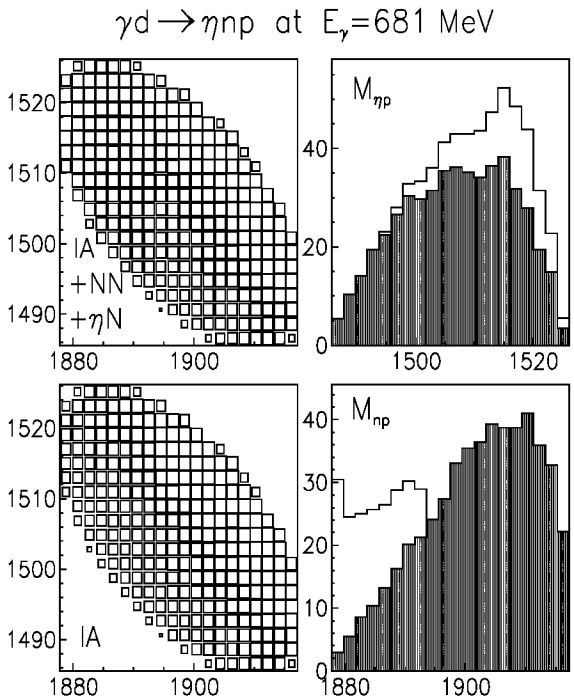

Fig. 2: Dalitz plots and invariant mass spectra for the reaction $\gamma d \to np\eta$, with an incident photon energy of 681 MeV. Same description of curves as in Fig. 1.

To extract more detailed informations about the contribution of the FSI close to threshold, it is illuminating to plot the corresponding invariant mass spectra. In Figs. 1 and 2 we show the spectra for two different photon energies, and include in the figures the calculation based on the impulse approximation alone for comparison. Fig. 1 clearly shows that at the small excess energy the FSI dominates the invariant mass spectra. At the higher photon energy, cf. Fig. 2, the FSI becomes less important compared to the contribution from the S_{11} resonance. In fact, the resonance even dominates the spectrum for higher values of the invariant np mass.

References:

[1] A. Sibirtsev, S. Schneider, Ch. Elster, J. Haidenbauer, S. Krewald, J. Speth, submitted to Phys. Rev. C, nucl-th/0111086.

[2] A. Sibirtsev, Ch. Elster, J. Haidenbauer, J. Speth, Phys. Rev. **C64**, 024006 (2001).

[3] R. Machleidt, Phys. Rev. **C63**, 024001 (2001).

[4] O. Krehl, C. Hanhart, S. Krewald, J. Speth, Phys. Rev. **C62**, 025207 (2000).

Instantons As Unitary Spin Maker

M. Napsuciale *, A. Wirzba and M. Kirchbach **

Flavor symmetry is presently understood on the basis of QCD and the structure of the quark mass matrix. In the zero quark mass limit, the light flavor sector of QCD acquires a three flavor chiral symmetry $U(3)_L \times U(3)_R$ which at the level of hadrons is assumed to be realized in the Goldstone phase. The associated Goldstone bosons are identified with the lightest pseudoscalar mesons.

The first problem one encounters in that scheme is the large mass of the η'. The way out of this problem is to take into account quantum corrections which spoil the conservation of the singlet axial current. Particularly relevant to this problem is the existence of Euclidean solutions with non-trivial topological properties (instantons) which also break the $U(1)_A$ symmetry. In fact, the most appealing explanation of the problem of the large η' mass is provided by the instanton induced quark-quark interaction [1].

The second problem concerns the different symmetries for pseudoscalar and axial vector mesons, on the one side, and vector and tensor mesons, on the other side.

Isoscalar vector mesons closely follow the flavor basis structure: $\phi = \bar{\psi}\lambda_s\psi = \bar{s}s$ and $\omega = \bar{\psi}\lambda_{ns}\psi = (\bar{u}u + \bar{d}d)/\sqrt{2}$. This contrasts the singlet-octet pattern followed by the isoscalar axial vector and pseudoscalar mesons. To explain this dilemma, the Okubo-Zweig-Iizuka (OZI) rule [2] was invoked that forbids the mixing of of quarkonia made of u or d quarks with quarkonia made of s or c quarks. In the absence of symmetry breaking terms one can freely use any basis for the generators of the group. The physically interesting basis is the one whose generators still reflect a residual symmetry of the system in the presence of symmetry breaking terms. In that regard, we have three sources of breaking $U(3)_L \times U(3)_R$ symmetry. The first one is the $U_A(1)$ symmetry breaking by quantum effects. Although the instanton induced interaction is suppressed at high energies due to the factor $\exp(-8\pi^2/g^2)$, it is always present and even becomes decisive at low energies. The second source is the spontaneous breaking of chiral symmetry occurring at the scale $\lambda_\chi \approx 4\pi f_\pi$. The third source is the non-vanishing quark mass matrix that explicitly violates three flavor chiral symmetry.

The problem of the conflicting flavor symmetries of the anomalous- and anomaly-free meson sectors was addressed e.g. in Ref. [3]. There, the (three) flavor symmetry for hadrons was concluded from the conserved vector current rather than from mass relations and shown to be $SU(2)_{ud} \otimes SU(2)_{cs} \otimes U(1_{udcs})$ in the limit of heavy *spectator* c quarks.

In the present paper [4], we have investigated the relevance of the instanton–induced determinantal 't Hooft interaction to the η–nucleon coupling $g_{\eta NN}$ within the framework of a three-flavor linear sigma model in the OZI–rule–respecting basis $\{(\bar{s}s), \frac{1}{\sqrt{2}}(\bar{u}u + \bar{d}d)\}$. Instantons, in combination with the spontaneous breaking of chiral symmetry, are shown to provide the major mechanism for the ideal mixing between pseudoscalar strange and non-strange quarkonia. As long as 't Hooft's interaction captures most of the basic features of the axial QCD gluon anomaly, we identify the anomaly as the main culprit for the appearance of octet flavor symmetry in the anomalous sectors of the pseudoscalar (and axial vector) mesons. Especially, the wave function of the physical η meson induced by the determinantal instanton-induced 't Hooft interaction is such that the η meson is close to the octet state. Within this context, unitary spin is shown to be an accidental symmetry due to anomalous gluon dynamics rather than a fundamental symmetry in its own right.

The model presented has the advantage that it allows for possible generalizations to non-ideal mixing angles and different values of the meson decay constants in the strange and non-strange sectors, respectively. It also allows to study consequences for the ηNN coupling. In two independent calculations, one based on the conventional derivative coupling of the flavor-eigenstates to the nucleon, and the other based on a careful study of the axial vector coupling *including anomaly contributions* (resulting from the 't Hooft interaction) to the nucleon, we obtained the magnitude of $g_{\eta NN}$. We found it, within error bars, to be stable against changes in the input parameters and in addition, to be be close to the ordinary $SU(3)$ results.

Though we find the η–nucleon coupling constant $g_{\eta NN}$ to obey a Goldberger-Treiman like relation, the latter does not take its origin from a (massless) pole dominance of the induced pseudoscalar form factor of the octet axial current. Rather it appears as a consequence of a subtle effect of of instanton induced flavor-mixing *during propagation* of the isoscalar pseudoscalars.

In having clarified the role of the axial gluon anomaly (as mimicked by 't Hooft's effective instanton induced interaction) for manufacturing the octet way, we have established the limits beyond which one has to extend the model in order to describe possible deviations of the $g_{\eta NN}$ value from its octet-Goldberger-Treiman-value. Among the possible candidates for such effects we emphasize the direct meson-instanton coupling and subleading $\bar{K}^{(*)}K^{(*)}$ loops of the type discussed in Ref. [5].

References:

[1] G. 't Hooft, Phys. Rev. Lett. **37**, 8 (1976); Phys. Rev. **D14**, 3432 (1976).
[2] S. Okubo, Phys. Lett. **5**, 165 (1963); G. Zweig, CERN Report No 8419 TH 412 (1964); J. Iizuka, Prog. Theor. Phys. Suppl. **37-38**, 21 (1966).
[3] M. Kirchbach, Phys. Rev. **D58** 117901 (1998).
[4] M. Napsuciale, A. Wirzba and M. Kirchbach, nucl-th/0105055, Nucl. Phys. A in press.
[5] H. J. Lipkin, Nucl. Phys. **B244**, 147 (1984); ibid. **B291**, 720 (1987); H. J. Lipkin and B. Zou, Phys. Rev. **D53**, 6693 (1996); B. Zou, Phys. Atom. Nucl. **59**, 1427 (1996).

* Instituto de Fisica, Universidad de Guanajuato, AP E-143, 37150, Leon, Guanajuato, Mexico
** Escuela de Fisica, Univ. Aut. de Zacatecas, AP C-580, Zacatecas, ZAC 98068 Mexico

Gravity as an Effective Field Theory

Barry R. Holstein

It is well known that the gravitational interaction is nonrenormalizable, meaning that there exists no consistent scheme to handle all the divergences which arise in a quantum version of the theory. However, if one is willing to work look only at the long distance, *i.e.*, low momentum component of the theory, then quantum gravity is fully realizable and has a form which is required by the fact that it is a quantum field theory. Gravity couples to the energy momentum tensor $T_{\mu\nu}$ of a particle. We have calculated the energy momentum tensor in a power series in α, using usual Feynman diagram techniques. These calculations are straightforward applications of QED[1]. The result is expressed in terms of form factors $F(q^2)$ of the various allowed Lorentz structures in the matrix element of $T_{\mu\nu}$. . The form factor is the momentum space description of the structure of the particle. Because the massless photon couples to gravity, this form factor has features not common in most other form factors. Normally, form factors can be expanded in a power series in q^2 around $q^2 = 0$, with the coefficients being related to the structure of the particle. For example, the coefficient of the term linear in q^2 is related to the "charge radius squared" of the particle, i.e.

$$< r^2 >= 6\frac{d}{dq^2}F(q^2)|_{q^2=0} \tag{1}$$

However, in the gravitational case, photonic diagrams yield *non-analytic* terms in the expansion of the form factor. In particular, we will find square-root and logarithmic non-analytic terms, i.e.

$$\begin{aligned} F(q^2) &= 1 + a\alpha\frac{q^2}{m^2}\sqrt{\frac{m^2}{-q^2}} \\ &+ b\alpha\frac{q^2}{m^2}\log(-q^2) + c\alpha\frac{q^2}{m^2} + \ldots \end{aligned} \tag{2}$$

where a,b,c are constants. These non-analytic terms cannot be represented by effective Lagrangians and can only arise from the long range propagation of massless particles. Note that they imply that the gravitational charge radius is infinite, which reflects the fact that the energy in the electric field extends out to infinity. These non-analytic terms generate the effects that we seek

The spatial distribution of energy, and hence the metric, will be recovered by a Fourier transformation to coordinate space. Generically the position dependent terms in the metric will be

$$\text{metric} \sim Gm\left[\frac{1}{r} + \frac{a\alpha}{mr^2} + \frac{b\alpha\hbar}{m^2r^3} + \frac{c\alpha}{m^2}\delta^3(x) + \ldots\right] \tag{3}$$

The leading piece in the form factor yields the usual "Newtonian" component of the metric. The analytic term in the form factor yields a delta function - i.e. no effect at large distances. However, the two non-analytic terms produce the effects that we are interested in. The square-root generates the classical correction in the metric of order α. We have shown that this produces precisely the terms required by Einstein's Equation. The logarithm generates something new which was not present in the classical solution - a term of order $G\alpha\hbar/mr^3$.

References:

[1] The calculations for spin 1/2 have previously performed by F. Berends, and R. Gastmans, Phys. Lett, **B55**, 311 (1975); Ann. Phys. (NY) **98**, 225 (1976) and by K. Milton, Phys. Rev. **D15**, 538 (1977). In the case of spin 0 previous evaluations were done by B. Kubis and U.-G. Meissner, Nucl. Phys. **A671**, 332 (2000) and Nucl. Phys. **A692**, 647 (2001). However, except for a brief discussion by Berends and Gastman the implications of the low q^2 region and its connection with coordinate space were not explored in these works.

[2] J.F. Donoghue, Phys. Rev. **D50**, 3874 (1994).

Photon-Hadron and Photon-Photon Physics in Ultraperipheral Relativistic Heavy Ion Collisions

G. Baur, K. Hencken*, and D. Trautmann*

In central collisions at relativistic heavy ion colliders like RHIC at Brookhaven and LHC at CERN/Geneva one aims at producing and detecting a new form of hadronic matter, the Quark Gluon Plasma. In [1] a complementary aspect of these collisions is discussed: *the ultraperipheral ones.* Due to coherence there are strong electromagnetic fields of short duration in such collisions. They give rise to photon–photon and photon–hadron collisions up to invariant mass regions hitherto unexplored experimentally. Together with the experimentalists S. Sadovsky and Yu. Kharlov a review was written for Physics Reports [2] to discuss these questions.
The Relativistic Heavy Ion Collider RHIC is now in operation in Brookhaven. A dedicated program exists to study these peripheral collisions [4]. The aspects of ultraperipheral collisions at RHIC with first experimental results was reviewed in [6]. Most recent references can be found in the proceedings of the Erice workshop on Electromagnetic Probes of Fundamental Physics,October 2001 [3].
It was suggested to use the CMS detector at LHC for photon-hadron and photon–photon physics at LHC [7, 8]. Some aspects of this were also discussed in connection with the Letter of Intent for FELIX [9].
These relativistic heavy ion colliders are also vector meson factories [10, 1, 6]. At RHIC the invariant mass region is similar to the one at HERA. A new energy regime will be entered at LHC.
In Fig. 1 we show differential cross sections for fermion pair production and hadron production in $\gamma\gamma$-collisions.
Bound-free e^+e^- pair production was studied in [11].

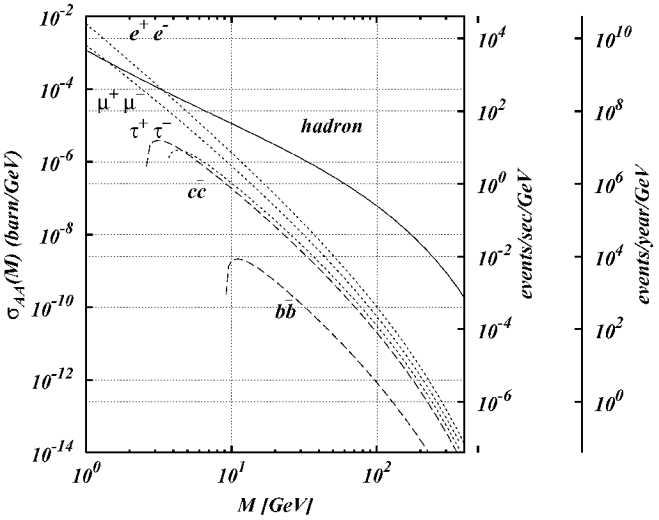

Figure 1: Cross section for fermion pair production as well as total hadron production at the LHC for Ca-Ca collisions. A luminosity of ($L = 4x10^{30}\mathrm{cm}^{-2}\mathrm{s}^{-1}$) was assumed. The process $\gamma\gamma \to hadrons$ is also shown. A "(heavy ion)year" is $10^6 s$. For further details see [2]

References:

[1] G. Baur, K. Hencken, and D. Trautmann, Topical Review, J. Phys. G **24**, 1657 (1998).

[2] G. Baur ,K.Hencken, D.Trautmann, S.Sadovsky and Yu.Kharlov, Phys. Rep. **in press**,

[3] Proceedings of the Erice Workshop on Electromagnetic Probes of Fundamental Physics, October 2001, to be published

[4] Star Peripheral Collision group, see, e.g., at `http://www.star.bnl.gov/STAR/html/pec_l/base.html`.

[5] K. Hencken, P. Stagnoli, D. Trautmann, and G. Baur, Nucl. Phys. B **82**, 409 (2000).

[6] S. R. Klein, Nonlinear QED Effects in Heavy Ion Collisions, LBNL-47144,physics/0012021

[7] G. Baur *et al.*, Photon-Photon Physics with heavy ions at CMS, CMS Note 1998/009, available from the CMS information server at http://cmsserver.cern.ch, 1998, Eur.Phys. J.C, in press

[8] G. Baur *et al.*, Heavy Ion Physics Programme in CMS, CMS NOTE 2000/060, 2000.
G. Baur, in *CMS Heavy Ion Meeting in St. Petersburg June11-14,2000* , edited by M. Bedjidian (2000), p. 207.
K. Hencken, in *CMS Heavy Ion Meeting in St. Petersburg*, edited by M. Bedjidian (2000), p. 219.CMS Document 2000-030

[9] K. Eggert *et al.*, FELIX Letter of Intent, CERN/LHCC 97–45, LHCC/I10, to appear in J. Phys. G (2001).

[10] S. Klein and J. Nystrand, Phys. Rev. C **60**, 014903 (1999).

[11] H.Meier, Z.Halabuka, K. Hencken, D. Trautmann, and G. Baur, Phys. Rev. A **63**, 032713 (2001).

*Institut für Theoretische Physik, Universität Basel, Klingelbergstrasse 82, CH 4056 Basel, Schweiz

Electron-positron pair production in external fields

A.Aste*, G.Baur, K. Hencken*, D. Trautmann*, and G. Scharf**

This work can be found in [1]. The problem of e^+e^- pair production by the collision of highly relativistic nuclei has attracted a lot of interest during the past few years. From the theoretical side, the result that the Dirac equation can be solved exactly in the electromagnetic background field created by two nuclei in the limit where the two nuclei are 'ultrarelativistic' [2, 3], seemed to lead to the unexpected consequence that the single pair cross section is equal to its Born value. The term 'ultrarelativistic' is used here for the limiting case where the Lorentz factor γ becomes large ($\gamma \to \infty$), i. e. the velocity of the colliding ions approaches the speed of light. In connection with the relativistich heavy ion colliders it was found that the impact parameter dependent probability in perturbation theory can become larger than one, which was shown to result in multiple pair production [4, 5, 6, 7, 8].
A series of papers on the same topic [9, 10, 11, 12] showed that there must be an error in the interpretation of the results found in [2]. It was shown by Baltz *et al.* [13] that the expression for pair production derived from the results in [2] describes the total number of produced pairs, and not the single pair production. Additionally, the importance of taking into account the vacuum-vacuum transition amplitude when going over from wave mechanics to the full external field problem with quantized electron field was pointed out, as was already discussed in [7, 8]. A recent work which treats the structure of Coulomb and unitarity corrections to the single and multiple pair production is [14].
We will derive in this paper the main results obtained in [13] in a very compact way using [15]. The correct expression for the multiplicity can be derived indeed in a very straightforward manner from the fundamental equations which define the S-matrix for the external field problem.
We establish the connection between the single-particle matrix elements from the solution of the Dirac equation and the pair production in a full many-body theory. The important point is discussed in the textbooks see e.g. [15, 16]. The (free) propagator of the Dirac equation is e.g. given in $Ch.2-5$ of [16]. We look for a kernel $K(x_2, x_1)$ of the Dirac equation such that

$$\Psi(t_2, \vec{x_2}) = \int d^3x_1 K(t_2, \vec{x_2}; t_1, \vec{x_1}) \gamma^0 \Psi(t_1, \vec{x_1})$$

$$\text{for } t_2 > t_1$$

This is the retarded kernel. The hole theory (which is mainly of historic interest)suggests a different Green function, the Feynman propagator, see e.g. [16, 17]. This appears in a natural way in the quantized relativistic field theory.

References:

[1] A. Aste et al. submitted to Eur. J.Phys. C, hep-ph/0112193

[2] B. Segev, J.C. Wells, Phys. Rev. C **59**, no. 5, 2753 (1999)

[3] A. J. Baltz, L. McLerran, Phys. Rev. C **58**, 1679 (1998)

[4] G. Baur, Phys. Rev. A **42**, no. 9, 5736 (1990)

[5] K. Hencken, D. Trautmann, G. Baur, Phys. Rev. C **59**, 841 (1999)

[6] M. J. Rhoades-Brown, J. Weneser, Phys. Rev. A **44**, 330 (1991)

[7] C. Best, W. Greiner, G. Soff, Phys. Rev. A **46**, 261 (1992)

[8] K. Hencken, D. Trautmann, G. Baur, Phys. Rev. A **51**, 998 (1995)

[9] D.Yu. Ivanov, K. Melnikov, Phys. Rev. D **57**, 4025 (1998)

[10] D.Yu. Ivanov, A. Schiller, V.G. Serbo, Phys. Lett. B **454**, 155 (1999)

[11] U. Eichmann, J. Reinhardt, W. Greiner, Phys. Rev. A **61**, 062710 (2000)

[12] R.N. Lee, A.I. Milstein, Phys. Rev. A **61**, 032103 (2000)

[13] A.J. Baltz, F. Gelis, L. McLerran, A. Peshier, Nucl. Phys. A **695**, 395 (2001)

[14] R.N. Lee, A.I. Milstein, V.G. Serbo, hep-ph/0108014

[15] G. Scharf, Finite quantum electrodynamics: the causal approach (Springer, New York, 1995) (second edition)

[16] C. Itzykson, J.-B. Zuber, Quantum Field Theory (McGraw-Hill, 1980), p. 89

[17] J.D. Bjorken and S. Drell Relativistic Quantum Mechanics

*Institut für Theoretische Physik, Universität Basel
** Institute for Theoretical Physics, University of Zürich

Accurate Studies of Pionium Interacting with Matter

T.A. Heim*, K. Hencken*, M. Schumann*, D. Trautmann*, and G. Baur

Target-elastic and target-inelastic electromagnetic cross sections for pionium scattering off various target materials are studied in [1] and [2]. Accurate predictions for this quantity are needed as a theoretical input in the analysis of the ongoing DIRAC experiment at CERN . This experiment aims at measuring the pionium lifetime, an important check on chiral perturbation theory [3].

To describe the excitation of the pionium atoms through the electromagnetic interaction with the target atoms we use the semi-classical approximation (SCA). In the rest-frame of the pionium, the much heavier target atoms move past with almost the speed of light on a straight-line trajectory $\vec{R} = \{b, 0, vt\}$ and are treated classically, whereas the pionium atom is situated at the origin of the coordinate system and is treated quantum-mechanically.

The non-relativistic Hamiltonian describing this system is

$$H = H_0 + H_{\rm int} \ , \tag{1}$$

where the first part, H_0, describes the pionium atom,

$$H_0 = \frac{\vec{p}^{\,2}}{2\mu} - \frac{e^2}{r} \ , \tag{2}$$

where μ is the reduced mass and $\vec{r}$ the relative coordinate. The second term in (1), $H_{\rm int}$, describes the interaction between the pionium and the target atom

$$H_{\rm int} = H_{\rm scalar} + H_{\rm mag} \ , \tag{3}$$

where the scalar interaction is given by

$$H_{\rm scalar} = e\left[\Phi(\vec{r}/2) - \Phi(-\vec{r}/2)\right] \ . \tag{4}$$

For the calculation of the higher order corrections only $H_{\rm scalar}$ will be considered, as it yields the main contribution to the cross-section. The effect of the magnetic interaction $H_{\rm mag}$ (and of relativistic corrections) are found to be much smaller than 1% [4].

The transition amplitude $a_{fi}(b)$ from an initial state $i = \{n_i, l_i, m_i\}$ to a final state $f = \{n_f, l_f, m_f\}$, where n, l, and m denote the principal, angular, and magnetic quantum numbers, respectively, is given in the sudden (or Glauber) approximation by

$$a_{fi}^G(b) = \int d^3r \, \psi_f^*(\vec{r}) \left[1 - \exp\left(i\chi(b,\vec{r})\right)\right] \psi_i(\vec{r}), \tag{5}$$

where

$$\chi(b,\vec{r}) = -\frac{1}{\hbar}\int_{-\infty}^{\infty} H_{\rm int}\,(b,\vec{r},t)dt \ . \tag{6}$$

The results for the breakup probabilities are shown in Fig. 1 as a function of the impact parameter b. The applicability of the Glauber theory is also tested by showing the difference of the first order results with and without taking the finite value of ω into account. The importance of higher order corrections increases

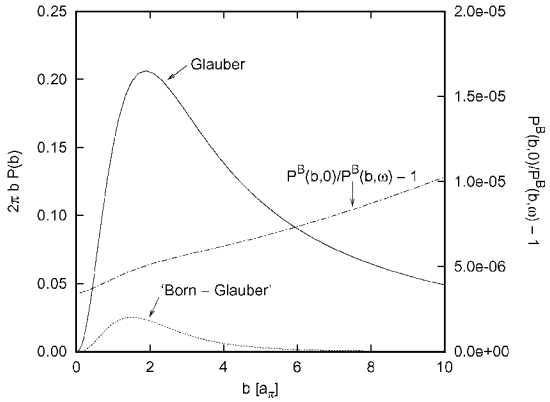

Figure 1: Comparison of the breakup probabilities for the transition $1s$–$2p$ of the pionium due to the Coulomb interaction with a Nickel (Z=28)atom. The slow convergence of $2\pi b|a_{fi}^G(b)|^2$ (solid line) is clearly visible, whereas the higher order terms (difference between first order (Born) and Glauber approximation, dotted line) are limited to small b. Also shown is the relative difference between the probabilities in first order with and without a finite ω. Whereas this difference increases with b, it is small in the region of b, where the higher order terms contribute appreciably.

with the charge number Z. For heavy nuclei they can be as large as 20% of the Born result [6].

References:

[1] T. Heim, K. Hencken, D. Trautmann, and G. Baur, *J. Phys. B* **33** (2000) 3583.

[2] HadAtom99 Workshop on Hadronic Atoms October 14–15,1999, Bern, Switzerland, available as hep-ph/9901381, see also the miniproceedings of HadAtom01, to be published

[3] see the homepage of the DIRAC experiment at HTTP://WWW.CERN.CH/DIRAC/.

[4] T.A. Heim, K. Hencken, D. Trautmann, and G. Baur, J.Phys.B 34(2001)3763

[5] Z. Halabuka, T.A. Heim, K. Hencken, D. Trautmann, and R.D. Viollier, *Nucl. Phys.* B **554** (1999) 86

[6] M. Schumann, T. Heim, K. Hencken, D. Trautmann and G.Baur, submitted to J.Phys.B

* Institut für Theoretische Physik, Universität Basel, Klingelbergstrasse 82, CH-4056 Basel, Switzerland

Coherent Coulomb excitation of relativistic nuclei in aligned crystal targets

V.R.Zoller*

There were several proposals [1, 2, 3, 4] of experiments on coherent Coulomb excitation of relativistic nuclei in crystal targets, $A\gamma \to A^*$. The central idea has been that crystals provide a periodic perturbation a frequency of which, ν, can be boosted by the Lorentz factor to the nuclear level splitting $\Delta E = E_1 - E_0$, so that the level populations would exhibit quantum beats. Specifically, a probability of excitation $P(N)$ was claimed to grow as $P(N) \propto N^2$, up to the crystal thicknesses $N = L/a \sim 10^4 - 10^5$, where a is the lattice spacing. This conclusion is based, however, on an evaluation of the transition amplitude in the plane wave Born approximation.

In a more consistent treatment of coherent $A \to A^*$ transitions one needs to include distortions due to the initial state Coulomb interactions (ISI) of the nucleus A and final state Coulomb interactions (FSI) of the excited nucleus A^*. Technically, the inclusion of distortions are reminiscent of the well known Glauber-Gribov shadowing effect [5, 6] and entails an attenuation of the coherent excitation amplitudes with growing crystal thickness. In our analysis we follow our early work on coherent transitions in crystals [7].

Consider the small-angle Coulomb scattering of ultrarelativistic nucleus (the mass number A, the charge Z_1 and the four-momentum p) moving along a crystal axis. The projectile-nucleus undergoes a correlated series of soft collisions which give rise to diagonal ($A \to A$, $A^* \to A^*$) and off-diagonal ($A \to A^*$, $A^* \to A$) transitions. The interatomic distances, $a \sim 3 - 5^o A$, are large, compared to the Thomas-Fermi screening radius $r \simeq 0.468 Z_2^{-1/3 o} A$, where Z_2 is the atomic number of the target atom and $\alpha = 1/137$. The relevant impact parameters, b, satisfy $b \ll a$, so that scattering by different atomic strings is incoherent.

Follwoing [3, 1, 2], we look for the electric dipole excitation $1/2^+ \to 1/2^-$ in the ^{19}F nucleus. The helicity-flip Born amplitude $t_B(\mathbf{q}_\perp)$ in the nucleus-atom collision is of the form $t_B(\mathbf{q}_\perp) = \sqrt{\alpha} dZ_2 q_\perp e^{i\phi}/(q_\perp^2 + \lambda^2)$, where $\lambda^2 = \mu^2 + \kappa^2$ and $\mu = 1/r$. The longitudinal momentum transfer $\kappa = (2M_A \Delta E + q_\perp^2)/2p$, defines the coherency length $l_c \sim \kappa^{-1}$.

Summation of multiple Coulomb scattering of ultrarelativistic particles can conveniently be performed in the eikonal approximation, in which

$$t(\mathbf{q}_\perp) = \sqrt{\alpha} dZ_2 \lambda e^{i\phi} \int bdb J_1(q_\perp b) K_1(\lambda b) \exp[i\chi(b)], \quad (1)$$

where $J_1(x)$ and $K_{0,1}(x)$ are the Bessel functions and the screened Coulomb phase shift function is $\chi(b) = -\beta K_0(\mu b)$, where $\beta = 2\alpha Z_1 Z_2$. Here we treat an excitation to a lowest order in the perturbation theory which is justified for all the practical purposes. Decays of excited state inside the target can safely be neglected.

Then, in the static lattice approximation, the full transition amplitude on a string of N identical atoms reads [7]

$$T(\mathbf{q}_\perp) = \sqrt{\alpha} dZ_2 \lambda S(q_\perp) e^{i\phi} I(q_\perp), \quad (2)$$

where

$$I(q_\perp) = \int bdb J_1(q_\perp b) K_1(\lambda b) \exp[-i\beta N K_0(\mu b)] \quad (3)$$

In eq.(2) $S(q_\perp)$ is the structure factor of the lattice

$$S(q_\perp) = \sin(\kappa N a/2)/\sin(\kappa a/2). \quad (4)$$

A careful inspection of the relevant parameters shows that coherent enhancement is present only in the contribution from the small impact parameters $b < r$. Here stationary phase approximation is applicable and yields

$$I(q_\perp) \simeq \frac{1}{\lambda q_\perp} \exp\left[-i\beta N \log\frac{q_\perp}{2\mu} + 2i\varphi\right], \quad (5)$$

where

$$\exp[2i\varphi] = \Gamma(1 + i\beta N/2)/\Gamma(1 - i\beta N/2). \quad (6)$$

Thus, for $q_\perp \gg \mu\beta N$ one finds no attenuation effect. At a larger $q_\perp$ the structure factor of a crystal enters the game. The final result for the excitation cross section reads

$$\sigma = \int dq_\perp^2 |T(\mathbf{q}_\perp)|^2 \propto N_c^2 \log(N/N_c), \quad (7)$$

where

$$N_c \ll N_n = \left[\frac{4\sqrt{6} p_n}{a\mu^2\beta^2}\right]^{1/3} \quad (8)$$

and $p_n = aM\Delta E/2\pi n$. For instance, for the W target one finds only a modest enhancement, $N_c \sim 30$, for the diamond target the enhancement is stronger, though: $N_c \sim 300$.

We conclude that not only the $q_\perp$-dependence of the coherent transition amplitude differs dramatically from the early predictions [2, 3], but the effect of the coherent enhancement is much weaker than predicted from Born approximation in [1, 2, 4].

The author thanks J. Speth and FZ-Juelich for hospitality and DFG (grant 436 RUS 17/119/01) for support. Partial support from INTAS (grant 97-30494) is gratefully acknowledged.

References:

[1] V.V. Okorokov and S.V. Proshin, *Investigation of the coherent excitation of the relativistic nuclei in a crystal*, Moscow, ITEP-13-1980

[2] Yu.L. Pivovarov, A.A. Shirokov and S.A. Vorobiev, Nucl. Phys. A509 (1990) 800 ;
Yu.L. Pivovarov and A.A. Shirokov, Sov. J. Nucl. Phys. 37 (1983) 653.

[3] R. Fusina and J.C. Kimball, Nucl. Instrum. Meth. B33 (1988) 77

[4] V.V. Okorokov, Yu.L. Pivovarov, A.A. Shirokov and S.A. Vorobev, *Proposal of experiment on coherent excitation of relativistic nuclei in crystals*, Moscow, ITEP-90-49, Fermilab Library.

[5] R.J. Glauber, in Lectures in Theoretical Physics, edited by W.E. Brittin et al., Interscience Publishers, Inc., New York, vol.1, p. 315, 1959.

[6] V.N. Gribov, Sov. Phys. JETP 29 (1969) 483; 30 (1970) 709.

[7] V.R. Zoller, JETP Lett. 64 (1996) 788.

* Institut for Theoretical and Experimental Physics, 117218 Moscow, Russia

How Empty Spaces Can Exert Forces on Each Other

A. Bulgac * and A. Wirzba

The present work [1] that had quite some echo in in newspaper articles [2] and bulletin boards [3] reports about a so far unknown force that acts on Buckminister fullerenes or *buckyballs* (soccerball-type molecules made of carbon-60 molecules), when they are immersed in liquid mercury. The force is explained by the fact that buckyballs or other particles flowing in mercury restrict the (quantum mechanical) freedom of movement of the conducting electrons of the liquid metal which could normally pass unhindered through this metal. Thus there is a formation and superposition of standing waves between the cavities, in case the conducting electrons are interpreted as matter waves. In this way the electrons exert a quantum pressure on and between the immersed particles, and the resulting change in energy can be perceived as a force between the particles that can be attractive or repulsive depending on their relative separation and orientation.

Indeed, this effect resembles the traditional Casimir effect that describes the attraction between two parallel, narrowly spaced metallic mirrors in vacuum. The latter force was predicted by the Dutch physicist H.B. Casimir in 1948 [4] and has only recently been quantitatively confirmed in experiment (for the altered system of a sphere and a plate) [5]. Because of Heisenberg's uncertainty relation the vacuum is not really empty, but contains fluctuating fields. Between the mirrors, however, only fluctuations are allowed with half-wave-lengths shorter than the distance between the mirrors. In this way an inequality between the fluctuating fields inside and outside the two mirrors is produced and the above described Casimir force results — a macroscopic manifestation of the laws of quantum mechanics.

In the present work this effect has been generalized to the interactions between cavities (literal empty regions of space) immersed in the background of non-interacting fermion matter fields. In fact, the Casimir energy is interpreted as energy-weighted integral of the geometry-dependent part of the density of states built from the modes of the corresponding fluctuating or real quantum fields. This topic is relevant to the physics of neutron star crusts (nuclei embedded in a neutron gas), to inhomogeneous quark–gluon plasma, to dilute Bose-Einstein-condensate bubbles inside the background of a Fermi-Dirac condensate, to the above-mentioned buckyballs in liquid mercury etc. In contrast to the standard effect, the new form of Casimir energy is neither attractive nor repulsive in character, but it changes depending on the relative arrangement and distances of various scatterers. As stated above, this effect can qualitatively be explained by the formation *and* superposition of standing matter waves between scatterers, where those waves dominate which have a wavelength comparable to the Fermi length. For more than two scatterers the pattern of possible standing waves becomes rather complicated. The simplest standing wave forms between two scatterers only. However a wave can scatter first off one scatterer, then off a second one and a third time off a third scatterer before coming back to the first scatterer and closing the cycle. The actual Casimir energy is given by a coherent sum over the effects of all possible matter waves among all scatterers. In this way one arrives at an extremely curious and somewhat unexpected picture. The matter filling up the space between the voids – even when it is nothing else but an ideal quantum gas and thus with no interactions of any kind – leads to an effective interaction between the empty regions of space.

While the evaluation of the Casimir energy for complicated geometries can be rather involved, the calculation simplifies for a system of non-overlapping cavities, since it can be mapped onto the quantum mechanical problem of the scattering of a point-particle of a fixed, but tunable initial energy from the very same cavity-geometry. With the help of Krein's trace formula [6, 7], the Casimir energy can then be extracted from the delay time of the scattered point particle, summed over all relevant initial energies. Although the cavity-systems can be very complicated, such that the scattering pattern for a classical particle would be totally chaotic, the calculations of this work show that the Casimir interaction energy in the case of more than two scatterers can be evaluated quite accurately as a sum of pairwise interactions between these scatterers [1]. As is known from Bohr's correspondence principle, for large initial energies the quantum mechanical scattering calculation can be very well approximated by the interference of periodic orbits running between and being reflected off the cavities. The effective interaction of the empty regions of space thus decreases with distance roughly for the same reason why in a game of billiards it is very difficult to make a long shot: long trajectories are very unstable. The increased instability of relatively long periodic orbits bouncing off more than two scatterers is what makes the three or more body interactions rather short–ranged.

References:

[1] A. Bulgac and A. Wirzba, Phys. Rev. Lett. **87**, 120404 (2001), nucl-th/0102018, FZJ-IKP(TH)-2001-4.

[2] Boston Globe, Sep. 25, 2001, page C2; Frankfurter Allgemeine Zeitung, Sep. 26, 2001, Nr. 224, p. N1; Salzburger Nachrichten, October 1, 2001.

[3] Physics News Update (*The AIP Bulletin of Physics News*), no. 556 #1, Sep. 13, 2001; Daily University Science News (*UniSci*), Sep. 19, 2001; Bild der Wissenschaft Online, Sep. 18, 2001; Pressemitteilung des Forschungszentrum Jülich, Oct. 9, 2001.

[4] H.B.G. Casimir, Proc. K. Ned. Akad. Wet. **51**, 793 (1948).

[5] S. Lamoureaux, Phys. Rev. Lett, **78**, 5 (1997); **81**, 5475(E) (1998); U. Mohideen and A. Roy, Phys. Rev. Lett. **81**, 4549 (1998); for a recent review, see: M. Bordag, U. Mohideen and V. M. Mostepanenko, Phys. Rep. **353**, 1 (2001), quant-ph/0106045.

[6] M.G. Krein, *Mat. Sborn. (N.S.)* **33**, 597 (1953); *Sov. Math.-Dokl.* **3**, 707 (1962); M.Sh. Birman and M.G. Krein, *Sov. Math.-Dokl.* **3**, 740 (1962).

[7] E. Beth and G.E. Uhlenbeck, Physica **4**, 915 (1937); J. Friedel, *Nuovo Cim. Ser. 10 Suppl.* **7**, 287 (1958). These results for the correction to the density of states are particular cases of the Krein formula [6].

* Department of Physics, University of Washington, Seattle, WA 98195–1560, USA

4. NUCLEAR PHYSICS AND OTHER TOPICS

Energy gap effect in the shell model with random two-body interactions

S. Drożdż* and M. Wójcik*

In the present study we address the question of a possible emergence of the effects of order in the two-body random ensembles of random matrices. One principal directly observable characteristics of such effects is the appearance of energy gaps at the edges of the spectrum. The model to be quantitatively explored here in this connection consists, similarly as in ref. [1], of six identical particles (all single particle energies are set to zero) operating in the *sd*-shell. From the nuclear spectroscopy point of view this corresponds to the ^{22}O nucleus. The statistics is collected from one thousand of RQE samples of two-body matrix elements. The resulting central result of our related investigations is shown in Fig. 1. Here the distribution of the ground state

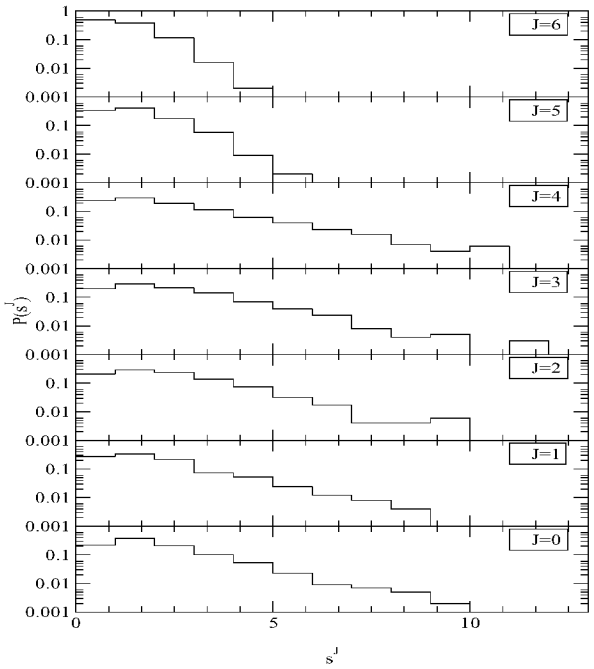

Fig. 1: Distributions of ground state energy gaps for successive J's.

(E_1^J) energy gaps $s^J = (E_2^J - E_1^J)/D^J$, for different J-sectors is shown. In this expression D^J denotes the average global level spacing among the remaining states, characteristic for a given J, $D^J = < E_{M_J}^J - E_1^J > /M_J$. In view of the results presented in our previous contribution it seems quite natural to see that there is a significant probability of nonzero ground state energy gaps relative to D^J. This can easily be traced back to the different distributions of states corresponding to the RQE relative to GOE (Gaussian-like versus semicircular). However, and this is very interesting, there is a nonzero probability for appearance of even very large (~ 10) gaps and that the large ground state energy gaps are more probable in the higher J-sectors ($J = 2-4$) than in the $J = 0$-sector. That this indicates more orderly ground states in the $J = 2-4$ sectors turns out consistent with their localization length which can be quantified in terms of the information entropy $K_l^J = -\sum_{\alpha=1}^{M_J} |a_{l,\alpha}^J|^2 \ln |a_{l,\alpha}^J|^2$ of an eigenstate labeled by l from the J-sector. The coefficients $a_{l,\alpha}^J$ denote the eigenvector components in the basis $|\alpha|$. Each K_l^J is normalised to its GOE limit, $K_{GOE}^J = \psi(M_J/2+1) - \psi(3/2)$, where ψ is the digamma function. Within our model the so-calculated and RQE ensemble averaged quantity for all the states versus their corresponding energies E_l^J is illustrated in Fig. 2. As anticipated, it is not $J = 0$ whose lowest eigenstate comes

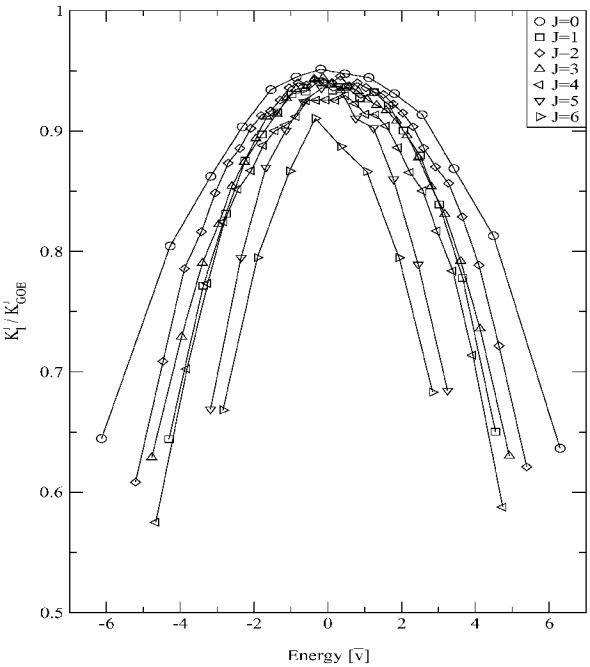

Fig. 2: The information entropy normalised to its GOE limit (K_l^J/K_{GOE}^J) for all the states l from various J-sectors (all positive parity) versus the energies (E_l^J) of those states. Circles correspond to $J = 0$, squares to $J = 1$, diamonds to $J = 2$, upwards oriented triangles to $J = 3$, left oriented triangles to $J = 4$, downwards oriented triangles to $J = 5$ and right oriented triangles to $J = 6$. Lines are drawn to guide the eye.

out most localised, i.e., most regular. The lowest states for several higher J values deviate much more from GOE. This in particular applies to $J = 2$ and, especially, to $J = 4$. This thus indicates more favorable conditions for the emergence of energy gaps for larger J than for $J = 0$ [2].

References:

[1] C.W. Johnson, G.F. Bertsch and D.J. Dean, Phys. Rev. Lett. **80**, 2749(1998).

[2] S. Drożdż and M. Wójcik, Physica A **301**, 291 (2001).

* Institut für Kernphysik, Forschungszentrum Jülich, D-52425 Jülich, Germany
Institute of Nuclear Physics, PL–31-342 Kraków, Poland

Coulomb Dissociation and Rare-Isotope Beams

G. Baur,K.Hencken*, D.Trautmann*, S.Typel** and H.H. Wolter***

Since the perturbation due to the electric field of the nucleus is exactly known, firm conclusions can be drawn from Coulomb dissociation measurements. Electromagnetic matrixelements and astrophysical S-factors for radiative capture processes can be extracted from experiments. We describe the basic theory, new results concerning higher order effects in the dissociation of neutron halo nuclei. Some new applications of Coulomb dissociation for nuclear astrophysics [1] and nuclear structure physics are discussed. Parts of this work are published in Ref.[2, 3, 4].

With increasing beam energy higher lying states can be excited with the Coulomb excitation mechanism. This can lead to Coulomb dissociation, in addition to Coulomb excitation of particle bound states. Such investigations are also well suited for secondary(radioactive) beams. Due to the time-dependent electromagnetic field the projectile is excited to a bound or continuum state, which can subsequently decay. If 1^{st} order electromagnetic excitation is the dominant effect, experiments can directly be interpreted in terms of electromagnetic matrix-elements, which also enter e.g. in radiative capture cross-sections The question of higher order effects is therefore very important. A good way to treat higher order effects in a general way is to solve the time-dependent Schrödinger equation [6]. We present new results for a simple and realistic model for Coulomb dissociation of neutron halo nuclei. We show that these effects are reassuringly small [5]. We also discuss new possibilities, like the experimental study of two-particle capture and applications to r- and rp-process nuclei, see also [7]. Low-lying dipole strength has been observed in weakly bound neutron rich nuclei(see [5] for further references) and their occurrence may be a systematic effect in proton-neutron asymmetric nuclei. This could affect significantly the r-process abundances [8]. Coulomb dissociation studies will be very useful in this context.

Electromagnetic excitation is also used at relativistic heavy ion accelerators to obtain nuclear structure information. Examples are the nuclear fission studies of radioactive nuclei and photofission of ^{208}Pb . Cross-sections for the excitation of the giant dipole resonance ("Weizsäcker-Williams process") at the relativistic heavy ion colliders RHIC and LHC(Pb-Pb) at CERN are huge , of the order of 100 b for heavy systems (Au-Au or Pb-Pb). The excited nuclei are lost from the beam. On the other hand, the effect is also useful as a luminosity monitor by detecting the neutrons in the forward direction and as a trigger on peripheral collisions. [9]

The intense source of quasi-real (or equivalent) photons has opened a wide horizon of related problems and new experimental possibilities especially for the present and forthcoming radioactive beam facilities to investigate efficiently photo-interactions with nuclei (single- and multiphoton excitations and electromagnetic dissociation).

A review is being prepared for Progress in Particle and Nuclear Physics [10].

References:

[1] G.Baur, C.A. Bertulani and H.Rebel, Nucl Phys.A458(1986)188

[2] G.Baur,S.Typel,H.H.Wolter,K.Hencken,and D.Trautmann, proceedings of the RCNP-TMU SYMPOSIUM on Spins in Nuclear and Hadronic Reactions , October 26-28 1999, World Scientific Publishing Company,(2000)p.119 ,edited by H.Yabu, T. Suzuki, and H. Toki, see also nucl-th/0001045

[3] G.Baur, K.Hencken, D.Trautmann, S.Typel, and H.H.Wolter nucl-th/008033 proceedings of the NATO Advanced Study Institute "Nuclei Far From Stability and Astrophysics" Predeal, Rumania 28.8.-8.9.2000,Kluwer Academic Publishers ,NATO Science Series, Physics and Chemistry Vol.17(2001)247

[4] G.Baur, K.Hencken, D.Trautmann S.Typel and H.H.Wolter, nucl-th/0011061, Proceedings of the International Workshop on Nuclear Physics, Erice 16.-24.9.2000,Progress in Particle and Nuclear Physics Vol.46 (2001) 99

[5] S.Typel and G.Baur, nucl-th/0101033, Phys.Rev C64(2001) 024601

[6] H. Utsunomiya et al. Nucl. Phys. A654(1999)928c, Y.Tokimoto et al. Phys. Rev. C53(2001)035801

[7] An International Accelerator Facility for Beams of Ions and Antiprotons. Conceptual Design Report. GSI November 2001.

[8] S. Goriely Phys. Lett. B436(1998)10

[9] M.Chiu et al. hep-ex/0109018

[10] G.Baur, K. Hencken and D.Trautmann Coulomb Dissociation in Hadron- and Astrophysics to be submitted to Progress in Particle and Nuclear Physics, deadline 15th April 2003

** NSCL,MSU,East Lansing

*** Sektion Physik, Universität München, D-85748 Garching, Germany

* Institut für Theoretische Physik, Universität Basel, Klingelbergstraße 82, CH-4056 Basel, Switzerland

Numerical Study of Poastacceleration Effects in the Coulomb Dissociation of Halo Nuclei

P.Banerjee*, G. Baur,K.Hencken**,R.Shyam*,and D.Trautmann**

We consider the breakup of a particle $a = (c + n)$ (deuteron, neutron-halo nucleus) consisting of a loosely bound neutral particle n and the core c (with charge Z_c) in the Coulomb field of a target nucleus with charge Z.

$$a + Z \to c + n + Z. \quad (1)$$

As a further simplification the $a = (c + n)$ system is assumed to be bound by a zero range force .
In the post-form CWBA the T-matrix for the reaction Eq. (1) can be written as [1]

$$T = \left\langle \chi^{(-)}_{\vec{q}_c} \psi_{\vec{q}_n} \middle| V_{nc} \middle| \chi^{(+)}_{\vec{q}_a} \phi_0 \right\rangle \quad (2)$$

$$= D_0 \int d^3R \chi^{(-)}_{\vec{q}_c}(\vec{R}) e^{-i\vec{q}_n \cdot \vec{R}} \chi^{(+)}_{\vec{q}_a}(\vec{R}), \quad (3)$$

with the "zero range constant" D_0 given by $D_0 = \frac{\hbar^2}{2\mu}\sqrt{8\pi\kappa}$. κ is related to the binding enegy and μ is the reduced mass of the $(c + n)$-system. The initial state is given by the incoming Coulomb wave function $\chi^{(+)}_{\vec{q}_a}$ with momentum $\vec{q}_a$ and the halo wave function ϕ_0. The final state is given by the independent motion of the core described by the outgoing Coulomb wave function $\chi^{(-)}_{\vec{q}_c}$ in the Coulomb field of the target nucleus Z with asymptotic momentum $\vec{q}_c$ and the free neutron with momentum $\vec{q}_n$, described by a plane wave. In these wave functions the Coulomb interaction is taken into account correctly to all orders. In our model there is no resonance structure in the $c + n$ continuum. This is clearly a good assumption for the deuteron and also for other neutron halo systems. A recent analysis of this matrix-element and its connections to the Born and semiclassical approximations was recently given in [2].
Eqs. (2), (3) include the effects of postacceleration. Postacceleration refers to a purely classical picture of the breakup process. The nucleus $a = (c + n)$ moves up the Coulomb potential, loosing the appropriate amount of kinetic energy. At the "breakup point" this kinetic energy (minus the binding energy) is supposed to be shared among the fragments according to their mass ratio (assuming that the velocities of c and n are equal). Running down the Coulomb barrier, the charged particle c alone (and not the neutron) gains back the Coulomb energy, resulting in its postacceleration. This simple picture will be modified in a quantal treatment, where a "breakup point" does not exist. A purely classical formula for this postacceleration, where the "breakup point" corresponds to the distance of closest approach is given in [3]. Postacceleration is clearly observed in low energy deuteron breakup, in the theoretical calculations as well as in the corresponding experiments [4].
Eq. (2) is also useful for the description of the Coulomb dissociation of halo nuclei at high beam energies, see [5]. Within this theory postacceleration effects become negligibly small in the high energy region. This is seen in Fig.1

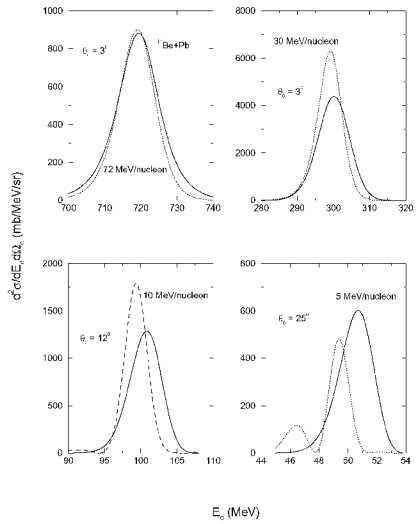

Figure 1: Double differential cross sections for various beam energies. The continuous line denotes the full calculation (eq. 2), the Born approximation is given by the dashed line. It is clearly seen how the postacceleration effect becomes less and less important for the higher beam energies

In addition to ^{11}Be Coulomb breakup it can also be applied e.g. to the ^{19}C Coulomb dissociation experiments [6]. We have disregarded here the finite range effects, they are important for a quantitative understanding of the data.

References:

[1] G.Baur and D.Trautmann, Nucl. Phys. A191(1972)321

[2] G.Baur, K. Hencken and D.Trautmann to be published in the Proceedings of ENAM2001, Haemeenlinna, Finland, nucl-th/0108013

[3] G.Baur, C.A. Bertulani and D. Kalassa Nucl. Phys. A550(1995)107

[4] G.Baur, F.Rösel ,D.Trautmann and R.Shyam, Physics . Reports 111(1984)333

[5] R.Shyam, P.Banerjee and G.Baur Nucl.Phys. A 540(1992)341

[6] T.Nakamura et al. Phys.Rev.Lett. 83(1999)1112

* SAHA Institute Calcutta
**Institut für Theoretische Physik, Universität Basel,
Klingelbergstraße 82, CH-4056 Basel, Switzerland

The Trojan Horse Method: a Tool for Nuclear Structure and Astrophysics

S. Typel*, G. Baur, and H.H. Wolter**

The idea of the Trojan Horse Method (THM) [1] is to extract the cross section of a two-body reaction $A+x \to C+c$, at low energies from a suitably chosen three-body reaction $A + a \to C + c + b$ (where $a = (b+x)$) with the help of nuclear reaction theory (like, e.g. DWBA). For recent discussions see [2], [3] and [4].

A striking parallelism of (d,p) spectra in the continuum region and neutron elastic scattering σ_l in partial wave l on the same target nucleus was observed in [5]. This was explained in a "Butler stripping theory" in ref. [6]. The "stripping enhancement factors" depend on the angular momentum l of the transferred neutron. It is defined by (see eq. 6 of [6])

$$\frac{d^2\sigma}{d\Omega_p dE_p} = \sum_l \sigma_l F_l(x,y)$$

where $\frac{d^2\sigma}{d\Omega_p dE_p}$ denotes the (d,p) double differential cross section and $x = q_n R_0$ and $y = qR_0$. The quantity q_n is the wave number corresponding to the neutron and $\vec{q} = \vec{Q_i} - \vec{Q_f}$. The cutoff radius is denoted by R_0. The "stripping enhancement factor" or "trojan horse factor" (THF) is given by

$$F_l(x,y) = C\frac{(yh_l(x)j_{l-1}(y) - xh_{l-1}(x)j_l(y))^2}{(x^2-y^2)^2}$$

with the factor $C = m_b m_a m_x \frac{Q_f}{Q_i} q_x^3 \frac{D_0^2}{16\pi^5\hbar^5}$. $D_0 = \frac{\hbar^2\eta^2}{2\mu}\sqrt{8\pi\eta}$ is the zero range constant related to the properties of the $a = (b + x)$ $(d = (p + n))$ system.

This "THF" depends essentially on the two kinematical variables x and y. The quantity y controls the kinematics of the (a,b) transfer reaction ("the Trojan horse"): for forward scattering there is a minimum value y_{min}, and y increases with scattering angle. The variable x refers to the $(A + x)$-system. It can become very small close to threshold and leads to the characteristic threshold behaviour of $F_l(x,y)$. This threshold behaviour is determined by the angular momentum barrier, which is very effective in the case of elastic scattering (close to threshold) and less so in the stripping case. For small values of x the spherical Hankel function behaves as $\frac{(2l-1)!!}{x^{l+1}}$.

For charged particle transfer, there is in addition the Coulomb barrier. The radial Butler integral which involves the Coulomb functions F_l and G_l cannot be done analytically as in the case of a neutral particle. Yet, there are methods to evaluate this integral very fast and work is in progress. The radial integrals show a characteristic $\exp(2\pi\eta_{Ax})$ dependence; this enhancement factor cancels the corresponding Gamow suppression factor in the $A+x \to C+c$ reaction. The parameter which governs the threshold behaviour is the Coulomb parameter $\eta_{Ax} = \frac{Z_A Z_x e^2 R_0 m_n}{\hbar^2 x}$. An interesting old study of (d,n) reactions is [7]. In this case, the corresponding (p,p) cross section is also known. It can serve as an interesting test case.

It is interesting to note that screening effects, which can affect low energy charged particle reactions, are generally absent in the THM method. This is nicely illustrated in Fig. 4 of [2], where the ^{7}Li$(p,\alpha)\alpha$ and ^{6}Li$(d,\alpha)\alpha$ reactions are also studied with the THM method [8, 9]. A formal proof that screening is unimportant in the THM method can be found by noting that in the expression for the T-matrix [10] there is a scattering wave function with the boundary conditions $\Psi^{(-)}_{Cc}$. The incoming channel $C+c$ has a high energy and is consequently little affected by the screening function $\exp(\pi\eta_{Cc}\frac{U_e}{E_{Cc}})$ where U_e is an electron-screening energy and E_{Cc} the energy in the $C + c$ channel, which is generally much higher than U_e. (For a scattering wave $\Psi^{(+)}_{Ax}$ this would be quite different: the corresponding screening function would involve $\exp(\pi\eta_{Ax}\frac{U_e}{E_{Ax}})$. For small E_{Ax} this would be a large screening effect.)

References:

[1] G. Baur, Phys. Lett. B178 (1986) 135

[2] Frank Strieder and Claus Rolfs. Key reactions in stellar burning: LUNA and other new approaches, NUPECC News, Vol. 11 No. 3 (2001) 5

[3] S. Austin, High Energy Approach to Low Energy Phenomena in Astrophysics, nucl-th/0201010

[4] G. Baur, S. Typel, H.H. Wolter, K. Hencken, and D. Trautmann, proceedings of the RCNP-TMU symposium on Spins in Nuclear and Hadronic Reactions, October 26-28, 1999, World Scientific Publishing Company (2000) 119, edited by H. Yabu, T. Suzuki, and H. Toki, see also nucl-th/0001045

[5] H. Fuchs et al., Phys. Lett. 37B (1971) 285

[6] G. Baur and D. Trautmann, Z. Physik 267 (1974) 103

[7] J. Bommer et al., Phys. Rev. C 128 (1975) 1069

[8] M. Lattuada et al., Astrophys. J. 562 (2001) 1076

[9] C. Spitaleri et al., Phys. Rev. C 63 (2001) 055801

[10] S.Typel and H.H. Wolter, Few Body Systems 29 (2000)7

* NSCL, Michigan State University, East Lansing, USA

** Sektion Physik, Universität München, Garching, Germany

Identifying complexity by means of matrices

S. Drożdż, J. Kwapień, J. Speth and M. Wójcik

Complexity is an interdisciplinary concept which, first of all, addresses the question of how order emerges out of randomness. By its very nature, even though central to the contemporary physics, this concept still lacks a precise definition. In qualitative terms it refers to diversity of forms, to emergence of coherent patterns out of randomness and also to some ability of frequent switching among such patterns. This normally involves many components, many different space and time scales, and thus such phenomena like chaos, noise, but, of course, also collectivity and criticality. In fact, due to all those elements, it seems most appropriate to search for a real complexity just at the interface of chaos and collectivity. Indeed, these two seemingly contradictory phenomena have to go in parallel, as they both are connected with existence of many degrees of freedom and a strong, often random, interaction among them.

Approaching complex systems, either empirically or theoretically, is typically based on analyzing large multivariate ensembles of parameters. For this reason, probably the most efficient formal frame to quantify the whole variety of effects connected with complexity is in terms of matrices. Since complexity is embedded in chaos, or even noise, the random matrix theory (RMT) provides then an appropriate reference. Its utility results predominantly from the fact that the degree of agreement quantifies the generic properties of a system, i.e., those connected with chaotic or noisy activity. For the complex systems this is expected to be a dominant component, but this component is not what constitutes an essence of complexity. From this perspective the deviations are even more relevant and more interesting as they reflect a creative and perhaps deterministic potential emerging from a noisy background of such systems.

For many reasons matrices provide a very practical and powerful tool in approaching and quantifying the related characteristics. Expressed in the most general form, in essentially all the cases of practical interest, the $n \times n$ matrices $\mathbf{W}$ used to describe the complex system are by construction designed as

$$\mathbf{W} = \mathbf{X}\mathbf{Y}^T, \tag{1}$$

where $\mathbf{X}$ and $\mathbf{Y}$ denote the rectangular $n \times m$ matrices. Such, for instance, are the correlation matrices whose standard form corresponds to $\mathbf{Y} = \mathbf{X}$. The more general case, of $\mathbf{X}$ and $\mathbf{Y}$ different, results in asymmetric correlation matrices with complex eigenvalues λ. As shown recently [1], such matrices also turn out to provide a very powerful tool in practical applications.

Further examples of matrices of similar structure include the Hamiltonian matrices of strongly interacting quantum many body systems such as atomic nuclei. This holds true [2] on the level of bound states where the problem is described by the Hermitian matrices, as well as for excitations embedded in the continuum [3]. Several neural network models also belong to this category of matrix structure.

As it has already been expressed above, several variants of ensembles of the random matrices provide an appropriate and natural reference for quantifying various characteristics of complexity. The bulk of such characteristics is expected to be consistent with RMT, and in fact there exists strong evidence that it is. Once this is established, even more interesting are however deviations, especially those signaling emergence of synchronous or coherent patterns, i.e., the effects connected with the reduction of dimensionality. In the matrix terminology such patterns can thus be associated with a significantly reduced rank k (thus $k \ll n$) of a leading component $\mathbf{W}_c$ of $\mathbf{W}$. A satisfactory structure of the matrix that would allow some coexistence of chaos or noise and of collectivity thus reads:

$$\mathbf{W} = \mathbf{W}_r + \mathbf{W}_c. \tag{2}$$

Of course, in the absence of $\mathbf{W}_r$, the second term ($\mathbf{W}_c$) of $\mathbf{W}$ generates k nonzero eigenvalues, and all the remaining ones $(n-k)$ constitute the zero modes. When $\mathbf{W}_r$ enters as a noise (random like matrix) correction, a trace of the above effect is expected to remain, i.e., k large eigenvalues and the bulk composed of $n-k$ small eigenvalues whose distribution and fluctuations are consistent with an appropriate version of random matrix ensemble. One likely mechanism that may lead to such a segregation of eigenspectra is that m in eq. (1) is significantly smaller than n, or that the number of large components makes it effectively small on the level of large entries w of $\mathbf{W}$. Another mechanism that may lead to a structure analogous to (2), is the presence of some systematic trend [4], in addition to noise, in the $\mathbf{X}$ and $\mathbf{Y}$ matrices.

Based on several examples of natural complex dynamical systems, like the strongly interacting Fermi systems, the human brain and the financial markets, we provide [5] evidence that such effects are indeed common to all the phenomena that intuitively can be qualified as complex. Complexity can thus be viewed as a trinity comprising coherence, chaos and a gap (probably not too large) between them. Coherence constitutes the essence as it makes patterns and structures, which is of primary interest and importance. Chaos is always present in any really interesting system and, in fact, it is even needed as it allows to quickly explore the whole available phase space, and thus to probe various possibilities and to switch from one pattern of activity to another. Finally, the gap between them allows the structures to be identifiable and to exist for some time. Thus all the three are needed in parallel. Such a combination probably makes a natural system most efficient in its evolution.

References:

[1] J. Kwapień, S. Drożdż, A.A. Ioannides, Phys. Rev. E 62 (2000) 5557.
[2] S. Drożdż, M. Wójcik, Physica A 301 (2001) 291.
[3] S. Drożdż, A. Trellakis, J. Wambach, Phys. Rev. Lett. 76 (1996) 4891.
[4] S. Drożdż, F. Grümmer, A.Z. Górski, F. Ruf, J. Speth, Physica A 287 (2000) 440.
[5] S. Drożdż, J. Kwapień, J. Speth, M. Wójcik, arXiv:cond-mat/012271, to be published in Physica A

Dynamics of financial correlations in the matrix representation

S. Drożdż, F. Grümmer, J. Kwapień, F. Ruf and J. Speth

In global terms the financial correlations can be classified as correlations in space and correlations in time, though of course they are somewhat interrelated. The first category so far studied involves for instance the correlations among the companies comprised by a single stock market. From practical perspective this type of correlations relates to the theory of optimal portfolios and risk management. Studying explicit correlations in time is at least as important because it is this type of correlations that directly reflects a nature of the financial dynamics. In the present application, we propose to use the concept of the correlation matrix such that it focuses entirely on the time-correlations, with the entries being constructed from the time-series of normalized price returns representing the consecutive trading days.

Our study is based on the DAX recordings with the frequency of 15 s during the period between Nov 28, 1997 and Sept 17, 1999. By taking the DAX intraday 15 s variation between the trading time 9:03 and 17:10, one obtains complete and equivalent time series representing different trading days during this calendar period.

A principal characteristic of interest is the structure of eigenspectrum. The resulting probability density of eigenvalues, shown in Fig. 1, displays a very interesting structure. There exist two almost degenerate eigenvalues visibly repelled from the others, i.e. well above the upper edge allowed for a purely random matrix (in our case this edge is at 2.19) which indicates that the dynamics develops certain time specific repeatable structures in the intraday trading. The bulk of the spectrum, however, agrees remarkably well with the bounds prescribed by purely random correlations. This, supported by outcomes of an independent test based on uncorrelated artificial time series, indicates that the statistical neighbouring recordings in our time series of 15 s DAX returns share essentially no common information and that a whole non-randomness can be associated with the two largest eigenvalues. An analogous study of the volatility correlations shows that even in this case the structure of eigenspectrum of the resulting matrix is consistent with purely random correlations. However, now one can identify three outlying eigenvalues and the largest of them is repelled significantly higher (Fig. 1).

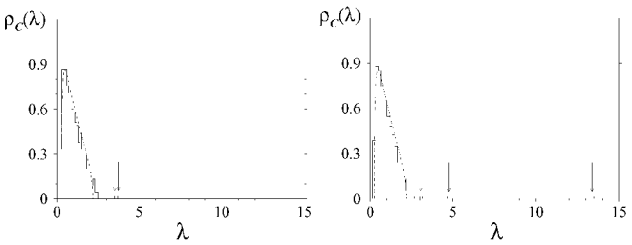

Fig. 1: The probability density of the eigenvalues of the correlation matrix calculated from the DAX returns (left) and DAX volatility (right). The null hypothesis of purely random correlations formulated in terms of theoretical distribution is indicated by the dashed lines.

The structure of eigenspectrum of a matrix is expected to be related to the distribution of its elements. For this reason in Fig. 2 we show the distributions of such elements corresponding to our two cases under consideration. In the case of index returns, this distribution is symmetric with respect to zero: a Gaussian like for small matrix elements, but sizably thicker than a Gaussian for large ones, where a power law with the index of about 5.5-5.7 provides a reasonable representation. It is these tails which generate the two largest eigenvalues seen in the left panel in Fig. 1. The volatility correlation matrix, on the other hand, reveals different distribution. First of all, the center of this distribution is shifted towards positive values and this is responsible for the largest eigenvalue. Secondly, this distribution is asymmetric. This originates from the fact that the volatility fluctuations are stongly asymmetric relative to their average value. The slope on the right hand side cannot be here reliably measured in terms of a single power law, but its even smaller value as compared to the case of returns is evident. On the other hand, on the negative side the distribution drops down faster than a Gaussian and, therefore, the separation between the two remaining large eigenvalues is significantly more pronounced than of their returns counterparts in Fig. 1.

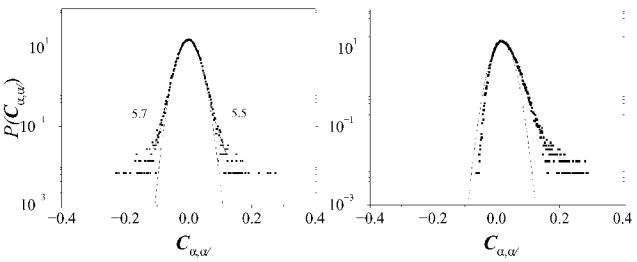

Fig. 2: Distribution of matrix elements for the correlation matrix calculated from the time series of returns (left) and from the time series of volatilities (right). The solid lines in the left panel indicate the power law fits to the tails of the distribution, while the dashed one represents a Gaussian best fit. The numbers reflect the corresponding scaling indices.

References:

[1] S. Drożdż, J. Kwapień, F. Grümmer, F. Ruf, J. Speth, Physica A **299** (2001) 144

[2] J. Kwapień, S. Drożdż, F. Grümmer, F. Ruf, J. Speth, e-print cond-mat/0108068, to appear in Physica A (2002)

[3] M.L. Mehta, Random Matrices, Academic Press, Boston, 1999

[4] A. Edelman, SIAM J. Matrix Anal. Appl. **9** (1988) 543; A.M. Sengupta, P.P. Mitra, Phys. Rev. E **60** (1999) 3389

Decomposing the stock market intraday dynamics

J. Kwapień, S. Drożdż, F. Grümmer, F. Ruf and J. Speth

One of the great challenges of econophysics is to properly quantify and, following this, to explain the nature of financial correlations and fluctuations. The efficient market hypothesis implies that they are dominated by noise. Indeed, the spectrum of the correlation matrix accounting for correlations among the stock market companies agrees very well with the universal predictions of random matrix theory. Locations of extreme eigenvalues differ however from these predictions and thus identify certain system-specific, non-random properties such as collectivity. Moreover, it is commonly accepted that the autocorrelation function of the financial time-series drops down to zero within few minutes, while the correlations in volatility remain positive for many weeks. On short time-scales the return distributions are definitely not Lévy stable but it turns out difficult to detect their convergence to a Gaussian on longer time-scales as expected from the central limit theorem. In addressing this sort of issues below we use the concept of the correlation matrix whose entries are constructed from the time series of price changes representing the consecutive trading days. The present study is based on high-frequency (15 s) DAX recordings.

In quantifying the differences among the eigenvectors corresponding to correlation matrix eigenvalues taken either from collective or from noisy part of the spectrum, it is instructive to look at the superposed time series of normalized returns:

$$g_{\lambda_k}(t_i) = \sum_{\alpha=1}^{N} \mathrm{sign}(v_\alpha^k)|v_\alpha^k|^2 g_\alpha(t_i), \qquad (1)$$

where $g_\alpha(t_i)$ denotes an original intraday signal corresponding to a day α and v_α^k is a component of k-th eigenvector. Three of such superposed time series are shown in Fig. 1. For a statistical value of k a superposed signal develops no coherent structures. The first two eigensignals differ however significantly and indicate the existence of very pronounced, repeatable structures at the well defined instants of time through many days. The first ($k = 1$) of them corresponds to the period just before closing in Frankfurt during the time interval considered here, and the second one ($k = 2$) to the period immediately after 14:30, which reflects the DAX response to the North-American financial news release exactly at this time.

The above decomposition of the stock market dynamics allows one to shed some more light on the issue of the probability distribution of price changes. That the nature of such changes is very complex can be concluded by looking for instance at the probability distributions of fluctuations associated with different returns 'eigensignals' $g_{\lambda_k}(t_i)$. Some examples are shown in Fig. 2. What one can clearly see is that the probability density of fluctuations connected with the bulk of the spectrum drops down much faster than the ones connected with the more collective ($k = 1, 2$) eigenvectors. This goes in parallel with the results of analysis of the original signals (not shown here), where we observe clear difference between tails of the return distribution for different periods of a trading day. Although typically the parameters of probability density functional are about consistent with those cited in the literature, a short, highly volatile period near 14:30 displays much thicker tails as compared to the periods of 'normal' activity, which seem to be still in the Lévy stable regime.

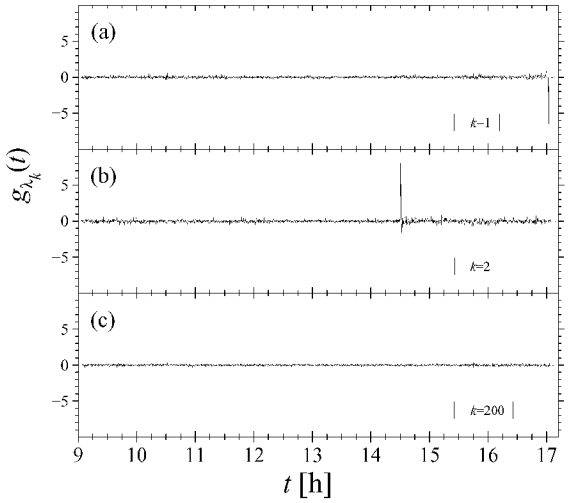

Fig. 1: The superposed time series of normalized returns calculated according to eq. (1) for $k = 1$ (a), $k = 2$ (b) and $k = 200$ (c).

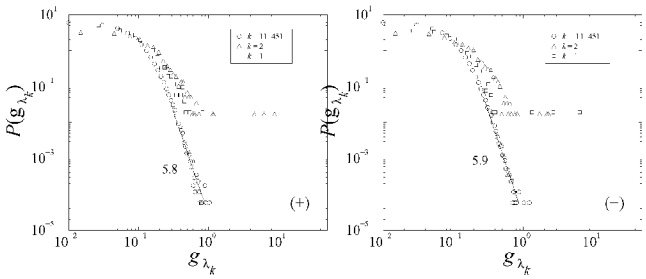

Fig. 2: Probability density functions of fluctuations of the superposed returns as expressed by the Eq. (1). Both positive (left) and negative (right) sides of those distributions are shown.

In summary, our analysis of the cross-day correlations in DAX shows that, in the observed evolution of the market, one can identify distinct components whose dynamics can be governed by different laws. These components manifests themselves mainly in several well defined short periods of time during the intraday trading, characterized by strong synchronous repeatable bursts of activity. The related return probability density functionals develop significantly larger values on the level of rare events than during periods of the normal activity both on the level of original data and the reconstructed eigensignals. This may constitute a principal reason for an observed extremely slow convergence to a Gaussian of the global return distribution on long-time scales.

References:

[1] S. Drożdż, J. Kwapień, F. Grümmer, F. Ruf, J. Speth, Physica A **299** (2001) 144

[2] J. Kwapień, S. Drożdż, F. Grümmer, F. Ruf, J. Speth, arXiv:cond-mat/0108068, to appear in Physica A (2002)

[3] M.L. Mehta, Random Matrices, Academic Press, Boston, 1999

[4] R.N. Mantegna, H. Eugene Stanley, An Introduction to Econophysics: Correlations and Complexity in Finance, University Press, Cambridge, 2000

Time-frequency analysis of binaural activation of the human auditory cortex

J. Kwapień and S. Drożdż

We performed a wavelet-based study of time-frequency properties of the magnetic collective activity of the auditory cortex during the external sound stimulation. Five healthy male volunteers participated in the magnetoencephalography (MEG) experiment consisting in delivery of series of 1-kHz sound stimuli to one ear. It is well known that, owing to the existence of the segregated neural pathways from ears to the auditory cortex, its stimulus-evoked activation is binaural even if only one ear was stimulated.

From the point of view of an observer studying the electromagnetic activity of the cortex, the neuronal synchronization implies the occurrence of process-characteristic Fourier frequencies in a recorded signal. The synchronized neurons share the same information; this can happen either due to a similar but independent activation of two different regions of the cortex, or due to a direct communication between these regions. The existence of relations between the MEG signals originating from different hemispheres can be proved, for example, by means of statistical methods like the mutual information, or, alternatively, by studying dependences between the frequency spectra of such signals. Fig. 1 shows typical single-trial and average MEG signals from the auditory cortex.

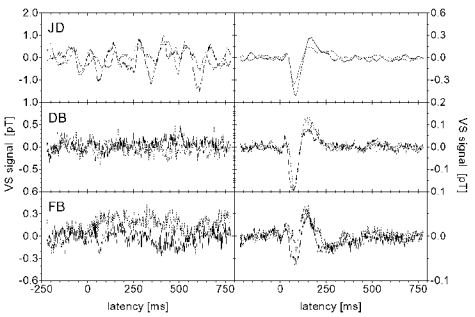

Fig. 1: Exemplary single-trial signals from the left and right hemispheres (left column) for three characteristic subjects, together with the corresponding average signals obtained from 120 trials (right column).

In human brain one usually deals with signals of nonstationary character, which manifests itself in temporal variability of frequency spectrum of the signal. Such data can be studied by means of the wavelet transform, employing various versions of wavelet functions that are localized both in time and in frequency. For a discrete real scalar signal $x(t)$ it reads

$$W(t_k,s) = \sum_{j=0}^{N-1} x(t_j)\psi\left[\frac{(j-k)\Delta t}{s}\right], \qquad (1)$$

where s is called the scale and a corresponds to the space or time translation. Wavelets of the same type but with different parameter values are grouped into families which comprise functions of all possible scales and translations. The wavelet transform results in the complex $W(a,s)$.

Although we found clear dissimilarity of the spectra for different hemispheres, the spectrum averaged over all the trials convincingly documents that the frequency transition

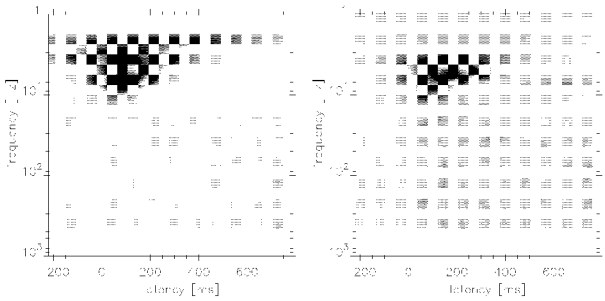

Fig. 2: Scalar product (2) as a function of latency and frequency for two exemplary subjects. The largest values are denoted by black pixels, while the smallest values by the white ones.

is triggered by the stimulus, and lasts for several hundred milliseconds. In our ealier analysis [1] we shown that signals from the opposite hemispheres are strongly related with each other, with this relation being entirely restricted to the evoked response interval. We found that this phenomenon carries signatures of a delayed synchronization. With the wavelet analysis, it is possible to make one step further, and determine the existence of correlations between the same frequency components of the signals from different hemispheres.

Dependence of the strength of the interhemispheric correlations, both on Fourier frequency of the signal components and on latency, is presented in a compact form in Fig. 2. This Figure presents exemplary 2-D plots of the scalar product defined by the equation

$$S(t_k,f) = \sum_{\alpha=1}^{120} |\tilde{W}_\alpha^{(L)}(t_k,f)|^2 |\tilde{W}_\alpha^{(R)}(t_k,f)|^2, \qquad (2)$$

where $|\tilde{W}_\alpha^{(L,R)}(t_k,f)|^2$ denotes the wavelet power spectrum of the signal from the trial α; the superscripts L,R indicate the hemispheres, while N is the length of the signal ($k = 0,..N-1$). The Figure shows that the strongest interhemispheric dependences are localized in the range from 2 Hz (or 3 Hz, depending on a subject) to about 10 Hz. The frequency at maximum $S(t_k,f)$ is subject-dependent (4-7 Hz). The signals correlate soon after the stimulus arrives and remain mutually related for approximately 300 ms.

In summary, we identified a pronounced repeatable stimulus-triggered transient in frequency content of the signals. This transient originates from an activation of frequencies restricted to the range 2-20 Hz, with a maximum varying from several to about 10 Hz, depending on a subject. The evoked activity in two hemispheres reveals similar frequency characteristics, both at the statistical and single-trial level; this forms the ground for the existence of the interhemisphere correlations.

References:

[1] J. Kwapień, S. Drożdż, L.C. Liu and A.A. Ioannides, Phys. Rev. E **58** (1998) 6359-6368

[2] J. Kwapień and S. Drożdż, Structures, Waves, Biomedical Engineering **10** (2001) 69-78

Nature of the mechanism generating order out of randomness

S. Drożdż* and M. Wójcik*

The nature of a mechanism generating order out of randomness constitutes one of the most fundamental issues of the contemporary physics. Theories based on various versions of ensembles of the random matrices provide one possible theoretical frame for studying such effects. In this context the recently identified [1] preponderance of the $J = 0$ ground states in strongly interacting Fermi systems, such as atomic nuclei, arising from random two-body interactions came as a surprise since there is no obvious pairing character in the assumed random force. Various possible explanations of this effect have been tested with no success, however. We investigate the origin of order in the low-lying spectra of many-body systems with random two-body interactions. Contrary to the common belief our study [2] based both on analytical as well as on numerical arguments shows that except for the most J-stretched states, the ground states in the higher J-sectors are more orderly than the ones in the $J = 0$-sector. A predominance of $J = 0$ ground states turns out to be the result of putting on together states with different characteristic energy scales from different J-sectors. In analytical terms our argument goes as follows. The interaction matrix elements $v^J_{\alpha,\alpha'}$ of good total angular momentum J in the shell-model basis $|\alpha\rangle$ can be expressed as:

$$v^J_{\alpha,\alpha'} = \sum_{J'} \sum_{ii'} c^{J\alpha\alpha'}_{J'ii'} g^{J'}_{ii'}. \tag{1}$$

The summation runs over all combinations of the two-particle states $|i\rangle$ coupled to the angular momentum J' and connected by the two-body interaction g. $g^{J'}_{ii'}$ denote the radial parts of the corresponding two-body matrix elements while $c^{J\alpha\alpha'}_{J'ii'}$ globally represent elements of the angular momentum recoupling geometry. In statistical ensembles of matrices the crucial factor determining the structure of eigenspectrum is the probability distribution $P_V(v)$ of matrix elements [3]. Especially relevant are the tails of such distributions since they prescribe the probability of appearance of the large matrix elements. From the point of view of the mechanism producing the energy gaps they are most effective in generating a local reduction of dimensionality responsible for such effects. In principle, the probability distribution of the shell model matrix elements is prescribed by their general structure expressed by the eq. (1), provided the probability distributions of both $g^{J'}_{ii'}$ and $c^{J\alpha\alpha'}_{J'ii'}$ are known. In general terms this structure can be considered to have the following form:

$$V = \sum_{i=1}^{N} V_i. \tag{2}$$

and each V_i to be a product of another two variables denoted as C_i and G_i. By making use of the convolution theorem the probability distribution $P_V(v)$ that V assumes a value equal to v can be expressed as $P_V(v) = F^{-1}[F(P_{V_1}(v_1)) \cdot F(P_{V_2}(v_2)) \cdot \ldots \cdot F(P_{V_N}(v_N))]$, where F denotes a Fourier transform, F^{-1} its inverse and $P_{V_i}(v_i)$ the probability distributions of individual terms V_i. Taking in addition into account the fact that

$$P_{V_i}(v_i) = \int dg_i P_{G_i}(g_i) P_{C_i}(v_i/g_i)/|g_i| \tag{3}$$

one can explicitly derive the form of $P_V(v)$ in several cases. Assuming all the above constituents are identically Gaussian distributed ($P_{V_i}(v_i) = K_0(|v_i|)/\pi$ and thus $F(P_{V_i}(v_i)) = 1/\sqrt{1+\omega^2}$) one arrives at

$$P_V(v) = \frac{|v|^{(N-1)/2} K_{(N-1)/2}(|v|)}{2^{(N-1)/2}\Gamma(N/2)\sqrt{\pi}}, \tag{4}$$

where K stands for the modified Bessel function. Asymptotically, for large v, this leads to $P_V(v) \sim \exp(-v) W^{N/2-1}(v)$, where W^L denotes a polynomial of order L. For such a global estimate the identical Gaussian distribution of $g^{J'}_{ii'}$ is consistent both with the Two-Body Random Ensemble (TBRE) and with the Random Quasiparticle Ensemble (RQE). The only anticipated difference originates from the fact that in the second case the variance of the distribution drops down with J' like the inverse of $2J' + 1$ which is expected to result in a smaller effective N as compared to TBRE. By contrast, in both versions of the above random ensembles the geometry expressed by $c^{J\alpha\alpha'}_{J'ii'}$ enters explicitly. However, the complicated quasi-random coupling of individual spins is believed to result in the so-called geometric chaoticity. An explicit verification shows [2] that the Gaussian may be considered quite a reasonable representation of the distribution of such factors for all combinations of J and J' with one exception for those which involve $J = 0$. In this later case the distribution of $c^{0\alpha\alpha'}_{J'ii'}$ resembles more a uniform distribution over a finite interval located symmetrically with respect to zero. These empirical facts justify well the estimates of $P_V(v)$ based on eq. (4) for $J \neq 0$ and not so well for $J = 0$. More appropriate in this particular case is to assume a uniform distribution of $c^{0\alpha\alpha'}_{J'ii'}$ over an interval confined by say $-c_0$ and c_0, i.e., $P_{C_i}(c_i) = 1/2c_0$, retaining $P_{G_i}(g_i)$ in its original Gaussian form of course. By making use of eqs. (2) and (3) one then obtains

$$P_V(v) = \frac{1}{\sqrt{2\pi}} \int_0^\infty \left[\frac{erf(c_0\omega/\sqrt{2})}{c_0\omega}\right]^N \cos(\omega v) d\omega \tag{5}$$

which for large v behaves like

$$P_V(v) \sim \exp(-v^2). \tag{6}$$

The probability of appearance of a large off-diagonal matrix element which in magnitude overwhelms the remaining ones is thus greater for $J \neq 0$ than for $J = 0$.

References:

[1] C.W. Johnson, G.F. Bertsch and D.J. Dean, Phys. Rev. Lett. **80**, 2749(1998).
[2] S. Drożdż and M. Wójcik, Physica A **301**, 291 (2001).
[3] S. Drożdż, S. Nishizaki, J. Speth and M. Wójcik, Phys. Rev. E **57**, 4016(1998).

* Institut für Kernphysik, Forschungszentrum Jülich, D-52425 Jülich, Germany
Institute of Nuclear Physics, PL–31-342 Kraków, Poland

Wave Chaos in Elastodynamic Cavity Scattering

A. Wirzba, N. Søndergaard* and P. Cvitanović**

The Gutzwiller semiclassical quantization of classically chaotic systems relates quantum observables such as spectral densities to sums over classical unstable periodic orbits [1, 2]. The work presented here [3] is a step towards a formulation of such approximate short-wavelength theory of wave chaos for the case of linear elastodynamics [4]. Why elastodynamics? The elastodynamics experiments initiated by Oxborrow *et al.* [5] attain Q values as high as $5 \cdot 10^6$, making spectral measurements in elastodynamics competitive with measurements in microwave cavities at liquid helium temperatures [6], and vastly superior to nuclear physics and room temperature microwave experiments for which the Q values are orders of magnitude lower, typically $\sim 10^2$–10^3. Elastodynamic experiments are also more flexible and much cheaper than the competitors in atomic physics, helium-cooled microwave cavities or solid state nano-devices.

So far, for elastodynamics there is neither an experimental demonstration of existence of unstable periodic orbits nor a theory that would predict them. While Oxborrow *et al.* measure accurately half a million spectral lines, the current theory has been barely adequate for computation of dozens of resonances. This unsatisfactory state of affairs is the *raison d'être* for the theoretical effort undertaken in this work.

While current experiments excel in measurements of eigenspectra of *compact resonators*, the periodic orbit theory computations of such bound system spectra are rendered difficult by presence of non-hyperbolic phase space regions. As our primary goal is to derive and test rules for replacing wave mechanics by the high-frequency ray-dynamic trajectories, we have instead concentrated in this work on the problem of *scattering* off cylindrical cavities, for which the classical dynamics is fully under control.

In the case of one cavity the exact scattering spectrum is known [7]. For the multiple cavities case we have generalized the S-matrix formalism developed for the quantum-mechanical n-disk scattering [8, 9, 10, 11], and have computed the exact scattering resonances and the Wigner time delays from the full elastodynamic wave-mechanical scattering matrix for a quasi-two-dimensional isotropic and homogenous elastodynamic slab with several cylindrical cavities.

We have then compared the exact results with the corresponding quantities calculated in the short-wavelength approximation, and discovered that the quantum-mechanical intuition failed us: the Rayleigh surface waves (which have no analog in the quantum scattering problem) dominate the spectrum, rendering even a two-disk elastodynamic scattering problem chaotic.

To the second order in the cumulant expansion of the exact multiscattering matrix, the short-wavelength ray-dynamics estimates and the exact Wigner time delays for the two-cavity system are in good agreement. In fact, in the high frequency limit both classical and complex periodic orbits contribute, with each complex orbit composed of sequences of classical particle trajectory segments with varying polarizations interspersed with surface wave segments. The shortest of these orbits suffice to interpret exact elastodynamic scattering resonances and Wigner time delays.

The two-cavity scattering system clearly demonstrates that surface orbits of Rayleigh type [12] dominate the leading part of the spectrum. They have no counterpart in quantum mechanics. In particular, the elastodynamic resonance spectrum for two-cavities scatterer is dominated by an infinite number of weakly attenuated complex periodic orbits of Rayleigh type, and is in that sense chaotic, contrary to the quantum mechanical case.

In contrast to the creeping rays [13] in the quantum mechanical case [14], so far we do not have a method to compute contributions of Rayleigh-type rays for arbitrary curved billiard boundaries, and extend the high-frequency approximation to lower frequencies. As long as this is so, we cannot state the full Gutzwiller-Voros type Zeta function for the elastodynamic case. Generalizations to anisotropic media (the highest Q-value experiments are performed on single crystals of quartz), and applications of the above ray-dynamics techniques to resonator geometries used in experiments remain open problems.

References:

[1] M.C. Gutzwiller, *Chaos in Classical and Quantum Mechanics* (Springer, New York, 1990).
[2] P. Cvitanović *et al.*, *Classical and Quantum Chaos*, `www.nbi.dk/ChaosBook/` (Niels Bohr Institute, Copenhagen, 2001).
[3] A. Wirzba, N. Søndergaard and P. Cvitanović, FZJ-IKP(TH)-2001-17, nlin.CD/0108053
[4] L.D. Landau and E.M. Lifshitz, *Theory of Elasticity* (Pergamon, Oxford, 1959).
[5] C. Ellegaard, T. Guhr, K. Lindemann, J. Nygaard and M. Oxborrow, Phys. Rev. Lett. **77**, 4918 (1996).
[6] H.-D. Gräf *et al.*, Phys. Rev. Lett. **69**, 1296 (1992); H. Alt *et al.*, Phys. Rev. Lett. **74** 62, (1995).
[7] J.L. Izbicki *et al.*, Wave Motion **28**, 227 (1998).
[8] M.V. Berry, Ann. Phys. (N.Y.) **131**, 163 (1981).
[9] P. Gaspard and S.A. Rice, J. Chem. Phys. **90**, 2225 (1989); **90**, 2242 (1989); **90**, 2255 (1989).
[10] A. Wirzba, CHAOS **2**, 77 (1992); Nucl. Phys. **A 560**, 136 (1993).
[11] A. Wirzba, Phys. Rep. **309**, 1 (1999).
[12] J.B. Keller and F.C. Karal, Jr., J. Acoust. Soc. Am. **36**, 32 (1964); J. Appl. Phys. **31**, 1039 (1960).
[13] W. Franz, Z. Naturforschung **9a**, 705 (1954).
[14] G. Vattay, A. Wirzba and P.E. Rosenqvist, Phys. Rev. Lett. **73**, 2304 (1994); P.E. Rosenqvist, G. Vattay and A. Wirzba, J. Stat. Phys. **83**, 243 (1996).

* Department of Physics & Astronomy, Northwestern University, Evanston, IL 60208-3112
and Theoretical Mechanics Department, University of Nottingham, Nottingham NG7 2RD, UK
** Center for Nonlinear Science, School of Physics, Georgia Institute of Technology, Atlanta, GA 30332-0430

III. Accelerator Division

5. COOLER SYNCHROTRON COSY

6. ION SOURCES, BEAM TRANSPORT, AND LINAC INJECTOR

7. SPECTROMETER BIG KARL

8. RADIATION PROTECTION

5. COOLER SYNCHROTRON COSY

Progress and Developments at COSY in 2001

U. Bechstedt, J. Dietrich, A. Lehrach, B. Lorentz, R. Maier,
D.Prasuhn, A.Schnase, H. Schneider, R.Stassen, H.J. Stein, H.Stockhorst, R.Tölle

Beam Time Statistics

With 7728 scheduled hours, of which 7251.5 were delivered, the reliability of all components of COSY was again illustrated. 76,1 % of the planned beamtime was used by experiments, the fraction of experimental beamtime with polarized protons being over 1/3.

Operation and Development

Also in 2001 the operation of the COSY accelerator facility could be successfully continued for internal as well as external experiments in hadron physics. Comprehensive studies were carried out to preserve the polarization of stored protons up to maximum momentum, resulting in an enlarged particle number at a high degree of polarization for the internal experiments EDDA and COSY 11, as well as for the external experiment TOF. In addition, the beam current of the polarized ion source could be increased further and the beam transmission in the external beamlines and cyclotron was improved. As a result, the number of stored protons reached up to $2 \cdot 10^{10}$ with a degree of polarization of 75% at 3.4 GeV/c. The experience gained in acceleration could also be used successfully to decelerate a polarized beam down to 1 GeV/c. Consequently, the EDDA experiment could take data not only in the upward but also in the downward ramp, which improved the statistics by nearly a factor of two. Further machine studies led to an increase in beam lifetime of more than one hour even without stochastic cooling. This result is very important for the internal experiments TRI and ANKE.

It was shown that the original COSY design momentum of 3.3 GeV/c could be extended to 3.65 GeV/c by carefully adjusting the machine parameters.

A series of machine experiments was specifically dedicated to electron cooling experiments in order to study the performance of electron cooling in COSY in more detail. The experiments [1] were carried out together with research visitors from Dubna and Novosibirsk, (members of the famous Novosibirsk group, the pioneers of electron cooling.) Focal points were the precise alignment of proton and electron beam [2], longitudinal cooling force measurements, limits for the proton current as function of the achievable emittances, proton beam instabilities during and after the cooling process [3], and further studies to increase the proton intensity by stacking. In all experiments the fast real time vectoranalyser developed in 1997 [4] turned out to be an outstanding device to observe the time evolution of beam distributions with great precision.

First adiabatic capture studies of an electron-cooled beam have been carried out. It turned out that the capture efficiency depends strongly on the instant at that the higher harmonic cavity is turned on and how fast the voltage is increased. Also, the ratio of the amplitudes of the first and third harmonic are expected to influence the capture efficiency. Here, further investigations are neccessary.

A beam profile monitor using a position sensitive micro channel plate (MCP) detector has been developed and was tested extensively [5].

A wall current monitor (WCM) that was formerly located in the ring, was installed in the experimental area of JESSICA for non-beam disturbing diagnostics of intensity and time structure of a fast extracted beam. Details of this broadband pick-up are presented in [6].

To investigate the beam position stability a round beam position monitor (BPM inner diameter 150 mm) from the same type of the COSY-ring monitors is now installed in the extraction beamline upstream to the JESSICA-target [6].

The control loop (Schneider Box) that keeps constant the counting rates in the ANKE experiment was further improved and successfully applied [7].

The work to realize a new injector for COSY was continued with high priority. This new injector aims to fill COSY with polarized and unpolarized protons or deuterons up to the space charge limit. A project study was carried out to establish the specifications of the new injector (superconducting linear accelerator with final energies between 50 and 60 MeV). The results were compiled in a conceptual design report [8] describing the machine as well as all necessary sub-systems including diagnostics, computer control and infra-structure.

Acceleration of a Stacked Beam

Figure 1 shows the stacking process over a period of

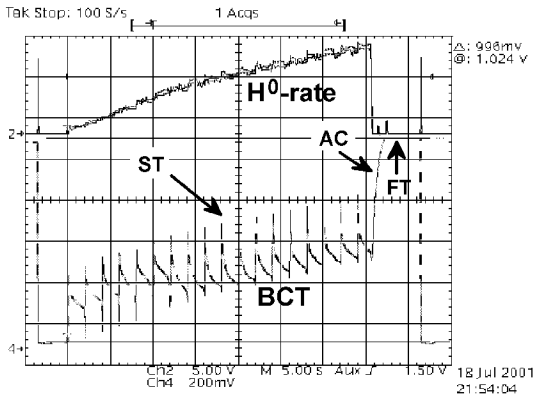

Fig. 1: Increasing beam current (BCT) during stacking (ST) of protons and acceleration (AC) to flat top (FT). During cooling the H^0 - rate is increasing. Horizontal scale: 5s/div.

about 30 s in which the beam current is increasing. Acceleration to the flat top momentum 1.57 GeV/c starts after 30 s. Such a stacked beam with about

$5 \cdot 10^{10}$ protons with emittances of about 3 μm is not stable [9]. However, its lifetime of about 2 s is sufficient for acceleration without losses in the beginning of the ramp if injection is stopped. This achievement will smoothen the way to the planned storage cell experiments that need low initial emittances and high proton currents, much more than the standard stripping injection at COSY can provide.

Fast Extraction of an Electron Cooled Beam

Fast kicker extraction is applied to deliver a short high intensity beam pulse to the JESSICA experiment that carries out studies for the ESS high power target. The successful fast kicker extraction [10] of an electron cooled beam for JESSICA since the year 1999 has demonstrated that the preparation of the proton beam at injection, i.e. reducing the beam size connected with an increase of phase space density can open new experimental possibilities at COSY.
The investigation of the fast kicker extraction was continued and a result is shown in figure 2. After about 18 s of cooling the beam is accelerated to 1.57 GeV/c. A fast kick is applied after 5 s flat top so that the beam bunch is kicked into the electrostatic septum within one turn.

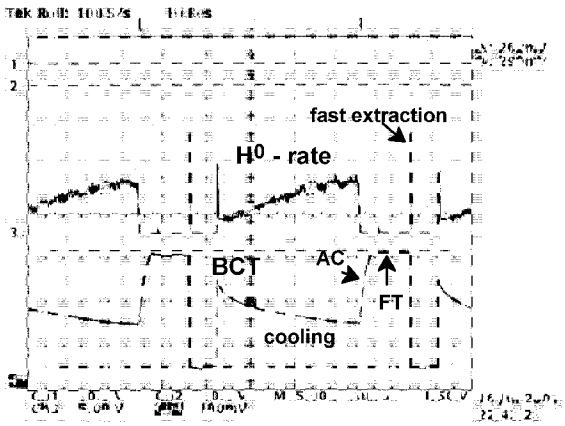

Fig. 2: Electron Cooling, acceleration (AC) to flat top (FT) and fast extraction after 5 s flat top. Horizontal scale: 5s/div.

It was proven that the required beam intensity of $2 \cdot 10^9$ protons in a pulse of 200 ns length could be reached.

Slow Extraction of an Electron Cooled Beam

In contrast to the fast kicker extraction method, stochastic extraction is capable for extracting the beam slowly over a long period of time. The beam particles are driven by swept noise into the 11/3 order resonance in the horizontal plane created by sextupoles [11]. In this extraction process the horizontal beam emittance is determined by the extraction mechanism, whereas the vertical emittance is determined solely by the optics of the COSY ring. Stochastic extraction is now applied routinely with an efficiency of more than 80% at proton momenta up to 3.4 GeV/c. This was achieved by theoretical as well as experimental studies of the extraction mechanism and improved diagnostic methods. In addition, careful optimizing the transmission of the external beamlines, tune and chromaticity adjustments as well as a careful positioning of the septa have significantly reduced beam losses to the external experiments. As a result, extraction rates up to 10^9 protons/s were measured. As requested by experiments, the proton beam was also slowly extracted over up to ten minutes.

Further, these improvements helped to extract a polarized beam of particular high quality to TOF.

By applying electron cooling at injection, it was possible to reduce the size of the extracted beam further, which significantly reduced the halo and thus the counting rates measured with the veto detectors at the experiment. This yielded a beam quality at the experiment BIG KRAL, which was never achieved before [12]. Figure 3 displays longitudinal spectra in a linear scale versus time of a beam with momentum 1.57 GeV/c observed at harmonic number 1000.

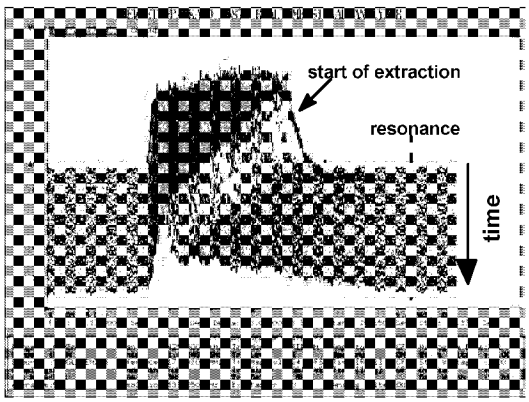

Fig.3: Time evolution of the beam distribution (linear scale) over app. ten seconds of stochastic extraction observed at the 1000th harmonic of the beam. The line marks the resonance where the beam density is zero.

The sweeping noise is moved with constant velocity from the higher frequency side into the waiting rectangularly shaped beam. The figure makes visible that the protons diffuse along a straight line into the resonance where they are extracted. During extraction the sharp low frequency edge moves through the stack. Note that the left-hand side of the stack is not affected. In figure 4 a snap shot shows a complete cycle in COSY. The beam is injected and electron-cooled as is visible in the increasing H^0 - rate. After loss-less acceleration to 1.57 GeV/c slow extraction starts after 5 s. The rectangularly shaped beam distribution and the constant sweep velocity of the extraction noise result in linear drop of the beam current. Hence, the mean spill is constant during extraction over nearly 10 s.

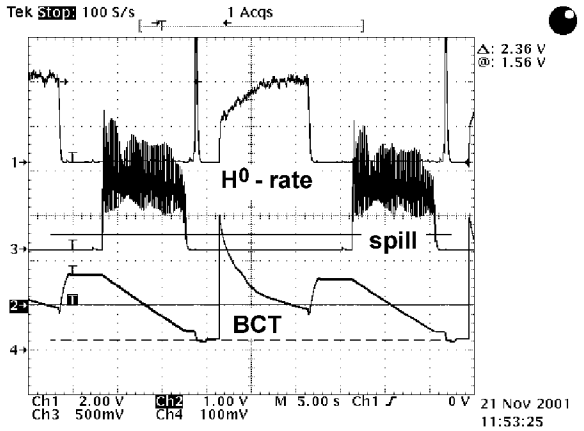

Fig. 4: At injection level the proton beam is electron-cooled as is visible in the increasing H^0- rate. After acceleration to 1.57 GeV/c the beam is slowly extracted. Horizontal scale: 5s/div.

Acknowledgement

We gratefully acknowledge the advice and help we received by our Russian colleagues I. Meshkov and A. Sidorin from Dubna and V. Parkhomchuk from Novosibirsk who participated in the electron cooling experiments. Their experience and engagement form the basis for a big step forward in understanding and applying electron cooling in COSY.

References

[1] J. Dietrich, R. Maier, I.N. Meshkov, V.V. Parkhomchuk, V.S. Kamerdjiev, D. Prasuhn, A. Sidorin, H.J. Stein, H. Stockhorst, J.D. Witt, *Laboratory Report* , in preparation

[2] A Sidorin, I.N. Meshkov, H.J. Stein, H. Stockhorst, *Natural neutralization in the e beam of the COSY electron cooler*, this Annual Report

[3] I.N. Meshkov, A. Sidorin, J. Dietrich, H.J. Stein, H. Stockhorst, R. Maier, D. Prasuhn, V.V Parkhomchuk, J.D. Witt, *Observation of instabilities of electron cooled p beams*, this Annual Report

[4] A. Schnase, J. Dietrich, F.-J. Etzkorn, R. Maier, H. Stockhorst, *VXI-based Realtime Vectoranalyser with embedded Risc-Workstation*, Annual Report 1997

[5] V. Kamerdjiev and J. Dietrich *Ionisation beam profile monitor*, this Annual Report

[6] J. Dietrich, K. Henn, I. Mohos, M. Simon *Beam position monitor in the extraction beamline to JESSICA*, this Annual Report

[7] U. Bechstedt et al., *Analogue Rate-Controller For ANKE*, this Annual Report

[8] *The Superconducting Injector LINAC for the Cooler Synchrotron COSY*, Conceptual Design Report, this Annual Report

[9] R. Maier, D. Prasuhn, H.J. Stein, J.D. Witt *Preparation of High-Intensity Low-Emittance Proton Beams by Electron Cooling in COSY*, IKP Annual Report 1999

[10] J. Dietrich, J. Bojowald, H. Labus, H. Lawin, I. Mohos *Fast Kicker Extraction at COSY-Jülich*, Proc. of the 7th Europ. Part. Acc. Conf., EPAC2000, June 2000, Vienna, Austria

[11] H. Stockhorst, A. Schnase, *Development of Beam Extraction*, IKP Annual Report 1995

[12] D. Prasuhn, H. Stockhorst, H.J. Stein, R. Maier, H. Machner and P.v. Rossen, *Electron Cooling and Slow Extraction,* this Annual Report

Electron Cooling and Slow Extraction

D.Prasuhn, H. Stockhorst, H. J. Stein, R. Maier, A. Magiera , H. Machner and P. v. Rossen

The COSY experiments GEM and TOF gain in resolution from a high brilliance beam at the target place. In order to increase the angular resolution veto counters with 3 mm small holes for the direct beam are installed close to the liquid hydrogen target cell. The accepted beam intensity in the experiment is then limited by the counting rate of the veto counter due to background or halo projectiles, i.e. extracted particles, which were scattered at the septum foil during the extraction process or hit the vacuum pipe somewhere on their way in the extraction beam line and were backscattered. From the experience in several experiments we know that the adjustment of the beam line magnets critically influences the counting rate on the veto counters. Especially the acceptance limitation in the vertical plane in the bending sections generates halo, which in normal cases could only be reduced to approximately 2.5% of the beam intensity.

So, after several accelerator tests with the electron cooled proton beam in COSY we set up an experiment to accelerate and extract the electron cooled beam. From beam transfer measurements and from the performance of the kicker extraction for JESSICA we know, that the small emittance of the electron cooled beam keeps preserved during the acceleration process. The extraction of the cooled beam was set up in the usual procedure with stochastic extraction. The cycle is displayed in figure 1.

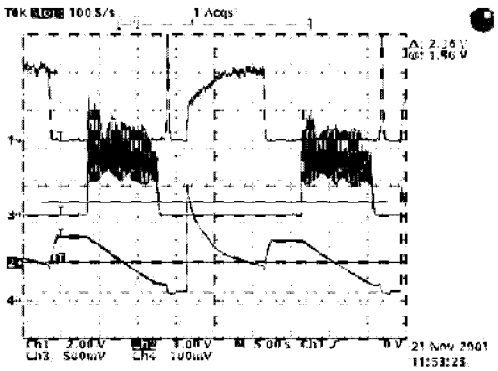

Fig. 1: The cycle for electron cooling and extraction. Trace 1 shows the H^0-counting rate from the electron cooling, trace 3 the counting rate from the external experiment, trace 4 the intensity signal of the circulating beam in COSY.

With an electron current of 250 mA it takes 10 s to cool the proton beam to the equilibrium emittances in the longitudinal and transverse planes. The intensity of the proton beam decreases during the cooling process to $1.2 \cdot 10^{10}$. They are bunched and accelerated without losses to 1571 MeV/c and extracted with an extraction efficiency of 80%. Extraction takes place over 10 s, which results in an intensity of 10^9 protons/s during the spill, but an averaged intensity of $5 \cdot 10^8$ protons/s.
The resulting beam spot on the viewer in the BIG KARL scattering chamber is shown in figure 2.

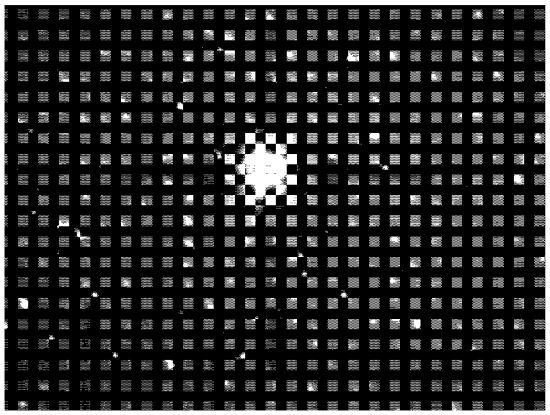

Fig. 2: The image of the electron cooled beam on the viewer in the BIG KARL scattering chamber. The marks indicate a distance of 2 mm from the origin of the cross.

But the real benefit of the extraction of the electron cooled beam is not the dimension of the beam spot but the disturbing halo. This could be decreased to less than $4 \cdot 10^{-4}$ of the beam intensity compared to 2.5% with the uncooled beam. Thus the primary beam intensity can be increased by a factor of 60 for the same veto counting rate. Table 1 compares the beam properties of the extracted beam with and without electron cooling.

	Without electron cooling	With electron cooling
Stored Beam Intensity	$4 \cdot 10^{10}$	$1 \cdot 10^{10}$
Shortest extraction time	10 s	10 s
Shortest cycle time	20 s	30 s
Extraction efficiency	75 %	80 %
Intensity in the spill	$3.0 \cdot 10^9$ p/s	$8.0 \cdot 10^8$ p/s
Cycle averaged beam intensity	$1.5 \cdot 10^9$ p/s	$2.7 \cdot 10^8$ p/s
Halo ratio for a 3 mm veto hole	$2.5 \cdot 10^{-2}$	$4.0 \cdot 10^{-4}$

Table 1: Comparison of parameters of the extracted beam with and without electron cooling

Observation of Instabilities of Electron Cooled Proton Beams

I.N. Meshkov[1], J. Dietrich, V.S. Kamerdjiev, R. Maier, V.V. Parkhomchuk[2], D. Prasuhn, A. Sidorin[1], H.J. Stein, H. Stockhorst, J.-D. Witt

At optimal settings of the COSY machine parameters the process of proton beam stacking can be used to increase the cooled p intensity [1]. After the cooling time of a first injected beam, a newly injected beam is cooled onto the stored cold beam. If the time interval between two consecutive injections is prolonged to more than 20 s, typical fast beam losses were observed which limit the attainable beam intensity. In Fig. 1 is shown an example where the injections occurred every 30 s. The lower curve represents the p beam current versus time measured by the beam current transformer (BCT monitor), the upper curve is the counting rate from the neutral particle detector (H^0 monitor) which serves as the characteristic signal for the cooling process. One can differentiate four characteristic time domains. (i) In the first 10 s during the cooling process a fast decay ($\tau \approx 3$ s) of the intensity of the freshly injected p beam. Then, (ii) a short period of about 7 s with almost constant p current and H^0 rate, indicating that cooling is accomplished. After 17 s (iii) a fast intensity drop of 50 % ($\tau \approx 2$ s) followed (iv) by a further, but slow intensity decrease (τ □ 10 s) of p current and H^0 rate.

Such a behaviour of the p beam has been observed earlier many times. The loss after injection might be related to the fact that in COSY the diameter of the injected p beam (stripping injection at $p_{inj} = 294$ MeV/c) is larger than the e beam diameter as well as to incoherent space charge limitations due to the shrinking diameter of the p beam. The second loss, occurring intensified at beam intensities above 5×10^9 p, is evidently connected with the high phase space density of the cooled beam. One can assume that the p beam becomes unstable which leads to particle losses.

In July 2001 we investigated the instability phenomenon the first time in some detail. The first hint of a peculiar behaviour of the stored cooled p beam was the appearance of a triple peak structure in the longitudinal Schottky spectrum. In Fig. 2 is shown a sequence of Schottky spectra recorded in the same time interval between two injections as shown in Fig. 1. The "classical" double peak, which appeared after some proper cooling, was followed by a structure with an additional third peak in the center. The central peak, which corresponds to the exact revolution frequency, appeared 8 s after injection. The triple peak structure was then present until the end of the 30 s cycle. In parallel to the longitudinal Schottky measurements, we

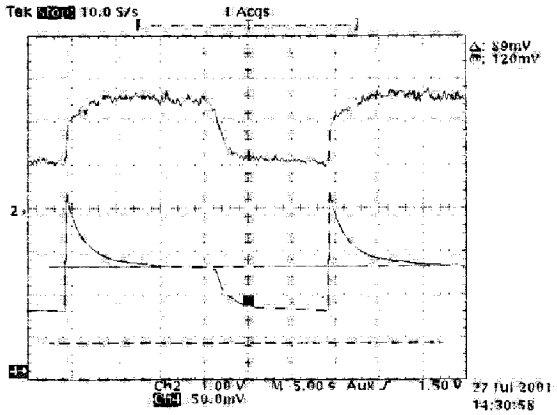

Fig.1: Proton beam current (lower curve) and H^0 count rate (upper curve) versus time at continuously repeated injections. Two consecutive injections are shown. Scaling: time 5 s/div, proton current 50 mV/div = 0.5 mA ≈ 6×10^9 protons, H^0 count rate 1 V/div = 3000 Hz. The dashed line indicates zero intensity for the proton beam.

investigated the transverse Schottky noise with the high-performance vector analyzer [2] which can measure, store and visualize the sequence of a large number of spectra in a moviefilm-like manner, see Fig. 3. The plot is shown in spectrogram mode, i.e. the degree of brightness (in the original plot different colors) is a measure for the signal strength. Recorded in the same period as shown in Fig.1, the tranverse Schottky spectrum in the betatron frequency range clearly demonstrates the process of instability development. Just after injection a weak signal of the horizontal betatron oscillation appears, shifting during the next 8 s by 1.4 kHz to a lower frequency ($\Delta Q_x = + 0.003$). Suddenly, after 8 s the f_x signal becomes very strong, exactly at the time when the central peak appears in the longitudinal Schottky spectrum. This transverse signal remains strong until at about 17 s it jumps to the tune of the vertical plane. This is the time when the second strong intensity loss occurs (see Fig.1). It is obvious that the transverse Schottky signals are caused by coherent oscillations of the p beam. They were also observed in the time domain by recording analog signals from three of the

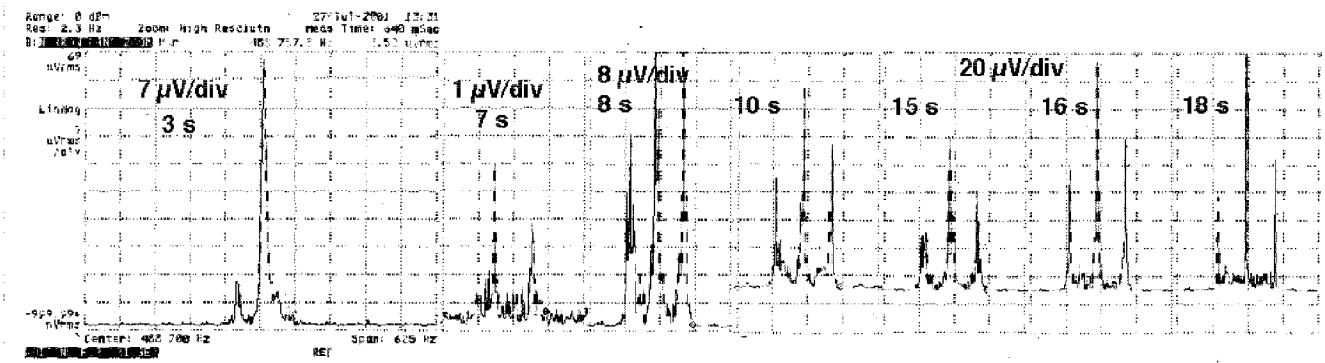

Fig. 2: Longitudinal Schottky noise spectra recorded by triggering at characteristic times after injection. Frequency scale 62.5 Hz/div., central peak frequency 488.7 kHz, amplitude scale linear. Note the different scaling for records at different times.

beam position monitors (BPM's) in the COSY ring. One was measuring the sum signal, the other two the difference signals in the horizontal and the vertical plane.

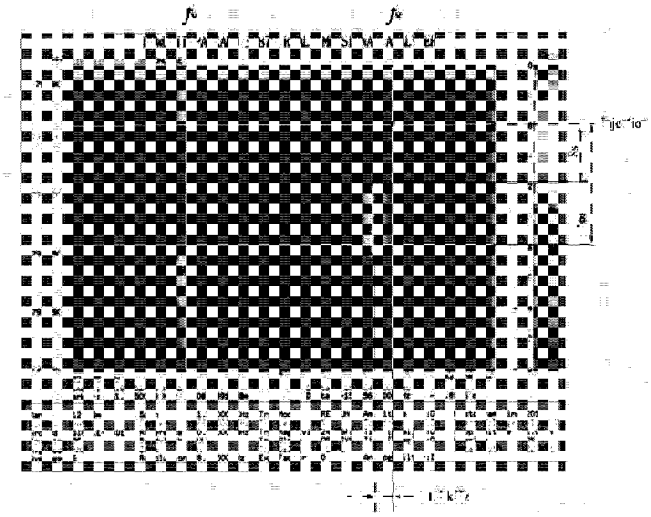

Fig. 3: Spectrogram of the transverse Schottky noise in the same time region as in Fig. 1. f_x = 676.92, f_y = 662.19 kHz are the horizontal and vertical betatron frequencies (measured tunes Q_x = 3.620, Q_y = 3.645), the black dot indicates injection time and frequency. The shift Δf = −1.4 kHz during cooling corresponds to a positive tune shift ΔQ_x = 0.003. 8 s after injection, at the same time when longitudinally the third peak appears, the f_x amplitude gets very strong remaining almost constant the next 8 s. Between 16 and 18 s the Schottky signal moves to the vertical tune and stays there until the end of the cycle. (In the electronic version the details can be made visible by copying and scaling-up the figure.)

In Fig 4 are shown oscillograms recorded at some of the characteristic times within the observed cycle. Without going into details, one can observe the following features. At 3 s the H signal is flat, but at 10 s it shows the betatron oscillations which at the same time is seen in the freqency domain (see Fig. 3). Between 16.0 and 16.5 s the transition of the oscillations from the horizontal to the vertical plane is occurring. Here, the transition appears more abrupt than seen in Fig. 3. The S signal is always present, but stronger and more regular when the transverse oscillations are seen.

All these interesting phenomena are experimental facts, definite conclusions, however, cannot be drawn at the moment. Many questions have been left open, for instance, we note that the strong fast loss (see Fig.1) could be suppressed by applying longitudinal electronic noise to the proton beam. Nevertheless, the life time of the proton beam was still much poorer than one would expect from the basic principle of electron cooling. Long life times are obtained only at low proton intensities ≤ 10^9 p. In addition, a dependence on the electron current was also found. The measurement results shown in this contribution were all obtained with 250 mA electron current corresponding to a volume density of 0.34×10^8 electrons/cm^3. When the electron current was increased the instability developed in shorter time accompanied with a stronger particle loss. The electron beam has not only the desired cooling effect but has also a parasitic influence on the p beam. Here, we refer to Ref. 3 where such aspects, known as the phenomenon of "electron heating", are addressed.

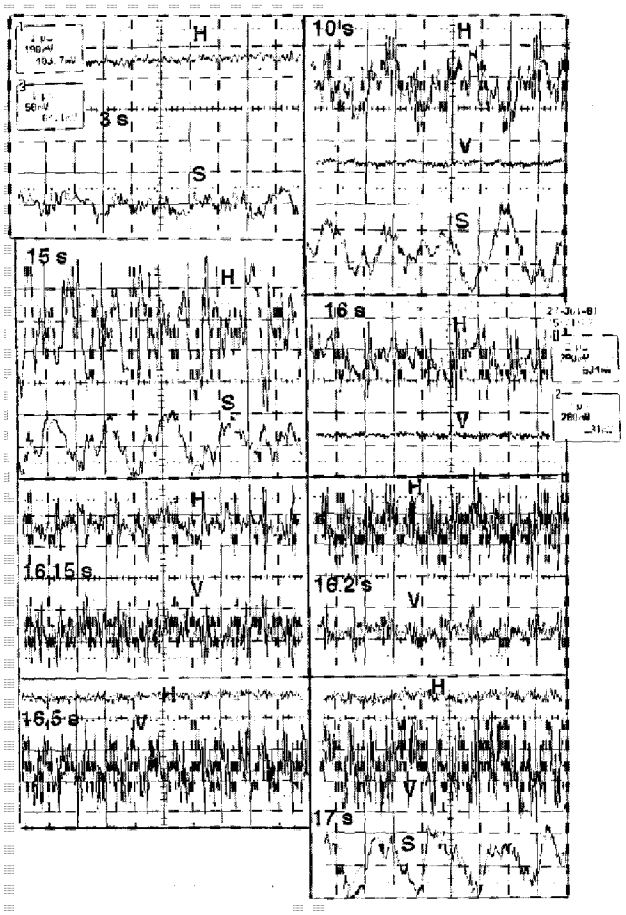

Fig. 4: BPM analog signals clearly demonstrating the collective oscillations of the p beam H denotes the horizontal difference signal, V the vertical difference signal, and S the sum signal from the BPM electrodes, time scale either 1 or 2 μs/div, amplitude scaling 50 mV/div for S and 100 or 200 mV/div for H and V.

Despite the unsolved problems, the electron cooling experiments in week 18 and week 30 of the year 2001 resulted in clear guidelines in which direction the investigations shall be continued [4]. This will be useful for a better understanding of the general problems of electron cooling as well as for the success of specific physics experiments at COSY [5].

References:

[1] U. Bechstedt et al., Progress and Development at COSY in 2001, this Annual Report.

[2] A. Schnase, VXI-based Realtime.Vectoranalyser with embedded Risc-Workstation, IKP Annual Report 1977, Report Jül-3505 (1998) 188.

[3] V.V. Parkhomchuk, New Insights in the Theory of Electron Cooling,.Nucl. Instrum. Methods Phys. Res. A441 (2000) 9-17.

[4] Results from the Electron Cooling Experiments 2001 at COSY, IKP Laboratory Report in preparation.

[5] D. Prasuhn et al., Electron Cooling and Slow Extraction, this Annual Report.

[1] JINR, Dubna

[2] Budker INP, Novosibirsk

Natural Neutralization in the Electron Beam of the COSY Electron Cooler

A. Sidorin[1], I.N. Meshkov[1], H.J. Stein, H. Stockhorst

The space charge of the electron beam inside the beam tube causes a potential depression on the axis of the electron beam lowering the energy of a cooled beam compared to the voltage setting of the cathode. The higher the electron current the higher the electron beam voltage has to be in order to keep the proton energy constant. The revolution frequency of the p beam is used to observe energy changes. In Fig. 1 is shown the necessary increase of the e beam voltage at increasing e beam current on the condition of constant revolution frequency.

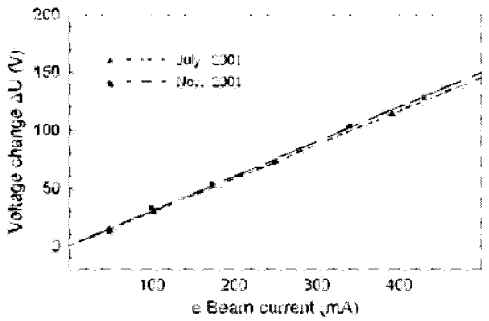

Fig. 1: Necessary e beam voltage change to achieve the same p beam revolution frequency at increasing e beam current.

The e beam considered as a homogeneously charged cylinder inside the round beam tube of the cooling section yields a slope of 45 V/100 mA whereas the measured slope is 30 V/100 mA. The difference is caused by partial neutralization of the e beam by positive ions trapped in the potential well formed by the geometry of the beam tubes. The diameter in the cooling section is twice larger than in the gun and the collector section. Evidently, the COSY electron cooler operates with a constant natural neutralization of 34%.

Theoretically, the space charge potential inside the e beam should be parabolic. The cooled p beam has a small enough diameter to be used for scanning the space charge parabola. Here, the shift of the p beam revolution frequency is used to make visible the potential change. Provided that e and p beam are well aligned, the minimum of the parabola indicates how well the p beam is centered inside the e beam. Fig. 2 shows a result for 200 mA e beam current. The minima of the fitted parabolas show that the p beam was about −2 mm horizontally and +1 mm vertically displaced from the e beam axis. Dispersion in the cooling section (− 6.3 m) causes an additional displacement of the p beam due to its energy change. In Fig. 3. are shown the measured parabolas corrected for dispersion [1], normalized to the same origin, and compared with the theoretical parabola for 200 mA current and 34% neutralization.

Optimal cooling requires a very precise alignment of p and e beam. The appropriate diagnostic tool for alignment is the neutral-particle profile detector [1]. Here, the widths of the H^0 transverse profiles which characterize the p beam divergence can be minimized. The results shown in Fig. 4 prove that already without aligment steering the p beam quality was sufficient for the displacement measurements. It is interesting to note that in the horizontal plane the H^0 width is extremely sensitive to small angle variations, whereas the dependence in the vertical plane is flat, at least within ± 0.4 mrad.

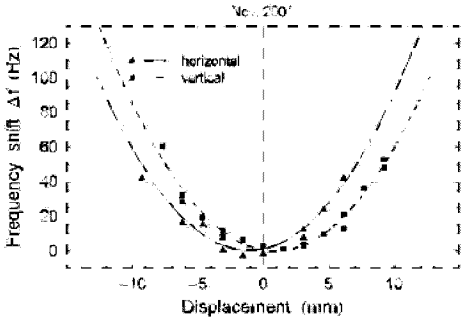

Fig. 2: Shift of the revolution frequency (f_0 = 488.657 kHz) by displacing the e beam from its natural zero position, e beam current 200 mA, angle steering coils inactive.

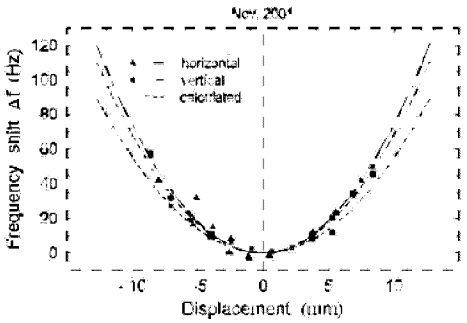

Fig. 3: Space charge parabolas corrected for dispersion and normalized to equal origin. The measured parabolas do agree well. The calculated parabola corresponds to a 200 mA e beam with 34% neutralization. The agreement with the calculated parabola is satisfying. Full agreement with the measured parabolas would be obtained with 20% neutralization.

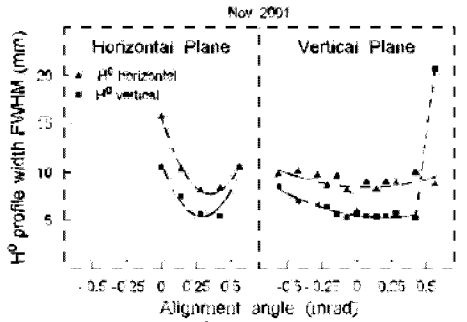

Fig. 4: Dependence of the H^0 width on the alignment of the e beam, position steering coils inactive. For the vertical plane the horizontal setting was + 0.35 mrad. The minima of the H^0 widths correspond to 2 σ emittances of about 0.5 μm obtained at low p beam intensity (≈ 10^9 p).

Finding the minima of the space charge parabolas and the minimum widths of the H^0 profiles is an easy exercise which guarantees the best cooling conditions. It should be performed before any electron cooling experiment or application is started.

References:

[1] Results from the Electron Cooling Experiments 2001 at COSY, IKP Laboratory Report in preparation.

[1] JINR, Dubna

Analogue Rate-Controller For ANKE

U. Bechstedt, P. Birx, M. Böhnke, J. Dietrich, H. Borsch, R. Hecker, K. Kruck, A. Lehrach, B. Lorentz, R. Maier, D. Prasuhn, J. Schmitz A. Schnase, H. Schneider*, R. Stassen, H. Stockhorst, R. Tölle,

For a high efficiency on the Solid Target the internal experiment ANKE needs an evenly distributed rate of protons. The involved steering magnets SV24 and SV34 are supplied by currents ramping with constant di/dt. That leads to a Gauss-shaped signal on the rate-meter (Figure 2).
Different distribution requires a complex calculation of set-values, conjoined with many hours for development. Because of this reason for ANKE a rate-controller is installed now. It keeps the rate on the target during the whole flat-top constant (Figure 3). Figure 1 shows the circuit in principle.

The principle of function

The controller compares the set-value adjusted for the experiment with the actual-value delivered by the rate-meter. As result it generates a correction signal. That will be added to the standard linear ramped current gives a new set-value for **one** of the involved steering power converters (presently SV24). Depending on building in of the target a vertical or horizontal acting correction element is integrated into the controlling-circuit.

The development of the controller includes the investigation into the dynamic properties of all components. As low-pass are considered the rate-meter, the du/dt-limiter and the combination of power converter and magnet. Beam, target and detector are regarded as proportional blocks. The controller itself acts with PI-behaviour.

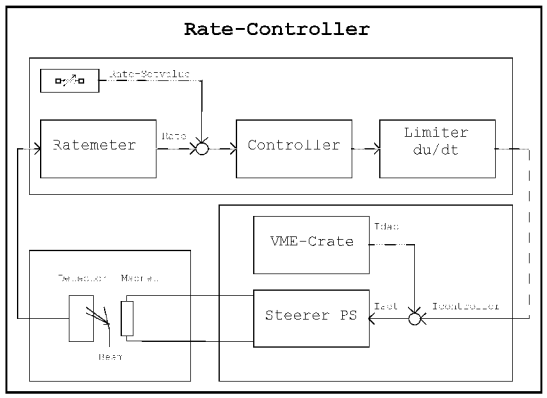

Figure 1: Block diagram of the rate-controller

Timing

During injection and acceleration the controller is disabled. Only after the preparation of beam properties is finished it becomes active. The Timing System of COSY provides the signal for the control. A skilful adjusted set-value allows the complete consumption of the beam, with constant rate, during flattop-phase.

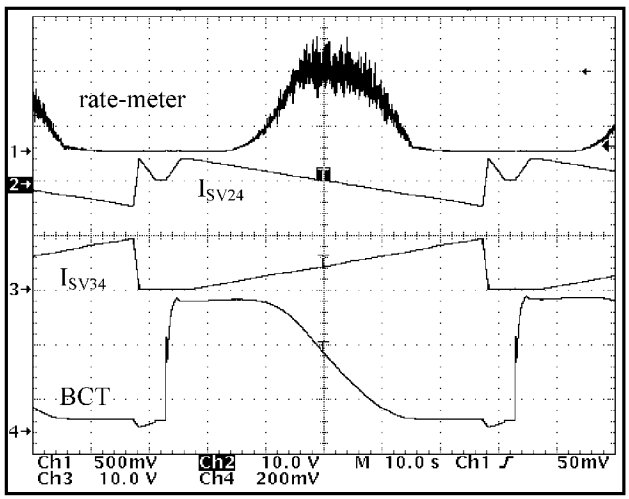

Figure 2: Signals without rate-controller

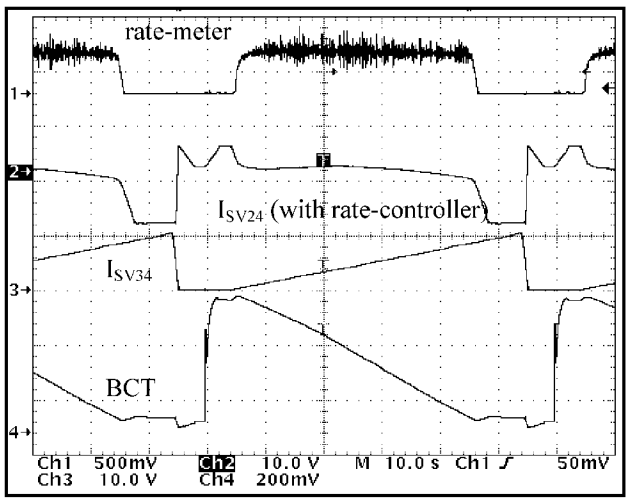

Figure 3: Signals with rate-controller

Upgrade of digital noise generation for Ultra Slow Extraction at COSY

A. Schnase, F.-J. Etzkorn, H. Stockhorst

At COSY, the slow extraction of the proton beam for extraction times longer than 10 seconds is usually performed by applying band limited noise to the beam.
Feedback of the spill signal measured by experiments who used the extracted proton beam show, that there is some variation of the particle flux.
The fluctuations in the order of 6 Hz seem to correspond to the repetition frequency of the synthesizer who generates the bandlimited noise for Ultra-Slow-Extraction (USE). A simplified layout of this system is shown in fig. 1.

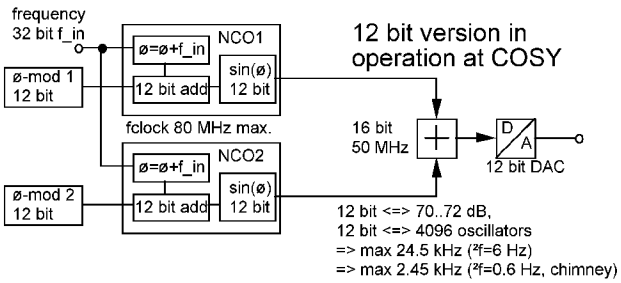

Fig. 1: Noise synthesis with 12 bit resolution

Triggered by mobile communication, the performance of digital-to-analogue converters improves. Therefore we re-arranged the system layout to upgrade from 12 bit to 16 bit signal paths. The set-up is shown in fig. 2.

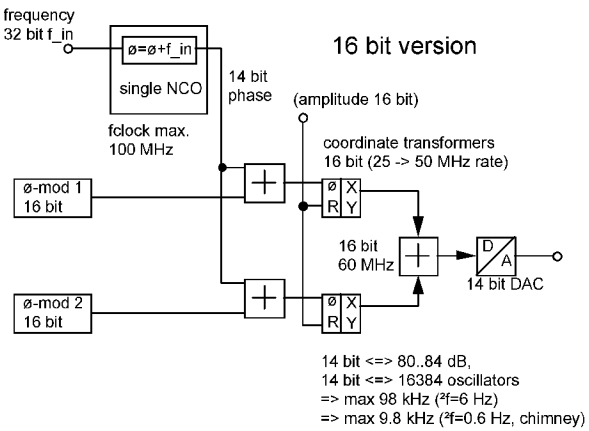

Fig. 2: Noise synthesis with 14/16 bit resolution

The VME-board shown in fig.4 uses 14 bit technology for the Digital-Analogue conversion and Numerical oscillator and 16 bit arithmetic for phase modulation and coordinate transformation at a maximum clock of 50 MHz. To obtain best performance, we found that the clock has to be less than 45 MHz. At higher rates, the coordinate transformers produce less accurate results.
When we started to compare the measured noise spectra of the 14/16 bit device to the 12 bit system, we found not much difference. Then we programmed noise-sequences with artificially reduced accuracy. We learned, that the measurement is already at the noise floor limit of the FFT-analyser HP 89440.

Then we measured with the VXI "HP 3587 Realtime Signal Analyzer" which has a higher dynamic range. Figure 3 shows the results, which are collected in the table below. The results confirm the improvement.

resolution of phase-modulation	8 bit	10 bit	12 bit	16 bit
dynamic range / dB	62.3	76.4	87.8	92.0

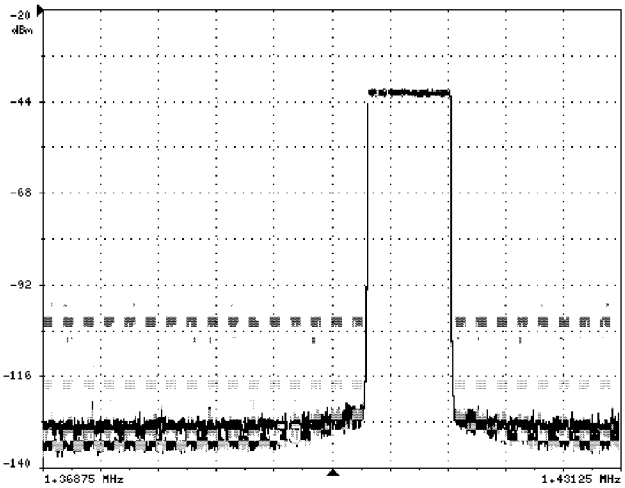

Fig. 3: Rectangular noise spectra with 12 dB/div.
From Top to Bottom: 8, 10, 12, and 16 bit phase-modulation,

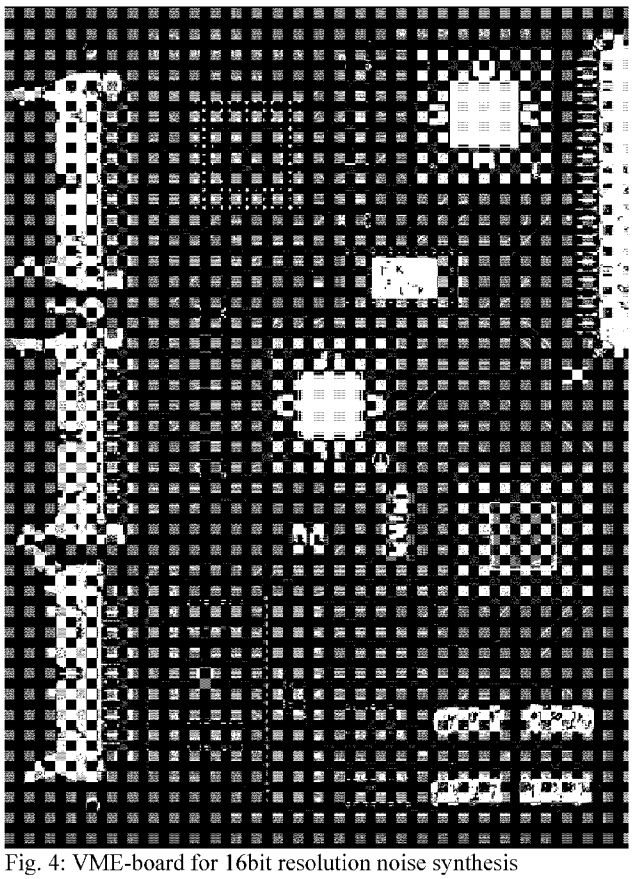

Fig. 4: VME-board for 16bit resolution noise synthesis

New detector for spill measurements

H.Labus, G.Lürken, I.Mohos, J.Dietrich

The new detector for spill measurements is designed to measure with one compact device high resolution time structure and absolute intensity of extracted proton beams with energies above 50 MeV . The detector is suited for different type of extraction, from ultra slow to kicker extraction, within an extremely wide intensity range from 0 to 10^{16}/s.

The device consists of two different detectors mounted in a steel pot of at least 92mm inner diameter which in this case is connected to an CF100 cylinder via a bellow and can be moved pneumatically to and from the measurement position within < 5s. The detectors works at normal air condition which is a great advantage concerning costs and service especially with large UHV-facilities. The wall of the steel pot is no real disadvantage as ultra slow extracted beams have uniform intensity and can not be detected with non disturbing devices as beam position monitors or wall current monitors which need a pulsed beam. The thickness of the steel pot is 1mm but can be made 0.1mm around the sensitive area of the detectors so even protons with energy below 50 MeV can be detected.

The first detector consists of two adjacent PMTs (photo multiplier tubes) each in variable light contact with a thin (2 to 5 mm) square shaped (65*65 mm for CF63 beam tubes) plastic scintillator. Coincidence between the PMTs yields background free absolute intensity in the range 0 to $5*10^6$/s. The variable light contact is performed by a switch selectable optical filter to reduce the light current to the PMTs by a factor of 10^4 to 10^6 to analyse the time structure of proton bursts from kicker extraction. In this case rates of 10^{16}/s may occur within 1 µs . Only the absolute intensity is then not available as the amplification of PMTs is normally unknown and not stable within an order of magnitude. The average anode current of one PMT reduced by its dark current is a measure of the proton rate if gamma background can be neglected. This measure is relative due the unknown PMT amplification and average number of photoelectrons per proton but can be calibrated by the absolute intensity from the coincidence rate between 10^4/s and 10^6/s. The dark current must be measured within the extraction time of one cycle before the measurement cycle to take into account the gamma background as good as possible. The total influence of the gamma background, which should normally be neglectable due to the small volume scintillators can be checked without beam. For rates above 10^8 the PMT amplification must be reduced by lowering the HV (high voltage) to stay below maximum anode current and within fair linearity. From dark current measurement as a function of HV the necessary HV reduction for 10 or 100 times lower amplification can be found. If the attenuation of the optical filter would be known also the particle number within a proton burst could be measured absolutely. This attenuation ($>10^5$) can be measured at stochastic extraction with high rates above 10^8/s by measuring the average anode current with and without optical filter .

The second detector is an ionisation chamber mounted in the gap between the scintillators, followed by a current voltage converter with programmable gain for absolute intensity measurements of the higher rates from 10^4/s to 10^{10}/s and fair time resolution from DC to some hundred Hz. There is still a certain advantage if an additional ionisation chamber is used. It is possible to compare its absolute extraction intensity with the values from the average anode current of the PMT above 10^5/s. Recombination losses due to the extremely high space charge up to 10^{12} ion pairs /cm^3 could be tested in an ionisation chamber with the kicker extraction. Simultaneous measurement with a wall current monitor could also answer this question. A much more practical advantage of an ionisation chamber is its use as a beam center and rough profile indicator if the electrode is divided into segments each with a separate electronic read out. In our case the electrode is divided in 6 segments (see Fig.1).

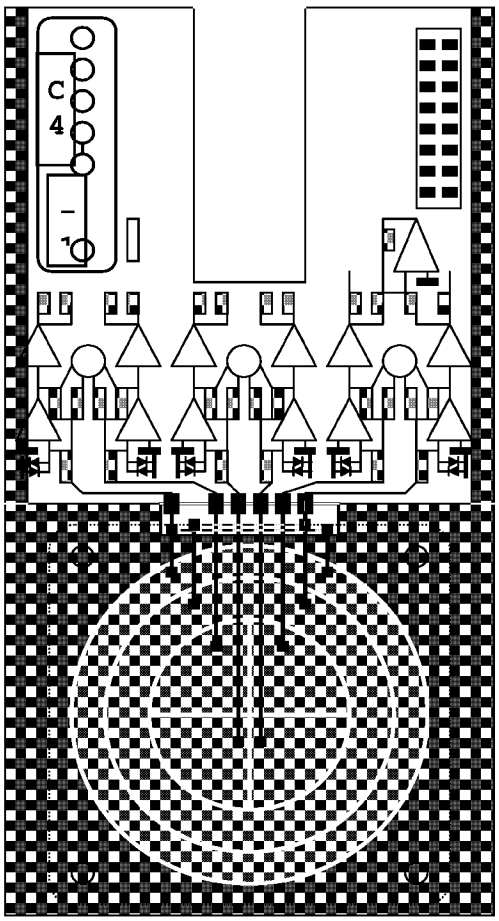

Figure 1: Platine for the ionisation chamber with 6 segments

6. ION SOURCES, BEAM TRANSPORT, AND LINAC INJECTOR

Ionisation beam profile monitor

V. Kamerdjiev and J. Dietrich

A profile monitor using a position sensitive micro channel plate (MCP) detector [1] has been developed at the University of Bonn [2] and was tested and modified at FZ-Jülich [3]. A parallel ion drift field is maintained in the 130 mm wide gap between two electrodes. Residual gas ions are drifted onto an MCP assembly that provides a charge gain of about 10^7. The secondary charge produced from each ion is collected by a wedge and strip anode. The anode signal is then integrated by a capacitor, amplified and delayed for proper gating during the digitization. The read out is done by means of a PC running a user friendly Cobold PC program [1] under Windows OS.

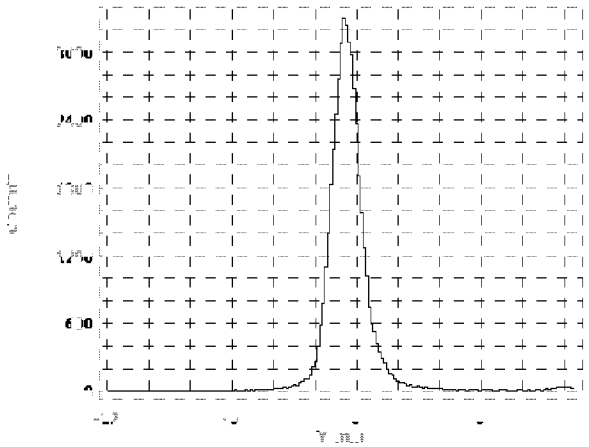

Figure 1: Vertical beam profile after electron cooling.

Since COSY operates with beam intensities up to 10^{11} protons and a vacuum of 10^{-10} mbar, there is a big risk of radiation damage of the detector. Hence the MCP voltage is switched on only during the measurement (typically a few seconds). Also a pneumatically driven protection screen is installed to prevent detector irradiation during the routine operation of the accelerator. Profile measurements have been carried out for beam intensities up to $2 \cdot 10^9$ protons. Fig.1 shows the vertical beam profile after electron cooling for 6×10^7 protons at 40 MeV.

The ionisation beam profile monitor is used in routine operation. However, the comparison with two other methods shows that in case of cooled beam the profile is wider then the one measured by H^0 monitor, but if the beam was not cooled the profile is narrower then the one measured with EDDA wire target. This fact has not been properly understood yet.

Monitor optics simulations show that potential distribution results in a slightly divergent effect on the residual gas ion trajectories (Fig. 2). The optics of this monitor is under further investigation. The lifetime of the channel plates and the event rate are crucial issues for the measurement of intense proton beams.

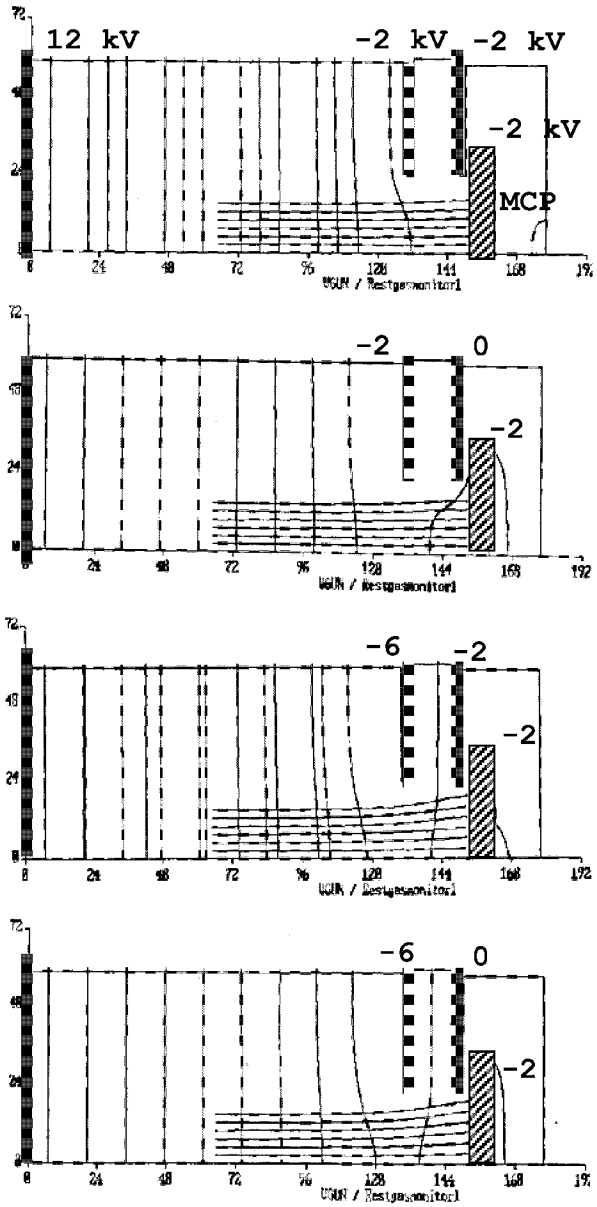

Figure 2: Trajectories of residual gas ions for different potential distributions calculated with the Herrmannsfeldt program EGUN (axis in [mm]).

References:

[1] RoentDek Handels GmbH, Frankfurt, Germany.
[2] M. Schulz-Rojahn," Messung von Strahlprofilen am internen COSY-Protonenstrahl mittels Restgasionisation", Doctor's thesis, Bonn, 1998.
[3] V. Kamerdjiev, Diploma thesis, FZ Jülich, 2000

Highly sensitive current measurement electronics

I. Mohos and J.Dietrich

The current measurement electronics (SME) consist of 32 precision low-noise integrating amplifiers with FET op amp, switchable integrating capacitors, and low leakage FET switches (Fig. 1). They integrate at the same time low-level input currents for a user-determined period, storing the resulting voltage on the integrating capacitor. Due to the very low noise and input leakage the electronics measure currents in order of pA. The input signal current can be positive or negative. Programmable timing controls the integration period, hold and reset functions to set the effective transimpedance gain and to reset (discharge) the integrator capacitor.

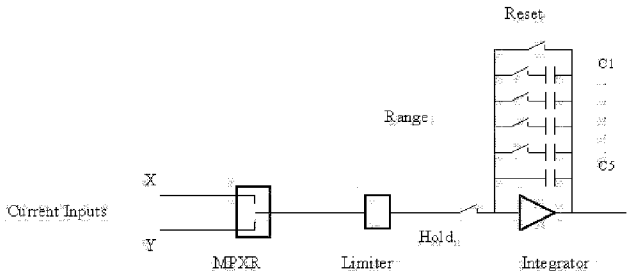

Figure 1:Schematic diagram of the i/U converter (1 of 32)

An input relay multiplexer selects the wire-plane for measurement. The trigger delay and integrating time is user programmable (1ms - 10 s), integrating capacitors between 10 pF and 100nF in five steps can be selected. A high resolution **(13bit+S)** ADC digitizes the integrator outputs sequentially. Automatic correction eliminates the integrator offsets depending on the integrating time and capacitor. The offset values measured in beam pauses are stored into a two dimensional array. After each current measurement the corresponding stored offset will be subtracted. The residual effective resolution after offset correction is better then **11bit+S.**

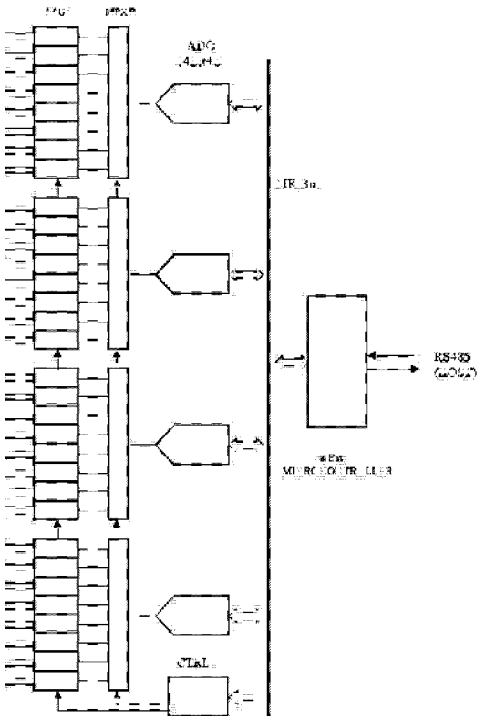

Figure 2: Functional parts of the front – end electronics SME

Microcontroller with firmware controls the timing, data acquisition and data transfer. RS485 serial interface connects the measurement electronics to the host computer (Fig. 2). The baud rate is also programmable (1.2-153.6 kBd). Modular **3U** shielding enclosures contain the integrating electronics in subgroups of 2x8 channels. The channel capability is expandable for 2 wire planes up to 128 wires each.

This development is the basis for high sensitive and stable current measurements like for profile grids, beam emittance analyser as used for beam diagnostics at COSY. The MTA-ITA-LAI (KFKI) Budapest has acquired the licence for this development and the first 2x32 channel system was built for a beam emittance analyser produced by the NTG Gelnhausen.

Beam position monitor in the extraction beamline to JESSICA

J. Dietrich, K. Henn, I. Mohos, M. Simon

In the cooler synchrotron COSY for beam extraction the so called stochastic extraction (ultra slow extraction) is realized. Now a fast beam extraction is routinely used for the experiment JESSICA (Jülich Experimental Spallation Target Setup in COSY Area) [1] is of great importance for prototyping the high power target of the European Spallation Source. For the experiments proton pulses with energy < 1.5 GeV, pulse length of < 1μs and intensity of more than 10^9 protons per pulse are needed.

For non-beam disturbing diagnostics of intensity and time structure of the kicked and extracted beam a wall current monitor (WCM), which was formerly located in the ring, was installed in the experimental area of JESSICA. The WCM is a broadband pick-up (100 kHz – 200 MHz) for detailed measurements of beam pulse intensity and shape.

In the case of slow extraction multi wire proportional chambers are used for beam profile and beam position measurements in the extraction beamlines. But for fast extraction (kicker extraction) other solutions are necessary.

To investigate the beam position stability a round beam position monitor (BPM inner diameter 150 mm) from the same type of the COSY-ring monitors is now installed in the extraction beamline to JESSICA before the target.

The WCM-electronics consists of a programmable broadband amplifier (0-66dB) with 70MHz upper cutoff frequency. The output signal is fed via coaxial cable to the COSY control room for oscilloscope investigations.

The used BPM-electronics is characterized by the broadband mode. Low noise preamplifiers match the capacitive pickups to the system impedance. Passive hybrid converts the pick-up signals into sum an difference signals. Programmable broadband amplifiers (0-66dB) enhence the signal level, low pass filters with 7 MHz cut-off integrate the broadband signals. Sum and difference signals will be digitized at the same time, where the sampling rate of the flash-ADCs is 20 MHz. The digitized data are buffered in 4k FIFO memories.

Configuration and data aquisition of the WCM and BPM are done on VXI-Bus systems. Recorded raw data and configuration parameters are send via network to a LINUX-workstation, where they are stored for later analysis. In addition online calculation of instensity and position is performed and the results are visualized in long-term-plots.

Fig.1 shows a very stable beam position in horizontal and vertical direction for the fast extraction mode of COSY. Unfortunately the beam position monitor gives only an informatioin about the centre of charge, not of the beam profile. The development of a fast non beam disturbing beam profile measuring device in the case of a high intensitive beam as it is necessary for the European spallation source is a great challenge.

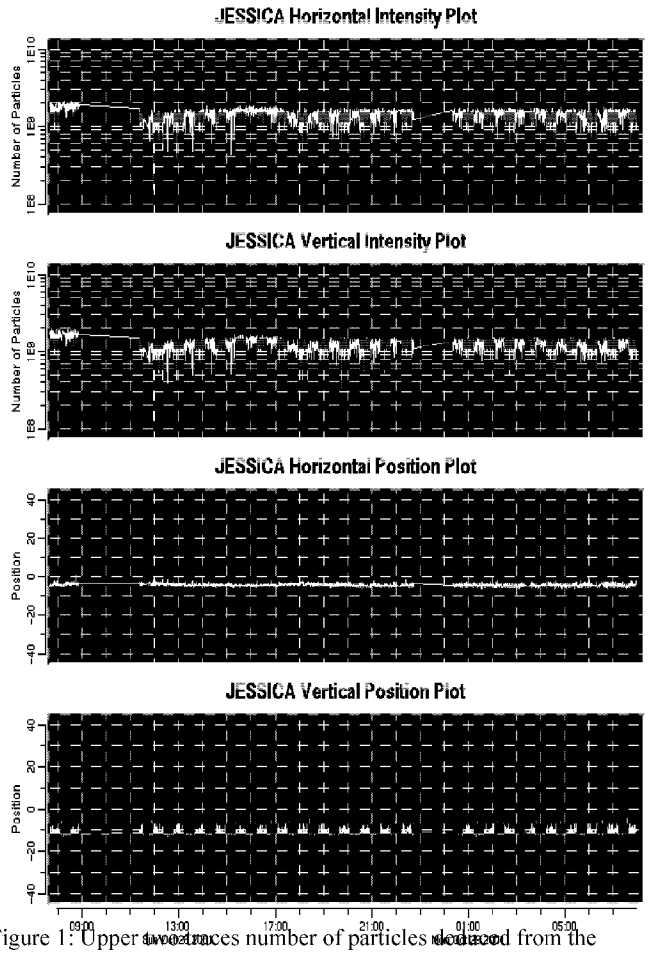

Figure 1: Upper two traces number of particles detected from the horizontal and vertical bem position monitor versus time (in hours). Lower two traces horizontal and vertical beam position before the JESSICA target in [mm] versus time.

References

[1] W.Breuer et al., IKP Annual Report 1998, Report Jül-3640 (1998)180

Magnets, Alignment and New Installations

U. Bechstedt, L. Conin, G. Dolfus, R. Enge, P. Faber, K. Jach, G. Krol, G. Langenberg, H. Pütz,
B. Erkes, D. Ruhrig, T. Sagefka, F. Scheiba

Similar to the past two years there were no very big new installations at COSY during the year 2001. A lot of smaller activities, however, as well as three accidents kept us busy.

Magnets

A basic quadrupole design was made for the planned injector linac for COSY. Two types of quadrupoles are needed with aperture diameters of 31 mm and 38 mm and gradients of 60 T/m and 45 T/m respectively.
For the storage cell of the polarized atomic beam target at ANKE additional vertical steering magnets are needed to bring the COSY beam through the small aperture of the cell. As there is no more space available for additional discrete steering magnets we made a design for additional coils on two quadrupole magnets. After preliminary tests 8 coils were manufactured by the central electrical workshop and installed on quadrupole magnets MQT 28 and MQT 32 of the cooler telescope.

Installations

After COSY 13 had finished the experimental program the scattering chamber was taken out of the COSY ring. It was replaced by a new scattering chamber for the PISA experiment constructed by colleagues from Krakow and manufactured by the central workshop of the research center. The chamber can be equipped with up to 8 detector arms. For the start of the experiment 2 arms had been installed. They are using so called bragg curve detectors filled with isobutene at a pressure of 300 mbar separated from the COSY UHV by two thin mylar foils. One of the foils is aluminized and serves as cathode of the detector.
During the first beam time in August one of these foils was destroyed and COSY was flooded with isobutene. Parts of the foils are now distributed inside the COSY vacuum system.
Only 4 weeks before one of the thin stainless steel foils at the polarimeter in the injection beam line was burst. During this accident it showed up that the electronics of the fast shutter to protect the ring against vacuum problems in the injection beam line did not work. This caused COSY to be flooded as well which damaged the hot cathode of the electron cooler. The cathode was successfully replaced during the shut down shifted to week 40 because of this repair.
Another problem caused by this accident showed up in November when the vacuum in the injection close to the polarimeter deteriorated drastically. This caused the fast shutter to close quite frequently until it finally was blocked and could not be opened again. Reason for the vacuum problem was a leak to the vacuum in the water cooling of one of the horizontal scrapers close to the polarimeter.
When we replaced the fast shutter it turned out that the vacuum valve from the injection beam line to COSY had a big leak. This caused COSY to be flooded with air again, again damaging the hot cathode of the electron cooler. It was successfully replaced during the shutdown in week 51.
Besides these activities a number of other smaller jobs had to be done: modification of the vacuum system for JESSICA from a diameter of 63 mm to 100 mm an installation of a beam position monitor to allow for the test with short beam pulses, repair of a vacuum leak at viewer 2 inside COSY as well as 2 vacuum leaks at ionization pumps, replacement of filaments of titanium sublimation pumps, opening of quadrupole MQU 7 for the dismantling and reinstallation of the scintillation detector inside the COSY 11 dipole chamber, turning of steering magnet SV 30 back as a vertical steering magnet, dismantling of the second electrostatic septum from the COSY ring to allow for the test with rf-contacts, openeing of the vacuum tube to get out an EDDA thin wire target lost from the target rod.

Alignment

Inside the COSY tunnel there were measurements for the installation of the PISA scattering chamber as well as for the internal experiments like COSY 11 and ANKE.
At the external target stations a lot of time was spent for the alignment of the components of the JESSICA target. Related to JESSICA as well was the alignment of the components of the modified bam line.
Like in the past years a part of the alignment activities was for both of the polarized ion sources.
At the end of the year there was a big task carried out together with an alignment company to extend our measurement grid to the area where the new injector linac for COSY will be set up. Nine additional fixed points were installed in the lorry gateway and measured with respect to each other. During the shutdown the COSY grid was remeasured and the new points were connected to the existing grid. The data evaluation giving the achieved error ellipses is still in progress.
At the same time the precision leveling done on a regular time schedule was carried out. We found a sink of the lorry gateway of approximately 5 mm within the last 10 years.

Ion Sources at COSY-Jülich

B. Dahmen, W. Derissen, R. Enge, H.P. Faber, O. Felden, N. Gad, R. Gebel, M. Glende, H. Hadamek, A. Müller, U. Rindfleisch, P. von Rossen, N. Rotert, Th. Sagefka, H. Singer, J. Bisplinghoff[1], P.D. Eversheim[1], D. Rosendaal[1]

The polarized proton/deuteron source[1,3], based on the colliding beams principle[2], has after an extensive redesign of major components, matured such, that it runs now in routine operation at the cooler synchrotron COSY[4,5]. Inside COSY a polarization of 70% at maximum momentum was reached[4]. In recent experimental runs up to $2.5 \cdot 10^{10}$ protons with a polarization of 86% were stored at the injection momentum of 295 MeV/c in the cooler synchrotron. The intensity of the accelerated beam in the cooler synchrotron on an internal target exceeded 3.5 mA at a momentum of 3200 MeV/c.

The total polarized beam time in 2001 sums up to about 2600 hours. For the first time the polarized H^- beam intensity exceeded 1 µA after cyclotron extraction. At the same time the number of the polarized protons in COSY[6] reached values up to $1.5 \cdot 10^{10}$ at maximum energy with a polarization of about 70%.

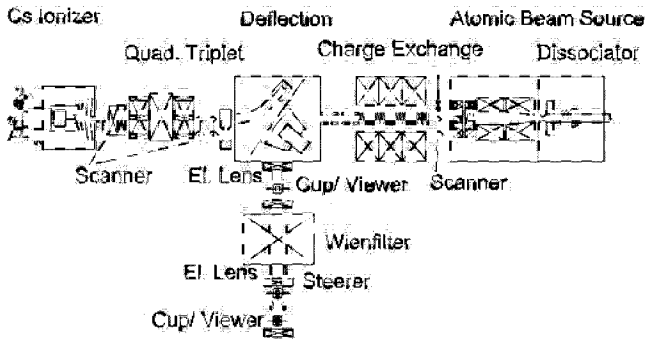

Figure 1: A schematic view of the COSY colliding beams polarized ion source.

This fundamental improvement was a consequence of a complete redesign of the original caesium ionizer[9] and a new pulsed operation that had been developed with pulse widths of about 20 ms over months to the point of routine operation. The electrically pulsed operation[11] of a caesium ionizer was already demonstrated in 1998[10]. The new caesium ionizer was set in operation for the first time in spring 2000. An additional pulsed electrode in front of the tungsten ionizer, that works similar to a grid of a triode, and an air-cooling circuit were integrated in the new setup. The caesium vapor is fed through a tube to the porous tungsten ionizer. The ionizer surface is operated at a temperature of typically 1050°C. The cooling system is able to decrease rapidly the Cs reservoir temperature from 400°C to 40°C in about 6 minutes, an essential prerequisite for efficient operation. The cooling capacity is sufficient to operate the Cs-reservoir down to 40°C with the thermal ionizer having its full operational temperature.

For the pulsed operation the temperature of the caesium reservoir had to be precisely controlled in the range from 35°C to 80°C, depending on the characteristics of the tungsten contact ionizer and the desired intensity. The tungsten contact ionizers are still under investigation to maximise the output, the repeatability and the long-term stability.

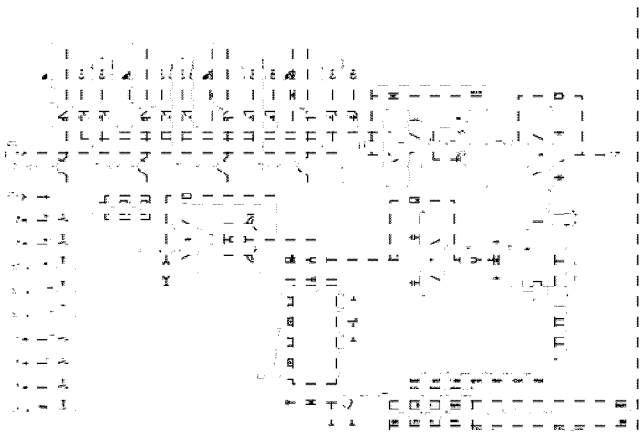

Figure 2: Control circuit for the wire positioning and current measurement of the caesium beam scanner module and micro controller for automatic profile scans.

The damaging effect of the Cs beam has been reduced through the pulsed operation by nearly two orders of magnitude, allowing an operation of 9 weeks without servicing of the caesium ionizer or other parts of the source.

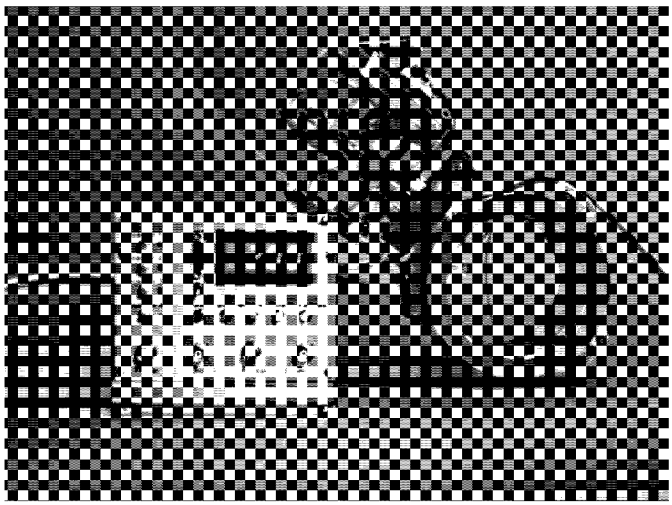

Figure 3: The caesium beam scanner module and micro controller for automatic profile scans.

Four caesium beam profile scanner modules, of which one is shown in figure 3, allow the online control of the cae-

sium beam envelopes, for the charged as well as the neutral beam. The scanner modules were described at the Erlangen workshop[8]. For the pulsed Cs beam the scanners are operated by a micro controller system. This system provides a readout of up to four scanner positions, the integrated charge per pulse and also synchronize the positioning of the wire scanner to the timing of the pulsed ionizer.

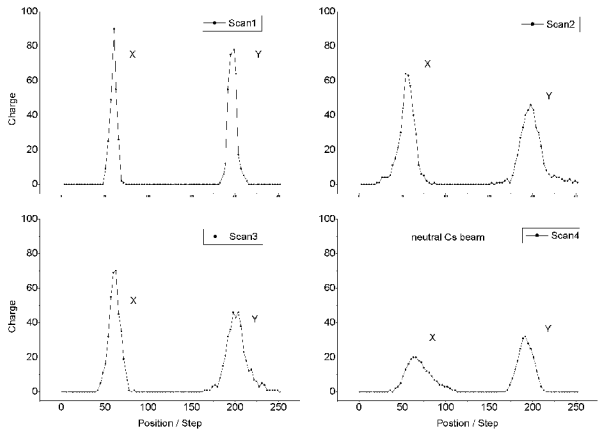

Figure 4: Beam profiles of the pulsed Cs beam taken at four different positions. The Scans 1 to 3 are taken with a resolution of 0.47 mm per step. The neutral Cs beam is scanned with 0.31 mm per step.

The beam is scanned over a width of 60 mm in both directions during one revolution. The fourth scanner for the neutral Cs beam scans over 40 mm. The scan is taken in vertical direction from bottom to top and in the horizontal direction from right to left. Figure 4 shows the result of the measurement of horizontal and vertical profiles at the four positions. The online acquired profiles give the size and the beam shapes. The 5 mm diameter beam, at a distance of 0.25 m after the ionizer, is imaged to a beam position of 9 mm at the entrance to the atomic beam part 3.5 m downstream. Profiles taken at different positions before and behind the quadrupole triplet allow to determine the alignment and the emittance of the caesium beam. This provides reliable information to judge the performance of the thermal ionizer module. Data taken with this system was also used to determine the parameters of the quadrupole system and to optimize the geometry of the caesium beam line for high transmission. A set of correcting dipoles have been added to remove residual beam displacements in the charge exchange region.

All original parts in the caesium beam section, figure 1, have been replaced by improved components. The new parts have been optimized in accordance with the operational experience.

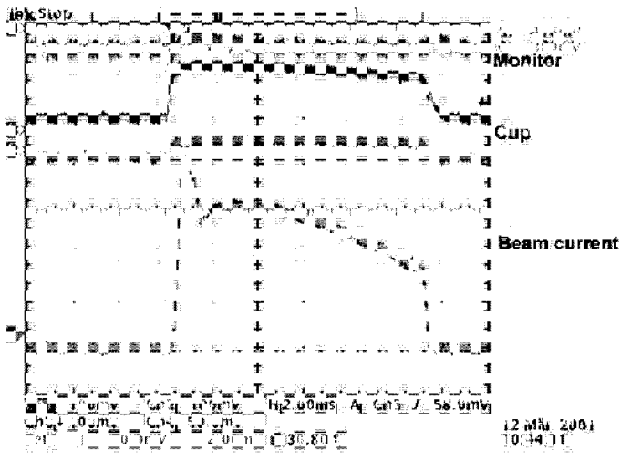

Figure 5: Trace 1 shows the achievable H^- intensity measured at the first cup in the source beam line. The scale from bottom to top is 100 µA.

The start up procedure of the caesium beam part is simplified by a set of beam diagnostic elements (see figure 1). Figure 5 shows an example for online monitoring of the polarized source. The caesium beam is monitored at the power supplies (Trace 3), including the load on the extraction (Trace 4). The beam is neutralized and the remaining charged part is dumped in a faraday cup (Trace 2).

The improved reliability and quality of the caesium beam permitted to further optimize the charge exchange and extraction system. Figure 5 shows the peak current measured at the first cup in beam line to the injector cyclotron to demonstrate the potential of the improved source. The beam was extracted at a potential of 4.5 keV and magnetically deflected by 90° to the cup, where an intensity of 30 µA was reached. First vector polarized deuteron beams were produced with this source.

References

[1] P.D. Eversheim et al. , Proceedings of Polarized Beams and Polarized Gas Targets, Köln; 224, 1995
[2] W. Haeberli, NIM 62, 355, 1968
[3] R. Weidmann et al., Rev. Sci. Instrum. 67 II 1357 1996
[4] A. Lehrach et al., NIM A 439 26 2000.
[5] D. Prasuhn et al., NIM A 441 167 2000.
[6] D. Prasuhn et al., Proceedings of PAC2001, Chicago, 2001, to be published.
[7] R. Gebel et al., Proceedings of Polarized Gas Targets and Polarized Beams, Urbana; 503 1997.
[8] R. Gebel et al., Proceedings of Polarized Sources and Targets,Erlangen; 86 1999
[9] S. Lemaitre et al., NIM A 408 345 1998.
[10] M. Eggert et al., Proceedings of Polarized Sources and Targets, Erlangen; 90, 1999.
[11] M. Eggert et al., NIM A 453 514 2000.

[1] Institut für Strahlen und Kernphysik, Universität Bonn

COSY-Superconducting Linac, the New Injector for COSY

U. Bechstedt, J. Dietrich, A. Facco*, O. Felden, R. Gebel, K. Henn, H. Jungwirth, A. Lehrach,
R. Maier, N. Markgraf, U. Pfister, D. Prasuhn, P. v. Rossen, A. Schempp**, A. Schnase,
H. Schneider, Y. Senichev, R. Stassen, H. Stockhorst, R. Tölle, E. Zaplatin, V. Zviagintsev*
*LNL-INFN, Legnaro, Italy; ** IAP Universität Frankfurt/Main, Germany

During the past year considerable effort was spent to set up the project to replace the injector cyclotron for COSY by a superconducting LINAC. The injector is being designed to deliver both polarized and unpolarized H^- and D^- beams at an energy of approximately 50 MeV and in pulses with a maximum beam current of 2 mA lasting up to 500 µs. For injection into COSY, we aim to achieve at least a pulsed beam current of 0.5 mA (average) over 200 µs. This provides in the order of 5×10^{11} particles for stripping and allows to significantly reduce emittance growth of the beam in COSY during the injection process. The maximum repetition rate is limited to 2 Hz, and the utilized duty factor of the injector will therefore not exceed a value of 10^{-3}.

Under the constraint to avoid the construction of new buildings, the only suitable place for the new injector is in the present service area at the south-eastern end of the COSY hall. From this area, the injector can be linked most directly and economically to the existing injection path into COSY. Such a choice also provides the required accessibility of all sections of the injector and minimizes interference with the operation of COSY during the construction period. The service area is used to unload trucks by either of the two cranes in the COSY hall and that functionality has to be maintained when the new injector is installed. Hence only an area of approximately 40 m length and 8 m width is available for the LINAC, including its support equipment and shielding.

A normal conducting LINAC would fit into the available space but has the drawback that D^- ions can only pass a H^- LINAC using the $2\beta\lambda$-mode. Unfortunately this implies that the final energy of D^- would be at best half that of H^-. Even if the H^- energy is chosen at 70 MeV, the D^- energy will not exceed 32 MeV, which is not acceptable for injection into COSY.

The concept of a superconducting LINAC with individually powered resonators changes this situation. RF power is generated in 3 kW solid state modules. As each resonator can be controlled individually in amplitude and phase, it is possible to reach a final energy of approximately 50 MeV with H^- as well as with D^- ions. This flexibility is affordable because of the relatively low RF power required. Superconducting cavities are much more expensive, however, and they need complex cryostats and cryogenic systems for operation.

The layout of the proposed injector is shown in fig. 1 and consists of five consecutive sections. The ion source section includes a source for polarized H^- and D^- ions (CIPIOS type) and a commercial multi-cusp source for unpolarized H^- and D^- ions. These ion sources have to be operated in the pulsed mode required. They are connected to the accelerating structures via the Low Energy Beam Transfer (LEBT) system in such a way that CIPIOS can be tuned and tested even when the injector is operated with unpolarized beams. To allow proper alignment of polarization directions, a Wien filter or alternatively a solenoid is included in the LEBT system.

An investigation of currently available ion sources for polarized H^- and D^- beams was carried out. For our requirements, the most attractive source is undoubtedly the type from A.S. Belov, which under the name of CIPIOS is also used for the cooler synchrotron at the Indiana University Cyclotron Facility (IUCF) in Bloomington. It operates at 25 kV extraction voltage and delivers an up to 1 mA (peak current) intense polarized H^- beam of 1.2 π mm mrad (normalized 90% emittance) as well as polarized D^- beams. The ion velocities in units of the velocity of light (β) are 0.0073 and 0.0052 respectively. The maximum pulse length achieved up to now is about 400 µs with potential for further improvement.

In the design of the LEBT beam line non-linear space charge effects are taken into account. As the magnetic rigidity is different for the two ion species, the ion-optical elements have to be adjustable over a wide range. The following section begins with electrostatic elements that focus the beam into an RF-quadrupole (RFQ) accelerator operating at 160 MHz. Such accelerators have the essential advantage that, in addition to providing acceleration, they simultaneously bunch the beam from the ion source without significant losses in beam intensity.

Since RFQ's have structures designed for one particular particle velocity profile, some scenarios were considered for operating the ion sources with equal ion velocities. From IUCF we know, however, that CIPIOS does not withstand higher voltages than 30 kV, and thus D^- ions cannot be made fast enough. On the other hand, H^- ions should not be made slower either, because the emittance degrades rapidly with decreasing extraction voltage. No alternative was found to be practical. Hence we rather accept different particle velocities at the exit of the ion source, which requires different RFQ structures for H^- and D^- operation, respectively. The two structures will be easily interchangeable.

A kinetic energy of 2.5 MeV was considered feasible for H^- injection into the LINAC (corresponding to 5 MeV for D^-). A combination of RFQ and booster cavity is the most compact design we found for this purpose. After this pre-acceleration, quadrupole magnets and a rebunching cavity match the beam to the needs of the LINAC in the transversal planes as well as longitudinally.
Different layouts of this LINAC were investigated. Our first approach was inspired by the recent developments in Legnaro/Italy (ALPI) where great experience in the design and operation of superconducting quarter wave resonators (QWR's) is available. We started our calculations using a

conservative peak acceleration gradient of only 6 MV/m. The resulting length of the LINAC is about 26 m, which together with all the other equipment required would hardly fit into the available space. We therefore considered "folding" the long LINAC structure into the service area. The result was that an isochronous and achromatic U-turn together with some rebunching cavities would be necessary, similar to those installed at ALPI. Such a solution would be quite inefficient and expensive in our case. In addition, the marginal gain in space for the LINAC had to be weighed against the drawback that one of the cranes would not be accessible for trucks in the service area. Hence that idea was rejected. Instead we introduced a 90° bend before the beam is bunched, that is between CIPIOS and the RFQ, but there would still not be enough space for the LINAC. Detailed simulations taking into account the 3D E- and B-field distributions of QWR's showed that the beam is strongly influenced by the transversal E- and B-field components. The main effect is transversal steering, mainly caused by the magnetic dipole moment of the field. This effect can nearly be compensated by proper arrangement of the QWR's. Another effect is the increase of the effective emittance leading to a star shape distribution of the beam in the transversal phase space. This is mainly caused by transversal electrical quadrupole moments. To minimize this effect one has to choose resonators with symmetric field distribution like half wave resonators.

As the practical field limits of superconducting resonators are not reached for our pulsed operation with the 6 MV/m layout, we finally decided to increase the peak acceleration gradient to about 8 MV/m, such that the peak surface field in the resonators is kept below a maximum acceptable value of 80 mT. The design of this LINAC has the following characteristics. It comprises a total number of 44 coaxial half wave resonators (HWR's) of which the first 14 operate at 160 MHz and the remaining 30 at 320 MHz. Three different HWR structures for the following optimum particle velocities are used. For the first two HWR's a β_s value of 0.092 is chosen, for the following twelve β_s = 0.118, and for the remaining thirty β_s = 0.224.

Four HWR's are grouped in each cryostat. Longitudinal beam dynamics requires the length of the unit cell of the LINAC (i.e. cryostat plus transversal focussing length between the cryostats) to be limited to 1.7 m. Stable acceleration can then be provided for both H^- and D^- beams by a proper choice of the RF phase for each HWR. Final energies of 52 MeV and 56 MeV can be reached in this way for H^- and D^- ions, respectively. The LINAC has only a total length of nearly 19 m and fits much more easily into the available space. In fact, two more cryostats could be added if required, as is shown in fig. 1.

After the LINAC, the beam is guided to a 90° magnetic bend with which alternatively the diagnostic section of the transfer beam line or the injection path into COSY can be chosen. All components of the transfer beam line should make ample provision for possible future extensions of the LINAC to higher energies. Components of the existing injection beam line (IBL) from the cyclotron will be incorporated as far as possible, because they meet such requirements anyway and would otherwise become redundant. Quadrupole doublets allow to shape a target spot in the diagnostic section as is needed for instance by a polarimeter. Also equipment for measuring the energy, emittance and time structure of the beam will be provided. At the end of this section, a beam dump is installed including additional shielding outside the existing wall of the COSY hall. In the beam line to COSY, debunchers could be used to minimize the momentum spread of the bunched beam if necessary.

Improved injection into COSY can make use of the installed bumper magnets. As the pulse duration will be shorter than 500 µs, injection into the flat-top field of the bumpers is possible. Then the whole beam is pulled off the stripper foil that is crossed by the ions up to 300 times in the process. Compared to the present situation, this avoids injection into the decaying field of the bumper magnets, which blows up the horizontal phase space excessively. So we expect a much smaller beam size in COSY at injection, even if we continue to use the present injection system.

Large parts of the injector have to be enclosed in a shielded tunnel with controlled access for radiation protection. Laterally a wall thickness of 2 m concrete is required for this purpose. For the roof we need 0.5 m thick concrete beams that overlap to reduce sky shine. The electronic equipment and power supplies for the injector will be installed in racks alongside the lateral shielding wall outside the tunnel. We also have to provide space for the cold box and heat exchangers as well as the dewar of the cryo-plant in this area. The compressor and the gas purifying system of this plant have to be installed outside the COSY hall due to excessive vibrations that would be detrimental to the operation of the LINAC. Last but not least, the existing electricity supply and water cooling systems of COSY have enough spare capacity to support the new injector together with the cyclotron JULIC and COSY itself.

The work done so far described in much more detail in [1]. The project aims to commission the new injector in 2005.

[1] The Superconducting Injector LINAC for the Cooler Synchrotron COSY, Conceptual Design Report, October 2001, edited by Helge Jungwirth.

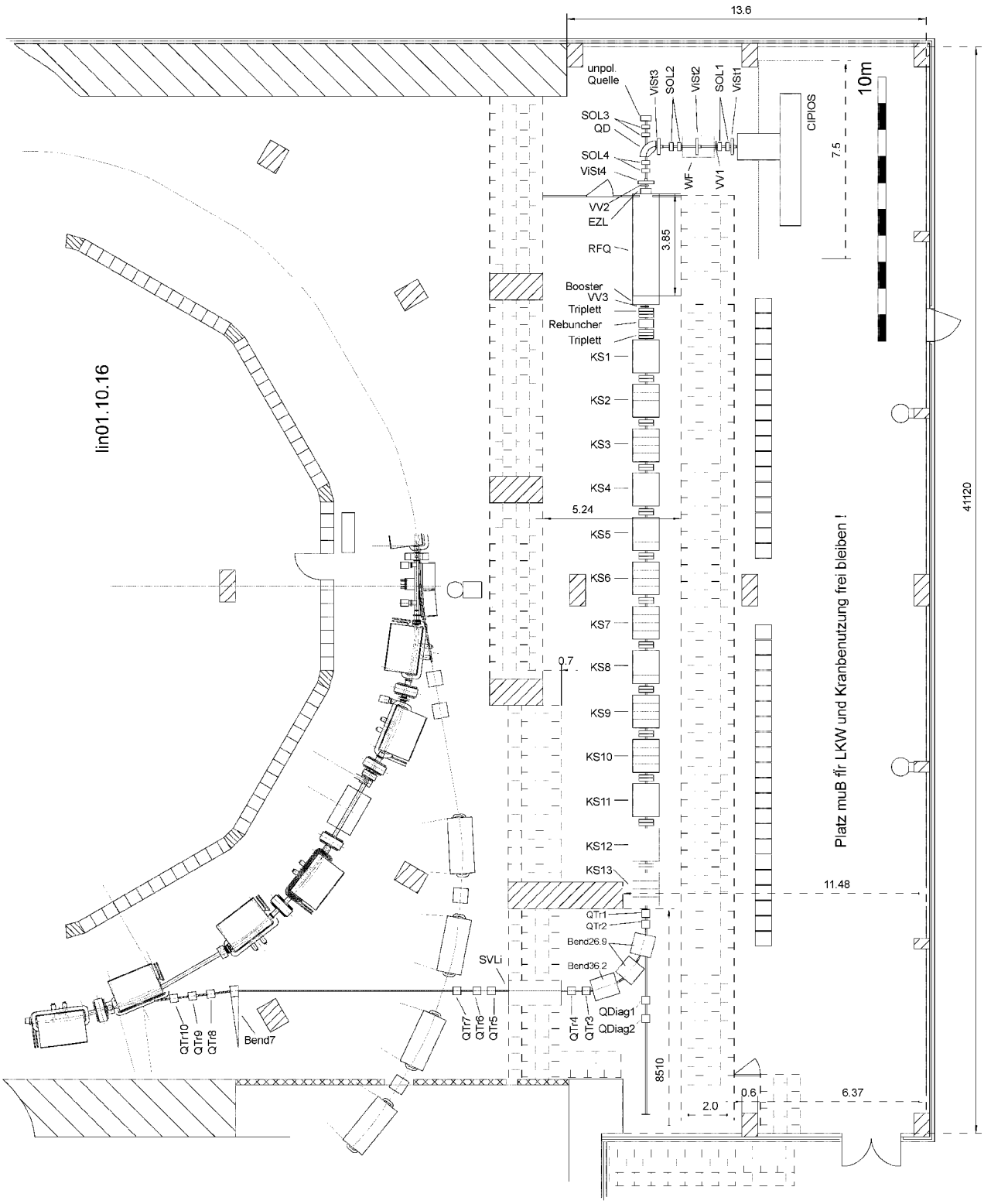

Fig. 1: Layout of the COSY-SCL injector

Some features of Beam Dynamics in Super-conducting Linac based on Quarter- and Half-Wave Cavities

Yu.Senichev, A.Bogdanov, W.Braeutigam, A.Lehrach, R.Maier, R.Tölle, E.Zaplatin,
Forschungszentrum Jülich GmbH, Institut für Kernphysik,
D-52425 Jülich, Germany

The Super-conducting Injector LINAC for COSY has to accelerate protons and deuteron particles that differ in mass by a factor of 2. There are two preferable types of linear accelerator structures appropriate for this purpose: the multi-gap structure with internal synchronization of gaps, such as an Alvarez structure and the system with external synchronizing of the different groups of structures with few gaps, for instance the super-conducting coaxial cavities. For our purpose the super-conducting cavity is more appropriate. We consider two options of linear accelerator based on the super-conducting quarter- and half-wave resonators. In both options the accelerator consists of two parts. In first and second parts we use the resonators with 160 MHz and 320 MHz frequencies correspondingly. Simultaneously the resonators are subdivided into the families with the same β relative velocity. We optimize the number of resonators in each group and each family. We discuss how to optimize for protons and deuterium particles simultaneously. We analyze the 6-dimensional beam dynamics in the real field calculated by MAFIA. The quarter-wave cavity technology is quite developed, but due to the dipole component of magnetic and electrical fields the beam is unstable in the transverse plane. We have developed the special method to compensate this effect. In the half-wave resonators such problem does not exist due to the field symmetry. For the transverse plane we examine the single, doublet and triplet systems. We investigate the parametric resonance arising in the longitudinal plane due to the drift space needed for the focusing elements and determine the space limitation.

I. Quarter-wave cavity

In both quarter- and half-wave cavities the motion equations are the same. To design the linac we integrate numerically 6D phase motion in the real components $E_x, E_y, E_z, B_x, B_y, B_z$ taken from MAFIA calculations.

In the quarter-wave cavity due to the construction we have the dipole H component. It is shifted relatively of E mode for 90 degrees in time, but nevertheless the particles are getting the uncompensated transverse kick, since H mode acts to the beam like π - mode. The total effect is dramatically bad for the beam and without compensation the bunch is shifted on 200 mm from axis (see fig.1), which one is unacceptable. Obviously, the method, which one could help to compensate the dipole mode, has to be based of RF field. Therefore we have analyzed the different schemes of the cavities placement[1]. The figure 1 shows the results of the particles tracking in the real field for the option "4 groups of cavities with drift between cryomodules 1m of length", when we launch the bunch represented by the empty phase ellipse in the longitudinal plane with the zero initial transverse deviation for x,y, dx/dz,dy/dz. The rotation of the cavities $(-90^o, 90^o, 90^0, -90^o)$ or inversely gives the minimum deviation of the bunch from the axis. However, under the commissioning we expect the problems with the tuning the quadrupoles and RF fields separately.

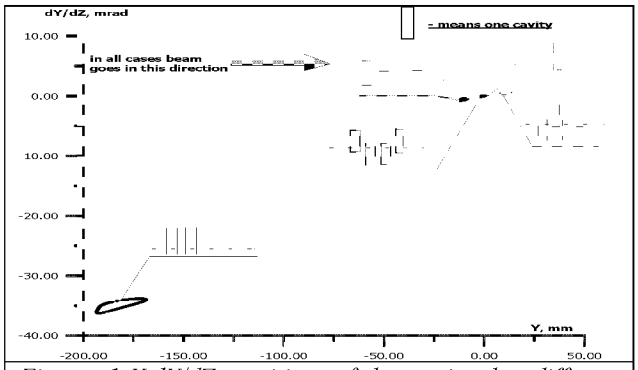

Figure 1:X,dX/dZ position of beam in the different scheme of compensation.

II Half-wave cavity

In half-wave cavity the dipole H mode is absent, therefore the position of beam on the exit of accelerator coincides with the geometrical centre (see fig.2).

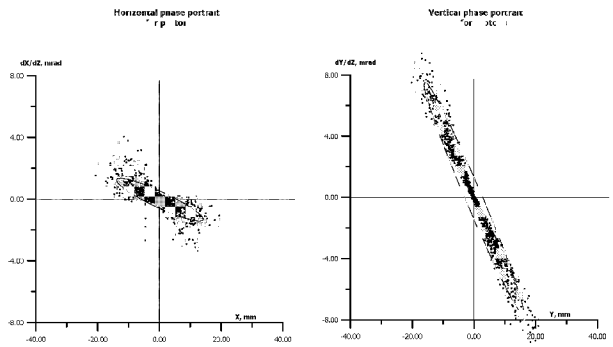

Fig.2: Horizontal and vertical portrait of beam on exit of linac

In the longitudinal plane in both options the motion is very non linear due to the absent of synchronism between the particle and RF wave. The RF gap size is adjusted to minimize this effect.

References

[1]W. Bräutigam, O. Felden, M. Glende, H. Jungwirth, A. Lehrach, R. Maier, S. Martin, A. Schnase, Yu. Senichev, R. Stassen, R. Tölle, E. Zaplatin, SC ACCELERATOR COMPONENTS FOR LIGHT ION LINACS, SuperConductiv Workshop, Tsukuba, 2001.

Low-β Superconducting RF Accelerating Structures

E. Zaplatin, W. Bräutigam, R. Maier, R. Stassen, Yu. Senichev

At present, many accelerators favour the use of SC cavities as accelerating RF structures. For some of them, like long pulse Spallation Source or Transmutation Facility SC structures might be the only option.
For the high energy parts of such accelerators the well-developed multi-cell elliptic cavities are the most optimal. For the low energy part the elliptic structures cannot be used because of their mechanic characteristics. There is a scope of different already proven low-β SC cavities. Here we investigate quarter-wave coaxial cavities (160 MHz, β=0.11 and 320 MHz, β=0.22), half-wave coaxial cavity in comparison with spoke cavity and based on spoke cavity geometry multi-cell H-cavities (700 MHz, β=0.2). All cavities optimised to reach the maximal possible accelerating electric field. The simulations of electrodynamics and structural analysis have been provided. The simulations also have been done for various vacuum and coupling port positions. Different cavity tuning schemes are under investigation.

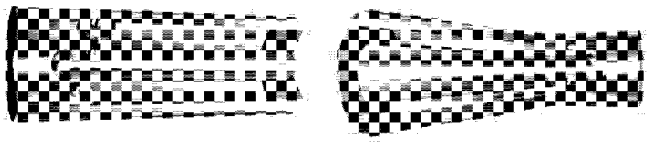

Fig.1: Plane and Conical Quarter-Wave Resonator.

Quarter-Wave RF Resonator (QWR, Fig.1) is a coaxial transmission line shortened by the terminating capacitance. The range of such structure application is for rather low β<0.2 and fundamental frequency under 300 MHz. The resonant frequency is defined by the line length, inner-outer radius ratio and capacitance. An accelerating field magnitude is limited by peak magnetic field that is defined mainly by the radius of the inner electrode. This favours the use of the cone QWR (Fig.1). The disadvantage of the cone cavity is larger longitudinal extension. On the other hand this may be compensated by the cross-cavity installation (Fig.2).

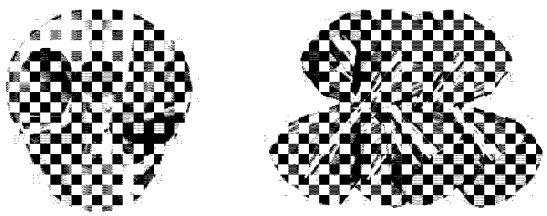

Fig.2: Half-Wave Resonator & Cross-Cavity Installation.

Another accelerating structure for this range of particle energy is a spoke resonator (Fig.3). The spoke cavity by definition is a coaxial half-wave length cavity with an outer conductor turned on ninety degrees so that its axe is directed along the beam path. An equivalent capacitance of such cavity is defined by the distance between conductors in the center of the cavity along this ax. A distribution of an electromagnetic field in such cavity is the same like in coaxial cavity. The range of application of this cavity is from 100 to 800 MHz of fundamental frequency and β=0.1-0.6. The limitations of application are defined mainly by the resonance capacitance grow for low-β values which in its turn reduces cavity diameter.

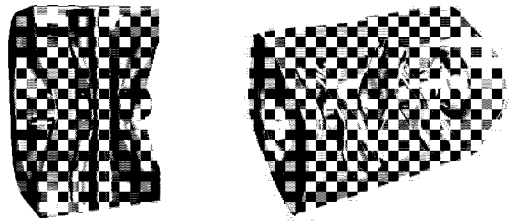

Fig.3: Spoke Half-Wave Resonator & 4-Gap H-Cavity.

The spoke cavity acceleration efficiency is defined by the magnetic field magnitude on the inner electrode surface like in the coaxial resonators. The comparison of cross-cavity half-wave conical resonator installation with the set of spoke cavities in terms of maximal reachable accelerating field favours the use of the first option[1].

Starting with the value β=0.2 there is a possibility to use multi-gap (bigger than two) accelerating structures. 4-gap and 10-gap cavities based on spoke resonator geometry are under investigation. Such structure could represent the same cylindrical or modified shape outer conductor loaded with several electrodes (Fig.3). But as soon as one adds at least another spoke in such structure it turns from the coaxial spoke cavity into H-type cavity, which is defined by the electromagnetic field distribution. The detailed results of multy-gap H-cavity optimisation are published elsewhere[2]. For 3D numerical simulation verification and cavity tuning investigation 10-gap H-cavity copper model (700 MHz, β=0.2) has been built. The cavity and end plates are made from the 3 mm and 1 mm copper sheet respectively. The spokes have been machined from the bulk copper. For the cavity tune the deformation of the end plates is used. The results of the numerical simulations and first model measurements are shown on Fig.4.

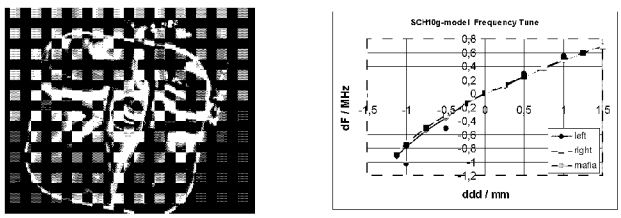

Fig.4: 10-gap H-cavity Copper Model & Frequency Tuning Shift.

References

[1] E. Zaplatin et al., "Very Low-β SC RF Cavities for Proton Linac", ESS 01-122-L, Jülich, December 2001.
[2] E. Zaplatin et al., "Low-β SC RF Cavity Investigations", *SCRF2001, Tsukuba, Japan, 2001.*

Beam Diagnostic for the new COSY-SCL Injector

J. Dietrich

Due to the relatively high pulse current and as a consequence of using superconducting cavities, beam diagnostic instrumentation is of great importance for operating the LINAC. The diagnostics will allow proper matching between the various sections of the machine, and to measure and help minimize beam losses. All beam measuring equipment has to meet two utilization criteria: During the injector testing period (independently of the COSY accelerator complex), measurements of the beam characteristics will be needed to determine suitable LINAC settings. This requires a precise and complete instrumentation (measurements of the beam intensity distribution in the three phase planes) to allow us to compare the actual beam properties with theoretical predictions. During operation we have to (i) check the stability of the standard values set for the beam parameters, and (ii) measure the parameters of newly set beams, if we want to change the beam characteristics. The LINAC design leaves relatively little space for installing diagnostic devices. Hence such devices must be specially designed to fit where access to the beam is possible. The more special types of diagnostic instrumentation that we plan to use can be described as follows. The table sums up the total requirements for the different sections of the injector.

Beam Current Transformer (FCT): Non-intercepting beam current monitoring will be done with beam current transformers, where the beam forms the primary (single turn) winding and the signal is developed across a secondary winding. Passive devices (not including any electronics) with a bandwidth of up to 2 GHz allow rise times as short as 175 ps with a droop of a few percent per millisecond and a sensitivity of up to 1.25 V/A (commercially available from BERGOZ).

Wire Scanner (*or Wire Grids,* WS): The transverse particle density distribution (beam profile) will be measured by stepping a pair of orthogonal wires across the beam pipe aperture. Since the direction of the drive is inclined at 45° to the horizontal, the single motion provides a scan in both planes. Data can be taken on successive LINAC pulses until the full scan is completed. The wire scanner provides the best compromise between range and resolution at low cost. Only one electronic channel is required for each plane. The wire scanners are very compact longitudinally, which is important in the matching section and between tanks and modules. Since only a small percentage of the beam intercepts the wires, this technique can be considered non-destructive.

Emittance Measurement Unit (EMU): The conventional method of measuring beam emittance makes use of a slit and multi-collector hardware. The slit is moved across the beam to define the position of a sample that spreads according to its divergence. The resulting distribution that is measured by the multi-collector (wire grid or sandwich target) represents the angular spread. The result is a direct measure of the transverse phase space in one plane. The measurement destructs the beam.

Wall Current Monitor (WCM): The beam generates an image current on the surface of the beam pipe. A ceramic gap is placed in the pipe and resistors are distributed azimuthally around it, connecting the separated pieces of the beam pipe. The image current flows through the resistors developing a voltage across them, which provides the bunch shape signal. The best example (at FNAL) has an upper frequency limit of 6 GHz before degradation by the signal cable becomes unaccaptable. It is a passive inexpensive device and can provide sufficient information about bunch shape and beam current.

Beam Position Monitor (BPM): Different types of beam position monitors are known. BPM's of the strip-line type are used at the BNL 200 MeV and FNAL LINAC's. In the BNL design, the strip-lines are cut to second harmonic for minimizing the BPM length along the beamline. Processing is done at the highest frequency possible after down conversion to obtain the best frequency response. In the Los Alamos APT project, so called 4-lobe microstrip transmission-line detectors are used, which measure the image currents of the beam travelling along the wall of the beam tube. The BPM's will be located inside a quadrupole between two successive cryostats of the LINAC. A further possibility would be to extract the beam signal inductively. Such devices allow to detect deviations of down to ± 0.1 mm from the required beam position. They can be combined with ring electrodes for the fast capacitive measurement of the beam phase.

Beam Loss Monitor (BLM): The beam loss monitor system is one of the most important diagnostic tools in a relativly high average current superconducting accelerator, where it is essential that beam losses can be kept as low as possible. While beam current transformers read the transmitted current or charge, they are not sufficiently sensitive to detect small deviations due to beam losses. Liquid scintillator photomultipliers have been used on some LINAC's in the past, but problems with reproducibility, aging, and calibration make them less suitable than ion chambers for use as beam loss monitors. The long

coaxial ion chambers used at BNL offer uniform coverage and linear fall-off with distance. They have been used in typical lengths between 15 m and 25 m, to increase the volume exposed to the radiation, but are not sensitive enough in the LINAC where the accelerating structures (shielding of the cryotanks) are located. However, they do have sufficient sensitivity for use in the transfer beamline. Proportional ion chambers with a typical gas gain of 10 3 may be needed in the accelerating region.

Laser Diagnostic (LD) for H^- (D^-): Beam diagnostics, especially non-destructive methods, are important for the performance and operation of an accelerator, in particular for high current pulsed H^- beams like in neutron spallation sources. The basis of beam diagnostic devices using a laser is that the threshold for photo-detaching an electron only amounts to about 0.75 eV, and that the photo-detachement cross section rises to about 4×10 -17 cm 2 for photons of about 1.5 eV (800 nm). A Q-switched laser (Nd:YAG) can neutralize a significant fraction of the beam in a single 10 ns wide pulse. The neutral beam maintains nearly identical characteristics like the parent H^- beam, including size, divergence, energy, energy spread and phase spread. A dipole magnet can separate the neutral beam from the H^- beam to allow diagnostics (e.g. with Multi Wire Proportional Chambers) on the neutral beam without intercepting the high current H^- beam. A non-intercepting beam profile monitor for H^- beams is currently being developed at Brookhaven National Laboratory. Experiments have been performed on the BNL LINAC to measure the transverse beam profile at 750 keV by using a Nd:YAG laser to photo-neutralize narrow beam slices. The laser beam is scanned across the ion beam neutralizing those portions struck by the laser. The electrons are removed from the ion beam and the beam current notch is measured. The same method could be used to make a notch in the beam for reducing the intensity injected into COSY. A defined time structure can be realized, which would be equivalent to micro-pulsing.

Particle Energy Monitor (Time-of-Flight): Capacitive pick-up pairs at each cryostat will be used to ascertain the particle energy by means of the time-of-flight between the pick-ups. Phase measurements on the 3rd harmonics of the bunch frequency (RF) with an accuracy of 1 degree enable about 5 ps time resolution. Energy increment after the accelerating cavities and the end-energy of the LINAC in the transport beam-line are monitored in real-time.

	FCT	FC	WCM	WS	EMU	BPM	V	CPU	BLM	LD
LEBT	1	1		1			1		1	
RFQ-LINAC	1			1					1	
LINAC	10			10		12		10	10	
Transport Line COSY	1	1	1	1		4			4	
Straight Transport Line	1	1		1	1	4			4	1

FCT = Fast Current Transformer
FC = Faraday Cup, Coaxial Faraday Cup (bunch structure)
WCM = Wall Current Monitor
WS = Wire Scanner or Wire Grids (profile monitor)
EMU = Emittance Measurement Unit (slit/collector)
BPM = Beam Position Monitor
V = Viewer (fluoresence screen)
CPU = Capacitive Pick – Up
BLM = Beam Loss Monitor
LD = Laser Diagnostic (MWPC multi wire proportional chamber, current transformer)

7. SPECTROMETER BIG KARL

Magnetic Spectrograph BIG KARL

J. Engel, R. Jahn, K. Kruck, H. Machner, R. Maier, U. Rindfleisch, P. v. Rossen, R. Tölle,
GEM- and MOMO-Collaboration

Modifications and additions have been made to the BIG KARL experimental area to keep it abreast with experimental demands.

A somewhat longer break resulted from a serious water leak, but did not interfere with the regular scheduled beam time.

The third quadruple of the entrance matching triplet had developed a major leak in the cooling system. These quadrupoles are high performance magnetic lenses that are capable of achieving poletip fields up to 1.3 Tesla. As a consequence the copper coils have to be run with very high current densities up to 40 A/mm^2. The narrow channels of the hollow copper conductors need subsequently a high water flow, which for this reason is very turbulent. Such a condition highly nurtures corrosion, and in combination with the relative thin walled conductors, leaks. Two leaks had already appeared close to the terminals in the year before. It was possible to repair them at that time with rubber pads being pressed against the conductor with a fixture. The new leak was of a more severe kind as it appeared deep in the middle of the epoxy resin covered coil. This made a simple repair impractical.

The entrance quadrupoles originated from DESY and were acquired partly from DESY and partly from CERN. Anticipating possible future problems spare quadrupoles had been stocked. This gave us the option to replace all three damaged coils of the third quadruple. After complete disassembly, the damaged coils have been exchanged against defect-free coils. Reassembly and recommissioning were performed successfully.

New wire chambers with high spatial and time resolution were ordered to resolve ^{7}Li and ^{7}Be in the focal plane of the spectrometer. These detectors are based on the avalanche principle using delay line coupled wires to extract the position information and are intended to operate with a gas pressure of 20 mbar inside a large vacuum chamber to minimize the effects due to multiple scattering. Although scheduled for delivery in this year insufficient wire quality has delayed their completion.

A new focal plane Cerenkov detector was designed and build by the HIRES collaboration for the focal plane to study exotic quark states according to the proposal of ref. 1. In a December run this detector underwent a first test done parasitically to the GEM isospin breaking experiment to evaluate the potential for pion suppression, an important prerequisite to later filter out kaon events.
The MOMO collaboration had a short run to finalize its program measuring the data for the two-kaon production based on the reaction pd $\rightarrow$ ^{3}He K^+ K^- by taking events being within 2 MeV of the Φ-threshold. Measurements that close to the threshold were enabled by the high luminosity reached at this target station after carefully optimizing the ultra slow extraction of the COSY cooler synchrotron. A preliminary analysis produced a cross section of 0.6 nbarn at this energy. Data reduction is in progress to complete the assessment of the entire dataset accumulated for this reaction.

GEM did successfully conduct final measurements to complete its data concerning the isospin breaking. The symmetry violation was studied measuring the reactions $p + d \rightarrow {}^3H + \pi^+$ and $p + d \rightarrow {}^3He + \pi^o$. ^{3}He and ^{3}H were recorded simultaneously, the first in the main focal plane and the latter at the side yoke of dipole D1 to eliminate uncertainties stemming from target thickness and/or beam normalization. The experimental refinements worked out in the previous runs made it possible to reduce the influence of any background to full satisfaction.

The data measured for a precision determination of the eta mass have gained just recently an enormous interest as in the meantime a measurement has surfaced that claims to be in contradiction to the value publised by the Particle Data Group. The BIG KARL spectrometer is, due to its specifications, formidably suited to best the published errors of this important quantity. At a workshop held to highlight essential experiments which should be performed at the spectrometer having no equal elsewhere a scheme was developed to eliminate for instance errors connected with the uncertainty of the beam momentum and the precise B*rho-value of the spectrometer (ref. 1). The analysis of the data is in progress.

Details concerning the topics mentioned are found elsewhere in this report.

References

[1] "Physics with Big Karl" Berichte des Forschungszentrums Jülich, Jül-3804, ISSN 0944-2952

8. RADIATION PROTECTION

Radiation protection

O.Felden, J.Göbbels, K.Krafft

Since August 2001 the modified laws governing radiation protection and safety are in effect. Their thorough revision has, as expected, led to some strong modifications. Although the thresholds for the different radiation protection areas (closed areas, controlled areas and supervised areas) were lowered by a factor of 2.5, there was no necessity to change the radiation protection areas inside and outside the IKP, because a certain safety margin had already been built into during the original planning. In table 1 the new thresholds are shown in comparison to the old values.

Another requirement of the new radiation protection ordinance is, that the effective dose of not occupationally exposed persons, staying in supervised areas must not exceed 1 mSv per year. This condition can be fulfilled too, as evidenced by our accounting of radiation levels done in previous years.

Another potential difficulty in connection with the new radiation protection ordinance is, that we have to renew the existing license to run COSY if we need to make changes to the accelerator or experiments.

	new thresholds	old thresholds
closed area	3 mSv/h	3 mSv/h
controlled area	6 mSv/a	15 mSv/a
supervised area	1 mSv/a	5 mSv/a

Table 1: New thresholds for the different radiation protection areas in comparison to the old values.

In order to allow access to the inner area of the COSY accelerator during its operation the local dose in the inner hall is permanently monitored for each individual of the group of persons having the right to access this area. The maximum accumulated dose must not exceed 1mSv per week during the presence of those persons in the inner part of the COSY hall. This dose is being measured with eight neutron monitors installed at the access doors to the accelerator ring and one neutron monitor, installed at the roof shielding of the COSY ring. The first neutron monitor (NM1) is located at the access door under the staircase that leads to the inner hall, NM2 at the experiment COSY11, NM3 at the electron-cooler, NM4 at the experiment ANKE, NM5 at the beam extraction, NM6 at the beam injection, NM7 at the experiment PISA and NM8 at the experiment EDDA.
The dose is measured permanently with the radiation surveillance system and the data is stored continuously in the personal safety system (PSA). Persons entering the inner hall must give notice of their entrance as well as their leave to the PSA via a magnetic strip card. The members of the group having the right for access wear in addition a film badge for neutron dosimetry.

The annual dose for each neutron monitor as well as the doses for the four quarters of the year are shown in the figure below.

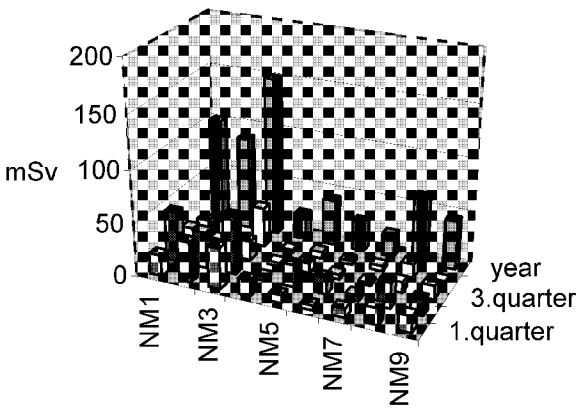

IV. EUROPEAN SPALLATION NEUTRON SOURCE (ESS)

9. TARGET PHYSICS

10. ACCELERATOR COMPONENTS

9. TARGET PHYSICS

Neutron Multiplicity Distributions for 1.2 GeV p + Al ...U

NESSI-Collaboration: C.-M. Herbach, D. Hilscher, U. Jahnke, V. Tishchenko (HMI-Berlin); A. Letourneau, A. Péghaire (GANIL-Caen); D. Filges, F. Goldenbaum, K. Nünighoff, N. Paul, H. Schaal, G. Sterzenbach, M. Wohlmuther (FZ-Jülich); L. Pienkowski (Univ. Warsaw); W.U. Schröder, J. Tõke, (Univ. Rochester)

Neutron multiplicity distributions in proton induced spallation reactions are a sensitive test of models describing such reactions. Previous measurements [1-3] studied in particular the neutron multiplicity distributions from thick targets thus providing a bench mark test of several high energy *transport* codes [4]. For testing the modeling of the primary intra nuclear cascade (INC) experimental data on thin targets are needed. Neutron multiplicity data are particularly important for deducing the excitation energy in peripheral reactions on heavier targets where little or no charged particles are emitted.

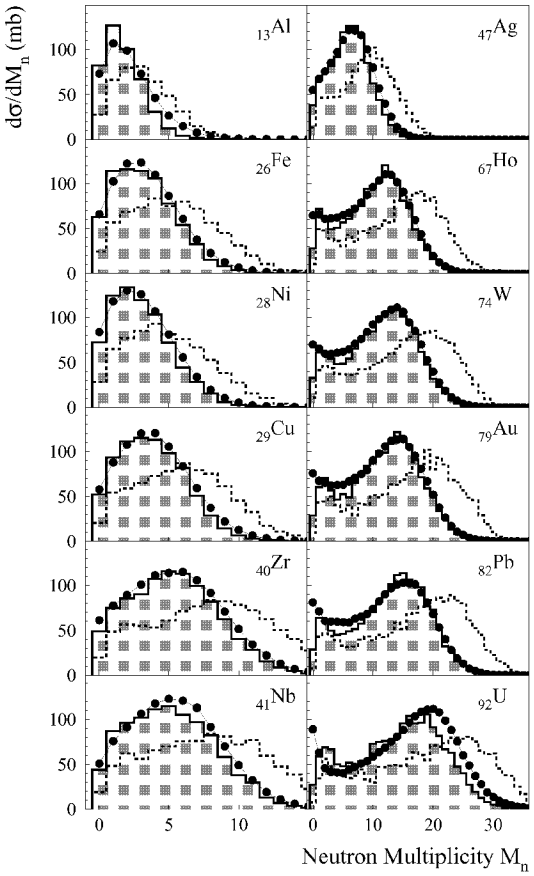

Fig. 1: Measured (•) and calculated (histogram) neutron multiplicity distributions. The calculated distributions are shown before (dashed histogram) and after folding with the neutron energy dependent detection efficiencies (shaded histogram). Note the different M_n-scales for the left and right panels.

Here we report on systematic measurements of 1.2 GeV proton induced spallation reactions on a large variety of targets: Al, Fe, Ni, Cu, Zr, Nb, Ag, Ho, W, Au, Pb, and U. The target thicknesses ranged from 0.1 to 1.0 g/cm^2 corresponding to reaction probabilities between 1 and 5×10^{-3} and consequently a negligible probability for secondary reactions. On the other hand the target thickness was large enough that the background contribution of spurious reactions outside the target was as low as 1.5 to 6% with an inelasticity threshold of about 2 MeV. This background was carefully measured separately with no target in the beam and subtracted from the measured distributions.

In Fig. 1 the measured neutron multiplicity distributions are compared with calculations with the INCL2.0 code [4] coupled with the GEMINI [4] evaporation code. In order to compare the calculated with the measured distributions the calculations were folded with the neutron energy dependent efficiency of the neutron detector BNB.

Generally the INCL2.0 calculations agree very well with the measured distributions. For heavier targets and low neutron multiplicities there exists a discrepancy between experiment and calculations. A similar discrepancy was reported previously [3] and was ascribed to the sharp cut off modeling of the nuclear density distribution in INCL2.0.

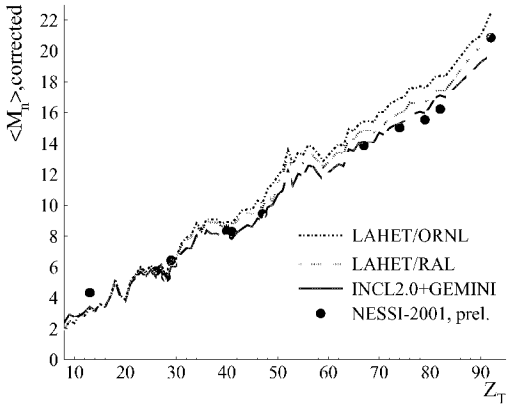

Fig. 2: Experimental (•) and calculated (lines) mean neutron multiplicities as a function of the target atomic number Z_T for 1.2 GeV proton induced spallation reactions. The measured mean multiplicities have been corrected for detection efficiency.

A good agreement with model calculations is observed for the mean neutron multiplicities as shown in Fig. 2. The measured mean neutron multiplicities have been corrected for detection efficiency. The detection efficiency is obtained by exploiting the neutron energy distributions as calculated with INCL2.0 and GEMINI. The LAHET calculations are shown for two different options of the employed Coulomb barriers (ORNL, RAL) [4]. The LAHET code tends to over predict the neutron production in heavier targets while INCL2.0+GEMINI agrees with the experimental results very well except for Al and U.

This work was supported by the HGF-Strategiefonds project "R&D for ESS", the French GEDEON project and the EU TMR-project ERB-FMRX-CT98-0244.

References:

[1] A. Letourneau et al., Nucl. Intr. Meth. B 170 (2000) 299.
[2] D. Hilscher et al., Nucl. Instr. Meth. A 414 (1998) 100.
[3] L. Pienkowski et al., Phys. Rev. C 56 (1997) 1909.
[4] D. Filges et al., Eur. Phys. J. A 11 (2001) 467, and references therein.

Systematics of Energy Dissipation in GeV Proton-Nucleus Reactions

NESSI-Collaboration: C.-M. Herbach, D. Hilscher, U. Jahnke, V. Tishchenko (HMI-Berlin); J. Galin, A. Letourneau, B. Lott, A. Péghaire (GANIL-Caen); D. Filges, F. Goldenbaum, R.-D. Neef, K. Nünighoff, N. Paul, H. Schaal, G. Sterzenbach (FZ-Jülich); L. Pienkowski (Univ. Warsaw); W.U. Schröder, J. Tõke (Univ. Rochester)

The NESSI-experiment combines two 4π detectors for neutrons and charged particles: the large spherical scintillator tank BNB (Berlin Neutron Ball) housing in its interior vacuum chamber a spherical array from 158 independent silicon detectors, the BSiB (Berlin Silicon Ball). These detectors register for each initiated reaction virtually all light particles which are evaporated from the excited target remnant in course of its de-excitation. The occurrence of the reaction itself is recognized with a very low threshold on inelasticity by the prompt scintillation light which it creates in BNB.

From the knowledge of the multiplicities of neutrons and light charged particles in the evaporation cascade we deduce[1] event-wise the amount of thermal excitation created in each reaction and therefrom we assemble the excitation energy distributions which are shown in Fig.1 for p+Au, as an example, and three incident energies, E_p= 0.8, 1.2 and 2.5 GeV. The differential cross sections $d\sigma/dE^*$ are quoted in absolute units since the number of incident protons as well as the number of induced reactions have also been gathered in the experiment.

The $d\sigma/dE^*$-distributions are rather broad and exhibit the typical 'horse's back- and -tail' shape with the Gaussian-like contribution from central collisions and the low-E^* component decreasing from low E^* towards higher E^* from peripheral collisions. The distributions extend to higher and higher excitation with increasing proton energy.

In Fig.1 we confront our data with simulations from two intra-nuclear cascade models, LAHET[2] and INCL[3]. It is obvious that, while the INCL model provides a good agreement with the experiment at all bombarding energies, the LAHET-code instead largely overestimates the cross section at high E^* for higher incident energy E_p.

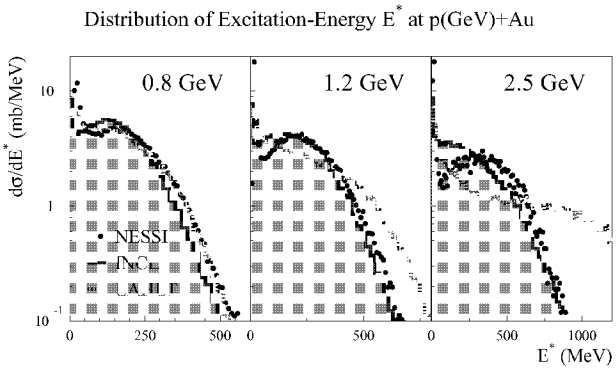

Fig. 1: Comparison of experimental (dots) and calculated excitation energy distributions for p+Au at E_p= 0.8, 1.2 and 2.5 GeV. The calculations have been performed with INCL[3] (dark histogram with shaded area) and with LAHET[2] (light histogram). It is noteworthy that the E^*-scale changes from panel to panel.

In order to provide an overview of the evolution of the E^*-spectra with increasing bombarding energy we consider the average excitation energy $<E^*>$ produced in each reaction. More specifically, we show in Fig.2 as a function of E_p the ratio $<E^*>/E_p$ which quantifies the efficiency of energy dissipation. Apart from the data for the p+Au reaction we have added first results with a much lighter target, Fe as an example, and once more we compare with the result of simulations with INC-models. The experimental data $<E^*>/E_p$ for p+Au decrease rapidly from 21% at 0.8 to only 11.5% at 2.5 GeV, while $<E^*>$ would still increase slowly from 170 to 290 MeV. The INCL-prediction follows this decrease very closely, as does the calculation with the model from Golubeva et al.[4].

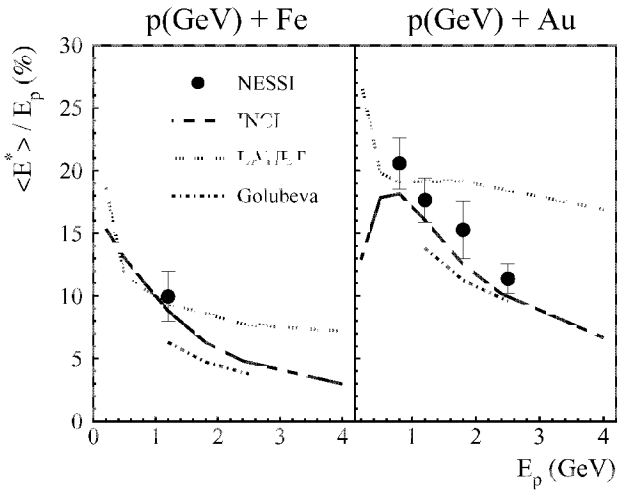

Fig. 2: Evolution of the energy dissipation, expressed by the ratio $<E^*>/E_p$ in the two reactions p+Fe, Au with bombarding energy E_p. Experimental data are shown as dots, results of calculations by lines.

The LAHET-simulation, however, provides good agreement with the experiment only at low incident energy, while at high E_p Fig.2 now reveals the full extend, i.e. a factor of 2, of discrepancy between the INC models. A closer inspection[1,5] of the INC predictions shows that the overestimation of the deposited excitation energy in LAHET correlates with an underestimation of the energy of directly emitted pions as well as nucleons.

This work was supported by the HGF-Strategiefonds project "R&D for ESS", the French GEDEON project and the EU TMR-project ERB-FMRX-CT98-0244.

References:

[1] M. Enke et al. Nucl. Phys. A 657 (1999) 317.
[2] R.E. Prael, H. Lichtenstein, Rep. LA-UR-89-3014,(1989)
[3] J. Cugnon et al. Nucl. Phys. A 620 (1997) 475.
[4] Ye.S. Golubeva et al. Nucl. Phys. A 483 (1988) 539.
[5] D. Filges et al. Eur. Phys. J. A 11 (2001) 467.

Emission of Composite Particles in the 2.5 GeV p + Au Spallation Reaction

NESSI-Collaboration: A. Letourneau, A. Böhm, J. Galin, B. Lott, A. Péghaire (GANIL-Caen); M. Enke, C.-M. Herbach, D. Hilscher, U. Jahnke, V. Tishchenko (HMI-Berlin); D. Filges, F. Goldenbaum, R.-D. Neef, K. Nünighoff, N. Paul, G. Sterzenbach (FZ-Jülich); L. Pienkowski (Univ. Warsaw); W.U. Schröder, J. Töke, (Univ. Rochester)

The investigation of composite-particle emission in spallation reactions has been pursued in detail with the help of the complementary tools of the NESSI experiment. On the one hand, the 4π coverage for neutron and light charged particle (lcp) detection allows an event-wise determination of the excitation energy E* of the heated target nucleus, on the other hand, a set of six low-threshold telescopes providing A and Z identification for the lcp (essentially H, He and Li isotopes) allows a precise characterization of all these particles as a function of E*. The experimental multiplicities for lcp's, ranging from p to ^{7}Li are shown as function of E* in Fig.1 and are compared with the result of a two-step simulation including an intra-nuclear cascade model, code INCL [1], followed by a statistical decay, code Gemini [2].

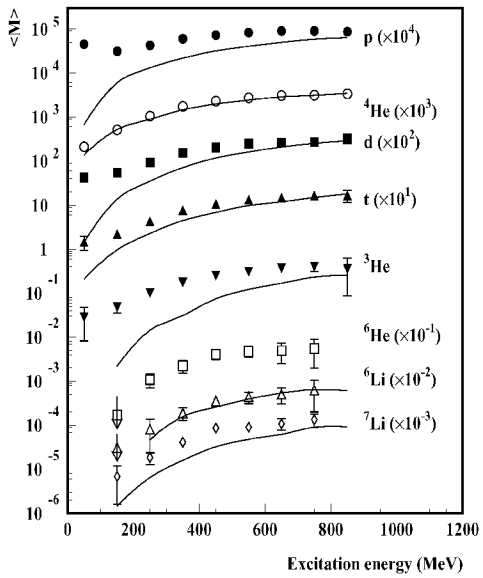

Fig. 1: Comparison of experimental (symbols) and calculated (solid lines) multiplicities of various H, He and Li isotopes as function of the excitation energy E*. A two-step model, INCL [1] combined with Gemini [2], has been used for the calculation which, however, does not allow for pre-equilibrium emission of composite particles. For protons direct emission is suppressed here for comparison.

This simulation which is restricted to evaporation can certainly not account for the observed yield of most particle species at low E*. The discrepancy between experiment and simulation is narrowing down, however, with increasing E*. At high E* some particles (e.g. ^{2}H, ^{3}H, ^{4}He, ^{6}Li) are mostly issued from a statistical emission, whereas others (^{1}H or ^{3}He) are emitted both, prior and past to the attainment of thermal equilibrium. Among all particles the two neighboring isotopes of He, ^{3}He and ^{4}He, exhibit extreme behaviors: the strongly bound ^{4}He is shown to be almost exclusively evaporated whatever E*, while ^{3}He is mostly of non-evaporative character whatever E*, with at best 50% of evaporative component at high E*.

This comparison thus reveals the strong deficiency of the intra-nuclear cascade models which do not consider pre-equilibribum emission of composite particles, direct emission prior to evaporation being a common feature of all ejected particles. Direct emission amounts to 61, 44, 34, 68 and 11% of the total emission for the most abundant lcp's: p, d, t, ^{3}He and ^{4}He, respectively.

The non-evaporative component of ^{3}He, together with that of ^{2}H and ^{3}H has been satisfactorily accounted for by building up composite particles by coalescence during the INC process [3].

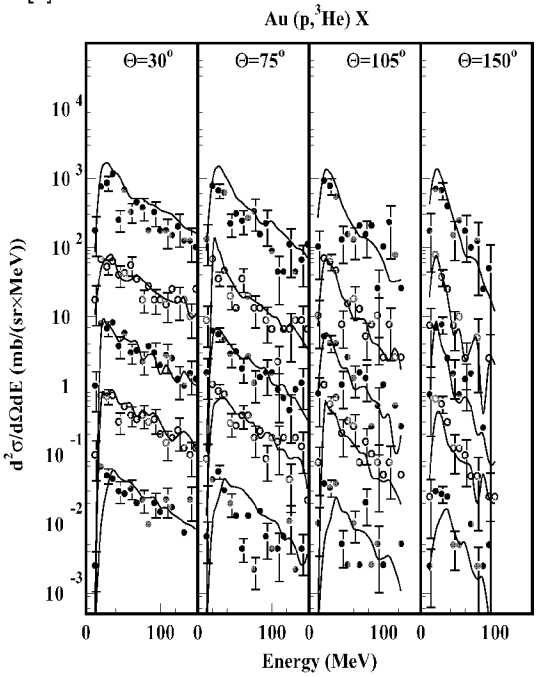

Fig. 2: Doubly differential cross sections for the emission of ^{3}He, observed at Θ= 30°, 75°, 105° and 150° and for five bins in E* (from top to bottom: E*= 0-220, 220-370, 370-470, 470-570, >570 MeV). The experimental data are indicated by dots, the simulation which now includes coalescence is shown as lines. A scaling factor 10^{i}, i= 0- 4 has been applied to the spectra in each panel, beginning with i= 0 at the bottom.

In Fig.2 we show for ^{3}He that not only the integrated cross section can thus be reproduced but also the doubly differential ones (at 4 emission angles) for several E* bins. While a similar good agreement is reached also for d and t, the coalescence concept in its present version seems to fail for the strongly bound ^{4}He.

This work was supported by the HGF-Strategiefonds project "R&D for ESS", the French GEDEON project and the EU TMR-project ERB-FMRX-CT98-0244.

References:

[1] J. Cugnon et al. Nucl. Phys. A 620 (1997) 475.
[2] R.J Charity et al. Nucl. Phys. A 483 (1988) 391.
[3] A. Letourneau, PhD-thesis, Caen, 2000 and to be publ.

Data Library of spallation products in proton induced reactions

PISA collaboration: V. Bollini, A. Bubak, D. Filges, F. Goldenbaum, K. Kilian, P. Kulessa, H. Machner, R.-D. Neef, H. Ohm, N. Paul, K. Pysz, H. Schaal, R. Siudak (FZJ-Jülich); R. Czyżykiewicz, A. Heczko, L. Jarczyk, B. Kamys, St. Kistryn, W. Klimala, A. Magiera, W. Migdał, B. Piskor-Ignatowicz, Z. Rudy, M. Wojciechowski (Jagellonian Univ. Kraków); A. Budzanowski, M. Kistryn, St. Kliczewski (INP Kraków); J. Kisiel, E. Stephan, W. Zipper (Univ. Silesia, Katowice); R. Barna, D. De Pasquale, A. Italiano (Messina Univ. and INFN, Messina); S. Förtsch, D. Steyn, T. Thovhogi (NAC Faure); J. Cugnon (Univ. de Liege); H. Hodde (Univ. Bonn)

During the past many experiments provided a huge set of production cross sections data in proton induced spallations reactions. Unfortunatelly among collected data there are not many cross sections for production of the lightest isotopes such as hydrogen or helium. A collections of such data for proton induced spallation processes in a wide energy range (up to several GeV) on thin targets will allow to test the validity and improve the predictions of INC (Intranuclear Cascade) and evaporation models currently available on the market. Such data are also very important and essential for assessment of material damage due to gas production and arising swellings or embrittlement. All this processes are very important for ESS (European Spallation Source) target constractions.

This was the motivation to start at the beginning of this year the creation of a data base for hydrogen and helium production cross sections in the framework of the HINDAS project (**H**igh and **I**ntermediate energy **N**uclear **D**ata for **A**ccelerator-driven **S**ystems). Now this data base is a compilation of experimental cross sections for proton-induced isotope production at energies from a few MeV to 10 GeV. There are also some data for energies up to 30 GeV. Presently, for proton-induced reactions, this compilation contains about 15,000 data points, for 38 targets of 50 elements. All data are derived from avaliable literature and private communications.

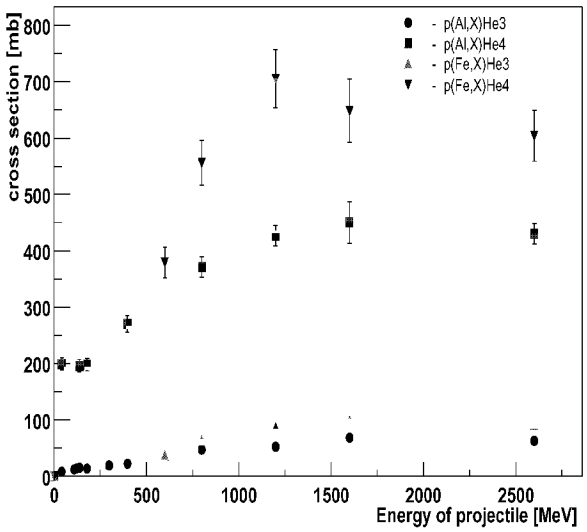

Fig. 1: Example 1 of data available from the data base: total cross sections for He isotopes production as function of incident proton energy.

Each record of the data base contains the following information: target, atomic mass of the target, atomic number of the target, proton energy of the projectile [MeV], error of the proton energy [MeV], type of ejectile, atomic mass of the nuclide, atomic number of the nuclide, total production cross section [mb], error of the production cross section [mb], angle, references, comments.

The whole database was orginally written in "excel format" (Microsoft Excel) and in this format is further developed. Actually this database is also availabe for users through the Web under address:

www.nuph.us.edu.pl/~pisa/baza/sign.html

In order to make the data base accessible through the web it was transfered to raw ASCII format.

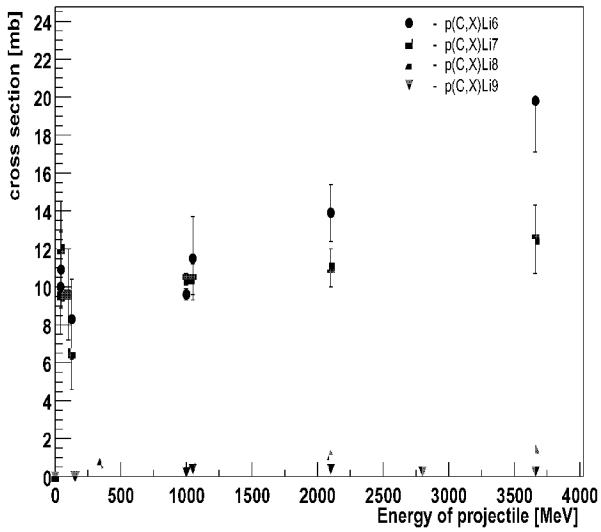

Fig. 2: Example 2 of data available from the data base: total cross sections for Li isotopes production as function of incident proton energy.

The users have two possibilities to select the data through the web page. So called simple selection and second one, more detailed, with more additional options. In the first case selection is available only under one condition (e.g. 'Target' **or** 'Proton energy of the projectile'). In the second one, there is possibility of the selection under a few conditions (e.g. 'Atomic mass of the target' **and** 'Atomic number of target' **and** 'Type of ejectile'). After applaing selection the data will be displayed in web page format. Downloading the selected data is possible as well. The downloaded file is in ASCII format. The library is continuously in progress and frequently updated.

This work is supported by the BMBF-Verbundforschung, the EU-LIFE program, the EU HINDAS project FIS5-1999-00150, and the EU TMR project ERB-FMRX-CT98-0244.

The first results from PISA experiment

PISA collaboration: V. Bollini, A. Bubak, D. Filges, F. Goldenbaum, K. Kilian, P. Kulessa, H. Machner, R.-D. Neef, H. Ohm, N. Paul, K. Pysz, H. Schaal, R. Siudak (FZJ-Jülich); R. Czyżykiewicz, A. Heczko, L. Jarczyk, B. Kamys, St. Kistryn, W. Klimala, A. Magiera, W. Migdał, B. Piskor-Ignatowicz, Z. Rudy, M. Wojciechowski (Jagellonian Univ. Kraków); A. Budzanowski, M. Kistryn, St. Kliczewski (INP Kraków); J. Kisiel, E. Stephan, W. Zipper (Univ. Silesia, Katowice); R. Barna, D. De Pasquale, A. Italiano (Messina Univ. and INFN, Messina); S. Förtsch, D. Steyn, T. Thovhogi (NAC Faure); J. Cugnon (Univ. de Liege); H. Hodde (Univ. Bonn)

The first run at 1.9 GeV incident proton energy and Au target was undertaken in August 2001 with the aim to test all experimental equipment, and to take first data of proton induced spallation reactions. The detecting arms [1] consisted of two multichannel plates working as a START and STOP detector for the time-of-flight measurement, a Bragg curve detector followed by three silicon detectors of 100, 300 and 4900 μm thickness for particle identification and kinetic energy measurement, and a set of double layer scintillation detectors ("phoswich").

It was expected that the TOF plus Bragg curve detectors provide identification of light heavy ions with mass up to 20 - 30 and kinetic energy starting from less than 1 MeV/amu. Unfortunately the experiment has been strongly hampered by the unexpected breakdown of a foil in the Bragg curve detector. Consequently only a part of the detecting system was tested. Here we present results obtained for two silicon detectors (100 and 300 μm) working as a telescope.

The light ejectiles (Z<7) were clearly visible in the coincidence spectra in the energy range given in the table below. Excellent Z identification has been achieved whereas only

Ejectile	He	Li	Be	B	C
E_{min} / MeV	12	25	40	50	65
E_{max} / MeV	30	60	90	125	155

moderate A identification has been possible (cf.Fig.1).

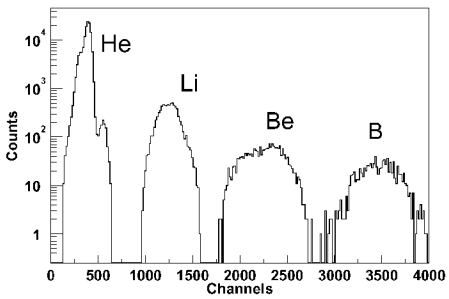

Fig. 1: Histogram of coincidence events for light heavy-ions with Z=2–5 registered by Si-telescope – obtained by projection of two-dimensional spectrum ΔE(Si1)-E(Si2) onto the ΔE(Si1) axis.

In Figs 2 and 3 the spectra of He and Be particles are presented as examples. For these two elements instability of ^{5}He and ^{8}Be allows for very good separation of ^{6}He and ^{7}Be from other isotopes. This enabled also to estimate the typical width of peaks in the spectra and thus allows to continue separation of other isotopes by fitting of Gaussian curves with fixed width parameter.

It is visible in Figs. 1 and 2 that separation of particles originating from ejectiles differing in the mass number by 1 unit is, in principle, possible even with silicon telescope alone. However, strong overlapping of Gaussian peaks calls for some improvement of the detecting system. The mass

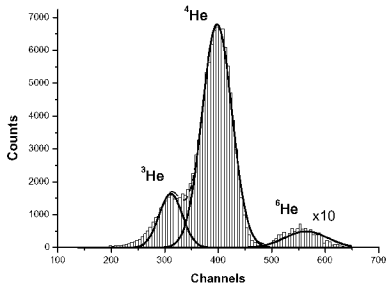

Fig. 2: The same histogram as in Fig. 1 but for He - ions. Solid lines show the Gaussian peaks fitted to the histogram.

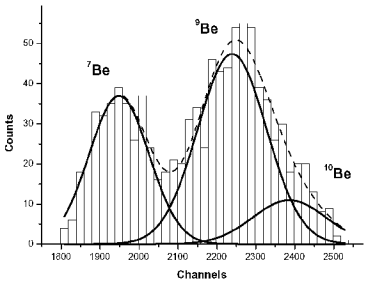

Fig. 3: The same histogram as in Fig.2 but for Be - ions

number identification can be significantly improved by increasing the energy resolution of silicon detector telescope and/or by adding independent information from time-of-flight (TOF) detectors. The former idea will be applied in the forthcoming experiments by cooling the silicon detectors to $\sim$ -20^{o}C to improve their energy resolution in comparison to presently achieved of about 7%. As discussed in a separate contribution to this Annual Report this should enable good mass resolution of light heavy ions (up to A $\sim$ 16) by silicon telescope alone and allow to measure spectra of these ions in energy range $\approx$ 3.5 MeV/amu - 50 MeV/amu. The ions with larger mass number and energy in the above range will be stopped in the gas of the Bragg-curve detector or in the first Si-detector of the telescope and therefore cannot be identified by Si-telescope itself. The previous tests of the Bragg curve detectors and phoswiches [2] showed that they allow to achieve a good energy resolution for the lowest and the highest energies of light ejectiles, respectively.

This work is supported by the BMBF-Verbundforschung, the EU-LIFE program, the EU HINDAS project FIS5-1999-00150, and the EU TMR project ERB-FMRX-CT98-0244.

References:

[1] IKP Annual Report 1999, p. 175-176
[2] IKP Annual Report 2000, p. 172-173

Bragg-curve and silicon detector telescope for PISA

PISA collaboration: V. Bollini, A. Bubak, D. Filges, F. Goldenbaum, K. Kilian, P. Kulessa, H. Machner, R.-D. Neef, H. Ohm, N. Paul, K. Pysz, H. Schaal, R. Siudak (FZJ-Jülich); R. Czyżykiewicz, A. Heczko, L. Jarczyk, B. Kamys, St. Kistryn, W. Klimala, A. Magiera, W. Migdał, B. Piskor-Ignatowicz, Z. Rudy, M. Wojciechowski (Jagellonian Univ. Kraków); A. Budzanowski, M. Kistryn, St. Kliczewski (INP Kraków); J. Kisiel, E. Stephan, W. Zipper (Univ. Silesia, Katowice); R. Barna, D. De Pasquale, A. Italiano (Messina Univ. and INFN, Messina); S. Förtsch, D. Steyn, T. Thovhogi (NAC Faure); J. Cugnon (Univ. de Liege); H. Hodde (Univ. Bonn)

It was planned to use in PISA experiment – devoted to investigation of proton induced spallation of nuclei – Bragg-curve detectors combined with time-of-flight measurement by 2 multi-channel-plates (MCP's) for particle identification and their energy determination [1]. Additionally the telescopes of 3 Si detectors and phoswiches are planned to be applied for detection of high energy light heavy-ions.

In the table below we present estimation of the energy range of ejectiles for two versions of the detecting system: 1) the system consisted of 2 MCP's, Bragg-curve detector (BCD), and telescope of 3 Si detectors of thickness 100 μm, 300μm, and 4900 μm, and 2) the Si telescope itself. The minimum energies of ejectiles which allow their identification are shown in the 2nd and 3rd column for the first and the second system, respectively. In both cases the maximum detection energy or to be more precise the punch through (4th column of the table) is determined by thickness of Si telescope . For heavier ejectiles the BCD is crucial for detection of the main part of the evaporation spectrum which is concentrated at energies close to the Coulomb barrier of ejectile-residual nucleus system. Furthermore, the BCD can serve as ΔE detector for ejectiles which are not stopped in the gas of BCD and give also signal in Si detectors. In Fig. 1 the coincidence spectra of energy registered in BCD versus energy deposited in first two Si detectors of thickness of 100 μm and 300 μm as calculated with the program package GEANT are presented. The discontinuities visible on the smooth lines of energy(BCD)-energy(Si1+Si2) dependence appear because of presence of the gas (isobutane) between Si1 and Si2 detectors. In Fig. 2 and Fig. 3 the coincidence spectra are presented obtained from two Si detectors (without taking into account information obtained from the Bragg curve detector). The lowest energy detected in BCD or in the first Si detector which still allows for distinguishing true signal from the detector noise is marked by a small arrow in Figs. 1 and 2. In all cases the following energy resolution of detectors was assumed; 2% for BCD, 4% for 100 μm Si, and 2% for 300 μm and 4900 μm Si. It is planned to use in experiment the silicon detectors cooled to temperature $\approx$ -20^{o}C what should enable to get energy resolution even better than assumed here. Thus it can be concluded that using such a telescope it is possible to identify Z and A of ejectiles to at least $\sim$ A=16.

Ejectile	E_{min}(MeV)		E_{max}(MeV)
	1^{st} system	2^{nd} system	both systems
Proton	5	5	30
^{4}He	5	12	130
^{7}Li	8.5	25	250
^{9}Be	11	40	400
^{11}B	12	50	530
^{12}C	15	65	700
^{20}Ne	25	150	1550
^{28}Si	35	240	2600

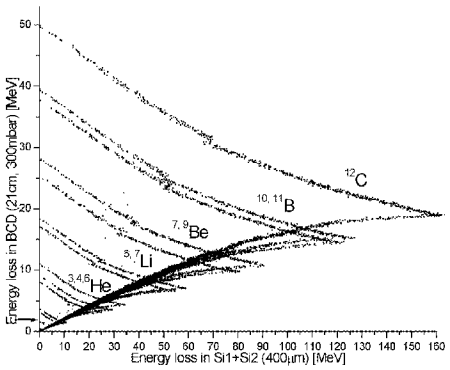

Fig. 1: Energy loss in BCD versus energy loss in the 1st and the 2nd Si detector for light heavy-ions with Z=2-5.

This work is supported by the BMBF-Verbundforschung, the EU-LIFE program, the EU HINDAS, and the EU TMR project.

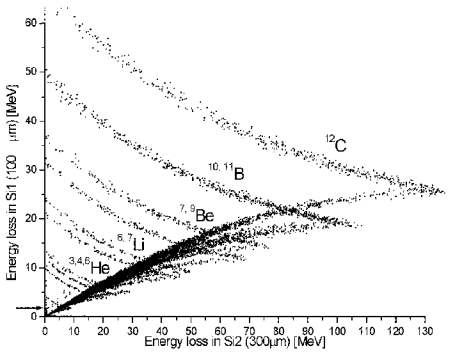

Fig. 2: Same as in Fig.1 but for energy loss in the 1st Si (100 μm) vs energy loss in the 2nd Si detector (300 μm).

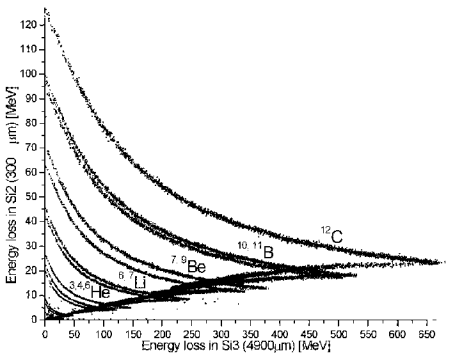

Fig. 3: The same as in Fig. 2 but for the second pair of silicon detectors (300 μm and 4900 μm).

References:

[1] IKP Annual Report 1999, p. 175-176

Investigations of the Neutronic Performance of the ESS Long Pulse Target Station

D. Filges, F. Goldenbaum, B. Haft (TU-Graz), R.-D. Neef, K. Nünighoff, Ch. Pohl, G. Sterzenbach, M. Wohlmuther (IKP)

In contrast to the ESS reference design [1] with four moderator positions the geometry for the long pulse target station provides only two moderators, an ambient temperature water moderator and a liquid para-H_2 moderator at 20 K. The thickness of the moderator is 5 cm. In case of the cold hydrogen moderator an extended water premoderator with a thickness of 2.5 cm is used. As a target a liquid Hg target -same as in the short pulse target station- was choosen. Also the reflector material (Pb with 15 Vol.-% D_2O and the dimensions (180 cm in diameter and height) are equal to the design of the short pulse target station.
The Monte-Carlo simulations are performed with MCNPX-code [2]. The obtained neutron flux- and current densities for an ambient water- and a cold para-H_2-moderator for the above mentioned geometry are listed in Tab. 1. The influence of several parameters

Moderator	$\hat{\Phi}$	$\hat{J}$	$\bar{\Phi}$	$\bar{J}$
	in $[n \cdot cm^{-2} \cdot s^{-1}]$			
para-H_2	$9.6{\cdot}10^{15}$	$1.7{\cdot}10^{15}$	$2.3{\cdot}10^{14}$	$6.9{\cdot}10^{13}$
Water	$7.2{\cdot}10^{15}$	$1.1{\cdot}10^{15}$	$3.0{\cdot}10^{14}$	$4.5{\cdot}10^{13}$

Table 1: *Peak and average thermal (E≤0.431 eV) neutron flux- and current densities.*

was also studied. Fig. 1 gives an impression of the influence of different reflector materials on the neutron current density. It can be seen that the highest current can be achieved when using a Be-reflector instead of a Pb-reflector. The maximum current of a Be-reflector is

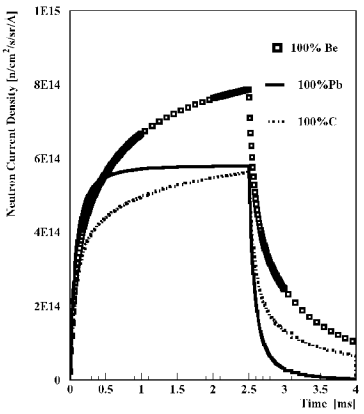

Fig. 1: *Time distributions of thermal neutron current densities for different reflector materials. In this case a liquid H_2-moderator was used.*

35 % higher than for a Pb-reflector. But the decay time will be much longer as compared to Pb. The decay constant of a graphite reflector with 153 μs is between Be with 198 μs and Pb with 95 μs. The advantage of the Pb reflector is the long period of constant neutron current during the pulse and a short decay time. In a further parameter study the influence of the moderator thickness was investigated. Extending the thickness of the para-H_2 moderator leads to an increase of the neutron current.

The possibility of a flux-trap target at ESS was investigated. In this case the target is splitted into two parts and the moderators are positioned at the gap between the front and back target [3, 4]. In contrast to the LANSCE [3] design with four moderators surrounding the gap ESS can only use two moderators. This is due to the horizontal beam instead of a vertical beam impinging on the target. Thus a four moderator design with its gain due to the interaction of all moderators is not feasible at ESS. As can be seen in Fig. 2 the flux-trap target yields a 10 % higher neutron flux density as compared to the above described reference design (wing geometry). But the technical effort to operate such a target is unjustified.
This work is partly supported by the TMR program of the European Community under contract No.:FMRX-CT98-0244.

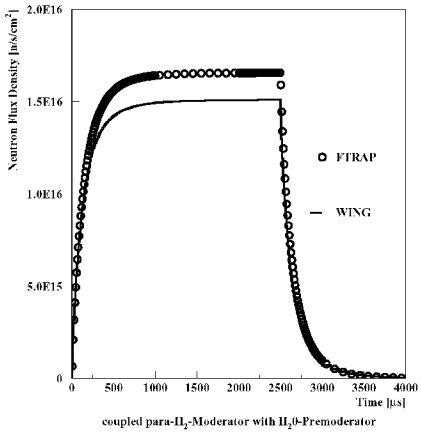

Fig. 2: *Comparison of a flux-trap (open circles) and a wing geometry (solid line). The neutron flux densities inside a premoderated para-H_2 moderator are plotted.*

References:

[1] ESS Volume III. The ESS Technical Study. ISBN 090-237-6-659, November 1996.

[2] H.G. HUGHES et al., *MCNPX–The LAHET/MCNP Code Merger*, X-Division Research Note XTM-RN(U)97-012, LA-UR-97-4891, Los Alamos National Laboratory (1997)

[3] G.J. Russel et al., *The LANSCE Target System*, ICANS-IX, p.177, Villigen, Switzerland, September 1986

[4] Y. Kiyanagi et al., *Neutronic studies on flux-trap moderators in spallation neutron sources*, NIM A 343(1994), 550-557

Investigations of the Neutronic Performance of the ESS Short Pulse Target Station

D. Filges, F. Goldenbaum, B. Haft (TU-Graz), R.-D. Neef, K. Nünighoff, Ch. Pohl, G. Sterzenbach, M. Wohlmuther

The neutronic performance of the the short pulse target station as described in [1] was investigated in more detail. In contrast to [1] all values are calculated for a perturbed system including e.g. beam holes. This modification leads to lower neutron flux- and current densities. The average and peak values are listed in

Moderator	$\hat{\Phi}$	$\hat{J}$	$\bar{\Phi}$	$\bar{J}$
	in $[n \cdot cm^{-2} \cdot s^{-1}]$			
para-H_2	$9.0{\cdot}10^{16}$	$2.5{\cdot}10^{16}$	$3.2{\cdot}10^{14}$	$9.2{\cdot}10^{13}$
Water	$1.3{\cdot}10^{17}$	$2.3{\cdot}10^{16}$	$3.1{\cdot}10^{14}$	$4.2{\cdot}10^{13}$

Table 1: *Peak and average thermal (E≤0.431 eV) neutron flux- and current densities for the coupled moderator setup.*

Tab. 1.

The simulations were performed for an ambient temperature water moderator and a 20 K cold liquid para-H_2 moderator. As a reflector a pure Pb cylinder with a diameter and height of 180 cm was used. For both moderator types a coupled, decoupled, and a decoupled-poisoned setup were considered and the wavelength dependence of the neutron current and

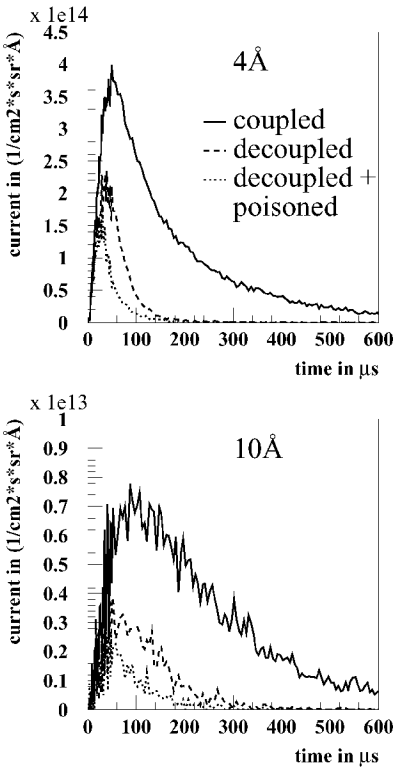

Fig. 1: *Time distributions of the neutron current density for 4 and 10 Å for the three different hydrogen moderator setups.*

peak width was investigated. As a decoupler a 1 mm thick Cd-layer was applied to decrease the pulse width. Further decrease of the pulse width can be achieved by additionally poisoning the moderator with a 0.5 mm thick Gd-layer in the midplane of the moderator. The influence of the different configurations on the time distribution of the neutron pulse are shown in Fig. 1 for a para-H_2-moderator for two wavelengths. The pulse width FWHM can be reduced to 69 % (61 %) for 4 Å (10 Å) when decoupling and poisoning the moderator. The decrease of the neutron current density when decoupling or poisoning the moderator -which is in an order of a factor 3- can also be seen. Further the broadening of the peak width for longer wavelength is evident. Fig. 2 gives an impression of the pulse

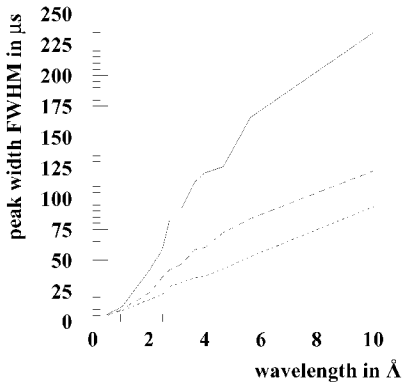

Fig. 2: *Neutron pulse widths (FWHM as function of wavelength for the three different hydrogen moderator setups. Legend see Fig. 1.*

width as a function of the wavelength for the three H_2-moderator configurations.

One of the interesting points is the feasability of poisoning in a real system. This has a strong impact on the expected life time of the poisoning layer inside a cold H_2 moderator which will burn up due to nuclear reactions. To estimate the burn-up of a Gd-layer a neutron flux Φ_{th}=$5{\cdot}10^{13}$ n/cm^{2}s at the poisoning surface was calculated. The neutron absorbing isotopes are ^{155}Gd and ^{157}Gd with a density of $4.6{\cdot}10^{20}$ atoms per cm^2. Assuming that all neutrons are absorbed in one of these isotopes the estimated lifetime -including breeding of ^{155}Gd and ^{157}Gd- is about 106 days.

This work is partly supported by the TMR program of the European Community under contract No.:FMRX-CT98-0244.

References:

[1] ESS Volume III. The ESS Technical Study. ISBN 090-237-6-659, November 1996.

[2] H.G.HUGHES et al., MCNPX–The LAHET/MCNP Code Merger, X-Division Research Note XTM-RN(U)97-012, LA-UR-97-4891, Los Alamos National Laboratory (1997)

Neutronic Investigations of Moderators with JESSICA

for the JESSICA-Collaboration: V. Bollini, A. Bubak, D. Filges, F. Goldenbaum, R.-D. Neef, K. Nünighoff, N. Paul, Ch. Pohl, D. Prasuhn, H. Schaal, G. Sterzenbach, M. Wohlmuther (IKP); H. Conrad (IFF); H. Soltner, H. Stelzer (ZAT); H. Tietze-Jaensch (ESS-CPT); B. Haft, W. Ninaus (TU-Graz); A. Smirnov (JINR-Dubna)

At the JESSICA experiment measurements with ambient temperature water and polyethylene moderators were performed. In the first phase the JESSICA experiment was used to measure the time of flight spectrum of the neutrons leaving the moderator surface. The shape of the time of flight spectra of the thermal neutrons was compared with MCNPX [1] simulations. As can be seen

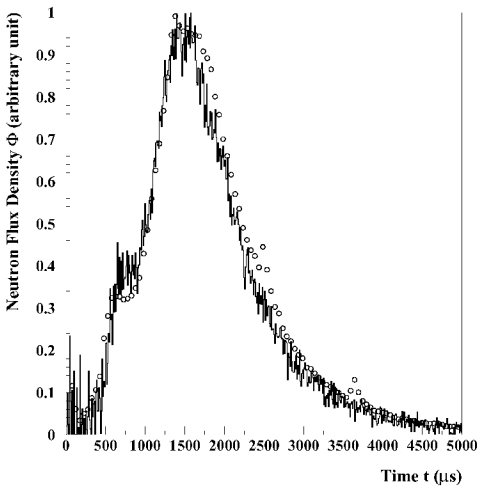

Fig. 1: *Comparsion of the thermal neutron time of flight spectra between experiment (open circles) and MCNPX (solid line). The peak values of the graphs are normalized to one.*

in Fig.1 both are in very good agreement. At the moment the comparison of absolute values is not possible because of difficulties in the determination of the exact number of protons per pulse and number of neutrons per pulse (efficiency, deadtime).

In the second phase a pyrolitic graphite crystal and a second neutron flight path perpendicular to the first flight path were installed. The

neutrons scattered at the crystal allow to study the time structure of the neutron pulses at several wavelengths. The sensitivity of the experiment to measure changes in the pulse width of the neutron pulse was demonstrated with a polyethylene moderator. When de-coupling and poisoning the moderator a decrease in both pulse widths and peak intensities was observed. For example the pulse width FWHM at 2.37 Å is 79.3 μs for a coupled polyethylene moderator and 70.7 μs for de-coupled poisoned one. A first test with a simple liquid nitrogen cooled ice moderator was performed. In Fig. 2 the time of flight spectra of the scattered neutrons are shown. It can be seen, that relative to the ambient water moderator the peak intensity increases at longer wavelengths for the ice moderator. From the time of flight spectrum the moderator temperature can be determined by transforming the data from $\phi(t)$ to $\phi(v)/v^3$ and t to v^2. From the semi-logarithmic graph of $\phi(v)/v^3$ versus v^2 the gradient of the regression line gives the moderator temperature. For an ambient temperature water moderator the experimental data results to a moderator temperature of 307 K which is slighlty higher than the real temperature of about 295 K. The moderator temperature derived from the ice moderator is 147 K. Fig. 3 shows the different regression lines for both moderators.

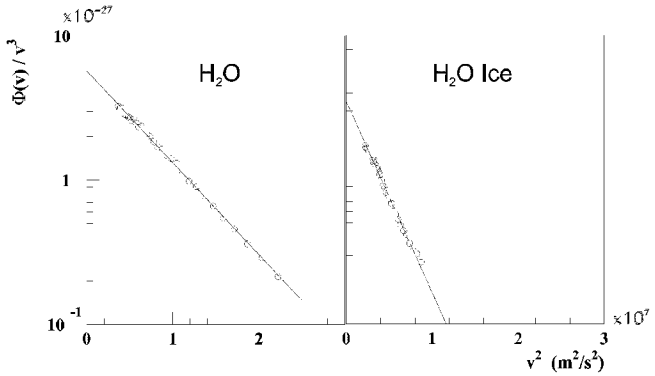

Fig. 2: *Regression lines for an ambient water moderator and a cold ice test moderator at liquid nitrogen temperature.*

These experiments demonstrate the feasibility of the JESSICA experiment to investigate the neutronic performance of advanced cold moderators. In the next beam times an ice moderator and a methan-hydrate moderator at ≈20 K will be studied.

This work is partly supported by the TMR program of the European Community under contract No.:FMRX-CT98-0244.

References:

[1] H.G.HUGHES et al., MCNPX–The LAHET/MCNP Code Merger, X-Division Research Note XTM-RN(U)97-012, LA-UR-97-4891, Los Alamos National Laboratory (1997)

10. ACCELERATOR COMPONENTS

Preliminary Design of ESS Target Beamlines

J.Y. Tang, A. Lehrach, R. Maier, S. Martin, S. Schwenke

1 Introduction

Since the ESS Technical Report [1] was published in 1996, the project goal has been modified. A new 5MW long pulse target station (LPTS) of 16.67Hz repetition rate and 2.5ms duration is added to take the beam directly from the Linac, and the original 10Hz target station is taken out as well as the muon target in the beamline to 50Hz short pulse target station (SPTS). Therefore, a new beam transfer system to the targets has been studied. The beam sizes at the targets should be in both cases 200mm (horizontal) and 60mm (vertical). The beamlines to these target stations have to be designed to accept 5MW beam power with different beam characteristics at the entrance.

2 Beamline to the Long Pulse Target Station

Two different types of ion sources (H^- and H^+ sources) for the LPTS are under consideration. Therefore, the extraction scheme to the LPTS has to be designed to accept both types of beams.

A kicker and two bumpers are used for fast switching between long pulse beam and short pulse beam. In the case of long pulse beam also in H^-, two strippers are inserted to convert the H^- beam into H^+ beam in the line to LPTS, whereas in the case of long pulse beam in H^+ no stripper is used. The bumpers bend the H^+ beam back into the linac axis. The two strippers in the switchyard to LPTS are very important, perhaps as critical as the one for ring injection. They have to assure nearly 100% conversion of H^- beam into H^+ beam. Since there is a section of emittance blow-up downstream, the beam halo created by H^0 and H^- beams after the first stripper can be kept in the main beam. The linac beam dump is along the linac axis on the same vertical level. This makes the linac commissioning and beam setup easier and safer because the kicker and the bumpers are switched off to dump both types of beams.

The LPTS is located horizontally along the linac axis on a different vertical level. The beam is lifted in an achromatic vertical bending section by 4.3m from the linac level (2.8m below ground) to the target level (1.5m above ground). A long section consisting of many modules (about 10 to 20) of quadrupoles and sextupoles is under study to blow up the transversal emittance from less than 1.0πmm.mrad to more than 10πmm.mrad with gaussian distribution. This procedure is very important to get the required beam profile stability at the target.

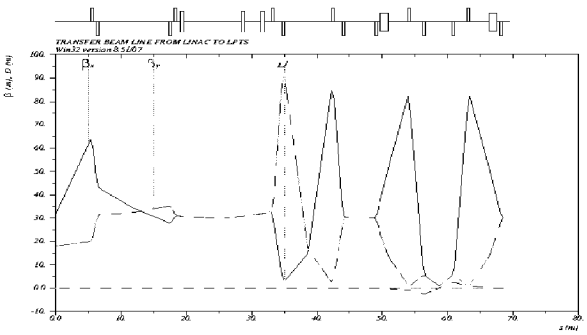

Figure 1, Beta functions and dispersions for the LPTS beamline

3 Beamline to the Short Pulse Target Station

The design of the beamline from the rings to the SPTS is based on the work done by V. Ziemann [2] with some modifications. Since the emittance is as big as 30πmm.mrad (r.m.s) and nearly equal in the horizontal and vertical planes, the 90° FODO design is a good solution for the main focusing structure.

The beam merging behind the two accumulator rings is done by bending down the beam from the upper ring with a combination of ordinary dipole, septum and kicker magnets. The beam dump is on the same vertical level like to lower ring. A 45° achromatic horizontal bending section directs the beam either to the SPTS or to the beam dump by switching off the first dipole magnet. As in the case of LPTS, an anti-symmetric vertical bending section lifts the beam by 4.3m to the target station. A section of about 40m is reserved for a possible muon target and is presently substituted by standard FODO modules.

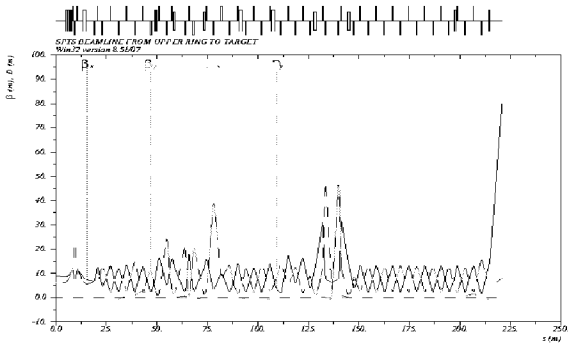

Figure 2, Beta functions and dispersions for the beamline SPTS-upper ring

4 Magnets, Beam dumps and Beam Diagnostics

Ordinary rectangular dipoles, septa, kickers, quadrupoles and non-linear magnets are used for beam guiding, beam focusing and beam preparation. Many dipoles and quadrupoles are powered in series to save costs and to increase the reliability of the whole system. Some correctors are needed for beam alignment.

There are two main beam dumps for the commissioning and the beam set-up of the linac and the two rings. It has not been determined yet what kind of beam dumps will be built: full power dumps of 10MW for the linac and 5MW for the rings or only dumps of 200kW for reduced repetition rate.

The beam diagnostics system is very important for machine commissioning and beam set-up as well as for safety control of the whole system. It includes beam position monitors, beam loss monitors, beam profile monitors and beam current monitors. We have to study what kind of beam diagnostic devices can work under ESS beam power conditions with reasonable lifetime and low beam interaction to avoid additional radiation.

Reference:

[1] ESS – A Next Generation Neutron Source for Europe – Volume III – The ESS Technical Study, ESS-96-53-M-3

[2] V. Ziemann, New Optics of ESS Target Beam Lines, ESS-96-54-R

Funneling System for the European Spallation Neutron Source ESS

Yu.Senichev, W.Bräutigam, R.Maier,
Forschungszentrum Jülich GmbH, Institut für Kernphysik,
D-52425 Jülich, Germany

A.Barsukov, O.Belyaev, Yu.Budanov, I.Grushichev,
V.Stepanov, V.Teplyakov, A.Zherebtsov, I.Zvonarev,
IHEP, Protvino, Russia

The funneling system allows reaching the required ESS beam intensity of 107 mA in peak per micro pulse, when two identically bunched beams are merged into a single beam with double intensity. Besides, in case of one frequency after funnelling the intensity in each bunch is lower.
Basic principle is based on the resonant method of the beams funnelling in the multi-gap deflector [1]. The new idea differs from another ones by the possibility to organize the π-mode standing wave deviation system. The method has the higher efficiency.

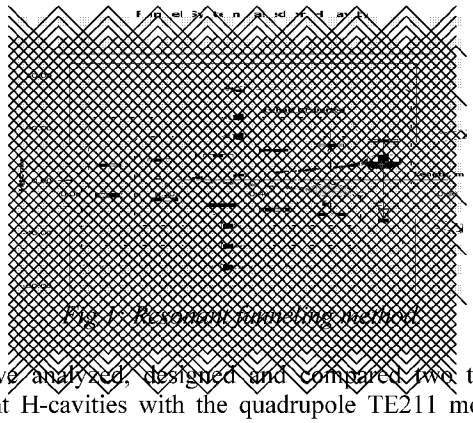

Fig.1: Resonant funneling method.

We have analyzed, designed and compared two types of different H-cavities with the quadrupole TE211 mode and the dipole TE111 mode. They both can provide the effective resonant merging of beams. The construction based on TE211 mode reminds the RFQ cavity, but instead of the modulated wanes we use the capacities connected to the wanes by the special order. Additionally we have developed the new construction of the funnel device, based on the lower TE111 mode, where the ratio between the cavity radius and the wavelength is smaller.

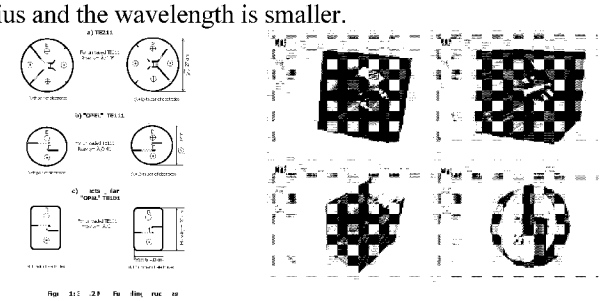

Fig.2: The different types of modes and cavities for beam funnelling.

Three different cavities with 352 MHz for funneling have been investigated experimentally. The field distribution, the tuning and the cooling system have been tested and compared with the numerical results.

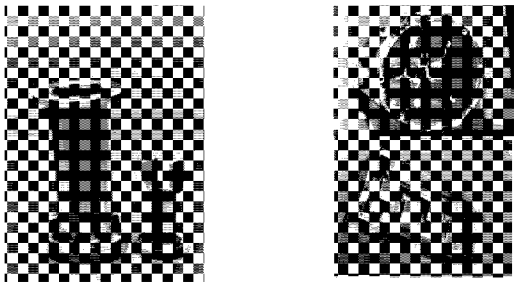

Fig.3: Three different cavities for funneling.

The transverse electrical field in the longitudinal direction has been calculated by MAFIA The angle and space deviations of bunches are determined by:

$$\Delta\left(\frac{dx}{dz}\right)=\frac{eE_1\cos\varphi}{2m_0c^2\gamma\beta^2}\cdot n\left(\frac{\beta\lambda}{2}\right)$$

$$\Delta x=\frac{eE_1\cos\varphi}{4m_0c^2\gamma\beta^2}\cdot n^2\left(\frac{\beta\lambda}{2}\right)^2$$

The beam dynamics has been calculated numerically in the real field for the energy 5 MeV and 25 MeV.

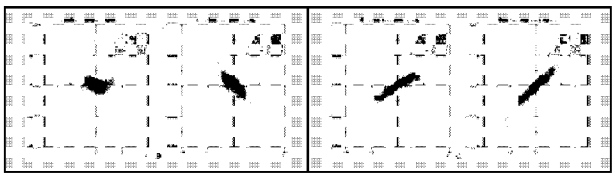

Fig.4: The phase portrait of beam on the entrance and exit of funneling

For both options the emittance growth does not exceed 2% and 10% in case of bunch frequency 350 MHz and 175 MHz correspondently.

References

[1] Yu. Senichev and W.Bräutigam, The resonant pi-mode multi-gap funneling and de-funneling systems, HEACC 2001, Tsukuba.

Pulsed power amplifier for ESS test of a 500 MHz superconducting cavity

H.G. Böge, W. A. Brocke*, H. Meier*, A. Schnase (IKP), H. Singer

In 1999 the Siemens UHF television transmitter which we got as a loan from ACCEL Instruments, Bergisch Gladbach, was installed. In 2000 this tube amplifier was brought "back to life" and modified for pulsed mode operation at the ESS superconducting test cavity. This set-up is shown in fig. 1.

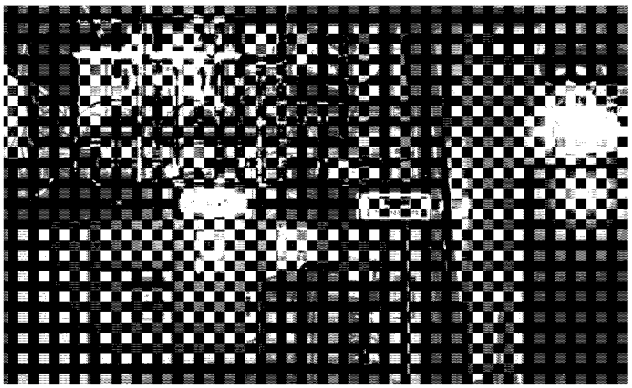

Fig. 1: Set-up of the UHF amplifier

When this amplifier was operated in Wuppertal University before, the coaxial output of the amplifier was directly connected to the cavity under test, which acted as a load and the power coupler representing the antenna.
Here, we test superconducting structures under pulsed conditions. This implies that we prevent the amplifier from being destroyed by the power reflected from the cavity during the filling time. Therefore a circulator, shown in fig. 2, guides the reflected power to a water-cooled load.

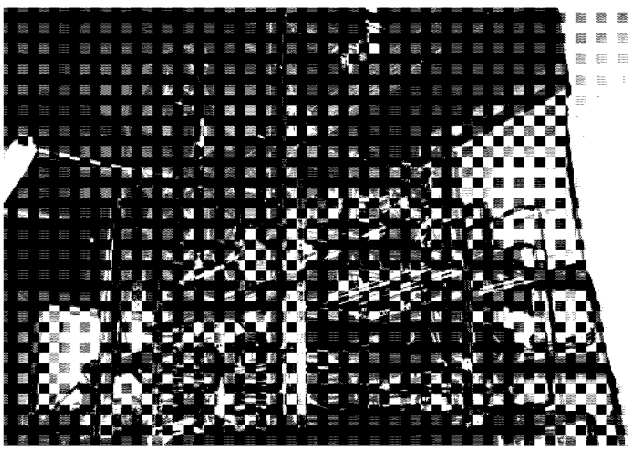

Fig. 2: Detail view of circulator and support construction

The circulator uses ferrites, which of course results in a temperature dependence of directivity. The operating range of the circulator is 30°C +/- 2°C, so a controlled heater for the cooling water increases the water temperature level to the specified value.
During operation of a superconducting cavity, X-ray emission occurs due to the high electric field strength. A motor driven coaxial 2 way switch (DPDT) connects the transmitter either to the cavity under test or to a water-cooled load designed for a maximum power of 50 kW. The fourth port of the switch serves as a test point to the cavity with low power. The position of the coaxial switch is monitored to fulfil safety regulations. The interlock assures that the transmitter may be operated only when it drives the water-cooled load, or when it is safe to operate the superconducting cavity in the concrete shielding area, e.g. all radiation protection rules are obeyed.
The interlock of the RF transmitter also monitors the water flow through the 3 water-cooled loads, the temperatures and the circulator state. If these conditions are met, the cavity vacuum is good enough, the temperature of the cavity coupler is not too high, the shielding area is locked, and the coax-switch is in the right position, then the RF may be applied to the test cavity.
This interlock is too slow to react in case of discharges. Therefore we added a GaAs-switch which reacts in less than 1 microsecond. This switch is combined with 4 logic inputs. Two of the inputs protect the circulator and the power coupler against discharges by the aid of optical detectors. The third input is usable for pulsing the amplifier and the fourth input is a spare. In the input signal path a 6dB attenuator helps to generate a voltage pattern that simulates the operation of a superconducting cavity under beam loading conditions.
Under cw operation, the transmitter delivers 25 kW, as specified for television operation. Under pulsed conditions with 50 Hz repetition rate and up to 5 ms on-time, we noticed, that the transmitter can deliver more power, but the output power decreases during the pulse. We improved this by increasing the capacitor value in the driver tube power supply. With this modification, it is possible now to achieve between 30 to 40 kW peak power.

For a given E-field in a cavity, the bandwidth is proportional and the filling time is reciprocal to the available power. To reduce the filling time from 2 to 5 ms (see [1]) at 30kW power to 0.5ms we need around 200 to 250 kW rf power at 50Hz repetition rate and 2ms pulse duration. For such an amplifier we asked several manufacturers:: Thomcast, Bertronix, and Rohde&Schwarz. Thomcast offers a solution with either 2 UHF-diacrodes or 2 IOTs which would satisfy our demands and could also be used for the low-ß superconducting cavities of an ESS-Linac, following the idea of driving one cavity per transmitter.

For the year 2001, it was intended to add a second power coupler to the superconducting cavity. But this plan was skipped in favour of another cryogenic vacuum vessel.

References

[1] K. Bongardt, "Pulsed Mode Operation of the FZJ 500 MHz sc Cavity Teststand", IKP Annual Report 1999

* FZ-Jülich, ZEL

Modifying digital phase measurement from RF to UHF frequencies

A. Schnase, F.-J. Etzkorn, H. Meier (ZEL)

The signal generation for the synchrotron cavities of COSY are based on DDS (Direct Digital Synthesis) concepts. Clock rates up to 100 MHz at digital resolutions between 12 to 16bit allow direct processing of RF signals up to 40 MHz. For beam- and cavity- phase measurements at COSY there exist proven designs which operate with clock rates up to 25 MHz. However, this is not enough for the frequencies of 160/320 MHz of the COSY injector LINAC or 500 MHz for the ESS-test set-up of a super-conducting 5-cell cavity.

Therefore, a frequency conversion by analogue mixers is necessary. Unfortunately, the performance of such mixers for measurement purposes is difficult to predict. A small matching error will degrade performance, and then design criteria are difficult to meet. Figure 1 shows a digital receiver, which combines digital boards already developed at COSY with commercially available signal sources and high-frequency components like mixers and filters.

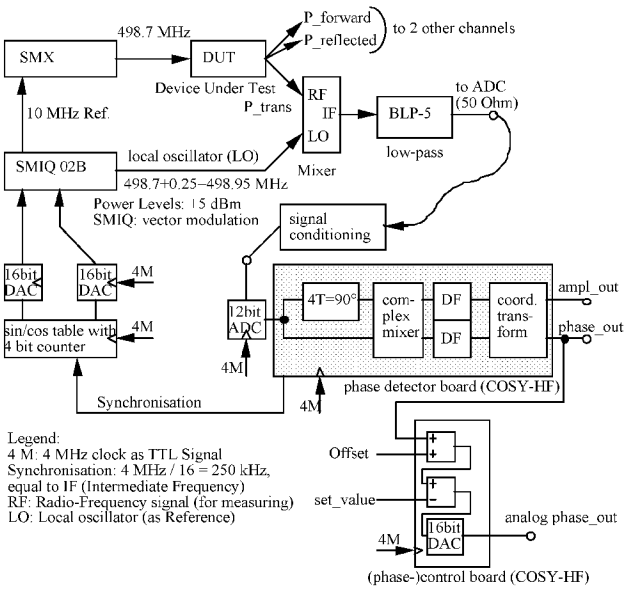

Fig. 1: Digital receiver with 12bit ADC and 16bit processing

The principle of this circuit is to mix the measurement information down to an intermediate frequency of 250kHz, and then sample and filter the result with a clock rate of 4MHz. The local oscillator will then operate at 250kHz offset to the measurement frequency. This frequency-offset is created with a vector-modulator, shown in fig. 2.

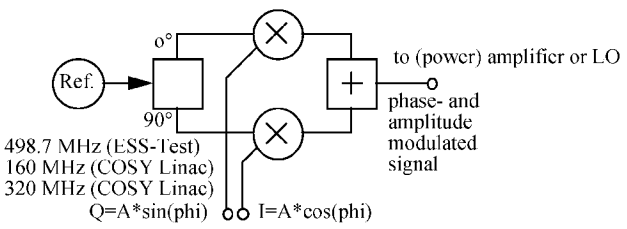

Fig. 2: Analogue vector modulator

This principle of a vector-modulator can also be applied to the control of amplitude and phase of high frequency cavities.

The measurement of the behaviour of a cavity under beam loading conditions requires the processing of 3 channels, which are shown in fig. 3. Then the digital modules to process the information can be arranged like in fig. 4 .

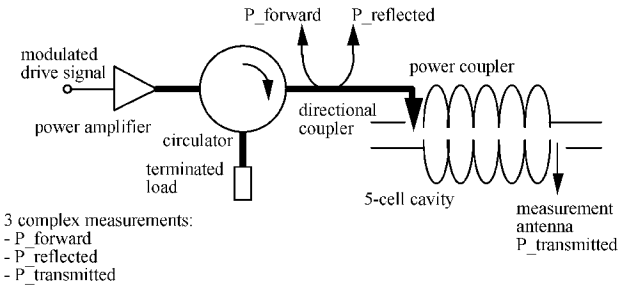

Fig. 3: Measurement parameters of a high frequency cavity

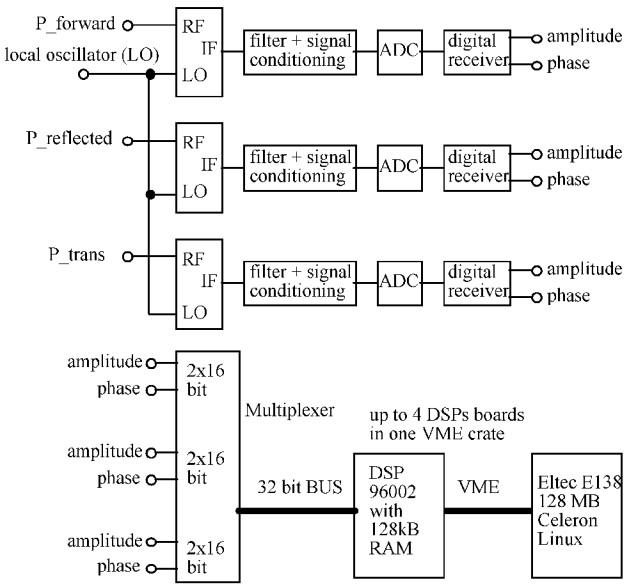

Fig. 4: Digital processing of measurements of one cavity

Finally, the components can be assembled together, and fig. 5 shows an example how a digital control system for a high frequency cavity can look like.

Of course, some questions related to components are still under investigation:

- The choice of the intermediate frequency (250kHz)
- The selection of a high quality ADC
- The choice of mixers and vector-modulators
- Signal conditioning

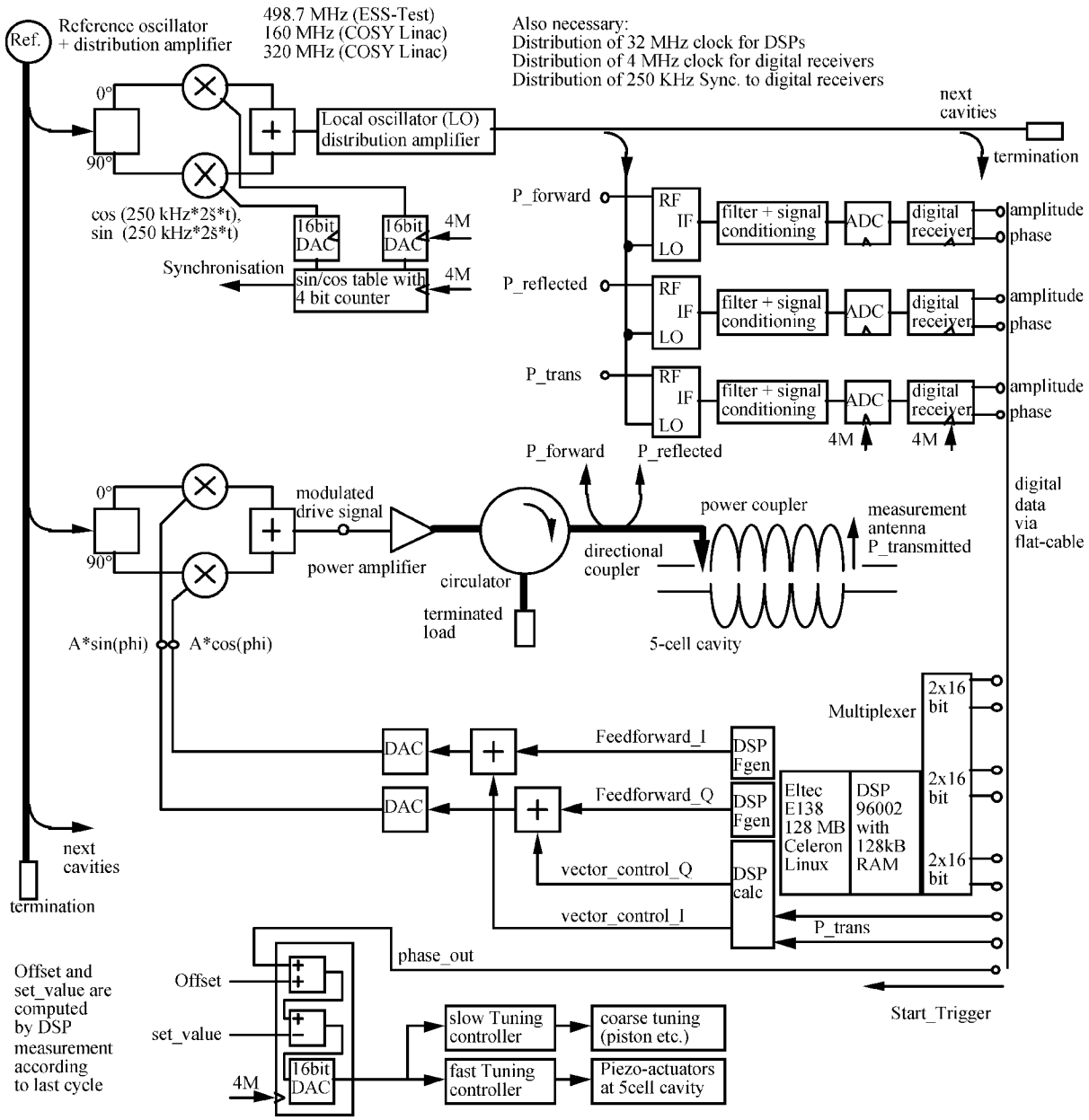

Fig. 5: A possible design of a digital control system module for one high frequency cavity

Analysis of Normal- and Superconducting Options for the ESS Low Energy Part of the Proton Linear Accelerator

Yu. Senichev, W. Bräutigam, R. Maier, E. Zaplatin

At present ESS project is reconsidered to give the new impulse to the development of the neutron source project in Europe. The super-conducting option of the high-energy part for the ESS linear accelerator is presently under discussion. Simultaneously, the new additional option of the proton beam long pulse is going to be implemented, what increases the RF duty cycle up to 15 – 20%. Therefore due to the power limit of cooling system the normal conducting accelerator structure of the low energy part has to have the required high shunt impedance. We have considered for the Low Energy Part Linac (20-200 MeV) the conventional E and H type DTL structures for 350 MHz and the super-conducting H type structure for 700 MHz. We compare each with another on the basis of the electrodynamics parameters of structures and the beam dynamics analysis.

I. Normal conducting option

In the accelerator with the high duty cycle the shunt impedance plays even the bigger role, since the structure is restricted by the maximum possible power dissipated by the cooling system, what brings up a question "yes" or "no". The maximum power losses is determined by the construction of the structure itself and it can be varied from 10kW/m and up to 50 kW/m. To increase the shunt impedance the outer sizes of drift tube have to be minimized as much as possible. For that there are two possibilities: one of them is the permanent quadrupole magnet installation inside of the drift tubes and another is the taking out the quadrupoles from the cavity, what means the accelerating and focusing functions are separated. We have done the MAFIA calculations for all these three options for 350 MHz frequency (see fig.1).

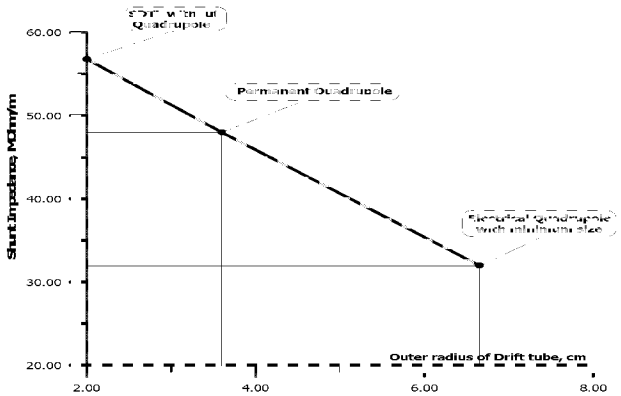

Fig.1: Shunt impedance of DTL structure with 350 MHz vs outer drift tube radius method.

1. SDTL and BDTL structures

The separated DTL Alvaretz structure is the DTL structure with the external quadrupoles located between cavities. Due to the external placement of the drift tube is easier optimized. Therefore the losses of power can be minimized so significantly. However, the length of such cavity is determined by the required transverse acceptance and it is reasonable from this point of view to take it $L = 5 \div 6\,\beta\lambda$. Thus, the structure has to be divided into many resonators and each one has to be fed by own generator. It leads to very expensive RF system, since each of them requires own RF control system. Additionally the effective longitudinal emittance grows with the number of resonators n as $\sqrt{n[\langle\delta\varphi\rangle^2 + \langle\delta A\rangle^2]}$ due RF amplitude δA and phase $\delta\varphi$ instabilities. The only solution is to join some number of cavities in one module by bridges, what is called BDTL structure. It is very compact cavity and the ratio between cavity and drift tube radius is quite reasonable to get the high shunt impedance. However, the cavities joined by the bridges create the new resonant system with the own eigen modes. Both the cavity and the bridge can be considered as the coupled cells. These modes have to be separated to have the uniform distribution of the field along the whole module (cavities with bridges). In case of $\pi/2$ mode of such resonant system the bridge plays the role of the coupling cell, where the field almost equals to zero and the cavity is the accelerating cell. We have analyzed the system of four cavities joined by three bridges by MAFIA. The results are appeared to be not so inspirational for the longer cavity (higher energy). It is because the frequency difference between $\pi/2$ and 0 modes is determined by the coupler window size a, the field in the region of window H and the stored energy in cavity W:

$$f_{\pi/2}^2 - f_0^2 \propto a^3 H^2 / W \qquad (1)$$

But the stored energy is increased with growth of the cavity length (it is proportional to β) and therefore the coupling goes down. After 20 MeV it is very significant effect. Additionally there is another possibility to get the high-coupled structure for the higher energy. It is CCDTL structure, when the number of drift tubes minimized up to one-two. However, such a structure is the tri-periodical structure requiring the special procedure of tuning, and the frequent separation of cavity by the transverse walls gives the significant contribution in the decreasing of the shunt impedance.

2. CHDTL structure with bridges

The next step has been done in direction of H cavities joined through the bridges in one module. Due to the lower quality factor of H cavities we hoped to get the structure with the higher coupling of the system "cavity-bridge-cavity". The cavity itself was based on CHDTL structure, developed by Ratzinger. The focusing elements are placed just between cavities. The number of drift tubes is determined as before by the required value of the transverse acceptance and it is about 10. The bridges play the role of the coupling cells and the fundamental mode of the system "cavity-bridge-cavity" is $\pi/2$. It means the magnetic and electric fields are shifted by $\pi/2$ from the cavity to the bridge and from the bridge to the next cavity. Therefore the bridges practically does not

affect to the total shunt impedance of whole system. However, in this structure we could not get the coupling coefficient higher of 1%. Due to this reason the maximum number of cavities joint by bridge was two only. Another disadvantage of this type structure is the high sensitivity of the shunt impedance value to the drift tube radius. For instance, the structure with 5 mm radius of the drift tube has 50-60 MOhm/m. But for our case, when we need 10 mm, the shunt impedance goes down to 25 MOhm/m. It is not enough for the structure with 15% duty cycle.

3. DTL with permanent magnet

From figure 1 we can see that DTL structure with the permanent magnet gives the shunt impedance around 45-50 MOhm/m, what meets to the satisfactory condition for the cooling system. However, from the beam dynamics point of view the permanent magnet is uncontrollable, and therefore we need simultaneously the steering system. But any additional element gives the increasing of the focusing period and therefore the beam radius increases as well. Simultaneously, we have found out the FFftrDDdtr lattice is more sensitive to the space charge due to the longer focusing period. Thus, the permanent magnet requires the larger aperture, what neutralizes all advantages of this option in comparison with the conventional DTL with the electrical quadrupoles.

II. Super-conducting structure

Thus, no one normal conducting structure meets to the requirements of the high duty cycle structure (>15%) for the energy region 20-200 MeV. Therefore it is reasonable to consider the super-conducting structure.

- First of all due to the higher acceleration rate the number of super-conducting cavities is smaller, and therefore we have the smaller number of the generators, which one is very important advantage in comparison with SDTL.
- Secondly, we have not problems with the shunt impedance.
- Finally, we can pass to the frequency 700 MHz just after the funneling, what makes sense from the point of view of the peak current decreasing in each bunch.

Analyzing the possible candidates of the super-conducting cavity for the low energy part of ESS we have taken the H cavity. For RF structure the electrode shape plays the significant role, since it affects to the maximum possible accelerating rate through the ratio of B_{peak} / E_{ac} and E_{peak} / E_{ac}. In previous papers [1] the spoke shape electrodes (fig. 2a) have been analyzed. Additionally we consider the tore-shape electrode [2] (fig 2b) due to more freedom in the electrodes tore-shape.

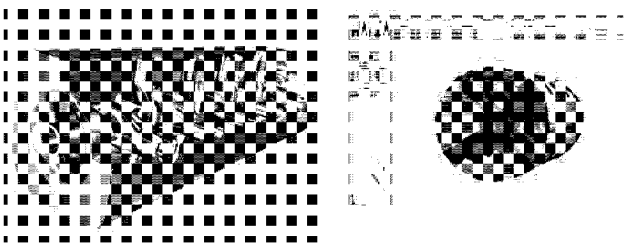

Fig.2:Spoke cavity(a) and tore cavity (b).

The H structure is one-resonator cavity, where the π shifted electrical field gap to gap is created by the alternating rotation of the electrodes in the transverse plane, but not as in the multi-cell elliptical E structure. The H cavity can be based on the dipole mode TE111 or the quadrupole mode TE211. Obviously, in case of the dipole mode the electrodes have to be rotated by 180^0 and for the quadrupole mode by 90^0. Due to the one resonator-cavity the coupling coefficient does not play any role. The critical wavelength λ_{cr}, the resonant wavelength λ and the cavity length $L \approx N_{gap}\beta\lambda/2$ determines the separation of the neighbouring modes:

$$\frac{\Delta f}{f} = \left(\frac{\lambda_{cr}}{\lambda}\right)^3 \frac{3}{\beta^2 N_{gap}^2} \qquad (2)$$

where N_{gap} is the number of accelerating gaps (what in principle is the same as N_{cell} in the elliptical cavity), β is the relative phase velocity. Thus, in the H cavity we have the strong factor $1/\beta^2$. The optimized ratio E_{peak} / E_{ac} and B_{peak} / E_{ac} depends on the number of electrodes inside cavity (fig.3). Taking into account the maximum magnetic field $B_{peak} = 60mT$, we can use the accelerating field $E_{ac} = 5 \div 8\, MeV/m$.

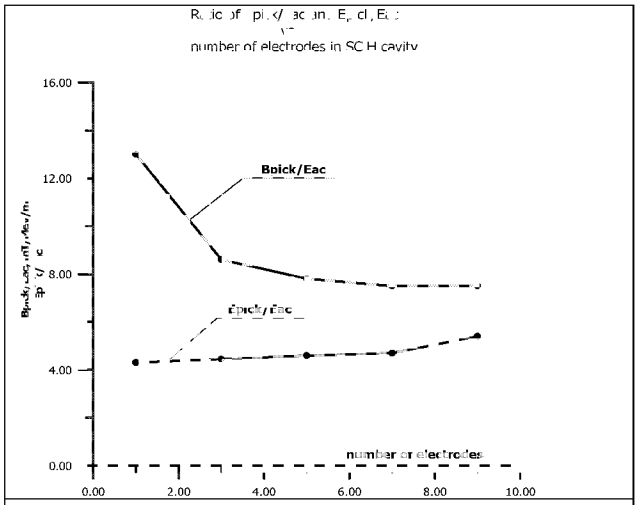

Figure 3: E_{peak} / E_{ac} and B_{peak} / E_{ac} vs electrodes number.

The number cells in one cavity is determined by the beam dynamics and equals 10 cells. The total number of SCH cavity for beam acceleration from 20 MeV to 200 MeV is 43. The maximum accelerating field is limited by the magnetic field and for reliability it is taken 5 MeV/m. The doublet focusing system is quite appropriated to this lattice.

References

[1] E.Zaplatin, A spoke RF cavity simulation with MAFIA, SCRF99, Santa Fe, USA, 1999.

[2] Yu.Senichev, ESS preprint ISSN 1433-559X ESS 01-120-LOctober 2001

V. Technical Developments

11. ELECTRONICS, SEMICONDUCTOR DETECTORS

11. ELECTRONICS, SEMICONDUCTOR DETECTORS

Electronics Laboratory

C.Berchem, J.Bojowald, N.Dolfus, W.Ernst, H.Labus, G.Lürken, R.Nellen, T.Sefzick

During the last year the activities of the IKP Electronics Laboratory focussed on three topics:

Electronics and Data Acquisition for experiments

Support for Experiments was given in several ways:
Analog readout electronics based in the ASD8-chip was developed in cooperation with the ZEL where the digital readout part was added. Currently, the system is adapted to the new multi-wire proportional chamber for ANKE and the straw chamber project at TOF. The latter also required development and prototyping of pre-amplifiers and signal converters. Electronics for a test detector consisting of 128 channels is in process.
The RAL111 based readout system at the ATRAP-I experiment at CERN was improved. The gained experience was used for the development of the ATRAP-II scintillating fiber hodoscope electronics, which consists of appr. 1800 channels and reads out 16-fold multi-anode photomultipliers. Ordering, receiving inspection, and calibration of 250 of the redesigned pre-amplifiers has already been done, as well as of the 8-fold analog signal cables, which required a special design. The new RAL111 readout boards are prototype tested and await production. The manufacture of high voltage cables meeting CERNs very strict safety requirements is under way.
For COSY-11 ordering, receiving inspection, and calibration of 50 discriminator modules for the new hexagonal drift chamber readout was done.
For ANKE assistance was provided for commissioning the wire chamber for negatively charged particles. Development and prototyping of inverting amplifiers for the so-called Dubna-chamber were completed successfully. Several interface and high voltage boards, needed for this experiment, were developed and produced.
At TOF and COSY-11 the data acquisition systems were successfully updated to the standard system delivered by ZEL, which required complete rebuilds of computer systems and data and trigger buses. Moreover, for JESSICA and for laboratory purposes small systems of the same type were set up.
For the widely used PC to CAMAC interfaces (DSPT 6001/6002) a replacement for the ISA card is needed, because modern PC's are not equipped with ISA slots anymore. A simple solution based on a standard PCI parallel card and a self-written Linux software driver has been developed and tested to perfect satisfaction.
The existing control and readout system for the cristal spectrometer at PSI has been improved. An additional new system implementing all improvements made to the first one is actually set up and tested.
For the TOF experiment the hardware (switch cabinets, cables) has been designed and produced. Implementing and programming of the Simatic S7 control system has been supported extensively.

COSY diagnostics

The prototype of a new spill detector, consisting of a pair of thin plastic scintillators and an ionisation chamber was successfully tested und proved its ability to measure time structure and intensity of the extracted COSY-beam (see article in this annual report).
Three ionisation chambers for beam disturbing diagnostics in the extraction beamlines have been built, one of them has already been installed. These chambers supplement the position measuring multi-wire chambers with an intensity measurement.
Additional ten multi-wire chambers have been built in collaboration with the Jagellonian University in Cracow. Production took place in Cracow, testing and calibration has been done in Jülich.
For the emittance measurement apparatus three additional sandwich targets consisting of 60 isolated Tantalum foils each were produced, where each foil is contacted with a ceramic isolated wire and read out individually. The targets differ in foil thickness. The existing electronics has been rewired completely.
The change-over from the HP-VEE control soft- and hardware to PC-based LABView systems has been completed to 95% and awaits installation on site. This change affects the tune measurement, beam energy measurement, and the phase measurement in the injection beamline.

Computer network

In the final stage the computer network of the IKP will provide about 730 lines based on fibre optics. The cables for this star layout network have been installed and equipped with sockets. Up to now 80 terminals have been taken into operation. The others will follow after purchase and installation of the necessary hardware (routers und interfaces).

Miscellaneous

Like every year substantial support has been given with regard to short term maintenance and repair or replacement of electronics. In some cases the urgent demand didn't allow a time-consuming outside repair procedure, in other cases the manufacturer doesn't even exists anymore, but the electronics can not be replaced easily.
Prototypes and small series of cables or electronics, for which an outside production was not reasonable, have been delegated to infrastructure facilities where possible, the rest has been done here, mainly by trainees and student auxiliary workers.

A Flexible Printed Board for the ASiST Chip Readout

L. Conin, N. Dolfus, G. Fiori, H. Hadamek, T. Krings, S. Merzliakov[1], A. Mussgiller, D. Protic, R. Schleichert

The readout electronics of the ANKE Silicon Tracking Telescope ASiST [1] is based on the chip combination VA32HDR_2 and TA32CG of the Norwegian company *ideas* [2]. The VA32HDR_2 houses 32 preamplifiers and 32 slow shaper amplifiers (2µs) whereas the TA32CG provides 32 corresponding fast shaper amplifiers (100ns) and discriminators to get timing and trigger signals.

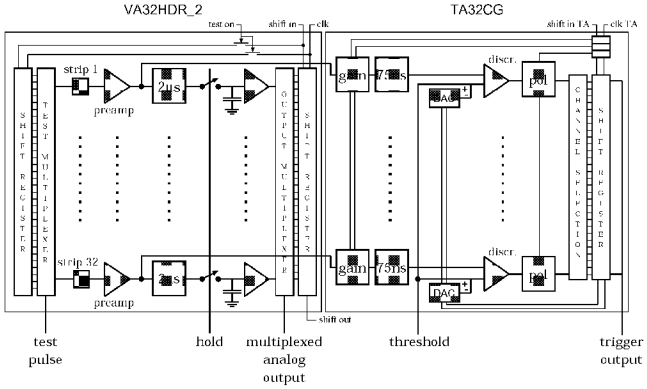

Fig. 1. The block diagram of the VA32HDR_2 and the TA32CG chips. The individual preamplifier outputs of the VA32HDR_2 are directly bonded to the inputs of the TA32CG. In the simplest trigger configuration the trigger output of the TA32CG directly serves to generate a hold signal for the VA32HDR_2.

In the in-vacuum prototype assembly of the ASiST, 7 chip-pairs (7*32=224 readout channels) are glued and some SMD components are soldered on a flexible printed board, the so-called Y-Flex [3]. Figure 2 shows a photo of a single foil. Each double-sided detector will be equipped with 2 of these foils. The material (**L**iquid **C**rystal **P**olymer, LCP) has been chosen for two reasons: First it is not magnetic or electrically conductive, which is important in the 1.6T environment of the ANKE spectrometer magnet. Second it is designed to incorporate a minimum amount of water. This feature is extremely attractive to minimize the pumping time to reach ultra high vacuum conditions.

Before bonding the chips, the foil is glued on a simple 0.635mm Al_2O_3 ceramic plate to have a rigid support in the region of the chips.
The total assembly of a single flexible printed board has been checked for its ultra-high vacuum compatibility. Figure 3 shows the rest-gas spectrum. The remaining gas components are no severe problem the COSY vacuum and can easily be pumped.

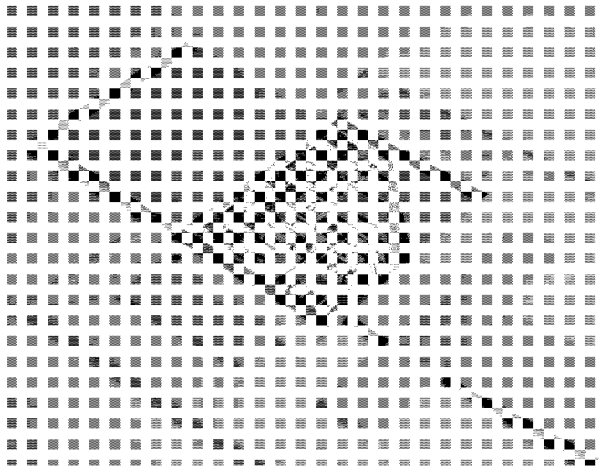

Fig. 2. The Y-Flex flexible printed board with 7 chip-pairs glued on it. To the left side the foil is directly glued to the detector. The right side interfaces to the vacuum feed-through.

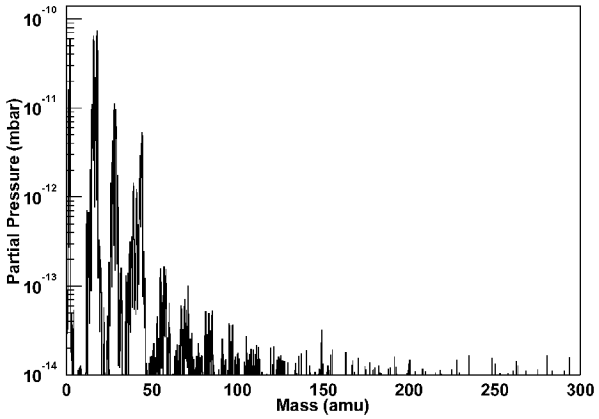

Fig. 3. The rest-gas spectrum of the Y-Flex flexible printed board. The total pressure at which the spectrum has been taken is $1.6*10^{-9}$mbar. The total assembly is fully UHV compatible.

References:

[1] S. Barsov et al., *The ANKE Silicon Spectator Tracker ASiST*, contribution to this report.
[2] A. Mussgiller et al., *Evaluation of front-end Chips for Silicon Strip Detectors*, Annual Report 1999 of the IKP, FZ-Juelich (1999), p.31.
[3] Yamaichi, Flexible Printed Circuit, http://www.yamaichi.de.

[1] JINR Dubna, Russia

Experimental Results from an ASiST Prototype

A. Mussgiller, S. Merzliakov[1], T. Krings, D. Protic, R. Schleichert

A prototype of the ANKE Silicon Spectator Tracker ASiST [1] has been assembled. The setup consists of 3 silicon-strip detectors. The first detector is 65µm thick, with an active area of 40*40mm^2, 40 strips on each side (Micron Semiconductors BB1 design). The second detector is 300µm thick, with an active area of 66.18*51.13mm^2 and 631+1023 strips (Micron Semiconductors Babar IV design). On the *n-side* there are 631 strips: 316 strips and 315 reciprocal strips. Strip plus reciprocal strip have a pitch of 105µm. Already on the detector they are bonded to 315 groups of 4 strips and a single group of 3 strips. Therefore 316 groups of strips (pitch 210µm) are bonded to a Kapton pitch-adapter that furthermore joins the groups to 40 channels: 38 channels in the center, each joining 8 groups, 2 channels at the border, each joining 6 groups. These 40 channels have been equipped with dedicated fast preamplifiers for timing measurements, which are not described here. On the *p-side* there are 1023 strips (512 strips, 511 reciprocal strips) with a pitch of 50µm. On the detector they are bonded together to 256 groups (pitch 200µm): 255 groups of 4 strips, 1 group with 3 strips. These 256 groups are bonded to a pitch-adapter foil. It joins the groups to the 7*32=224 readout-channels of the flexible printed circuit described below: 192 single-group channels in the center, 2*16 channels at the borders, each joining 2 groups.

The last layer is a 5500µm thick single-sided Si(Li) detector with 200 strips and an active area of 47*23mm^2.

The setup has been installed and included into the common ANKE read-out system during a beam-time in September 2001. At a COSY energy of T_p=500MeV data has been taken for the reaction $\vec{p}d \rightarrow pX$. Figure 1 shows a typical pedestal distribution in the experimental environment. Without any correction the width (FWHM) is about 53keV. Applying an offline common-mode correction the width of the pedestal distribution can be reduced to about 33keV.

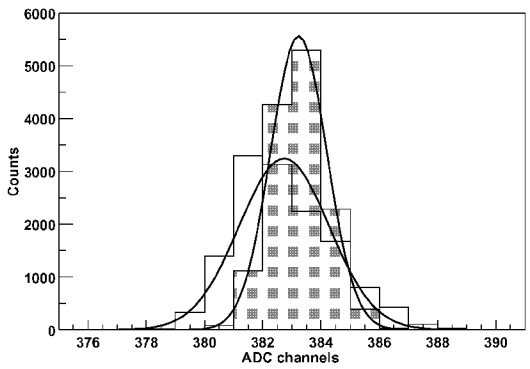

Fig. 1: The typical pedestal distributions measured in ADC channels (15keV/channel): σ=1.54 ADC-channels without common correction, σ=0.96 ADC-channels with an off-line common correction.

Figure 2 shows the energy loss in the first 65µm thin layer versus the energy loss in the second 300µm thick layer. All channels have been energy calibrated by a simple linear approximation taking the pedestal value as zero energy loss and the punch-through points (2.2MeV in 65µm and 6.3MeV in 300µm silicon). The 40 channels of the 65µm (p-side) and the 224 channels of the 300µm (p-side) are summed in the spectrum.

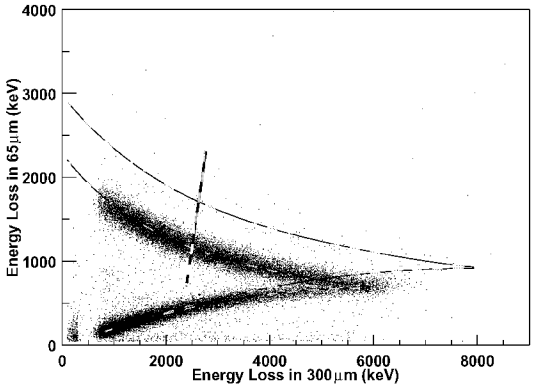

Fig. 2: Energy loss in the 65µm versus the energy loss in the 300µm thick detector. In addition are drawn the SRIM calculations for the energy losses of protons and deuterons.

Even with this simple calibration, not taking into account the non-linearity of the electronic chips, a single narrow proton band appears. The minimum detected proton energy can be extracted to be about 2.5MeV. No deuterons are seen because the telescope is installed in the backward hemisphere of the target where scattered deterons are absent. Nevertheless, the proton-deuteron separation by their energy losses in the first two layers under forward angles of the telescope can be expected to be pretty good as deduced from Figure 3. The energy resolution along the line in Figure 2 is shown to be ~160keV FWHM, which proofs the good performance of the 65µm thick detector.

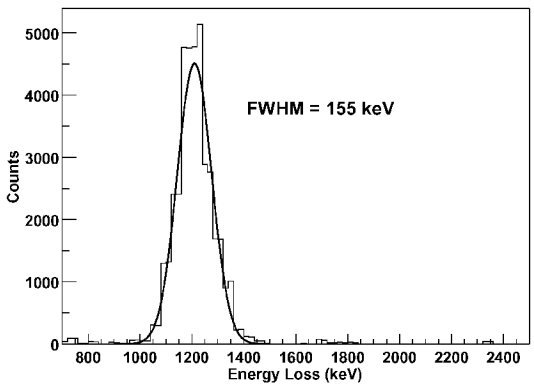

Fig. 3: Projection along the line in Figure 2 results in an energy resolution of about 160keV FWHM

References:

[1] S. Barsov et al., *The ANKE Silicon Spectator Tracker ASiST*, contribution to this report.

[1] JINR Dubna, Russia

VI. Scientific Council COSY

Prof. Dr. P. Braun-Munzinger (Chairman)	GSI Darmstadt
Dr. A. Bringer	IFF, FZ Jülich
Prof. Dr. L. Cardman	JLab, USA
Prof. Dr. H. Coenen	INC, FZ Jülich
Prof. Dr. J. Domingo	Jlab, USA
Prof. Dr. D. v. Harrach	University of Mainz
Prof. Dr. D. W. Hertzog	University of Illinois, USA
Prof. Dr. E. Hilger	University of Bonn
Prof. Dr. Y. Nagai	University of Osaka, Japan
Prof. Dr. O. Riska	University of Helsinki, Finland
Prof. Dr. A. W. Thomas	University of Adelaide, Australia
Dr. D. Trines	DESY Hamburg
Dr. H. Wenninger	CERN, Switzerland

VII. Program Advisory Committee (for COSY)

Dr. B. Friman	GSI Darmstadt
Prof. Dr. M. Garcon	Saclay, France
Prof. Dr. E. Grosse	FZ Rossendorf
Prof. Dr. C. Guaraldo	INFN Frascati, Italy
Prof. Dr. M. Harakeh (Chairman)	KVI Groningen, The Netherlands
Prof. Dr. T. Johansson	Svedberg Laboratory, Sweden
Prof. Dr. S. Kullander	University of Uppsala, Sweden
Prof. Dr. R. Landua	CERN; Switzerland
Prof. Dr. V. Metag	University of Giessen
Prof. Dr. H.O. Meyer	IUCF Bloomington, USA
Prof. Dr. U. Mosel	University of Giessen
Dr. E. Radermacher	CERN, Switzerland
Prof. Dr. K. Rith	University of Erlangen
Prof. Dr. C. Wilkin	University College London, UK

VIII. COLLABORATIONS

COSY-EDDA-Collaboration*
Spokesmen: J. Bisplinghoff, F. Hinterberger, W. Scobel

O. Felden, R. Gebel, M. Glende, R. Maier, D. Prasuhn, P. v. Rossen:
Institut für Kernphysik, Forschungszentrum Jülich, D-52425 Jülich

J. Bisplinghoff, M. Busch, C. Dahl, P.D. Eversheim, R. Gross-Hardt, F. Hinterberger, R. Jahn, A. Meinerzhagen, H. Rohdjeß, D. Rosendaal, H.J. Trelle, K. Ulbrich, E. Weise, R. Ziegler:
Institut für Strahlen- und Kernphysik, Universität Bonn

F. Bauer, K. Büßer, T. Colberg, L. Demirörs, O. Eyser, J. Greiff, E. Jonas, H. Krause, C. Lehmann, J. Lindlein, C. Pauly, N. Schirm, W. Scobel, A. Wellinghausen, T. Wolf:
I. Institut für Experimentalphysik, Universität Hamburg

*supported by BMFT-Verbundforschung; University Program of Forschungszentrum Jülich

COSY-11 Collaboration*
Spokesman: M. Wolke

D. Grzonka, K. Kilian, C. Kolf, W. Oelert, G. Schepers, T. Sefzick, P. Winter, M. Wolke:
Institut für Kernphysik, Forschungszentrum Jülich, D-52425 Jülich

P. Wüstner:
Zentrallabor für Elektronik, Forschungszentrum Jülich, D-52425 Jülich

H.H. Adam, I. Geck, A. Khoukaz, N. Lang, T. Lister, C. Quentmeier, R. Santo, S. Steltenkamp:
Institut für Kernphysik, Westfälische Wilhelms-Universität, D-48149 Münster

R. Czyzykiewicz, M. Janusz, L. Jarczyk, B. Kamys, P. Moskal, J. Smyrski, A. Strzalkowski:
Institute of Physics, Jagellonian University, PL-30059 Cracow

A. Budzanowski:
Institute of Nuclear Physics, PL-31342 Cracow

P. Kowina, M. Siemaszko, W. Zipper:
Institute of Physics, Silesian University, PL-40007 Katowice

*supported by BMFT-Verbundforschung; International Bureau of the BMBF, DLR-Bonn;
University Program of Forschungszentrum Jülich

COSY-13 Collaboration*
Spokesman: B. Kamys

W. Borgs, M.Hartmann, H.R. Koch, P. Kulessa, R. Maier, H. Ohm, D. Prasuhn, J. Stein, H. Ströher:
Institut für Kernphysik, Forschungszentrum Jülich, D-52425 Jülich

L. Jarczyk, B. Kamys, Z. Rudy, A. Strzalkowski:
M.Smoluchowski Institute of Physics, Jagellonian University, Cracow, Poland

K. Pysz:
H.Niewodniczanski Institute of Nuclear Physics, Radzikowskiego 152, PL-31342 Cracow, Poland

W. Cassing:
Institut für Theoretische Physik, Universität Gießen

*supported by International Bureau of KfK Karlsruhe; TEMPUS-Program

ANKE* (0^0-Facility)
Spokesman: M. Büscher

U. Bechstedt, G. Borchert, W. Borgs, M. Büscher, J. Dietrich, S. Dymov, D. Gotta, D. Grzonka, M. Hartmann, V. Hejny, M. Karnadi, V. Kleber, H.R. Koch, K. Kruck, P. Kulessa, I. Lehmann, B. Lorentz, Y. Maeda, R. Maier, M. Mikirtichyants, A. Mussgiller, M. Nekipelov, R. Nellen, H. Ohm, D. Prasuhn, D. Protić, F. Rathmann, R. Schleichert, H. Schneider, G. Schug, H. Seyfarth, A. Sibirtsev, K. Sistemich, H.J. Stein, H. Ströher, K.-H. Watzlawik:
Institut für Kernphysik, Forschungszentrum Jülich, D-52425 Jülich

G. Hansen, F. Klehr, H. Stechemesser:
Zentralabteilung Allgemeine Technologie, Forschungszentrum Jülich, D-52425 Jülich

R. Baldauf, M. Drochner, W. Erven, H. Kleines, H. Loevenich, J. Sakardi, P. Wüstner, K. Zwoll:
Zentrallabor für Elektronik, Forschungszentrum Jülich, D-52425 Jülich

V. Dimitrov, N. Langenhagen, H. Müller, B. Rimarzig, Chr. Schneider, J. Seibert:
Zentralinstitut für Kernforschung, Rossendorf, D-01474 Dresden

N. Koch, S. Lorenz, F. Schmidt, E. Steffens:
Physikalisches Institut II, Universität Erlangen-Nürnberg, D-91058 Erlangen

W. Cassing,:
Institut für Theoretische Physik, Universität Gießen, D-35392 Gießen

R. Engels, H. Paetz gen. Schieck:
Institut für Kernphysik, Universität Köln, D-50937 Köln

H.-H. Adam, A. Khoukaz, N. Lang, Th. Lister, T. Mersmann, C. Quentmeier, R. Santo:
Institut für Kernphysik, Universität Münster, D-48149 Münster

L. Jarczyk, B. Kamys, St. Kistryn, Z. Rudy, J. Smyrski, A. Strzalkowski:
Institute of Physics, Jagellonian University, Cracow, Poland

K. Pysz:
Institute of Nuclear Physics, Radzikowskiego 152, PL-31342 Cracow, Poland

V. Abazov, A. Churin, O. Gorchakov, A. Kacharava, N. Kadagidze, V.I. Komarov, V. Kruglov, A. Kulikov, V. Kurbatov, V. Leontiev, G. Macharashvili, S. Merzliakov, A. Petrus, Yu. Uzikov, A. Volkov, S. Yaschenko, B. Zalikhanov, N. Zhuravlev:
Joint Institute of Nuclear Research, Dubna, Russia

S. Trusov, V. Yazkov:
Dubna Branch of the Moscow State University, Dubna, Russia

V. Abaev, S. Barsov, S. Belostotski, O. Grebenyuk, V. Koptev, A. Kovalov, P. Kravchenko, P. Kravtsov, S. Mikirtichyants, V. Nelubin, A. Vassiliev:
Petersburg Nuclear Physics Institute, Gatchina, Russia

V. Chernetzky, V. Chernyshev, M. Chumakov, P. Fedorets, A. Gerasimov, V. Goryachev, L. Kondratyuk:
Institute for Theoretical and Experimental Physics, Moscow, Russia

Ye.S. Golubeva, V. Grishina:
Institute for Nuclear Research, Russian Academy of Sciences, Moscow, Russia

C. Wilkin:
Physics Department, Univ. College London, London WC1 6BT

N. Amaglobeli, B. Chiladze, M. Nioradze:
High Energy Physics Institute, Tbilisi State University, Tbilisi, Georgia

I. Zychor:
Soltan Institute for Nuclear Studies, PL-05400 Swierk, Polen

*supported by Land Nordrhein-Westfalen, BMFT (Verbundforschung; Forschungszentrum, WTZ mit Polen und Russland), DFG, INTAS, Collaborators

COSY-GEM-Collaboration*
Spokesman: H. Machner

S. Abdel-Samad, J. Bojowald, D. Filges, K. Kilian, Th. Krings, H. Machner, R. Maier, D. Protic, P. v. Rossen:
Institut für Kernphysik, Forschungszentrum Jülich, D-52425 Jülich

K. Zwoll:
Zentralinstitut für Elektronik, Forschungszentrum Jülich, D-52425 Jülich

J. Ernst, R. Jahn, J. Urban:
Institut für Strahlen- und Kernphysik, Universität Bonn

D. Frekers:
Institut für Kernphysik, Universität Münster

P. Hawranek, L. Jarczyk, S. Kistryn, W. Klimala, A. Magiera, J. Smyrski, A. Strzalkowski, A. Wronska:
Jagellonian University, Cracow, Poland

A. Budzanowski, S. Kliczweski, R. Siudak:
Institute of Nuclear Physics, Cracow, Poland

B.J. Lieb:
Physics Department, GMU, Fairfax, Virginia, USA

L.C. Liu:
LANL, T. Division, Los Alamos, USA

H. Nann:
IUCF, Bloomington, Indiana, USA

A. Chatterjee, B.K. Jain, S.S. Kapoor, B.J. Roy:
BARC Trombay, Bombay, India

J. Ilieva, T. Kutsarova, E. Pentchev:
Institute of Nuclear Research and Nuclear Energy, Sofia, Bulgaria

D. Kolev. R. Tsenov, G. Vankova:
Univ. Sofia, Sofia, Bulgaria

G. Martinska, M. Ulicny:
P. P. J. Safarik Univ., Kosice, Slovakia

M. Kracikova:
Technical Univ. Kosice, Kosice, Slovakia

L. Golovanov, D. Kirillov, L. Sitnik, N. Piskunov:
Laboratory for High Energies, JINR Dubna, Russia

*supported by University Program of Forschungszentrum Jülich ; International Bureau of the BMBF, DLR-Bonn

COSY-TOF Collaboration*
Coordinator: E. Roderburg

M. Abdel-Bary, S. Abdel-Samad, D. Filges, A. Gillitzer, H. Hadamek, , D. Hesselbarth, U. Johnen, K. Kilian, R. Klein, S. Marwinski, H.P. Morsch, R. Nellen, N. Paul, E. Roderburg, T. Sefzick, H. Uehlemann, P. Wintz:
Institut für Kernphysik, Forschungszentrum Jülich GmbH, D-52425 Jülich

H. Kämmerling:
Zentralabteilung Technologie, Forschungszentrum Jülich GmbH, D-52425 Jülich

M. Drochner, P. Wüstner:
Zentrallabor für Elektronik, Forschungszentrum Jülich GmbH, D-52425 Jülich

H. Koch, S. Mauro, W. Meyer, A. Wilms:
Institut für Experimentalphysik, Ruhr-Universität Bochum, D-44780 Bochum

H. Dutz: Physikalisches Institut der Universität Bonn, D-53115 Bonn

K.-Th. Brinkmann, H. Freiesleben, R. Jäkel, B. Jakob, L. Karsch, E. Kuhlmann, P. Schönmeier, M. Schulte-Wissermann, G.Y. Sun, M. Würschig-Pörsel:
T.U. Dresden, D-01062 Dresden

M. Müller-Veggian:
Fachhochschule Jülich, D-52428 Jülich

H. Clement, A. Erhardt, E. Dorochkevitch, J. Kress, R. Meier, G.J. Wagner, G. Zangh:
Physikalisches Institut, Universität Tübingen, D-72076 Tübingen

S. Dshemuchadse, K. Möller, L. Naumann:
Institut für Kern- und Hadronenphysik, FZ Rossendorf, D-01314 Dresden

W. Eyrich, M. Fritsch, W. Schroeder, F. Stinzing, M. Wagner, S. Wirth:
Physikalisches Institut, Universität Erlangen-Nürnberg, D-91058 Erlangen

A. Filippi, S. Marcello:
INFN I-10125 Torino

P. Zupranski:
Soltan Institut for Nuclear Studies, PL-00681 Warsaw

*supported by BMFT-Verbundforschung; University Program of Forschungszentrum Jülich GmbH

COSY-MOMO-Collaboration*
Spokesman: R. Jahn

H. Machner, P. v. Rossen, R. Tölle: Institut für Kernphysik, Forschungszentrum Jülich, D-52425 Jülich

F. Bellemann, J. Bisplinghoff, J. Ernst, F. Hinterberger, R. Ibald, R. Jahn, R. Joosten, J. Munkel, D. Rosendaal, H. Schnitker:
Institut für Strahlen- und Kernphysik, Universität Bonn

L. Jarczyk, A. Magiera, J. Smyrski, A. Strzalkowski:
Institute for Physics, Jagellonian University, Cracow, Poland

A. Kozela: University of Cracow, Poland

C. Wilkin: University of London, England

*supported by BMFT-Verbundforschung; University Program of Forschungszentrum Jülich;

NESSI Collaboration (European Spallation Source (ESS))*
Spokesman: U. Jahnke

D. Filges, F. Goldenbaum, R.-D. Neef, K. Nünighoff, N. Paul, H. Schaal, G. Sterzenbach, M. Wohlmuther:
Institut für Kernphysik, Forschungszentrum Jülich, D-52425 Jülich

C.-M. Herbach, D. Hilscher, U. Jahnke, V. Tishchenko:
Hahn-Meitner-Institut Berlin, Glienickerstr. 100, D-14109 Berlin

J. Galin, A. Letourneu, A. Péghaire
GANIL (IN2P3-CNRS, DSM-CEA), BP 5027, F-14076 Caen-Cedex, France

L. Pienkowski: University of Warsaw, Pl-02-097 Warszawa, Poland

W.U. Schröder, J. Töke: University of Rochester, Rochester, New York 14627, USA

*supported by EU-TMR-Program and Helmholtz Strategiefonds

JESSICA-Collaboration*
Spokesman: K. Nünighoff

H. Conrad, J. Dietrich, D. Filges, F. Goldenbaum, G. Hansen, H. Klein, S. Martin, R.D. Neef, K. Nünighoff, N. Paul, Ch. Pohl, D. Prasuhn, H. Schaal, H. Stelzer, H. Tietze-Jaensch, H. Ullmaier, M. Wohlmuther:
Forschungszentrum Jülich, D-52425 Jülich

E. Iverson, P.K. Job: Argonne National Laboratory (USA)

B. Haft, W. Nienhaus, E. Schachinger: Techn. Univ. Graz (Austria)

Y. Oyama, N. Watanabe: JAERI (Japan)

M. Furusaka: KEK (Japan)

A.V. Belushkin, A. Smirnov, V. Soukhanov: FLNP, JINR, Dubna (Russia)

P. Ferguson, E. Pitcher, G. Russell: Los Alamos National Laboratory (USA)

T. Gabriel, T. Lucas: Oak Ridge National Laboratory (USA)

S.M. Bennington, T. Broome, H. Jones: RAL (UK)

Y. Kiyanagi: University of Hokkaido (Japan)

*supported by EU-TMR-Program, Helmholtz Strategiefonds

PISA Collaboration*
Spokesmen: B. Kamys and F. Goldenbaum

V. Bollini, A. Bubak, D. Filges, F. Goldenbaum, K. Kilian, P. Kulessa, H. Machner, R.-D. Neef, H. Ohm, N. Paul, K. Pysz, H. Schaal, R. Siudak:
Institut für Kernphysik, Forschungszentrum Jülich, D-52425 Jülich

R. Czyzykiewicz, A.Heczko, L. Jarczyk, B. Kamys, St. Kistryn, W. Klimala, A. Magiera, W. Migdal, B. Piskor-Ignatowicz, Z. Rudy, M. Wojciechowski:
M. Smoluchowski Institute of Physics, Jagellonian University, PL-30059 Kraków

A. Budzanowski, M. Kistryn, St. Kliczewski:
H. Niewodniczanski Institute of Nuclear Physics, PL-31342 Kraków

J. Kisiel, E. Stephan, W. Zipper:
Institute of Physics, University of Silesia, PL-40007 Katowice

R. Barna, D. De Pasquale, A. Italiano:
Dipartimento di Fisisca, Messina University and Instituto Nazionale di Fisica Nucleare, Sezione di Catania, Grupo Collegato di Messina, I-98166 Vill. S. Agata (Messina)

S. Förtsch, D. Steyn, T. Thovhogi:
National Accelerator Centre, PO Box 72, Faure, 7131 South Africa

J. Cugnon:
Institut de Physique, Universite de Liege, B-4000 Liege

H. Hodde:
Institut für Strahlen- und Kernphysik, Universität Bonn, D-53115 Bonn

*supported by BMFT-Verbundforschung, EU-TMR-Program, EU-LIFE-Program, HINDAS-Program

CELSIUS/WASA Collaboration
Spokesman: S. Kullander

H. Calen, C. Ekström, K. Fransson, J. Greiff, A. Kupse, P. Marciniewski, R. Ruber:
The Svedberg Laboratory, Uppsala, Sweden

L. Gustafsson, B. Höistad, M. Jacewicz, A. Jansson, T. Johansson, S. Keleta, I. Koch, S. Kullander, Th. Thörngren-Engblom, J. Zlomanczuk:
Department of Radiation Sciences, Uppsala, Sweden

K. Kilian, W. Oelert, T. Sefzick:
Institut für Kernphysik, Forschungszentrum Jülich, Jülich, Germany

A. Turnowiecki, Z. Wilhelmi:
Institute of Experimental Physics, Warsaw, Poland

Z. Zabicrowski:
Institute of Nuclear Studies, Lodz, Poland

J. Stepaniak:
Soltan Institute for Nuclear Studies, Warsaw, Poland

A. Bondar, L. Kurdadze, A. Kuzmin, S. Oreshkin, B. Shwartz, V. Sidorov, A. Sukhanov:
Budker Institute of Nuclear Physics, Novosibirsk, Russia

D. Bogoslawsky, G. Ivanov, E. Jiganov, A. Kuznetsov, B. Morosov, J. Petukhov, S. Sandukovsky, V. Tikhomirov:
Joint Institute for Nuclear Research Dubna, Moscow, Russia

V. Sopov, V. Tchernychev:
Institut of Theoretical and Experimental Physics, Moscow, Russia

N. Kimura, A. Yamamoto, H. Yamaoka:
National Laboratory for High Energy Physics, Tsukuba, Japan

M. Gornov, V. Grebenev, Y. Gurov, R. Shafigullin:
MEPHI, Moscow, Russia

C. Bergholtz, P.E. Tegner, K. Wilhelmsen:
Department of Physics, Stockholm University, Sweden

H. Clement, J. Pätzold, G. Wagner:
Physikalisches Institut, Universität Tübingen, Germany

L. Demirörs, C. Pauly, W. Scobel:
Institut für Experimentalphysik, Universität Hamburg, Germany

B. Nefkens: UCLA, Los Angeles, USA

AD-2 Collaboration (ATRAP)*
Spokesman: G. Gabrielse

G. Gabrielse, T. Roach, J. N. Tan, C. Storry, J. Tan, J. Estrada, P. Yesley, P. Oxley, N. Bowden, M. Wessels, A. Speck:
Department of Physics, Harvard University, Cambridge, MA 02138, USA

H. Kalinowsky: Univ. Bonn, ISKP, D-53115 Bonn

T.W. Hänsch, K. Eikeman, J. Walz: Max-Planck-Institut für Quantenoptik, D-85748 Garching

W. Oelert, T. Goetz, D. Grzonka, G. Schepers, T. Sefzick:
Institut für Kernphysik, Forschungszentrum Jülich, D-52425 Jülich

*supported by BMFT-Verbundforschung, National Science Foundation (USA)

ZEUS Collaboration
Spokesman: R. Klanner, Deutsches Elektronen-Synchrotron (DESY), D-22603 Hamburg

D. Filges, R.D. Neef:
Institut für Kernphysik, Forschungszentrum Jülich, D-52425 Jülich
and 49 national and international institutions

EUROBALL-Collaboration

R.M. Lieder: Institut für Kernphysik, Forschungszentrum Jülich, D-52425 Jülich

P. von Brentano: Institut für Kernphysik, Universität zu Köln, D-50937 Köln

D. Schwalm: MPI für Kernphysik Heidelberg, Postfach 103980, D-69029 Heidelberg

J. Gerl: GSI Darmstadt, Postfach 110552, D-64291 Darmstadt

H. Hübel: Institut für Kernphysik, Universität Bonn, D-53115 Bonn

K.P. Lieb: II. Physikalisches Institut, Universität Göttingen, D-37073 Göttingen

F. Dönau: Institut für Kern- und Hadronenphysik, Forschungszentrum Rossendorf, D-01314 Rossendorf

J. Lisle: Department of Physics, Victoria University of Manchester, Manchester M13 9PL, UK

P. Nolan: Department of Physics, Univ. of Liverpool, Liverpool L69 3BX, UK

J. Simpson: Daresbury Laboratory, Warrington WA4 4AD, UK

C. Rossi-Alvarez: Istituto Nazionale di Fisica Nucleare, Padova, I-35131 Padova, Italy

G. deAngelis: Istituto Nazionale di Fisica Nucleare, Lab. Nazonali di Legnaro, I-35020 Legnaro, Italy

M. Pignanelli: Istituto Nazionale di Fisica Nucleare, Sezione di Milano, I-20133 Milano, Italy

C. Fahlander: Department of Physics, University of Lund, S-22362 Lund, Sweden

A. Johnson: Manne Siegbahn Institute of Physics, S-10405 Stockholm, Sweden

J. Nyberg: The Svedberg Laboratory, S-75121 Uppsala, Sweden

B. Herskind: NBI, University of Copenhagen, DK-1350 Copenhagen, Denmark

F. Beck: ihres Strasbourg, F-67037 Strasbourg, France

F. Hannachi, Institut de Physique Nucleaire, CSNSM, F-91405 Orsay, France

TMR Gamma-Tracking Detector Collaboration
Coordinator: R.M. Lieder

R.M. Lieder, W. Gast, H.M. Jäger, L. Mihailescu:
Institut für Kernphysik, FZ Jülich, D-52425 Jülich, Germany

J. Eberth, G. Pascovici, H.G. Thomas, N. Warr, D. Weisshaar:
Institut für Kernphysik, Universität zu Köln, D-50937 Köln, Germany

F. Beck, D. Curien, G. Duchêne, E. Pachoud, I. Piqueras:
IReS Strasbourg, F-67037 Strasbourg, France

C. Rossi Alvarez, D. Bazzacco, M. Bellato, Th. Kroell, Ch. Manea, B. Quintana, R. Venturelli:
INFN, Sezione di Padova, I-35131 Padova, Italy

D.R. Napoli, D. Rosso, P. Spolaore:
INFN, Laboratori Nazionali di Legnaro, I-35020 Legnaro, Italy

A. Geraci, A. Pullia, G. Ripamonti:
Dip. Elettronica e Informazione, Politecnico di Milano, I-20133 Milano, Italy

F. Camera, S. Leoni, B. Million, O. Wieland, A. Bracco, M. Pignanelli, S. Brambilla:
INFN, Sezione di Milano, I-20133 Milano, Italy

J. Lisle, A.G. Smith, R. Well:
Schuster Laboratory, University of Manchester, Manchester M13 9PL, UK

P. Nolan, A. Boston, D. Cullen, M. Descovich:
Oliver Lodge Laboratory, University of Liverpool, Liverpool L69 3BX, UK

B. Cederwall, E. Ideguchi, J. van der Marel:
Department of Physics, Kungliga Tekniska Högskolan Stockholm, S-100 44 Stockholm, Sweden

J. Nyberg:
Department of Neutron Research, Uppsala University, S-75120 Uppsala, Sweden

B. Herskind, G. Sletten, J. Wilson:
Niels Bohr Institute, University of Copenhagen, DK-2100 Copenhagen, Denmark

R. Henck, D. Gutknecht, K. Jääskeläinen, M.-O. Lampert:
Eurisys Mesures, F-67834 Tanneries, France

IX. Personnel

Scientific Staff

Prof. Dr. G. Baur (TH)
(a.o. Prof. At the Univ. of Basel)

DP V. Baru (TH)

Dr. U. Bechstedt (LI)

DP. A. Bogdanov (LI)
(since April 25, 2001)

Dr. J. Bojowald (Ec)

DP V. Bollini (E1)
(since Feb. 6, 2001)

Dr. K. Bongardt (LI)

DI. N. Bongers (LI)

Prof. G. Borchert (E2)
(suspended for 2001)

DI. W. Bräutigam (LI)

DP A. Bubak (E1)
(since Feb. 20, 2001)

Dr. M. Büscher (E2)

Dr. P. Büttiker (TH)

Dr. habil. J. Dietrich (LI)

Dr. A. Djalois (E1)

DP S. Dymov (E2)

Prof. Dr. Ch. Elster (TH)

Dr. E. Epelbaum (TH)
(until November 30, 2001)

Dr. K. Fan (LI)
(since April 11, 2001)

Dr. O. Felden (Rp)

Prof. Dr. D. Filges (E1)
(apl. Prof. at the Univ. Wuppertal)

DP M. Frink (TH)

DP A. Gasparian (TH)

Dr. W. Gast (E1)

Dr. R. Gebel (LI)

Dr. A. Gillitzer (E1)

Dr. M. Glende (LI)

Dipl. T. Götz (E1)
(until Dec. 31st, 2001)

Dr. F. Goldenbaum (E1)

Dr. D. Gotta (E2)

Dr. F. Grümmer (TH)

Dr. D. Grzonka (E1)

Dr. J. Haidenbauer (TH)

Dr. C. Hanhart (TH)
(since February 1st, 2001)

Dr. M. Hartmann (E2)

Dr. V. Hejny (E2)

DI. K. Henn (LI)

DP M. Hennebach (E2)

DP D. Hesselbarth (E1)
(until July 16, 2001)

DP I. Ivanov (TH)

DI H.-N. Jungwirth (LI)
(since March 1st, 2001)

A. Y. Kamenev (E2)
(since October 25, 2001)

DP. V. Kamerdjiev (LI)

I. Keshelashvili (E2)
(since November 30, 2001)

Prof. Dr. K. Kilian (E1)
(Prof. at the Univ. Bonn)

DP V. Kleber (E2)

Dr. V. Klemt (TH)

Dr. R. Koch (E2)

Dipl. C. Kolf (E1)
(until Dec. 31st, 2001)

DP H. Krebs (TH)

Prof. Dr. S. Krewald (TH)
(apl. Prof. at the Univ. of Bonn)

DP B. Kubis (TH)

Dr. P. Kulessa (E2)

Dr. J. Kwapien (TH)
(since October 1st, 2001)

Dr. H. Labus (Ec)
(until Dec. 31st, 2001)

H.-R. Langohr (E1)

Dr. H. Lawin (LI)

DP I. Lehmann (E2)

Dr. A. Lehrach (LI)

DI B. Lensing (E1)
(since April 17, 2001)

Prof. Dr. R. M. Lieder (E1)
(apl. Prof. at the Univ. Bonn)

Dr. B. Lorentz (LI)

Prof. Dr. H. Machner (E1)
(Honorar Prof. at the Univ. Essen)

Dr. Y. Maeda (E2)
(since March 1st, 2001)

Prof. Dr. R. Maier (LI)
(Prof. at the Univ. Bonn)

DI J. Majewski (E1)
(since June 18, 2001)

N. Markgraf (LI)
(since July 2, 2001)

Dr. S. Martin (LI)

Dokt. S. Marwinski (E1)
(until Jan. 31st, 2001)

Prof. Dr. Ulf-G. Meißner (TH)
(apl. Prof. at the Univ. of Bonn)

DP L. Mihailescu (E1)

DP M. Mikirtytchiants (E2)

DI. I. Mohos (LI)

Dr. H.-P. Morsch (E1)

A. Motzke (TH)
since March 9, 2001

Dr. R.-D. Neef (E1)

DP M. Nekipelov (E2)

Prof. Dr. N. N. Nikolaev (TH)

DI K. Nünighoff (E1)

Prof. Dr. W. Oelert (E1)
(apl. Prof. at the Univ. Bochum)

Dr. H. Ohm (E2)

Dr. J. Oller (TH)
until December 31st, 2001

DI N. Paul (E1)

DP F. Pavlov (TH)
until September 7, 2001

L. Platter (TH)
since January 15, 2001

DI Ch. Pohl (E1)

Dr. D. Prasuhn (LI)

DP.H.-J. Probst (Rp)
(until February 28, 2001)

DP D. Protić (Dt)

Dr. K. Pysz (E1)
(since July 1st, 2001)

Dr. F. Rathmann (E2)

Dr. E. Roderburg (E1)

Dr. P. v. Rossen (LI)

DP F. Sassen (TH)

Dr. H. Schaal (E1)

Dr. W. Schäfer (TH)
until January 31, 2001

Dr. G. Schepers (E1)

Dr. R. Schleichert (E2)

Dr.-Ing. A. Schnase (LI)

DI. H. Schneider (LI)

DP S. Schneider (TH)

DI. G. Schug (LI)

S. Schwenke (LI)
(since November 5, 2001)

Dr. T. Sefzick (E1)

Dr. Y. Senichev (LI)

Dr. H. Seyfarth (E2)

Dr. A. Sibirtsev (TH)

Prof. K. Sistemich (E2)
(until March 31, 2001)

Prof. Dr. J. Speth (TH)
(apl. Prof. at the Univ. of Bonn

DI. R. Stassen (LI)

Dr. H.-J. Stein (E2)

G. Sterzenbach (E1)

Dr. H. Stockhorst (LI)

Prof. Dr. H. Ströher (E2)
(apl. Prof. at the Univ. of Cologne)

Prof. Dr. J. Tang (LI)
(since August 12, 2001)

Dr. R. Tölle (LI)

DP M. Walzl (TH)
until April 30, 2001

Dr. K.-H. Watzlawik (E2)

Dipl. P. Winter (E1)

Dr. P. Wintz (E1)

DI M. Wohlmuther (E1)

Dr. (HGF) M. Wolke (E1)

Dr. E. Zaplatin (LI)

Technical and Administrative Staff

M. Sc. M. Abd El-Bary (E1)
(NRC, AEA, Egypt)

M. Sc. S.M. Abd El Samad
(NRC, AEA, Egypt) (E1)

C. Berchem (Ec)
P. Birx (LI)

R. Bley (Ad)

H.-G. Böge (LI)

M. Böhnke (LI)

DI W. Borgs (E2)

J. Borsch (LI)

DI. R. Brings (LI)

P. Brittner (LI)

J. But (Ws)

M. Comuth (Ad)

L. Conin (LI)

B. Dahmen (LI)

C. Deliege (LI)

W. Derissen (Cd)

N. Dolfus (Ec)

G. D`Orsaneo (E2)

R. Enge (LI)

J. Engel (LI)

B. Erkes (LI)

W.-R. Ermer (E2)

W. Ernst (Ec)
K. Esser (Ad)
DI. F.-J. Etzkorn (LI)

H.-P. Faber (LI)

G. Fiori (Dt)

H.-W. Firmenich (Ws)

N. Gad (LI)

D. Gehsing (LI)

S. Geisler (Cd)
(until Oct. 31st, 2001)

J. Göbbels (Rp)

H. Hadamek (Ws)

R. Hecker (LI)

E. Heßler (Cd)
(since Sept. 17, 2001)

M. Holona (Ws)

K.-D. Jach (LI)

DI H.-M. Jäger (E1)

H.J. Jansen (Ws)

R. Janssen (Ad)

Dipl. (FH) U. Johnen (E1)
(until June 30, 2001)

M. Karnadi (E2)

DI R. Klein (E1)
(until April 30, 2001)

K. Krafft (Rp)

M. Kremer (Ws)

Th. Krings (Dt)

G. Krol (LI)

M. Küven (Ws)

S. Müller (Ad)
(since April 1st, 2001)

G. Roes (Ad)

F. Schultheiß (Ws)

D. Spölgen (Ws)
(until July 31st, 2001)

D. Spölgen (E2)
(since August 1st, 2001)

J. Strehl (Ws)

J. Uehlemann (E1)
(since Feb. 1st, 2001)

DI. T. Vashegyi (LI)

K.-P. Wieder (E2)

DI. J.-D. Witt (LI)

M. Zander (LI)
(until September 30, 2001)

H. Zens (LI)

Research Visitors
(for one week to six months):

Anagnostopoulos (E2)
from July 28 to August 31st, 2001
(University Ioannina, Greece)

Dr. V. Balanutsa (E2)
from March 11 to April 8, 2001
from August 19 to September 16, 2001
from November 12 to December 12, 2001
(Institute for Theoretical and Experimental Physics, Moscow)

Dr. S. Barsov (E2)
from March 4 to May 2nd, 2001
from July 22nd to September 16, 2001
from October 14 to November 18, 2001
(St. Petersburg Nucl. Phys. Inst., Gatchina, St. Petersburg)

Prof. V. Baryshevsky (E2)
from December 9 to 16, 2001
(Research Institute of Nuclear Problems, Minsk, Belarus)

Dr. T. Batsch (E1)
from Nov. 19 to Nov. 24, 2001
(Soltan Institute, Otwock, Poland)

Prof. A. Belov (LI)
from May 26 to June 2, 2001
(INR, Moskau, Russia)

E. Bialkowski (E1)
from July 8 to July 21, 2001
from August 19 to Sept. 15, 2001
(INP, Krakow, Poland)

Dr. A. Boukharov (E2)
from January 21st to February 8th, 2001
from March 25 to April 8, 2001
from May 20 to June 3rd, 2001
from September 3rd to 24, 2001
from October 1st to 22nd, 2001
from December 2nd to 9, 2001
(Moscow Power Engineering Institute, Moscow)

Dr. O. Brovko (LI)
from July 7 to July 29, 2001
(JINR, Dubna, Russia)

Dr. V. Chernetsky (E2)
from March 11 to April 8, 2001
from October 1st to 29, 2001
from November 19 to December 20, 2001
(Institute for Theoretical and Experimental Physics, Moscow)

Prof. V. Chernyshev (E2)
from January 21st to February 24, 2001
from March 25 to April 15, 2001
from May 20 to June 10, 2001
from September 3rd to October 29, 2001
from November 26 to December 24, 2001
(Institute for Theoretical and Experimental Physics, Moscow)

Dr. B. Chiladze (E2)
from May 23rd to June 6, 2001
(High Energy Phys. Inst., Tbilisi State University, Tbilisi, Georgia)

Dr. M. Chumakov (E2)
from May 20 to June 3rd, 2001
from November 19 to December 9, 2001
(Institute for Theoretical and Experimental Physics, Moscow)

R. Czyzykiewicz (E1)
from August 15 to August 29, 2001
from Sept. 21 to Oct. 20, 2001
from Nov. 19 to Dec. 2, 2001
(Jagellonian Univ., Krakow, Poland)

Dr. B. Julia Diaz (Th)
from September 3 to September 28, 2001
(University of Salamanca, Spain)

Dr. V. Dimitrov
from September 21st to October 4, 2001
from October 9 to 23rd, 2001
(Forschungszentrum Rossendorf, Dresden)

Prof. Dr. S. Drozdz (Th)
(DLR-Fellow)
from March 19 to March 31, 2001
from June 10 to June 15, 2001
since October 1, 2001
(University of Krakow, Poland)

Prof. Dr. J.W. Durso (Th)
from June 29 to November 2, 2001
(Mount Holyoke College, Hadley, MA, USA)

Prof. W. Falk (E1)
from Nov. 1 to Nov. 30, 2001
(Univ. of Manitoba, Canada)

Pavel Fedorets (E2)
from September 3rd,2000 to July 2nd, 2001
from September 2nd to December 23rd, 2001
(Institute for Theoretical and Experimental Physics, Moscow)

Dr. L. Freindl (E1)
from April 19 to May 4, 2001
(INP Krakow, Poland)

Prof. V. Gaidash (LI)
from May 26 to June 2, 2001
from August 11 to August 18, 2001
(INR, Moskau, Russia)

Prof. Dr. S. Gerasyuta (Th)
From November 4 to December 16, 2001
(University of St. Petersburg, Russia)

Prof. Dr. S. Gevorkyan (Th)
(INTAS-Fellow)
from November 16 to December 11, 2001
(Yerevan Physical Institute, Armenia)

Prof. Dr. I. Ginzburg (Th)
from October 21 to November 3, 2001
(S.L. Sobolev Institute, Novosibirsk, Russia)

Dr. V. Glagolev (E2)
from December 9 to 19, 2001
(Joint Institute for Nuclear Research, Dubna, Moscow)

Dr. E. Golubeva (E2)
from September 3rd to October 14, 2001
(Institute for Theoretical and Experimental Physics, Moscow)

Dr. V. Goryachev (E2)
from May 7 to June 4, 2001
(Institute for Theoretical and Experimental Physics, Moscow)

Dr. V. Grishina (E2)
from April 14 to May 20, 2001
from August 26 to October 8, 2001
(Institute for Theoretical and Experimental Physics, Moscow)

Dr. L. Gusev (E2)
from January 14 to February 4, 2001
from April 8 to May 13, 2001
from September 24 to October 22nd, 2001
(Institute for Theoretical and Experimental Physics, Moscow)

Dr. A. Hassan (E1)
from June 22 to Sept. 14, 2001
(NRC, AEA, Cairo, Egypt)

DP P. Hawranek (E1)
Research sholarship
(Univ. Krakow, Poland)

A. Heczko (E1+LI)
from March 7 to March 31, 2001
from July 1 to July 31, 2001
from August 1 to August 11, 2001
(Univ. Krakow, Polen)

Prof. Dr. B. Holstein (Th)
(Humboldt-Fellow)
from September 3 to Dezember 15, 2001
(University of Massachussetts, USA)

Dr. V. Iakuchev (LI)
from May 26 to June 2, 2001
(INR, Moskau, Russia)

Dr. Y. Ilieva (E1)
from April 12 to May 5, 2001
(INRE, Sofia, Bulgaria)

Prof. Dr. B. Ioffe (Th)
(Humboldt-Fellow)
from March 21 to June 20, 2001
(ITEP Moscow, Russia)

M. Janusz (E1)
from August 19 to August 26, 2001
from Sept. 18 to Sept. 30, 2001
(Jagellonian Univ., Krakow, Poland)

Prof. L. Jarczyk (E1 + E2)
from February 18 to 24, 2001
from August 6 to September 1st, 2001
(Jagellonian University Cracow, Poland)

V. Jha (E1)
from August 5 to Sept. 2, 2001
(BARC Indien)

P. Kalinak (E1)
from April 19 to April 30, 2001
from Dec. 3 to Dec. 18, 2001
(Univ. Kosice, Slovakia)
Prof. B. Kamys (E1)
from August 12 to Sept. 16, 2001
(Univ. Krakow, Poland)

Prof. S. Kamerdzhiev (Th)
from September 24 to December 23, 2001
(IPPE, Obninsk, Russia)
Russia)

Prof. B. Kamys (E2)
from February 18 to 24, 2001
from August 12 to September 8. 2001
(Jagellonian University Cracow, Poland)

Dr. A. Katcharava (E2)
from April 29 to May 12, 2001
from August 1st to December 31st, 2001
(Universität Erlangen-Nürnberg)

Dr. Z. Khorguashvili (E2)
from May 23rd to June 6, 2001
from December 4 to 25, 2001
(Georgian Academy of Sciences, Tbilisi, Georgia)

Dr. D. Kirillov (E1)
from April 09 to April 30, 2001
from Nov. 11 to Dec. 16, 2001
(JINR Dubna, Rußland)

Dr. J. Kisiel (E1)
from August 15 to August 29, 2001
(Univ. Silesia, Katowice, Poland)

Dr. M. Kistryn (E1)
from March 7 to March 18, 2001
from June 6 to June 10, 2001
from July 16 to August 26, 2001
(INP Krakow, Poland)

Dr. S. Kistryn (E1)
from August 9 to August 29, 2001
(Univ. Krakau, Polen)

Dr. St. Kliczewski (E1)
from March 11 to March 18, 2001
from April 1 to May 5, 2001
from June 19 to July 7, 2001
from July 24 to August 28, 2001
from Oct. 15 to Dec. 20, 2001
(Kernforschungszentrum Krakow, Poland)

Dr. A. Klimala (E1)
from April 17 to May 5, 2001
from August 6 to August 31, 2001
from Oct. 15 to Oct. 26, 2001
from Nov. 5 to Dec. 17, 2001
(Jagellonian Univ. of Krakow, Poland)

Dr. D. Kolev (E1)
from Nov. 25 to Dec. 16, 2001
(University of Sofia, Sofia, Bulgaria)

Prof. V. Komarov (E2)
from January 17 to February 22nd, 2001
from April 19 to June 18, 2001
from September 17 to October 29, 2001
from December 2nd to 23rd, 2001
(Joint Inst. for Nucl. Res., Dubna, Moscow)

Prof. Dr. L. Kondratyuk (Th + E2)
from February 11 to March 3, 2001
from April 14 to May 13, 2001
from August 26 to October 8, 2001
(Institute for Theoretical and Experimental Physics, Moscow)

Dr. E. Konobeevski (E2)
from November 25 to December 2nd, 2001
(Russian Academy of Sciences, Moscow)

Prof. V. Koptev (E2)
from January 15 to March 14, 2001
from April 15 to May 16, 2001
from July 29 to August 29, 2001
from September 23rd to November 21st, 2001
from December 3rd to 21st, 2001
(St. Petersburg Nucl. Phys. Inst., Gatchina, St. Petersburg)

DP P. Kowina (E1)
Research sholarship
(Univ. of Katowice, Poland)

Dr. V. Kozlov (E1)
from April 19 to June 19, 2001
from Oct. 15 to Dec. 14, 2001
(Moscow State Univ., Russia)

Dr. P. Kravchenko (E2)
from October 28 to November 13, 2001
(St. Petersburg Nucl. Phys. Inst., Gatchina, St. Petersburg)

Dr. M. Kravcikova (E1)
from April 19 to April 30, 2001
from Nov. 22 to Dec. 3, 2001
(Technische Universität Kosice, Slovakia)

Dr. P. Kravtsov (E2)
from February 4 to April 1st, 2001
from September 19 to November 21st, 2001
(St. Petersburg Nucl. Phys. Inst., Gatchina, St. Petersburg)

Prof. Dr. G. Krein (Th)
from October 8 toOctober 28, 2001
(UNESP Sao Paulo, Brasil)

Prof. Dr. A. Kudryavtsev (Th)
from April 16 to May 23, 2001
(ITEP Moscow, Russia)

Dr. A. Kulikov (E2)
from January 15 to February 20, 2001
from August 8 to 22nd, 2001
from September 19 to October 3rd, 2001
(Joint Inst. for Nucl. Res., Dubna, Moscow)

Prof. Dr. E. Kuraev (Th)
(INTAS-Fellow)
from August 10 to August 30, 2001
(JINR Dubna, Russia)

Dr. V. Kurbatov (E2)
from January 17 to February 2nd, 2001
from March 17 to 31st, 2001
from April 1st to 30, 2001
from July 29 to August 26, 2001
from September 21st to October 4, 2001
(Joint Inst. for Nucl. Res., Dubna, Moscow)

Prof. T. Kutsarova (E1)
from April 29 to May 8, 2001
from Nov. 23 to Dec. 13, 2001
(INRE, Sofia, Bulgaria)

Dr. J. Kwapien (Th)
(DLR-Fellow)
from March 19 to March 31, 2001
(University of Krakow, Poland)

M. Lesiak (E1)
from Nov. 19 to Dec. 1, 2001
(Univ. Krakow, Poland)

Prof. J. Lieb (E1)
from April 27 to May 15, 2001
from Nov. 26 to Dec. 14, 2001
(George Mason University, VA, USA)

Dr. G. Macharashvili (E2)
from January 17 to February 22nd, 2001
from March 17 to 31st, 2001
from April 1st to 30, 2001
from July 30 to August 27, 2001
from September 15 to October 29, 2001
(Joint Inst. for Nucl. Res., Dubna, Moscow)

Dr. A. Magiera (E1)
from April 17 to May 5, 2001
from August 6 to Sept. 2, 2001
(Univ. Krakow, Poland)

Prof. Dr. S. Manayenkov (Th)
from March 5 to April 29, 2001
(NPI St. Petersburg, Gatchina, Russia)

S. Marcello (E1)
from May 18 to May 22, 2001
(INFN Torino, Italy)

Prof. G. Martinska (E1)
from April 19 to April 30, 2001
from Nov. 22 to Dec. 3, 2001
(Univ. of Kosice, Slowakia)

Dr. S. Merzliakov (E2)
from January 15 to March 7, 2001
from March 28 to May 16, 2001
from June 26 to August 19, 2001
from September 20 to November 19, 2001
from November 13 to December 24, 2001
(Joint Inst. for Nucl. Res., Dubna, Moscow)

Prof. I. Meshkov (LI)
from April 30 to May 13, 2001
from July 19 to July 29, 2001
(JINR, Dubna, Russia)

W. Migdal (E1)
from March 7 to March 19, 2001
from June 4 to June 9, 2001
from July 8 to August 5, 2001
(Jagellonian Univ. of Krakow, Poland)

Dr. S. Mikirtytchiants (E2)
from January 17 to April 30, 2001
from July 22nd to August 26, 2001
from September 23rd to December 21st, 2001
(St. Petersburg Nucl. Phys. Inst., Gatchina, St. Petersburg)

Dr. A. Misiak (LI)
from July 1 to July 31, 2001
(Univ. Krakau, Poland)

Dr. T. Morek (E1)
from Nov. 12 to Nov. 26, 2001
(Univ. Warsaw, Poland)

Dr. P. Moskal (E1)
Research Sholarship
(Jagellonian Univ. of Krakow, Poland)

Prof. M. Moszynski (E1)
from August 29 to Sept. 2, 2001
(Soltan Inst., Warsaw, Poland)

Prof. Dr. K. Nakayama (Th)
from May 10 to August 10, 2001
(University of Georgia, Athens, USA)

Prof. Dr. H. Nann (E1)
from June 28 to July 13, 2001
(IUCF Bloomington, USA)

S. Nedev (E1)
from April 12 to April 26, 2001
from July 1 to Dec. 31, 2001
(Sofia, Bulgaria)

Dr. V. Nelyubin (E2)
from April 25 to May 20, 2001
(St. Petersburg Nucl. Phys. Inst., Gatchina, St. Petersburg)

Dr. L. Netchaeva (LI)
from August 11 to August 18, 2001
(INR, Moskau, Russia)

Prof. M. Nioradze (E2)
from February 10 to 24, 2001
from May 23rd to June 6, 2001
from December 5 to 18, 2001
(High Energy Phys. Inst., Tbilisi State University, Tbilisi, Georgia)

Prof. Dr. J Niskanen (Th)
from June 10 to June 19, 2001
from December 10 to December 19, 2001
(University of Helsinki, Finland)

Dr. S. Orfanitski (E1)
from April 19 to June 19, 2001
from Oct. 15 to Dec. 14, 2001
(Moscow State Univ., Russia

Dr. E. Oset (Th)
from July 15 to August 14, 2001
(University of Valencia, Spain)

Dr. J. Palomar (Th)
from June 1 to June 26, 2001
from July 7 to August 31, 2001
(University of Valencia, Spain)

Dr. A. Parfenov (LI)
from December 3 to December 12, 2001
(JINR, Dubna, Russia)

Dr. V. Parkhomchuk (LI)
from April 30 to May 13, 2001
(INP, Novosibirsk, Russia)

Dr. A. Pasternak (E1)
from Febr. 27 to March 27, 2001
from August 2 to Oct. 2, 2001
since Dec. 10, 2001
(Ioffe Institute St. Petersburg, Russia)

Dr. O. Petrus (E2)
from January 15 to March 7, 2001
from July 9 to August 21st, 2001
from September 16 to October 31st, 2001
(Joint Inst. for Nucl. Res., Dubna, Moscow)

Dr. P. Piirola (Th)
from October 7 to December 12, 3001
(University of Helsinki, Finland)

B. Piskor-Ignatowicz (E1)
from August 15 to August 29, 2001
(Jagellonian Univ., Krakow, Poland)

Dr. N. Piskunov (E1)
from May 18 to May 22, 2001
from Nov. 16 to Dec. 16, 2001
(JINR Dubna, Rußland)

Dr. S. Podchasky (E2)
from January 21st to February 4, 2001
from March 19 to April 8, 2001
from May 20 to June 3rd, 2001
from September 3rd to October 1st, 2001
from November 12 to December 23rd, 2001
(Institute for Theoretical and Experimental Physics, Moscow)

E. Podsvirova (E1)
from Jan. 10 to March 28, 2001
from August 1 to Oct. 28, 2001
(Ioffe Institute St. Petersburg, Russia)

Dr. K. Pysz (E1 + E2)
from February 1st to 28, 2001
from March 7 to March 18, 2001
(Jagellonian University Cracow, Poland)
Dr. A. Rakityanski (Th)
(INTAS-Fellow)
from August 10 to August 30, 2001
(JINR Dubna, Russia)

Dr. R. Rapp (Th)
from June 16 to July 14, 2001
(SUNY at Stony Brook, USA)

Prof. K. Rashid (E2)
from June 10 to July 15, 2001
(Quaid-I-Azam University, Islamabad, Pakistan)

Dr. B. Roy (E1)
Research Sholarship
(BARC Indien)

T. Rozek (E1)
from Dec. 9 to Dec. 22, 2001
(Univ. Silesia, Katowice, Poland)

Dr. Z. Rudy (E1 + E2)
from February 18 to 24, 2001
from August 6 to September 1st, 2001
(Jagellonian University Cracow, Poland)

Prof. N.Ya. Ruhlyada (LI)
from December 16 to December 23, 2001
(INPE, Obninsk, Russia)

Prof. T. Rzaca-Urban (E1)
from July 15 to August 5, 2001
(Univ. of Warsaw, Poland)
Prof. A. Sidorin (LI)
From April 22 to May 13, 2001
From July 19 to July 29, 2001
(JINR, Dubna, Russia)

Dr. W. Schäfer (Th)
from April 17 to April 24, 2001
from July 25 to August 14, 2001
from November 21 to November 26, 2001
(NORDITA, Copenhagen, Denmark)

Dr. I. Selioujenkov (E2)
from September 3rd to October 1st, 2001
(Institute for Theoretical and Experimental Physics, Moscow)

Dr. S. Sherman (E2)
from December 12 to 23rd, 2001
(St. Petersburg Nucl. Phys. Inst., Gatchina, St. Petersburg)

Dr. M. Siemaszko (E1)
from March 24 to April 8, 2001
(Univ. Silesia, Katowice, Poland)

Dr. I. Sitnik (E1)
from April 16 to April 8, 2001
(JINR Dubna, Rußland)

Dr. R. Siudak (E1)
from Febr. 21 to Febr. 25, 2001
from April 1 to May 5, 2001
from June 5 to June 9, 2001
since June 9, 2001
(Jagellonian Univ. of Krakow, Poland)

M. Smiechowicz (E1)
from Dec. 5 to Dec. 19, 2001
(Jagellonian Univ., Krakow, Poland)

Dr. J. Smyrski (E2)
from January 2nd to 8, 2001
from January 21st to 30, 2001
(Jagellonian University Cracow, Poland)

Dr. E. Stephan (E1)
from August 13 to August 29, 2001
(Univ. Silesia, Katowice, Poland)

Prof. Z. Sujkowski (E2)
from November 18 to 21st, 2001
(Soltan Inst. for Nucl. Studies, Swierk-Otwock, Poland)

R. Sworst (E1)
from Dec. 5 to Dec. 19, 2001
(Jagellonian Univ., Krakow, Poland)

Dr. A. Szczurek (Th)
(DLR-fellow)
from March 12 to April 11, 2001
(University of Krakow, Poland)

Dr. V. Tarassov (E2)
from May 20 to June 20, 2001
(High Energy Phys. Inst., Tbilisi State University, Tbilisi, Georgia)

Dr. N. Tchernov (E2)
from December 12 to 23rd, 2001
(St. Petersburg Nucl. Phys. Inst., Gatchina, St. Petersburg)

Prof. Dr. R. Tegen (Th)
from September 3 to October 20, 2001
(University of Witwatersrand, South Africa)

Dr. P.-E. Tegner (E1)
from Nov. 19 to Nov. 30, 2001
(Univ. Stockholm, Sweden)

Dr. G. Tertychny (Th)
from October 15 to December 12, 2001
(IPPE, Obninsk, Russia)

Dr. V. Trofimov (E2)
from December 12 to 23rd, 2001
(St. Petersburg Nucl. Phys. Inst., Gatchina, St. Petersburg)

Prof. R. Tsenov (E1)
from Nov. 25 to Dec. 16, 2001
(University of Sofia, Sofia, Bulgaria)

Dr. K. Tsushima (Th)
from May 21 to July 2, 2001
(University of Adelaide, Australia)

DP M. Ulicny (E1)
Research sholarship
(Univ. of Kosice, Slowakia)

Dr. J. Urban (E1)
(Univ. of Kosice, Slowakia)

Dr. W. Urban (E1)
from July 15 to August 5, 2001
(Univ. of Warsaw, Poland)

Dr. Y. Uzikov (E2)
from February 4 to March 16, 2001
from April 19 to June 9, 2001
from August 8 to October 27, 2001
from November 14 to December 22nd, 2001
(Joint Inst. for Nucl. Res., Dubna, Moscow)

G. Vankova (E1)
from April 16 to May 16, 2001
from Nov. 16 to Dec. 16, 2001
(Univ. Sofia, Sofia, Bulgaria)

Dr. A. Vassiliev (E2)
from February 4 to March 21st, 2001
from October 17 to December 23rd, 2001
(St. Petersburg Nucl. Phys. Inst., Gatchina, St. Petersburg)

Dr. T. Venkova (E1)
from August 1 to August 31, 2001
from Nov. 10 to Nov. 30, 2001
(INRE, Sofia, Bulgarien)

Prof. C. Wilkin (E2)
from February 17 to 24, 2001
from November 8 to 14, 2001
(University College London, U. K.)

Dr. A. Wirzba (Th)
since January 1, 2001
(SUNY at Stony Brook, USA)

M. Wisniowski (E1)
from Nov. 19 to Dec. 1, 2001
(Jagellonian Univ., Krakow, Poland)

Dr. D. Wolski (E1)
from Nov. 19 to Nov. 24, 2001
(Soltan Inst., Otwock, Poland)

A. Wronska (E1 + E2)
from January 30 to February 10, 2001
from April 17 to May 5, 2001
(Jagellonian University Cracow, Poland)

Dr. S. Wyngaardt (Th)
from April 29 to June 27, 2001
since October 30, 2001
(University of Stellenbosch, South Africa)

Dr. U. Yakshiev (Th)
(INTAS-Fellow)
from July 7 to September 6, 2001
(University of Tashkent, Uzbekistan)

Dr. S. Yaschenko (E2)
from January 15 to March 16, 2001
from March 27 to December 31st, 2001
(Universität Erlangen-Nürnberg)

Dr. B.G. Zakharov (Th)
(DFG-fellow)
since December 16, 2001
(Landau Inst. for Theor. Phys., Moscow, Russia)

Dr. B. Zalikhanov (E2)
from January 16 to April 15, 2001
from July 7 to September 7, 2001
from October 4 to January 4, 2002
(Joint Inst. for Nucl. Res., Dubna, Moscow)

Dr. N. Zhuravlev (E2)
from December 2nd to 10, 2001
(Joint Inst. for Nucl. Res., Dubna, Moscow

Prof. W. Zipper (E1)
from Febr. 21 to Febr. 25, 2001
from June 4 to June 9, 2001
from August 15 to August 29, 2001
(University of Silesia, Katowice, Poland)

Dr. V. Zoller (Th)
(DFG fellow)
from September 28 to December 21, 2001
(ITEP, Moscow, Russia)

P. Zupranski (E1)
from April 2 to April 8, 2001
from May 14 to May 25, 2001
from August 27 to August 20, 2001
(Soltan Inst., Warschau, Poland)

Dr. I. Zychor (E2)
from January 29 to March 28, 2001
from July 1st to August 24, 2001
from October 8 to November 30, 2001
(Soltan Inst. for Nucl. Studies, Swierk-Otwock, Poland)

X. Publications
Journals

IKP-
Abaev, V.; Büscher, M.; Dymov, S.; Hartmann, M.; Kacharava, A.; Komarov, V. I.; Koptev, V.; Kurbatov, V.; Mikirtychiants, S.; Nekipelov, M.; Petrus, A.; Ströher, H.; Uzikov, Yu. N.; Wilkin, C.; Yaschenko, S.
Spin-triplet final-state dominance in $pp \rightarrow pn\pi^+$ reaction at 492 MeV
Physics Letters B 521 (2001) 158 - 164
20.45.0

IKP-
COSY-TOF Collaboration
S. Abd El-Samad, M. Abdel-Bary, K.-Th. Brinkmann, H. Clement, S. Dshemuchadse, H. Dutz, W. Eyrich, A. Erhardt, D. Filges, A. Filippi, H. Freiesleben, M. Fritsch, J. Georgi, A. Gillitzer, D. Hesselbarth, B. Jakob, L. Karsch, K. Kilian, H. Koch, J. Kreß, E. Kuhlmann, S. Marcello, S. Marwinski, S. Mauro, W. Meyer, P. Michel, K. Möller, H. Mörtel, H.P. Morsch, L. Naumann, Ch. Plettner, M. Richter, E. Roderburg, A. Schamlott, P. Schönmeier, M. Schulte-Wissermann, W. Schröder, F. Stinzing, M. Steinke, G.Y. Sun, G.J. Wagner, M. Wagner, A. Wilms, S. Wirth
Production of ω mesons in proton-proton collisions
Physics Letters B 522 (2001) 16-21
20.45.0

IKP-
Ananthanarayan, B., Büttiker, P.
Comparison of πK scattering in SU(3) chiral perturbation theory and dispersion relations
Eur. Phys. J. C19 (2001) 517
20.80.0

IKP-
Ananthanarayan, B., Büttiker P., Moussallam B.
πK sum rules and the SU(3) chiral expansion
Eur. Phys. J. C22 (2001) 133
20.80.0

IKP-
Barsov, S. et al., [ANKE Collaboration],
ANKE, a new facility for medium energy hadron physics at COSY-Jülich,
Nucl. Instrum. Meth. A462 (2001) 364
20.80.0

IKP-
Baru, V.V.; Gasparian, A.M; Haidenbauer, J.; Kudryavtsev, A.E; Speth, J.
On the Migdal-Watson approach to FSI effects in meson production
NN collisions
Yad. Fiz., 64 (2001), p. 633-638
20.80.0

IKP-
Bernard, V.; Hemmert, T.R.; Meißner, Ulf-G.
Ordinary and radiative muon capture on the proton and the pseudoscalar form factor of the nucleon
Nuclear Physics, A686 (2001), p. 290-316
20.80.0

IKP-
Bernard, V.; Kaiser, N.; Meißner, Ulf-G.
Aspects of near-threshold neutral pion photoproduction off protons
European Physical Journal, A11 (2001), p. 209-216
20.80.0

IKP-
Bernard, V., Elouadrhiri, L, Meißner, Ulf-G.
Axial structure of the nucleon
J. Phys. G28 (2002) R1-R35
20.80.0

IKP-
M. Betigeri, J. Bojowald, A. Budzanowski, A. Chatterjee, J. Ernst, L. Freindl, D. Frekers, W. Garske, K. Grewer, A. Hamacher, J. Ilieva, L. Jarczyk, K. Kilian, S. Kliczewski, W. Klimala, D. Kolev, T. Kutsarova, J. Lieb, H. Machner, A. Magiera, H. Nann, L. Pentchev, H.S. Plendl, D. Protic, B. Razen, P. von Rossen, B. J. Roy, R. Siudak, J. Smyrski, R.V. Srikantiah, A. Strzalkowski, R. Tsenov, K. Zwoll
Simultaneous Measurements breaking via External π^0-η meson Mixing
Nucl. Physics A690 (2001) 473-493
20.45.0

IKP-
M. Betigeri, J. Bojowald, A. Budzanowski, A. Chatterjee, J. Ernst, L. Freindl, D. Frekers, W. Garske, K. Grewer, A. Hamacher, J. Ilieva, L. Jarczyk, K. Kilian, S. Kliczewski, W. Klimala, D. Kolev, T. Kutsarova, J. Lieb, H. Machner, A. Magiera, H. Nann, L. Pentchev, H.S. Plendl, D. Protic, B. Razen, P. von Rossen, B. J. Roy, R. Siudak, A. Strzalkowski, R. Tsenov, K. Zwoll
Differential Cross Section Measurement for the $pp \rightarrow d\pi^+$ reaction at 850 MeV/c
Phys. Review C 63 (2001) 044011
20.45.0

IKP-
R. Bilger, W. Brodowski, H. Calén, H. Clement, J. Dyring, C. Ekström, G. Fäldt, K. Fransson, J. Greiff, L. Gustafsson, B. Höistad, M. Jacewicz, J. Johanson, A. Johansson, T. Johansson, K. Kilian, I. Koch, S. Kullander, A. Kupsc, P. Marciniewski, B. Morosov, W. Oelert, R.J.M.Y. Ruber, P. Sundberg, B. Shwartz, J. Stepaniak, A. Sukhanov, P. Thörngren-Engblom, A. Turowiecki, G.J. Wagner, Z. Wilhelmi, C. Wilkin, J. Zabierowski, J. Zlomanczuk
Cross sections of the $pp \rightarrow pp\pi^0$ reaction between 310 and 425 MeV
Nuclear Physics A 693 (2001) 633-662
20.50.0

IKP-
Büscher, M.; Ioffe, B. L.; Koptev, V.; Nekipelov, M.; Sibirtsev, A.; Sistemich, K.; Speth, J. and Ströher, H.
Phenomenological analysis of K^+-meson production in proton-nucleus collisions
Physical Review C, Vol. 65 (2002) 014603
20.45.0

IKP-
Bulgac, A., Wirzba, A.
Casimir interaction among objects immersed in a fermionic environment
Phys. Rev. Lett., 87, (2001) 120404 1-4
20.80.0

IKP-
Cloth, P.; Filges, D. and the members of the ZEUS Collaboration:
Measurement of Inclusive Prompt Photon Photoproduction at HERA
Phys.Lett.B472, (2000) 175-188
20.48.0

IKP-
Drozdz, S., Grümmer F., Ruf, F., Speth, J.
Towards identifying the world stock market cross-correlations: DAX versus Dow Jones
Physica A 294 (2001) 226-234
20.80.0

IKP-
Drozdz, S., Kwapien, J., Grümmer, F. Ruf, F., Speth, J.
Quantifying the dynamics of financial correlations
Physica A 299 (2001) 144
20.80.0

IKP-
Drozdz, S., Wojcik, M.
Nature of order from random two-body interactions
Physica A 301 (2001) 291
20.80.0

IKP-
J. Eberth, G. Pascovici, H.G. Thomas, N. Warr, D. Weisshaar, D. Habs, P. Reiter, P. Thirolf, D. Schwalm, C. Gund, H. Scheit, M. Lauer, P. Van Duppen, S. Franchoo, M. Huyse, R. M. Lieder, W. Gast, J. Gerl, K.P. Lieb and MINIBALL COLLABORATION
A Ge detector array for radioactive ion beam facilities
Progress in Particle and Nuclear Physics 46 (2001) 389-398
20.10.0

IKP-
Elster, Ch., Glöckle, W., Fachruddin, I.
Nucleon-nucleon scattering in a three-dimensional approach
Nucl. Phys. A689, 507c (2001)
20.80.0

IKP-
Epelbaum, E.; Kamada, H.; Nogga, A.; Witala, H.; Glöckle, W.; Meißner, Ulf-G.
Three- and four-nucleon systems from chiral effective field theory
Physical Review Letters, 86 (2001) p. 4787-4790
20.80.0

IKP-
Fachruddin, I., Elster Ch., Glöckle W.
New Forms of Deuteron Equations and Wave Functions
Phys. Rev. C63, 054003-1 (2001).
20.80.0

IKP-
Fachruddin, I. Elster, Ch., Glöckle, W.
Nucleon-nucleon scattering in a three-dimensional approach
Nucl. Phys. A689 (2001), 507c (2001)
20.80.0.

IKP-
Fettes, N.; Meißner, Ulf-G.
Pion-nucleon scattering in an effective chiral field theory with explicit spin-3/2 fields
Nuclear Physics, A679 (2001), p. 629-670
20.80.0

IKP-
Fettes, N.; Meißner, Ulf-G.
Towards an understanding of isospin violation in pion-nucleon scattering
Physical Review, C63 (2001), p. 045201
20.80.0

IKP-
Fettes, N.; Meißner, Ulf-G.
Complete analysis of pion-nucleon scattering in chiral perturbation theory to third order
Nuclear Physics, A693 (2001), p. 693-709
20.80.0

IKP-
D. Filges, F. Goldenbaum, M. Enke, J. Galin, C.-M. Herbach, D. Hilscher, U. Jahnke, A. Letourneau, B. Lott, R.-D. Neef, K. Nünighoff, N. Paul, A. Péghaire, L. Pienkowski, H. Schaal, U. Schröder, G. Sterzenbach, A. Tietze, V. Tishchenko, J. Toke, M. Wohlmuther
Spallation neutron production and the current intra-nuclear cascade and transport codes
Eur. Phys. J. A. 11, 467-490 (2001)
20.90.0

IKP-
Gabrielse,G.; Estrada,J.; Tan,J.N.; Yesley,P.; Bowden,N.S.; Oxley,P.; Roach,T.; Storry,C.H.; Wessels,M.; Tan,J.; Grzonka,D.; Oelert,W.; Schepers,G.; Sefzick,T.; Breunlich,W.H.; Cargnelli,M.; Fuhrmann,H.; King,R.; Ursin,R.; Zmeskal,J.; Kalinowsky,H.; Wesdorp,C.; Walz,J.; Eikema,K.S.E.; Haensch,T.W.
First positron cooling of antiprotons
Physics Letters B, 507 (2001), p.1-4
20.50.0

IKP-
Gardner, S.; Meißner, Ulf-G.; Valencia, G.
Watson's theorem and electromagnetism in $K \to \pi\pi$
Physics Letters, B500 (2001), p. 44-50
20.80.0

IKP-
Gasparian, A.M.; Haidenbauer, J.; Hanhart, C.; Kondratyuk, L.; Speth, J.
Near threshold Λ and Σ production n in pp collisions
Nucl. Phys., A684 (2001) p. 397c-399c
20.80.0

IKP-
Ginzburg, I.F., Ivanov I.P.
CP-odd anomalous interactions of Higgs boson in its production at photon colliders
Eur. Phys. J. C22 (2001) 411
20.80.0

IKP-
Grishina, V. Yu.; Kondratyuk, L. A.; Büscher, M.; Cassing, W.; Ströher, H.
$a_0(980)$-$f_0(980)$ mixing and isospin violation in the reactions pN $\longrightarrow$ da_0, pd $\longrightarrow$ ^{3}He/^{3}Ha_0 and dd $\longrightarrow$ ^{4}He a_0
Physics Letters B 521 (2001) 217 – 224
20.45.0

IKP-
D. Grzonka, K. Kilian
Overview of the experimental program of strangeness production at COSY
Nuclear Physics A691 (2001) 473c-482c
20.45.0

IKP-
Hadjimichef, D.; Haidenbauer, J.; Krein, G.
Long- and medium-range components of the nuclear force in quark-model based calculations
Phys. Rev. C, 63 (2001) p. 035204 1-8
20.80.0

IKP-
Hanhart C., Phillips, D.R., Reddy, S. and Savage, M.J.
Extra dimensions, SN1987A, and nucleon nucleon scattering data,
Nucl. Phys. B595 (2001) 335
20.80.0

IKP-
Hanhart, C., Phillips, D.R. and Reddy, S.
Neutrino and axion emissivities of neutron stars from nucleon nucleon scattering data,
Phys. Lett. B499 (2001) 9
20.80.0

IKP-
Hanhart, C., Miller, G.A., Myhrer, F., Sato, T. and van Kolck, U.
Toy model for pion production in nucleon-nucleon collisions
Phys. Rev. C63 (2001) 044002
20.80.0

IKP-
Hanhart, C., Pons, J.A., Phillips, D.R. and Reddy, S.
The likelihood of GODs' existence: Improving the SN 1987a constraint on the size of large compact dimensions
Phys. Lett. B509} (2001) 1
20.80.0

IKP-
Heim, Thomas A., Hencken, K., Trautmann, D., Baur, G.
Pionium interacting with matter: Magnetic terms and relativistic corrections
Journ. of Phys. B: At. Mol. Opt. Phys. 34 (2001) 3763
20.80.0

IKP-
Ivanov I.P., Nikolaev, N.N.
Deep Inelastic Scattering in k-factorization and the anatomy of the differential gluon structure function of the proton
Phys. Atom. Nucl. 64 (2001) 753; Yad. Fiz. 64 (2001) 813
20.80.0

IKP-
Krusche, B.; Ahrens, J.; Beck, R.; Kamalov, S.; Metag, V.; Owens, R. O.; Ströher, H.
Coherent π^0-photoproduction from atomic nuclei
Phys. Lett. B 526 (2002) 287
20.50.0

IKP-
Kubis, B.; Meißner, Ulf-G.
Baryon form factors in chiral perturbation theory
European Physical Journal, C18 (2001), p. 747-756
20.80.0

IKP-
Kubis, B., Meißner, Ulf-G.
Isospin-violation in pion-kaon scattering
Nucl. Phys. A699 (2002) 709-731
20.80.0

IKP-
Kubis, B.; Meißner, Ulf-G.
Low energy analysis of the nucleon electromagnetic form factors
Nuclear Physics, A679 (2001), p. 698-734
20.80.0

IKP-
Krewald, S., Speth, J., Wang, Z.S.
A meson-theoretical Explanation of the $f_0(980)$ Production Puzzle in the Reaction $\pi \_ p \rightarrow \pi^0 \pi^0 n$
Phys. of Atomic Nuclei, Vol. 64, No. 4, 2001
20.80.0

IKP-
R.M. Lieder, W. Gast, H.M. Jäger, L. Mihailescu, M. Rossewij, J. Eberth, G. Pascovici, H.G. Thomas, D. Weisshaar, F. Beck, D. Curien, G. Duchene, E. Pachoud, I. Piqueras, C. Rossi Alvarez, D. Bazzacco, M. Bellato, Th. Kröll, Ch. Manea, B. Quintana, R. Venturelli, D.R. Napoli, D. Rosso, P. Spolaore, A. Geraci, A. Pullia, G. Ripamonti, F. Camera, B. Million, O. Wieland, J. Lisle, A.G. Smith, R. Well, P. Nolan, A. Boston, D. Cullen, M. Descovich, T. Enqvist, B. Cederwall, E. Ideguchi, J. van der Marel, J. Nyberg, B. Herskind, G. Sletten, J. Wilson, R. Henck, D. Gutknecht and K. Jääskeläinen
The TMR network project Development of gamma-ray tracking detectors
Nuclear Physics A682 (2001) 279c-285c
20.10.0

IKP-
R.M. Lieder, W. Gast, H.M. Jäger, L. Mihailescu, M. Rossewij, J. Eberth, G. Pascovici, H.G. Thomas, D. Weisshaar, F. Beck, D. Curien, G. Duchene, E. Pachoud, I. Piqueras, C. Rossi Alvarez, D. Bazzacco, M. Bellato, Th. Kröll, Ch. Manea, B. Quintana, R. Venturelli, D.R. Napoli, D. Rosso, P. Spolaore, A. Geraci, A. Pullia, G. Ripamonti, F. Camera, S. Leoni, B. Million, O. Wieland, A. Bracco, M. Pignanelli, S. Brambilla, J. Lisle, A.G. Smith, R. Well, P. Nolan, A. Boston, D. Cullen, M. Descovich, T. Enqvist, B. Cederwall, E. Ideguchi, J. van der Marel, J. Nyberg, B. Herskind, G. Sletten, J. Wilson, R. Henck, D. Gutknecht and K. Jääskeläinen
Gamma-Ray Tracking Arrays Progress in Particle and Nuclear Physics 46 (2001) 399-407
20.10.0

IKP-
R.M. Lieder, W. Gast, H.M. Jäger, L. Mihailescu, M. Rossewij, J. Eberth, G. Pascovici, H.G. Thomas, D. Weisshaar, F. Beck, D. Curien, G. Duchene, E. Pachoud, I. Piqueras, C. Rossi Alvarez, D. Bazzacco, M. Bellato, Th. Kröll, Ch. Manea, B. Quintana, R. Venturelli, D.R. Napoli, D. Rosso, P. Spolaore, A. Geraci, A. Pullia, G. Ripamonti, F. Camera, S. Leoni, B. Million, O. Wieland, A. Bracco, M. Pignanelli, S. Brambilla, J. Lisle, A.G. Smith, R. Well, P. Nolan, A. Boston, D. Cullen, M. Descovich, T. Enqvist, B. Cederwall, E. Ideguchi, J. van der Marel, J. Nyberg, B. Herskind, G. Sletten, J. Wilson, R. Henck, D. Gutknecht and K. Jäskelinen
Development of Gamma-Ray Tracking Detectors
Acta Physica Polonica B32 (2001) 2395-2401
20.10.0

IKP-
Meier, H., Halabuka, Z., Hencken, K., Trautmann, D., Baur, G.
Bound-free electron-positron production in relativistic heavy ion collisions
Phys. Rev. A63 (2001) 032713
20.80.0

IKP-
Meißner, Ulf-G.; Oller, J.A.
Chiral dynamics in the presence of bound states: kaon-nucleon interactions revisited
Physics Letters, B500 (2001) p. 263-272
20.80.0

IKP-
Meißner, Ulf-G.; Oller, J.A.
$J/\Psi \rightarrow \phi\pi\pi\left(K\overline{K}\right)$ decays, chiral dynamics and OZI violation
Nuclear Physics, A679 (2001) p. 671-697
20.80.0

IKP-
Meißner, Ulf-G.; Oller, J.A.
S-wave $\Lambda\pi$ phase shift is not large
Physical Review, D64 (2001) p. 014006
20.80.0

IKP-
Meißner, Ulf-G.; Epelbaum, E.; Glöckle, W.
The nucleon-nucleon interaction from effective field theory
Nuclear Physics, A684 (2001), p. 371c-376c
20.80.0

IKP-
Messchendorp, J.G., Sibirtsev, A., Cassing, W., Metag, V. and Schadmand, S.
Studying the omega-mass in-medium in γ + A to π^0 γ + X reactions
Eur. Phys. J. A11 (2001) 95
20.80.0

IKP-
T. Morek, J. Srebrny, Ch. Droste, M. Kowalczyk, T. Rzaca-Urban, K. Starosta, W. Urban, R. Kaczarowski, E. Ruchowska, M. Kisielinski, A. Kordyasz, J. Kownacki, M. Palacz, E. Wesolowski, W. Gast, R.M. Lieder, P. Bednarczyk, W. Meczynski and J. Styczen
Investigation of the K = 8- isomer in 132Ce
Phys. Rev. C63 034302-1 (2001)
20.10.0

IKP-
Moskal,P.; Adam,H.-H.; Budzanowski,A.; Grzonka,D.; Jarczyk,L.; Khoukaz,A.; Kilian,K.; Kowina,P.; Lang,N.; Lister,T.; Oelert,W.; Quentmeier,C.; Santo,R.; Schepers,G.; Sefzick,T.; Sewerin,S.; Siemaszko,M.; Smyrski,J.; Strzalkowski,A.; Wolke,M.; Wuestner,P.; Zipper,W.
Monitoring of the accelerator beam distributions for internal target facilities
Nuclear Instruments and Methods A, 466 (2001), p. 448-455
20.45.0

IKP-
Moskal,P.; Adam,H.-H.; Budzanowski,A.; Götz,T.; Grzonka,D.; Jarczyk,L; Khoukaz,A.; Kilian,K.; Kolf,C., Kowina,P., Lang,N.; Lister,T.; Oelert,W.; Quentmeier,C.; Santo,R.; Schepers,G.; Sefzick, T.; Siemaszko,M.; Smyrski,J.; Steltenkamp,S.; Strzakowski,A.; Winter,P.; Wolke,M.; Wüstner,P.; Zipper,W.
On the close to threshold meson production in neutron-neutron collisions
Physics Letters B, 517 (2001), p.295-298
20.45.0

IKP-
Nakayama, K.; Haidenbauer, J.; Speth, J.
The reactions $pn \to d\omega$ and $pn \to d\phi$ near threshold
Phys. Rev. C, 63 (2001), p. 015201 1-7
20.80.0

IKP-
Nakayama, K.; Haidenbauer, J.; Speth, J.
The reactions $pn \to d\omega$ and $pn \to d\phi$ and the role of the OZI rule
Nucl. Phys., A689 (2001) p. 402c-405c
20.80.0

IKP-
Nikolaev, N.N.
Color transparency
Nucl. Phys. Proc. Suppl. 99A (2001) 249
20.80.0

IKP-
Nikolaev, N.N.
TESLA: The superconducting electron-positron linear collider with an integrated X-ray laser laboratory
Technical Design Report, Part 6, Chapter 2 TESLA-N Study Group: H. Abramowicz et al. THERA: Electron-proton scattering at root(s) approximately 1 TeV, DESY-01-011FB, DESY-2001-011FB, DESY-TESLA-2001-23FB, DESY-TESLA-FEL-2001-05FB, ECFA-2001-209FB, March 2001. 62pp
20.80.0

IKP-
Nikolaev, N.N., Schäfer W., Schwiete, G.
Coherent production of hard dijets on nuclei in QCD
Phys. Rev. D63 (2001) 014020
20.80.0

IKP-
Nikolaev,, N.N., Zoller, V.R.
How open charm production probes the rightmost hard BFKL pole exchange
Phys. Lett. B509 (2001) 283
20.80.0

IKP-
Nowak, M.A., Rho, M., Wirzba, A., Zahed, I.
$\pi^0 \to \gamma\gamma$ in dense QCD
Physics Letters B 497 (2001), 85 – 90
20.80.0

IKP-
Oller, J.A., Oset, E., Palomar, J.E.
Pion and kaon vector form factors
Phys. Rev. D63 (2001) 114009
20.80.0

IKP-
Quentmeier,C.; Adam,H.-H.; Balewski,J.T.; Budzanowski,A.; Grzonka,D.; Jarczyk,L.; Khoukaz,A.; Kilian,K.; Kowina,P.; Lang,N.; Lister,T.; Moskal,P.; Oelert,W.; Santo,R.; Schepers,G.; Sefzick,T.; Sewerin,S.; Siemaszko,M.; Smyrski,J.; Strzalkowski,A.; Wolke,M.; Wuestner,P.; Zipper,W.
Near Threshold K+K- Meson-Pair Production in Proton-Proton Collisions
Physics Letters B, 515 (2001), p.276-282
20.45.0

IKP-
Schmidt, A.; Achenbach, P.; Ahrens, J.; Arends, H. J.; Beck, R.; Bernstein, A. M.; Hejny, V.; Kotulla, M.; Krusche, B.; Kuhr, V.; Leukel, R.; MacGregor, I. J. D.; McGeorge, J. C.; Metag, V.; Olmos de León, V. M.; Rambo, F.; Siodlaczek, U.; Ströher, H.; Walcher, Th.; Weiß, J.; Wissmann, F. and Wolf, M.
Test of Low-Energy Theorems for H($\vec{\gamma}$,π^0)^{1}H in the Threshold Region
Physical Review Letters, Vol. 87, Number 23 (2001) 232501
20.50.0

IKP-
Sibirtsev, A., Elster, C., Haidenbauer, J. and Speth, J.
Incoherent photoproduction of η-mesons from the deuteron near threshold
Phys. Rev. C64 (2001) 024006
20.80.0

IKP-
Sibirtsev, A. et. Al (DIANA Collaboration)
Evidence of elementary processes for hyperon production in low-energy antiproton annihilation on Xenon nuclei
Nucl. Phys. A683, 305 (2001)
20.80.0

IKP-
Speth, J., Hanhart, C., Krehl, O.
The Structure of the Roper Resonance
Nucl. Physics A680 (2001) 328c-334c
20.80.0

IKP-
Szczurek, A., Nikolaev, N.N., Schäfer, W., Speth, J.
Mapping the proton unintegrated gluon distribution in dijets correlations in real and virtual photoproduction at HERA.
Phys. Lett. B500 (2001) 254
20.80.0

IKP-
Szczurek, A., Uleshenko V., Speth, J.
$\bar{d} - \bar{u}$ Asymmetry and semi-inclusive production of pions in deep inelastic scattering
Phys. Rev. D63 (2001) 114005-1
20.80.0

IKP-
Typel, S., Baur, G.
Higher Order Effects in Electromagnetic Dissociation of Neutron Halo Nuclei
Phys.Rev. C64 (2001) 024601
20.80.0

IKP-
Uzikov; Yu. N.; Komarov; V. I., Rathmann; F., Seyfarth, H.
Singlet-to-triplet ratio in the deuteron breakup reaction pd $\longrightarrow$ pnp at 585 MeV
Physics Letters B 524 (2002), p. 303 – 307
20.45.0

IKP-
Walzl, M.; Meißner, Ulf-G.
Elastic electron-deuteron scattering in chiral effective field theory
Physics Letters, B513 (2001), p. 37-45
20.80.0

IKP-
Walzl, M.; Meißner, Ulf-G.; Epelbaum, E.
Charge-dependent nucleon-nucleon potential from chiral effective field theory
Nuclear Physics, A693 (2001), p. 663-692
20.80.0

IKP-
Weiß, J.; Achenbach, P.; Ahrens, J.; Annand, J. R. M.; Beck, R.; Hejny, V.; Kellie, J. D.; Kleber, V.; Kotulla, M.; Krusche, B.; Kuhr, V.; Leukel, R.; Metag, V.; Olmos de Léon, V. M.; Rambo, F.; Schmidt, A.; Siodlaczek, U.; Ströher, H.; Wissmann, F. and Wolf, M.
Exclusive measurement of coherent η-photoproduction from the deuteron
European Physical Journal A, 11 (2001), p. 371 – 374
20.50.0

IKP-
Wise, T.; Haeberli, W.; Lorentz, B.; Quin, P. A.; Rathmann, F.; Schwartz, B.;Walker, T. G; Wellinghausen, A.; Balewski, J. T.; Doskow, J.; Meyer, H. O.; Pollock, R. E.; v. Przewoski, B.; Rinckel, T.; Saha, Swapan K.; Pancella, P. V.
Nuclear Polarization of Hydrogen Molecules from Recombination of Polarized Atoms
Physical Review Letters, Vol. 87, Number 4 (2001)
20.50.0

IKP-
Zakharov, B.G.
On the energy loss of high-energy quarks in a finite-size quark-gluon plasma
JETP Lett. 73 (2001) 49, Pisma Zh. Eksp. Teor. Fiz. 73 (2001) 55
20.80.0

IKP-
Zoller, V.R.
Diffractive beauty photoproduction as a short distance probe of QCD pomeron
Phys. Lett. B509 (2001) 69
20.80.0

Proceedings, Reports

IKP-
Baur, G., Hencken, K., Trautmann, D., Typel, S., Wolter, H.H.
The past and future of coulomb dissociation in hadron- and astrophysics
Proceedings of the NATO Advanced Study Institute "Nuclei Far From Stability and Astrophysics", Predeal, Rumania, 28.8.-8.9.2000, Kluwer Academic Publishers
NATO Science Series Physics and Chemistry-Vol.17, D. Poenaru, H. Rebel, J. Wentz, eds.(2001) p. 247-258
20.80.0

IKP-
Baur, G., Hencken, K., Trautmann, D., Typel, S., Wolter, H. H.
Electromagnetic dissociation as a tool for nuclear structure and astrophysics
Proceedings of the International Workshop of Nuclear Physics, 22th Course Radioactive Beams for Nuclear and Astro Physics Erice, Sicily, 16-24.9.2000, Progress in Particle and Nuclear Physics Vol 46(2001) 99-108
20.80.0

IKP-
M. Betigeri, J. Bojowald, A. Budzanowski, A. Chatterjee, M. Drochner, J. Ernst, L. Freindl, D. Frekers, W. Garske, K. Grewer, A. Hamacher, J. Ilieva, L. Jarczyk, G. Kemmerling K. Kilian, S. Kliczewski, W. Klimala, D. Kolev, T. Kutsarova, J. Lieb, H. Machner, A. Magiera, H. Nann, L. Pentchev, H.S. Plendl, D. Protic, B. Razen, P. von Rossen, B. J. Roy, R. Siudak, J. Smyrski, A. Strzalkowski, R. Tsenov, P.A. Zolnierczuk, K. Zwoll
Meson Production in p+d Reactions
Proc. Few Body Conf., Evora, Portugal, Nuc. Phys. A689 (2001) 398c
20.45.0

IKP-
Betz, M.; Veit, E.A.; Haidenbauer, J.
Importance of Δ exchange in $p\bar{p}$ annihilation: Comparison between the two-pion and three-pion channels, in ``Hadrons Physics 2000: Topics on the structure and interaction of hadronic systems", edited by F.S. Navarra et al.
(World Scientific, Singapore, 2001), p. 367-370
20.80.0

IKP-
Büscher, M.; Kleber, V., Nekipelov, M; Kulessa, P.
Proceedings of the „2nd ANKE Workshop on strangeness production in pp and pA interactions“, 21./22.6.2001, Gatchina, Russland
Berichte des Forschungszentrums Jülich 3922, ISSN 0944-2952, Institut für Kernphysik
20.45.0

IKP-
Cloth, P.; Filges, D. and the members of the ZEUS Collaboration:
Measurement of Dijet Production in Neutral Current Deep Inelastic Scattering at High Q^2 and Determination of α_s
Report, DESY-01-018, February 2001
20.48.0

IKP-
Cloth, P.; Filges, D. and the members of the ZEUS Collaboration:
Study of the Effective Transverse Momentum of Partons in the Proton Using Prompt Photons in Photoproduction at HERA,
Report, DESY-01-043, March 2001
20.48.0

IKP-
Cloth, P.; Filges, D. and the members of the ZEUS Collaboration:
Multiplicity Moments in Deep Inelastic Scattering at HERA,
Report, DESY-01-053, April 2001
20.48.0

IKP-
Cloth, P.; Filges, D. and the members of the ZEUS Collaboration:
Measurement of the Neutral Current Cross Section and F_2 Structure Function for Deep Inelastic e^+p Scattering at HERA,
Report, DESY-01-064, May 2001
20.48.0

IKP-
Cloth, P.; Filges, D. and the members of the ZEUS Collaboration:
Properties of Hadronic Final States in Diffractive Deep Inelastic ep Scattering at HERA
Report, DESY-01-064, May 2001
20.48.0

IKP-
Dietrich, J.
COSY: Schnelle Teilchenextraktion für ESS-Target-Forschung in Jülich
FZJ-Intern, Nr.4, Dezember 2000
20.30.0

IKP-
Elster, Ch., Fachruddin, I., Glöckle, W.
Three dimensional calculations of the NN System
American Physics Society Meeting, April 2001
Washington DC, Bulletin J15.013
20.80.0

IKP-
Elster, Ch., Liu, H., Glöckle, W.
Three body bound state calculations with three body forces without angular momentum decomposition
Europhysics Conference on "Computational Physics", Aachen, Germany, 5.-8.9.2001,
Book of Abstracts, NIC Series Vol. 8, F. Hossfeld, K. Binder (Edts), p. A22
20.80.0

IKP-
W. Gast, R.M. Lieder, L. Mihailescu and M. Rossewij
Digital Triggering and Timing for Tracking Arrays
Verhandl. DPG (VI) 36, 34 (2001)
Book of Conference Contributions
20.10.0

IKP-
Gillitzer, A.
Deeply bound pionic atoms
Structure of Hadrons
XXIX Int. Workshop on Gross Properties of Nuclei and Nuclear Excitations
Proceedings Hirschegg, Austria, Jan. 14-20,2001, p. 56
20.45.0

IKP-
D. Gronzka, K. Kilian
Meson baryon production and interaction
16th International Conference on Few-Body Problems in Physics (FB16),
Taipei, Taiwan, China
Nucl. Physics A684 (2001), p. 130-138
20.45.0

IKP-
D. Gronzka, K. Kilian
Future Physics Program at COSY
Structure of Hadrons
XXIX Int. Workshop on Gross Properties of Nuclei and Nuclear Excitations
Proceedings Hirschegg, Austria, Jan. 14-20,2001, p. 330-339
20.45.0

IKP-
Haidenbauer, J.; Melnitchouk, W.; Speth, J.
A meson exchange model for the YN interaction, in "Mesons & Light Nuclei", AIP Conference Proceedings of the 8th Conference, edited by J. Adam et al., no. 603 (2001), p. 421-424
20.80.0

IKP-
Julia-Diaz, B.; Fernandez, F.; Valcarce, A.; Haidenbauer, J.
Quark model study of the triton bound state, in "Mesons & Light Nuclei", AIP Conference Proceedings of the 8th Conference, edited by J. Adam et al. ,no. 603 (2001), p. 267-270
20.80.0

IKP-
Jungwirth, H.N. for the COSY-team
First Deuteron Beam at COSY
COSY NEWS, No.10 (July 2001), p. 7-8
20.30.0

IKP-
Krewald S., Speth, J., Wang, Z.S.
A meson-theoretical explanation of the $f_0(980)$ production puzzle in the reaction $\pi - p \rightarrow \pi^0 \pi^0 n$
Proceedings 16th International IUPAP Conference on FEW BODY PROBLEMS IN PHYSICS, 6.-10.3.2000, Taipei, Taiwan, Hrsg. C.Y.Cheung, Y.K.Ho, T.S.H.Lee and S.N.Yang, Nucl. Phys. A 484 (2001) 429c
20.80.0

IKP-
Krewald, S., Schneider, S., Speth, J.
Two Pion Production in the Jülich model
Int. Conference NSTAR 2001 -Proceedings of the Workshop "The Physics of excited Nucleons, Mainz, Germany, 7.-10.3.2001
World Scientific Konferenzband, hrsg. D. Drechsel & L. Tiator, p. 93-99, ISBN 981-02-4760-5
20.80.0

IKP-
Kulessa, P.; Cassing, W.; Kamys, B.; Ohm, H.; Pysz, K.; Rudy, Z.; Ströher, H.
Nonmesonic decay of the heavy hypernuclei produced in the p+Au reaction
Bormio, Italien, 22. – 27.1.2001
Proceedings of the XXXIX International Winter Meeting on Nuclear Physics, Universitá Degli Studi Di Milano, p. 349
20.45.0

IKP-
R.M. Lieder, H. Brands, W. Gast, H.M. Jäger, L. Mihailescu, T. Rzaca-Urban, Z. Marcinkowska, W. Urban, T. Morek, Chr. Droste, S. Chmel, D. Bazzacco, G. Falconi, R. Menegazzo, S. Lunardi, C. Rossi Alvarez, G. deAngelis, E. Farnea, A. Gadea, D.R. Napoli and Z. Podolyak
Investigation of Magnetic Rotation around 142Gd
Proceedings of the International Symposium on Nuclear Structure Physics,
Editors: R. Casten, J. Jolie, U. Kneissl, P. Lieb
World Scientific, New Jersey (2001) p. 375 – 376
20.10.0

IKP-
Lieder, R.M. for the Gamma-Ray Tracking Detector Collaboration
Development of Gamma-Ray Tracking Detectors
Proc. Int. Conf. and NATO Advanced Research Workshop on High Spin Physics 2001, Warsaw, vol. 1, p. 3 (2001), Book of Conference Contributions
20.10.0

IKP-
R.M. Lieder, T. Rzaca-Urban, H. Brands, W. Gast, H.M. Jäger, L. Mihailescu, Z. Marcinkowska, W. Urban, T. Morek, Chr. Droste, S. Chmel, D. Bazzacco, G. Falconi, R. Menegazzo, S. Lunardi, C. Rossi Alvarez, G. deAngelis, E. Farnea, A. Gadea, D.R. Napoli and Z. Podolyak
Investigation of Magnetic Rotation around 142Gd
International Symposium on Nuclear Structure Physics, Göttingen (2001)
Abstract, Book of Conference Contributions
20.10.0

IKP-
R.M. Lieder for the Gamma-Ray Tracking Detector Collaboration
Development of Gamma-Ray Tracking Detectors
Negotiation DPG (VI) 36, 34 (2001)
Book of Conference Contributions
20.10.0

IKP-
H. Machner, M. Betigeri, J. Bojowald, A. Budzanowski, A. Chatterjee, M. Drochner, J. Ernst, L. Freindl, D. Frekers, W. Garske, K. Grewer, A. Hamacher, J. Ilieva, L. Jarczyk, K. Kilian, S. Kliczewski, W. Klimala, D. Kolev, T. Kutsarova, J. Lieb, H. Machner, A. Magiera, H. Nann, L. Pentchev, H.S. Plendl, D. Protic, B. Razen, P. von Rossen, B. J. Roy, R. Siudak, J. Smyrski, R.V. Srikantiah, A. Strzalkowski, R. Tsenov, K. Zwoll
Meson Production in p+d Reactions
Proc. Int. Symposium on Nuclear Physics, Bombay, India, Dec. 2000
Pramana 57 (2001) 399
20.45.0

IKP-
Meißner, Ulf-G.
Theory of the nucleon spin polarizabilities
GHD 2000 –
Proceedings of the Symposium on the Gerasimov-Drell-Hearn sum rule and the nucleon spin structure in the resonance region, Drechsel, D. and Tiator, L. (eds), World Scientific Publ. Singapore, 2001, S. 47-56
20.80.0

IKP-
Meißner, Ulf-G.; Epelbaum, E.; Glöckle, W.
The nucleon-nucleon interaction from effective field theory
Proceedings of the 16th International Conference on Few-Body Problems in Physics
Nuclear Physics, A684 (2001) S.371-376
20.80.0

IKP-
Meißner, Ulf-G.
Chiral QCD: Baryon Dynamics, in "At the Frontier of Particle Physics-Handbook of QCD
M. Shifman (ed.), World Scientific, Singapore, 2001, Vol. I, p. 417-506
20.80.0

IKP-
L. Mihailescu
Principle and methods for gamma-ray tracking with large volume Ge detectors
Jül-report 3871 (2001)
20.10.0

IKP-
L. Mihailescu, W. Gast and R.M. Lieder
Position Sensitivity with Coaxial Ge Detectors
Verhandl. DPG (VI) 36, 25 (2001) und Poster
Book of Conference Contributions
20.10.0

IKP-
L. Mihailescu, W. Gast and R.M. Lieder
Gamma-ray Imaging with Low Fold Segmented Semiconductor Detectors
IEEE-NSS Conference record, Nov 2001
Book of Conference Contributions
20.10.0

IKP-
L. Mihailescu, W. Gast, H. Jäger and R.M. Lieder
Pulse Shape Analysis Methods for Resolving Multiple Interactions
Proceedings of the TMR User Meeting 2001, University of Liverpool
20.10.0

IKP-
T. Morek, J. Srebrny, Ch. Droste, M. Kowalczyk, T. Rzaca-Urban, K. Starosta, W. Urban, R. Kaczarowski, E. Ruchowska, M. Kisielinski, A. Kordyasz, J. Kownacki, M. Palacz, E. Wesolowski, M. Wolinska, W. Gast, R.M. Lieder, P. Bednarczyk, W. Meczynski and J. Styczen
Investigation of the K = 8- Isomers in N=74 Isotones on Beam of the Warsaw Cyclotron
Proc. Int. Conf. and NATO Advanced Research Workshop on High Spin Physics 2001, Warsaw, vol. 1, p. 28 (2001)
Book of Conference Contributions
20.10.0

IKP-
Nikolaev, N.N.
Diffractive DIS: Where are we?
Int. Conference on New Trends in High Energy Physics
Yalta, Crimea, Ukraine, 22.-29.9.2001
Proceedings, ed. By P.N. Bogolytubov, G.V. Bugrij, L.L. Enkovszky, Kiev-2001, p. 201-218
20.80.0

IKP-
R. Novotny, R. Beck, W. Döring, V. Hejny, A. Hofstaetter, M. Korzhik, V. Metag, K. Römer, H. Ströher
Electromagnetic calorimetry with $PbWO_4$ in the energy regime below 1 GeV
Proceedings of the Fourth Euroconference – Luminescent Detectors and Transformers of Ionizing Radiation (LUMDETR´2000)
Radiat. Meas. 33, 5 (2001) 615-618
20.45.0

IKP-
Rathmann, F.; Dymov, S.; Engels, R.; Jansen, P.; Kacharava, A.; Klehr, F.; Kleines, H.; Komarov, V.; Koptev, V.; Kravtsov, P.; Kulikov, A.; Kurbatov, A., Lorentz, B.; Macharashvili, G.; Mikirtytchiants, M.; Nekipelov, M.; Nelyubin, V.; Prasuhn, D.; Petrus, A.; Sarkadi, J.; Seyfarth, H.; Paetz gen. Schieck, H.; Schult, O.; Steffens, E.; Ströher, H.; Uzikov, Yu.; Vassiliev, A.; Yaschenko, S.; Zalikhanov, B., and Zwoll, K. for the ANKE Collaboration
The Polarized Internal Gas Target for the Deuteron Break-up Experiment of ANKE at COSY Jülich
Proceedings Advance Study Institute on Symmetries and Spin 2001
Czechoslovak Journal of Physics, Vol. 52 (2002) Suppl. A1
20.45.0

IKP-
T. Rzaca-Urban in collaboration with research groups from IKP, Jülich, LNL Legnaro, Universities of Warsaw, Padova and Bonn
Search for Magnetic Rotation in the A ~ 140 region
Proc. Int. Conf. and NATO Advanced Research Workshop on High Spin Physics 2001, Warsaw, vol. 1, p. 15 (2001)
Book of Conference Contributions
20.10.0

IKP-
Wirzba, A.
Cooper-mesons in the color-flavor-locked superconducting phase of dense QCD in "Nucleus-Nucleus Collisions"
Proceedings of the Conference "Bologna 2000 - Structure of the Nucleus at the Dawn of the Century", Bologna, Italy, 29.5.-3.6. 2000, eds. G.C. Bonsignori, M. Bruno, A. Ventura, D. Vretena, World Scientific, Singapore 2001, p. 83-90
20.80.0

Talks/Poster

Invited Talks

IKP-
Baur, G.
Theory of coulomb dissociation
Workshop on Direct Reactions with Exotic Nuclei
ECT* Trento, Italy, 19.2.-2.3.2001
20.80.0

IKP-
Baur, G., Hencken, K., Trautmann, D.
A realistic solvable model for the coulomb dissociation of neutron halo nuclei
ENAM2001, 3rd International Conference on Exotic Nuclei and Atomic Masses
Hämeenlinna, Finland, 2.-7.7.2001
20.80.0

IKP-
Baur, G.
Coulomb dissociation: principles and application to nuclear astrophysics
Euro Summer School:Experimental Nuclear Astrophysics
Santa Tecla, Italy, 30.9.-7.10.2001
20.80.0

IKP-
Baur, G.
Physics opportunities in ultraperipheral heavy ion collisions at LHC
Int. Workshop, "Electromagnetic Probes of Fundamental Interactions",
Erice, Sicily, 16.-21.10.2001
20.80.0

IKP-
Bräutigam, W.; Brings, R.; Gad, N.; Gebel, R.; Jungwirth, H.N.; Maier, R.; Rindfleisch, U.
Extraction of D^- Beams from the Cyclotron JULIC for Injection into the Cooler Synchrotron COSY
Cyclotrons 2001 (16^{TH} International Conference on Cyclotrons and Their Applications)
MSU, East Lansing, MI, 12.-17.05.2001
20.30.0

IKP-
Bräutigam, W.; Conrad, H.; Filges, D.; Hansen, G.; Maier, R.; Martin, S.; Ullmaier, H.
Description and Results of the Actual R&D Work for the Development of the European Spallation Source (ESS) at FZ-Juelich
AccApp & ADTTA01 "Nuclear Applications in the New Millenium"
November 11-15, 2001, Reno Hilton Hotel, Reno, Nevada
20.91.0

IKP-
Bräutigam, W.; Felden, O.; Glende, M.; Jungwirth, H.N.; Lehrach, A.; Maier, R.; Martin, S.; Schnase, A.; Senichev, Y.; Stassen, R.; Tölle, R.; Zaplatin, E.
A. Facco, V. Zviagyntsev, INFN Laboratori Nazionali di Legnaro, Legnaro, Padova 35020, Italy
SC Accelerator Components for Light Ion LINACS
The 10^{th} Workshop on RF Superconductivity SRF 2001, September 6 – 11, 2001, Tsukuba, Japan (in Press)
20.91.0

IKP-
Brovko, O.I.; Dietrich, J.; Krasnov, V.A.; Meshkov, I.N.; Mohos, I.; Parfenov, A.N.; .Pavlov, V.A.
Non Disturbing Beam Profile-Position Monitor
Proc. of the 6^{th} International Workshop "Relativistic Nuclear Physics: From Hundreds of MeV to TeV", Varna (Bulgaria), September 2000
20.30.0

IKP-
Büscher, M.
Untersuchung der K^+ Produktion in pp und pA Kollisionen mit ANKE
Arbeitstreffen „Hadronen und Kerne"
Schloss Pommersfelden; 24. – 28.9.2001
20.45.0

IKP-
Büscher, M.
Strangeness production in pp and pA-collisions at ANKE
Workshop on Strangeness Production
Groningen, Niederlande, 2. – 3.11.2001
20.45.0

IKP-
Büttiker, P.
Dispersive analysis of πK scattering
HadAtom01, Int. Workshop on Hadronic Atoms
Bern, Switzerland, 11.-12.10.2001
20.80.0

IKP-
Büttiker, P.
Chiral and dispersive description of pion kaon scattering
Int. Workshop on Effective Field Theories of QCD
Physikzentrum Bad Honnef, Germany, 26.-30.11.2001
20.80.0

IKP-
Dietrich, J.; Bojowald, J.; Kamerdjiev, V.; Mohos, I.
Recent Beam Diagnostic Developments at COSY-Jülich
2001 Particle Accelerator Conference, PAC2001, June 18-22, Chicago
20.30.0

IKP-
Dietrich, J.
Das Kühler-Synchrotron COSY-Jülich
Universität Dortmund, Fachbereich Physik, 23.10.2001
20.30.0

IKP-
Drozdz, S.
Quantifying dynamics of financial correlations
NATO Advanced Research Workshop on 'Application of Physics in Economic Modelling'
Prague, Czech, 8-10.2.2001
20.80.0

IKP-
Drozdz, S.
Dynamics of financial fluctuations
Int. Conf. on 'Interdisciplinary Study and Complexity', Mexico City, 22.-26.10.2001
20.80.0

IKP-
Drozdz, S.
Characteristics of correlations in Natural complex dynamical systems
Int. Conf. on 'Horizons in Complex Systems', Messina (Sicily), 5.-8.12.2001
20.80.0

IKP-
Elster, Ch.
Incoherent photoproduction of η-mesons from the deuteron near threshold
CANU-Meeting, Bad Honnef, Germany, 17.-18.12.2001
20.80.0

IKP-
Epelbaum, E.
Two- three- and four-nucleon systems in chiral effective field theory
Instituto Superior Tecnico, Lisbon, Portugal, 5.3.2001
20.80.0

IKP-
Epelbaum, E.
Recent progress in chiral effective field theory: resonance saturation for 4N-operators
Few-Body Physics at Low and Moderate Energies: Open Questions Beyond Computational Problems, Trento, Trieste, 25.6.-6.7.01
20.80.0

IKP-
Epelbaum, E.
Chiral dynamics in few-nucleon systems
International Conference Mesons and Light Nuclei 2001
Prag, Czech, 2.-6.7.2001
20.80.0

IKP-
Epelbaum, E.
Chiral Theory Applied to Nucleon-Nucleon Systems
LOWq: Workshop on Electromagnetic Nuclear Reactions at Low Momentum Transfer Halifax, Canada, 23.8.-25.8.01
20.80.0

IKP-
Epelbaum, E.
Nuclear forces from chiral EFT: recent developments
Int. Workshop on "Effective Field Theories of QCD"
Physikzentrum Bad Honnef, Germany, 26.-30.11.2001
20.80.0

IKP-
Filges, D.:
Spallation Physics and Neutronics for Spallation Targets
ENEA-Workshop on Target Technologies for Spallation Sources,
Brasimore, Italy, February 9, 2001 (internationale Konferenz)
20.90.0

IKP-
Filges, Detlef (Autor), S. Bennigton, B. Haft, R. D. Neef, K. Nünighoff
Neutron Performance of the ESS Target Moderator Reflector System
2nd ESS SAC Meeting at the Donostia Int. Physics Center (DIPC)/University of the Basque Country, San Sebastian, Spain, March 7-8, 2001 (internationale Konferenz)
20.90.0

IKP-
Filges, D. (Autor), S. Bennigton, B. Haft, R. D. Neef, K. Nünighoff,
Particle Transport Simulations of the Neutronic Performance of Moderators of the ESS Mercury Target-Moderator-Reflector System
ESS-SAC/ENSA Workshop on "Scientific Trends in Condensed Matter Research and Instrumentation Opportunities at ESS", Engelberg, Switzerland, May 3-5,2001
20.90.0

IKP-
Filges, D.:
European Spallation Source (ESS) – Eine Neutronenquelle für das 21. Jahrhundert
Universität Stuttgart, Institut für Kernenergetik und Energiesysteme,
Stuttgart, June 1, 2001 (sonstiger Vortrag)
20.90.0

IKP-
Filges, Detlef et al., S. Bennigton, B. Haft, R. D. Neef, K. Nünighoff,
Neutronic Performance of SPTS – Status and Outlook
7th General Meeting in Seggau, Sept. 27-29, 2001 (internationale Konferenz)
20.90.0

IKP-
Filges, Detlef, W. Bräutigam, H. Conrad, G. Hansen, R. Maier, S. Martin, H. Ullmaier
Description and Results of Current R&D Work for the Development of the European Spallation Source (ESS) at FZ-Jülich
Nuclear Applications in the New Millennium, Accelerator Applications ANS-Conference,
Reno, USA, Nov. 10-15, 2001 (internationale Konferenz)
20.90.0

IKP-
Filges, Detlef
Experimental Investigations on Spallation Physics
Seminar Talk, SNS-ORNL, USA, Nr. 20, 2001
20.90.0

IKP-
Gebel. R.; Felden, O.; Glende, M.; Maier, R.; v. Rossen, P.
Eversheim, P.D. (Uni Bonn)
New Developments at the Polarized Ion Source of COSY-Jülich
International Workshop on Polarized Sources and Targets, PST 2001
Nashville, Indiana, USA, September 30 - October 4, 2001
20.30.0

IKP-
Gillitzer, A.
Deeply bound pionic atoms
XXIX Int. Workshop on Gross Properties of Nuclei and Nuclear Excitations
Hirschegg, Austria, Jan. 14-20,2001
20.45.0

IKP-
Gillitzer, A.
Tiefgebundene pionische Zustände in Sn
Arbeitstreffen Hadronen und Kerne
Pommersfelden, 24.-28.09.2001
20.45.0

IKP-
A. Gillitzer
Die Untersuchung gebundener Meson-Kern-Zustände an TOF
19. CANU Arbeitstreffen Bad Honnef 17. -18. 12. 2001
20.45.0

IKP-
Goldenbaum, Frank et al., K. Nünighoff
Spallation Neutron Production and Validation of Transport Codes
Int. Conf. on Nuclear Data for Science and Technology
Tsukuba, Ibaraki, Japan, Oct. 7-12,2001 (internationale Konferenz)
20.90.0

IKP-
Gotta, D.
A Possibility of protonium X-ray spectroscopy at the AD
Second International Workshop on Atomic Collisions and Spectroscopy with Slow Antiprotons (PBAR01)
Aarhus, Danmark, September 14-15, 2001
20.50.0

IKP-
Gotta, D.
First results from the new pionic hydrogen experiment
Workshop on Molecular Effects in the Exotic Hydrogen Cascade
Villigen, Schweiz, 26. – 27.11.2001
20.50.0

IKP-
Hanhart, C.
Constraints on high energy phenomena from low energy nuclear physics
Very High Energy Phenomena in the Universe, XXIst Moriond Workshop, Les Arcs 1800, France, 24.1.2001
20.80.0

IKP-
Hennebach, M.
The new pionic hydrogen experiment at PSI
2nd Int. Workshop on Hadronic Atoms
Bern, Schweiz, 11. – 12.10.2001
20.50.0

IKP-
Hejny, V.
Development of a compact photon detector for ANKE at COSY
6th Int. Conf. On Inorganic Scintillators and their use in Scientific and Industrial Applications
Charmonix, 16. – 21.9.2001
20.45.0

IKP-
Holstein, B.
Aristotle as right: heavier objects fall faster
University of Copenhagen, Copenhagen, Denmark, 23.10.2001
University of Helsinki, Helsinki, Finland, 29.10.2001
University of Liege, Liege, Belgium, 31.10.2001
Forschungszentrum Jülich, Jülich, Germany, 19.11.2001
20.80.0

IKP-
Holstein, B.
Allowed eta decay and chiral symmetry'
Eta Physics Symposium,
University of Uppsala, Uppsala, Sweden, 26.10.2001
20.80.0

IKP-
Holstein, B.
Gravity as an effective field theory
Effective Field Theory Workshop, Bad Honnef, Germany, 26.11.2001
20.80.0

IKP-
Holstein, B.
Neutrinos and the standard model
Neutrino Workshop, ECT*, Trento, Italy, 3.12.2001
20.80.0

IKP,
Holstein, B.
Chiral symmetry at MAMI,"
University of Mainz, Germany, 12.12.2001
20.80.0

IKP-
Ivanov, I.
Possible Odderon discovery at HERA via charge asymmetry in diffractive $\pi+\pi$-photoproduction
DIS 2001 - IX International Workshop on Deep Inelastic Scattering, Bologna, Italy, 27.4.-1.5.2001
20.80.0

IKP-
Jungwirth, H.N. (als Co-Autor)
Conradie, J.L.; Botha, A.H.; Celliers, P.J.; Cronje, P.M.; Delsink, J.L.G.; Villiers, J.G.de; Plessis, H.du; Toit, J.S.du; Fourier, D.T.; Hogan, M.E.; Kohler, I.H.; Müller, A.; Rohwer, P.F.; Smit, H.A.; Theron, P.J.; Niekerk*, M.J.van (NAC, Faure, South Africa)
New Priorities and Developments at NAC
Cyclotrons 2001 (16^{TH} International Conference on Cyclotrons and Their Applications)
MSU, East Lansing, MI, 12.-17.05.2001
20.30.0

IKP-
Kilian, K.
Future Physics Program at COSY
Structure of Hadrons
XXIX Int. Workshop on Gross Properties of Nuclei and Nuclear Excitations
Hirschegg, Austria, Jan. 14-20,2001, (int. Konferenz)
20.45.0

IKP-
K. Kilian
Meson baryon production and interaction
16^{th} International Conference on Few-Body Problems in Physics (FB16),
Taipei, Taiwan, China, 6.-10.03.2001
20.45.0

IKP-
Koning, A.; Beijers, H.; Benlliure, J.; Bersillon, O; Cugnon, J.; Duijvestijn, M.; Eudes, Ph.; Filges, D.; Haddad, F.; Lebrun, C.; Lecolley, F.-R.; Leray, S.; Meulders, J.-P.; Michel, R.; Neef, R.; Nolte, R.; Olsson, N.; Ramström, E.; Schmidt, K.-H.; Schuhmacher, H.; Slypen, I.; Synal, H.-A.; Weinreich, R.:
HINDAS, A European Nuclear Data Program for Accelerator-Driven Systems
Nuclear Applications in the New Millennium, Accelerator Applications ANS-Conference,
Reno, USA, Nov. 10-15, 2001 (internationale Konferenz)
20.90.0

IKP-
Krebs, H.
Pion Electroproduction on the Deuteron Near the Threshold
Int. Workshop on "Effective Field Theories of QCD"
Bad Honnef, Germany, 26.-30.11.2001
20.80.0

IKP-
Krewald, S.
The Jülich model
NSTAR 2001 – International Workshop on the Physics of Excited Nucleons, Universität Mainz, 7.-10.3.2001
20.80.0

IKP-
Krewald, S.
Two-pion production on the nucleon
MENU2001 - 9th International Symposium on Meson-Nucleon Physics and the Structure of the Nucleon
George Washington University, Washington, USA,
26.-31.7.2001
20.80.0

IKP-
Krewald, S.
Two-pion production – A tool to investigate exotic hadrons
International Workshop, "Quarks and Hadrons in Continuum Strong QCD"
Universität Tübingen, Germany, 3.-6.9.2001
20.80.0

IKP-
Krewald, S.
Two-pion production - a tool to investigate exotic hadrons
Int. Conference on "Quarks and Hadrons in Continuum Strong QCD", Universität Tübingen, Germany, 3.-6.9.2001
20.80.0

IKP-
Kubis, B.
Isospin violaton in low-energy pion-kaon scattering
Int. Workshop on "Effective Field Theories of QCD"
Physikzentrum Bad Honnef, Germany, 26.-30.11.2001
20.80.0

IKP-
Kulessa, P.
Nonmesonic decay of the Λ hyperon in heavy hypernuclei
Strange Quarks in Matter (SQM 2001)
Frankfurt a. M., 24. – 29.9.2001
20.45.0

IKP-
Kwapien, J.
Decomposing financial return distributions
Int. Conference 'New Economic Windows', Salerno (Italy), 13.-15.9.2001
20.80.0

IKP-
Lehrach, A.
Luccio, A.U.; MacKay, W.W.; Roser, T. (BNL, USA)
Spin Resonance Crossing in the Relativistic Heavy Ion Collider (RHIC)
2001 Particle Accelerator Conference, PAC2001, June 18-22, Chicago
20.30.0

IKP-
Lehrach, A.; Maier, R.
Siberian Snake for the Cooler Synchrotron COSY
2001 Particle Accelerator Conference, PAC2001, June 18-22, Chicago
20.30.0

IKP-
Lehrach, A. (als Co-Autor)
Zelenski A., Alessi J., Huang H., Kponou A., LoDestro V. (BNL, USA)
Klenov V., Kokhanovski S., Zubets V. (INR Moscow)
Levy P., Wight G. (TRIUMF)
Mori Y , M. Okamura (KeK, Japan)
A new Optically Pumped Polarized H- Ion Source for the RHIC spin physics
International Workshop on Polarized Sources and Targets (PST2001), Nashville, Indiana, USA, September 30 - October 4, 2001,
20.30.0

IKP-
Lehrach, A. (als Co-Autor)
Mackay W.W., Ahrens L.A., Bai M., Bunce G., Courant E., Deshpande A., Drees A., Fischer W., Huang H., Kurita K., Luccio A.U., Makdisi Y., Pilat F., Ptitsyn V.I., Roser T., Saito N., Satogata T., Tepikian S., Trbojevic D., Tsoupas N., van Zeijts J. (BNL, USA), Spinka H., Underwood D. (ANL), Alekseev I., Kanavets V., Svirida D., Lozowski B. (ITEP Moscow), Ranjbar V. (IUCF, USA), Imai K., Tojo J. (Kyoto University), Fields D. (LANL)
Commissioning and Future Plans for Polarized Protons in RHIC
2001 Particle Accelerator Conference, PAC2001, June 18-22, Chicago
20.30.0

IKP-
Lehrach, A. (als Co-Autor)
Fischer W., Bai M., Blaskiewicz M, Brennan J.M., Cameron P., Connolly R., Parzen G., Tepikian S., Zeno K., van Zeijts J. (BNL, USA)
Measurements of Intra-Beam Scattering Growth Times with Gold Beam below Transition in RHIC
2001 Particle Accelerator Conference, PAC2001, June 18-22, Chicago
20.30.0

IKP-
Lehrach, A. (als Co-Autor)
M. Bai, A.U. Luccio, W.W. MacKay, T. Roser, N. Tsoupas (BNL, USA)
Spin Flipping in RHIC
2001 Particle Accelerator Conference, PAC2001, June 18-22, Chicago
20.30.0

IKP-
Lehrach, A. (als Co-Autor)
Trbojevic D., Ahrens L.A., Bai M., Blaskiewicz M., Brennan M., Cameron P., Cardona J., Connolly R., Drees A., Fischer W., Fliller R.P., Ganetis G., Glenn J.W., Hahn H., Hayes T., Kewisch J., MacKay W.W., Peggs S., Ptitsyn V.I., Roser T., Satogata T., Shea T., Smith K., Tepikian S., Tsoupas N., de Long J., van Zeijts J. (BNL, USA)
Commissioning of the Relativistic Heavy Ion Collider,
2001 Particle Accelerator Conference, PAC2001, June 18-22, Chicago
20.30.0

IKP-
Lehrach, A. (als Co-Autor)
Bai M., Blaskiewicz M., Roser T., van Asselt W. (BNL, USA)
Measurement of Non-linearities using Spectrum Analysis of Driven Betatron Oscillation
2001 Particle Accelerator Conference, PAC2001, June 18-22, Chicago
20.30.0

IKP-
Lieder, R.M.
On the way to a 4pi gamma-ray tracking array
Seminarvortrag im Department of Physics, Warsaw, 20.4.2001, international
20.10.0

IKP-
Lieder, R.M.
Development of gamma-ray tracking detectors for AGATA (Advanced Gamma-Ray Tracking Array)
Seminarvortrag im Heavy Ion Laboratory, Warsaw University 7.6.2001, international
20.10.0

IKP-
Lieder, R.M.
Introduction: The TMR network project "Development of gamma-ray tracking detectors"
TMR User Meeting 2001, Oliver Lodge Laboratory, University of Liverpool, 12.9.2001, international
20.10.0

IKP-
Lieder, R.M.
On the way to a 4p i gamma-ray tracking array
Workshop on Shapes, Rotation and temperature in Atomic Nuclei
Niels Bohr Institute, University of Copenhagen
7.12.2001, international
20.10.0

IKP-
Machner, H.
Light meson production in pp and pd interactions
Relativistic Nuclear Physics, From Hundreds of MeV to TeV
Varna, Bulgarien, 10-16.09.2001
20.45.0

IKP-
Machner, H.
Meson production in in p+d reactions
MENU01, Advisory Committee
Washington D. C., 26.-31.07.2001
20.45.0

IKP-
Machner, H.
Schwellennahe Mesonenproduktion an COSY
Festkolloqium zum 65. Geburstag von Prof. J. Ernst
Universität Bonn
20.45.0

IKP-
Machner, H.
Meson Production in p+d reactions
Arbeitstreffen Hadronen und Kerne
Pommersfelden, 24.-28.09.2001
20.45.0

IKP-
Maier, R.
Beschleunigergestützte Neutronenquellen: Die Europäische Spallationsquelle (ESS)
Universität Dortmund, 23.01.2001
20.30.0

IKP-
Meißner, Ulf-G.
Chiral dynamics
International April meeting of the American Physical Society, Washington D.C., USA, 28.4.-1.5.2001
20.80.0

IKP-
Meißner, Ulf-G.
Theory of axial form factors
Workshop on Hadron form factors
Physikzentrum Bad Honnef, Germany, 17.-19.4.2001
20.80.0

IKP-
Meißner, Ulf-G.
Few-nucleon systems: New results from chiral effective field theory
International Workshop on Nuclear Forces and Few-Nucleon Systems, Institute for Nuclear Theory, Seattle,
USA, 11.-16.6.2001
20.80.0

IKP-
Meißner, Ulf-G.
Progress in meson-nucleon physics: Status and perspectives
9th International Symposium on Meson-Nucleon Physics and the Structure of the Nucleon
Washigton D.C., USA, 26.-31.7.2001
20.80.0

IKP-
Meißner, Ulf-G.
Progress in meson-nucleon physics: Status and perspectives
opening talk, Ninth International Symposium on Meson-Nucleon Physics and the Structure of the Nucleon Center for Nuclear Studies, The George Washington University, Washington D.C., USA, 26.-31.7.2001
20.80.0

IKP-
Meißner, Ulf-G.
Pion production in chiral perturbation theory
Plenary Talk, Workshop on “Chiral Fluctuations in Chiral Matter”, Orsay, France, 26.-28.9.2001
20.80.0

IKP-
Meißner, Ulf-G.
Theory of Pion nucleon xcattering
International Workshop “Hadatom 01”, Universität Bern, Switzerland, 12.10.2001
20.80.0

IKP-
Mihailescu, L.
Tracking and Imaging of Gamma-rays with Large Volume Semiconductor Detectors
Seminarvortrag im Space Sciences Laboratory, University of California,
Berkeley, 2.8.2001
20.10.0

IKP-
Mihailescu, L.
Tracking and Imaging of Gamma-rays with Large Volume Semiconductor Detectors
Seminarvortrag im Lawrence Livermore National Laboratory, Livermore, 3.8.2001
20.10.0

IKP-
Mihailescu, L.
Tracking and Imaging of Gamma-rays with Large Volume Semiconductor Detectors
Seminarvortrag im Los Alamos National Laboratory, Los Alamos, 8.8.2001
20.10.0

IKP-
Mikirtychiants, M.
The polarized gas target for ANKE at COSY-Jülich
9th Int. Conf. on Polarized Sources and Targets (PST 01)
Nashville, Indiana, 30.9. – 4.10.2001
20.45.0

IKP-
Mikirtychiants, M.
The polarized gas target for ANKE at COSY-Jülich
IX Workshop on High Energy Spin Physics (SPIN 01)
Dubna, Russland, 2. – 7.8.2001
20.45.0

IKP-
Mohos, I.; Bojowald, J.; Dietrich, J.; Klehr, F.
New Schottky-Pickup for COSY-Jülich
Beam Diagnostics and Instrumentation for Particle Accelerators, DIPAC2001, Grenoble, May 2001
20.30.0

IKP-
Morsch, P.
Structure of baryon resonances from hadronic and eletromanetic probes
Structure of Hadrons, Hirschegg 14.-20.01.2001
20.45.0

IKP-
Morsch, P.
Structure of the Roper resonance from α-proton and π-N scattering
Workshop NSTAR 2001, the physics of excited nucleans, Mainz 7.-10.3.2001
20.45.0

IKP-
Morsch, P.
N* resonances and the MOMO puzzle
CANU-Meeting, Bad Honnef 17.-18.12.2001
20.45.0

IKP-
Moskal,P.* fuer die COSY-11 Kollaboration
Experimental Results on Strangeness Production in elementary Proton-Proton Collisions at COSY
6th International Conference On Strange Quarks in Matter: 2001 - A Flavorspace Odyssey (SQM2001); internationale Konferenz
Frankfurt, 25.-29.9.2001
Konferenzband zur Veroeffentlichung vorgesehen bei Institute of Physics IoP Publishing
20.45.0

IKP-
Nikolaev, N.N.
Unifying aspects of polarization of vector mesons from hard production in DIS and at Tevatron
Third International Conference on Perspectives in Hadronic Physics, Miramare-Trieste, Italy, 7.-11.5.2001
20.80.0

IKP-
Nikolaev, N.N.
Connection between diffraction and small x
XXXI Intern. Symposium on Multiparticle Dynamics
Datong, China, 1.-7.9.2001
20.80.0

IKP-
Nikolaev, N.N.
Diffractive DIS: Where are we?
Int. Conference on New Trends in High Energy Physics
Yalta, Crimea, Ukraine, 22.-29.9.2001
20.80.0

IKP-
Nünighoff, Kay et al.:
Status of JESSICA Collaboration
7th ESS General Meeting in Seggau, Sept. 27-29, 2001 (internationale Konferenz)
20.90.0

IKP-
Nünighoff, Kay, D. Filges, F. Goldenbaum, M. Enke, J. Galin, C.-M. Herbach, D. Hilscher, U. Jahnke, A. Letourneau, B. Lott, R.-D. Neef, K. Nünighoff, N. Paul, A. Péghaire, L. Pienkowski, H. Schaal, U. Schröder, G. Sterzenbach, A. Tietze, V. Tishchenko, J. Toke, M. Wohlmuther
Experimental and Theoretical Investigations to Improve the Predictive Power of Nuclear Reaction Models in Spallation Neutron Production
Nuclear Applications in the New Millennium, Accelerator Applications ANS-Conference,
Reno, USA, Nov. 10-15, 2001 (internationale Konferenz)
20.90.0

IKP-
Oelert,W.
Trapping of Antiprotons -Application of cooling to very low temperatures -
ATRAP - on it's way to cold Antihydrogen
255th International WE-Heraeus Seminar on Beam Cooling and Related
Topics (ECOOL 2001); internationale Konferenz
Bad Honnef, 13.-18.5.2001
Konferenzband zur Veroeffentlichung vorgesehen beim Forschungszentrum Juelich
Schriften des Forschungszentrums Juelich, Reihe: Matter and Materials
20.50.0

IKP-
Oelert,W.
Antimaterie - die gespiegelte Materie als Antrieb zur Grundlagenforschung
Westfaelische Volkssternwarte und Planetarium
Recklinghausen, 28.3.2001
20.50.0

IKP-
Oller, J.
Chiral lagrangians with resonances
Workshop on the Physics of Excited Nucleons
Johannes Gutenberg-Universität, Mainz, Germany,
7-10.3.2001
20.80.0

IKP-
Oller, J.
Pion and kaon form factors
Workshop on Hadron Form Factors
Bad Honnef, Germany, 17.-19.4.2001
20.80.0

IKP-
Oller, J.
Overview of The chiral unitary approach
Eurodaphne Workshop on Nonperturbative Methods in Chiral Theories, University of Valencia-CSIC, IFIC, Valencia, Spain, 28-30.6.2001
20.80.0

IKP-
Oller, J.
In-medium chiral perturbation theory
Int. Workshop on "Effective Field Theories of QCD"
Bad Honnef, Germany, 26.-30.11.2001
20.80.0

IKP-
Prasuhn, D.
Cooling at COSY
Workshop on Beam Cooling and Related Topics,
Bad Honnef, 13. – 18.05.2001
20.38.0

IKP-
Rathmann, F.
Overview of gas target development
9th Int. Conf. on Polarized Sources and Targets (PST 01)
Nashville, Indiana, 30.9. – 4.10.2001
20.45.0

IKP-
Schaal, Hartwig:
Shielding Calculations
7th ESS General Meeting in Seggau, Sept. 27-29, 2001
(internationale Konferenz)
20.90.0

IKP-
Schleichert, R.
A self-triggering silicon tracking telescope for spectator proton detection
IEEE Nuclear Science Symposium 2001
San Diego, USA, 4. – 10.11.2001
20.45.0

IKP-
Schnase, A. (als Co-Autor)
Yoshii, M.; Ezura, E.; Hashimoto, Y.; Ohmori, C.; Mori, Y.; Takagi, A.; KEK, Japan
Yamamoto, M.; JAERI, Japan
Digital Control For KEK-PS MA Loaded RF System
PAC 2001, Chicago, USA, 18.06-22.06.2001
20.30.0

IKP,
Schneider, S.
The reaction $n\pi \rightarrow \pi\pi N$ in a meson-exchange model
University of Helsinki, Finland, 18.10.2001
20.80.0

IKP-
Senichev, Y.; Bräutigam, W.
Pichoff, N.; Uriot, D., CEA Saclay
The ESS-CONCERT Funnel Line
PAC2001, Chicago, USA, 18.06-22.06.2001
20.91.0

IKP-
Senichev, Y.; Bräutigam, W.
Resonant Multi-Gap Funneling and De-Funneling Systems
HEACC2001, Tsukuba, Japan, 26.03.-30.03.2001
20.91.0

IKP-
Speth, J.
Pions in hadronic physics
University of New South Wales, Sydney, Australia, 5.3.2001
20.80.0

IKP-
Speth, J.
Microscopic analysis of giant resonances in Ca and Ni isotopes
International Nuclear Physics Conference 2001 (INPC), Berkeley, USA, 30.7.-3.8.2001
20.80.0

IKP-
Speth, J.
Pions in hadronic physics
George Washington University, USA, 4.9.2001
20.80.0

IKP-
Speth, J.
Pions in hadronic physics
Jefferson Lab., Newport News, USA, 7.9.2001
20.80.0

IKP-
Speth, J.
Pion-nucleon reactions (Two-pion production)
Jefferson Lab., Newport News, USA, 21.9.2001
20.80.0

IKP-
Speth, J.
Pions in hadronic physics
University of Helsinki, Finnland, 8.10.2001
20.80.0

IKP-
Ströher, H.
Electromagnetic production of eta and eta´
Workshop on Eta Physics
Uppsala, 25. – 27.10.2001
20.50.0

IKP-
Ströher, H.
Hadronic meson production on free and bound nucleons at COSY-Jülich
XXVII Mazurian Lakes School of Physics
Krzyze, Polen, 9. – 13.9.2001
20.45.0

IKP-
Ströher, H.
Development of a compact photon detector for ANKE at COSY Jülich
Int. Symp. on Electromagnetic Interactions in Nuclear and Hadron Physics
Osaka, Japan, 4. – 7.12.2001
20.45.0

IKP-
Szczurek, A.
Towards mapping the proton unintegrated gluon distribution in dijets correlations in real and virtual photoproduction at HERA
International Workshop on "Deep Inelastic Scattering and QCD", Bologna, Italy, 27.4.-1.5.2001
20.80.0

IKP-
Tietze-Jaensch, H.; Conrad, H,; Dietrich, J.; Filges, D.; Haft, B.; Hansen, G.; Maier, R.; Paul, N; Pohl, C.; Prasuhn, D.; Smirnov, A.; Stelzer, K.; Ullmaier, H.
JESSICA, the ESS-like target/reflector mock-up and cold moderator test facility
15th Meeting of the International Collaboration on Advanced Neutron Sources,
November 6-9, 2000, p.829
Tsukuba, Japan
20.91.0

IKP-
Wirzba, A.
In-medium chiral perturbation theory (Invited Talk)
The force from nothing: Casimir interactions between bubbles in the fermi-sea
VIII Mexican Workshop on Particles and Fields, Zacatecas, Mexico, 14.-20.11.2001
20.80.0

IKP-
Wolke,M. fuer die COSY-11 Kollaboration
Threshold Strangeness Production Studies in Proton-Proton Collisions
at the COSY-11 Facility Workshop on Strangeness Production; internationale Konferenz
KVI, Groningen, Niederlande, 2.-3.11.2001
20.45.0

IKP-
Zaplatin, E.; Bräutigam, W.; Stassen, R.
Low-β SC RF Cavity Investigations
The 10^{th} Workshop on RF Superconductivity SRF 2001, September 6 – 11, 2001, Tsukuba, Japan
20.91.0

Conference Contributions and others

IKP-
Baru, V.
η -meson production in nucleon-nucleon collisions
Deutsche Physikalische Gesellschaft, Frühjahrstagung
Erlangen, Germany, 19.-23.3.2001
20.80.0

IKP-
Baur, G.
Coulomb dissociation and Nuclear Astrophysics
Forschungszentrum Karlsruhe, Germany, 16.3.2001
20.80.0

IKP-
Baur, G.
Production of fast antihydrogen
IKP-Beiratssitzung, Forschungszentrum Jülich, Germany, 7.5.2001
20.80.0

IKP-
Baur, G.
Coulombdissoziation und Nukleare Astrophysik
Universität Stuttgart, Germany, 7.6.2001
20.80.0

IKP-
Baur, G.
Coulomb Dissociation, a tool for nuclear structure and astrophysics
Yukawa International Seminar on Physics of Unstable Nuclei
Kyoto, Japan, 5.-10.11.2001

IKP-
Bräutigam, W.
Superconducting Accelerator Technology for COSY and ESS
Vortrag am 17. November 2001 am NAC National Accelerator Centre, Faure, South Africa
29.91.0

IKP-
K. Th. Brinkmann
Omega-Produktion im Proton-Proton Stoß
DPG Frühjahrstagung Erlangen 19.3. - 23.3. 2001
20.45.0

IKP-
K.-Th. Brinkmann
Erzeugung pseudoskalarer und vektorieller Mesonen in pp-Stößen
Arbeitstreffen "Hadronen und Kerne" Pommersfelden
24. - 28.9. 2001
20.45.0

IKP-
Büscher, M.
Status of K^+ measurements with ANKE at COSY-Jülich
Compilation of existing data
First results of the ROC-model calculations
Planned a_0/f_0 measurements at ANKE
2nd ANKE Workshop on "Strangeness production in pp and pA interactions at ANKE
PNPI, Gatchina, Russland, 21. – 22.6.2001
20.45.0

IKP-
Büttiker, P.
Dispersion relations for π K scattering
Institut de Physique Nucleaire, Université Paris-Sud
Paris, France, 9.3.2001
20.80.0

IKP-
Büttiker, P.
π K scattering and dispersion relations
Nonperturbative Methods in Chiral Theories
International Eurodaphne workshop, Valencia, Spain,
28.6.2001
20.80.0

IKP-
H. Clement
Zweipion-Produktion im Nukleon-Nukleon Stoß
19. Canu Arbeitstreffen Bad Honnef 17. -18. 12. 2001
20.45.0

IKP-
Dietrich, J.
Extraktion eines kurzgepulsten COSY-Protonenstrahls für JESSICA
ESS-Tag, 10.-11.Mai 2001, Monschau
20.30.0

IKP-
Elster, Ch.
Incoherent photoproduction of η-mesons from the deuteron near threshold
14th Midwest Nuclear Theory Get-Together
Argonne National Laboratory, Argonne, USA, October 2001
20.80.0

IKP-
Elster, Ch.
Three body bound state calculations with three body forces without angular momentum decomposition
Europhysics Int. Conference on Computational Physics, Aachen Germany, 5.-8.9.2001
20.80.0

IKP-
Filges, D.; Neef, R.-D.; Nünighoff, K.; Pohl, C.; Haft, B.; Bennington, S.:
H_2 and H_2O Moderator Neutron Performance Monte-Carlo Simulations for the ESS Reference Target-Moderator-Reflector-System
Workshop on Moderator Concepts and Optimization for Spallation Neutron Sources, HMI Berlin, March 12-14, 2001
(internationale Konferenz)
20.90.0

IKP-
Filges, D.; Pohl, C.; Goldenbaum, F.:
Proton Beam Monitoring
3rd JESSICA Workshop, HMI Berlin, March 15, 2001
(internationale Konferenz)
20.90.0

IKP-
Filges, D.:
Nukleare Untersuchungen und Target Design
ESS-HGF-Projekt Treffen, HMI Berlin, March 16, 2001
(internationale Konferenz)
20.90.0

IKP,
Frink, M.
Analysis of the pion-kaon sigma term
Int. Workshop on "Effective Field Theories of QCD"
Bad Honnef, Germany, 26.-30.11.2001
20.80.0

IKP-
M. Fritsch
Hyperon-Produktion in den Kanälen pp -> K Lambda p und pp -> K Sigma0
p an COSY-TOF
DPG Frühjahrstagung Erlangen 19.3. - 23.3. 2001
20.45.0

IKP-
M. Fritsch
Hyperon-Produktion an COSY-TOF
Arbeitstreffen "Hadronen und Kerne" Pommersfelden
24. - 28.9. 2001
20.45.0

IKP-
Gasparian, A.M.
Kaon production in pion-nucleon scattering
Deutsche Physikalische Gesellschaft, Frühjahrstagung Erlangen, Germany, 19.-23.3.2001
20.80.0

IKP-
Gasparian, A.M.
Theoretical explanation for the energy dependence of the Λ / Σ^o cross section ratio
Extended COSY-11 Collaboration Meeting, Jagellonian University, Cracow, Poland, 20.-24.6.2001
20.80.0

IKP-
Gast, W.
``Digital Triggering and Timing for Tracking Arrays"
DPG Spring Meeting, Erlangen, March 19-22, 2001
20.10.0

IKP-
Gast, W.
``Pulse Shape Analysis for Tracking Detectors"
Workshop on Gamma-Ray Tracking, University of Massachusetts, Lowell,
June 22-23, 2001
20.10.0

IKP-
Gast, W.
``Digital Signal Processing for Gamma-Ray Tracking"
TMR 2001 User Meeting on Gamma-Ray Tracking Detectors, University of Liverpool, Liverpool, Sept. 12-14, 2001
20.10.0

IKP-
Gotta, D.
The new pionic hydrogen experiment at PSI
Seminar Institut für Teilchenphysik, ETH Zürich, 4.12.2001
20.50.0

IKP-
Haft, B.; Pohl, C.:
Energy and Time Spectra for Various JESSICA Testmoderators
3rd JESSICA Workshop, HMI Berlin, March 15, 2001
(internationale Konferenz)
20.90.0

IKP-
Haidenbauer, J.
Theoretical aspects of the reactions $pp \to ppK^+K^-$ and $pp \to ppa_o / f_o$
Extended COSY-11 Collaboration Meeting, Jagellonian University, Cracow, Poland, 20.-24.6.2001
20.80.0

IKP-
Haidenbauer, J.
A meson-exchange model for the YN interaction
International Conference on Mesons and Light Nuclei, Prague, Czech Republic, 2.-6.7.2001
20.80.0

IKP-
Haidenbauer, J.
Meson production in nucleon-nucleon collisions
International Workshop, University of Helsinki,
Finland 5.10.2001
20.80.0

IKP-
Haidenbauer, J.
Strangeness production in pp reactions
International Workshop on Strangeness production, KVI, Groningen, The Netherlands, 2.-3.11 2001
20.80.0

IKP-
Hanhart, C.
Near threshold meson production in NN collisions
Frühjahrstagung der Deutschen Physikalischen Gesellschaft, Erlangen, Germany, 22.3.2001
20.80.0

IKP-
Hanhart, C.
Meson production in nucleon-nucleon collisions
Universität München, Germany, 12.6.2001
20.80.0

IKP-
Hanhart, C.
The reaction NN→NNπ in chiral perturbation theory
University of Washington, Seattle, USA, 23.8.2001
20.80.0

IKP-
Hanhart, C.
Meson production in nucleon-nucleon collisions
Arbeitstreffen "Hadronen und Kerne",
Schloß Pommersfelden, Germany 24.-28.9.2001
20.80.0

IKP-
Hanhart, C.
Meson production in nucleon-nucleon collisions
CANU-Meeting, Bad Honnef, Germany, 17.-18.12.2001
20.80.0

IKP-
Hartmann, M.
Measurements with the K-detection system
2nd ANKE Workshop on "Strangeness production in pp and pA interactions at ANKE
PNPI, Gatchina, Russland, 21. – 22.6.2001
20.45.0

IKP-
D. Hesselbarth
Messung der Reaktionsdynamik der Lambda Produktion im Proton-Proton Stoß
DPG Frühjahrstagung Erlangen 19.3. - 23.3. 2001
20.45.0

IKP-
Ivanov, I.
Spin-orbit coupling in vector mesons probed by hard diffractive VM production
International Workshop on Low x Physics- 2001
Crakow, POLAND, 27.-30.6.2001
20.80.0

IKP-
B. Jakob
Untersuchung von pp-Reaktionen an der Pionenproduktionsschwelle mit dem COSY-TOF
Physikerinnentagung Dresden 15.-18. 11. 2001
20.45.0

IKP-
Kamerdjiev, V.
Ein Restgasmonitor für COSY
Winterseminar Beschleunigerphysik der Goethe-Universität Frankfurt am Main, Riezlern, 6.3.2001
20.30.0

IKP-
Khoukaz,A.* fuer die COSY-11 Kollaboration
Die Reaktion p d --> 3He eta nahe der Produktionsschwelle
Fruehjahrstagung der Deutschen Physikalischen Gesellschaft (DPG);
nationale Konferenz, Erlangen, 19.-23.3.2001
Verhandlungen der DPG (VI), 36 (2001)
20.45.0

IKP-
Khoukaz,A.* fuer die COSY-11 Kollaboration
Near Threshold K+K- Meson-Pair Production in Proton-Proton Collisions
Mesons & Light Nuclei '01; internationale Konferenz Prag, Tschechische Republik, 3.-6.7.2001
Konferenzband zur Veroeffentlichung vorgesehen bei American Institute of Physics, AIP Conference Proceedings
20.45.0

IKP-
Kleber, V.
Results of the measurements on pp --> d a_0^+ (980)
2nd ANKE Workshop on "Strangeness production in pp and pA interactions at ANKE
PNPI, Gatchina, Russland, 21. – 22.6.2001
20.45.0

IKP-
Kleber, V.
K^+ and a_0^+ production at ANKE
19. CANU Arbeitstreffen, Bad Honnef, 17. – 18.12.2001
20.45.0

IKP-
Koch, R.
Luminosities during ANKE experiments (A-dependence)
2nd ANKE Workshop on "Strangeness production in pp and pA interactions at ANKE
PNPI, Gatchina, Russland, 21. – 22.6.2001
20.45.0

IKP-
J. Kreß
Exklusive Messung der Reationen pp -> pp pi+ pi- und pp -> d pi0 pi+
mit polarisierten Protonen an COSY-TOF
DPG Frühjahrstagung Erlangen 19.3. - 23.3. 2001
20.45.0

IKP-
Krewald, S.
Two-Pion production
Special Research Center for the Subatomic Structure of Matter, University of Adelaide, Australia, 17.10.2001
20.80.0

IKP-
Kubis, B.
Baryon form factors in chiral perturbation theory
Workshop on Hadron Form Factors
Physikzentrum Bad Honnef, Germany, 17.4.-19.4.2001
20.80.0

IKP-
Kubis, B.
Isospin violation in pion-kaon scattering
HadAtom01, Int. Workshop on Hadronic Atoms
Bern, Switzerland, 11.-12.10.2001
20.80.0

IKP-
Kubis, B.
Analysis of isospin violation in near-threshold pion-kaon scattering, Bern, Switzerland, 2.11.2001
20.80.0

IKP-
E. Kuhlmann
Hyperon Production at the Proton Synchrotron COSY
International Nuclear Physics Conference INPC 2001, Berkeley CA/USA
20.45.0

IKP-
Kulessa, P.
COSY-13: A summary of results
19. CANU Arbeitstreffen, Bad Honnef, 17. – 18.12.2001
20.45.0

IKP-
Lehrach, A.
Polarization at COSY and RHIC
IKP-Beirat, 7.5.2001
20.30.0

IKP-
Lehrach, A.
Superconducting Injector Linac for the Cooler Synchrotron COSY
09.08.2001, Argonne National Laboratory, Chicago, USA
20.30.0

IKP-
Lieder, R.M.
The TMR network project "Development of gamma-ray tracking detectors"
Contributed Talk at the International Conference and NATO Advanced
Research Workshop High Spin Physics 2001, Warsaw, 6.2.2001, international
20.10.0

IKP-
Lieder, R.M.
The TMR network project "Development of gamma-Ray Tracking Detectors"
Frühjahrstagung 2001 der Deutschen Physikalischen Gesellschaft, Fachverband Hadronen und Kerne, Erlangen, 6.3.2001, national
20.10.0

IKP-
Maier, R.
Seltsame Teilchen im Visier
Vortrag bei der Fachtagung zur Stärkung des mathematisch-naturwissenschaftlich-technischen Unterrichts in NRW, 26.11.2001, ZB des FZ-Jülich
20.30.0

IKP-
Maier, R.
Statusbericht zum CONCERT Beschleunigerteam
ESS-Tage, Monschau 10-11.05.2001
20.30.0

IKP-
Maier, R.
HEBT to LP Target & Protection
7th ESS-Meeting in Seggau, Österreich, 26.09. – 29.09.2001
20.91.0

IKP-
S. Marwinski
Schwellennahe eta-Mesonproduktion im Proton-Proton-Stoß am COSY-TOF-Flugzeitspektrometer
DPG Frühjahrstagung Erlangen 19.3. - 23.3. 2001
20.45.0

IKP-
Meißner, Ulf-G.
Chirale Dynamik
Universität Bonn, Germany, 15.11.2001
20.80.0

IKP-
Meißner, Ulf-G.
Zur Theorie der Reaktionen $pp \to dK^+\overline{K}^0$ und $pp \to d\pi^+\eta$
CANU-Treffen, Bad Honnef, Germany 17.-18.12.2001
20.80.0

IKP-
L. Mihailescu
Pulse Shape Analysis Methods for Resolving Multiple Interactions
Contributed Talk at the TMR User Meeting 2001
Oliver Lodge Laboratory, University of Liverpool, 12.9.2001
20.10.0

IKP-
L. Mihailescu
Gamma-ray Imaging with Low Fold Segmented Semiconductor Detectors
Contributed Talk at the IEEE-NSS Conference, San Diego 6.11.2001
20.10.0

IKP-
Moskal,P. fuer die COSY-11 Kollaboration
Interaction of eta Mesons with Protons
Fruehjahrstagung der Deutschen Physikalischen Gesellschaft (DPG); nationale Konferenz
Erlangen, 19.-23.3.2001
Verhandlungen der DPG (VI), 36 (2001)
20.45.0

IKP-
Moskal,P. fuer die COSY-11 Kollaboration
Influence of the stochastically cooled beam on the experimental conditions at internal target facilities
255th International WE-Heraeus Seminar on Beam Cooling and Related Topics (ECOOL 2001); internationale Konferenz
Bad Honnef, 13.-18.5.2001
Konferenzband zur Veroeffentlichung vorgesehen bei Forschungszentrum Juelich
Schriften des Forschungszentrums Juelich, Reihe: Matter and Materials
20.45.0

IKP-
Moskal,P. fuer die COSY-11 Kollaboration
Study of the eta-proton interaction via the reaction p p --> p p eta
9th International Symposium on Meson-Nucleon Physics and the Structure of the Nucleon (MENU 2001); internationale Konferenz
Washington DC, USA, 26.-31.7.2001
Konferenzband zur Veroeffentlichung vorgesehen in pi N Newsletter, 16 (2001)
20.45.0

IKP-
Moskal,P.* fuer die COSY-11 Kollaboration
A Study of the eta-proton Interaction at COSY-11
19. CANU Arbeitstreffen; nationale Konferenz
Bad Honnef, 17.-18.12.2001
20.45.0

IKP-
Mussgiller, A.
Target-near counters for spectator tagging
Future spectator and vertex counters for ANKE
2nd ANKE Workshop on "Strangeness production in pp and pA interactions at ANKE
PNPI, Gatchina, Russland, 21. – 22.6.2001
20.45.0

IKP-
Neef, R.D.:
A Neutron Generator for JESSICA
3rd JESSICA Workshop, HMI Berlin, March 15, 2001 (internationale Konferenz)
20.90.0

IKP-
Nekipelov, M.
Data on K^+ production in pA collisions from ANKE
2nd ANKE Workshop on "Strangeness production in pp and pA interactions at ANKE
PNPI, Gatchina, Russland, 21. – 22.6.2001
20.45.0

IKP,
Nikolaev, N.N.
Diffractive deep inelastic scattering at small x
XXXV Annual Winter School on Nuclear and Particle Physics of St.Petersburg Nuclear Physics Institute, Repino, Russia, 19.-25.2.2001
20.80.0

IKP-
Nünighoff, Kay, Ch. Pohl
Monte Carlo Simulation for Neutron Scattering Instruments
Workshop Monte Carlo Simulation, HMI Berlin, Berlin,
June 25-28, 2001
20.48.0

IKP-
E. Roderburg
Ergebnisse der eta-Produktion am Flugzeitspektrometer
19. Canu Arbeitstreffen Bad Honnef 17. -18. 12. 2001
20.45.0

IKP-
Sassen, F.
$\pi\pi$ -Scattering up to 1.6 GeV
Deutsche Physikalische Gesellschaft (Frühjahrstagung)
Erlangen, Germany, 20.3.2001
20.80.0

IKP-
Sassen, F.
Die Produktion des f0(980) $\pi^p \rightarrow \pi^0 \pi^0 n$
CANU-Meeting, Bad Honnef, 18.12.01
20.80.0

IKP-
Schepers,G.; Grzonka,D.; Kalinowsky,H.*; Oelert,W.; Sefzick,T.
ATRAP, auf dem Weg zu kaltem Antiwasserstoff
Fruehjahrstagung der Deutschen Physikalischen Gesellschaft (DPG); nationale Konferenz, Erlangen, 19.-23.3.2001
Verhandlungen der DPG (VI), 36 (2001)
20.50.0

IKP-
Schnase, A.
Ideen zum Beam Chopping (Low energy part of Linac)
ESS-Tage, Monschau 10-11.05.2001
20.91.0

IKP-
Schneider, S.
Two-pion production on the proton in hadronic processes
Deutsche Physikalische Gesellschaft (Frühjahrstagung)
Erlangen, Germany, 20.3.2001
20.80.0

IKP-
Sibirtsev, A.
Compilation of available data on strangeness production in proton-nucleus collisions and folding model calculations
International Workshop on Strangeness Production in pp and pA interactions at ANKE,
Gatchina, Russia, 21-22.6.2001
20.80.0

IKP-
Smyrski,J.* fuer die COSY-11 Kollaboration
Recent results from the COSY-11 experiment on near-threshold meson production in pp and pd collisions
International Nuclear Physics Conference (INPC 2001); internationale Konferenz, Berkeley, USA, 30.7.-3.8.2001
Konferenzband zur Veroeffentlichung vorgesehen bei American Institute of Physics, AIP Conference Proceedings
20.45.0

IKP-
Speth, J.
Some topics in econophysics
University of Adelaide, Australia, 27.2.2001
20.80.0

IKP-
Stassen, R.
Experimentelle Untersuchungen zur aktiven Lorentz-Force-Kompensation
ESS-Tage, Monschau 10-11.05.2001
20.30.0

IKP-
Stassen R.
Pulsed SC cavity control,
Vortrag, 7th ESS-Meeting in Seggau, Österreich,
26.09. – 29.09.2001
20.91.0

IKP-
Ströher, H.
Physics with ANKE at COSY Jülich
4th Workshop on the Scientific Cooperation between JINR and German Research Centres
Dubna, Russland, 21. – 22. November 2001
20.45.0

IKP-
M. Wagner
Sigma+ Produktion an COSY-TOF
DPG Frühjahrstagung Erlangen 19.3. - 23.3. 2001
20.45.0

IKP-
M. Wagner
Strangness-Produktion an TOF
19. Canu Arbeitstreffen Bad Honnef 17. -18. 12. 2001
20.45.0

IKP-
Winter,P. fuer die COSY-11 Kollaboration
Erste Ergebnisse zur eta-Produktion mit polarisierten Protonen an COSY-11
19. CANU Arbeitstreffen; nationale Konferenz
Bad Honnef, 17.-18.12.2001
20.45.0

IKP-
S. Wirth
Strangeness Production at the Time-of-Flight Spectrometer COSY-TOF
MENU 2001 Washington DC/USA 26.7. - 31.7.2001
20.45.0

IKP-
Wirzba, A.
Casimir interaction among objects immersed in a fermionic environment, Open University, Milton Keynes, United Kingdom, 11.6.2001
20.80.0

IKP,
Wirzba, A.
Cavity scattering in elastodynamics: wave versus ray dynamics
Center of Nonlinear Science, Georgia Institute of Technology (USA), 20.8.2001
20.80.0

IKP-
Wirzba, A.
Casimir interaction among objects immersed in a fermionic environment
Fifth Intern. Workshop on Quantum Field Theory under the Influence of External Conditions
Universität Leipzig, Germany, 10.-14.9.2001
20.80.

IKP-
Wirzba, A.
Die Kraft aus dem Nichts: Casimir-Wechselwirkungen zwischen Blasen im Fermi-See
TU München, Garching, Germany, 31.10.2001
20.80.0

IKP-
Wolke,M. fuer die COSY-11 Kollaboration
Schwellennahe Mesonenproduktion in der Proton-Proton-Wechselwirkung an COSY-11
XXXII. Arbeitstreffen "Kernphysik"; nationale Konferenz
Schleching, 1.-8.3.2001
20.45.0

IKP-
Wolke,M. fuer die COSY-11 Kollaboration
Schwellennahe Strangeness Dissoziation im Proton-Proton Stoß
Fruehjahrstagung der Deutschen Physikalischen Gesellschaft (DPG); nationale Konferenz
Erlangen, 19.-23.3.2001
Verhandlungen der DPG (VI), 36 (2001), S.59
20.45.0

IKP-
Wolke,M. fuer die COSY-11 Kollaboration
Hyperon and Kaon-Antikaon Production in Proton-Proton Scattering Close to Threshold at the COSY-11 Facility
VII International Conference on Hypernuclear and Strange Particle, Physics (HYP2000); internationale Konferenz
Turin, Italien, 23.-27.10.2000
20.45.0

IKP-
Wolke,M. fuer die COSY-11 Kollaboration
Strangeness-Produktion in Schwellennähe mit COSY-11
Arbeitstreffen 'Hadronen und Kerne'; nationale Konferenz
Pommersfelden, 24.-28.9.2001
20.45.0

Poster:

IKP-
Filges, Detlef (for the PISA-Collaboration)
PISA-Poster
7th ESS General Meeting in Seggau, Sept. 27-29, 2001
20.90.0

IKP-
Herbach, C.-M.; Böhm, A.; Enke, M.; Filges, D.; Galin, J.; Goldenbaum, F.; Hilscher, D.; Jahnke, U.; Letourneau, A.; Lott, A.; Neef, R.-D.; Nünighoff, K.; Paul, N.; Peghaire, A.; Pienkowski, L.; Schaal, H.; Schröder, W.U.; Sterzenbach, G.; Tishchenko, V.; Töke, I.:
Decay of Excited Nuclei in Proton Incuced Spallation Reactions
DPG-Frühjahrstagung, Physik der Hadronen und Kerne, Erlangen, March 19-23, 2001
20.90.0

IKP-
Hilscher, Dieter (for the NESSI-Collaboration)
NESSI-Experiment
7th ESS General Meeting in Seggau, Sept. 27-29, 2001
20.90.0

IKP-
Lehrach, A.
Spin Resonance Crossing in the Relativistic Heavy Ion Collider (RHIC)
PAC2001, Chicago, USA, 18.06-22.06.2001
20.30.0

IKP-
Lehrach, A.
Siberian Snake for the Cooler Synchrotron COSY
PAC2001, Chicago, USA, 18.06-22.06.2001
20.30.0

IKP-
R.M. Lieder, T. Rzaca-Urban, H. Brands, W. Gast, H.M. Jäger, L. Mihailescu, Z. Marcinkowska, W. Urban, T. Morek, Chr. Droste, S. Chmel, D. Bazzacco, G. Falconi, R. Menegazzo, S. Lunardi, C. Rossi Alvarez, G. deAngelis, E. Farnea, A. Gadea, D.R. Napoli and Z. Podolyak
Investigation of Magnetic Rotation around 142Gd
International Symposium on Nuclear Structure Physics, Göttingen (2001)
20.10.0

IKP-
L. Mihailescu, W. Gast and R.M. Lieder
Position Sensitivity with Coaxial Ge Detectors
Verhandl. DPG (VI) 36, 25 (2001) und Poster
Buch der Konferenzbeitrge
20.10.0

IKP-
Prasuhn, D.; Bechstedt, U. Dietrich, Gebel, R.; Henn, K.; Lorentz, B.; Maier, R.; Schnase, A.; Schneider, H.; Stassen, R.; Stockhorst, H.; Tölle, R.
Status of the Cooler Synchrotron COSY Juelich
PAC2001, Chicago, USA, 18.06-22.06.2001
20.30.0

IKP-
Stassen, R.; Bräutigam, W.; Felden, O.; Glende, M.; Maier, R.; Meier, H.; Schnase, A.; Schug, G.; Singer, H.
Superconductive Test Cavity for the ESS
PAC2001, Chicago, USA, 18.06-22.06.2001
20.91.0

IKP-
Stassen, R.; Bräutigam, W.; Felden, O.; Glende, M.; Lehrach, A.; Maier, R.; Schnase, A.; Schug, G.; Senichev, Y.; Tölle, R.; Zaplatin, E.
Superconductive Activities at COSY FZJ
SRF2001, Tsukuba, Japan, 06.09.-11.09.2001
20.91.0

Lectures at Universities

WS 2000/2001

IKP-
Filges, D.
Physik II, Atom- und Kernphysik
Universität Wuppertal, V2, Ü2 (Vorlesung+Übung)
20.48.0/20.90.0

IKP-
Gillitzer, A., Kilian, K.
Atomic Physics, 2-stündig
Rheinische Friedrich-Wilhelms-Universität Bonn
20.45.0

IKP-
Gillitzer, A., Kilian, K., Klempt E.
Übungen zur Atomphysik, 2-stündig
Rheinische Friedrich-Wilhelms-Universität Bonn
20.45.0

IKP-
Gillitzer, A., Kilian, K., Lieder, R.
Diplompraktikum experimentelle Mittelenergiephysik
und Kernspektroskopie, ganztägig
Rheinische Friedrich-Wilhelms-Universität Bonn
20.45.0

IKP-
Maier, R.
Anwendung von Teilchenbeschleunigern
Vorlesung
Universität Bonn
20.30.0

IKP-
Wolke,M., Wintz, P.
Uebungen zur Atomphysik
Fachgruppe Physik-Astronomie
Rheinische Friedrich-Wilhelms-Universität Bonn
20.45.0

SS 2001

IKP,
Baur, G.
Spontane Symmetriebrechung und Higgs-Mechanismus in
Teilchen-und Festkörperphysik
Universität Basel, V2
20.80.0

IKP-
Dietrich, J.
Strahldiagnose in der Beschleunigerphysik
Vorlesung
Universität Dortmund, Institut für Beschleunigerphysik und
Synchrotronstrahlung
11.-13. Juni und 2.-4. Juli 2001
20.30.0

IKP-
Elster, Ch.
General Physics: Electricity and Magnetism (Vorlesung)
Ohio University, V3
20.80.0

IKP-
Filges, D.
Seminar über Abschirmprobleme von
Teilchenbeschleunigern
Universität Wuppertal, V2 (Seminar)
20.90.0

IKP-
Gillitzer, A., Gothe, R.
Hadronen- und Kernphysik, 2-stündig
Rheinische Friedrich-Wilhelms-Universität Bonn
20.45.0

IKP-
Gillitzer, A., Kilian, K., Lieder, R.
Diplompraktikum experimentelle Mittelenergiephysik
und Kernspektroskopie, ganztägig
Rheinische Friedrich-Wilhelms-Universität Bonn
20.45.0

IKP-
Krewald, S.
Einführung in die Theoretische Hadronenphysik
Universität Bonn, V2
20.80.0

IKP-
Machner, H.
Kern- und Elementarteilchenphysik, 6-stündig
Universität Essen
20.45.0

IKP-
Meißner, Ulf-G.
Theoretische Elektrodynamik
Universität Bonn, V4, Ü4
20.80.0

IKP-
Speth, J.
Theoretische Elektrodynamik
Universität Bonn, V4, Ü4
20.80.0

WS 2001/2002

IKP-
Baur, G.
Coulomb Dissoziation und Nukleare Astrophysik
Universität Basel, V2
20.80.0

IKP,-
Elster, Ch.
Relativistic Quantum Mechanics
Ohio University, V3
20.80.0

IKP-
Filges, D.
Physik II, Atom- und Kernphysik
Universität Wuppertal, V2, Ü2 (Vorlesung+Übung)
20.48.0/20.90.0

IKP-
Gillitzer, A.
Experimentelle Fragestellungen der
nuklearen Astrophysik, 2-stündig
Rheinische Friedrich-Wilhelms-Universität Bonn
20.45.0

IKP-
Gillitzer, A., Kilian, K., Lieder, R.
Diplompraktikum experimentelle Mittelenergiephysik
und Kernspektroskopie, ganztägig
Rheinische Friedrich-Wilhelms-Universität Bonn
20.45.0

IKP-
Maier, R.
Teilchenbeschleuniger I
Vorlesung
Universität Bonn
20.30.0

IKP,-
Meißner, Ulf-G.
Quantenmechanik I
Quantenfeldtheorie
Universität Bonn, V4, Ü4
20.80.0

IKP-
Krewald, S.
Einführung in die Theorie der schwachen Wechselwirkung
Universität Bonn, V2
20.80.0

IKP-
Rathmann, F.
Experimentelle Methoden der Spin-Physik (mit Exkursion)
Universität Erlangen
20.45.0

IKP-
Speth, J.
Quantenmechanik I
Universität Bonn, V4, Ü4
20.80.0

IKP-
Ströher, H.; Gotta, D.; Büscher, M.
Elementarteilchenphysik (mit Exkursion FZJ)
Universität zu Köln
20.45.0

IKP-
Wirzba, A.
Einführung in die Hadronenphysik
Technische Universität Darmstadt,
V3, Lv. Nr. 05.367.1
20.80.0

Diploma

IKP-
Frink, M.
Analyse des Pion-Kaon Sigma Terms
Diplomarbeit, Universität Bonn, Oktober 2001
20.80.0

IKP-
Götz, T.
Untersuchungen zum Photon-Detektionssystem des ATRAP-Experimentes
Diplomarbeit, Rheinische Friedrich-Wilhelms-Universität Bonn, Dezember 2001
Berichte des Forschungszentrums Jülich, Juel-
20.50.0

IKP-
Johnen, U.
Lichtausbeute gewundener Plastikszintillatoren
Diplomarbeit, Fachhochschule Aachen, Abteilung Juelich, Juni 2001
20.45.0

IKP-
Kolf,C.
Spurrekonstruktion in der Hexagonal-Driftkammer am Experiment COSY-11
Diplomarbeit, Rheinische Friedrich-Wilhelms-Universität Bonn, Dezember 2001
Berichte des Forschungszentrums Juelich, Juel-3941
20.45.0

IKP-
Pavlov, F.
Scattering on polarized nucleons on polarized deuterons in the lightcone dynamics
Diplomarbeit, St. Petersburg Technical University, August 2001
20.80.0

IKP-
Sassen, F.
Dispersionstheoretische Behandlung von 3-Meson-Vertexfunktionen
Diplomarbeit, Universität Bonn, Juli 2001
20.80.0

IKP-
Schneider, S.
Zwei-Pion-Produktion am Proton in hadronischen Prozessen
Universität Bonn, Diplomarbeit, Januar 2001
20.80.0

IKP-
Winter,P.
Erste Messung der Analysierstaerke A_y in der Reaktion p(pol) p --> p p eta am Experiment COSY-11
Diplomarbeit, Rheinische Friedrich-Wilhelms-Universität Bonn, Dezember 2001
Berichte des Forschungszentrums Juelich, Juel-3943
20.45.0

Dissertations

IKP-
Abdel El-Samad, S.-M.
Improving the Properties of Cryogenic Targets for External Cooler Synchrotron (COSY)
Forschungszentrum Jülich
Universität Bonn, Dissertation
20.45.0

IKP-
Mihailescu, L.
Principles and methods for gamma-ray tracking with large volume Ge-detectors
Forschungszentrum Jülich, 2001
Berichte des Forschungszentrums Jülich, ISSN 0944-2952
Universität Bonn, Dissertation
Jül-report 3871 (2001)
20.10.0

IKP-
Nünighoff, Kay
Experimente und Theorien zur Neutronenproduktion in Schwermetalltargets – Anwendbarkeit von Monte-Carlo Simulationsverfahren zur sicherheitstechnischen Auslegung der Europäischen Spallationsneutronenquelle ESS
Forschungszentrum Jülich, 2001
Berichte des Forschungszentrums Jülich, Okt. 2001, ISSN 0944-2952
Universität Wuppertal, Dissertation, Januar 2001
JUEL-3916
20.90.0

IKP-
Tietze, Annegret:
Grundlegende Untersuchungen sicherheitsrelevanter Materialbelastungen zum Targetsystem der "Europäischen Spallations-Neutronenquelle (ESS)" – Vergleich Experiment und Theorie –
Forschungszentrum Jülich, 2001, Universität Wuppertal, Dissertation, Januar 2001
JUEL-3857
20.90.0

XI. INDEX OF AUTHORS